LHCb-ANA-2015-023
7th October 2015
Final

Prompt charm production in pp collisions at $\sqrt{s} = 13\,\text{TeV}$ in 2015 data

C. Burr[1,2], S. Easo[1,3], M. Gersabeck[4], V. Gligorov[3], D. Müller[4], A. Pearce[1,4], P. Spradlin[5].

[1] *STFC Rutherford Appleton Laboratory, Didcot, United Kingdom*
[2] *School of Physics and Astronomy, University of Southampton, Southampton, United Kingdom*
[3] *European Organization for Nuclear Research (CERN), Geneva, Switzerland*
[4] *School of Physics and Astronomy, University of Manchester, Manchester, United Kingdom*
[5] *School of Physics and Astronomy, University of Glasgow, Glasgow, United Kingdom*

LHCb-ANA-2015-023
07/10/2015

Abstract

Production cross sections of prompt open charm hadrons are measured on $\sqrt{s} = 13\,\text{TeV}$ pp collision data corresponding to an integrated luminosity of $(4.98 \pm 0.19)\,\text{pb}^{-1}$ collected during the early 50 ns running period of Run 2. The cross sections of D^0, D^+, D_s^+, and D^{*+} mesons are measured in bins of charm hadron transverse momentum p_T and rapidity y computed in the pp collision rest frame. The total $c\bar{c}$ cross section is determined from these using known fragmentation fractions and is found to be

$$\sigma(pp \to c\bar{c}X) = 2940 \pm 3\ (\text{stat}) \pm 180\ (\text{syst}) \pm 160\ (\text{frag})\,\mu\text{b}.$$

Status of the analysis note

Items that have been struck through (like ~~this~~) have been deleted in later drafts.

Draft 1.0

This draft explains the measurement procedure. Main items that require work in the future are:

- Section 2: this will be filled as the theory predictions become available. A first draft for one prediction is expected in the coming weeks;
- Section 3: description of the `NoBias` 'backup' data;
- Section 3.1: description of the Turbo stream;
- Section 4.3: offline processing remains to be described;
- Section 5.6.4: PID efficiencies remain to be calculated on data;
- Section 7: Systematic uncertainty plans remain to be finalised and eventually calculated;
- Section 9: Results to be included after data taking; and
- Appendix A: Yield tables for full 2011 dataset and results comparisons.

Draft 2.0

The physics issues now addressed in this version are:

- Section 1: D^0 cross check limited to D^{*+}-tagged decays (untagged $D^0 \to K^-\pi^+\pi^-\pi^+$ is not selected);
- Section 1: Be more explicit about intended p_{T}-y binning and the set of proposed measurements;
- Section 2: This now contains a first set of theory predictions. These will be refined once the accompanying documentation is available.
- Section 4: Trigger selection updated with latest selection, stripping selection aligned with trigger cuts;

- Section 5.2.1 and 7.5: Evaluate tracking efficiency correction and associated systematic uncertainty;
- Section 7.3: Method for evaluating systematic uncertainties due to PID calibration sample size and binning schema added and evaluated on a mock-up calibration sample;
- Section 8: Add 2011 $\sqrt{s} = 7\,\text{TeV}$ cross-check, details on the fitter validation; and
- Appendix E: Describe PDF factorisation study.

This draft includes some editorial changes and clarifications, including:

- All equations are now numbered;
- Section 1: Explaining and referencing use of ISO 31-11 set notation;
- Section 3.2: Clarify Turbo stream data flow;
- Section 3.3: Explain background category values 0 and 10;
- Section 4: Moved stripping selection to appendix, as it is not expected to be used in the nominal analysis; and
- Section 8: Moved 2011 $\sqrt{s} = 7\,\text{TeV}$ cross check from appendix to main body of the note.

The known outstanding issues are:

- Section 2: We are expecting predictions from two additional theory groups. Our binning schemas have been provided and we will include descriptions and predictions once they are available;
- Section 7: There are some systematic uncertainties still to be described and evaluated, and we still need to produce a list of approximate expected magnitudes;
- Section 8.3: There is some bias in the fitted signal yield uncertainty; and
- Appendix E: The fit observables appear to be correlated, and this is not yet accounted for in the fit or otherwise proven to be irrelevant.

Other items requiring more work are marked as "TODO: ".

Draft 3.0

The physics issues now addressed in this version are:

- Section 7: Add table containing estimates of systematic uncertainty sizes from most source, and give more detail on determination of selection and tracking systematic uncertainty evaluation; and
- ~~Section ??: Add study of signal mass PDF parameters varying with p_{T} and y~~ removed in Draft 4.0 due to removal of mass fit.

This draft includes some editorial changes and clarifications, including:

- Section 4.2: Clarify splitting of `D2HHH` trigger lines.

The known outstanding issues are:

- Section 2: We are expecting predictions from two additional theory groups. Our binning schemas have been provided and we will include descriptions and predictions once they are available;
- Section 6: There are no plots of fits to the 2015 validation data taken in June, due to several bugs in the Tesla processing step that require the data to be reprocessed;
- Section 5.2.2: The Monte Carlo truth matching inefficiency has been computed but is not yet taken in to account;
- Section 7: There are some systematic uncertainties still to be described and evaluated;
- Section 8.3: There is some bias in the fitted signal yield uncertainty; and
- Appendix E: The fit observables appear to be correlated, and this is not yet accounted for in the fit or otherwise proven to be irrelevant.

Other items requiring more work are marked as "TODO: ".

Draft 4.0

The physics issues now addressed in this version are:

- Section 6: Fitter has been substantially changed in response to finding correlations between the charm hadron mass and $\ln \chi^2_{\mathrm{IP}}$ observables;
- Section 7: Revised correlations in the propagation of hadronic interaction uncertainty on the tracking corrections;
- Section 7: Updated the PID binning scheme uncertainty to incorporate the size of the reference sample in the study; and
- Section 7: Refined correlations between 7 TeV and 13 TeV. Correlations are only assumed for the tracking, branching ratios and luminosity as individual numbers are not recoverable.

This draft includes some editorial changes and clarifications, including:

- Observable name changed from $\log \mathrm{IP}\ \chi^2$ to $\ln \chi^2_{\mathrm{IP}}$ for consistency with the paper;
- Section 3 has been updated with the L0 efficiencies, luminosities, and application versions that are all known now that the data have been taken; and
- ~~Section ?? has only two columns of sub-figures with the main figures extending across multiple pages.~~

The known outstanding issues are:

- Section 6: There are no fits for untagged and tagged D^0 modes, nor for any of the cross-check modes; and
- Section 8.3: The toy studies, so far performed only on the D_s^+ fit, do not show optimal pulls.

Draft 5.0

The physics issues now addressed in this version are:

- Changed D_s^+ control mode from $D_s^+ \to \pi^-\pi^+\pi^+$ to $D_s^+ \to K^-K^+\pi^+$ excluding the ϕ resonance;

- Section 2: Add description of the three theory predictions to be used in the publication;
- Section 3: The data-taking has been completed, information updated to reflect this;
- Section 6: Fitting procedure for D^{*+} is now described;
- Section 7: Almost all systematics have now been computed and are given where available;
- Section 8.3: The observed bias in the fitted prompt signal yield values and uncertainties has been resolved;
- Section 8.2: Added study to check for abnormal candidate multiplicity;
- Section 9: Differential cross-sections for all modes are now given, along with some relative 13 TeV/7 TeV results.

The known outstanding issues are:

- Section 7: The systematic associated to the choice of fit PDFs is still missing;
- Section 9: The integrated $\sigma(H_c)$ cross-sections are missing, as is the integrated $\sigma(c\bar{c})$ cross-section.

Draft 6.0

The physics issues now addressed in this version are:

- All results have been updated to reflect the status of the paper in circulation; and
- New ratio results as in the latest PAPER draft (version 5.2).

This draft includes some editorial changes and clarifications, including:

- Due to the new binning scheme, table size has increased significantly. To improve readability of the main body, only tables for $D^0 \to K^-\pi^+$ are shown, remaining tables have been moved to the appendix.

Contents

1 Introduction **1**

2 Theory **4**
2.1 FONLL (Cacciari et al.) . . . 4
2.2 POWHEG+NNPDF3.0L (Gauld et al.) . . . 5
2.3 GMVFNS (Spiesberger et al.) . . . 7

3 Data **10**
3.1 Trigger strategy . . . 10
3.2 Data flow . . . 11
3.3 Simulation . . . 12
3.3.1 Truth matching . . . 13
3.4 Crossing angle correction . . . 14

4 Selection **16**
4.1 Discriminating variables . . . 16
4.2 Trigger . . . 18
4.2.1 HLT1 reconstruction and selection . . . 19
4.2.2 HLT2 reconstruction and selection . . . 20
4.3 Offline processing . . . 21

5 Efficiencies **25**
5.1 LHCb acceptance . . . 25
5.2 Reconstruction . . . 26
5.2.1 Tracking efficiency correction . . . 26
5.2.2 Monte Carlo truth matching inefficiency . . . 27
5.3 Trigger . . . 33
5.4 Offline selection . . . 33
5.4.1 Boosted decision tree . . . 33
5.5 Combination of efficiencies and their statistical uncertainty . . . 34
5.6 PID calibration . . . 34
5.6.1 Definitions . . . 36
5.6.2 Estimating the efficiency . . . 36
5.6.3 Optimising the binning in the track variables . . . 40
5.6.4 PID efficiencies . . . 42
5.7 Signal window efficiency . . . 46

6 Yield extraction **48**
6.1 Definition of species . . . 48
6.2 Strategy . . . 48
6.3 Construction of probability density functions . . . 49
6.4 Mode-specific details . . . 58
6.5 Fit results . . . 59

7 Systematic uncertainties **91**
7.1 Finite Monte Carlo sample size . . . 91
7.2 Monte Carlo modelling . . . 91
7.3 PID calibration . . . 92
7.3.1 Calibration sample size . . . 93
7.3.2 Binning scheme . . . 93
7.4 Luminosity . . . 98
7.5 Tracking efficiency correction . . . 99
7.6 Branching fractions . . . 100
7.7 Fit model . . . 100
7.8 Correlations and summary . . . 101
7.9 Correlations between 7 TeV and 13 TeV measurements . . . 101

8 Validation **104**
8.1 Dependence of background $\ln \chi^2_{\mathrm{IP}}$ on mass . . . 104
8.2 Number of candidates per event . . . 104
8.3 Checks for fitter biases . . . 106
8.4 Relative cross-sections using 2011 $\sqrt{s} = 7$ TeV data . . . 111

9 Results **129**
9.1 Integrated cross-sections . . . 129
9.2 Total $c\bar{c}$ cross-section . . . 129
9.3 Relative cross-sections . . . 132

A Efficiency tables for modes other than $D^0 \to K^-\pi^+$ **155**
A.1 Tracking correction . . . 155
A.2 MC selection efficiency . . . 162
A.3 PID selection efficiency . . . 168
A.4 Signal window efficiency . . . 174

B Individual per systematic tables **180**
B.1 Finite Monte Carlo statistic . . . 180
B.2 PID calibration sample size . . . 188
B.3 PID binning . . . 196
B.4 Tracking correction . . . 204

C Stripping selections **212**

D Probability density functions **218**

E Factorization of the PDFs **222**

F Fits in p_{T}-y bins **225**
F.1 $D^0 \to K^-\pi^+$ . . . 225
F.2 $D^+ \to K^-\pi^+\pi^+$ . . . 244
F.3 $D^+ \to K^-K^+\pi^+$ . . . 263
F.4 $D_s^+ \to \phi\pi^+$ . . . 281
F.5 $D_s^+ \to K^-K^+\pi^+$ . . . 299
F.6 $D^{*+} \to D^0\pi^+$ with $D^0 \to K^-\pi^+$ . . . 317
F.7 $D^{*+} \to D^0\pi^+$ with $D^0 \to K^-\pi^+\pi^-\pi^+$ . . . 336

G Tables of generator cut efficiencies **355**
G.1 $D^0 \to K^-\pi^+$ . . . 355
G.2 $D^0 \to K^-\pi^+\pi^-\pi^+$ . . . 360
G.3 $D^+ \to K^-\pi^+\pi^+$ . . . 365
G.4 $D^+ \to \phi\pi^+$ . . . 370
G.5 $D_s^+ \to \phi\pi^+$ . . . 375
G.6 $D_s^+ \to \pi^-\pi^+\pi^+$ . . . 380
G.7 $D^{*+} \to D^0\pi^+$, $D^0 \to K^-\pi^+$ . . . 385
G.8 $D^{*+} \to D^0\pi^+$, $D^0 \to K^-\pi^+\pi^-\pi^+$ . . . 390

H Monte Carlo modelling systematic **395**
H.1 An example with $D^0 \to K^-\pi^+$ . . . 395
H.2 $D^0 \to K^-\pi^+$ distributions and result . . . 402
H.3 $D^{*+} \to D^0\pi^+$ with $D^0 \to K^-\pi^+$ distributions and result . . . 410
H.4 $D^{*+} \to D^0\pi^+$ with $D^0 \to K^-\pi^+\pi^-\pi^+$ distributions and result . . . 420
H.5 $D^+ \to K^-\pi^+\pi^+$ distributions and result . . . 434
H.6 $D^+ \to K^-K^+\pi^+$ distributions and result . . . 444
H.7 $D_s^+ \to K^-K^+\pi^+$ distributions and result . . . 454

H.8 $D_s^+ \to \phi\pi^+$ distributions and result 464
H.9 $D_s^+ \to K^-K^+\pi^+$ excluding ϕ distributions and result 474

References **484**

List of Figures

2.1 Prediction for the absolute (top) D^0 and (bottom) D^+ cross-sections at $\sqrt{s} = 13\,\text{TeV}$ as described in the text, provided by [1]. 9
4.1 Schematic of impact parameter computation 19
5.1 Tracking correction table 27
5.2 $D^0 \to K^-\pi^+$ mass distributions for different background categories . 30
5.3 $D^+ \to K^-\pi^+\pi^+$ mass distributions for different background categories 31
5.4 $D^{*+} \to D^0\pi^+$ mass distributions for different background categories . 32
5.5 Example of PID track momentum dependence 41
5.6 PID calibration binning optimisation for $K^\pm$ tracks 43
5.7 PID calibration binning optimisation for $\pi^\pm$ tracks 44
6.1 Signal window and sideband definitions for $D^0 \to K^-\pi^+$ 50
6.2 Signal window and sideband definitions for $D^+ \to K^-\pi^+\pi^+$ 51
6.3 Signal window and sideband definitions for $D^+ \to K^-K^+\pi^+$ 52
6.4 Signal window and sideband definitions for $D_s^+ \to \phi\pi^+$ 53
6.5 Signal window and sideband definitions for $D_s^+ \to K^-K^+\pi^+$ 54
6.6 Signal window and sideband definitions for $D^{*+} \to D^0\pi^+$ with $D^0 \to K^-\pi^+$ 55
6.7 Signal window and sideband definitions for $D^{*+} \to D^0\pi^+$ with $D^0 \to K^-\pi^+\pi^-\pi^+$ 56
6.8 Integrated $\ln\chi^2_{\text{IP}}$ prefits for $D^0 \to K^-\pi^+$ 61
6.9 Integrated $\ln\chi^2_{\text{IP}}$ prefits for $D^+ \to K^-\pi^+\pi^+$ 62
6.10 Integrated $\ln\chi^2_{\text{IP}}$ prefits for $D^+ \to K^-K^+\pi^+$ 63
6.11 Integrated $\ln\chi^2_{\text{IP}}$ prefits for $D_s^+ \to \phi\pi^+$ 64
6.12 Integrated $\ln\chi^2_{\text{IP}}$ prefits for $D_s^+ \to K^-K^+\pi^+$ 65
6.13 Integrated $\ln\chi^2_{\text{IP}}$ prefits for $D^{*+} \to D^0\pi^+$ with $D^0 \to K^-\pi^+$ 66
6.14 Integrated $\ln\chi^2_{\text{IP}}$ prefits for $D^{*+} \to D^0\pi^+$ with $D^0 \to K^-\pi^+\pi^-\pi^+$ . . 67
6.15 Integrated mass fit for $D^0 \to K^-\pi^+$ 68
6.16 Integrated $\ln\chi^2_{\text{IP}}$ fit for $D^0 \to K^-\pi^+$ 69
6.17 Integrated mass fit for $D^+ \to K^-\pi^+\pi^+$ 70
6.18 Integrated $\ln\chi^2_{\text{IP}}$ fit for $D^+ \to K^-\pi^+\pi^+$ 71
6.19 Integrated mass fit for $D^+ \to K^-K^+\pi^+$ 72
6.20 Integrated $\ln\chi^2_{\text{IP}}$ fit for $D^+ \to K^-K^+\pi^+$ 73
6.21 Integrated mass fit for $D_s^+ \to \phi\pi^+$ 74
6.22 Integrated $\ln\chi^2_{\text{IP}}$ fit for $D_s^+ \to \phi\pi^+$ 75
6.23 Integrated mass fit for $D_s^+ \to K^-K^+\pi^+$ 76
6.24 Integrated $\ln\chi^2_{\text{IP}}$ fit for $D_s^+ \to K^-K^+\pi^+$ 77

6.25 Integrated fit to D^0 mass for $D^{*+} \to D^0\pi^+$ with $D^0 \to K^-\pi^+$ 78
6.26 Integrated δm fit for $D^{*+} \to D^0\pi^+$ with $D^0 \to K^-\pi^+$ 79
6.27 Integrated $\ln \chi^2_{\rm IP}$ fit for $D^{*+} \to D^0\pi^+$ with $D^0 \to K^-\pi^+$ 80
6.28 Integrated fit to D^0 mass for $D^{*+} \to D^0\pi^+$ with $D^0 \to K^-\pi^+\pi^-\pi^+$. 81
6.29 Integrated δm fit for $D^{*+} \to D^0\pi^+$ with $D^0 \to K^-\pi^+\pi^-\pi^+$ 82
6.30 Integrated $\ln \chi^2_{\rm IP}$ fit for $D^{*+} \to D^0\pi^+$ with $D^0 \to K^-\pi^+\pi^-\pi^+$ 83
7.1 Comparision data/KDE distributions in p 95
7.2 Comparision data/KDE distributions in η 96
7.3 1D efficiencies with KDE efficiency projection 97
7.4 Example for finely binned calib. for kaons 97
7.5 Example for finely binned calib. for pions 98
7.6 Integrated PID syest. uncert. for $D^0 \to K^-\pi^+$ 99
8.1 PDF factorization plots for the background two-dimensional fits . . . 105
8.2 Distribution of pull parameters for $D^0 \to K^-\pi^+$ PDF 107
8.3 Distribution of pull parameters for $D^+ \to K^-\pi^+\pi^+$ PDF 108
8.4 Distribution of pull parameters for $D_s^+ \to \phi\pi^+$ PDF 109
8.5 Distribution of pull parameters for $D^{*+} \to D^0\pi^+$ with $D^0 \to K^-\pi^+$ PDF 110
8.6 Example $\ln \chi^2_{\rm IP}$ prefits for $D^0 \to K^-\pi^+$ using 2011 data 113
8.7 Example $\ln \chi^2_{\rm IP}$ prefits for $D^+ \to K^-\pi^+\pi^+$ using 2011 data 114
8.8 Example $\ln \chi^2_{\rm IP}$ prefits for $D_s^+ \to \phi\pi^+$ using 2011 data 115
8.9 Example $\ln \chi^2_{\rm IP}$ prefits for $D^{*+} \to D^0\pi^+$ using 2011 data 116
8.10 Example fit projections for $D^0 \to K^-\pi^+$ using 2011 data 117
8.11 Example fit projections for $D^+ \to K^-\pi^+\pi^+$ using 2011 data 118
8.12 Example fit projections for $D_s^+ \to \phi\pi^+$ using 2011 data 119
8.13 Example fit projections for $D^{*+} \to D^0\pi^+$ using 2011 data 120
8.14 Total efficiencies for $D^0 \to K^-\pi^+$ for 2011 123
8.15 Total efficiencies for $D^+ \to K^-\pi^+\pi^+$ for 2011 123
8.16 Total efficiencies for $D_s^+ \to \phi\pi^+$ for 2011 124
8.17 Total efficiencies for $D^{*+} \to D^0\pi^+$ for 2011 124
8.18 2011 cross-check results for $D^0 \to K^-\pi^+$ 125
8.19 2011 cross-check results for $D^+ \to K^-\pi^+\pi^+$ 126
8.20 2011 cross-check results for $D_s^+ \to \phi\pi^+$ 127
8.21 2011 cross-check results for $D^{*+} \to D^0\pi^+$ 128

9.1 Integrated cross-section measurements (black diamonds) as well as their average (black circle and blue band) shown (left) based on the D^0 and D^+ cross-sections and theory predictions (red squares) [1, 2] for $0 < p_{\mathrm{T}} < 8\,\mathrm{GeV}/c$ and (right) for all four mesons for $1 < p_{\mathrm{T}} < 8\,\mathrm{GeV}/c$. The "absolute" predictions are based on calculations of the 13 TeV cross-section, while the "scaled" predictions are based on calculations of the 13 to 7 TeV ratio multiplied with the LHCb measurement. . . 131
9.2 Differential cross-sections for D^0 . . . 137
9.3 Differential cross-sections for D^+ . . . 137
9.4 Differential cross-sections for D_s^+ . . . 138
9.5 Differential cross-sections for D^{*+} . . . 138
9.6 Cross-sections relative between 13 TeV and 7 TeV for D^0 . . . 139
9.7 Cross-sections relative between 13 TeV and 7 TeV for D^+ . . . 140
9.8 Cross-sections relative between 13 TeV and 7 TeV for D_s^+ . . . 141
9.9 Cross-sections relative between 13 TeV and 7 TeV for D^{*+} . . . 142
9.10 Ratios of cross-section measurements of (top) D^+, (middle) D_s^+, and (bottom) D^{*+} mesons with respect to the D^0 cross-sections. The blue bands indicate the corresponding ratios of fragmentation fractions. The ratios are given as a function of p_{T} and different symbols indicate different ranges in y. . . . 147
9.11 Ratios of cross-section measurements of (top) D^{*+}, and (middle) D_s^+ mesons with respect to D^+ cross-sections, and (bottom) D_s^+ over D^{*+} mesons. The blue bands indicate the corresponding ratios of fragmentation fractions. The ratios are given as a function of p_{T} and different symbols indicate different ranges in y. . . . 148
E.1 PDF factorization plots for the background three-dimensional fits . . 222
E.2 PDF factorization plots for the background two-dimensional fits . . . 223
E.3 PDF factorization plots for the background three-dimensional fits . . 224
F.0 $\ln \chi^2_{\mathrm{IP}}$ fits per p_{T}-y bin for $D^0 \to K^-\pi^+$ . . . 243
F.0 $\ln \chi^2_{\mathrm{IP}}$ fits per p_{T}-y bin for $D^+ \to K^-\pi^+\pi^+$ . . . 262
F.0 $\ln \chi^2_{\mathrm{IP}}$ fits per p_{T}-y bin for $D^+ \to K^-K^+\pi^+$ . . . 280
F.0 $\ln \chi^2_{\mathrm{IP}}$ fits per p_{T}-y bin for $D_s^+ \to \phi\pi^+$ . . . 298
F.0 $\ln \chi^2_{\mathrm{IP}}$ fits per p_{T}-y bin for $D_s^+ \to K^-K^+\pi^+$ . . . 316
F.0 $\ln \chi^2_{\mathrm{IP}}$ fits per p_{T}-y bin for $D^{*+} \to D^0\pi^+$ with $D^0 \to K^-\pi^+$ . . . 335
F.0 $\ln \chi^2_{\mathrm{IP}}$ fits per p_{T}-y bin for $D^{*+} \to D^0\pi^+$ with $D^0 \to K^-\pi^+\pi^-\pi^+$ . . . 354
H.1 Data MC agreement for D0_DIRA_OWNPV in 2015 MagDown $D^0 \to K^-\pi^+$ . . . 403

H.2 Data MC agreement for D0_ENDVERTEX_CHI2/D0_ENDVERTEX_NDOF in 2015 MagDown $D^0 \to K^-\pi^+$ . . . 403
H.3 Data MC agreement for D0_Loki_AMINDOCA in 2015 MagDown $D^0 \to K^-\pi^+$ . . . 404
H.4 Data MC agreement for D0_Loki_BPVVDCHI2 in 2015 MagDown $D^0 \to K^-\pi^+$ . . . 404
H.5 Data MC agreement for D0_h1_TRACK_CHI2NDOF in 2015 MagDown $D^0 \to K^-\pi^+$ . . . 405
H.6 Data MC agreement for D0_h2_TRACK_CHI2NDOF in 2015 MagDown $D^0 \to K^-\pi^+$ . . . 405
H.7 Data MC agreement for D0_h1_ETA in 2015 MagDown $D^0 \to K^-\pi^+$. 406
H.8 Data MC agreement for D0_h2_ETA in 2015 MagDown $D^0 \to K^-\pi^+$. 406
H.9 Data MC agreement for D0_h1_P in 2015 MagDown $D^0 \to K^-\pi^+$ . . 407
H.10 Data MC agreement for D0_h2_P in 2015 MagDown $D^0 \to K^-\pi^+$ . . 407
H.11 Data MC agreement for D0_h1_PT in 2015 MagDown $D^0 \to K^-\pi^+$. 408
H.12 Data MC agreement for D0_h2_PT in 2015 MagDown $D^0 \to K^-\pi^+$. 408
H.13 Data MC agreement result for 2015 MagDown $D^0 \to K^-\pi^+$ 409
H.14 Data MC agreement for Dst_ENDVERTEX_CHI2/Dst_ENDVERTEX_NDOF in 2015 MagDown $D^{*+} \to D^0\pi^+$ with $D^0 \to K^-\pi^+$ . . . 411
H.15 Data MC agreement for Dst_pi_TRACK_CHI2NDOF in 2015 MagDown $D^{*+} \to D^0\pi^+$ with $D^0 \to K^-\pi^+$ . . . 411
H.16 Data MC agreement for D0_FDCHI2_OWNPV in 2015 MagDown $D^{*+} \to D^0\pi^+$ with $D^0 \to K^-\pi^+$ . . . 412
H.17 Data MC agreement for Dst_pi_PT in 2015 MagDown $D^{*+} \to D^0\pi^+$ with $D^0 \to K^-\pi^+$ . . . 412
H.18 Data MC agreement for D0_DIRA_OWNPV in 2015 MagDown $D^{*+} \to D^0\pi^+$ with $D^0 \to K^-\pi^+$ . . . 413
H.19 Data MC agreement for D0_ENDVERTEX_CHI2/D0_ENDVERTEX_NDOF in 2015 MagDown $D^{*+} \to D^0\pi^+$ with $D^0 \to K^-\pi^+$ . . . 413
H.20 Data MC agreement for D0_Loki_DOCAMAX in 2015 MagDown $D^{*+} \to D^0\pi^+$ with $D^0 \to K^-\pi^+$ . . . 414
H.21 Data MC agreement for D0_h1_TRACK_CHI2NDOF in 2015 MagDown $D^{*+} \to D^0\pi^+$ with $D^0 \to K^-\pi^+$ . . . 414
H.22 Data MC agreement for D0_h2_TRACK_CHI2NDOF in 2015 MagDown $D^{*+} \to D^0\pi^+$ with $D^0 \to K^-\pi^+$ . . . 415
H.23 Data MC agreement for D0_h1_ETA in 2015 MagDown $D^{*+} \to D^0\pi^+$ with $D^0 \to K^-\pi^+$ . . . 415

H.24 Data MC agreement for D0_h2_ETA in 2015 MagDown $D^{*+} \to D^0\pi^+$ with $D^0 \to K^-\pi^+$ . . . 416
H.25 Data MC agreement for D0_h1_P in 2015 MagDown $D^{*+} \to D^0\pi^+$ with $D^0 \to K^-\pi^+$ . . . 416
H.26 Data MC agreement for D0_h2_P in 2015 MagDown $D^{*+} \to D^0\pi^+$ with $D^0 \to K^-\pi^+$ . . . 417
H.27 Data MC agreement for D0_h1_PT in 2015 MagDown $D^{*+} \to D^0\pi^+$ with $D^0 \to K^-\pi^+$ . . . 417
H.28 Data MC agreement for D0_h2_PT in 2015 MagDown $D^{*+} \to D^0\pi^+$ with $D^0 \to K^-\pi^+$ . . . 418
H.29 Data MC agreement result for 2015 MagDown $D^{*+} \to D^0\pi^+$ with $D^0 \to K^-\pi^+$ . . . 419
H.30 Data MC agreement for Dst_ENDVERTEX_CHI2/Dst_ENDVERTEX_NDOF in 2015 MagDown $D^{*+} \to D^0\pi^+$ with $D^0 \to K^-\pi^+\pi^-\pi^+$ . . . 421
H.31 Data MC agreement for Dst_pi_TRACK_CHI2NDOF in 2015 MagDown $D^{*+} \to D^0\pi^+$ with $D^0 \to K^-\pi^+\pi^-\pi^+$ . . . 421
H.32 Data MC agreement for D0_Loki_BPVLTIME in 2015 MagDown $D^{*+} \to D^0\pi^+$ with $D^0 \to K^-\pi^+\pi^-\pi^+$ . . . 422
H.33 Data MC agreement for Dst_pi_PT in 2015 MagDown $D^{*+} \to D^0\pi^+$ with $D^0 \to K^-\pi^+\pi^-\pi^+$ . . . 422
H.34 Data MC agreement for D0_DIRA_OWNPV in 2015 MagDown $D^{*+} \to D^0\pi^+$ with $D^0 \to K^-\pi^+\pi^-\pi^+$ . . . 423
H.35 Data MC agreement for D0_ENDVERTEX_CHI2/D0_ENDVERTEX_NDOF in 2015 MagDown $D^{*+} \to D^0\pi^+$ with $D^0 \to K^-\pi^+\pi^-\pi^+$ . . . 423
H.36 Data MC agreement for D0_Loki_DOCAMAX in 2015 MagDown $D^{*+} \to D^0\pi^+$ with $D^0 \to K^-\pi^+\pi^-\pi^+$ . . . 424
H.37 Data MC agreement for D0_h1_TRACK_CHI2NDOF in 2015 MagDown $D^{*+} \to D^0\pi^+$ with $D^0 \to K^-\pi^+\pi^-\pi^+$ . . . 424
H.38 Data MC agreement for D0_h2_TRACK_CHI2NDOF in 2015 MagDown $D^{*+} \to D^0\pi^+$ with $D^0 \to K^-\pi^+\pi^-\pi^+$ . . . 425
H.39 Data MC agreement for D0_h3_TRACK_CHI2NDOF in 2015 MagDown $D^{*+} \to D^0\pi^+$ with $D^0 \to K^-\pi^+\pi^-\pi^+$ . . . 425
H.40 Data MC agreement for D0_h4_TRACK_CHI2NDOF in 2015 MagDown $D^{*+} \to D^0\pi^+$ with $D^0 \to K^-\pi^+\pi^-\pi^+$ . . . 426
H.41 Data MC agreement for D0_h1_ETA in 2015 MagDown $D^{*+} \to D^0\pi^+$ with $D^0 \to K^-\pi^+\pi^-\pi^+$ . . . 426
H.42 Data MC agreement for D0_h2_ETA in 2015 MagDown $D^{*+} \to D^0\pi^+$ with $D^0 \to K^-\pi^+\pi^-\pi^+$ . . . 427

H.43 Data MC agreement for D0_h3_ETA in 2015 MagDown $D^{*+} \to D^0\pi^+$ with $D^0 \to K^-\pi^+\pi^-\pi^+$ . . . 427
H.44 Data MC agreement for D0_h4_ETA in 2015 MagDown $D^{*+} \to D^0\pi^+$ with $D^0 \to K^-\pi^+\pi^-\pi^+$ . . . 428
H.45 Data MC agreement for D0_h1_P in 2015 MagDown $D^{*+} \to D^0\pi^+$ with $D^0 \to K^-\pi^+\pi^-\pi^+$ . . . 428
H.46 Data MC agreement for D0_h2_P in 2015 MagDown $D^{*+} \to D^0\pi^+$ with $D^0 \to K^-\pi^+\pi^-\pi^+$ . . . 429
H.47 Data MC agreement for D0_h3_P in 2015 MagDown $D^{*+} \to D^0\pi^+$ with $D^0 \to K^-\pi^+\pi^-\pi^+$ . . . 429
H.48 Data MC agreement for D0_h4_P in 2015 MagDown $D^{*+} \to D^0\pi^+$ with $D^0 \to K^-\pi^+\pi^-\pi^+$ . . . 430
H.49 Data MC agreement for D0_h1_PT in 2015 MagDown $D^{*+} \to D^0\pi^+$ with $D^0 \to K^-\pi^+\pi^-\pi^+$ . . . 430
H.50 Data MC agreement for D0_h2_PT in 2015 MagDown $D^{*+} \to D^0\pi^+$ with $D^0 \to K^-\pi^+\pi^-\pi^+$ . . . 431
H.51 Data MC agreement for D0_h3_PT in 2015 MagDown $D^{*+} \to D^0\pi^+$ with $D^0 \to K^-\pi^+\pi^-\pi^+$ . . . 431
H.52 Data MC agreement for D0_h4_PT in 2015 MagDown $D^{*+} \to D^0\pi^+$ with $D^0 \to K^-\pi^+\pi^-\pi^+$ . . . 432
H.53 Data MC agreement result for 2015 MagDown $D^{*+} \to D^0\pi^+$ with $D^0 \to K^-\pi^+\pi^-\pi^+$ . . . 433
H.54 Data MC agreement for Dp_DIRA_OWNPV in 2015 MagDown $D^+ \to K^-\pi^+\pi^+$ . . . 435
H.55 Data MC agreement for Dp_ENDVERTEX_CHI2/Dp_ENDVERTEX_NDOF in 2015 MagDown $D^+ \to K^-\pi^+\pi^+$ . . . 435
H.56 Data MC agreement for Dp_FDCHI2_OWNPV in 2015 MagDown $D^+ \to K^-\pi^+\pi^+$ . . . 436
H.57 Data MC agreement for Dp_Loki_BPVLTIME in 2015 MagDown $D^+ \to K^-\pi^+\pi^+$ . . . 436
H.58 Data MC agreement for Dp_h1_TRACK_CHI2NDOF in 2015 MagDown $D^+ \to K^-\pi^+\pi^+$ . . . 437
H.59 Data MC agreement for Dp_h2_TRACK_CHI2NDOF in 2015 MagDown $D^+ \to K^-\pi^+\pi^+$ . . . 437
H.60 Data MC agreement for Dp_h3_TRACK_CHI2NDOF in 2015 MagDown $D^+ \to K^-\pi^+\pi^+$ . . . 438
H.61 Data MC agreement for Dp_h1_ETA in 2015 MagDown $D^+ \to K^-\pi^+\pi^+$ 438
H.62 Data MC agreement for Dp_h2_ETA in 2015 MagDown $D^+ \to K^-\pi^+\pi^+$ 439

H.63 Data MC agreement for Dp_h3_ETA in 2015 MagDown $D^+ \to K^-\pi^+\pi^+$ 439
H.64 Data MC agreement for Dp_h1_P in 2015 MagDown $D^+ \to K^-\pi^+\pi^+$ 440
H.65 Data MC agreement for Dp_h2_P in 2015 MagDown $D^+ \to K^-\pi^+\pi^+$ 440
H.66 Data MC agreement for Dp_h3_P in 2015 MagDown $D^+ \to K^-\pi^+\pi^+$ 441
H.67 Data MC agreement for Dp_PT_First in 2015 MagDown $D^+ \to K^-\pi^+\pi^+$ 441
H.68 Data MC agreement for Dp_PT_Second in 2015 MagDown $D^+ \to K^-\pi^+\pi^+$ . . . 442
H.69 Data MC agreement for Dp_PT_Third in 2015 MagDown $D^+ \to K^-\pi^+\pi^+$ 442
H.70 Data MC agreement result for 2015 MagDown $D^+ \to K^-\pi^+\pi^+$ 443
H.71 Data MC agreement for Dp_DIRA_OWNPV in 2015 MagDown $D^+ \to K^-K^+\pi^+$ . . . 445
H.72 Data MC agreement for Dp_ENDVERTEX_CHI2/Dp_ENDVERTEX_NDOF in 2015 MagDown $D^+ \to K^-K^+\pi^+$ . . . 445
H.73 Data MC agreement for Dp_FDCHI2_OWNPV in 2015 MagDown $D^+ \to K^-K^+\pi^+$ . . . 446
H.74 Data MC agreement for Dp_Loki_BPVLTIME in 2015 MagDown $D^+ \to K^-K^+\pi^+$ . . . 446
H.75 Data MC agreement for Dp_h1_TRACK_CHI2NDOF in 2015 MagDown $D^+ \to K^-K^+\pi^+$ . . . 447
H.76 Data MC agreement for Dp_h2_TRACK_CHI2NDOF in 2015 MagDown $D^+ \to K^-K^+\pi^+$ . . . 447
H.77 Data MC agreement for Dp_h3_TRACK_CHI2NDOF in 2015 MagDown $D^+ \to K^-K^+\pi^+$ . . . 448
H.78 Data MC agreement for Dp_h1_ETA in 2015 MagDown $D^+ \to K^-K^+\pi^+$ 448
H.79 Data MC agreement for Dp_h2_ETA in 2015 MagDown $D^+ \to K^-K^+\pi^+$ 449
H.80 Data MC agreement for Dp_h3_ETA in 2015 MagDown $D^+ \to K^-K^+\pi^+$ 449
H.81 Data MC agreement for Dp_h1_P in 2015 MagDown $D^+ \to K^-K^+\pi^+$ 450
H.82 Data MC agreement for Dp_h2_P in 2015 MagDown $D^+ \to K^-K^+\pi^+$ 450
H.83 Data MC agreement for Dp_h3_P in 2015 MagDown $D^+ \to K^-K^+\pi^+$ 451
H.84 Data MC agreement for Dp_PT_First in 2015 MagDown $D^+ \to K^-K^+\pi^+$ 451
H.85 Data MC agreement for Dp_PT_Second in 2015 MagDown $D^+ \to K^-K^+\pi^+$ . . . 452
H.86 Data MC agreement for Dp_PT_Third in 2015 MagDown $D^+ \to K^-K^+\pi^+$ . . . 452
H.87 Data MC agreement result for 2015 MagDown $D^+ \to K^-K^+\pi^+$ . . . 453
H.88 Data MC agreement for Ds_DIRA_OWNPV in 2015 MagDown $D_s^+ \to K^-K^+\pi^+$ . . . 455

H.89 Data MC agreement for Ds_ENDVERTEX_CHI2/Ds_ENDVERTEX_NDOF in 2015 MagDown $D_s^+ \to K^-K^+\pi^+$ . . . 455
H.90 Data MC agreement for Ds_FDCHI2_OWNPV in 2015 MagDown $D_s^+ \to K^-K^+\pi^+$ . . . 456
H.91 Data MC agreement for Ds_Loki_BPVLTIME in 2015 MagDown $D_s^+ \to K^-K^+\pi^+$ . . . 456
H.92 Data MC agreement for Ds_h1_TRACK_CHI2NDOF in 2015 MagDown $D_s^+ \to K^-K^+\pi^+$ . . . 457
H.93 Data MC agreement for Ds_h2_TRACK_CHI2NDOF in 2015 MagDown $D_s^+ \to K^-K^+\pi^+$ . . . 457
H.94 Data MC agreement for Ds_h3_TRACK_CHI2NDOF in 2015 MagDown $D_s^+ \to K^-K^+\pi^+$ . . . 458
H.95 Data MC agreement for Ds_h1_ETA in 2015 MagDown $D_s^+ \to K^-K^+\pi^+$ 458
H.96 Data MC agreement for Ds_h2_ETA in 2015 MagDown $D_s^+ \to K^-K^+\pi^+$ 459
H.97 Data MC agreement for Ds_h3_ETA in 2015 MagDown $D_s^+ \to K^-K^+\pi^+$ 459
H.98 Data MC agreement for Ds_h1_P in 2015 MagDown $D_s^+ \to K^-K^+\pi^+$ 460
H.99 Data MC agreement for Ds_h2_P in 2015 MagDown $D_s^+ \to K^-K^+\pi^+$ 460
H.100 Data MC agreement for Ds_h3_P in 2015 MagDown $D_s^+ \to K^-K^+\pi^+$ 461
H.101 Data MC agreement for Ds_PT_First in 2015 MagDown $D_s^+ \to K^-K^+\pi^+$ 461
H.102 Data MC agreement for Ds_PT_Second in 2015 MagDown $D_s^+ \to K^-K^+\pi^+$ . . . 462
H.103 Data MC agreement for Ds_PT_Third in 2015 MagDown $D_s^+ \to K^-K^+\pi^+$ 462
H.104 Data MC agreement result for 2015 MagDown $D_s^+ \to K^-K^+\pi^+$ . . . 463
H.105 Data MC agreement for Ds_DIRA_OWNPV in 2015 MagDown $D_s^+ \to \phi\pi^+$ . . . 465
H.106 Data MC agreement for Ds_ENDVERTEX_CHI2/Ds_ENDVERTEX_NDOF in 2015 MagDown $D_s^+ \to \phi\pi^+$ . . . 465
H.107 Data MC agreement for Ds_FDCHI2_OWNPV in 2015 MagDown $D_s^+ \to \phi\pi^+$ . . . 466
H.108 Data MC agreement for Ds_Loki_BPVLTIME in 2015 MagDown $D_s^+ \to \phi\pi^+$ . . . 466
H.109 Data MC agreement for Ds_h1_TRACK_CHI2NDOF in 2015 MagDown $D_s^+ \to \phi\pi^+$ . . . 467
H.110 Data MC agreement for Ds_h2_TRACK_CHI2NDOF in 2015 MagDown $D_s^+ \to \phi\pi^+$ . . . 467
H.111 Data MC agreement for Ds_h3_TRACK_CHI2NDOF in 2015 MagDown $D_s^+ \to \phi\pi^+$ . . . 468
H.112 Data MC agreement for Ds_h1_ETA in 2015 MagDown $D_s^+ \to \phi\pi^+$ . . 468

H.113 Data MC agreement for Ds_h2_ETA in 2015 MagDown $D_s^+ \to \phi\pi^+$ . . 469
H.114 Data MC agreement for Ds_h3_ETA in 2015 MagDown $D_s^+ \to \phi\pi^+$ . . 469
H.115 Data MC agreement for Ds_h1_P in 2015 MagDown $D_s^+ \to \phi\pi^+$ . . . 470
H.116 Data MC agreement for Ds_h2_P in 2015 MagDown $D_s^+ \to \phi\pi^+$ . . . 470
H.117 Data MC agreement for Ds_h3_P in 2015 MagDown $D_s^+ \to \phi\pi^+$ . . . 471
H.118 Data MC agreement for Ds_PT_First in 2015 MagDown $D_s^+ \to \phi\pi^+$. 471
H.119 Data MC agreement for Ds_PT_Second in 2015 MagDown $D_s^+ \to \phi\pi^+$ 472
H.120 Data MC agreement for Ds_PT_Third in 2015 MagDown $D_s^+ \to \phi\pi^+$. 472
H.121 Data MC agreement result for 2015 MagDown $D_s^+ \to \phi\pi^+$ 473
H.122 Data MC agreement for Ds_DIRA_OWNPV in 2015 MagDown $D_s^+ \to K^-K^+\pi^+$ excluding ϕ 475
H.123 Data MC agreement for Ds_ENDVERTEX_CHI2/Ds_ENDVERTEX_NDOF in 2015 MagDown $D_s^+ \to K^-K^+\pi^+$ excluding ϕ 475
H.124 Data MC agreement for Ds_FDCHI2_OWNPV in 2015 MagDown $D_s^+ \to K^-K^+\pi^+$ excluding ϕ 476
H.125 Data MC agreement for Ds_Loki_BPVLTIME in 2015 MagDown $D_s^+ \to K^-K^+\pi^+$ excluding ϕ 476
H.126 Data MC agreement for Ds_h1_TRACK_CHI2NDOF in 2015 MagDown $D_s^+ \to K^-K^+\pi^+$ excluding ϕ 477
H.127 Data MC agreement for Ds_h2_TRACK_CHI2NDOF in 2015 MagDown $D_s^+ \to K^-K^+\pi^+$ excluding ϕ 477
H.128 Data MC agreement for Ds_h3_TRACK_CHI2NDOF in 2015 MagDown $D_s^+ \to K^-K^+\pi^+$ excluding ϕ 478
H.129 Data MC agreement for Ds_h1_ETA in 2015 MagDown $D_s^+ \to K^-K^+\pi^+$ excluding ϕ 478
H.130 Data MC agreement for Ds_h2_ETA in 2015 MagDown $D_s^+ \to K^-K^+\pi^+$ excluding ϕ 479
H.131 Data MC agreement for Ds_h3_ETA in 2015 MagDown $D_s^+ \to K^-K^+\pi^+$ excluding ϕ 479
H.132 Data MC agreement for Ds_h1_P in 2015 MagDown $D_s^+ \to K^-K^+\pi^+$ excluding ϕ 480
H.133 Data MC agreement for Ds_h2_P in 2015 MagDown $D_s^+ \to K^-K^+\pi^+$ excluding ϕ 480
H.134 Data MC agreement for Ds_h3_P in 2015 MagDown $D_s^+ \to K^-K^+\pi^+$ excluding ϕ 481
H.135 Data MC agreement for Ds_PT_First in 2015 MagDown $D_s^+ \to K^-K^+\pi^+$ excluding ϕ 481

H.136 Data MC agreement for Ds_PT_Second in 2015 MagDown $D_s^+ \to K^-K^+\pi^+$ excluding ϕ 482
H.137 Data MC agreement for Ds_PT_Third in 2015 MagDown $D_s^+ \to K^-K^+\pi^+$ excluding ϕ 482
H.138 Data MC agreement result for 2015 MagDown $D_s^+ \to K^-K^+\pi^+$ excluding ϕ 483

List of Tables

1.1 Summary of $\sqrt{s} = 7\,\text{TeV}$ charm cross section analysis results 3
3.1 List of fills and L0 rates. 11
3.2 List of event types simulated for each decay mode 13
4.1 HLT1 `1Track` selection 20
4.2 $D^0 \to K^-\pi^+$ HLT2 selection 21
4.3 $D^0 \to K^-\pi^+\pi^-\pi^+$ HLT2 selection 22
4.4 Common D^{*+} HLT2 selection 22
4.5 $D^+ \to h^-h^+h^+$ HLT2 selection 23
5.1 Tracking efficiency correction for $D^0 \to K^-\pi^+$. Shown uncertainties are due to the size of the simulated sample. 28
5.2 Truth matching efficiencies 29
5.3 MC selection efficiency $D^0 \to K^-\pi^+$ 35
5.4 Total PID selection efficiency for $D^0 \to K^-\pi^+$ in bins of D^0 p_T and y. Shown uncertainties are due to the size of the calibration sample. . . 45
5.5 Signal window requirement efficiencies for $D^0 \to K^-\pi^+$ 47
6.1 Prompt signal yields for $D^0 \to K^-\pi^+$ 84
6.2 Prompt signal yields for $D^+ \to K^-\pi^+\pi^+$ 85
6.3 Prompt signal yields for $D^+ \to K^-K^+\pi^+$ 86
6.4 Prompt signal yields for $D_s^+ \to \phi\pi^+$ 87
6.5 Prompt signal yields for $D_s^+ \to K^-K^+\pi^+$ 88
6.6 Prompt signal yields for $D^{*+} \to D^0\pi^+$ with $D^0 \to K^-\pi^+$ 89
6.7 Prompt signal yields for $D^{*+} \to D^0\pi^+$ with $D^0 \to K^-\pi^+\pi^-\pi^+$ 90
7.1 Monte Carlo modelling systematic results 92
7.2 Branching ratios 100
7.3 Systematic uncertainties summary 102
8.1 Relative number of events in % split into different candidate multiplicities. Each event is identified by a unique `runNumber-eventNumber` combination. 104
8.2 Prompt signal yields for $D^0 \to K^-\pi^+$ in 2011 data 121
8.3 Prompt signal yields for $D^+ \to K^-\pi^+\pi^+$ in 2011 data 121
8.4 Prompt signal yields for $D_s^+ \to \phi\pi^+$ in 2011 data 122
8.5 Prompt signal yields for $D^{*+} \to D^0\pi^+$, with $D^0 \to K^-\pi^+$, in 2011 data 122
9.1 Integrated charm hadron cross-sections 130
9.2 Charm hadron fragmentation fractions 130
9.3 Differential cross-sections for D^0 133
9.4 Differential cross-sections for D^+ 134

9.5 Differential cross-sections for D_s^+ 135
9.6 Differential cross-sections for D^{*+} 136
9.7 Relative cross-sections for $D^0 \to K^-\pi^+$ 143
9.8 Relative cross-sections for $D^+ \to K^-\pi^+\pi^+$ 144
9.9 Relative cross-sections for $D_s^+ \to \phi\pi^+$ 145
9.10 Relative cross-sections for $D^{*+} \to D^0\pi^+$ with $D^0 \to K^-\pi^+$ 146
9.11 The ratios of differential production cross-sections in 10^{-2} for prompt D^+ and D^0 mesons in bins of (y, p_T). The first uncertainty is statistical, and the second is the total systematic. 149
9.12 The ratios of differential production cross-sections in 10^{-2} for prompt D_s^+ and D^0 mesons in bins of (y, p_T). The first uncertainty is statistical, and the second is the total systematic. 150
9.13 The ratios of differential production cross-sections in 10^{-2} for prompt D^{*+} and D^0 mesons in bins of (y, p_T). The first uncertainty is statistical, and the second is the total systematic. 151
9.14 The ratios of differential production cross-sections in 10^{-2} for prompt D_s^+ and D^+ mesons in bins of (y, p_T). The first uncertainty is statistical, and the second is the total systematic. 152
9.15 The ratios of differential production cross-sections in 10^{-2} for prompt D^{*+} and D^+ mesons in bins of (y, p_T). The first uncertainty is statistical, and the second is the total systematic. 153
9.16 The ratios of differential production cross-sections in 10^{-2} for prompt D_s^+ and D^{*+} mesons in bins of (y, p_T). The first uncertainty is statistical, and the second is the total systematic. 154
A.1 Tracking efficiency correction for $D^+ \to K^-\pi^+\pi^+$. Shown uncertainties are due to the size of the simulated sample. 156
A.2 Tracking efficiency correction for $D^+ \to K^-K^+\pi^+$. Shown uncertainties are due to the size of the simulated sample. 157
A.3 Tracking efficiency correction for $D_s^+ \to \phi\pi^+$. Shown uncertainties are due to the size of the simulated sample. 158
A.4 Tracking efficiency correction for $D_s^+ \to K^-K^+\pi^+$ no ϕ. Shown uncertainties are due to the size of the simulated sample. 159
A.5 Tracking efficiency correction for $D^{*+} \to D^0\pi^+$ with $D^0 \to K^-\pi^+$. Shown uncertainties are due to the size of the simulated sample. . . . 160
A.6 Tracking efficiency correction for $D^{*+} \to D^0\pi^+$ with $D^0 \to K^-\pi^+\pi^-\pi^+$. Shown uncertainties are due to the size of the simulated sample. . . . 161
A.7 MC selection efficiency $D^+ \to K^-\pi^+\pi^+$ 162
A.8 MC selection efficiency $D^+ \to K^-K^+\pi^+$ 163

A.9 MC selection efficiency $D_s^+ \to \phi\pi^+$ 164
A.10 MC selection efficiency $D_s^+ \to K^-K^+\pi^+$ 165
A.11 MC selection efficiency $D^{*+} \to D^0\pi^+$ with $D^0 \to K^-\pi^+$ 166
A.12 MC selection efficiency $D^{*+} \to D^0\pi^+$ with $D^0 \to K^-\pi^+\pi^-\pi^+$ 167
A.13 Total PID selection efficiency for $D^+ \to K^-\pi^+\pi^+$ in bins of D^+ p_{T} and y. Shown uncertainties are due to the size of the calibration sample. 168
A.14 Total PID selection efficiency for $D^+ \to K^-K^+\pi^+$ in bins of D^+ p_{T} and y. Shown uncertainties are due to the size of the calibration sample. 169
A.15 Total PID selection efficiency for $D_s^+ \to \phi\pi^+$ in bins of D_s^+ p_{T} and y. Shown uncertainties are due to the size of the calibration sample. . . 170
A.16 Total PID selection efficiency for $D_s^+ \to K^-K^+\pi^+$ in bins of D_s^+ p_{T} and y. Shown uncertainties are due to the size of the calibration sample. 171
A.17 Total PID selection efficiency for $D^{*+} \to D^0\pi^+$, with $D^0 \to K^-\pi^+$, in bins of D^{*+} p_{T} and y. Shown uncertainties are due to the size of the calibration sample. 172
A.18 Total PID selection efficiency for $D^{*+} \to D^0\pi^+$, with $D^0 \to K^-\pi^+\pi^-\pi^+$, in bins of D^{*+} p_{T} and y. Shown uncertainties are due to the size of the calibration sample. 173
A.19 Signal window requirement efficiencies for $D^+ \to K^-\pi^+\pi^+$ 174
A.20 Signal window requirement efficiencies for $D^+ \to K^-K^+\pi^+$ 175
A.21 Signal window requirement efficiencies for $D_s^+ \to \phi\pi^+$ 176
A.22 Signal window requirement efficiencies for $D_s^+ \to K^-K^+\pi^+$ 177
A.23 Signal window requirement efficiencies for $D^{*+} \to D^0\pi^+$ with $D^0 \to K^-\pi^+$ 178
A.24 Signal window requirement efficiencies for $D^{*+} \to D^0\pi^+$ with $D^0 \to K^-\pi^+\pi^-\pi^+$ 179
B.1 MC stat. uncert. $D^0 \to K^-\pi^+$ 181
B.2 MC stat. uncert. $D^+ \to K^-\pi^+\pi^+$ 182
B.3 MC stat. uncert. $D^+ \to K^-K^+\pi^+$ 183
B.4 MC stat. uncert. $D_s^+ \to \phi\pi^+$ 184
B.5 MC stat. uncert. $D_s^+ \to K^-K^+\pi^+$ 185
B.6 MC stat. uncert. $D^{*+} \to D^0\pi^+$, $D^0 \to K^-\pi^+$ 186
B.7 MC stat. uncert. $D^{*+} \to D^0\pi^+$, $D^0 \to K^-\pi^+\pi^-\pi^+$ 187
B.8 PID syst. uncert. from cal. size $D^0 \to K^-\pi^+$ 189
B.9 PID syst. uncert. from cal. size $D^+ \to K^-\pi^+\pi^+$ 190
B.10 PID syst. uncert. from cal. size $D^+ \to K^-K^+\pi^+$ 191
B.11 PID syst. uncert. from cal. size $D_s^+ \to \phi\pi^+$ 192
B.12 PID syst. uncert. from cal. size $D_s^+ \to K^-K^+\pi^+$ 193

B.13 PID syst. uncert. from cal. size $D^{*+} \to D^0\pi^+$ with $D^0 \to K^-\pi^+$ . . . 194
B.14 PID syst. uncert. from cal. size $D^{*+} \to D^0\pi^+$ with $D^0 \to K^-\pi^+\pi^-\pi^+$ 195
B.15 PID syst. uncert. from binning $D^0 \to K^-\pi^+$ 197
B.16 PID syst. uncert. from binning $D^+ \to K^-\pi^+\pi^+$ 198
B.17 PID syst. uncert. from binning $D^+ \to K^-K^+\pi^+$ 199
B.18 PID syst. uncert. from binning $D_s^+ \to \phi\pi^+$ 200
B.19 PID syst. uncert. from binning $D_s^+ \to K^-K^+\pi^+$ 201
B.20 PID syst. uncert. from binning $D^{*+} \to D^0\pi^+$ with $D^0 \to K^-\pi^+$ . . . 202
B.21 PID syst. uncert. from binning $D^{*+} \to D^0\pi^+$ with $D^0 \to K^-\pi^+\pi^-\pi^+$ 203
B.22 Tracking syst. uncert. $D^0 \to K^-\pi^+$ 205
B.23 Tracking syst. uncert. $D^+ \to K^-\pi^+\pi^+$ 206
B.24 Tracking syst. uncert. $D^+ \to K^-K^+\pi^+$ 207
B.25 Tracking syst. uncert. $D_s^+ \to \phi\pi^+$ 208
B.26 Tracking syst. uncert. $D_s^+ \to K^-K^+\pi^+$ no ϕ 209
B.27 Tracking syst. uncert. $D^{*+} \to D^0\pi^+$, $D^0 \to K^-\pi^+$ 210
B.28 Tracking syst. uncert. $D^{*+} \to D^0\pi^+$, $D^0 \to K^-\pi^+\pi^-\pi^+$ 211
C.1 $D^0 \to K^-\pi^+$ stripping selection 214
C.2 $D^0 \to K^-\pi^+\pi^-\pi^+$ stripping selection 215
C.3 $D^+ \to h^-h^+h^+$ stripping selection 216
C.4 $D_{(s)}^+ \to \phi\pi^+$ stripping selection 217
G.1 Efficiency of DaughtersInLHCb for D^0 in MagDown event type 27163003 ($D^{*+} \to D^0(K^-\pi^+)\pi^+$) 356
G.2 Efficiency of DaughtersInLHCb for D^0 in MagDown event type 27163003 ($D^{*+} \to D^0(K^-\pi^+)\pi^+$) 357
G.3 Efficiency of DaughtersInLHCb for D^0 in MagUp event type 27163003 ($D^{*+} \to D^0(K^-\pi^+)\pi^+$) 358
G.4 Efficiency of DaughtersInLHCb for D^0 in MagUp event type 27163003 ($D^{*+} \to D^0(K^-\pi^+)\pi^+$) 359
G.5 Efficiency of DaughtersInLHCb for D^0 in MagDown event type 27265002 ($D^{*+} \to D^0(K^-\pi^+\pi^-\pi^+)\pi^+$) 361
G.6 Efficiency of DaughtersInLHCb for D^0 in MagDown event type 27265002 ($D^{*+} \to D^0(K^-\pi^+\pi^-\pi^+)\pi^+$) 362
G.7 Efficiency of DaughtersInLHCb for D^0 in MagUp event type 27265002 ($D^{*+} \to D^0(K^-\pi^+\pi^-\pi^+)\pi^+$) 363
G.8 Efficiency of DaughtersInLHCb for D^0 in MagUp event type 27265002 ($D^{*+} \to D^0(K^-\pi^+\pi^-\pi^+)\pi^+$) 364
G.9 Efficiency of DaughtersInLHCb for D^+ in MagDown event type 21263010 ($D^+ \to K^-\pi^+\pi^+$) 366

G.10 Efficiency of DaughtersInLHCb for D^+ in MagDown event type 21263010 ($D^+ \to K^-\pi^+\pi^+$) . . . 367
G.11 Efficiency of DaughtersInLHCb for D^+ in MagUp event type 21263010 ($D^+ \to K^-\pi^+\pi^+$) . . . 368
G.12 Efficiency of DaughtersInLHCb for D^+ in MagUp event type 21263010 ($D^+ \to K^-\pi^+\pi^+$) . . . 369
G.13 Efficiency of DaughtersInLHCb for D^+ in MagDown event type 21263002 ($D^+ \to K^-K^+\pi^+$) . . . 371
G.14 Efficiency of DaughtersInLHCb for D^+ in MagDown event type 21263002 ($D^+ \to K^-K^+\pi^+$) . . . 372
G.15 Efficiency of DaughtersInLHCb for D^+ in MagUp event type 21263002 ($D^+ \to K^-K^+\pi^+$) . . . 373
G.16 Efficiency of DaughtersInLHCb for D^+ in MagUp event type 21263002 ($D^+ \to K^-K^+\pi^+$) . . . 374
G.17 Efficiency of DaughtersInLHCb for D_s^+ in MagDown event type 23263020 ($D_s^+ \to K^-K^+\pi^+$) . . . 376
G.18 Efficiency of DaughtersInLHCb for D_s^+ in MagDown event type 23263020 ($D_s^+ \to K^-K^+\pi^+$) . . . 377
G.19 Efficiency of DaughtersInLHCb for D_s^+ in MagUp event type 23263020 ($D_s^+ \to K^-K^+\pi^+$) . . . 378
G.20 Efficiency of DaughtersInLHCb for D_s^+ in MagUp event type 23263020 ($D_s^+ \to K^-K^+\pi^+$) . . . 379
G.21 Efficiency of DaughtersInLHCb for D_s^+ in MagDown event type 23263011 ($D_s^+ \to \pi^-\pi^+\pi^+$) . . . 381
G.22 Efficiency of DaughtersInLHCb for D_s^+ in MagDown event type 23263011 ($D_s^+ \to \pi^-\pi^+\pi^+$) . . . 382
G.23 Efficiency of DaughtersInLHCb for D_s^+ in MagUp event type 23263011 ($D_s^+ \to \pi^-\pi^+\pi^+$) . . . 383
G.24 Efficiency of DaughtersInLHCb for D_s^+ in MagUp event type 23263011 ($D_s^+ \to \pi^-\pi^+\pi^+$) . . . 384
G.25 Efficiency of DaughtersInLHCb for D^{*+} in MagDown event type 27163003 ($D^{*+} \to D^0(K^-\pi^+)\pi^+$) . . . 386
G.26 Efficiency of DaughtersInLHCb for D^{*+} in MagDown event type 27163003 ($D^{*+} \to D^0(K^-\pi^+)\pi^+$) . . . 387
G.27 Efficiency of DaughtersInLHCb for D^{*+} in MagUp event type 27163003 ($D^{*+} \to D^0(K^-\pi^+)\pi^+$) . . . 388
G.28 Efficiency of DaughtersInLHCb for D^{*+} in MagUp event type 27163003 ($D^{*+} \to D^0(K^-\pi^+)\pi^+$) . . . 389

G.29 Efficiency of DaughtersInLHCb for D^{*+} in MagDown event type 27265002 ($D^{*+} \to D^0(K^-\pi^+\pi^-\pi^+)\pi^+$) 391
G.30 Efficiency of DaughtersInLHCb for D^{*+} in MagDown event type 27265002 ($D^{*+} \to D^0(K^-\pi^+\pi^-\pi^+)\pi^+$) 392
G.31 Efficiency of DaughtersInLHCb for D^{*+} in MagUp event type 27265002 ($D^{*+} \to D^0(K^-\pi^+\pi^-\pi^+)\pi^+$) 393
G.32 Efficiency of DaughtersInLHCb for D^{*+} in MagUp event type 27265002 ($D^{*+} \to D^0(K^-\pi^+\pi^-\pi^+)\pi^+$) 394
H.1 Monte Carlo modelling systematic yields for $D^0 \to K^-\pi^+$ D0_DIRA_OWNPV 395
H.2 Monte Carlo modelling systematic yields for $D^0 \to K^-\pi^+$ D0_ENDVERTEX_CHI2/D0_ENDVE
H.3 Monte Carlo modelling systematic yields for $D^0 \to K^-\pi^+$ D0_Loki_AMINDOCA 396
H.4 Monte Carlo modelling systematic yields for $D^0 \to K^-\pi^+$ D0_Loki_BPVVDCHI2 397
H.5 Monte Carlo modelling systematic yields for $D^0 \to K^-\pi^+$ D0_h1_TRACK_CHI2NDOF 397
H.6 Monte Carlo modelling systematic yields for $D^0 \to K^-\pi^+$ D0_h2_TRACK_CHI2NDOF 398
H.7 Monte Carlo modelling systematic yields for $D^0 \to K^-\pi^+$ D0_h1_ETA 398
H.8 Monte Carlo modelling systematic yields for $D^0 \to K^-\pi^+$ D0_h2_ETA 399
H.9 Monte Carlo modelling systematic yields for $D^0 \to K^-\pi^+$ D0_h1_P . 399
H.10 Monte Carlo modelling systematic yields for $D^0 \to K^-\pi^+$ D0_h2_P . 400
H.11 Monte Carlo modelling systematic yields for $D^0 \to K^-\pi^+$ D0_h1_PT . 400
H.12 Monte Carlo modelling systematic yields for $D^0 \to K^-\pi^+$ D0_h2_PT . 401
H.13 Per bin differences for Monte Carlo modelling systematic example . . 401

1 Introduction

Measurements of $c\bar{c}$ and $b\bar{b}$ cross sections test the predictions of quantum chromodynamics (QCD), and as the rapidity range available to LHCb is unique at the LHC, such measurements are complementary to those made by other experiments. In addition, charm cross section measurements are used as inputs to background estimations in atmospheric neutrino experiments [3], and to determine the parton distribution functions [4].

This analysis note documents the efforts to measure the double differential cross sections of various promptly produced open charm hadrons at a centre-of-mass energy of $\sqrt{s} = 13\,\text{TeV}$. The cross section is measured in bins of charm hadron transverse momentum $p_{\text{T}} = \sqrt{p_x^2 + p_y^2}$ and rapidity $y = 1/2 \ln (E + p_z)/(E - p_z)$, as computed in the rest frame of the proton-proton collision.

A measurement of prompt open charm cross sections has been made using a dataset corresponding to an integrated luminosity of $14.96\,\text{nb}^{-1}$ collected in 2010 at a centre-of-mass energy of $\sqrt{s} = 7\,\text{TeV}$ [5]. This analysis follows a similar methodology, which is thoroughly documented in the corresponding analysis note [6] and whose results are briefly summarised in Table 1.1. The analysis of data collected in 2015 will be fully described within this note.

The open charm hadrons used for this measurement are D^0, D^+, D_s^+, and D^{*+}. As a cross-check, two final states of each hadron are reconstructed, and the full measurement is made on both. The two measurements should agree, and the results of only one final state per hadron will be published[1]. These decay modes are $D^0 \to K^-\pi^+$ and $D^0 \to K^-\pi^+\pi^-\pi^+$, $D^+ \to K^-\pi^+\pi^+$ and $D^+ \to K^-K^+\pi^+$, $D_s^+ \to \phi\pi^+$ and $D_s^+ \to K^-K^+\pi^+$ excluding the ϕ contribution, and $D^{*+} \to D^0\pi^+$ with the same two $D^0 \to K^-\pi^+$ and $D^0 \to K^-\pi^+\pi^-\pi^+$ final states. (Only the D^{*+}-tagged $D^0 \to K^-\pi^+\pi^-\pi^+$ mode is selected, as a cross-check with the tagged $D^0 \to K^-\pi^+$ mode is sufficient to evaluate any problems that would appear in the untagged modes.) Unless otherwise stated, the addition of the charge conjugate process is implied throughout this note.

As charm hadrons can be produced both promptly from the pp collision and in the decays of B hadrons, we statistically separate the two contributions through extended maximum likelihood fits to the charm hadron χ^2_{IP} in order to measure the prompt yields. Aside from the explicit measurement of the D^{*+} production cross-section, no attempt is made to distinguish prompt hadrons produced from prompt excited charm resonances from those produced directly in the pp collision.

[1] This does not impact greatly on sensitivity as the cross-check channels are generally Cabibbo-suppressed decay modes which have significantly lower signal yields.

The analysis will reconstruct and select the various charm decays, measure the size of the prompt signal component N, and then compute the efficiency ϵ of each step, from the geometrical limitations imposed by the LHCb detector acceptance, to the selection cuts. Combined with a measurement of the collected integrated luminosity $\mathcal{L}$ and the branching fraction $\mathcal{B}$ of the decay mode f in question, the cross section for a single charm hadron H_c in a given p_{T}-y bin i can be computed as

$$\sigma_i(H_c) = \frac{N_i(H_c \to f)}{\epsilon_i(H_c \to f) \cdot \mathcal{B}(H_c \to f) \cdot \mathcal{L}}. \tag{1.1}$$

Double differential cross sections can then be determined using the width of the bin in p_{T}, Δp_{T}, and the width of the bin in rapidity, Δy, in which the yield and efficiency measurements were made

$$\left.\frac{\partial^2 \sigma(H_c)}{\partial p_{\mathrm{T}} \partial y}\right|_i = \frac{\sigma_i(H_c)}{\Delta p_{\mathrm{T}} \Delta y}. \tag{1.2}$$

In addition to this absolute $c\bar{c}$ cross section, the theory community has expressed an interest in being provided with the $\sqrt{s} = 13\,\mathrm{TeV}$ measurements relative to the $\sqrt{s} = 7\,\mathrm{TeV}$ measurements made on data taken in 2010, that is

$$\sigma_{i,\mathrm{rel}}(H_c) = \frac{\sigma_{i,13\,\mathrm{TeV}}(H_c)}{\sigma_{i,7\,\mathrm{TeV}}(H_c)}. \tag{1.3}$$

For the charm hadrons used in this analysis, the 2010 measurement used a bin width of 1 GeV in p_{T} and 0.5 in y. We adopt a compatible binning for this analysis, only extending the kinematic ranges or subdividing bins, such that the relative measurement may be simply computed from the published 2010 results. Throughout this note, bin boundaries are given using the ISO 31-11 standard, where, for example, the half-open interval $a \leq x < b$ is denoted $[a, b[$ [7].

We intend to measure the absolute cross sections of D^0, D^+, D_s^+, and D_s^+ hadrons in bins of width 0.5 in rapidity in the range $y \in [2.0, 4.5[$, and then in bins of different widths in transverse momentum in the range $p_{\mathrm{T}} \in [0, 30[$. These widths are 0.25 GeV in 0 GeV until 3 GeV, 0.5 GeV from 3 GeV until 5 GeV, and 1 GeV from 5 GeV until 30 GeV. The reason for using varying bin widths is to resolve any structure in the cross section at low p_{T}, where some was seen in the $\sqrt{s} = 7\,\mathrm{TeV}$ measurement.

In addition, we intend to measure the $\sqrt{s} = 13\,\mathrm{TeV}$ cross-sections relative between modes, such as $\sigma(D^0)/\sigma(D^+)$, and relative between bins, where every measurement is normalised to a single 'central' bin. The motivation for making these additional measurements also comes from the theory community.

Having outlined the general analysis, Section 2 shall describe the theoretical models available for comparison with the data. The data itself will then be discussed in

Table 1.1: Summary of $\sqrt{s} = 7\,\mathrm{TeV}$ charm cross section analysis results grouped by charm hadron H_c and integrated across all measured p_T-y bins [5].

H_c	$\sigma(pp \to H_c)$ [$\mu\mathrm{b}^{-1}$]
D^0	1661 ± 129
D^+	645 ± 74
D_s^+	197 ± 31
D^{*+}	677 ± 83
Λ_c^+	233 ± 77

Section 3, including details on the running conditions of the LHC, the trigger strategy, and which simulated samples are used. The selection applied to the candidates will follow in Section 4, including a brief description of how the charm hadron candidates are reconstructed. In Section 5 the efficiencies of each reconstruction and selection stage will be described and given, and the fitting framework that counts the yields of the various signal and background components after the full selection will be shown in Section 6. The sources of systematic uncertainty in the analysis will be enumerated and evaluated in Section 7. Several validations of the analysis are presented in Section 8, and finally the results of the measurement will be given in Section 9.

2 Theory

In the course of this analysis, we have been in contact with three groups of theorists who provided predictions for the production cross-sections that we measure: Cacciari et al. (FONLL)[2], Gauld et al. (POWHEG+NNPDF3.0L)[1], and Spiesberger et al. (GMVFNS)[8]. (In parentheses are nicknames by which we will refer to the sets of predictions in the following discussion.) Two of these groups, Cacciari et al. and Spiesberger et al., previously provided the predictions used in the 7 TeV measurements [5, 6].

In this section, and only this section, the acronym PDF stands for parton distribution function.

2.1 FONLL (Cacciari et al.)

The FONLL predictions were provided in the form of D^0, D^+, and D^{*+} production cross-sections (integrated over the bin, not differential) for pp collisions at $\sqrt{s} = 13\,\text{TeV}$ and at 7 TeV for each bin in a partition of the phase space $p_\text{T} < 30\,\text{GeV}$ and $2.0 < y < 4.5$. Each calculated cross-section is accompanied by a range that represents an uncertainty interval to account for uncertainties in the PDF set, the charm quark mass, and the renormalisation and factorisation scales. These FONLL calculations of the meson production cross-sections assume unit transition probabilities from a primary charm quark to the exclusive hadron state. Cacciari et al. also provided ratios of the $\sqrt{s} = 13\,\text{TeV}$ cross-sections to the 7 TeV cross-sections with accompanying uncertainties, which take into account the correlations in the theoretical uncertainties. Finally, Cacciari et al. provided total charm quark production cross-sections for $\sqrt{s} = 13\,\text{TeV}$ and 7 TeV in the charm phase space $p_\text{T} < 8\,\text{GeV}$ and $2.0 < y < 4.5$, and the ratio of the two cross-sections:

$$
\begin{aligned}
\sigma(pp \to cX; 13\,\text{TeV})_{p_\text{T}<8\,\text{GeV},2.0<y<4.5} &= 1.56^{+2.42}_{-1.41}\ \text{mb} \\
\sigma(pp \to cX; 7\,\text{TeV})_{p_\text{T}<8\,\text{GeV},2.0<y<4.5} &= 1.01^{+1.55}_{-0.86}\ \text{mb} \\
R_{13/7}(pp \to cX)_{p_\text{T}<8\,\text{GeV},2.0<y<4.5} &\equiv \frac{\sigma(pp \to cX; 13\,\text{TeV})_{p_\text{T}<8\,\text{GeV},2.0<y<4.5}}{\sigma(pp \to cX; 7\,\text{TeV})_{p_\text{T}<8\,\text{GeV},2.0<y<4.5}} \\
&= 1.5491^{+0.0502}_{-0.0547}
\end{aligned}
$$

These phase-space-integrated numbers illustrate some features of the binned estimates. They are dominated by the low-p_T region where the cross-sections are largest, but the relative theoretical uncertainties in this region approach 100% (in some cases, the uncertainty intervals even have unphysical negative cross-sections as their lower

limits). However, there is a large degree of correlation in these uncertainties that cancel in the ratios.

Ref. [2] and the papers that it cites (especially Ref. [9]) describe the FONLL calculations in detail. This paper also includes the D^+ cross-section tables that were provided to us. Cacciari et al. elected to not include the D^0 and D^{*+} tables in their paper. As explained in the appendix of Ref. [2],

> Cross sections and ratios for D^0 and D^{*+} are not included here [in Ref. [2]] for brevity, but are qualitatively very similar and can be obtained from the authors.

As described in Ref. [9], in the FONLL framework, 'one matches fixed next-to-leading order (NLO) [perturbative] QCD [calculations] with all-order resummation to next-to-leading log (NLL) accuracy in the limit where the the transverse momentum (p_{T}) of the heavy quark is much larger than its mass (m).' The predictions provided to us for this work use the NNPDF3.0 NLO PDF set [10].

These FONLL calculations of the meson production cross-sections assume unit transition probabilities from a primary charm quark to the exclusive hadron state. For comparison to the current measurements, they have been multiplied by transition probabilities measured at e^+e^- colliders operating at a centre-of-mass energy close to the $\Upsilon(4S)$ resonance [11]: $f(c \to D^0) = 0.565 \pm 0.032$, $f(c \to D^+) = 0.246 \pm 0.020$, $f(c \to D^{*+}) = 0.224 \pm 0.028$, and $f(c \to D_s^+) = 0.080 \pm 0.017$. Note that the transition probabilities do not sum up to unity, since, *e.g.*, $f(c \to D^0)$ has an overlapping contribution from $f(c \to D^{*+})$.

As for the 7 TeV analysis [5, 6], FONLL predictions for the D_s^+ production cross-sections were not provided. The analysts of those previous measurements obtained estimates for the D_s^+ production cross-sections by scaling the D^{*+} predictions by $f(c \to D_s^+)$. In recent discussions with Cacciari et al., the theorists suggested that D_s^+ production might be more similar to D^+ production than to D^{*+} production.

TODO: Check the 7 TeV results to determine whether the shape of the D_s^+ differential production is more consistent with that of D^{*+} or with that of D^+.

2.2 POWHEG+NNPDF3.0L (Gauld et al.)

The POWHEG+NNPDF3.0L predictions were provided in the form of D^0 and D^+ production cross-sections (integrated over the bin, not differential) for pp collisions at $\sqrt{s} = 13\,\mathrm{TeV}$ for each bin in a partition of the phase space $p_{\mathrm{T}} < 30\,\mathrm{GeV}$ and $2.0 < y < 4.5$. The values that were provided represent the sum of the production

cross-sections of the stated hadron and its charge conjugate. Each calculated cross-section is accompanied by a range that represents an uncertainty interval to account for uncertainties in the PDF set, the charm quark mass, and the renormalisation and factorisation scales. Gauld et al. also provided ratios of the D^0 $\sqrt{s} = 13\,\text{TeV}$ cross-sections to D^0 7 TeV cross-sections computed with the the same method. These ratios are accomapnied by uncertainties that take into account the correlations in the theoretical uncertainties. Finally, Gauld et al. provided D^0 production cross-sections and ratios integrated over the phase space of LHCb's 7 TeV cross-section measurement, $p_{\text{T}} < 8\,\text{GeV}$ and $2.0 < y < 4.5$. The total production cross-section of $D^0 + \overline{D}^0$ is given as

$$\sigma(pp \to (D^0 \text{ or } \overline{D}^0)X; 13\,\text{TeV})_{p_{\text{T}}<8\,\text{GeV},2.0<y<4.5} = 1.10^{+2.08}_{-0.90}\text{ mb},$$

which Gauld et al. divide by $2f(c \to D^0) = 2(0.565 \pm 0.032)$ (citing the transition probability assumed by the 7 TeV measurement [5]) to arrive at an estimate for the $c\bar{c}$ production cross-section:

$$\sigma(pp \to c\bar{c}X; 13\,\text{TeV})_{p_{\text{T}}<8\,\text{GeV},2.0<y<4.5} = 0.97^{+1.84}_{-0.79}\text{ mb}.$$

The ratio of the integrated D^0 cross-section at $\sqrt{s} = 13\,\text{TeV}$ to that at 7 TeV was computed more precisely by Gauld et al. as

$$R_{13/7}(pp \to (D^0 \text{ or } \overline{D}^0)X)_{p_{\text{T}}<8\,\text{GeV},2.0<y<4.5} = 1.39^{+0.12}_{-0.29}.$$

Gauld et al. used this more precise ratio and LHCb's measured integrated $c\bar{c}$ cross-section from Ref. [5] to compute more precise predictions for the integrated cross-sections for D^0 and for $c\bar{c}$:

$$\sigma(pp \to (D^0 \text{ or } \overline{D}^0)X; 13\,\text{TeV})_{p_{\text{T}}<8\,\text{GeV},2.0<y<4.5} = 2.24^{+0.31}_{-0.52}\text{ mb},$$
$$\sigma(pp \to c\bar{c}X; 13\,\text{TeV})_{p_{\text{T}}<8\,\text{GeV},2.0<y<4.5} = 1.98^{+0.25}_{-0.45}\text{ mb},$$

where the uncertainties are the sum in quadrature of the theory and experimental uncertainties.

Ref. [1] describes the POWHEG+NNPDF3.0L calculations in detail. This paper includes tables of double differential cross-sections multiplied by bin-width in y for D^0 and D^+, $\frac{\mathrm{d}^2\sigma}{\mathrm{d}y\,\mathrm{d}p_{\text{T}}}\Delta y$, that are equivalent to the bin-integrated cross-sections that Gauld et al. provided to us. The paper also includes the table of D^0 cross-section ratios for $\sqrt{s} = 13\,\text{TeV}$ to 7 TeV that were provided to us. The work in Ref. [1] proceeded in two steps. First, the authors produced an improved version of the NNPDF3.0 NLO PDF set [10] by reweighting the set so that FONLL calculations at $\sqrt{s} = 7\,\text{TeV}$ matched LHCb's charm cross-section measurements [5]. The resulting PDF set, which Gauld

et al. designated NNPDF3.0+LHCb, has a significant improvement in the uncertainties for the gluon distribution at small Bjorken-x. Next, the NNPDF3.0+LHCb PDF set was used with a NLO Monte Carlo integrator to obtain predictions of production cross-sections of exclusive heavy-flavor states (*i.e.*, D^0 and D^+). Gauld et al. compared the output of two NLO Monte Carlo programs: POWHEG [12] and MadGraph5_aMC@NLO [13]. Each was interfaced to Pythia8 [12] with the Monash 2013 tune [14] to match the NLO calculations to Pythia8 parton showers. The results of the two MC programs were found to be consistent. The main values provided to us for our comparisons and published in Ref. [1] are those from POWHEG. Fig. 2.1 shows the POWHEG+NNPDF3.0L D^0 and D^+ cross-section predictions.

2.3 GMVFNS (Spiesberger et al.)

The GMVFNS predictions were provided in the form of D^0, D^+, D^{*+}, D_s^+, and Λ_c^+ differential production cross-sections $\mathrm{d}\sigma/\mathrm{d}p_\mathrm{T}$ for pp collisions at $\sqrt{s} = 13\,\mathrm{TeV}$ integrated over each 0.5 unit y bin in the range $2.0 < y < 4.5$ for each of 27 evenly-spaced p_T values in the range $3.5 \leq p_\mathrm{T} \leq 29.5\,\mathrm{GeV}$. The values that were provided represent the average differential production cross-sections of the stated hadron and its charge conjugate. Each calculated differential cross-section is accompanied by a range that represents an uncertainty interval that accounts for uncertainties of the renormalisation scale and the two factorisation scales. Spiesberger et al. did not provide estimates for $p_\mathrm{T} < 3\,\mathrm{GeV}$; in this region the scale uncertainties become huge (as also seen in the FONLL predictions).

Ref. [8] describes the general-mass-variable-flavor-number scheme (GMVFNS) calculations in detail. At this time, the specific predictions that were provided by Spiesberger et al. for this analysis have not been published by the authors (Ref. [8] presents the previous calculations for pp collisions at $\sqrt{s} = 7\,\mathrm{TeV}$). The GMVFNS provides NLO predictions of charm production. Its framework includes the convolution with fragmentation functions describing the transition $c \to H_c$ that are normalised to the respective total transition probabilities (Ref. [15] for $c \to D^0$ and D^+, and Ref. [16] for $c \to D_s^+$ and Λ_c^+). The fragmentation functions are results of fits to production measurements at e^+e^- colliders, where no attempt was made in the fit to separate direct production and feed-down from higher resonances. The predictions provided to us for this work use the CT10 PDF set [17].[2]

[2]Note that the $\sqrt{s} = 7\,\mathrm{TeV}$ predictions in the authors' Ref. [8] use the CTEQ6.6 PDF set [18] and the predictions provided to the analysists of LHCb's $\sqrt{s} = 7\,\mathrm{TeV}$ measurement [5, 6] used the CTEQ6.5 PDF set [19] for most predictions and the CTEQ6.5c2 set [20] for D^0 to study the effects of intrinsic charm.

In order to compare our measurements to these predictions, the differential cross-sections must be integrated over the p_T ranges of the measurement bins. As for the 7 TeV analysis, this is done by numeric integration of a cubic interpolating spline through the theoretical point estimates of $(1/p_\mathrm{T})\mathrm{d}\sigma/\mathrm{d}p_\mathrm{T}$.[3] The factor $1/p_\mathrm{T}$ stabilizes the interpolation in the region where the differential cross-sections change most rapidly. In detail, for each combination of charm hadron species H_c and rapidity bin j, we estimate the functional form of the weighted differential production cross-section, $I_j(p_\mathrm{T}; H_c)$

$$I_j(p_\mathrm{T}; H_c) \equiv \frac{1}{p_\mathrm{T}} \left.\frac{\mathrm{d}\sigma}{\mathrm{d}p_\mathrm{T}}\right|_j$$

by fitting a cubic interpolating spline through the $\mathrm{d}\sigma/\mathrm{d}p_\mathrm{T}$ values provided by Spiesberger et al. divided their associated p_T values. Then for each p_T bin i, ${p_\mathrm{T}}^{i,\mathrm{min}} < p_\mathrm{T} < {p_\mathrm{T}}^{i,\mathrm{max}}$, with ${p_\mathrm{T}}^{i,\mathrm{min}} > 3\,\mathrm{GeV}$, the cross-section for the (p_T, y) bin (i, j) is calculated by numeric integration of the spline function multiplied by p_T:

$$\sigma(H_c)_{i,j} = \int_{{p_\mathrm{T}}^{i,\mathrm{min}}}^{{p_\mathrm{T}}^{i,\mathrm{max}}} p_\mathrm{T} \cdot I_j(p_\mathrm{T}; H_c)\,\mathrm{d}p_\mathrm{T}.$$

We calculate uncertainty intervals for the integrated cross-section values $\sigma(H_c)_{i,j}$ by applying the same procedure to the sets of lower and upper limits of the uncertainty intervals provided by Spiesberger et al.. Given the theorists' set of lower (upper) limits for the differential cross-section, $\mathrm{d}\sigma^{\mathrm{min(max)}}/\mathrm{d}p_\mathrm{T}$, we fit cubic interpolating splines

$$I_j^{\mathrm{min(max)}}(p_\mathrm{T}; H_c) \equiv \frac{1}{p_\mathrm{T}} \left.\frac{\mathrm{d}\sigma^{\mathrm{min(max)}}}{\mathrm{d}p_\mathrm{T}}\right|_j$$

which are integrated to estimate the lower (upper) limit of an uncertainty interval for $\sigma(H_c)_{i,j}$

$$\sigma(H_c)_{i,j}^{\mathrm{min(max)}} = \int_{{p_\mathrm{T}}^{i,\mathrm{min}}}^{{p_\mathrm{T}}^{i,\mathrm{max}}} p_\mathrm{T} \cdot I_j^{\mathrm{min(max)}}(p_\mathrm{T}; H_c)\,\mathrm{d}p_\mathrm{T}.$$

[3] In correspondence with Spiesberger et al., the theorists recommended that dividing the differential cross-section estimates by a 'suitable' power of p_T and integrating a linear interpolating function of those values would yield very accurate results.

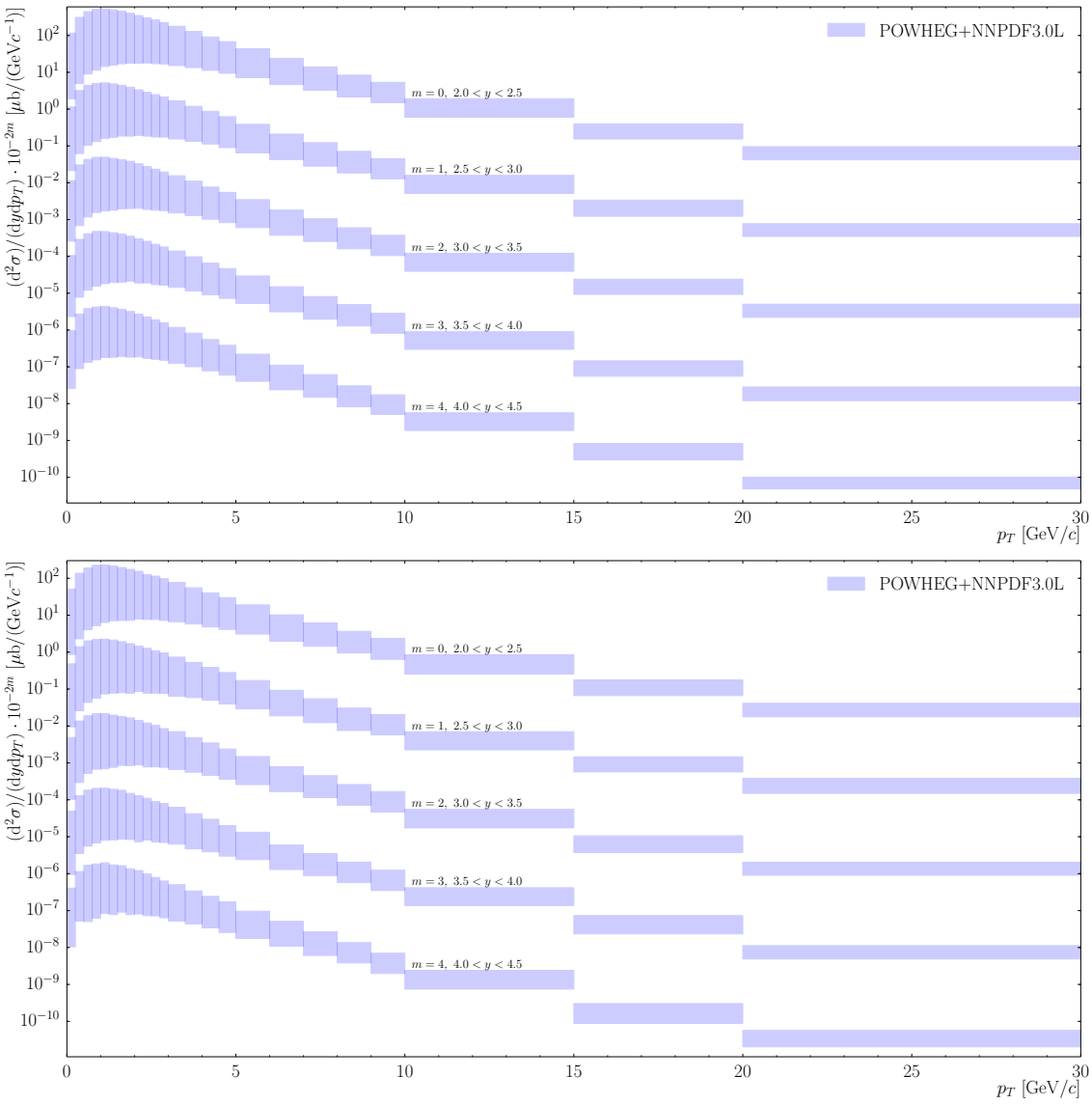

Figure 2.1: Prediction for the absolute (top) D^0 and (bottom) D^+ cross-sections at $\sqrt{s} =$ 13 TeV as described in the text, provided by [1].

3 Data

The dataset used for the analysis corresponds to an integrated luminosity of $(4.98 \pm 0.19)\,\mathrm{pb}^{-1}$ of proton-proton collisions at a centre of mass energy of $\sqrt{s} = 13\,\mathrm{TeV}$. It was collected during the 50 ns bunch-spacing early-running period of Run 2 of the LHC.

3.1 Trigger strategy

The LHCb Run 2 trigger consists of three stages: a hardware (L0) trigger which can use information from the calorimeter, muon, and pile-up systems; a software (HLT1) trigger which can use information from all subdetectors and processes all events selected by L0 in real-time; and a software (HLT2) trigger which runs asynchronously on events selected by HLT1 and performs a final selection using the full offline-quality alignment, calibration, and detector reconstruction. The L0 trigger is also able to deliver a fixed rate of randomly selected events, a fact this analysis will exploit.

The trigger strategy for this analysis is defined within these three stages:

1. L0: A '`NOBIAS`' trigger which fires at a determined rate on beam-beam bunch crossings;

2. HLT1: A single-track trigger which selects L0 events based on track transverse momentum; displacement from the primary proton-proton interaction region, and track quality; and

3. HLT2: A set of exclusive trigger lines which fully reconstruct each type of signal process being analyzed.

Each level of the trigger requires the previous one to have fired: the HLT1 single-track line only runs on events selected by the `NOBIAS` L0 trigger; and the HLT2 lines require that the single track which caused HLT1 to fire is part of the signal candidate which causes HLT2 to fire.

The specific selection criteria for the HLT lines are described in 4.2. For the L0 trigger, the selected rate of events was not constant throughout the datataking period because of a need to minimize deadtime depending on the LHC fill structure. This rate varied within 250–350 kHz. The known fill structure determines the total rate of beam-beam crossings, which is then combined with the selected `NOBIAS` rate to give the effective efficiency of the L0 trigger for a given fill. The overall efficiency of the L0 trigger is then determined as the luminosity-weighted average of the efficiencies for the individual fills

$$\bar{\epsilon}_{\mathrm{L0}} = \frac{\sum_{\mathrm{Fills}} \epsilon_{\mathrm{L0},i} \mathcal{L}_i}{\sum_{\mathrm{Fills}} \mathcal{L}_i}. \tag{3.1}$$

Table 3.1: List of fills used in analysis, the HLT TCK used in the fill, the integrated luminosity ("lumi.") collected in the fill, the L0 `NOBIAS` rate during the fill, and the corresponding effective L0 efficiency ("eff.").
The uncertainty on each luminosity, provided by the luminosity group, is 3.9%.

Fill	Runs	HLT TCK	Lumi. collected	L0 `NOBIAS` rate	L0 `NOBIAS` eff.
3976	157340–157397	`0x00F9014E`	$(628 \pm 24)\,\mathrm{nb}^{-1}$	250 kHz	20.58 %
3981	157558–157597	`0x00F9014E`	$(1101 \pm 43)\,\mathrm{nb}^{-1}$	300 kHz	10.84 %
3988	157697–157710	`0x00F9014E`	$(931 \pm 36)\,\mathrm{nb}^{-1}$	300 kHz	10.84 %
3992	157805–157819	`0x00F9014E`	$(1310 \pm 51)\,\mathrm{nb}^{-1}$	350 kHz	7.84 %
3996	157895–157909	`0x00F9014E`	$(999 \pm 39)\,\mathrm{nb}^{-1}$	350 kHz	7.84 %

This information is summarized in Table 3.1, which can be used to compute the effective L0 efficiency as $\bar{\epsilon}_{\mathrm{L0}} = 10.67\%$, given the total collected luminosity of $\sum_{\mathrm{Fills}} \mathcal{L}_i = (4.98 \pm 0.19)\,\mathrm{pb}^{-1}$. The effective luminosity used in this measurement is then

$$\mathcal{L}_{\mathrm{eff.}} = \bar{\epsilon}_{\mathrm{L0}} \cdot \sum_{\mathrm{Fills}} \mathcal{L}_i = (531 \pm 21)\,\mathrm{nb}^{-1}. \tag{3.2}$$

3.2 Data flow

Events containing candidates selected by any of the exclusive HLT2 lines are saved to the 'Turbo' stream, along with the selection reports of the HLT2 candidates that fired the lines.[4] The raw files are processed in two ways: with Tesla v1r8, which recreates the HLT2 candidates from the selection reports as objects consumable by the `DecayTreeTuple` algorithm; and with Brunel v47r9 and DaVinci v36r7p6, which run the offline reconstruction and stripping selection, ignoring the HLT2 candidates. Using Tesla is considerably quicker, as no further reconstruction is needed, and simpler to analyse as any differences between the HLT2 and offline reconstruction are irrelevant.

The HLT2 candidates from the Turbo stream are then made into ROOT ntuples with DaVinci v36r7p7.

[4]The full event is stored along with the HLT2 selection reports during the 'commissioning' phase of the Turbo stream. After this, in the beginning of 2016, it is expected that only the selection reports will be saved, in order to reduce disk space.

3.3 Simulation

Monte Carlo (MC) events are generated for each decay mode used in the analysis. The event types used for each mode, the corresponding decay file nicknames, and the number of generated events saved to disk are given in Table 3.2.

The events are generated with Pythia 8 and Gauss v47r2, with the conditions set to mimic the 50 ns bunch spacing used during the data taking, with an average number of *pp* interactions per bunch crossing ν of 1.6, corresponding to average number of *visible pp* interactions per bunch crossing μ of 1.1. Spillover, detector signals caused by particles from the previous or subsequent beam crossings, is not simulated, as it is assumed to be a negligible effect with a 50 ns bunch spacing (discussed in Section 5.2.1). Unstable particles are decayed by EvtGen, and all particles are transported through a simulation of the detector geometry by Geant4 and the detector response is recorded. The responses are converted into the format produced by the real detectors by Boole v29r7. The trigger software Moore v23r7p5 is then run using the trigger configuraiton key (TCK) `0x40f9014e`, and then the reconstruction is run using Brunel v47r9. The simulation version is `Sim08h` and the reconstruction version is `Reco15em`.

The output of the simulation is DSTs. These are processed with DaVinci v36r7p7, where for each decay mode three ROOT ntuples are produced: one containing the decay tree of the generated signal particles; one containing the decay tree of the generated signal particles whose final state particles are fully reconstructed as long tracks, which can be matched with true signal MC particles of the correct identity, and that originate from the signal charm parent; and one containing the candidates passing the relevant HLT2 line. The second, truth-matched ntuple should contain a subset of the latter, but the ntuple containing HLT2 candidates may not necessarily contain a subset of the truth-matched.

The TCK used in the MC productions, `0x40f9014e`, is nearly identical to the one used during data-taking, and in particular contains the same particle identification (PID) requirements. This is problematic, as the PID variables are known to be poorly modelled in the MC, and so efficiency determinations are not possible.[5] To circumvent this problem, we use the truth-matched Brunel output, as the parity between offline and online reconstruction should make the HLT2 reconstruction equivalent to that in Brunel.

[5]One could perform relative PID efficiency studies, rather than the absolute measurements described in Section 5.6, but this would require PID calibration MC, which is not available at the time of this writing.

Table 3.2: List of event types simulated for each decay mode with number of generated events saved to disk. The D^{*+} samples are used for both the D^{*+} studies and the untagged D^0 studies. Decay file names ending with "`,pt10GeV`" apply generator level cuts that require the signal charm hadron to have a p_{T} greater than 10 GeV, in addition to the `DaughtersInLHCb` cuts usually applied.

Decay mode	Event type	Nickname	Number (million)
$D^{*+} \to (D^0 \to K^-\pi^+)\pi^+$	27163003	`Dst_D0pi,Kpi=DecProdCut`	2.5
$D^{*+} \to (D^0 \to K^-\pi^+\pi^-\pi^+)\pi^+$	27265002	`Dst_D0pi,Kpipipi=DecProdCutMINT`	2.5
$D^+ \to K^-\pi^+\pi^+$	21263010	`D+_K-pi+pi+=res,DecProdCut`	2.5
$D^+ \to K^-K^+\pi^+$	21263002	`D+_K-K+pi+=res,DecProdCut`	2.5
$D_s^+ \to \phi\pi^+$	23263020	`Ds+_K-K+pi+=res,DecProdCut`	2.5
$D^{*+} \to (D^0 \to K^-\pi^+)\pi^+$	27163003	`Dst_D0pi,Kpi=DecProdCut,pt10GeV`	1
$D^{*+} \to (D^0 \to K^-\pi^+\pi^-\pi^+)\pi^+$	27265002	`Dst_D0pi,Kpipipi=DecProdCutMINT,pt10GeV`	1
$D^+ \to K^-\pi^+\pi^+$	21263010	`D+_K-pi+pi+=res,DecProdCut,pt10GeV`	1
$D^+ \to K^-K^+\pi^+$	21263002	`D+_K-K+pi+=res,DecProdCut,pt10GeV`	1
$D_s^+ \to \phi\pi^+$	23263020	`Ds+_K-K+pi+=res,DecProdCut,pt10GeV`	1

3.3.1 Truth matching

Each charm hadron candidate, in all ntuples, is flagged as either secondary or prompt, based on whether the charm hadron was produced in a decay chain containing a heavier long-lived hadron. This check is done by `MCTupleToolPrompt`, which traverses up the full MC ancestry tree, marking the charm hadron as secondary if an ancestor has a lifetime greater than 0.1 fs.

The truth-matching is performed using the `mcMatch` LoKi functor, which compares the reconstructed candidate with an ASCII decay descriptor, and defines a positive match as one where the selected stable tracks are associated to true MC particles, where those particles originate from a common parent, and where the particle identities have been correctly assigned. An arbitrary number of additional photons originating from the signal particle are allowed to be missing in the truth-matched final state. This allows us to filter candidates based on their true identity. The background category tool is used to classify the output of the trigger, which is not required to pass an `mcMatch` requirement, and define a 'true signal decay' as one with a background category value of either zero or ten. These values correspond to:

0 All final state Particle objects in the signal candidate decay chain are associated to an `MCParticle` with the same particle ID, all associated `MCParticles` have

the same top-level (excluding quarks) `MCParticle` parent, and the top-level `MCParticle` parent has same particle ID as signal candidate `Particle`; and

10 Same as 0 but one or more intermediate resonances (*e.g.* the ϕ in $D_s^+ \to \phi\pi^+$) are present in the `MCParticle` chain but not present in the signal candidate `Particle` chain, or vice-versa.

Photons generated from PHOTOS are ignored when computing the background category value.

3.4 Crossing angle correction

Due to the non-zero crossing angles of the two proton beams provided by the LHC, the pp collision frame is boosted with respect to the laboratory frame. As this measurement is made in bins of charm hadron transverse momentum and rapidity measured in the pp collision rest frame, a correction must be applied to the p_{T} and y measured in the laboratory frame.

Two crossing angles are defined per beam: θ_h is the angle made with the z axis in the horizontal xz plane, and θ_v is the angle made with the z axis in the vertical yz plane. With $\theta_h = 0$ and $\theta_v = 0$ we have

$$p^{\mu}_{z+} = \begin{pmatrix} E_{\mathrm{Beam}} \\ 0 \\ 0 \\ p_{\mathrm{Beam}} \end{pmatrix} \quad \text{and} \quad p^{\mu}_{z-} = \begin{pmatrix} E_{\mathrm{Beam}} \\ 0 \\ 0 \\ -p_{\mathrm{Beam}} \end{pmatrix}, \tag{3.3}$$

where $z\pm$ indicates the beam moves to increasing or decreasing z, E_{Beam} is the nominal beam energy of $\sqrt{s}/2 = 6.5\,\mathrm{TeV}$, and p_{Beam} is the beam momentum as $p^2_{\mathrm{Beam}} = E^2_{\mathrm{Beam}} - m^2_{\mathrm{Proton}}$. With non-zero crossing angles, the beam four vectors become

$$p^{\mu}_{z+} = \begin{pmatrix} E_{\mathrm{Beam}} \\ p_{\mathrm{Beam}} \sin\theta_{h,+} \\ p_{\mathrm{Beam}} \sin\theta_{v,+} \\ p_{\mathrm{Beam}}\sqrt{1 - \sin^2\theta_{h,+} - \sin^2\theta_{v,+}} \end{pmatrix} \quad \text{and}$$

$$p^{\mu}_{z-} = \begin{pmatrix} E_{\mathrm{Beam}} \\ -p_{\mathrm{Beam}} \sin\theta_{h,-} \\ -p_{\mathrm{Beam}} \sin\theta_{v,-} \\ -p_{\mathrm{Beam}}\sqrt{1 - \sin^2\theta_{h,-} - \sin^2\theta_{v,-}} \end{pmatrix}, \tag{3.4}$$

where $\theta_{h,\pm}$ and $\theta_{v,\pm}$ are defined to allow for asymmetrical crossing angles between the two beams. The centre-of-mass four vector p^{μ}_{CoM} is then the sum of p^{μ}_{z+} and p^{μ}_{z-}.

Charm hadron candidates are boosted into the centre-of-mass rest frame, and the system is then rotated to make the boosted beam axes coincide with the laboratory z axis. The transverse momentum and rapidity are then recomputed. Whenever charm hadron p_{T} or y are mentioned, it is the pp rest frame quantities that are used.

In the data sample used, the only non-zero crossing angle was in the xz plane and this was symmetric between the two beams. The crossing angle values when the magnet was in the down polarity were $\theta_{h,+} = \theta_{h,-} = 790\,\mu\mathrm{rad}$ and $\theta_{v,+} = \theta_{v,-} = 0$, and were $\theta_{h,+} = \theta_{h,-} = 210\,\mu\mathrm{rad}$ and $\theta_{v,+} = \theta_{v,-} = 0$ in the up polarity.[6]

[6] We do not use data taken with the up polarity, but the crossing angles are given here for completeness.

4 Selection

For a faster turn-around during data taking, our strategy is to implement most of the required selection criteria in the exclusive charm HLT2 lines, with only a minimal number of additional criteria applied offline.

This section shall begin by listing the variables used in the selection, and shall then describe the online trigger selections. A set of stripping selections has also been defined, intended to be used if the new `TurboStream` fails. They can be found in Appendix C and the HLT2 lines are based on those stripping lines.

4.1 Discriminating variables

We consider there to be three major differences between charm hadron decays we wish to select: the invariant mass of the charm hadron, its lifetime, and the topology of its decay, *i.e.* how many particles it decays into and any additional decay substructure. These three properties broadly drive selection differences between the modes.

For charm hadrons with higher masses, the search window in invariant mass will be centred on a higher value, and the transverse momentum available to the decay products will be higher for a given topology. A longer lifetime means a larger mean separation of the decay vertex from the production vertex, and larger child impact parameter with respect to the production vertex. Higher multiplicity decays, *i.e.* those with more particles in the final state, will have lower average child momenta and more combinatorial backgrounds.

The baseline selection was developed from existing charm cross section stripping selections with the following list of selection variables, where 'parent' refers to the charm hadron and 'child' refers to its decay products.

Child track χ^2 per degree of freedom

The χ^2 per degree of freedom of the child track returned by the Kalman fit. This variable discriminates between real and fake (ghost) tracks.

Child transverse momentum

Momentum transverse to the beamline, *i.e.* in the xy-plane in the LHCb coordinate system. Children of charm hadrons will generally have a higher p_{T} than prompt stable particles produced directly from the pp collision.

Child momentum

Total momentum p. Must be within the range of acceptable particle identification performance and fall within the kinematic spectrum of the particle identification (PID) calibration samples.

Child pseudorapidity

Pseudorapidity η, related to angle θ made with the beamline as $-\ln(\tan\frac{\theta}{2})$. Must be within the range of acceptable particle identification performance and fall within the kinematic spectrum of the PID calibration samples.

Child χ^2_{IP}

Impact parameter (IP) with respect to the primary vertex (PV) is the distance of closest approach of the track, extrapolated to the PV, as shown in Figure 4.1. Prompt stable particles produced directly from the pp collision will have a low impact parameter, whereas particles produced in long-lived charm decays will not generally have trajectories pointing back to the PV, and will therefore have high impact parameters.

The 'χ^2' is computed as $\Delta^{\mathrm{T}}\Sigma^{-1}\Delta$, where Δ is the difference in the position vectors of the track and the vertex, and Σ is the sum of the covariance matrices of the track and vertex fits.

Child PID

Particle identification information as the combined response of the calorimeters, muon stations, and RICH detectors. In this analysis the delta-log-likelihood (DLL) set of PID variables is used. The alternative ProbNN variables are not available in the trigger, and we wish to maximise the similarities between the trigger and stripping selections.

Predicted Cherenkov rings from tracks reconstructed by the tracking system are compared with the photons detected by the RICHs. A global likelihood fit is then performed across all radiators and tracks, and a likelihood, relative to the pion hypothesis, is assigned to each track for each particle hypothesis.

Pairwise child distance of closest approach

For a set of tracks physically originating from a common vertex, the largest distance between any two tracks, the DOCA, should be small.

Pairwise child distance of closest approach χ^2

This variable is used in one trigger line and relates to DOCA as χ^2_{IP} relates to IP.

Parent reconstructed mass

Invariant mass, either computed before the vertex fit as the sum of the child four-momenta, or after as the mass of the fitted vertex. In a selected sample, a peaking structure is expected within the reconstructed mass spectrum around the nominal charm hadron invariant mass. To confidently describe the combinatorial

background, the window around the nominal mass should be many times wider than the resolution on this peak.

Parent vertex quality

Quality of the vertex fit. A larger χ^2 value means a lower probability that the input tracks originated from the same spatial point, which would be true if the tracks were the product of a particle decay.

Parent vertex displacement

Displacement of the decay vertex from the production vertex, assumed to be the PV, as either the reconstructed lifetime $c\tau$ or the vertex displacement χ^2, where the latter is computed in the same way as the track χ^2_{IP}. The 'χ^2' is computed as $\Delta^{\mathrm{T}}\Sigma^{-1}\Delta$, where Δ is the difference in the spatial positions of the two vertices, and Σ is the sum of the covariance matrices of the two vertex fits.

Parent direction angle

If the decay products are chosen correctly, and the decay vertex position is correctly reconstructed, then the momentum vector of the parent should point in the same direction as the displacement vector between the production vertex and the decay vertex. The angle between the momentum and displacement vectors, called the direction angle (DIRA), should be small for a correctly reconstructed signal decay. (It is the cosine of the direction angle that is usually called "DIRA", which should be very close to 1 for a correctly reconstructed signal decay.)

The χ^2_{IP} of the parent H_c discriminates both between prompt and secondary charm and between prompt charm and combinatorial background. However, it is not used in the selection as it is used in the yield extraction, described in Section 6, where access to the full χ^2_{IP} range is beneficial.

4.2 Trigger

As discussed in Section 3.1, the L0 trigger selects beam-beam crossings randomly, and so its efficiency for each fill is a function of the selection rate and the LHC filling scheme. Events selected by the L0 trigger are further selected by the HLT based on reconstructed information from the tracking and RICH subdetectors.

The HLT selection is split into two parts. The first, HLT1, selects events containing a single, high transverse momentum (p_{T}), good quality track which is displaced from the primary proton-proton interaction vertex. The second, HLT2, reconstructs

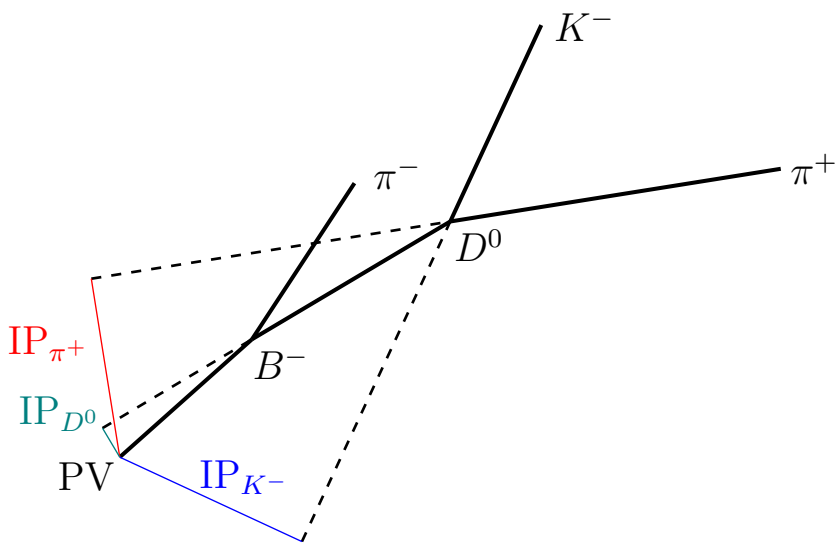

Figure 4.1: Definition of the impact parameter variable, as described in Section 4.1. The non-zero length of the impact parameter vector is characteristic of charm hadrons from B decays.

and fully selects the relevant signal candidate. In addition to documenting the selection criteria used by these triggers, this section will also briefly recap the detector reconstruction strategy used in the HLT. The efficiencies of these selections are documented in Section 5.3.

4.2.1 HLT1 reconstruction and selection

The HLT1 trigger stage has to process the full output rate of the L0 trigger and so does not have time to perform the full offline event reconstruction. The performed reconstruction relevant to this analysis is:

1. The full offline charged particle (track) reconstruction inside the VELO subdetector, including the Kalman fitting of reconstructed track trajectories (which assumes a track p_{T} of 400 MeV);

2. The full offline reconstruction of proton-proton collision vertices (primary vertices) based exclusively on the reconstructed VELO tracks, regardless of whether they are later promoted to long tracks; and

3. The reconstruction and Kalman fit of all VELO tracks in the TT and downstream (IT, OT) tracking detectors. VELO tracks are first extrapolated to the TT, and

Table 4.1: Requirements made on the track that fires the HLT1 `1Track` trigger line.

Particle	Variable	Cut value	LoKi functor
Any track	p_{T}	$> 800\,\mathrm{MeV}$	`PT`
	p	$> 3\,\mathrm{GeV}$	`P`
	Track χ^2	< 3	N/A
	χ^2_{IP}	> 10	`BPVIPCHI2`
	VELO hits	> 9	`TrIDC('isVelo')`

if at least two matching hits are found they are further extrapolated through the magnetic field within a search window restricted to a minimum transverse momentum of 800 MeV.

Because only tracks with a transverse momentum above 800 MeV are fully reconstructed, it would be inefficient to try and fully reconstruct the signal decays at this stage. Instead, a single track is searched for which meets the criteria given in Table 4.1. The presence of such a track is sufficient to identify the presence of a heavy flavour (charm or beauty) hadron decay in the event, and to reduce the rate of `NOBIAS` L0 triggers by approximately a factor of 6.5. A further efficient selection of those charm hadron decays which are of interest to this analysis, however, requires a more complete detector reconstruction.

4.2.2 HLT2 reconstruction and selection

The HLT2 trigger stage processes events selected by HLT1. It runs asynchronously, processing events not only during LHC fills but also during the inter-fill gaps, by using hard disks located in the HLT computing cluster nodes to buffer events. This leads to an increase in the effective processing power available to HLT2 of roughly a factor of two to three, and allows it to perform the full offline detector reconstruction. In addition, the asynchronous nature of HLT2 processing allows the detector to be aligned and calibrated in real-time before HLT2 runs, further bringing HLT2 closer to the optimal offline performance.

In principle, the HLT2 selections should then simply be identical to the rectangular criteria of the stripping selections described in Appendix C. For this reason, the HLT2 selection imposes rectangular criteria in order to select the signal decays of interest.

The following trigger lines are used in the analysis:

- A trigger line which selects $D^0 \to K^-\pi^+$ decay candidates;

Table 4.2: Selection requirements made in the $D^0 \to K^-\pi^+$ HLT2 trigger line. The track χ^2 criterion is applied in the reconstruction and listed here for completeness. The DIRA requirement, $\cos\theta > 0.99985$, is approximately equivalent to a cut of $\theta < 17.32\,\text{mrad}$.

Particle	Variable	Cut value	LoKi functor
$\pi^\pm$, $K^\pm$	p_T	$> 250\,\text{MeV}$	`PT`
	p	$p > 2\,\text{GeV}$	`P`
	Track χ^2	< 3	N/A
	χ^2_IP	> 16	`BPVIPCHI2`
$\pi^\pm$	$\text{DLL}_{K-\pi}$	< 5	`PIDK - PIDpi`
$K^\pm$	$\text{DLL}_{K-\pi}$	> 5	`PIDK - PIDpi`
D^0	$m(K^-\pi^+)$	$1784\,\text{MeV} < m < 1944\,\text{MeV}$	`in_range(m1,m,m2)`
	$K^\pm$ to $\pi^\pm$ DOCA	$< 0.1\,\text{mm}$	`AMINDOCA`
	Vertex fit χ^2	< 10	`VFASPF(VCHI2/VDOF)`
	Direction angle	> 0.99985	`BPVDIRA`
	Vertex displacement	$VD\chi^2 > 49$	`BPVVDCHI2`

- A trigger line which adds a charged pion to these $D^0 \to K^-\pi^+$ candidates to select $D^{*+} \to D^0\pi^+$ candidates;
- A trigger line which selects $D^0 \to K^-\pi^+\pi^-\pi^+$ candidates and then adds a charged pion to select $D^{*+} \to D^0\pi^+$ candidates (note that unlike in the two-body case, there is no line which selects untagged $D^0 \to K^-\pi^+\pi^-\pi^+$ candidates); and
- A set of trigger lines which select the $D^+ \to K^-\pi^+\pi^+$, $D^+ \to K^-K^+\pi^+$, and $D_s^+ \to K^-K^+\pi^+$ decay candidates, one line per mode.

The main difference with respect to the stripping is that, for the sake of simplicity, there is no dedicated $D_s^+ \to \phi\pi^+$ trigger. The specific selection criteria are given in Tables 4.2, 4.3, 4.4, and 4.5. The selection criteria given for the D^{*+} vertex selection are common to both D^0 decay modes.

4.3 Offline processing

Further offline requirements are imposed on the events passing the respective HLT2 lines. All final state particles in all modes which have PID cuts applied to them

Table 4.3: Selection requirements made in the HLT2 $D^0 \to K^-\pi^+\pi^-\pi^+$ line. The DIRA requirement, $\cos\theta > 0.99985$, is approximately equivalent to a cut of $\theta < 17.32\,\text{mrad}$.

Particle	Variable	Cut value	LoKi functor
$\pi^\pm$, $K^\pm$	p_T	$> 200\,\text{MeV}$	`PT`
	p	$p > 2\,\text{GeV}$	`P`
	Track χ^2	< 3	N/A
	χ^2_IP	> 4	`BPVIPCHI2`
$\pi^\pm$	$\text{DLL}_{K-\pi}$	< 5	`PIDK - PIDpi`
$K^\pm$	$\text{DLL}_{K-\pi}$	> 5	`PIDK - PIDpi`
D^0	$m(K^-\pi^+\pi^-\pi^+)$	$1784\,\text{MeV} < m < 1944\,\text{MeV}$	`in_range(m1,m,m2)`
	DOCA	$< 0.1\,\text{mm}$	`AMINDOCA`
	Vertex fit χ^2	< 10	`VFASPF(VCHI2/VDOF)`
	Direction angle	> 0.99985	`BPVDIRA`
	Vertex displacement	$\tau > 0.10\,\text{ps}$	`BPVLTIME()`

Table 4.4: Common selection requirements made on HLT2 D^{*+} candidates.

Particle	Variable	Cut value	LoKi functor
$\pi^\pm$	p_T	$> 100\,\text{MeV}$	`PT`
	Track χ^2	< 3	N/A
D^{*+}	$m(D^{*+}) - m(D^0)$	$130\,\text{MeV} < m < 160\,\text{MeV}$	`in_range(m1,m,m2)`
	Vertex fit χ^2	< 25	`VFASPF(VCHI2/VDOF)`

Table 4.5: Selection requirements made in the three-body HLT2 lines. The lines are split into D^+ ($D^+ \to K^-\pi^+\pi^+$, $D^+ \to K^-K^+\pi^+$) and D_s^+ ($D_s^+ \to K^-K^+\pi^+$) decays according to the mass window. Cuts of the form $x > x_1$, x_2, x_3 require that all particles satisfy $x > x_1$, at least two satisfy $x > x_2$, and at least one satisfies $x > x_3$. The DIRA requirement, $\cos\theta > 0.9994$, is approximately equivalent to a cut of $\theta < 34.64\,\mathrm{mrad}$.

Particle	Variable	Cut value	LoKi functor
$\pi^\pm$, $K^\pm$	p_T	> 200, 400, 1000 MeV	`PT`
	p	$p > 2\,\mathrm{GeV}$	`P`
	Track χ^2	< 3	N/A
	χ^2_IP	> 4, 10, 50	`BPVIPCHI2`
$\pi^\pm$	$\mathrm{DLL}_{K-\pi}$	< 5	`PIDK - PIDpi`
$K^\pm$	$\mathrm{DLL}_{K-\pi}$	> 5	`PIDK - PIDpi`
D^+	$m(h^-h^+h^+)$	$1789\,\mathrm{MeV} < m < 1949\,\mathrm{MeV}$	`in_range(m1,m,m2)`
D_s^+	$m(h^-h^+h^+)$	$1889\,\mathrm{MeV} < m < 2049\,\mathrm{MeV}$	`in_range(m1,m,m2)`
D^+/D_s^+	Vertex fit χ^2	< 25	`VFASPF(VCHI2/VDOF)`
	Direction angle	> 0.9994	`BPVDIRA`
	Vertex displacement	$VD\chi^2 > 16$ AND $\tau > 0.150\,\mathrm{ps}$	`BPVVDCHI2 & BPVLTIME()`

are required to be within the fiducial region of phase-space, $3 \leq p < 100\,\text{GeV}$ and $2 \leq \eta < 5$, mainly given by the constraints of the PID calibration procedure described in Section 5.6. Furthermore, the PID cut on pions (excluding the slow pion in D^{*+} decays) is tightened to $\text{DLL}_{K-\pi} < 3$. Additionally, a cut on the ghost probability (specifically the `TRACK_GhostProb`) of < 0.3 is applied on all final state tracks to reduce combinatorial background.

As the three-body modes $D^+_{(s)}$ decays still exhibit a large combinatorial background component after these cuts, especially in the low charm hadron p_T region, the vertex χ^2 and direction angle cuts are tightened to < 6 and > 0.9999 respectively.

5 Efficiencies

The efficiency chain defines the fraction of prompt signal candidates that pass each stage of the selection. The chain is defined in steps grouped by physical requirements and those imposed by software, and each step is relative to the previous one. This starts with the efficiency of a signal hadron to decay within the LHCb acceptance, $\epsilon_{\text{Acceptance}}$, having been produced in a pp collision. The efficiency of such a decay to be fully reconstructed is the reconstruction efficiency is $\epsilon_{\text{Reconstruction}}$, corrected for data-MC differences with ρ_{Tracking}, and then the efficiency of the reconstructed decay to be triggered through L0, HLT1, and HLT2 is the trigger efficiency $\epsilon_{\text{Trigger}}$. Finally, there is the efficiency of triggered candidates to pass through the offline selection (and the BDT requirements if applicable), and the requirements imposed on PID variables, which we split as $\epsilon_{\text{Offline}}$, ϵ_{PID}, and ϵ_{BDT}.

Assuming that the selections within each step are uncorrelated with all others, the total efficiency in a p_{T}-y bin $\epsilon_i(H_c \to f)$, used in the total cross section formula in Equation 1.1, is the product of the individual efficiencies

$$\epsilon_i(H_c \to f) = \epsilon_{\text{Acceptance}} \times \epsilon_{\text{Reconstruction}} \times \rho_{\text{Tracking}} \times \epsilon_{\text{Trigger}} \times \epsilon_{\text{Offline}} \times \epsilon_{\text{PID}}. \tag{5.1}$$

where each efficiency ϵ is dependent on the charm hadron H_c and the final state f, and is conditional on the previous step, *i.e.* the efficiencies are evaluated in this order.

As the full distributions of the selection variables are not available once a selection has been made on them, and we only have access to hadron candidates after the stripping, we must rely on Monte Carlo simulations, described in Section 3.3, to evaluate most of the efficiencies. The validity of the computed efficiencies relies on the MC accurately modelling the selection variables. The extent to which this assumption does (and does not) hold will be discussed in the context of systematic uncertainties in Section 7.2.

In this section we shall detail how the efficiency of each selection step is computed, and give p_{T}-y efficiency tables for each open charm hadron and final state. The notation for conditional yields will be used throughout, where $N_{A|B}$ denotes the prompt signal yields after process A given that process B preceded A.

5.1 LHCb acceptance

An acceptance efficiency arises due to the finite spatial acceptance of the LHCb detector. By instrumenting the forward region in the pseudorapidity range $2 < \eta < 5$, any particles flying outside this region are not detected. As there is no way to access

these particles in data, simulated data must be used. The acceptance is modelled by the `DaughtersInLHCb` generator-level cut, which requires that all stable charged H_c child particles have $10 < \theta < 400\,\text{mrad}$, where θ is the polar angle of the particle momentum vector, and that they all point in same z direction. This is applied to all generated signal samples, and any decays failing this cut are rejected. By counting the number of charm hadrons passing and failing the cut, the acceptance efficiency is defined as

$$\epsilon_{\text{Acceptance}} = \frac{N_{\texttt{DaughtersInLHCb}|\text{Generated}}}{N_{\text{Generated}}}. \tag{5.2}$$

Appendix G has tables for the efficiency of generator-level cuts for all MC event types that were used in this analysis.

5.2 Reconstruction

Given a set of child tracks flying within the LHCb acceptance, the fraction of final states fully reconstructed is the reconstruction efficiency. This includes the physical creation of 'hits' in the various tracking detectors, as well as the construction of tracks in software.

We compute the reconstruction efficiency by counting the number of truth-matched reconstructed decays, and comparing this with the number of decays passing the acceptance cuts defined in Section 5.1

$$\epsilon_{\text{Reconstruction}} = \frac{N_{\text{Reconstructed}|\texttt{DaughtersInLHCb}}}{N_{\texttt{DaughtersInLHCb}|\text{Generated}}}. \tag{5.3}$$

The truth-matching is described in Section 3.3.

5.2.1 Tracking efficiency correction

It is known that the tracking, or track reconstruction, efficiency is not correctly modelled in simulated data, and so the LHCb tracking group produces correction tables that analysts can apply to their efficiencies from data [21]. Figures 5.1 shows the corrections in bins of track momentum p and pseudorapidity η for each track individually. The actual correction factor ρ_{Tracking} which is used in Equation (5.1) to compute the total efficiency depends on the actual decay as it is depend on the kinematics and the number of the final state particles. Hence, a calibration procedure, in which every track in the reconstructed Monte Carlo sample is assigned its individual correction factor, is performed. In each event, the factors of all final state tracks are multiplied to obtain the event correction factor which is then averaged over all events

to obtain ρ_{Tracking}. For this average, event weights are assigned which reweight the distribution in the number of hits in the SPD detector to match the distribution seen in data.

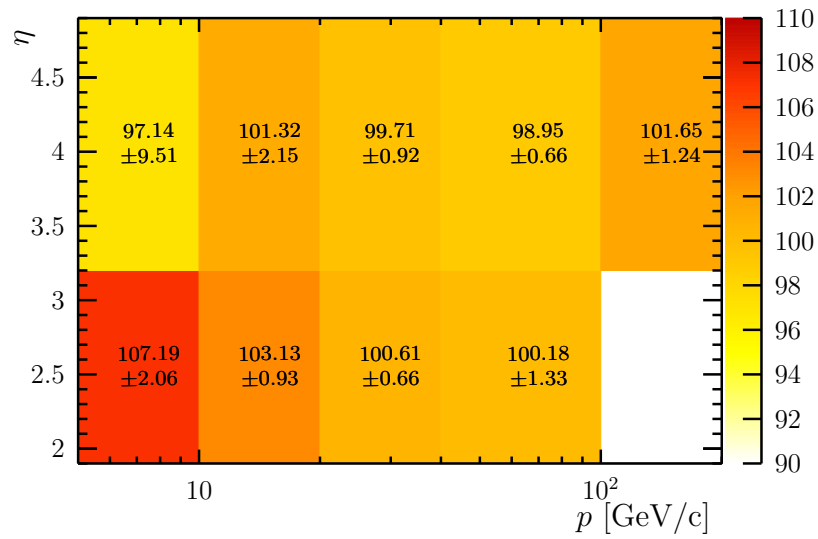

Figure 5.1: Per track correction factors obtained from 2015 data processed with `Reco15em` *and including a* < 0.3 *cut on the ghost probability (*`TRACK_GhostProb`*). Quoted uncertainties are due statistical uncertainties due to the size of the calibration mode and differences between the methods used.*

The actual procedure, including the evaluation of the statistical uncertainty due to limited Monte Carlo size, is identical to the PID calibration procedure described in Section 5.6.

The obtained tracking correction factors are given in Table 5.1 for $D^0 \to K^-\pi^+$, Table A.1 for $D^+ \to K^-\pi^+\pi^+$, Table A.2 for $D^+ \to K^-K^+\pi^+$, Table A.3 for $D_s^+ \to \phi\pi^+$, Table A.4 for $D_s^+ \to K^-K^+\pi^+$, Table A.5 for $D^{*+} \to D^0\pi^+$ with $D^0 \to K^-\pi^+$ and Table A.6 for $D^{*+} \to D^0\pi^+$ with $D^0 \to K^-\pi^+\pi^-\pi^+$.

A set of systematic uncertainties is also provided by the tracking group and are going to be discussed in Section 7.5.

5.2.2 Monte Carlo truth matching inefficiency

The LHCb Monte Carlo truth matching deems a reconstructed particle matched to an MC particle if there is an overlap of at least 70% between the hits created

Table 5.1: Tracking efficiency correction for $D^0 \to K^-\pi^+$. Shown uncertainties are due to the size of the simulated sample.

p_{T} [MeV/c]	y [2, 2.5[	[2.5, 3[	[3, 3.5[	[3.5, 4[	[4, 4.5[
[14000, 15000[	102.72 ± 0.06	102.08 ± 0.07	101.75 ± 0.06	101.78 ± 0.05	102.48 ± 0.08
[13000, 14000[	102.97 ± 0.05	102.06 ± 0.05	101.61 ± 0.05	101.63 ± 0.04	102.43 ± 0.05
[12000, 13000[	103.22 ± 0.04	102.01 ± 0.04	101.41 ± 0.04	101.49 ± 0.03	102.28 ± 0.04
[11000, 12000[	103.54 ± 0.04	102.11 ± 0.03	101.23 ± 0.04	101.39 ± 0.03	102.16 ± 0.04
[10000, 11000[	103.91 ± 0.03	102.18 ± 0.03	100.98 ± 0.04	101.17 ± 0.02	102.04 ± 0.03
[9000, 10000[	104.35 ± 0.03	102.43 ± 0.03	100.75 ± 0.04	101.02 ± 0.03	101.90 ± 0.03
[8000, 9000[	104.67 ± 0.09	102.68 ± 0.09	100.46 ± 0.08	100.73 ± 0.07	101.72 ± 0.06
[7000, 8000[	105.47 ± 0.06	102.98 ± 0.06	100.34 ± 0.06	100.32 ± 0.07	101.42 ± 0.05
[6000, 7000[	106.19 ± 0.05	103.27 ± 0.06	100.44 ± 0.07	100.06 ± 0.06	101.25 ± 0.04
[5000, 6000[	107.19 ± 0.05	103.83 ± 0.05	100.64 ± 0.04	99.58 ± 0.04	100.72 ± 0.03
[4000, 5000[	108.14 ± 0.05	104.42 ± 0.04	101.19 ± 0.03	99.28 ± 0.03	100.26 ± 0.03
[3500, 4000[	108.95 ± 0.06	105.12 ± 0.04	101.70 ± 0.04	99.35 ± 0.03	99.96 ± 0.04
[3000, 3500[	109.25 ± 0.07	105.71 ± 0.04	102.21 ± 0.04	99.60 ± 0.03	99.70 ± 0.03
[2500, 3000[	110.04 ± 0.06	106.35 ± 0.04	102.68 ± 0.03	99.93 ± 0.03	99.47 ± 0.03
[2000, 2500[	110.68 ± 0.06	107.05 ± 0.04	103.18 ± 0.03	100.35 ± 0.03	99.25 ± 0.03
[1500, 2000[	111.82 ± 0.06	107.80 ± 0.04	103.80 ± 0.03	100.73 ± 0.03	99.22 ± 0.03
[1000, 1500[	113.12 ± 0.05	108.71 ± 0.04	104.41 ± 0.03	100.93 ± 0.03	99.20 ± 0.03
[0, 1000[	114.14 ± 0.03	110.31 ± 0.03	105.66 ± 0.03	101.33 ± 0.03	99.38 ± 0.02

Table 5.2: Efficiency $1/\rho_{truth}$ of the truth matching requirement applied to the simulated data.

Mode	$1/\rho_{truth}$ [%]
$D^0 \to K^-\pi^+$	98.68 ± 0.06
$D^+ \to K^-\pi^+\pi^+$	96.53 ± 0.58
$D^+ \to K^-K^+\pi^+$	97.91 ± 0.07
$D_s^+ \to \phi\pi^+$	98.53 ± 0.13
$D_s^+ \to K^-K^+\pi^+$	97.92 ± 0.08
$D^{*+} \to D^0\pi^+$, $D^0 \to K^-\pi^+$	96.85 ± 0.09
$D^{*+} \to D^0\pi^+$, $D^0 \to K^-\pi^+\pi^-\pi^+$	97.63 ± 0.40

by the reconstructed particle and those created by the MC particle. This 70% is somewhat arbitrary, and leads to an inefficiency in the truth matching, *i.e.* some reconstructed particles are not marked as 'matched' despite truly belonging to MC particles, and hence to an underestimation to the efficiency and an inflation of the final measurement.

The magnitude of the size of the inefficiency can be determined by counting the number of signal yields that fail the truth matching requirement. Figure 5.2 shows the D^0 mass distributions for the various background category values, of which we only consider values of 0 and 10 as signal. The only background category above 10 to show a signal-like structure is 60, which means the truth-matching tool classified the decays as 'ghosts', *i.e.* containing at least one track that was determined to be a ghost track.

Figures 5.3 and 5.4, show the same information as Figure 5.2 but for $D^+ \to K^-\pi^+\pi^+$ and $D^{*+} \to D^0\pi^+$, with $D^0 \to K^-\pi^+$. These plots demonstrate that the truth matching efficiency is mode-dependent, and so is evaluated per-mode. Due to the limited Monte Carlo statistics, the inefficiency is assumed to be constant across the charm hadron p_{T}-y bins.

Given that the number of correctly matched signal decays is N, and the number of incorrectly labelled signal decays is U, the selection efficiency defined in Equation 5.3 is incorrect by a factor $\rho_{truth} = (U + N)/N$. We compute U for each mode by a fitting the charm hadron mass spectrum of the Monte Carlo which fails the truth matching. Table 5.2 lists the obtained efficiencies.

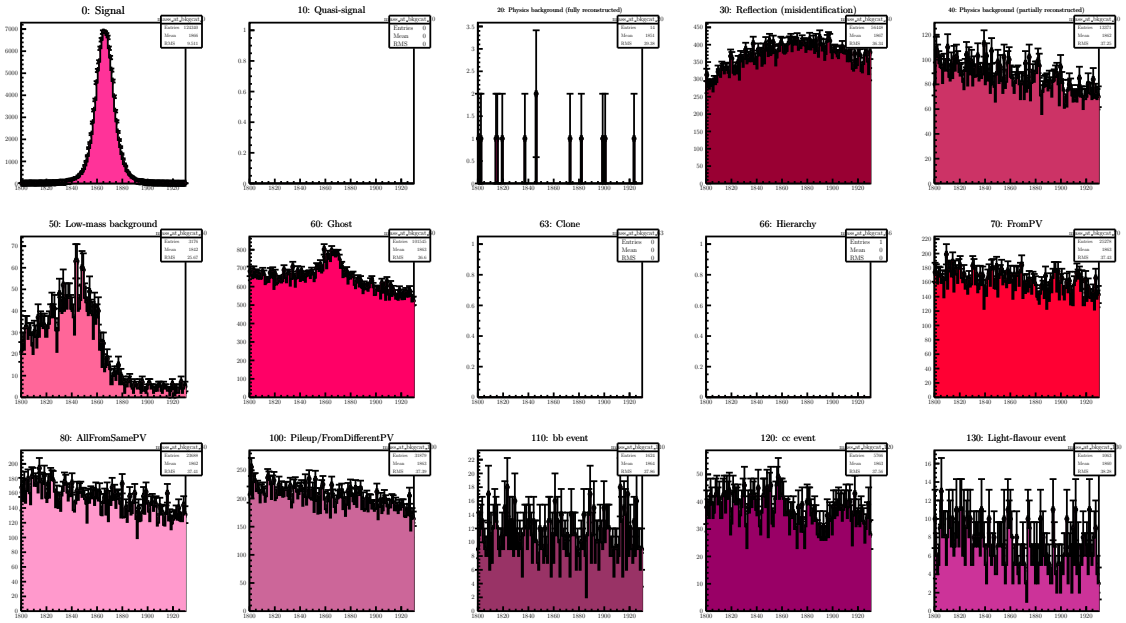

Figure 5.2: $D^0 \to K^-\pi^+$ mass distributions for all the possible background categories values. Any signal-like peaking structures in background categories other than 0 or 10 indicate an inefficiency in the truth matching.

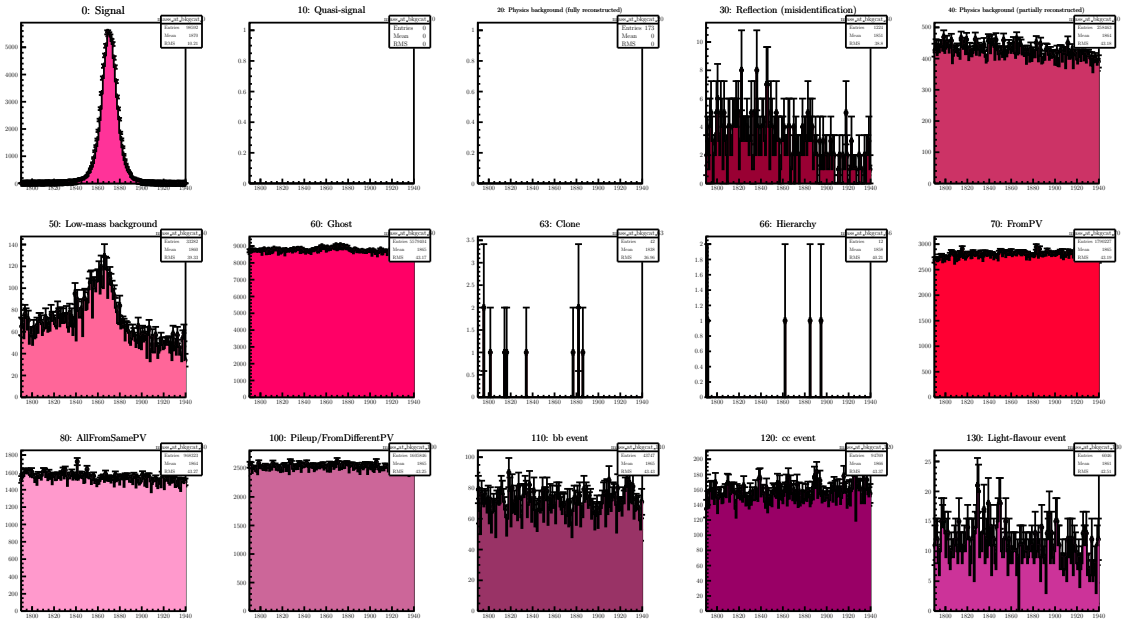

Figure 5.3: $D^+ \to K^-\pi^+\pi^+$ mass distributions for all the possible background categories values. Any signal-like peaking structures in background categories other than 0 or 10 indicate an inefficiency in the truth matching.

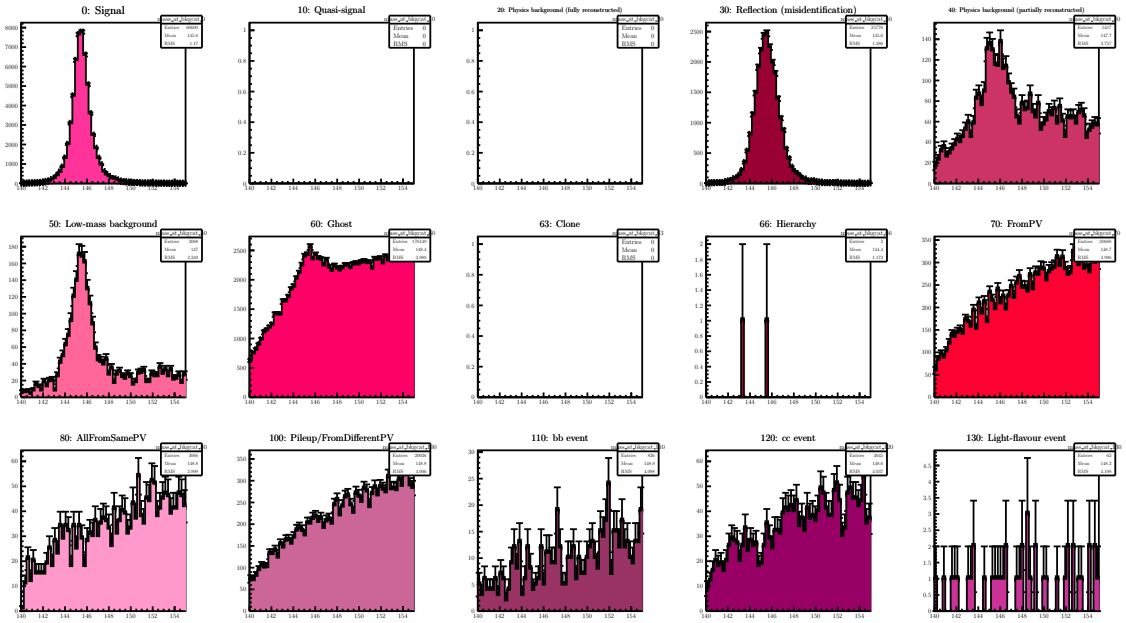

Figure 5.4: $D^{*+} \to D^0\pi^+$, with $D^0 \to K^-\pi^+$, δm distributions for all the possible background categories values. Any signal-like peaking structures in background categories other than 0 or 10 indicate an inefficiency in the truth matching.

5.3 Trigger

The three stages of the trigger, L0, HLT1, and HLT2, each carry a related efficiency. The L0 efficiency ϵ_{L0} is described in Section 4.2. As it is a function of the known selection rate and LHC filling scheme, simulated data is not needed to evaluate it. The HLT1 and HLT2 efficiency, however, do require simulated data as the efficiencies depend on variables to which we do not have access after the trigger.

The efficiency for the HLT1 and HLT2 selection is combined into a single trigger efficiency, defined by the number of true signal decays passing the trigger and those entering

$$\epsilon_{\mathrm{Trigger}} = \epsilon_{\mathrm{L0}} \times \frac{N_{\mathrm{Triggered|Reconstructed}}}{N_{\mathrm{Reconstructed|}\texttt{DaughtersInLHCb}}}. \tag{5.4}$$

As detailed in Section 5.6, the PID efficiency is evaluated using a data-driven method and hence not included in the trigger efficiency evaluated on simulated data.

5.4 Offline selection

As in the case of the trigger efficiency, the efficiency of the offline selection $\epsilon_{\mathrm{Offline}}$ can only be evaluated on simulated data, and is the ratio of truth-matched signal decays passing the selection to those entering it

$$\epsilon_{\mathrm{Offline}} = \frac{N_{\mathrm{Offline|Triggered}}}{N_{\mathrm{Triggered|Reconstructed}}}. \tag{5.5}$$

Here, the offline selection is defined as the rectangular recangular selection applied on the trigger candidates, excluding the tightened requirement on pion PID. The PID efficiencies are evaluated separately in Section 5.6 due to the data-driven approach available, which is preferable to relying on MC modelling. For modes applying a BDT selection, its efficiency is studied separately due to the different nature of the multivariate discriminant in comparison to the other selection variables.

5.4.1 Boosted decision tree

The boosted decision tree accepts a set of variables as input, and returns a single number called the BDT discriminant (or just the "output"). If the efficiency of a cut on the BDT discriminant is evaluated on simulated data, in the same manner as in Section 5.4 for the stripping efficiency, then it should be sufficient to ensure that the signal distributions of the input variables are well modelled in order for the output to be similarly well modelled.

This assumption is tested in the context of systematic uncertainties in Section 7.2, but for this section we only need to define the BDT efficiency:

$$\epsilon_{\mathrm{BDT}} = \frac{N_{\mathrm{BDT|Stripped}}}{N_{\mathrm{Stripped|Triggered}}}. \tag{5.6}$$

5.5 Combination of efficiencies and their statistical uncertainty

Aside of the acceptance and the PID efficiency, all other selection criteria are estimated on the same simulated data sample for the respective mode. Hence, the number of events passing a certain stage in the selection is fully correlated (it is the same number) to the number of events entering in the next stage. To avoid having to include those correlations explicitely, the final efficiency ϵ_{MC} is computed in one step, incorporating all selections evaluated on the simulated data.

Due to the finite size of the calibration sample, the statistical uncertainty on the selection efficiency give a non-negligible contribution to the systematic uncertainties of this measurement and hence care is necessary when evaluating this uncertainty. As binomial uncertainties fail to model this uncertainty correctly in case of very low efficiencies and limited sample size, the uncertainties are estimated from the posteriori [7] probability for ε, assuming a binomial distribution for the number of passing events given the total number of events and ε and a flat prior in ε. This posteriori probability is also used in the Monte Carlo error propagation to obtain the uncertainties on the measured cross-sections. Tables 5.3 and A.7–A.12 give the per-bin efficiencies for each mode.

5.6 PID calibration

This analysis places PID requirements on all child kaons and pions, except soft pions from D^{*+} decays, as these cuts significantly reduce the amount of background passing the selection. Signal Monte Carlo samples, used previously to estimate the efficiencies of all other selection criteria, cannot be used in the determination of the PID efficiencies as comparisons of MC simulations and real data reveals a large disagreement in the PID variables. Therefore, a data-driven method to estimate the efficiencies is described and applied in this section.

All presented studies and the stated results are based on the PIDCalib framework with version v9r2 of the `PIDPerfScripts` package.

[7] Given by $P(\varepsilon) \propto \varepsilon^p (1-\varepsilon)^{t-p}$ with $p(t)$ being the number of passing (total) events. This is the Beta function with $\alpha = p+1$ and $\beta = t-p+1$.

Table 5.3: Total MC selection efficiency for $D^0 \to K^-\pi^+$ in bins of D^0 p_{T} and y.

p_{T} [MeV/c]	y $[2, 2.5[$	$[2.5, 3[$	$[3, 3.5[$	$[3.5, 4[$	$[4, 4.5[$
$[14000, 15000[$	$11.44^{+0.38}_{-0.37}$	$16.68^{+0.51}_{-0.49}$	$4.03^{+0.31}_{-0.29}$	$0.00^{+0.04}_{-0.00}$	$0.00^{+0.08}_{-0.00}$
$[13000, 14000[$	$11.20^{+0.32}_{-0.32}$	$17.46^{+0.43}_{-0.42}$	$5.91^{+0.31}_{-0.30}$	$0.00^{+0.03}_{-0.00}$	$0.00^{+0.05}_{-0.00}$
$[12000, 13000[$	$11.33^{+0.27}_{-0.27}$	$18.46^{+0.36}_{-0.36}$	$8.20^{+0.30}_{-0.29}$	$0.00^{+0.02}_{-0.00}$	$0.00^{+0.03}_{-0.00}$
$[11000, 12000[$	$11.21^{+0.22}_{-0.22}$	$18.96^{+0.31}_{-0.30}$	$10.68^{+0.27}_{-0.27}$	$0.08^{+0.03}_{-0.02}$	$0.00^{+0.02}_{-0.00}$
$[10000, 11000[$	$10.29^{+0.18}_{-0.17}$	$18.96^{+0.25}_{-0.24}$	$13.99^{+0.25}_{-0.24}$	$0.76^{+0.08}_{-0.07}$	$0.00^{+0.01}_{-0.00}$
$[9000, 10000[$	$9.84^{+0.17}_{-0.17}$	$18.73^{+0.24}_{-0.24}$	$16.32^{+0.25}_{-0.25}$	$1.78^{+0.11}_{-0.10}$	$0.00^{+0.01}_{-0.00}$
$[8000, 9000[$	$9.09^{+0.48}_{-0.46}$	$19.24^{+0.69}_{-0.67}$	$18.91^{+0.76}_{-0.74}$	$3.56^{+0.43}_{-0.39}$	$0.00^{+0.08}_{-0.00}$
$[7000, 8000[$	$9.54^{+0.39}_{-0.37}$	$17.68^{+0.53}_{-0.51}$	$19.08^{+0.59}_{-0.58}$	$8.00^{+0.47}_{-0.45}$	$0.00^{+0.05}_{-0.00}$
$[6000, 7000[$	$8.20^{+0.28}_{-0.27}$	$16.44^{+0.39}_{-0.38}$	$19.34^{+0.45}_{-0.44}$	$10.54^{+0.39}_{-0.38}$	$0.27^{+0.09}_{-0.07}$
$[5000, 6000[$	$6.55^{+0.19}_{-0.18}$	$14.68^{+0.28}_{-0.27}$	$17.72^{+0.32}_{-0.32}$	$12.18^{+0.31}_{-0.30}$	$1.40^{+0.13}_{-0.12}$
$[4000, 5000[$	$5.28^{+0.13}_{-0.13}$	$13.18^{+0.20}_{-0.19}$	$14.72^{+0.22}_{-0.22}$	$11.97^{+0.22}_{-0.22}$	$2.50^{+0.12}_{-0.12}$
$[3500, 4000[$	$4.22^{+0.13}_{-0.13}$	$11.40^{+0.21}_{-0.21}$	$12.78^{+0.23}_{-0.23}$	$10.27^{+0.23}_{-0.23}$	$3.54^{+0.16}_{-0.16}$
$[3000, 3500[$	$3.29^{+0.10}_{-0.10}$	$9.68^{+0.17}_{-0.17}$	$11.01^{+0.19}_{-0.19}$	$8.99^{+0.19}_{-0.18}$	$3.57^{+0.14}_{-0.14}$
$[2500, 3000[$	$2.54^{+0.08}_{-0.08}$	$7.59^{+0.13}_{-0.13}$	$9.34^{+0.15}_{-0.15}$	$7.03^{+0.15}_{-0.14}$	$2.88^{+0.11}_{-0.11}$
$[2000, 2500[$	$1.90^{+0.06}_{-0.06}$	$5.81^{+0.11}_{-0.10}$	$6.94^{+0.12}_{-0.12}$	$5.43^{+0.11}_{-0.11}$	$2.35^{+0.09}_{-0.08}$
$[1500, 2000[$	$1.29^{+0.05}_{-0.05}$	$4.51^{+0.09}_{-0.08}$	$5.63^{+0.10}_{-0.10}$	$4.12^{+0.09}_{-0.09}$	$1.63^{+0.07}_{-0.06}$
$[1000, 1500[$	$0.97^{+0.04}_{-0.04}$	$3.61^{+0.07}_{-0.07}$	$4.49^{+0.08}_{-0.08}$	$3.42^{+0.08}_{-0.08}$	$1.42^{+0.06}_{-0.06}$
$[0, 1000[$	$0.71^{+0.03}_{-0.03}$	$2.91^{+0.06}_{-0.06}$	$3.92^{+0.07}_{-0.07}$	$3.13^{+0.07}_{-0.07}$	$1.20^{+0.06}_{-0.06}$

5.6.1 Definitions

Throughout this chapter, a set of terms is repeatedly used and hence defined in the following. A *track* refers to a final state object of the studied decay upon which a PID requirement is imposed. The performance of the LHCb particle identification detectors depends on the kinematics of the incident particle and hence each track is characterised by its momentum p and pseudorapidity η. In addition to the kinematics, the performance also varies between different events due to differences in the detector occupancy, described by the number of hits in the SPD detector `nSPDHits`.

The *reference sample* refers to the sample for which the efficiency of a specific PID selection should be determined. Therefore, it should have the same kinematics and `nSPDHits` distributions as the decay which is actually studied. Due to the abundance of signal in this analysis, the fully selected data sample for the specific mode is used as a reference sample after extracting the signal contribution using the sWeight method. As will be discussed in the next section, under certain conditions it is possible to choose a reference sample which already had PID requirements applied to it.

Lastly, the *calibration sample* contains tracks of known type without any PID requirements imposed on them. These tracks are taken from decays which can be selected with a high purity. Calibration pions and kaons are taken as the child tracks of the $D^0 \to K^-\pi^+$ decay, where the pion is defined as the track having the same electric charge as the soft pion from the tagging $D^{*+} \to D^0\pi^+$ decay, whilst the kaon must have the opposite charge. In order to obtain the pure signal contribution in the respective samples, a mass fit is performed and every event in the calibration sample is sWeighted according to the results of the fit.

5.6.2 Estimating the efficiency

This section describes the actual method used to obtain the PID efficiencies. At first, the simplest case with only one final state track with a PID requirement is discussed. This will be extended to cover events with PID requirements imposed on several final state tracks. Additionally, the application of the calibration method using PID selected reference samples is discussed.

Only one track with a PID requirement

Due to the dependence of the PID performance on the kinematics of the process, the PID selection efficiency can vary significantly for different processes even though the same cut value is imposed. Therefore, it is not sufficient to create a one-dimensional table per particle type and PID variable mapping specific cut values to an efficiency

computed from the number of events passing this cut in the calibration sample. Instead, a reweighting of the calibration sample to match the distributions in the kinematics and in `nSPDHits` in the reference sample is necessary. To achieve this, the calibration as well as reference sample is binned in those variables. In each of those bins i, the efficiency of a track to pass the PID cut is defined as

$$\epsilon_i = \frac{C_i'}{C_i}, \tag{5.7}$$

where C_i refers to the number of tracks in the calibration sample in the ith bin of which C_i' tracks pass the cut. Therefore, the efficiency for all tracks which fall into the same bin is assumed to be the constant and hence the choice of the binning can substantially change the result of the calibration. Section 7.3 will discuss the strategy being used in this analysis to optimise the binning scheme. In order to calculate the efficiency in the reference sample, a weight ω_i is applied to every bin in the calibration sample

$$\omega_i = \frac{R_i}{C_i} \cdot \frac{C}{R}, \tag{5.8}$$

where C_i (R_i) is the number of calibration (reference) tracks in the ith bin and C (R) is the total number of tracks in the respective sample. Using this weight, the efficiency in the reference sample can be computed

$$\epsilon_{PID} = \frac{\sum\limits_{i \in \text{bins}} \omega_i C_i \epsilon_i}{\sum\limits_{i \in \text{bins}} \omega_i C_i}. \tag{5.9}$$

Multiple tracks with a PID requirement

This analysis applies PID requirements on all final state tracks and hence cannot employ Equation (5.9) directly as more than one calibration sample is involved. Therefore, Equation (5.9) is modified by substituting the weight ω_i:

$$\epsilon_{PID} = \frac{\sum\limits_{i \in \text{bins}} R_i \epsilon_i}{\sum\limits_{i \in \text{bins}} R_i} = \frac{1}{R} \sum_{i \in \text{bins}} R_i \epsilon_i. \tag{5.10}$$

This is further rewritten in terms of a_{ij}, that is the weight of the jth event in the ith bin in the reference sample (in this analysis determined using the sWeight method):

$$\epsilon_{PID} = \frac{1}{R} \sum_{i \in \text{bin}} \sum_{j} a_{ij} \epsilon_i = \frac{1}{R} \sum_{e \in \text{events}} a_e \epsilon_e \text{ with } \epsilon_e = \epsilon_{f(e)}, \tag{5.11}$$

where the sum in the numerator has been expanded and rearranged to run over all events in the reference sample with $f(e)$ giving the corresponding bin and a_e being the weight for event e. By doing so, the PID calibration can be separated into two steps:

1. Each event in the reference sample is assigned the probability that an event having these kinematics has to pass the cut; and

2. The reweighting itself is done by averaging those probabilities over all events in the reference sample.

This per event efficiency can now be easily extended to incorporate multiple PID cuts as it is probability of an event to pass all applied PID cuts:

$$\epsilon_e = \prod_{p \in \text{part.}} \epsilon_{f_p(e)}, \tag{5.12}$$

where f_p gives the bin in the calibration sample for a particle of type p.

The uncertainty on a single track efficiency $\Delta\epsilon_i$ is given by the binomial uncertainty computed from C_i and C_i' in the corresponding reference sample. The statistical uncertainty on the efficiency of the entire event comprised of several final state tracks with PID cuts applied to them is then derived by using Gaussian error propagation:

$$\Delta\epsilon_e = \epsilon_e \sqrt{\sum_{p \in \text{part.}} \sum_{k \in \text{part.}} \rho_{pk} \cdot \frac{\Delta\epsilon_{f_p(e)}}{\epsilon_{f_p(e)}} \cdot \frac{\Delta\epsilon_{f_k(e)}}{\epsilon_{f_k(e)}}}. \tag{5.13}$$

Events in different bins of the calibration sample are statistically independent and thus the correlation term is given by

$$\rho_{pk} = \begin{cases} 1 & \text{if } p \text{ and } k \text{ are same type of particle and } f_p(e) = f_k(e), \\ 0 & \text{otherwise.} \end{cases} \tag{5.14}$$

The overall uncertainty $\Delta\epsilon$ on the PID efficiency consists of two components: the uncertainty due to the finite size of the calibration sample σ_C^{PID} and the finite size of

the reference sample σ_R^{PID}. The first contribution is included as the uncertainty on the weighted sample mean while the latter takes into account the spread of sample mean ϵ with respect to the true efficiency.

In this analysis, the two components are treated separately: the uncertainty due to the calibration sample size is estimated using a toy study, which also takes into account the correlation between the different tracks within one event, and included as a systematic uncertainty – discussed in Section 7.3.1. The finite reference sample size leads to the statistical uncertainty on the PID efficiency ε. The quoted uncertainty ε can be interpreted as a mean over the finite sample and hence is spread around the true mean which would be the result if the reference sample would be infinitely large. Therefore, this uncertainty is given by the estimated uncertainty on the sample mean:

$$\left(\sigma_R^{PID}\right)^2 = \frac{\sum a_e^2}{\left(\sum a_e\right)^2} \cdot \frac{\sum a_e}{\left(\sum a_e\right)^2 - \sum a_e^2} \cdot \sum \left(\epsilon_e - \epsilon_{PID}\right)\left(\epsilon_e - \epsilon_{PID}\right) a_e \ . \tag{5.15}$$

Using a PID selected reference sample

As stated before, this analysis uses the fully selected data sample as a reference to compute the PID efficiencies. This selection includes cuts on PID variables and thus it is not immediately obvious how this affects the result of the reweighting. Therefore, the impact is again first studied for only one PID selected final state track before being extended to the general case.

Assuming those PID cuts are also applied to the calibration sample, a new weight for the ith bin can be defined:

$$\omega_i' = \frac{R_i''}{C_i''} \cdot \frac{C''}{R''}, \tag{5.16}$$

where the double prime notation is chosen to indicate that the cut applied to the data is not required to be identical to the cut for which the efficiency should be estimated. Using the definition of the efficiency per bin, this can be rewritten:

$$\omega_i' = \frac{R_i \epsilon_i''}{C_i \epsilon_i''} \cdot \frac{C''}{R''} = \frac{R_i}{C_i} \cdot A \frac{C}{R} = A \cdot \omega_i. \tag{5.17}$$

A is a scale-factor relating the relative yield in the reference and calibration before and after the PID cut which is applied to the reference sample. Therefore, this scale-factor depends on the chosen cut-value but is the same for all bins and hence

cancels in the calculation of the desired efficiency ϵ. However, this is only valid if the condition

$$S''_i = \epsilon''_i S_i \quad \forall\ i \in \text{bins}\ , \tag{5.18}$$

where S represents either the calibration or reference sample, holds. Hence, $S''_i \neq 0$ must be true for all bins with $S_i \neq 0$ so the PID cut applied to the reference sample must not exclude any regions in the p-η-`nSPDHits` phase-space.

However, this method can only be applied directly to a measurement if PID selections are applied to one final state only. Nonetheless, the efficiency can be derived by weighting each event in the PID selected reference sample by $1/\epsilon''_i$:

$$\epsilon_{PID} = \frac{1}{\sum\limits_{e\in\text{events}} \frac{a_e}{\epsilon''_e}} \sum_{e\in\text{events}} \frac{a_e}{\epsilon''_e}\epsilon_e. \tag{5.19}$$

In this analysis, the PID selection applied to the reference sample is the one we are estimating the efficiency for and thus $\epsilon''_e = \epsilon_e$. Therefore, this simplifies to

$$\frac{1}{\epsilon_{PID}} = \frac{1}{R} \sum_{e\in\text{events}} \frac{a_e}{\epsilon_e} \tag{5.20}$$

and the uncertainty on $1/\epsilon$ can be computed as before by substituting $\epsilon_e \to 1/\epsilon_e$. Furthermore, the overall contribution to the statistical uncertainty on the measured cross-section is already included as the uncertainty on yield from the fit and hence the statistical uncertainty due to the reference sample size (given in Equation (5.15)) is not applied.

5.6.3 Optimising the binning in the track variables

The binning scheme, which splits the p-η-`nSPDHits` phase-space to reweight the calibration sample, is an important ingredient in the calibration procedure. As stated before, the calibration procedure assumes that the efficiency ϵ_i is correct for all tracks in the ith bin of the calibration histogram. Obviously, the only general solution which would satisfy this assumption is a binning scheme with infinitely small bins. However, due to the finite size of the calibration sample, this is impossible to achieve.

Therefore, bins should:

- Be as small as necessary such that the condition that the PID efficiency is constant within a given bin is satisfied;
- Be as large as possible to achieve small uncertainties on the individual ϵ_i; and

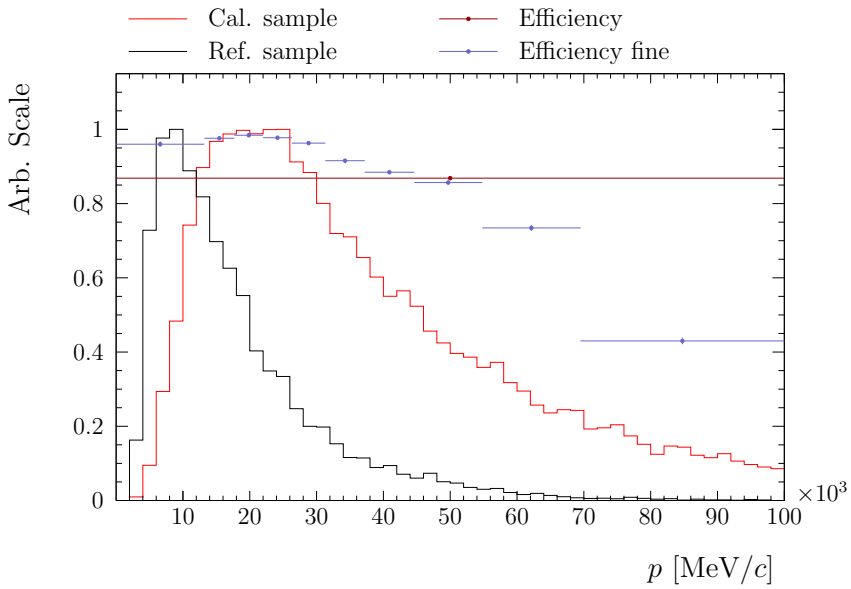

Figure 5.5: Example figure to illustrate different binning scheme in track momentum p for $K^{\pm}$ tracks with a cut of $DLL_{K-\pi} > 5$. The distribution in the calibration (reference) sample is shown in red (black). The fully selected $\sqrt{s} = 7\,\mathrm{TeV}$ $D^{+} \to K^{-}\pi^{+}\pi^{+}$ data is used as the reference sample. The distributions are shown to check the coverage of the reference sample phase space. The red points indicate the efficiency in the studied binning scheme while the blue ones show the efficiency in 10 equal probability sub-bins obtained by dividing each red bin. Clearly, one bin for the entire p range is insufficient and does not approximate the actual dependence illustrated by the finer binning.

- Avoid unphysical values for ϵ_i caused by statistical fluctuations in the bin in combination with the sWeights in the calibration sample.

All those requirements are easily fulfilled if the size of the calibration sample is large. Unfortunately, this is not the case for the early measurement run period and hence in this analysis.

Figure 5.5 illustrates the dependence of the efficiency for $\mathrm{DLL}_{K-\pi} > 5$ applied to a charged kaon track on the momentum p of the particle.

As can be seen, a single bin in track momentum is insufficient to describe the dependence and hence a finer binning is required. While the binning shown in blue is a more reasonable choice, a binning simply using equal probability bins blindly adds bins based solely on the distribution in the calibration sample. The region around the peak of the distribution is finely binned even though it appears to be almost flat and hence fewer, larger bins would suffice in this region. Therefore, this analysis uses

an iterative procedure to determine a suitable binning scheme:

1. Start with one bin covering the entire range;
2. Compute the χ^2 between the efficiency in the bin and the ten sub-bins (see Figure 5.5), if the p-value is smaller than 0.001, the bin is divided;
3. A bin is divided by testing possible bin boundaries obtained by splitting the bin into 20 equal probability sub-bins. The new boundary is the one minimising the sum of the respective χ^2 in the new bins and must yield two new bins with at least 2000 events each.
4. Repeat from step 2 until all bins pass the p-value requirement or all possible division fail the required number of events; and
5. Merge neighbouring bins if the corresponding efficiencies agree within 3σ.

This procedure is done separately for p, η and `nSPDHits` to obtain the binning in each of the dimensions. The cut-off values for the minimal number of events per bin and the p-value of the χ^2 comparison are only preliminary and will be retuned for the actual calibration data.

The results of the binning procedure are shown in Figure 5.6 for kaon and in Figure 5.7 for pion tracks. As can be seen, the procedure yields large bins in regions with approximately flat dependence on the chosen variable. The insufficient description of the efficiency for high track momentum and pseudorapidity, shown in Figures 5.6a and 5.6b, is a result of the limited statistic available in those bins. Once the actual calibration data is available, the shown binning schemes will be refined and improved.

5.6.4 PID efficiencies

In the following, the PID efficiency tables are given for all studied modes. The central values are computed for each charm hadron in a given p_{T}-y bin by multiplying together the PID efficiencies of all of the child tracks. As described above, the statistical uncertainty on the reference sample size is already incorporated in the uncertainty on the fit yields. Therefore, the uncertainties given in the tables are due to the size of the calibration sample and constitute one of the systematic uncertainties in this measurement. The estimation of the uncertainty is described in detail in Section 7.3.1.

The obtained PID efficiencies using the calibration procedure described above are given in bins of charm hadron p_{T} and y in Table 5.4 for $D^0 \to K^-\pi^+$, Table A.13 for $D^+ \to K^-\pi^+\pi^+$, Table A.14 for $D^+ \to K^-K^+\pi^+$, Table A.15 for $D_s^+ \to \phi\pi^+$,

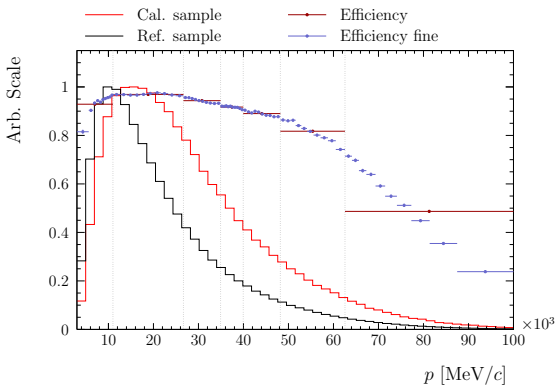

(a) Momentum

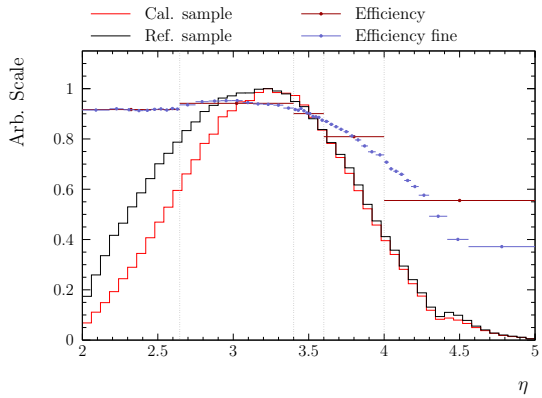

(b) Pseudorapidity

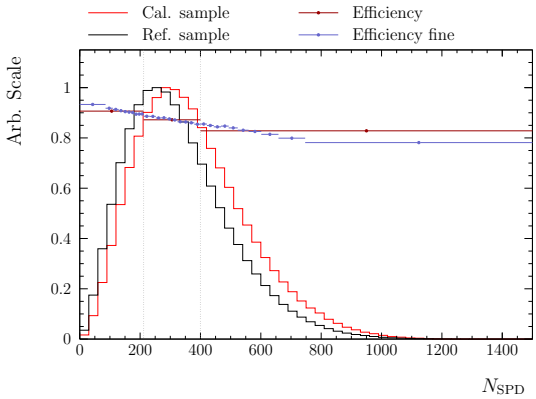

(c) No. of hits in the SPD

Figure 5.6: Results for the binning scheme for $K^{\pm}$ tracks with a PID cut of $DLL_{K-\pi} > 5$. The fully selected $D^0 \to K^-\pi^+$ sample is shown as the reference distribution. The resulting efficiencies are given by the red points. A finer binning (which is too fine for being used in the 3D binning scheme) is shown in blue to illustrate how well the binning scheme approximates the true dependence. Due to the procedure being independent of the actual decay mode, the same binning scheme is used for all other modes.

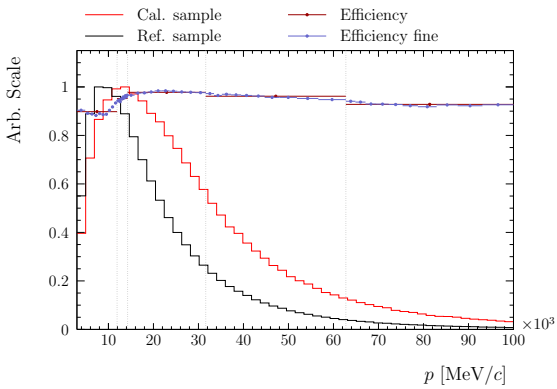

(a) Momentum

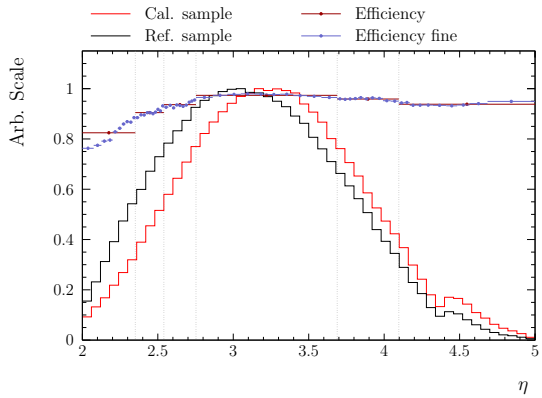

(b) Pseudorapidity

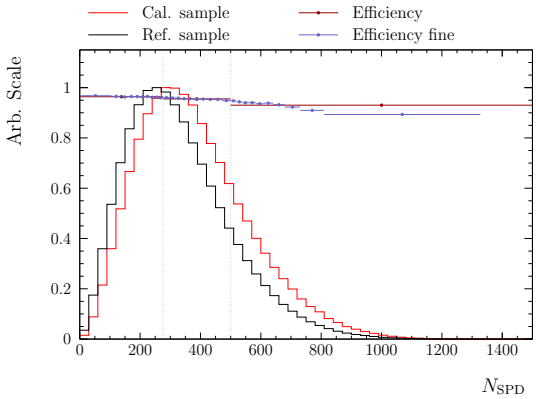

(c) No. of hits in the SPD

Figure 5.7: Results for the binning scheme for $\pi^{\pm}$ tracks with a PID cut of $DLL_{K-\pi} < 3$. The fully selected $D^0 \to K^-\pi^+$ sample is shown as the reference distribution. The resulting efficiencies are given by the red points. A finer binning (which is too fine for being used in the 3D binning scheme) is shown in blue to illustrate how well the binning scheme approximates the true dependence. Due to the procedure being independent of the actual decay mode, the same binning scheme is used for all other modes.

Table 5.4: Total PID selection efficiency for $D^0 \to K^-\pi^+$ in bins of D^0 p_{T} and y. Shown uncertainties are due to the size of the calibration sample.

	y				
p_{T} [MeV/c]	$[2, 2.5[$	$[2.5, 3[$	$[3, 3.5[$	$[3.5, 4[$	$[4, 4.5[$
$[14000, 15000[$	60.97 ± 0.80	57.54 ± 1.20	60.31 ± 0.41	-	-
$[13000, 14000[$	65.67 ± 0.51	58.93 ± 0.96	64.55 ± 0.37	-	-
$[12000, 13000[$	69.54 ± 0.44	64.17 ± 0.66	66.18 ± 0.33	-	-
$[11000, 12000[$	72.34 ± 0.37	69.92 ± 0.47	68.96 ± 0.30	60.38 ± 0.65	-
$[10000, 11000[$	73.33 ± 0.30	74.37 ± 0.29	71.52 ± 0.25	56.65 ± 0.45	-
$[9000, 10000[$	78.76 ± 0.22	77.74 ± 0.24	74.72 ± 0.22	53.34 ± 0.28	-
$[8000, 9000[$	81.68 ± 0.19	83.08 ± 0.15	76.91 ± 0.19	57.29 ± 0.26	-
$[7000, 8000[$	83.73 ± 0.16	87.33 ± 0.10	80.01 ± 0.15	61.07 ± 0.22	-
$[6000, 7000[$	85.85 ± 0.14	90.18 ± 0.07	83.81 ± 0.11	64.66 ± 0.19	43.96 ± 0.27
$[5000, 6000[$	86.12 ± 0.13	91.66 ± 0.06	88.16 ± 0.08	68.45 ± 0.16	43.59 ± 0.25
$[4000, 5000[$	85.25 ± 0.13	92.17 ± 0.06	91.55 ± 0.05	72.98 ± 0.14	50.62 ± 0.25
$[3500, 4000[$	83.91 ± 0.14	91.80 ± 0.06	92.95 ± 0.05	77.58 ± 0.11	56.20 ± 0.25
$[3000, 3500[$	83.28 ± 0.15	91.18 ± 0.07	93.15 ± 0.05	80.63 ± 0.10	59.19 ± 0.25
$[2500, 3000[$	82.82 ± 0.16	90.46 ± 0.08	93.13 ± 0.05	84.09 ± 0.09	62.42 ± 0.23
$[2000, 2500[$	82.55 ± 0.17	89.75 ± 0.09	92.90 ± 0.06	86.90 ± 0.09	65.14 ± 0.21
$[1500, 2000[$	82.67 ± 0.18	89.14 ± 0.10	92.70 ± 0.08	88.55 ± 0.10	70.87 ± 0.19
$[1000, 1500[$	82.94 ± 0.18	88.53 ± 0.13	92.36 ± 0.10	89.09 ± 0.12	75.97 ± 0.19
$[0, 1000[$	82.79 ± 0.18	87.38 ± 0.16	92.28 ± 0.10	89.87 ± 0.14	80.52 ± 0.24

Table A.16 for $D_s^+ \to K^-K^+\pi^+$, Table A.17 for $D^{*+} \to D^0\pi^+$ with $D^0 \to K^-\pi^+$ and Table A.18 for $D^{*+} \to D^0\pi^+$ with $D^0 \to K^-\pi^+\pi^-\pi^+$.

5.7 Signal window efficiency

As described in Section 6, the number of prompt signal candidates is measured by fitting the $\ln \chi^2_{\mathrm{IP}}$ distribution of candidates in a signal window defined in the mass distribution. The efficiency of this requirement is evaluated by computing the fractional integral of the signal component of the PDF fitted to the mass distribution, where the fractional integral across the entire fitted mass range is defined to be unity. In the case of the D^{*+} measurement, there is an additional requirement that the candidates used in the $\ln \chi^2_{\mathrm{IP}}$ fit fall in a signal window defined in the $\delta m = m(D^{*+}) - m(D^0)$ distribution. The efficiency of this δm signal window requirement is computed in the same way as for the mass signal window requirement, except the signal component of the PDF fitted to the δm distribution is used.

The integral of a probability density function is a number. To assign an uncertainty to this number, the fractional integral is recomputed in a series of 200 pseudo-experiments whereby the shape parameters of the signal PDF are varied within their uncertainties. Within each toy study, each shape parameter is assigned a value sampled from a Gaussian distribution with a mean as the 'nominal' value of that parameter, the value found by the fit, and with a width as the uncertainty on that nominal value. The variance on the deviation of the integrals, with respect to the integral computed using the nominal shape parameter values, is taken as the square of the uncertainty on the nominal integral value.

As the shape of some mass signal PDFs are p_{T}-y bin dependent, as described in Section 6.4, the signal window efficiency is computed for each p_{T}-y bin. Tables 5.5 and A.19–A.24 give the per-bin efficiencies for each mode.

Table 5.5: Signal window requirement efficiencies, in percent, for $D^0 \to K^-\pi^+$.

	y				
p_{T} [MeV/c]	$[2, 2.5[$	$[2.5, 3[$	$[3, 3.5[$	$[3.5, 4[$	$[4, 4.5[$
$[14000, 15000[$	95.64 ± 0.41	95.22 ± 0.42	97.60 ± 0.33	97.79 ± 0.04	97.79 ± 0.04
$[13000, 14000[$	95.98 ± 0.32	96.24 ± 0.26	93.58 ± 0.25	97.79 ± 0.04	97.79 ± 0.04
$[12000, 13000[$	96.62 ± 0.21	96.09 ± 0.23	93.90 ± 0.28	97.79 ± 0.04	97.79 ± 0.04
$[11000, 12000[$	96.58 ± 0.18	96.53 ± 0.16	96.01 ± 0.31	96.30 ± 0.10	97.79 ± 0.04
$[10000, 11000[$	96.78 ± 0.14	96.73 ± 0.12	95.68 ± 0.24	92.90 ± 1.08	97.79 ± 0.04
$[9000, 10000[$	96.92 ± 0.10	96.78 ± 0.09	96.19 ± 0.15	93.76 ± 0.16	97.79 ± 0.04
$[8000, 9000[$	97.35 ± 0.06	96.84 ± 0.07	96.16 ± 0.11	94.62 ± 0.45	97.79 ± 0.04
$[7000, 8000[$	97.41 ± 0.05	97.09 ± 0.06	96.32 ± 0.08	95.28 ± 0.23	97.79 ± 0.04
$[6000, 7000[$	97.44 ± 0.05	97.20 ± 0.05	96.47 ± 0.07	95.53 ± 0.14	93.76 ± 0.34
$[5000, 6000[$	97.58 ± 0.04	97.41 ± 0.04	96.72 ± 0.05	95.72 ± 0.09	93.33 ± 0.20
$[4000, 5000[$	97.68 ± 0.04	97.53 ± 0.04	96.89 ± 0.05	95.66 ± 0.07	93.61 ± 0.07
$[3500, 4000[$	97.77 ± 0.04	97.60 ± 0.04	97.00 ± 0.05	95.82 ± 0.07	93.63 ± 0.09
$[3000, 3500[$	97.81 ± 0.04	97.68 ± 0.04	97.09 ± 0.04	95.93 ± 0.07	93.67 ± 0.08
$[2500, 3000[$	97.84 ± 0.04	97.72 ± 0.04	97.17 ± 0.04	95.93 ± 0.06	93.74 ± 0.13
$[2000, 2500[$	97.91 ± 0.04	97.76 ± 0.04	97.28 ± 0.04	96.11 ± 0.06	93.61 ± 0.17
$[1500, 2000[$	97.97 ± 0.04	97.82 ± 0.04	97.36 ± 0.04	96.26 ± 0.06	93.70 ± 1.90
$[1000, 1500[$	97.99 ± 0.04	97.86 ± 0.04	97.46 ± 0.04	96.60 ± 0.06	95.28 ± 0.15
$[0, 1000[$	98.02 ± 0.04	97.92 ± 0.04	97.56 ± 0.04	96.79 ± 0.06	95.38 ± 0.17

6 Yield extraction

The number of fully selected prompt signal candidates for a given charm hadron and decay mode in a given p_{T}-y bin is determined by a one-dimensional binned extended maximum likelihood fit to the charm hadron $\ln \chi^2_{\mathrm{IP}}$ distribution in the mass signal region of the fully selected dataset. This is performed simultaneously across all p_{T}-y bins using the RooFit framework.

6.1 Definition of species

The species of interest for this analysis is *prompt* signal, that is a charm hadron originating from the pp interaction point, whilst a signal decay originating from the decay of a long-lived b-hadron is *secondary* signal. Combinatorial background is comprised of random combinations of tracks which have satisfied the full selection criteria. For the D^{*+} hadrons, two additional species of data are considered: *random soft pion* background, where a background soft pion from the event has been combined with the relevant *prompt* signal charm hadron to form a fake prompt resonant candidate, and *secondary soft pion* background, where a background soft pion from the event has been combined with the relevant *secondary* signal charm hadron to form a fake secondary resonant candidate.

6.2 Strategy

The prompt signal yield in each p_{T}-y bin is measured by an binned extended maximum likelihood fit to the $\ln \chi^2_{\mathrm{IP}}$ distribution. This variable can discriminate between prompt and secondary signal as the generating probability density functions (PDFs) will be displaced with respect to one another (charm hadrons produced via b-decays will not point back to the PV, in general). The combinatorial background, however, is much harder to discriminate against and model in $\ln \chi^2_{\mathrm{IP}}$, as it will contain a mixture of $\ln \chi^2_{\mathrm{IP}}$ values.

The prompt and secondary signal distributions are modelled by continuous, parametric PDFs, whose functional form will be given in Section 6.3. Rather than attempting to parameterise the combinatorial background distribution, a kernel density estimate (KDE), or template, PDF is created from the $\ln \chi^2_{\mathrm{IP}}$ distribution in the lower and upper sidebands of the reconstructed charm hadron mass. In the case of the D^{*+} measurements, the upper sideband of the delta mass distribution, the difference between the reconstructed D^{*+} mass and the reconstructed D^0 mass $\delta m = m(D^{*+}) - m(D^0)$, is used instead. This approach assumes that the $\ln \chi^2_{\mathrm{IP}}$ shape

in the signal region is the same as that in the sidebands, *i.e.* that the mass and $\ln \chi^2_{\mathrm{IP}}$ are uncorrelated in the background sample. This assumption is validated in Section 8.1.

The 'signal region' in the long-lived charm hadron mass distribution is defined as a $\pm 20\,\mathrm{MeV}$ window centred on the nominal rest mass of the given charm hadron, taken to be $m_{D^0} = 1864.84\,\mathrm{MeV}$, $m_{D^+} = 1869.61\,\mathrm{MeV}$, and $m_{D_s^+} = 1968.30\,\mathrm{MeV}$. The 'lower sideband' is a $20\,\mathrm{MeV}$-wide window with an upper bound $20\,\mathrm{MeV}$ below the centre of the signal window, and the 'upper' sideband is a $20\,\mathrm{MeV}$-wide window with a lower bound $20\,\mathrm{MeV}$ above the centre of the signal window. For the D^{*+} measurements, the 'signal region' is defined as a window $\pm 3\,\mathrm{MeV}$ wide, centred on the nominal δm value of $145.43\,\mathrm{MeV}$. The 'upper sideband', or just 'sideband' as a 'lower sideband' region is not defined, is defined as a $4.5\,\mathrm{MeV}$-wide window with a lower bound $4.5\,\mathrm{MeV}$ above the centre of the signal region. Figures 6.1–6.7 give a graphical representation of the signal and sideband regions for each mode.

The integral of the $\ln \chi^2_{\mathrm{IP}}$ background template PDF is constrained to be near the number of background candidates in the sample taken from the sidebands. This is measured by binned extended maximum likelihood fits to the charm hadron mass distribution, or the δm distribution in the D^0 mass signal region for the D^{*+} measurements.

To avoid any complications due to correlations between the background template PDF and the fitted data, only the data in signal region is used in the final fit. For the D^{*+} measurements, the signal region requirement is made in both the mass and the δm distributions.

6.3 Construction of probability density functions

For each one-dimensional mass and δm fit, we assign one PDF per discriminatory species: signal and combinatorial background. In both the mass and δm distributions, the prompt and secondary signal shapes are assumed to be identical, and for the δm fits the combinatorial background is assumed to be indistinguishable from random soft pion backgrounds. The total PDF is constructed as the sum of per-species PDFs, weighted by the respective species' yields

$$f(m) = \sum_{\mathrm{Species}} N_{\mathrm{Species}} \cdot f_{\mathrm{Species}}(m), \tag{6.1}$$

$$f(\delta m) = \sum_{\mathrm{Species}} N_{\mathrm{Species}} \cdot f_{\mathrm{Species}}(\delta m). \tag{6.2}$$

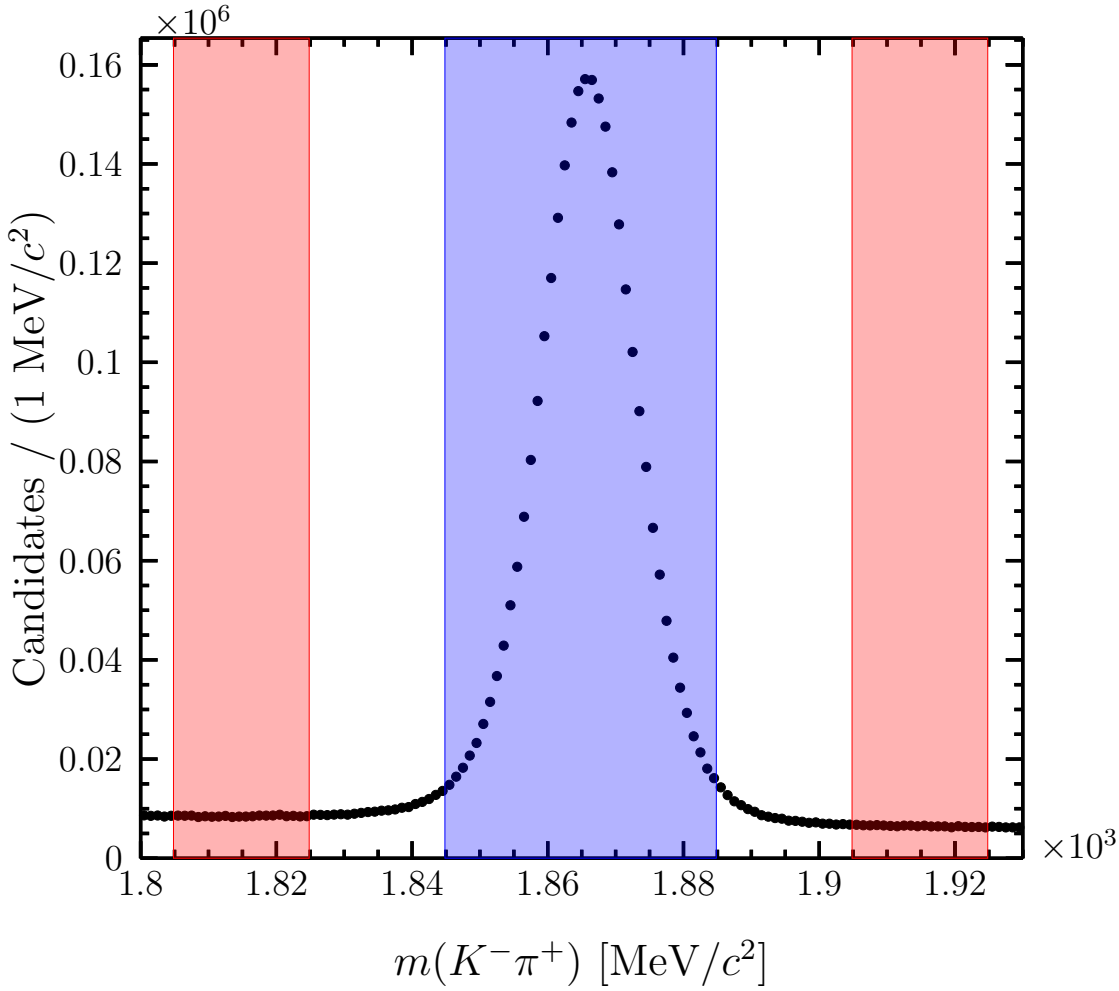

Figure 6.1: Definition of signal window, in blue, and sidebands, in red, for $D^0 \to K^-\pi^+$ candidates. The signal window is $\pm 20\,MeV$ either side of the nominal D^0 mass of 1864.84 MeV [22]. The upper and lower sidebands are each 20 MeV wide, with the lower sideband ending 40 MeV below the nominal D^0 mass and the upper sideband beginning 40 MeV above the nominal D^0 mass. The full dataset is shown.

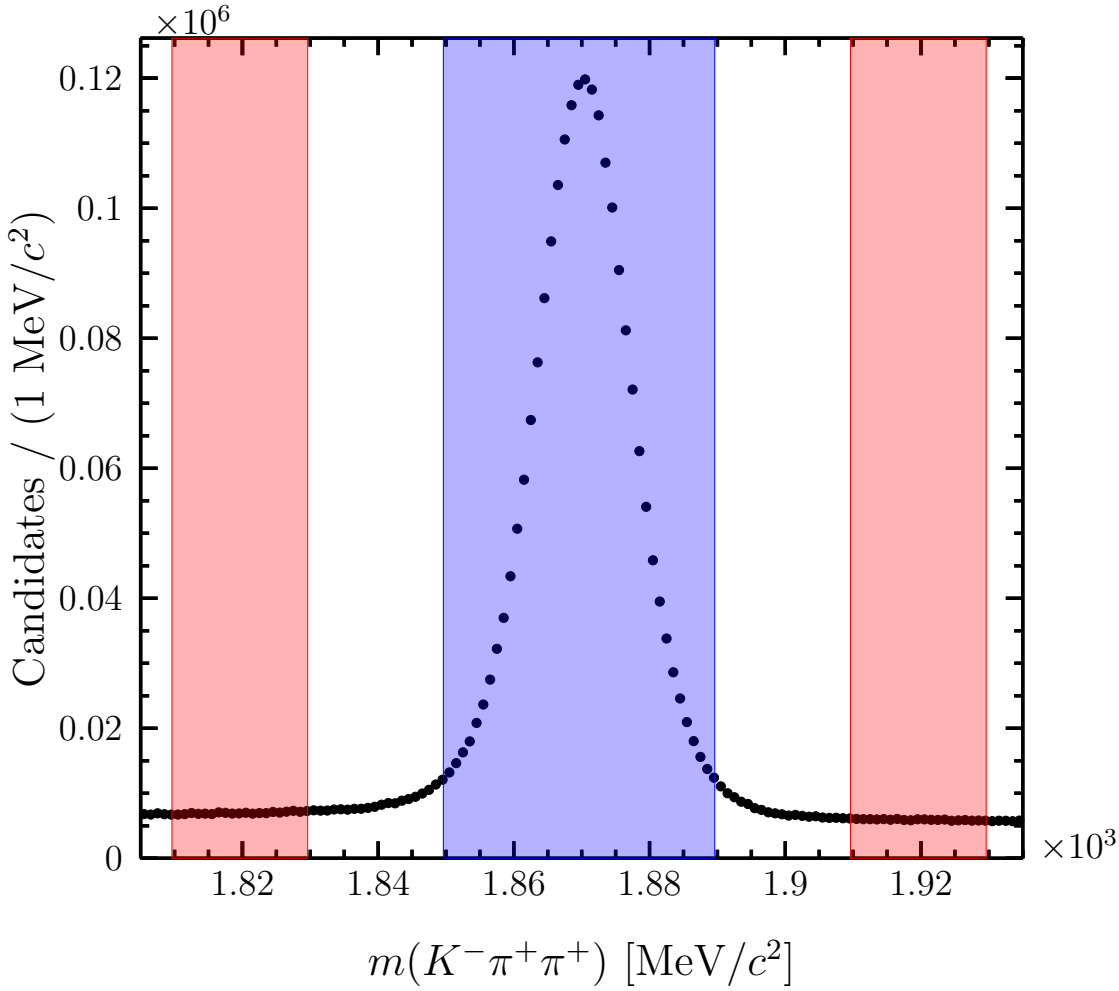

Figure 6.2: Definition of signal window, in blue, and sidebands, in red, for $D^+ \to K^-\pi^+\pi^+$ candidates. The signal window is $\pm 20\,MeV$ either side of the nominal D^+ mass of 1869.61 MeV [22]. The upper and lower sidebands are each 20 MeV wide, with the lower sideband ending 40 MeV below the nominal D^+ mass and the upper sideband beginning 40 MeV above the nominal D^+ mass. The full dataset is shown.

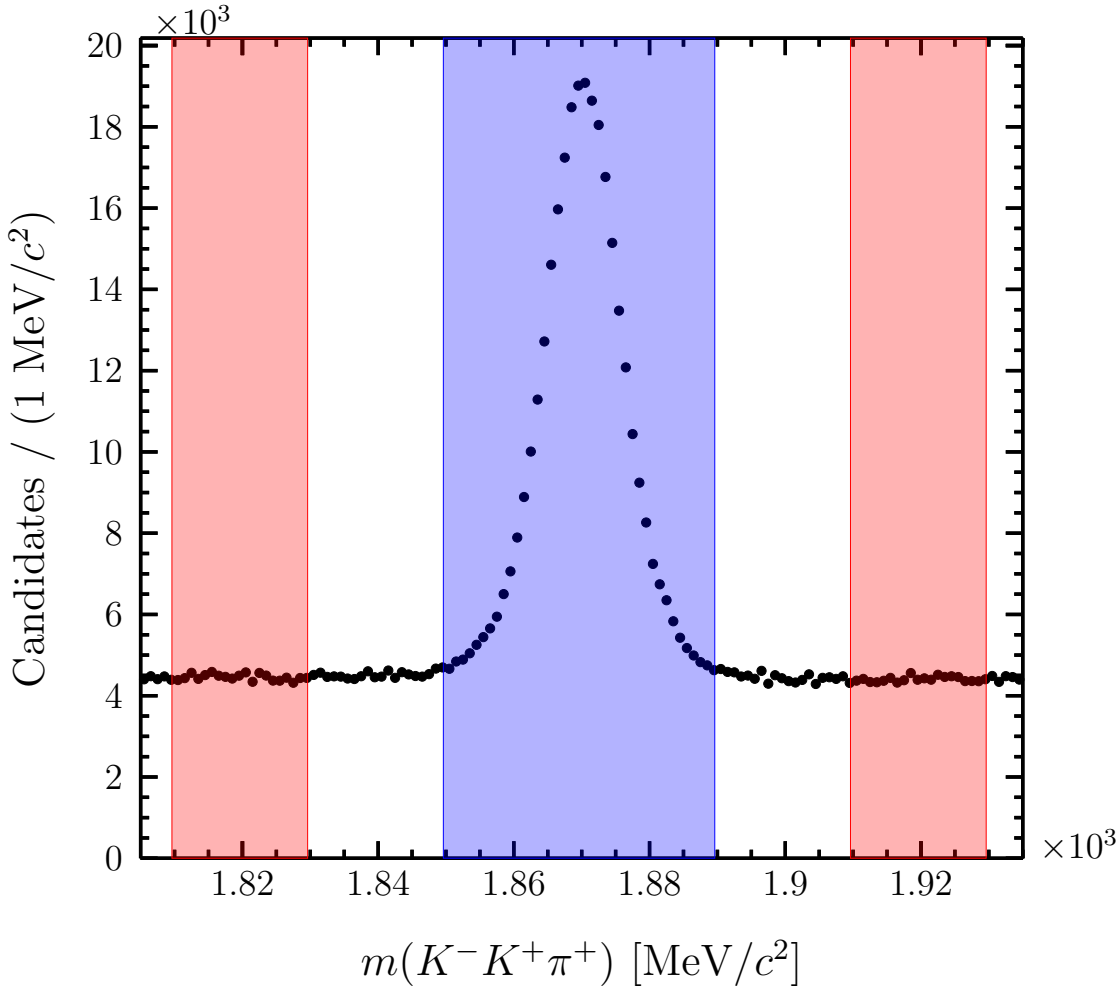

Figure 6.3: Definition of signal window, in blue, and sidebands, in red, for $D^+ \to K^-K^+\pi^+$ candidates. The signal window is $\pm 20\,MeV$ either side of the nominal D^+ mass of 1869.61 MeV [22]. The upper and lower sidebands are each 20 MeV wide, with the lower sideband ending 40 MeV below the nominal D^+ mass and the upper sideband beginning 40 MeV above the nominal D^+ mass. The full dataset is shown.

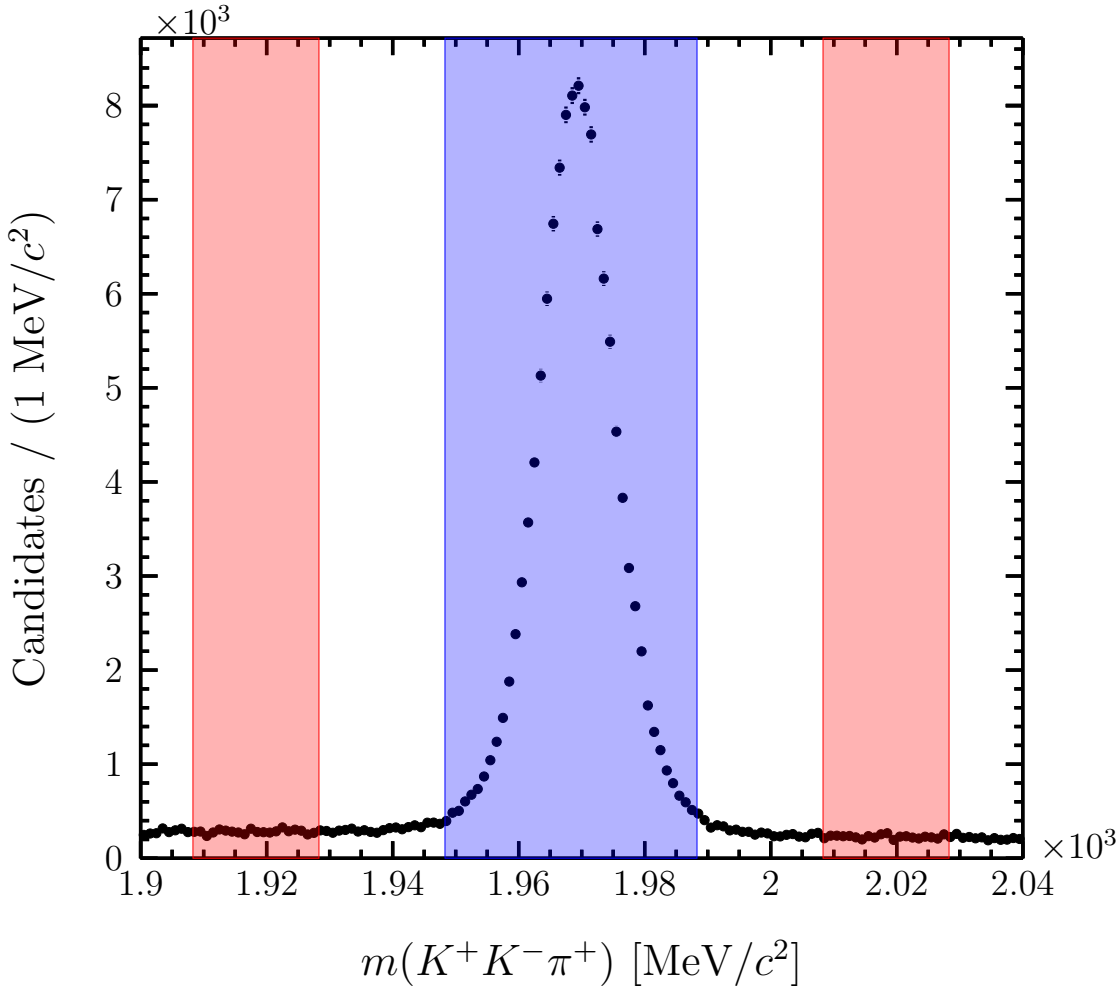

Figure 6.4: Definition of signal window, in blue, and sidebands, in red, for $D_s^+ \to \phi\pi^+$ candidates. The signal window is $\pm 20\,\mathrm{MeV}$ either side of the nominal D_s^+ mass of 1968.30 MeV [22]. The upper and lower sidebands are each 20 MeV wide, with the lower sideband ending 40 MeV below the nominal D_s^+ mass and the upper sideband beginning 40 MeV above the nominal D_s^+ mass. The full dataset is shown.

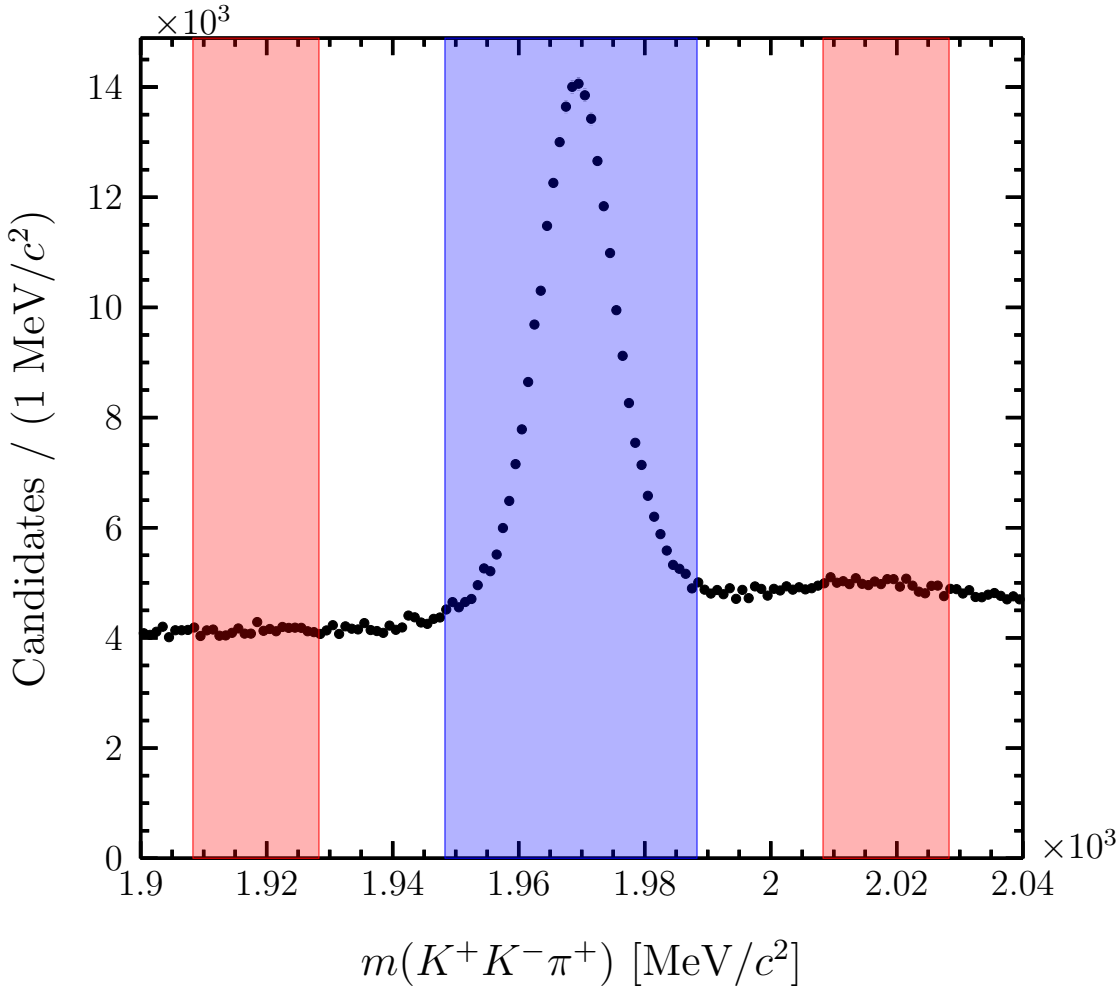

Figure 6.5: Definition of signal window, in blue, and sidebands, in red, for $D_s^+ \to K^-K^+\pi^+$ candidates. The signal window is $\pm 20\,MeV$ either side of the nominal D_s^+ mass of 1968.30 MeV [22]. The upper and lower sidebands are each 20 MeV wide, with the lower sideband ending 40 MeV below the nominal D_s^+ mass and the upper sideband beginning 40 MeV above the nominal D_s^+ mass. The full dataset is shown.

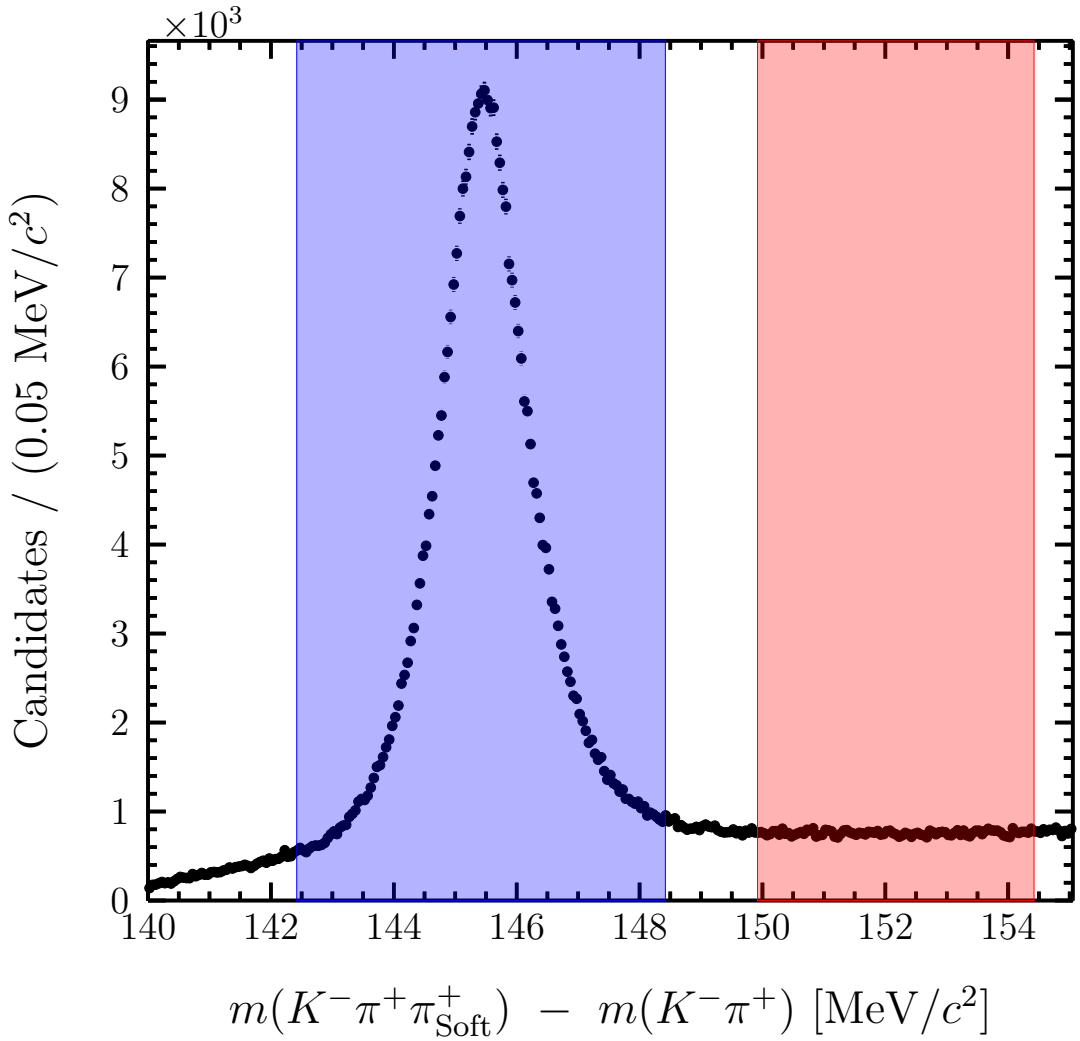

Figure 6.6: Definition of signal window, in blue, and sidebands, in red, for $D^{*+} \to D^0\pi^+$, with $D^0 \to K^-\pi^+$, candidates. The signal window is $\pm 3\,MeV$ either side of the nominal $\delta m = m(D^{*+}) - m(D^0)$ mass of 145.43 MeV [22]. The upper sideband is 4.5 MeV wide, beginning 4.5 MeV above the nominal δm value. The full dataset within the D^0 signal region, defined in Section 6.2 and shown in Figure 6.1, is shown.

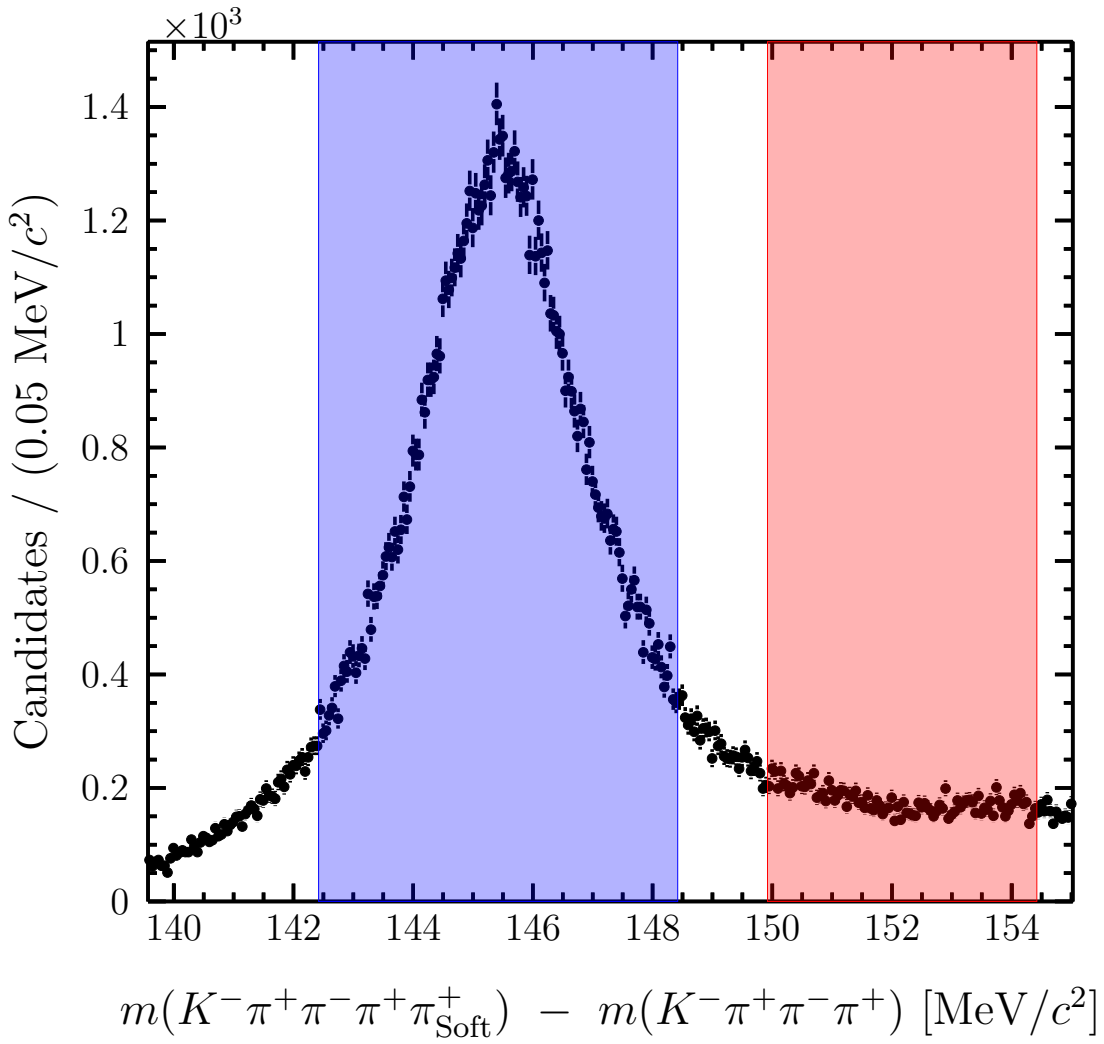

Figure 6.7: Definition of signal window, in blue, and sidebands, in red, for $D^{*+} \to D^0\pi^+$, with $D^0 \to K^-\pi^+\pi^-\pi^+$, candidates. The signal window is $\pm 3\,MeV$ either side of the nominal $\delta m = m(D^{*+}) - m(D^0)$ value of 145.43 MeV [22]. The upper sideband is 4.5 MeV wide, beginning 4.5 MeV above the nominal δm value. The full dataset within the D^0 signal region, defined in Section 6.2, is shown. The full dataset within the D^0 signal region, defined in Section 6.2 and shown in Figure 6.1, is shown.

For every mass fit, the background PDF is taken to be a first-order polynomial, and the signal PDF is mode-dependent, given in Section 6.4.

The joint combinatorial and random soft pion background in the δm fits is an empirical function of the form

$$f_{\mathrm{DST}}(x; \delta m_0, A, B) = e^{B \cdot \delta m} \cdot (x - \delta m_0)^A, \tag{6.3}$$

where δm_0 is a threshold value fixed to the charged pion rest mass $m_{\pi^\pm} = 139.57\,\mathrm{MeV}$ [22] and the parameter B is fixed to zero. The signal PDF is mode-dependent, given in Section 6.4.

For each one-dimensional $\ln \chi^2_{\mathrm{IP}}$ fit, we assign one PDF per discriminatory species: prompt signal, secondary signal, and combinatorial background. The total PDFs are constructed as the sum of per-species PDFs, weighted by the respective species' yields

$$f(\ln \chi^2_{\mathrm{IP}}) = \sum_{\mathrm{Species}} N_{\mathrm{Species}} \cdot f_{\mathrm{Species}}(\ln \chi^2_{\mathrm{IP}}). \tag{6.4}$$

The constraint on the background yield, discussed in Section 6.2, is applied by multiplying $f(\ln \chi^2_{\mathrm{IP}})$ by a Gaussian function whose mean is the number of background candidates N measured by the mass fit and whose width is the uncertainty on N returned by the fitter.

One such PDF, $f(\ln \chi^2_{\mathrm{IP}})$, and background constraint is constructed per p_{T}-y bin, and the likelihood is formed as the product of these such that each PDF is fitted simultaneously when the negative log-likelihood is minimised. The benefit of this construction is that some shape parameters can be shared across bins, reducing the uncertainty on the fit parameters. Which parameters are shared across bins and which are fitted independently is mode-dependent, given in Section 6.4.

We choose to model the prompt signal $\ln \chi^2_{\mathrm{IP}}$ distribution with a modified Gaussian distribution f_{AGE}, where the width is allowed to be asymmetric with respect to the mean and the tails are described by exponential functions

$$f_{\mathrm{AGE}}(x; \mu, \sigma, \epsilon, \rho_{\mathrm{L}}, \rho_{\mathrm{R}}) = \begin{cases} e^{\frac{\rho_{\mathrm{L}}^2}{2} + \rho_{\mathrm{L}} \cdot \frac{x-\mu}{(1-\epsilon)\cdot\sigma}} & x < \mu - (\rho_{\mathrm{L}} \cdot \sigma \cdot (1-\epsilon)), \\ e^{-\left(\frac{x-\mu}{\sqrt{2}\cdot\sigma\cdot(1-\epsilon)}\right)^2} & \mu - (\rho_{\mathrm{L}} \cdot \sigma \cdot (1-\epsilon)) \leq x < \mu, \\ e^{-\left(\frac{x-\mu}{\sqrt{2}\cdot\sigma\cdot(1+\epsilon)}\right)^2} & \mu \leq x < \mu + (\rho_{\mathrm{R}} \cdot \sigma \cdot (1+\epsilon)), \\ e^{\frac{\rho_{\mathrm{R}}^2}{2} - \rho_{\mathrm{R}} \cdot \frac{x-\mu}{(1+\epsilon)\cdot\sigma}} & x \geq \mu + (\rho_{\mathrm{R}} \cdot \sigma \cdot (1+\epsilon)). \end{cases} \tag{6.5}$$

The parameter where μ is the mode of the distribution, σ is the average of the left and right Gaussian widths, ϵ is the asymmetry of the left and right Gaussian widths,

and $\rho_{L(R)}$ is the exponent for the left (right) tail. The secondary signal distribution is modelled by a Gaussian distribution f_{SGS} with mean μ and width σ

$$f_{\mathrm{SGS}}(x;\mu,\sigma) = e^{-\frac{(x-\mu)^2}{2\sigma^2}}. \tag{6.6}$$

These shapes are motivated by the $\ln\chi^2_{\mathrm{IP}}$ distributions for prompt and secondary signal decays observed in the MC samples.

Given the large number of parameters to be fitted, some shape parameters are fixed to values obtained from 'prefits' to samples of prompt and secondary signal MC. The set of parameters that are fixed is mode-dependent, given in Section 6.4.

6.4 Mode-specific details

As different modes exhibit different features in the mass, δm, and $\ln\chi^2_{\mathrm{IP}}$ distributions, several aspects of the respective fits are different between modes. This sections gives the list of parameters that are split between p_{T}-y bins, and the list of parameters that are allowed to float after the prefit to MC data, for each mode.

Fit details for D^0

For the $D^0 \to K^-\pi^+$ mode, the signal shape in the mass fit is the sum of a Gaussian and a Crystal Ball function, sharing a common mean but allowed to have different widths. The mean and width of the signal mass PDF are split across p_{T}-y bins, as is the slope of the background mass PDF. The mean of the $\ln\chi^2_{\mathrm{IP}}$ prompt signal PDF and the width of the secondary signal PDF are also split across p_{T}-y bins. The mean and width of the prompt signal $\ln\chi^2_{\mathrm{IP}}$ PDF and all parameters of the secondary signal $\ln\chi^2_{\mathrm{IP}}$ PDF are floated in the fit, and all other $\ln\chi^2_{\mathrm{IP}}$ shape parameters fixed to the values from MC.

Prefits to the prompt signal and secondary signal data samples in $\ln\chi^2_{\mathrm{IP}}$ are given in Figure 6.8 for the $D^0 \to K^-\pi^+$ mode.

Fit details for D^+

For the $D^+ \to K^-\pi^+\pi^+$ mode, the signal shape in the mass fit is the sum of a Gaussian and a Crystal Ball function, sharing a common mean but allowed to have different widths. The mean of the signal mass PDF as well as the width of the Crystal Ball component in the mass PDF are split across p_{T}-y bins, as is the slope of the background mass PDF. The mean of the $\ln\chi^2_{\mathrm{IP}}$ prompt signal and secondary signal distributions are split across p_{T}-y bins. The mean and tail parameters of the signal

$\ln \chi^2_{\mathrm{IP}}$ PDF, are floated during the final fit, with all other shape parameters fixed to the values from MC.

For the $D^+ \to K^-K^+\pi^+$ mode, the signal shape in the mass fit is a Double Gaussian: the sum of two Gaussian functions sharing a common mean but allowed to have different widths. The width of the Crystal Ball component in the mass PDF and the slope of the background mass PDF are split across p_{T}-y bins. The mean of the $\ln \chi^2_{\mathrm{IP}}$ prompt signal and secondary signal distributions are split across p_{T}-y bins. The mean and tail parameters of the signal $\ln \chi^2_{\mathrm{IP}}$ PDF, are floated during the final fit, with all other shape parameters fixed to the values from MC.

Prefits to the prompt signal and secondary signal data samples in $\ln \chi^2_{\mathrm{IP}}$ are given in Figure 6.9 for the $D^+ \to K^-\pi^+\pi^+$ mode, and in Figure 6.10 for the $D^+ \to K^-K^+\pi^+$ mode.

Fit details for D_s^+

For the $D_s^+ \to \phi\pi^+$ and $D_s^+ \to K^-K^+\pi^+$ modes, the mean of the $\ln \chi^2_{\mathrm{IP}}$ prompt signal and secondary signal distributions are split across p_{T}-y bins. The mean and left tail parameter of the signal $\ln \chi^2_{\mathrm{IP}}$ PDF and all parameters of the secondary PDF are floated during the final fit, with all other shape parameters fixed to the values from MC.

Prefits to the prompt signal and secondary signal data samples in $\ln \chi^2_{\mathrm{IP}}$ are given in Figure 6.11 for the $D_s^+ \to \phi\pi^+$ mode, and in Figure 6.12 for the $D_s^+ \to K^-K^+\pi^+$ mode.

Fit details for D^{*+}

For the D^{*+}-tagged $D^0 \to K^-\pi^+$ and $D^0 \to K^-\pi^+\pi^-\pi^+$ modes, the mean of the $\ln \chi^2_{\mathrm{IP}}$ prompt signal and secondary signal distributions are split across p_{T}-y bins. The mean and tail parameters of the signal $\ln \chi^2_{\mathrm{IP}}$ PDF, are floated during the final fit, with all other shape parameters fixed to the values from MC.

Prefits to the prompt signal and secondary signal data samples in D^0 $\ln \chi^2_{\mathrm{IP}}$ are given in Figure 6.13 for the $D^0 \to K^-\pi^+$ mode, and in Figure 6.14 for the $D^0 \to K^-\pi^+\pi^-\pi^+$ mode.

6.5 Fit results

For each fit, the covariance matrix is checked to be positive definite, and the goodness-of-fit within each p_{T}-y bin is checked visually to ensure that the negative log-likelihood

converge to a sensible minimum. Integrated mass, δm, and $\ln \chi^2_{\mathrm{IP}}$ fits are given in Figures 6.15–6.30. Prompt signal yields per p_{T}-y bin are given in Tables 6.1–6.7

The $\ln \chi^2_{\mathrm{IP}}$ fits in each p_{T}-y have been omitted from this section for brevity, but are given in Appendix F.

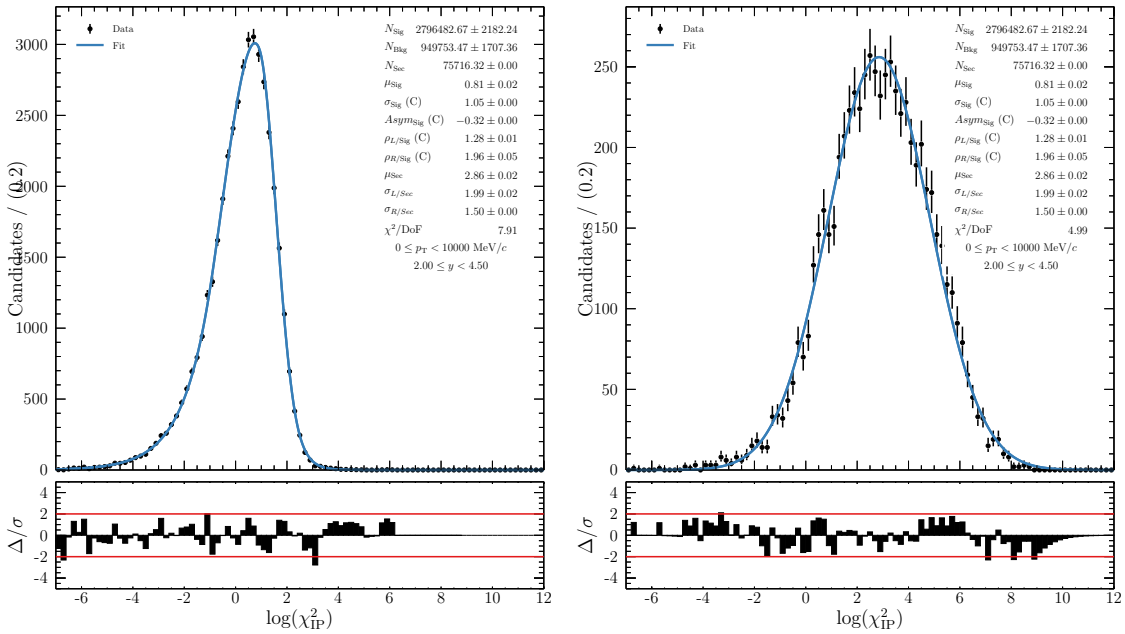

(a) Prompt signal *(b) Secondary signal*

Figure 6.8: Integrated $\ln \chi^2_{\mathrm{IP}}$ *prefits for* $D^0 \to K^-\pi^+$ *in the prompt signal and secondary signal sample. The data and fit curves shown are the sum of the individual* p_{T}*-*y *bin contributions.*

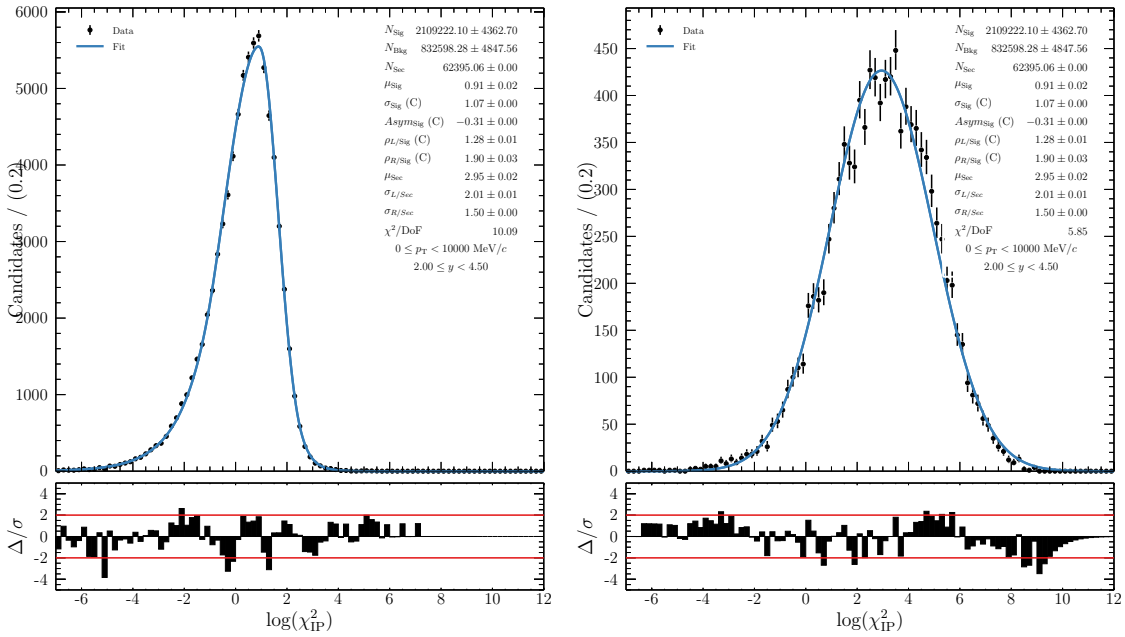

(a) Prompt signal *(b) Secondary signal*

Figure 6.9: Integrated $\ln \chi^2_{\mathrm{IP}}$ *prefits for* $D^+ \to K^-\pi^+\pi^+$ *in the prompt signal and secondary signal sample. The data and fit curves shown are the sum of the individual* p_{T}*-*y *bin contributions.*

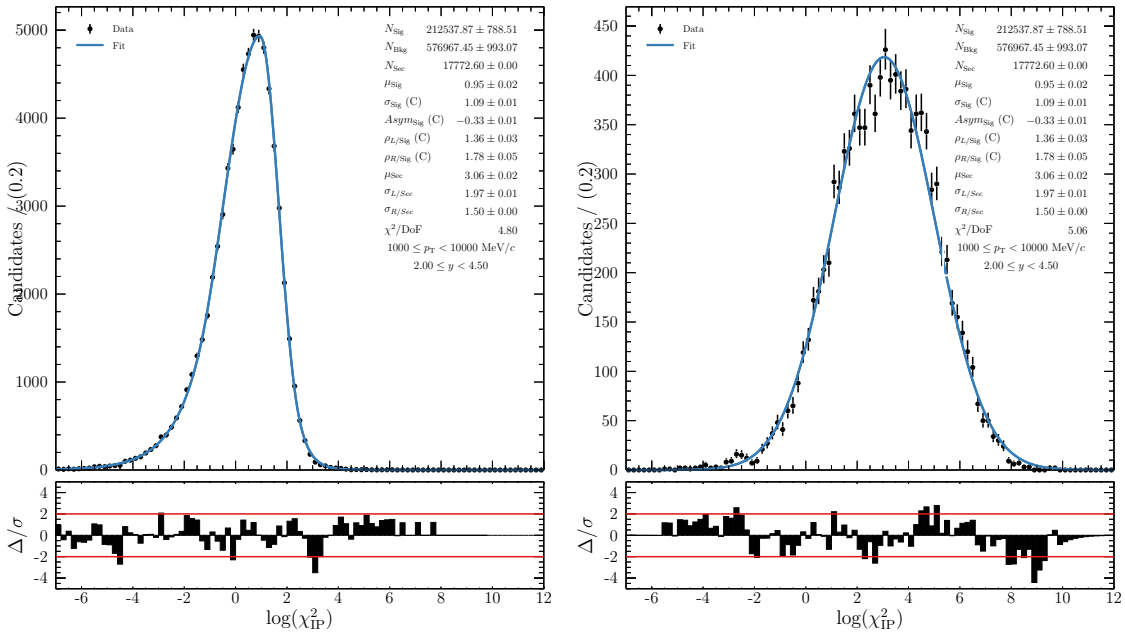

(a) Prompt signal *(b) Secondary signal*

Figure 6.10: Integrated $\ln \chi^2_{\mathrm{IP}}$ *prefits for* $D^+ \to K^- K^+ \pi^+$ *in the prompt signal and secondary signal sample. The data and fit curves shown are the sum of the individual* p_{T}*-*y *bin contributions.*

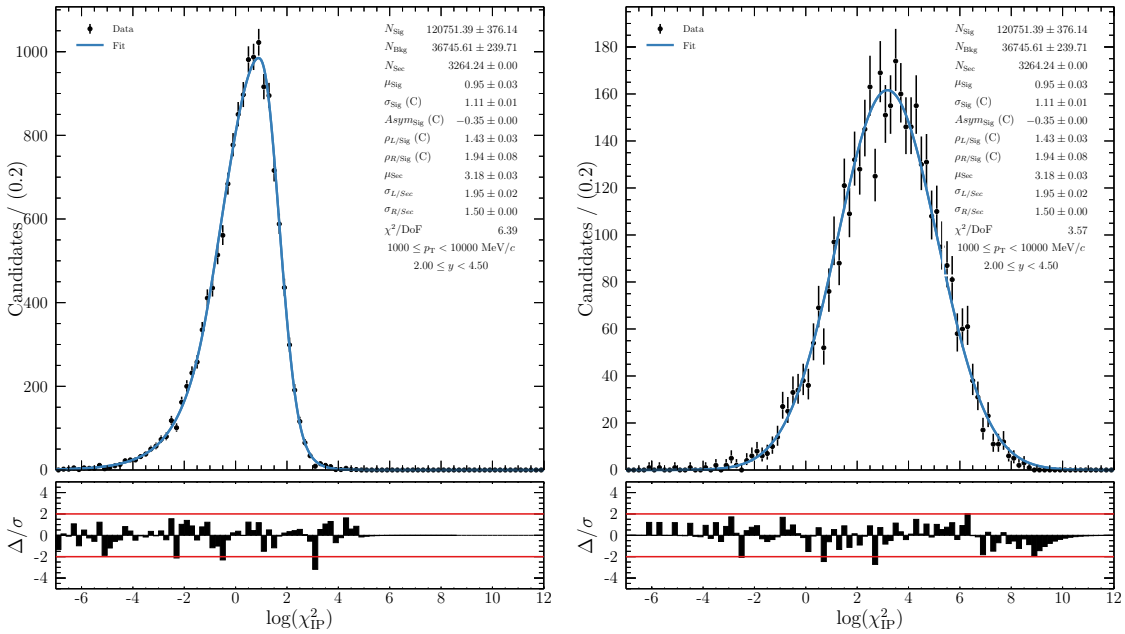

(a) Prompt signal *(b) Secondary signal*

Figure 6.11: Integrated $\ln \chi^2_{\mathrm{IP}}$ *prefits for* $D^+ \to \phi\pi^+$ *in the prompt signal and secondary signal sample. The data and fit curves shown are the sum of the individual* p_{T}*-*y *bin contributions.*

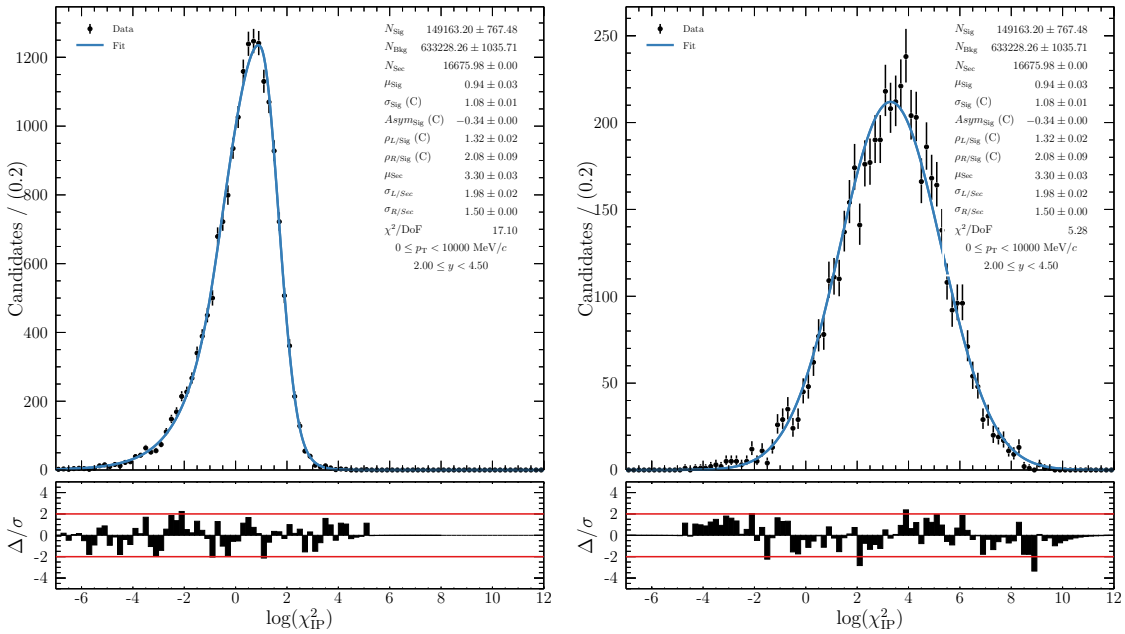

(a) Prompt signal *(b) Secondary signal*

Figure 6.12: Integrated $\ln \chi^2_{\mathrm{IP}}$ *prefits for* $D_s^+ \to K^- K^+ \pi^+$ *in the prompt signal and secondary signal sample. The data and fit curves shown are the sum of the individual* p_{T}*-*y *bin contributions.*

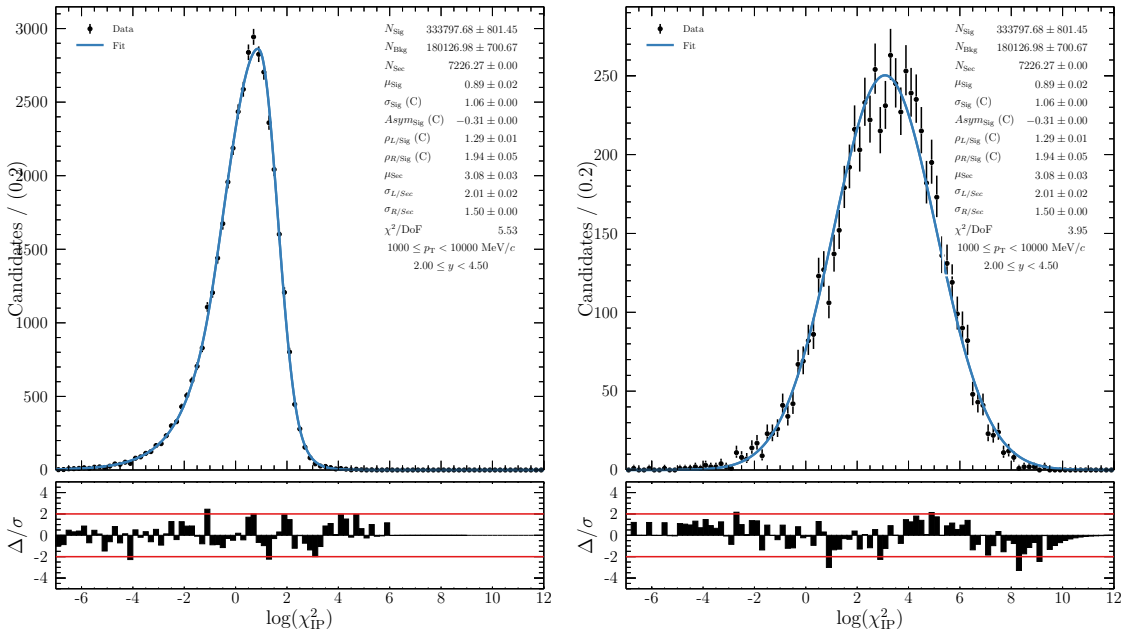

(a) Prompt signal *(b) Secondary signal*

Figure 6.13: Integrated $\ln \chi^2_{\mathrm{IP}}$ *prefits for* $D^{*+} \to D^0\pi^+$*, with* $D^0 \to K^-\pi^+$*, in the prompt signal and secondary signal sample. The data and fit curves shown are the sum of the individual* p_{T}*-*y *bin contributions.*

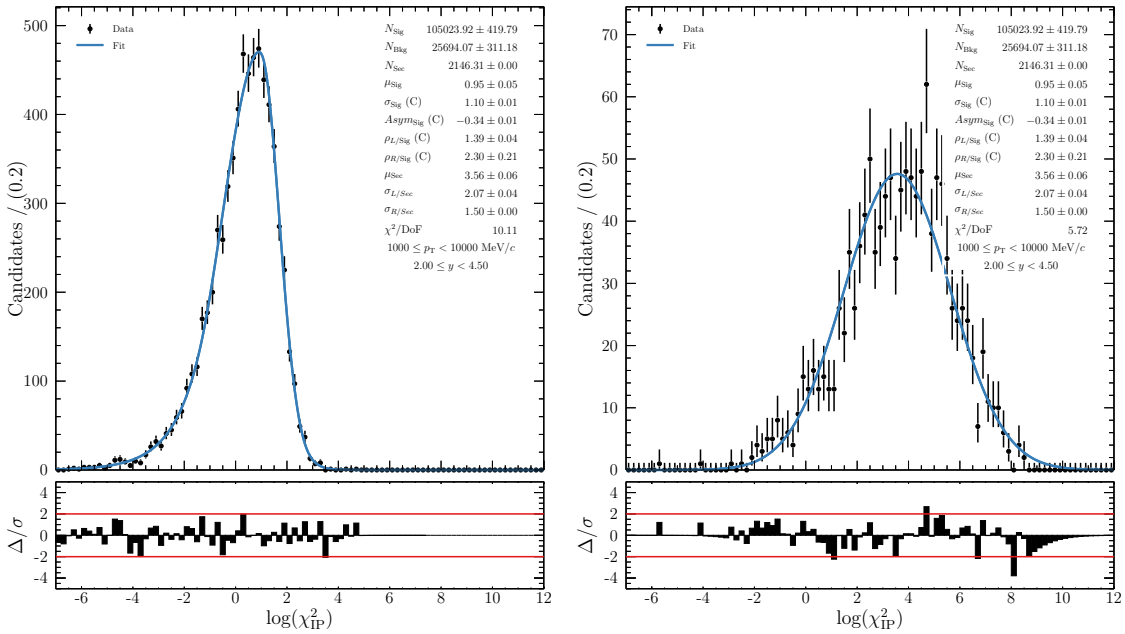

(a) Prompt signal *(b) Secondary signal*

Figure 6.14: Integrated $\ln \chi^2_{\mathrm{IP}}$ *prefits for* $D^{*+} \to D^0\pi^+$*, with* $D^0 \to K^-\pi^+\pi^-\pi^+$*, in the prompt signal and secondary signal sample. The data and fit curves shown are the sum of the individual* p_{T}*-*y *bin contributions.*

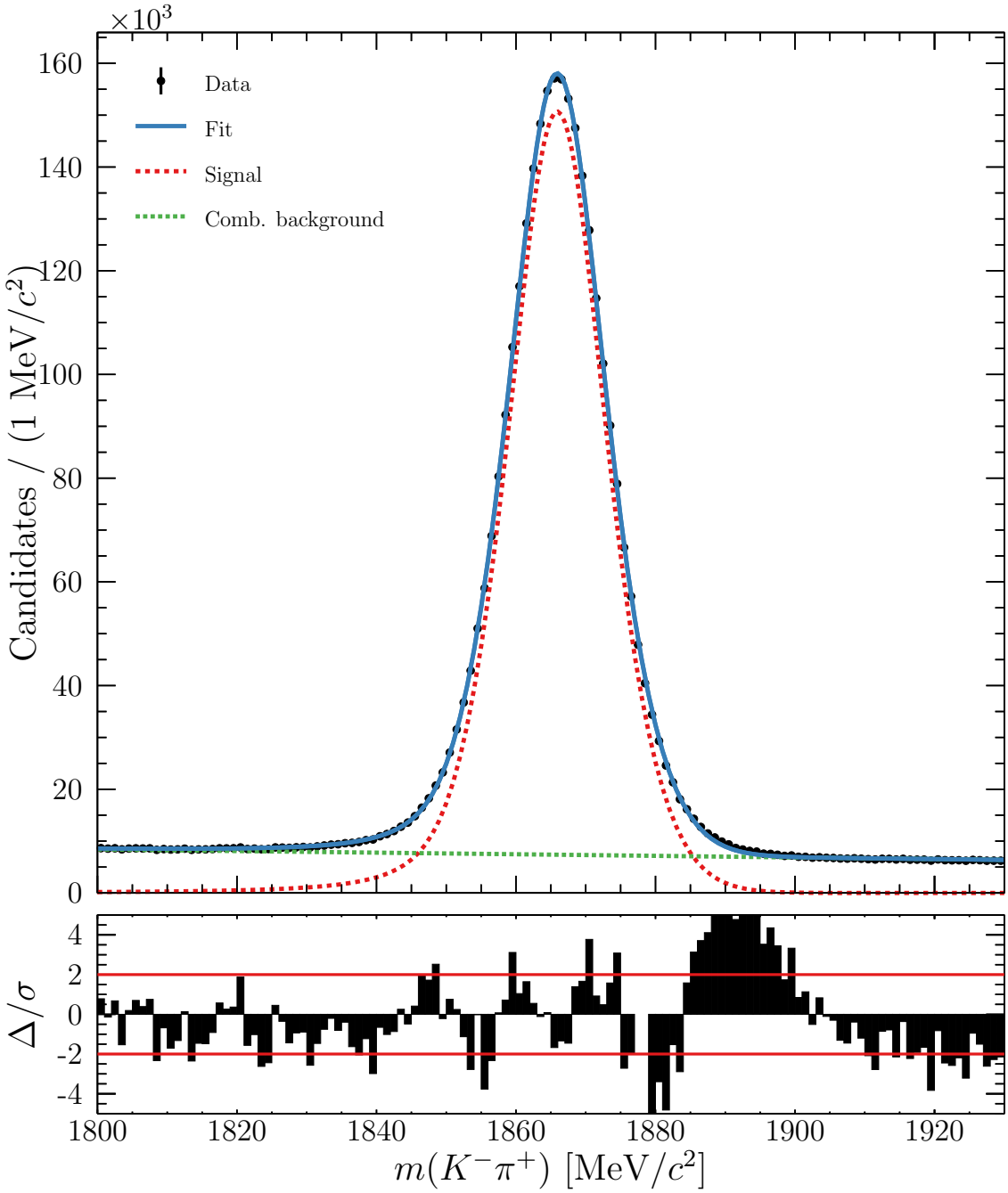

Figure 6.15: Integrated mass fit result for $D^0 \to K^-\pi^+$. The data and curve shown are the sum across all p_{T}-y bins. Per-bin fits are given in Appendix F.1.

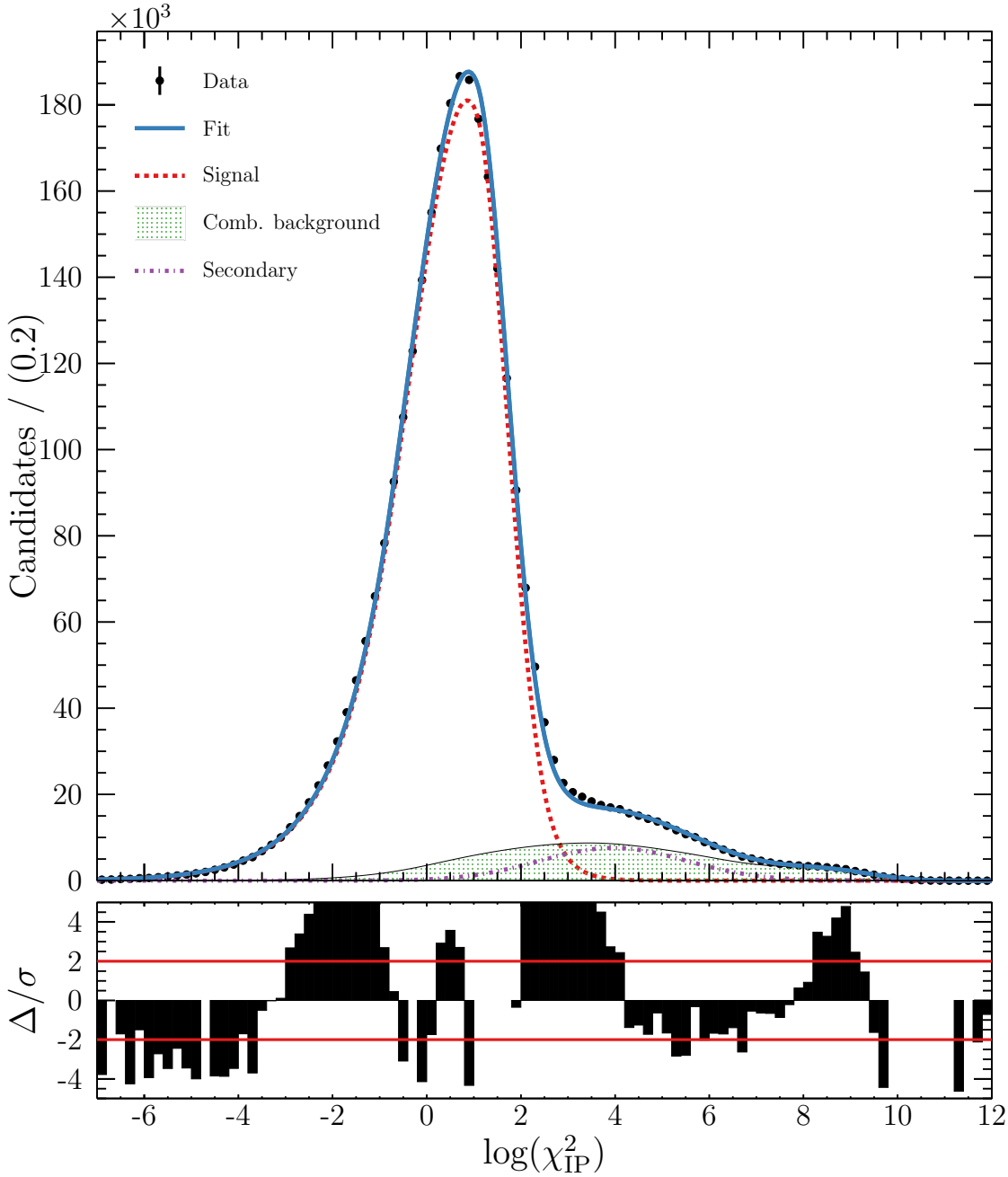

Figure 6.16: Integrated $\ln \chi^2_{\mathrm{IP}}$ *fit result for* $D^0 \to K^-\pi^+$*. The data and curve shown are the sum across all* p_{T}*-*y *bins. Per-bin fits are given in Appendix F.1.*

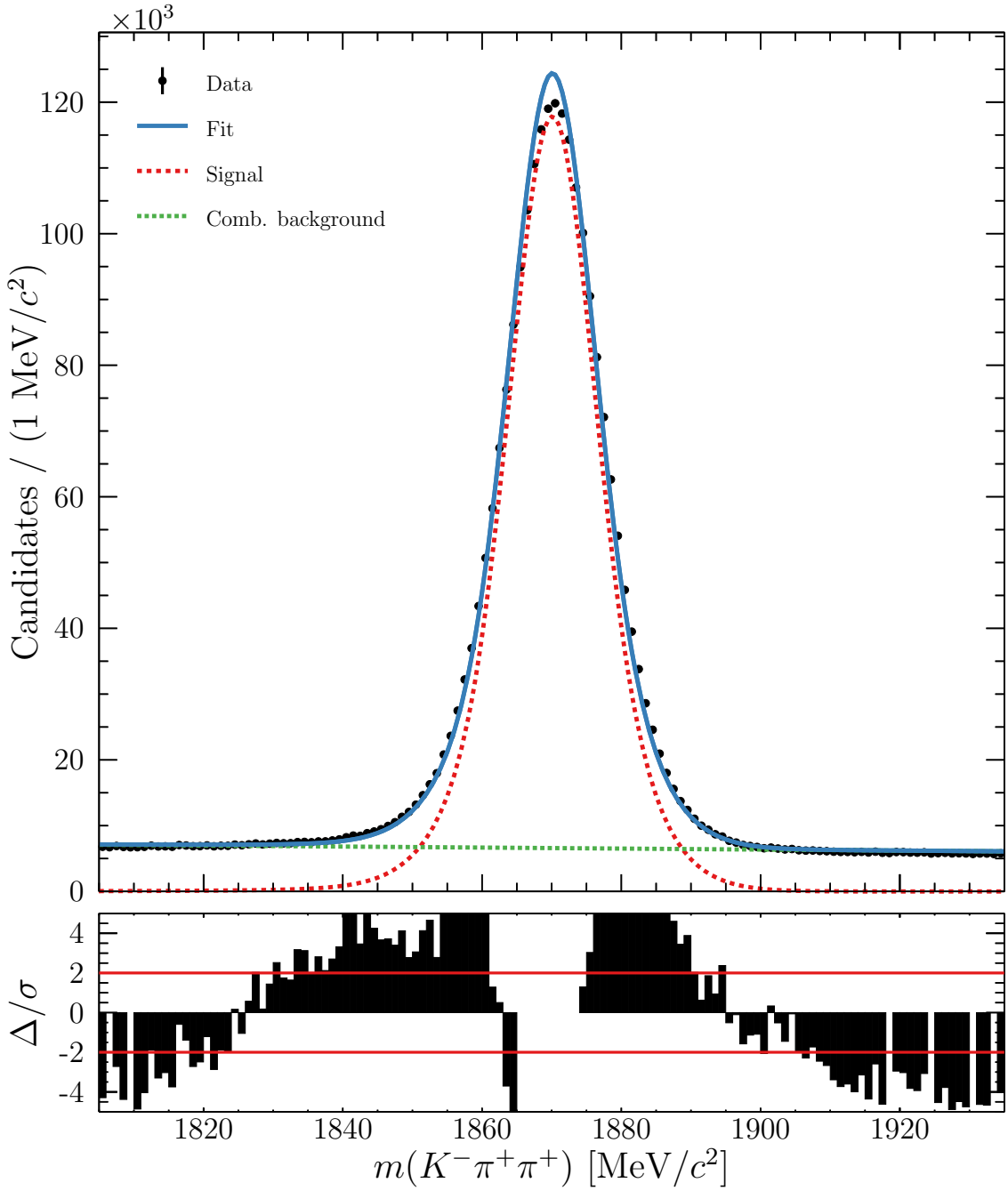

Figure 6.17: Integrated mass fit result for $D^+ \to K^-\pi^+\pi^+$. The data and curve shown are the sum across all p_{T}-y bins. Per-bin fits are given in Appendix F.2.

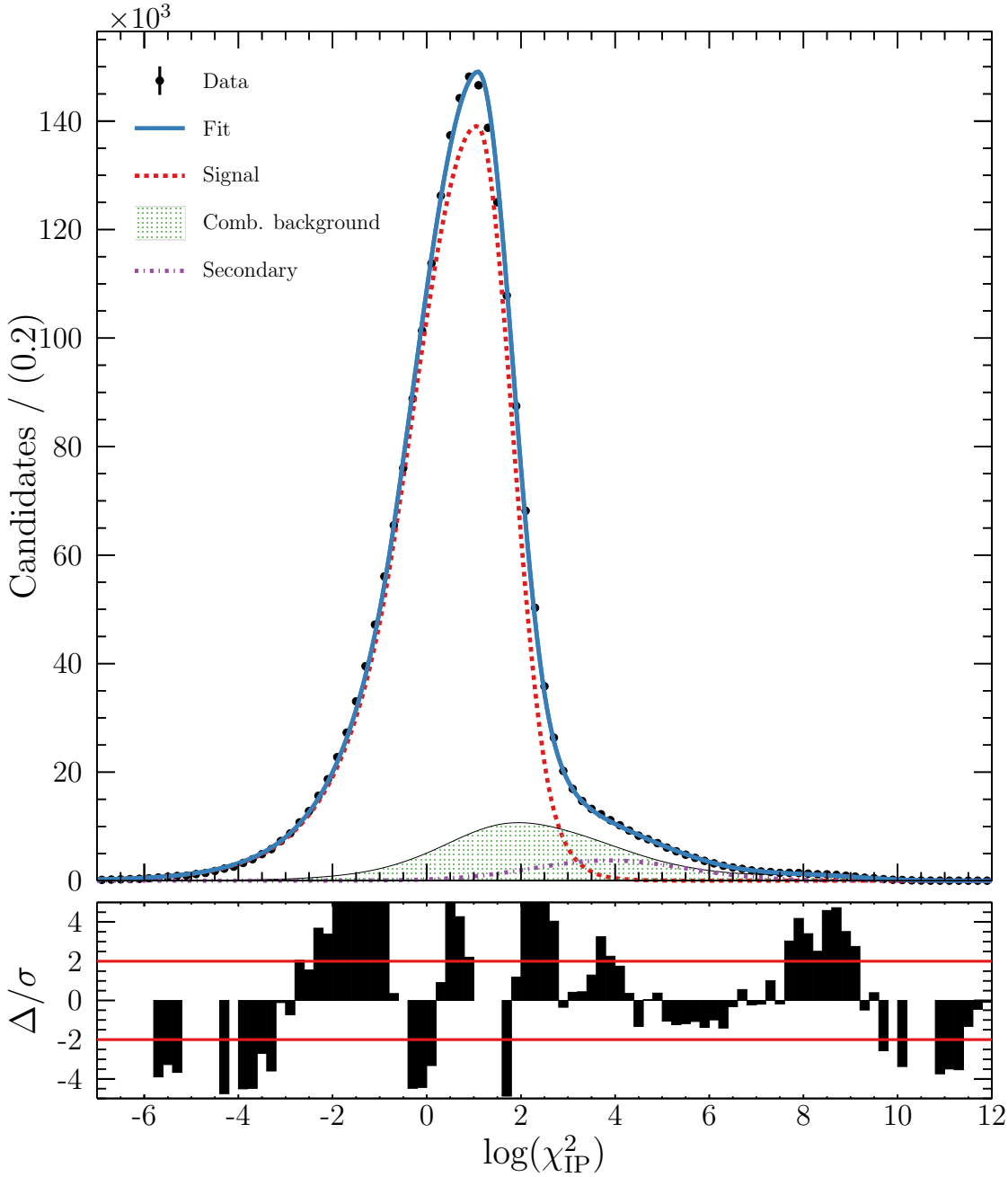

Figure 6.18: Integrated $\ln \chi^2_{\mathrm{IP}}$ *fit result for* $D^+ \to K^-\pi^+\pi^+$*. The data and curve shown are the sum across all* p_{T}*-*y *bins. Per-bin fits are given in Appendix F.2.*

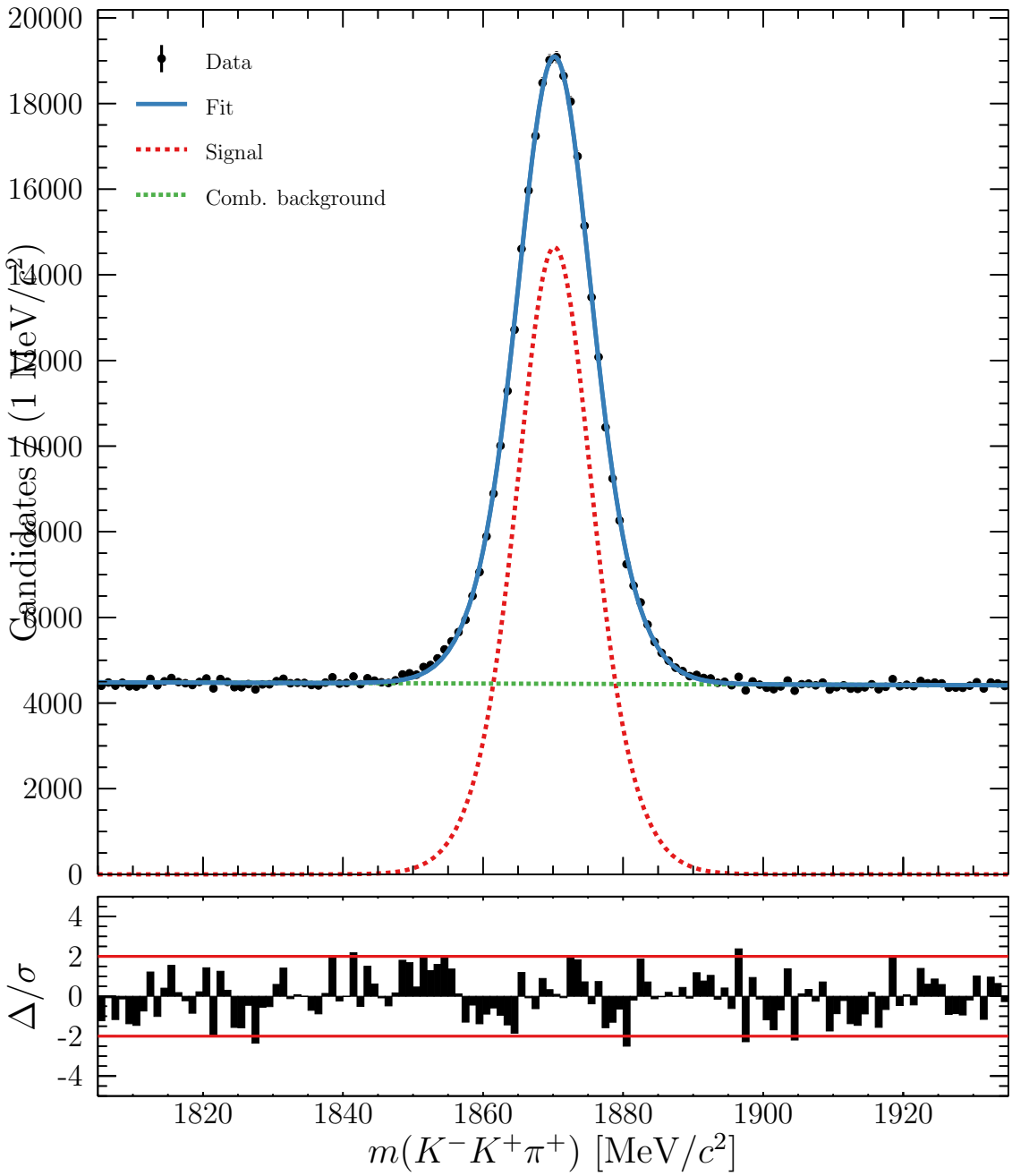

Figure 6.19: Integrated mass fit result for $D^+ \to K^-K^+\pi^+$. The data and curve shown are the sum across all p_T-y bins. Per-bin fits are given in Appendix F.3.

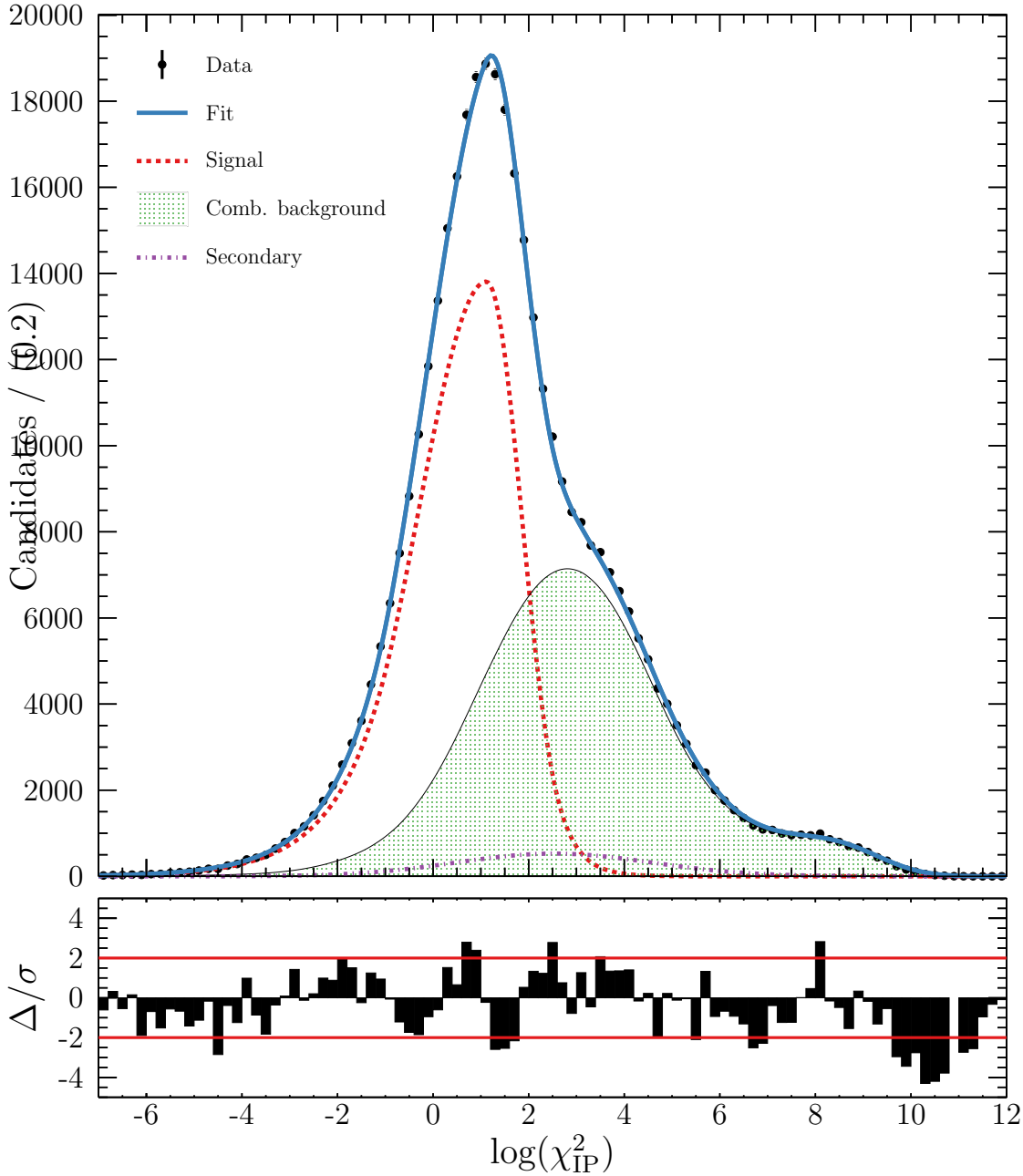

Figure 6.20: Integrated $\ln \chi^2_{\mathrm{IP}}$ *fit result for* $D^+ \to K^- K^+ \pi^+$*. The data and curve shown are the sum across all* p_{T}*-*y *bins. Per-bin fits are given in Appendix F.3.*

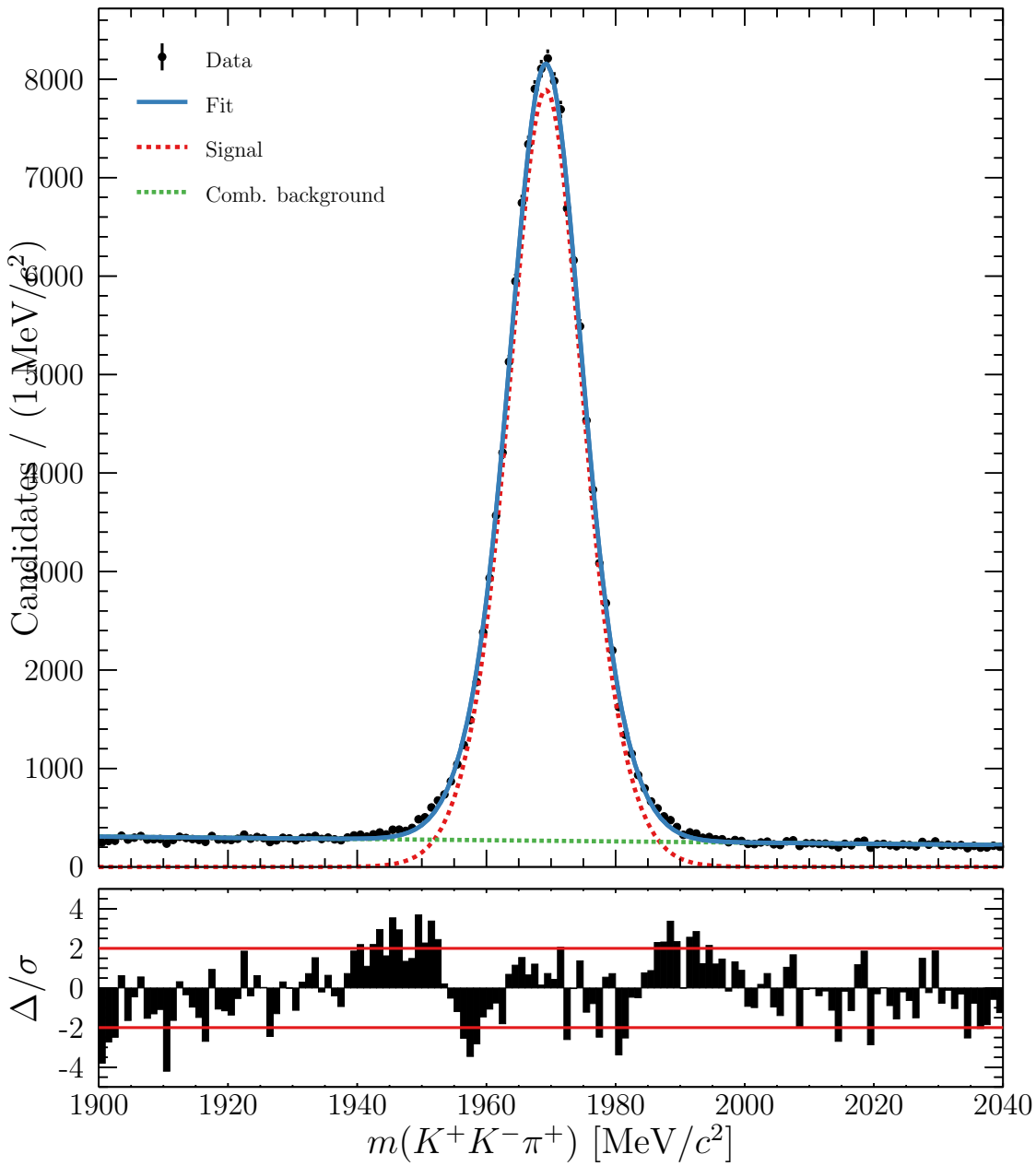

Figure 6.21: Integrated mass fit result for $D_s^+ \to \phi\pi^+$. The data and curve shown are the sum across all p_{T}-y bins. Per-bin fits are given in Appendix F.4.

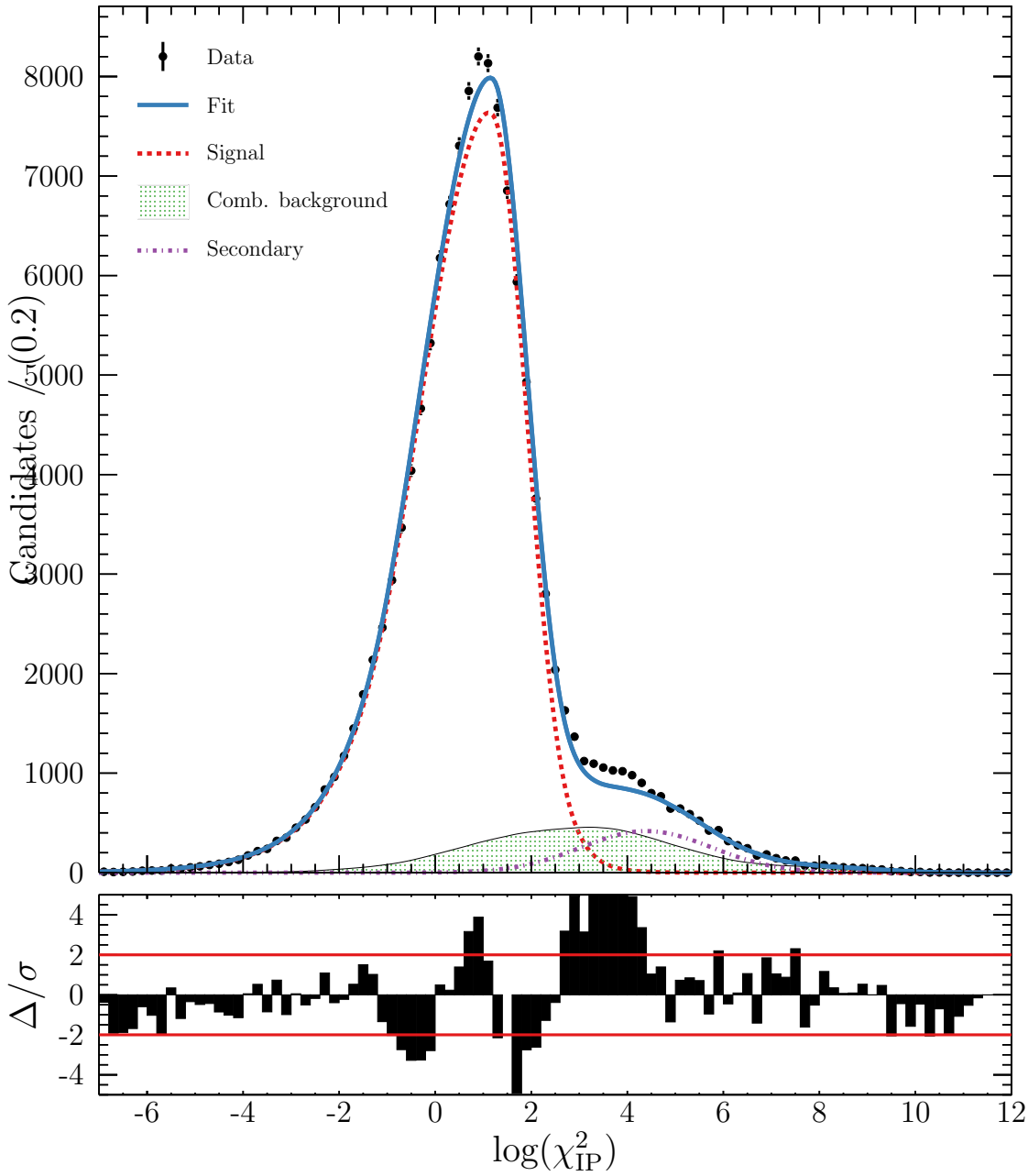

Figure 6.22: Integrated $\ln \chi^2_{\mathrm{IP}}$ *fit result for* $D_s^+ \to \phi\pi^+$*. The data and curve shown are the sum across all* p_{T}*-*y *bins. Per-bin fits are given in Appendix F.4.*

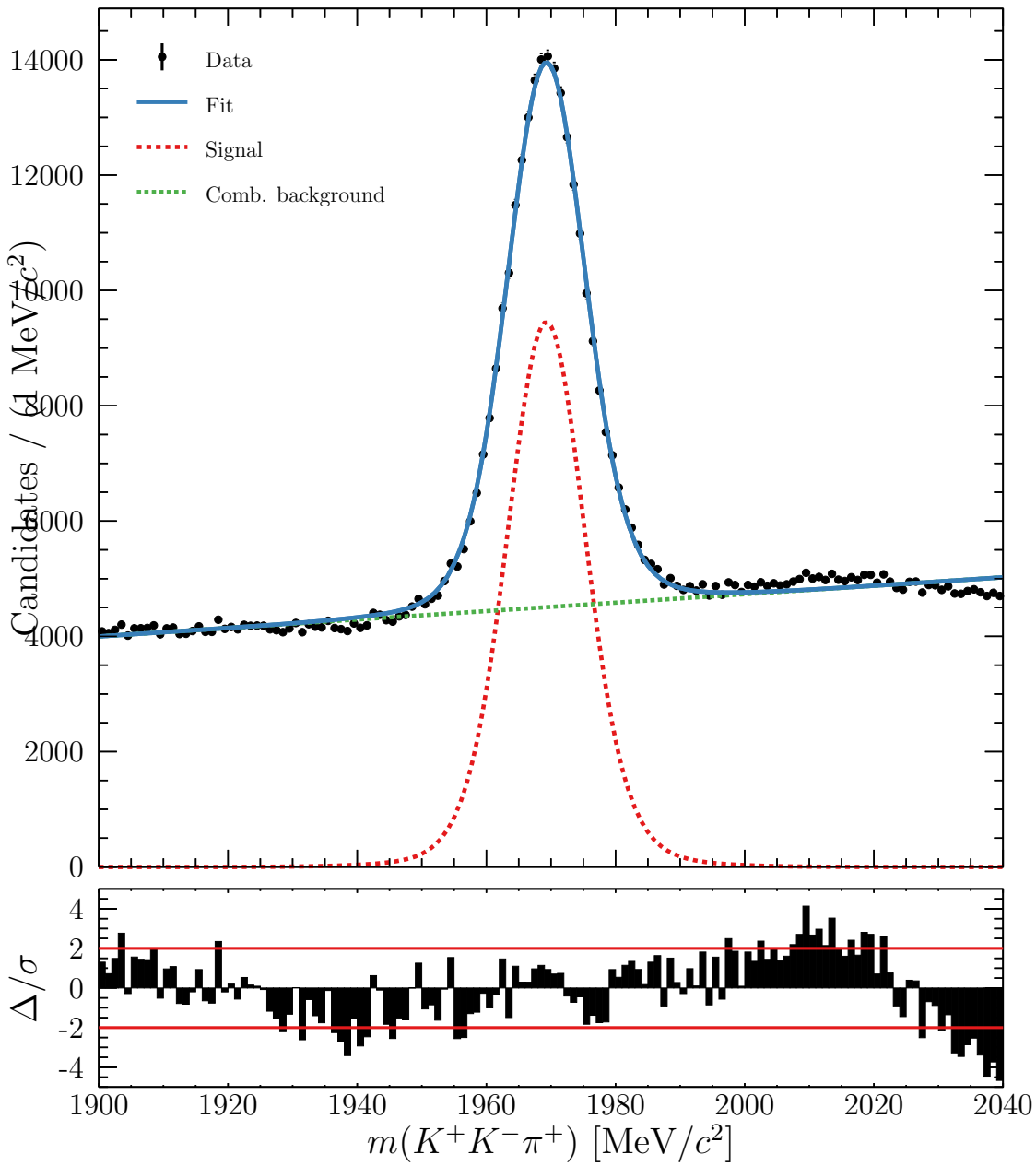

Figure 6.23: Integrated mass fit result for $D_s^+ \to K^-K^+\pi^+$. The data and curve shown are the sum across all p_T-y bins. Per-bin fits are given in Appendix F.5.

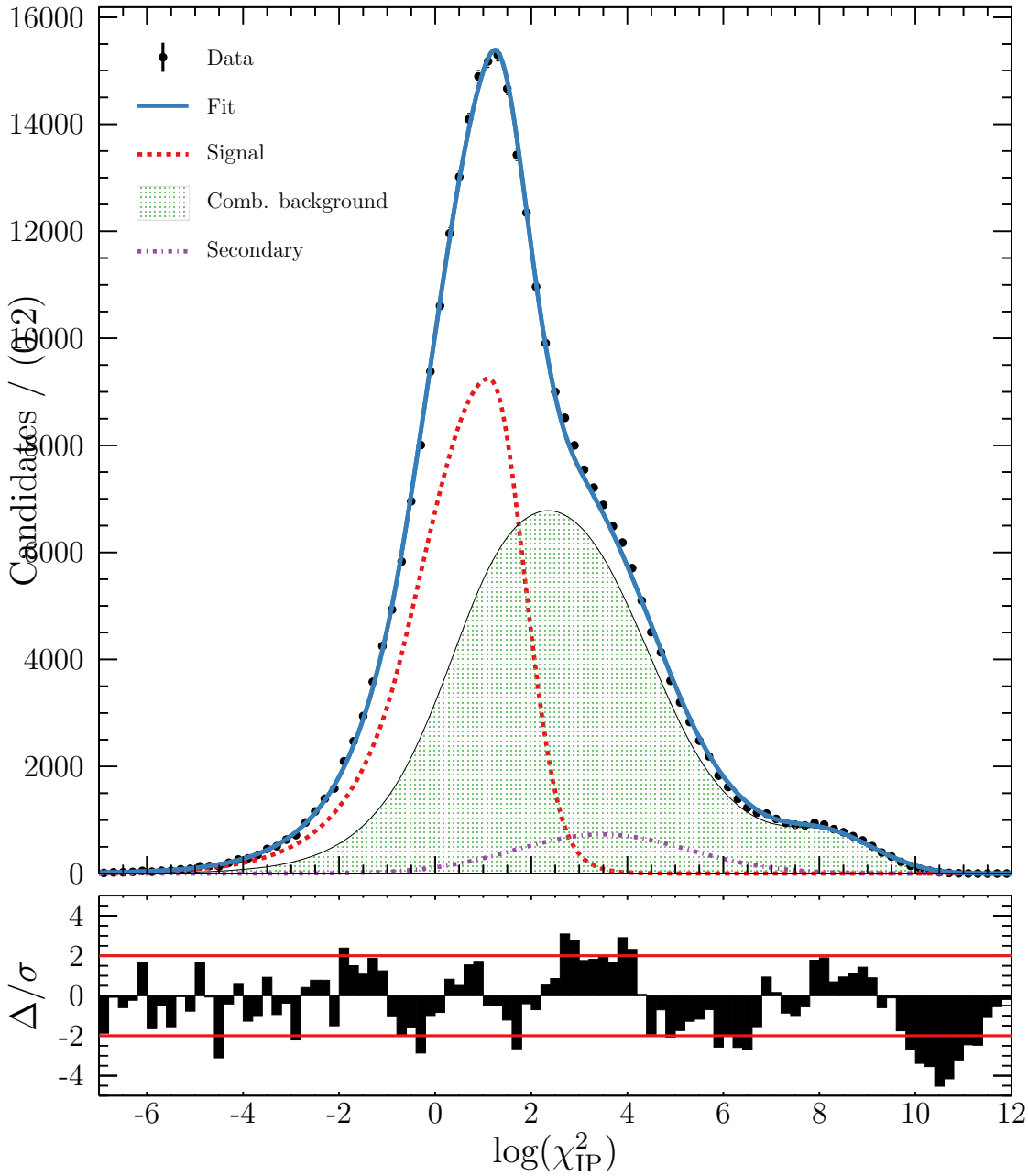

Figure 6.24: Integrated $\ln \chi^2_{\mathrm{IP}}$ *fit result for* $D_s^+ \to K^- K^+ \pi^+$*. The data and curve shown are the sum across all* p_{T}*-*y *bins. Per-bin fits are given in Appendix F.5.*

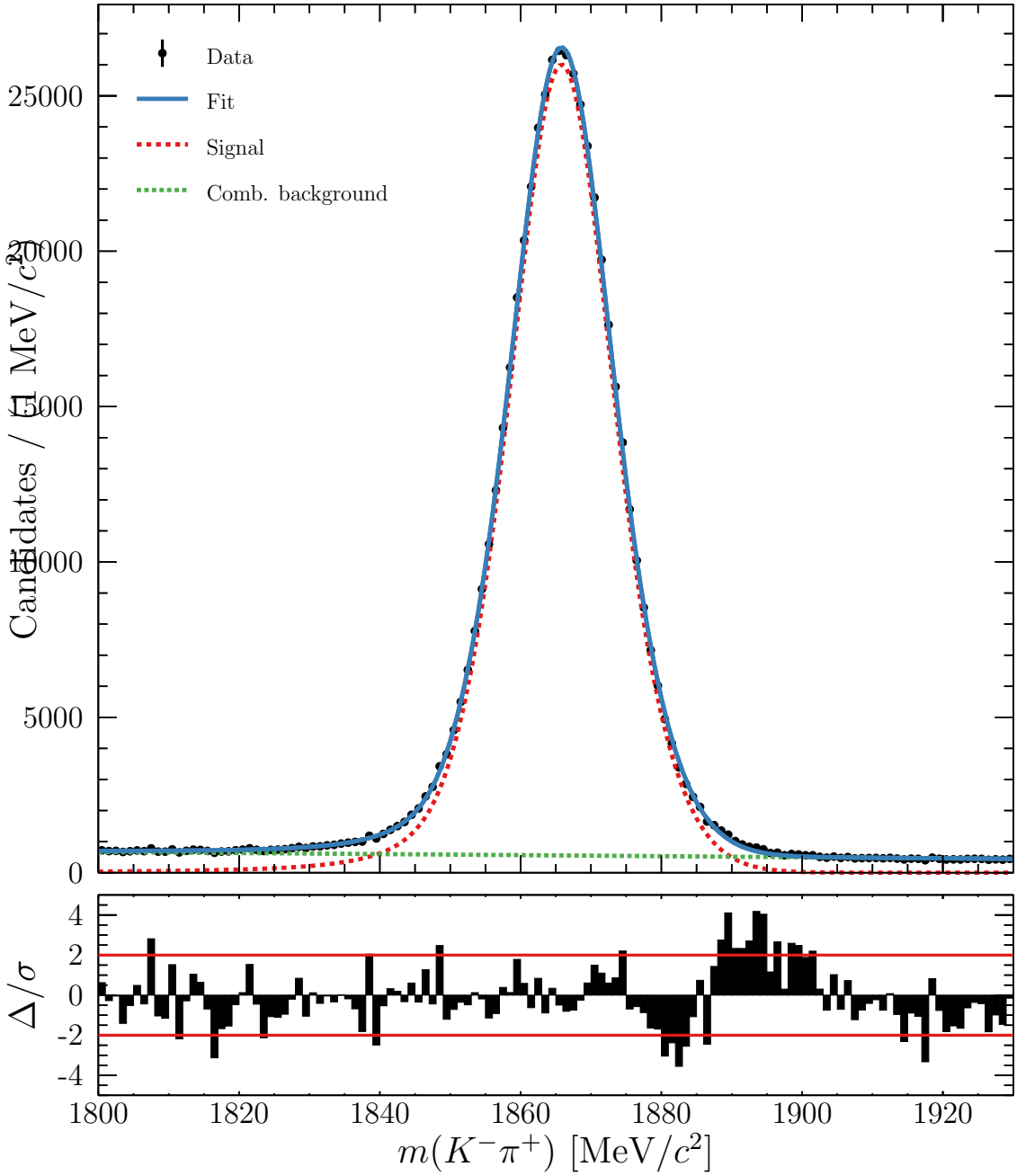

Figure 6.25: Integrated D^0 mass fit result for $D^{*+} \to D^0\pi^+$ with $D^0 \to K^-\pi^+$. The data and curve shown are the sum across all p_{T}-y bins. Per-bin fits are given in Appendix F.6.

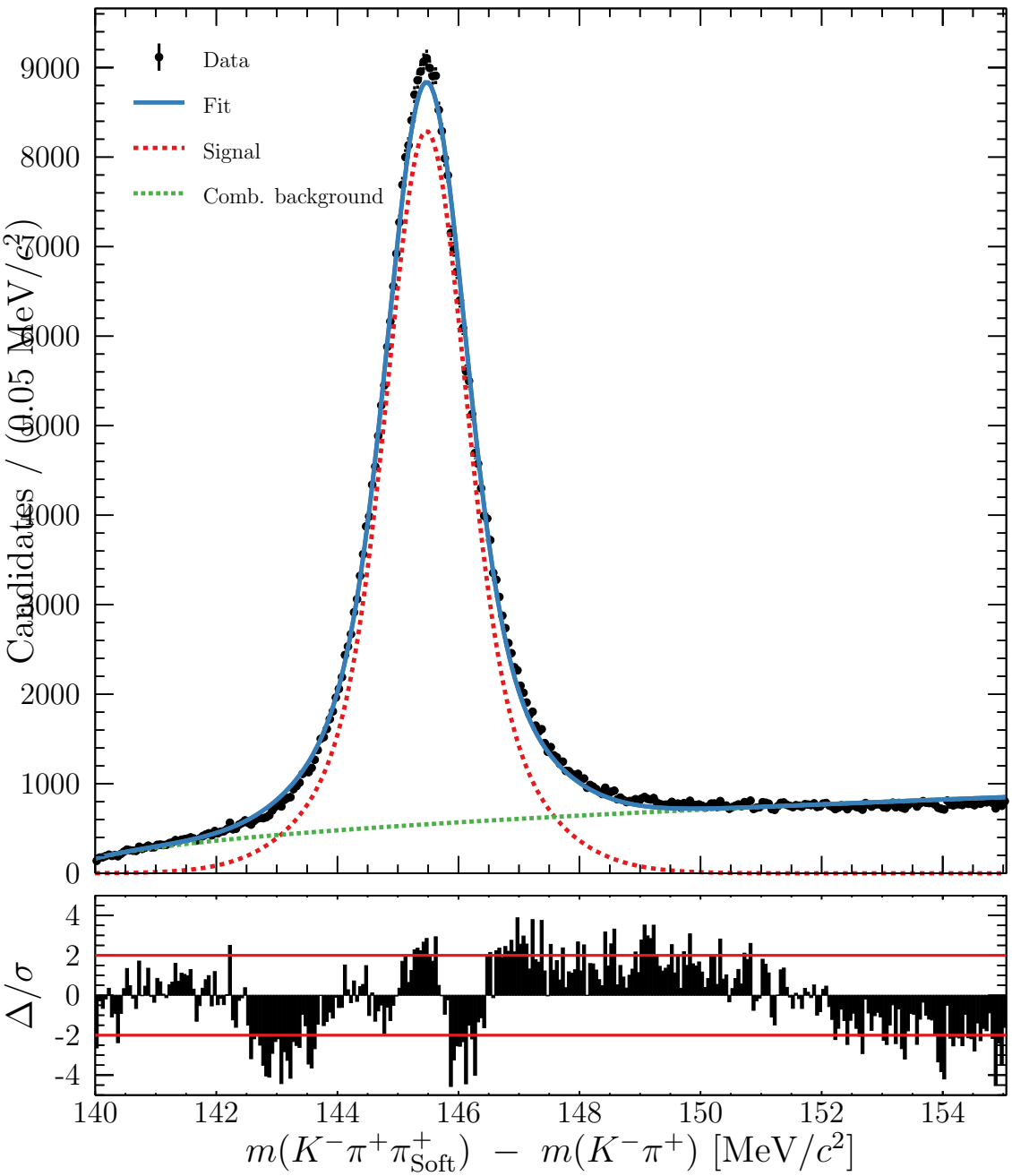

Figure 6.26: Integrated δm fit result for $D^{*+} \to D^0\pi^+$ with $D^0 \to K^-\pi^+$. The data and curve shown are the sum across all p_{T}-y bins. Per-bin fits are given in Appendix F.6.

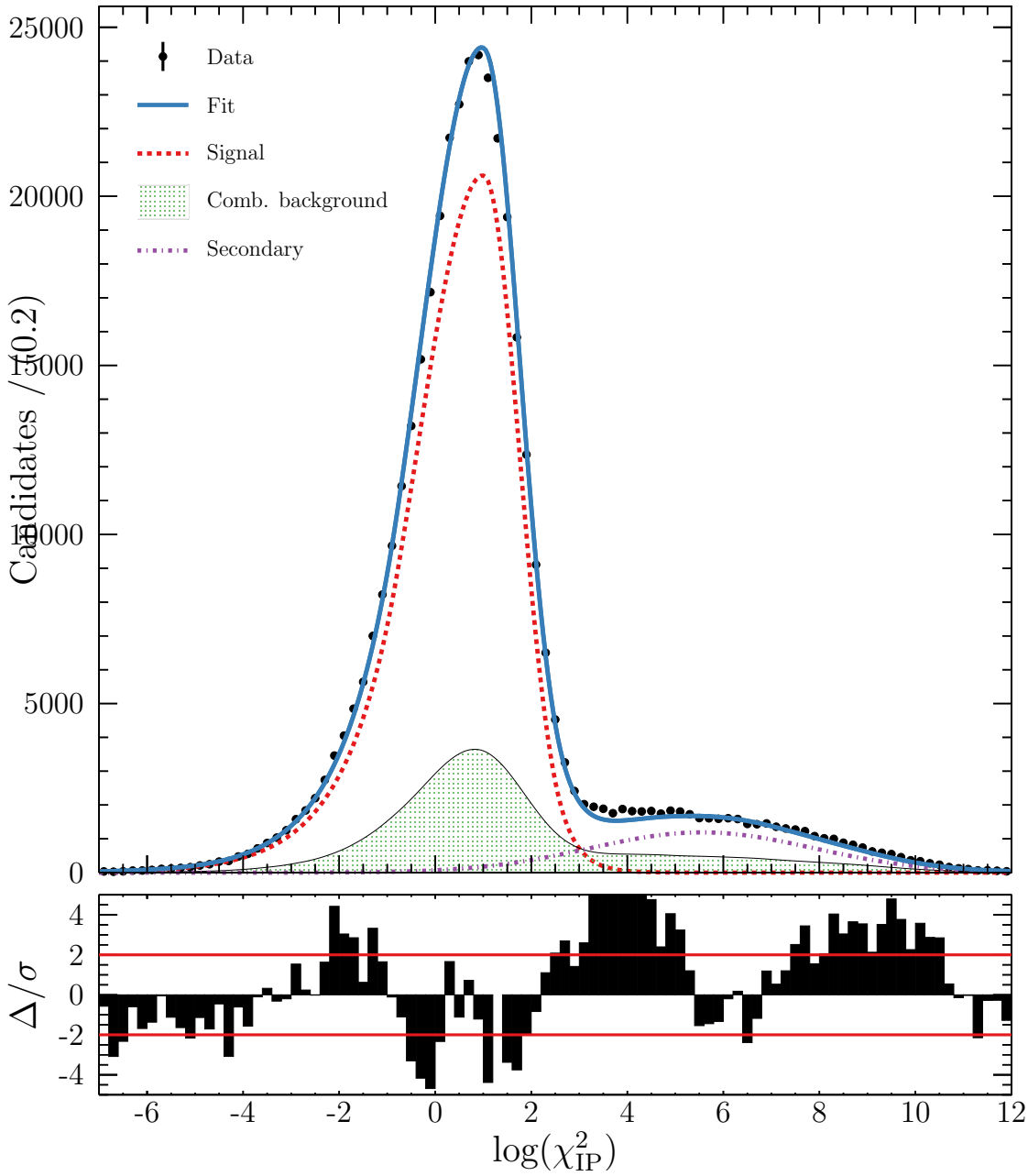

Figure 6.27: Integrated fit result for $D^{*+} \to D^0\pi^+$ with $D^0 \to K^-\pi^+$. The data and curve shown are the sum across all p_{T}-y bins. Per-bin fits are given in Appendix F.6.

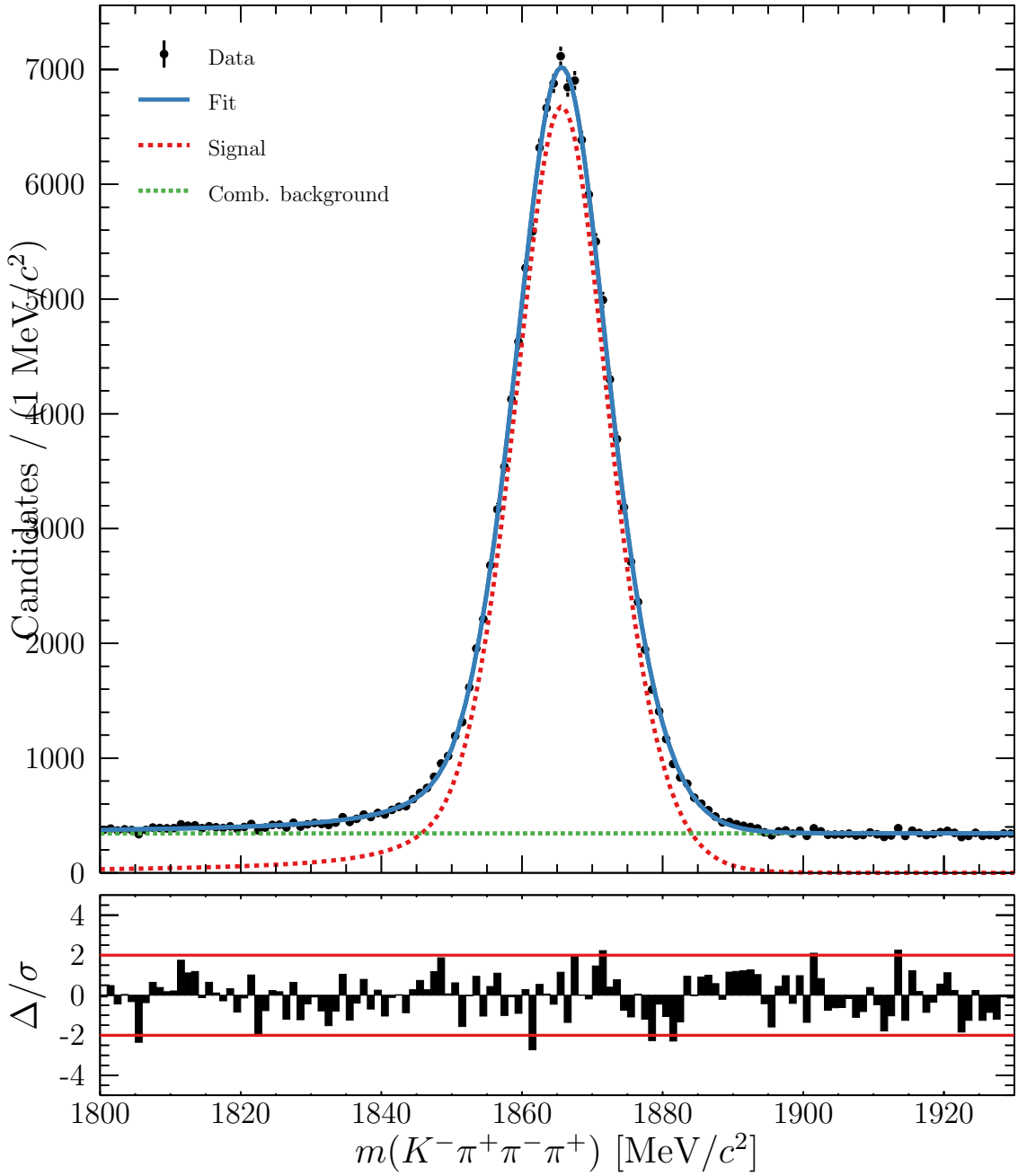

Figure 6.28: Integrated D^0 mass fit result for $D^{*+} \to D^0\pi^+$ with $D^0 \to K^-\pi^+\pi^-\pi^+$. The data and curve shown are the sum across all p_{T}-y bins. Per-bin fits are given in Appendix F.7.

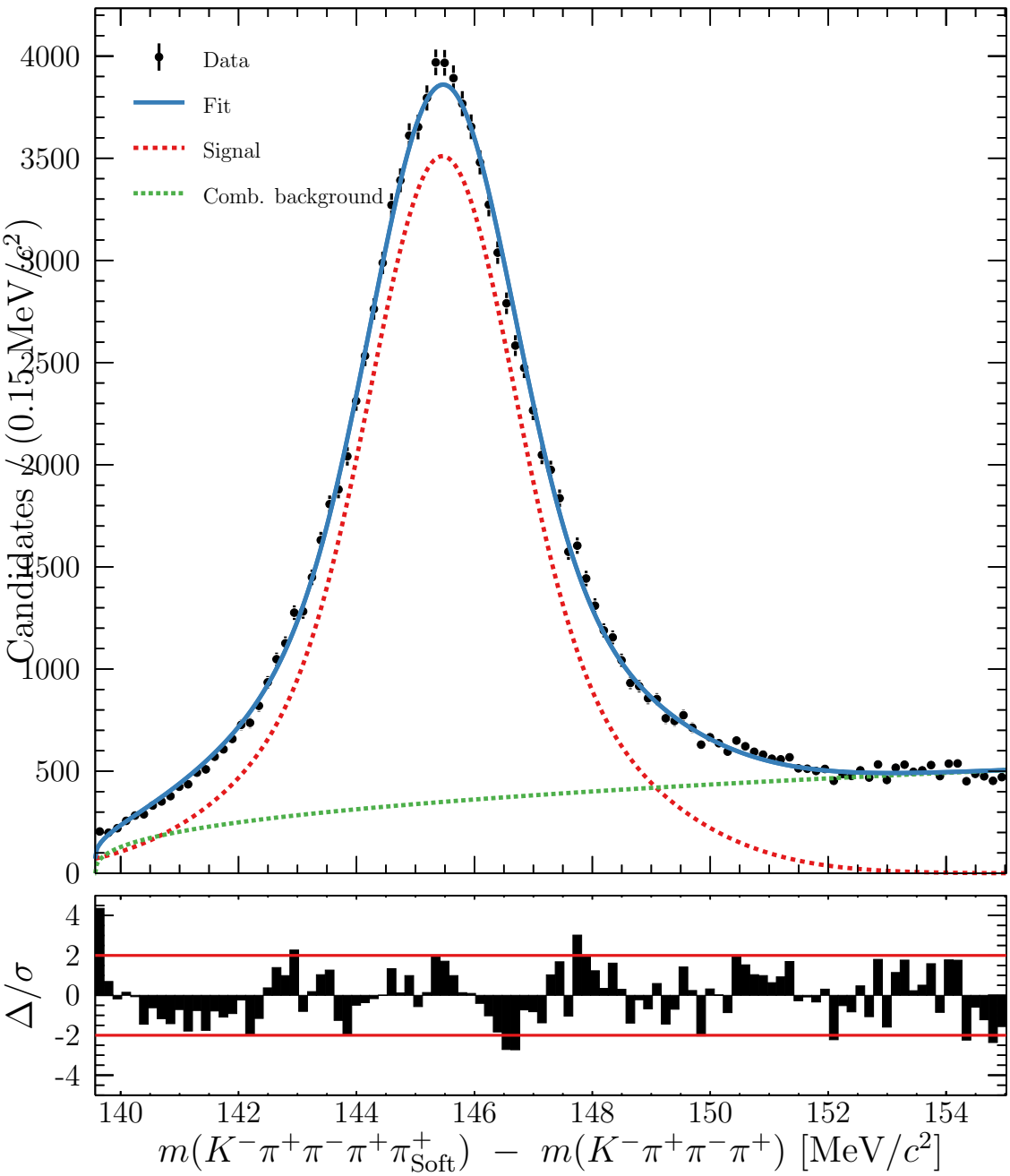

Figure 6.29: Integrated δm fit result for $D^{*+} \to D^0\pi^+$ with $D^0 \to K^-\pi^+\pi^-\pi^+$. The data and curve shown are the sum across all p_{T}-y bins. Per-bin fits are given in Appendix F.7.

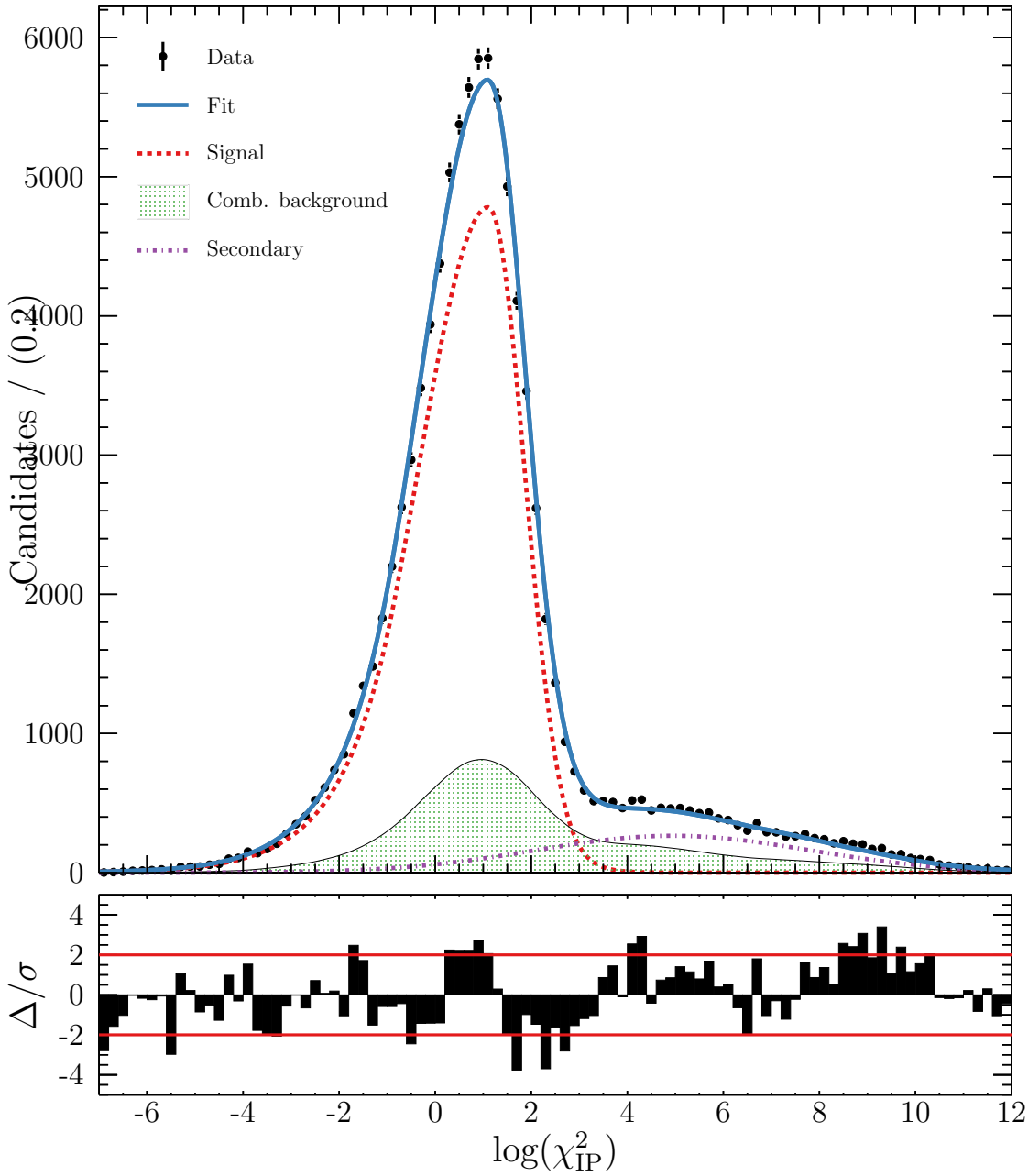

Figure 6.30: Integrated fit result for $D^{*+} \to D^0\pi^+$ with $D^0 \to K^-\pi^+\pi^-\pi^+$. The data and curve shown are the sum across all p_{T}-y bins. Per-bin fits are given in Appendix F.7.

Table 6.1: Prompt signal yields for $D^0 \to K^-\pi^+$ in D^0 p_{T}-y bins.

	y				
p_{T}[MeV/c]	$[2, 2.5[$	$[2.5, 3[$	$[3, 3.5[$	$[3.5, 4[$	$[4, 4.5[$
$[0, 1000[$	20295.1 ± 144.3	85915.6 ± 296.7	108762.8 ± 338.9	69423.1 ± 286.3	17231.2 ± 146.6
$[1000, 1500[$	22076.1 ± 146.4	84863.4 ± 288.0	99895.3 ± 315.6	60678.9 ± 253.8	14912.0 ± 127.7
$[1500, 2000[$	27541.6 ± 162.9	96616.0 ± 306.4	107675.0 ± 326.1	64377.2 ± 258.2	15276.8 ± 139.8
$[2000, 2500[$	30112.8 ± 170.3	102153.9 ± 314.1	106706.8 ± 323.9	62189.8 ± 251.9	14353.6 ± 121.8
$[2500, 3000[$	31717.6 ± 174.7	98096.1 ± 307.8	97047.6 ± 308.5	54351.4 ± 233.6	11766.5 ± 109.5
$[3000, 3500[$	30599.5 ± 171.7	85551.9 ± 287.4	80487.3 ± 281.3	44439.4 ± 210.3	8562.1 ± 92.7
$[3500, 4000[$	27959.6 ± 164.5	70870.5 ± 262.0	63571.7 ± 249.9	34106.7 ± 183.9	5294.9 ± 72.8
$[4000, 5000[$	44803.1 ± 208.1	98506.2 ± 309.6	85477.3 ± 290.1	41937.1 ± 203.3	3991.8 ± 63.1
$[5000, 6000[$	30134.5 ± 171.1	56346.6 ± 234.9	47003.3 ± 214.7	18970.9 ± 136.5	671.0 ± 26.1
$[6000, 7000[$	19097.3 ± 136.2	32445.0 ± 178.8	25491.8 ± 157.8	7509.4 ± 85.9	39.4 ± 6.0
$[7000, 8000[$	12009.6 ± 108.5	18628.2 ± 135.1	13670.4 ± 115.6	2459.0 ± 49.1	-
$[8000, 9000[$	7567.6 ± 86.7	10865.7 ± 103.2	7249.0 ± 84.2	684.0 ± 26.1	-
$[9000, 10000[$	4834.7 ± 69.3	6422.5 ± 79.4	3807.3 ± 60.9	165.0 ± 12.4	-
$[10000, 11000[$	2994.0 ± 54.8	3893.1 ± 62.0	1877.8 ± 42.9	32.0 ± 5.6	-
$[11000, 12000[$	1908.5 ± 43.6	2517.2 ± 50.0	894.3 ± 29.8	-	-
$[12000, 13000[$	1248.6 ± 35.5	1575.9 ± 39.4	424.5 ± 20.2	-	-
$[13000, 14000[$	860.8 ± 29.7	970.8 ± 31.1	181.6 ± 12.7	-	-
$[14000, 15000[$	545.7 ± 23.9	614.8 ± 24.8	71.9 ± 8.3	-	-

Table 6.2: Prompt signal yields for $D^+ \to K^-\pi^+\pi^+$ in D^+ p_{T}-y bins.

	y				
p_{T}[MeV/c]	$[2, 2.5[$	$[2.5, 3[$	$[3, 3.5[$	$[3.5, 4[$	$[4, 4.5[$
$[0, 1000[$	27.4 ± 0.6	896.1 ± 30.3	2521.3 ± 59.8	1986.3 ± 60.7	500.9 ± 30.1
$[1000, 1500[$	634.8 ± 18.5	11356.3 ± 114.5	21688.7 ± 168.6	16232.3 ± 156.4	3456.0 ± 72.4
$[1500, 2000[$	3992.6 ± 59.6	39694.3 ± 212.2	61834.7 ± 275.3	44371.3 ± 248.7	9910.9 ± 116.1
$[2000, 2500[$	10480.0 ± 110.0	70602.6 ± 279.3	97940.1 ± 341.0	66211.2 ± 294.2	15313.5 ± 140.0
$[2500, 3000[$	15099.3 ± 131.8	83476.8 ± 299.9	104997.7 ± 349.0	68397.3 ± 292.4	16822.2 ± 143.0
$[3000, 3500[$	17456.3 ± 141.5	78317.4 ± 289.6	90967.2 ± 323.3	58170.0 ± 264.0	14340.8 ± 129.1
$[3500, 4000[$	17630.7 ± 141.8	67089.0 ± 266.4	74708.7 ± 293.6	46375.5 ± 230.5	11168.4 ± 111.9
$[4000, 5000[$	30324.1 ± 173.7	98395.5 ± 333.0	101765.4 ± 345.2	61086.4 ± 264.0	12317.5 ± 116.9
$[5000, 6000[$	22682.4 ± 152.8	59566.7 ± 253.5	57770.9 ± 252.7	32290.2 ± 189.9	4498.5 ± 68.8
$[6000, 7000[$	16400.1 ± 132.7	34514.4 ± 190.4	32702.9 ± 188.1	15932.9 ± 131.4	1212.6 ± 31.9
$[7000, 8000[$	10852.7 ± 107.2	21643.7 ± 152.2	18830.9 ± 141.7	7318.9 ± 87.3	252.5 ± 10.3
$[8000, 9000[$	7493.8 ± 86.5	13428.1 ± 118.8	11080.8 ± 107.4	3189.4 ± 55.0	37.2 ± 1.9
$[9000, 10000[$	4977.7 ± 68.6	8586.9 ± 93.8	6672.3 ± 81.9	1343.8 ± 32.6	-
$[10000, 11000[$	3317.0 ± 54.0	5365.0 ± 72.4	3821.8 ± 60.1	475.5 ± 16.5	-
$[11000, 12000[$	2346.3 ± 43.7	3495.3 ± 57.1	2274.5 ± 44.0	183.4 ± 7.2	-
$[12000, 13000[$	1567.9 ± 33.7	2332.4 ± 44.5	1249.5 ± 30.7	56.2 ± 2.2	-
$[13000, 14000[$	1090.9 ± 26.6	1559.8 ± 34.8	743.3 ± 21.1	11.4 ± 0.6	-
$[14000, 15000[$	768.1 ± 21.2	1046.7 ± 26.7	415.2 ± 13.3	2.8 ± 0.2	-

Table 6.3: Prompt signal yields for $D^+ \to K^-K^+\pi^+$ in D^+ p_{T}-y bins.

	y				
p_{T}[MeV/c]	$[2, 2.5[$	$[2.5, 3[$	$[3, 3.5[$	$[3.5, 4[$	$[4, 4.5[$
$[1000, 1500[$	48.6 ± 7.7	466.7 ± 29.4	648.6 ± 39.0	424.8 ± 35.3	75.1 ± 12.8
$[1500, 2000[$	468.0 ± 25.4	3067.4 ± 72.9	4102.2 ± 86.2	2349.4 ± 65.3	465.4 ± 27.7
$[2000, 2500[$	1484.7 ± 45.5	7626.7 ± 108.3	9222.1 ± 119.5	5342.6 ± 90.1	1012.9 ± 38.9
$[2500, 3000[$	2574.6 ± 59.1	10145.2 ± 120.7	11294.9 ± 124.6	6687.1 ± 95.4	1386.5 ± 43.2
$[3000, 3500[$	2881.8 ± 62.5	9678.3 ± 114.7	9921.6 ± 114.1	6024.1 ± 88.4	1288.7 ± 40.5
$[3500, 4000[$	2925.1 ± 62.1	8025.6 ± 103.0	7969.7 ± 101.0	5002.4 ± 78.9	947.5 ± 34.7
$[4000, 5000[$	4861.4 ± 80.3	11514.8 ± 121.3	11089.0 ± 116.3	6391.2 ± 88.1	1004.1 ± 35.6
$[5000, 6000[$	3319.1 ± 66.4	6821.1 ± 92.6	6347.0 ± 86.7	3358.8 ± 62.9	412.8 ± 22.2
$[6000, 7000[$	2262.2 ± 54.4	3899.2 ± 69.6	3591.6 ± 64.9	1620.3 ± 43.5	88.8 ± 10.5
$[7000, 8000[$	1424.8 ± 43.4	2433.4 ± 54.6	1932.0 ± 47.7	735.8 ± 29.5	17.4 ± 4.5
$[8000, 9000[$	1010.2 ± 36.0	1469.4 ± 42.0	1074.9 ± 35.6	344.7 ± 19.9	1.9 ± 1.4
$[9000, 10000[$	626.5 ± 28.1	914.7 ± 33.0	707.0 ± 28.7	100.0 ± 10.8	-
$[10000, 11000[$	399.3 ± 22.6	575.7 ± 26.3	419.3 ± 21.7	44.8 ± 7.1	-
$[11000, 12000[$	254.9 ± 17.9	363.7 ± 20.7	247.2 ± 16.5	21.6 ± 4.8	-
$[12000, 13000[$	186.5 ± 14.8	258.4 ± 17.2	148.0 ± 13.2	9.2 ± 3.1	-
$[13000, 14000[$	107.1 ± 11.3	175.0 ± 13.9	69.8 ± 9.0	-	-
$[14000, 15000[$	106.2 ± 11.0	99.8 ± 10.8	35.8 ± 6.3	1.1 ± 1.4	-

Table 6.4: Prompt signal yields for $D_s^+ \to \phi\pi^+$ in D_s^+ p_{T}-y bins.

	y				
p_{T}[MeV/c]	$[2, 2.5[$	$[2.5, 3[$	$[3, 3.5[$	$[3.5, 4[$	$[4, 4.5[$
$[1000, 1500[$	15.5 ± 3.8	235.5 ± 16.7	325.5 ± 19.6	135.6 ± 13.4	12.2 ± 3.9
$[1500, 2000[$	286.0 ± 18.0	1714.8 ± 44.6	1939.5 ± 48.7	964.2 ± 34.5	125.8 ± 13.3
$[2000, 2500[$	846.4 ± 30.5	3804.6 ± 65.3	4116.9 ± 68.9	2203.8 ± 51.1	306.1 ± 20.1
$[2500, 3000[$	1343.7 ± 38.3	5206.2 ± 75.7	5441.2 ± 77.7	2877.5 ± 56.7	487.6 ± 23.7
$[3000, 3500[$	1557.2 ± 41.1	5187.6 ± 74.9	5170.0 ± 75.4	2854.4 ± 56.0	479.1 ± 23.1
$[3500, 4000[$	1632.7 ± 42.2	4497.8 ± 69.5	4338.3 ± 68.4	2485.2 ± 51.9	393.3 ± 21.3
$[4000, 5000[$	2859.7 ± 55.5	6990.5 ± 86.2	6254.1 ± 81.7	3530.1 ± 61.7	577.9 ± 25.1
$[5000, 6000[$	2302.1 ± 49.7	4482.3 ± 69.1	3869.6 ± 64.2	2156.4 ± 47.9	254.0 ± 16.5
$[6000, 7000[$	1503.1 ± 40.1	2729.5 ± 53.8	2233.0 ± 48.6	1093.2 ± 34.2	75.3 ± 8.8
$[7000, 8000[$	987.9 ± 32.7	1591.3 ± 41.1	1314.7 ± 37.3	510.8 ± 23.3	12.9 ± 3.4
$[8000, 9000[$	658.8 ± 26.5	998.4 ± 32.6	816.6 ± 29.1	252.1 ± 16.1	-
$[9000, 10000[$	449.8 ± 21.6	615.0 ± 25.5	500.5 ± 23.1	111.9 ± 10.7	-
$[10000, 11000[$	301.8 ± 17.6	401.3 ± 20.4	261.8 ± 16.4	34.3 ± 5.9	-
$[11000, 12000[$	190.5 ± 14.2	260.7 ± 16.5	179.4 ± 13.6	10.0 ± 2.9	-
$[12000, 13000[$	147.0 ± 12.2	149.7 ± 12.6	106.5 ± 10.2	4.0 ± 1.3	-
$[13000, 14000[$	79.1 ± 9.0	139.8 ± 12.0	56.0 ± 7.5	2.0 ± 0.4	-
$[14000, 15000[$	50.8 ± 7.2	85.1 ± 9.3	27.6 ± 5.0	-	-

Table 6.5: Prompt signal yields for $D_s^+ \to K^-K^+\pi^+$ in D_s^+ p_{T}-y bins.

	y				
p_{T}[MeV/c]	$[2, 2.5[$	$[2.5, 3[$	$[3, 3.5[$	$[3.5, 4[$	$[4, 4.5[$
$[1000, 1500[$	13.9 ± 12.5	166.6 ± 43.3	510.0 ± 51.6	249.2 ± 37.4	85.4 ± 28.1
$[1500, 2000[$	60.5 ± 34.2	1481.6 ± 86.7	2289.9 ± 101.9	1512.3 ± 81.6	223.8 ± 28.6
$[2000, 2500[$	433.8 ± 47.1	3504.0 ± 107.3	4806.1 ± 125.3	3044.4 ± 98.5	532.3 ± 41.3
$[2500, 3000[$	915.1 ± 63.2	5283.9 ± 122.2	6569.3 ± 123.0	3693.3 ± 89.8	724.6 ± 39.9
$[3000, 3500[$	1115.2 ± 62.2	5650.8 ± 116.4	6330.7 ± 113.4	3682.8 ± 89.1	667.7 ± 37.3
$[3500, 4000[$	1317.8 ± 65.5	5405.1 ± 103.6	5704.9 ± 102.9	3212.2 ± 76.6	498.5 ± 31.7
$[4000, 5000[$	2779.2 ± 84.8	8828.6 ± 124.1	8515.8 ± 121.8	4587.5 ± 90.6	543.7 ± 32.2
$[5000, 6000[$	2283.7 ± 70.6	5706.3 ± 97.1	5213.5 ± 93.0	2511.5 ± 65.6	153.2 ± 19.0
$[6000, 7000[$	1747.1 ± 57.4	3775.5 ± 75.2	3106.1 ± 69.6	1218.1 ± 43.9	36.5 ± 9.8
$[7000, 8000[$	1249.2 ± 46.8	2418.5 ± 58.3	1834.8 ± 51.3	549.2 ± 29.3	8.3 ± 3.6
$[8000, 9000[$	837.1 ± 37.7	1496.0 ± 47.5	1172.8 ± 43.9	241.9 ± 19.0	2.0 ± 1.3
$[9000, 10000[$	557.1 ± 30.8	943.9 ± 36.5	604.0 ± 29.1	83.7 ± 11.4	-
$[10000, 11000[$	418.0 ± 25.2	602.5 ± 29.6	346.3 ± 22.1	28.2 ± 6.4	-
$[11000, 12000[$	266.3 ± 20.5	399.0 ± 23.5	212.5 ± 16.9	13.6 ± 3.8	-
$[12000, 13000[$	195.4 ± 16.3	266.5 ± 18.9	115.5 ± 12.3	3.8 ± 2.1	-
$[13000, 14000[$	131.4 ± 14.3	173.3 ± 15.3	69.9 ± 9.7	-	-
$[14000, 15000[$	83.8 ± 11.6	121.9 ± 13.2	29.4 ± 6.5	-	-

Table 6.6: Prompt signal yields for $D^{*+} \to D^0\pi^+$, with $D^0 \to K^-\pi^+$, in D^{*+} p_{T}-y bins.

p_{T}[MeV/c]	y [2, 2.5[	[2.5, 3[	[3, 3.5[	[3.5, 4[	[4, 4.5[
[0, 1000[	-	-	158.0 ± 37.9	131.2 ± 26.8	67.5 ± 13.3
[1000, 1500[	-	617.6 ± 38.4	5410.9 ± 99.1	3597.0 ± 81.9	906.9 ± 39.6
[1500, 2000[	-	2850.3 ± 70.2	12161.6 ± 136.7	7734.4 ± 109.7	1671.2 ± 51.0
[2000, 2500[	104.1 ± 14.0	6008.0 ± 94.6	17360.0 ± 157.5	10193.0 ± 122.2	2081.5 ± 55.2
[2500, 3000[	569.0 ± 27.8	8808.4 ± 109.4	17603.7 ± 156.8	9582.9 ± 116.1	1953.2 ± 52.2
[3000, 3500[	1051.3 ± 36.9	9979.4 ± 113.5	15968.1 ± 144.8	8296.6 ± 105.9	1554.1 ± 44.9
[3500, 4000[	1500.9 ± 42.9	10200.1 ± 112.5	13504.2 ± 130.3	6867.1 ± 93.6	999.6 ± 35.7
[4000, 5000[	3507.4 ± 64.4	16731.6 ± 141.9	18674.3 ± 150.5	8970.9 ± 104.6	891.6 ± 32.6
[5000, 6000[	3104.5 ± 59.7	11315.9 ± 114.5	10812.5 ± 112.0	4464.0 ± 72.1	214.8 ± 15.4
[6000, 7000[	2323.8 ± 51.7	7310.8 ± 91.1	5945.4 ± 82.2	1851.2 ± 46.1	23.3 ± 5.3
[7000, 8000[	1783.6 ± 44.4	4415.1 ± 70.1	3457.0 ± 62.1	831.8 ± 30.3	-
[8000, 9000[	1296.1 ± 37.3	2747.5 ± 54.9	1924.7 ± 46.1	267.9 ± 16.9	-
[9000, 10000[	778.4 ± 29.5	1764.8 ± 43.4	1129.0 ± 34.8	80.7 ± 9.2	-
[10000, 11000[	611.5 ± 25.7	1023.1 ± 33.5	612.2 ± 25.3	18.5 ± 4.4	-
[11000, 12000[	404.4 ± 20.6	664.7 ± 26.9	285.9 ± 17.2	4.0 ± 0.6	-
[12000, 13000[	266.0 ± 16.5	458.7 ± 21.9	158.0 ± 12.9	-	-
[13000, 14000[	206.2 ± 14.7	245.1 ± 16.2	83.7 ± 9.3	-	-
[14000, 15000[	120.6 ± 11.4	183.5 ± 14.0	26.2 ± 5.0	-	-

Table 6.7: Prompt signal yields for $D^{*+} \to D^0\pi^+$, with $D^0 \to K^-\pi^+\pi^-\pi^+$, in D^{*+} p_{T}-y bins.

	y				
p_{T}[MeV/c]	$[2, 2.5[$	$[2.5, 3[$	$[3, 3.5[$	$[3.5, 4[$	$[4, 4.5[$
$[0, 1000[$	-	-	-	-	3.5 ± 0.5
$[1000, 1500[$	-	1.0 ± 0.9	14.7 ± 5.2	14.7 ± 5.0	-
$[1500, 2000[$	-	24.4 ± 5.8	178.6 ± 15.7	85.6 ± 11.9	-
$[2000, 2500[$	2.0 ± 1.1	177.1 ± 15.7	738.1 ± 31.6	321.0 ± 22.3	34.7 ± 6.9
$[2500, 3000[$	15.6 ± 4.0	727.3 ± 29.6	1672.2 ± 46.6	697.8 ± 31.2	79.0 ± 10.3
$[3000, 3500[$	59.4 ± 8.0	1385.3 ± 40.4	2797.8 ± 58.2	1171.5 ± 39.1	106.0 ± 12.0
$[3500, 4000[$	102.6 ± 10.9	2067.0 ± 49.2	3294.6 ± 62.4	1357.4 ± 41.7	142.6 ± 14.1
$[4000, 5000[$	520.4 ± 23.8	5100.1 ± 76.2	6712.9 ± 88.2	2819.6 ± 58.2	329.4 ± 20.2
$[5000, 6000[$	703.7 ± 27.9	5026.6 ± 74.6	5418.1 ± 78.3	2310.3 ± 52.2	225.3 ± 16.7
$[6000, 7000[$	769.0 ± 28.8	3980.0 ± 66.1	3851.0 ± 66.0	1523.1 ± 42.2	142.6 ± 12.7
$[7000, 8000[$	672.3 ± 27.0	2840.3 ± 56.1	2685.6 ± 54.6	1027.2 ± 34.5	67.4 ± 9.0
$[8000, 9000[$	580.5 ± 25.1	2186.4 ± 48.6	1714.5 ± 43.6	670.1 ± 27.5	27.0 ± 5.5
$[9000, 10000[$	463.5 ± 22.4	1346.8 ± 38.3	1213.2 ± 36.3	361.0 ± 20.1	12.0 ± 3.4
$[10000, 11000[$	365.6 ± 19.8	971.0 ± 32.6	756.0 ± 28.7	190.1 ± 14.7	1.8 ± 1.4
$[11000, 12000[$	288.0 ± 17.5	644.1 ± 26.5	521.6 ± 23.7	100.1 ± 10.6	-
$[12000, 13000[$	176.2 ± 13.9	437.2 ± 22.2	347.7 ± 19.3	61.0 ± 8.1	-
$[13000, 14000[$	146.5 ± 12.6	314.3 ± 18.5	229.5 ± 15.6	23.8 ± 5.2	-
$[14000, 15000[$	100.9 ± 10.5	236.3 ± 15.8	131.3 ± 11.9	7.2 ± 3.1	-

7 Systematic uncertainties

This section will describe and evaluate the systematic uncertainties in the analysis. Each of the sources for systematic uncertainties discussed below gives rise to one of the terms on the right side of equation 1.1 (or one of the its components in case of the efficiency). These uncertainties are then propagated by adding an additive nuisance parameter on the respective term. As some of the uncertainties found in the measurement are quite large and hence assumptions on the validity of linear Gaussian error propagation are not valid, Monte Carlo error propagation is used to propagate the uncertainties. The probability density functions for the nuisance parameters are modelled typically modelled using Gaussian distributions centered at $\mu = 0$ with a σ corresponding to the size of the systematic variation on the respective term.

7.1 Finite Monte Carlo sample size

This analysis relies on Monte Carlo samples to estimate most of the efficiencies and hence a systematic uncertainty on those efficiencies arises from the finite size of the Monte Carlo sample. As the set of events is unique for each bin and mode, this systematic uncertainty is fully uncorrelated. As already discussed in Section 5.5, the posteriori probability for the estimated efficiency is described by the Beta distribution and hence the corresponding nuisance parameter is modelled by this distribution after shifting it such that the most probable value coincides with zero.

The resulting relative systematic uncertainties are given in Table B.1 for $D^0 \to K^-\pi^+$, in Table B.2 for $D^+ \to K^-\pi^+\pi^+$, in Table B.3 for $D^+ \to K^-K^+\pi^+$, in Table B.4 for $D_s^+ \to \phi\pi^+$, in Table B.5 for $D_s^+ \to K^-K^+\pi^+$, in Table B.6 for $D^{*+} \to D^0\pi^+$ with $D^0 \to K^-\pi^+$ and in Table B.7 for $D^{*+} \to D^0\pi^+$ with $D^0 \to K^-\pi^+\pi^-\pi^+$.

7.2 Monte Carlo modelling

If the simulated data does not correctly model the selection variables, the selection efficiencies that are evaluated on MC will be wrong. Small deviations of the MC from the distributions in data can lead to small deviations from the true efficiencies, and these deviations need to be evaluated and assigned as systematic uncertainties.

In order to separate the signal and background contributions to a specified variable the sPlot method was used [23]. The resulting histograms which compare the simulated distribution to those obtained from data are shown in part (a) of the Figures in Appendix H.

The value a given variable which corresponds to a 50% efficiency of the fully

Table 7.1: Relative error on each kinematic bin due to the Monte Carlo modelling systematic

Mode	Relative error
$D^0 \to K^-\pi^+$	1.0%
$D^{*+} \to D^0\pi^+$ with $D^0 \to K^-\pi^+$	2.5%
$D^{*+} \to D^0\pi^+$ with $D^0 \to K^-\pi^+\pi^-\pi^+$	2.7%
$D^+ \to K^-\pi^+\pi^+$	0.3%
$D^+ \to K^-K^+\pi^+$	0.8%
$D_s^+ \to \phi\pi^+$	0.4%
$D_s^+ \to K^-K^+\pi^+$	2.5%
$D_s^+ \to K^-K^+\pi^+$ without ϕ	0.9%

selected candidates is found. This can then be applied to the real data with the expectation that the ratio between the yields on either side of the cut value will be 1.

For each event the signal sWeight is bootstrapped with corrections made for the PID efficiency of each track where relevant. These weights are then summed over to obtain a yield for the upper and lower half of each variable, for each kinematic bin.

For each transverse momentum and rapidity bin the yield corresponding to a tighter cut is corrected to obtain a new efficiency corrected yield, with the necessary uncertainty from the Monte Carlo statistics included. A difference is then found by subtracting the total yield from this efficiency corrected yield. This process is repeated for each variable used in the selection and the $N_{p_\mathrm{T}\ \mathrm{bins}} \cdot N_{y\ \mathrm{bins}} \cdot N_{\mathrm{selection\ variables}}$ differences are summed to give the total systematic which is independently applied to every kinematic bin. An example of this process is shown for $D^0 \to K^-\pi^+$ in Appendix H.1 along with a comparison of the distributions observed for each variable.

7.3 PID calibration

There are three assumptions made during the PID calibration procedure described in Section 5.6:

- The PID efficiency is constant within a calibration bin;
- The PID efficiency is independent of the source of the tracks; and
- The PID efficiency is wholly parameterised by track momentum p, pseudorapidity η, and event multiplicity.

The breakdown of these assumptions will lead to incorrect PID efficiencies, and the magnitude of the deviation from the true PID efficiency can be assigned as a systematic uncertainty. There is also a statistical uncertainty arising from the finite calibration sample size, which we will propagate to our measurement as a systematic uncertainty.

7.3.1 Calibration sample size

The efficiency in each bin i of the calibration histogram ε_i has a statistical uncertainty due to the size of the used calibration sample. To model the correlations between the tracks within a single event using the same calibration bins as well as the correlation between different events using (partly) the same calibration bins correctly, toy studies are performed to propagate the uncertainty of the individual ε_i to an uncertainty on the overall uncertainty ε. Each of those bins contains a different, exclusive set of calibration events and hence fluctuates independently. In each toy sample, a new efficiency $\varepsilon_{i,\text{toy}}$ is drawn from a Gaussian distribution with $\mu = \varepsilon_i$ and $\sigma = \Delta\varepsilon_i$. The entire calibration procedure is then repeated using those $\varepsilon_{i,\text{toy}}$ to obtain a new overall efficiency ε_{toy} per toy sample. σ_C^{PID} is then given by the standard deviation of the obtained ε_{toy} from 10000 toy experiments. A common set of toy calibration histograms is generated which is used for determining the uncertainty in each bin and for each mode, allowing to determine the correct correlations. As different bins and modes have different kinematic distributions for their final state particles, the correlation is found to be significant only for neighbouring p_T-y bins within one mode and negligible between different modes.

The resulting relative uncertainty $\sigma_C^{PID}/\varepsilon$ is given in Table B.8 for $D^0 \to K^-\pi^+$, in Table B.9 for $D^+ \to K^-\pi^+\pi^+$, in Table B.10 for $D^+ \to K^-K^+\pi^+$, in Table B.11 for $D_s^+ \to \phi\pi^+$, in Table B.12 for $D_s^+ \to K^-K^+\pi^+$, in Table B.13 for $D^{*+} \to D^0\pi^+$ with $D^0 \to K^-\pi^+$ and in Table B.14 for $D^{*+} \to D^0\pi^+$ with $D^0 \to K^-\pi^+\pi^-\pi^+$ The distribution in the PID efficiency obtained from the toy study is used as the distribution of the corresponding nuisance parameter after shifting it such that the most probable value is zero.

7.3.2 Binning scheme

Even though this analysis employs an automated method to find a binning scheme which describes the efficiencies in the calibration as good as possible taking into account the size of the calibration samples. However, Figures 5.6 and 5.7 show a clear deviation between the chosen binning scheme and a finer binning scheme when projecting the efficiency in one dimension. The quoted efficiencies ε_i in each bin in

the calibration histogram is the average efficiency of the calibration sample in this bin. Therefore, this can lead to a substantial systematic uncertainty if the distributions in the reference and calibration sample are different and hence the average is not in same in both samples.

To estimate this, a Kernel Density Estimate (KDE) based, data-driven approach is used. As the overall dependence of the efficiency on the number of hits in the SPD is small for the PID cuts used in this analysis (compared to the p and η dependence), the effect of the binning scheme is estimated using a two-dimensional binning scheme in p and η. `Meerkat` [24] is used to derive the probability densities $P^{(\mathrm{cut})}_{K/\pi}(p,\eta)$ describing the calibration sample before and after the PID cut and for K and $\pi^{\pm}$ respectively. Figures 7.1 and 7.2 show the distributions in the calibration sample for kaons and the obtained KDE.

Using the obtained KDE approximations of the probability density functions before and after the respective PID cut, the efficiency ε_i in a bin i in the calibration histogram can be written as:

$$\varepsilon_i = \frac{C'}{C} \cdot \frac{\int_{\mathrm{bin}} P^{\mathrm{cut}}(p,\eta)\,\mathrm{d}p\mathrm{d}\eta}{\int_{\mathrm{bin}} P(p,\eta)\,\mathrm{d}p\mathrm{d}\eta}\ , \tag{7.1}$$

where C and C' are the total of events in the calibration sample and the number of events passing the PID selection respectively. In Figure 7.3, the resulting one-dimensional projections plotted in a very fine binning are shown next to the binned efficiencies and a good agreement is seen between the efficiencies in the actual calibration sample and the KDE model.

To estimate the uncertainty due to the binning scheme, a set of two-dimensional calibration histograms is created from the KDEs. Figures 7.4 and 7.5 show examples of those calibration histograms alongside the nominal histogram which is created using the nominal histogram and filled from the KDE. It is in very good agreement with the calibration histogram obtained directly from the calibration sample. The actual uncertainty is then obtained by comparing the results of the PID calibration using the finer binned histograms to the ones obtained using the nominal binning scheme. Typically, a converging behaviour of the obtained PID efficiency is seen with increasing number of bins used in the calibration histograms (seen in Figure 7.6 for $D^0 \to K^-\pi^+$). The systematic uncertainty on the quoted PID efficiency is then estimated as the difference of the nominal and converged value and propagated using a Gaussian assumption for the corresponding nuisance parameter. As each mode has a different composition of final state particles, the systematic uncertainty is evaluated for each mode and bin separately and discussed in the following.

Cross-checks have been performed using toy data generated from the KDE itself.

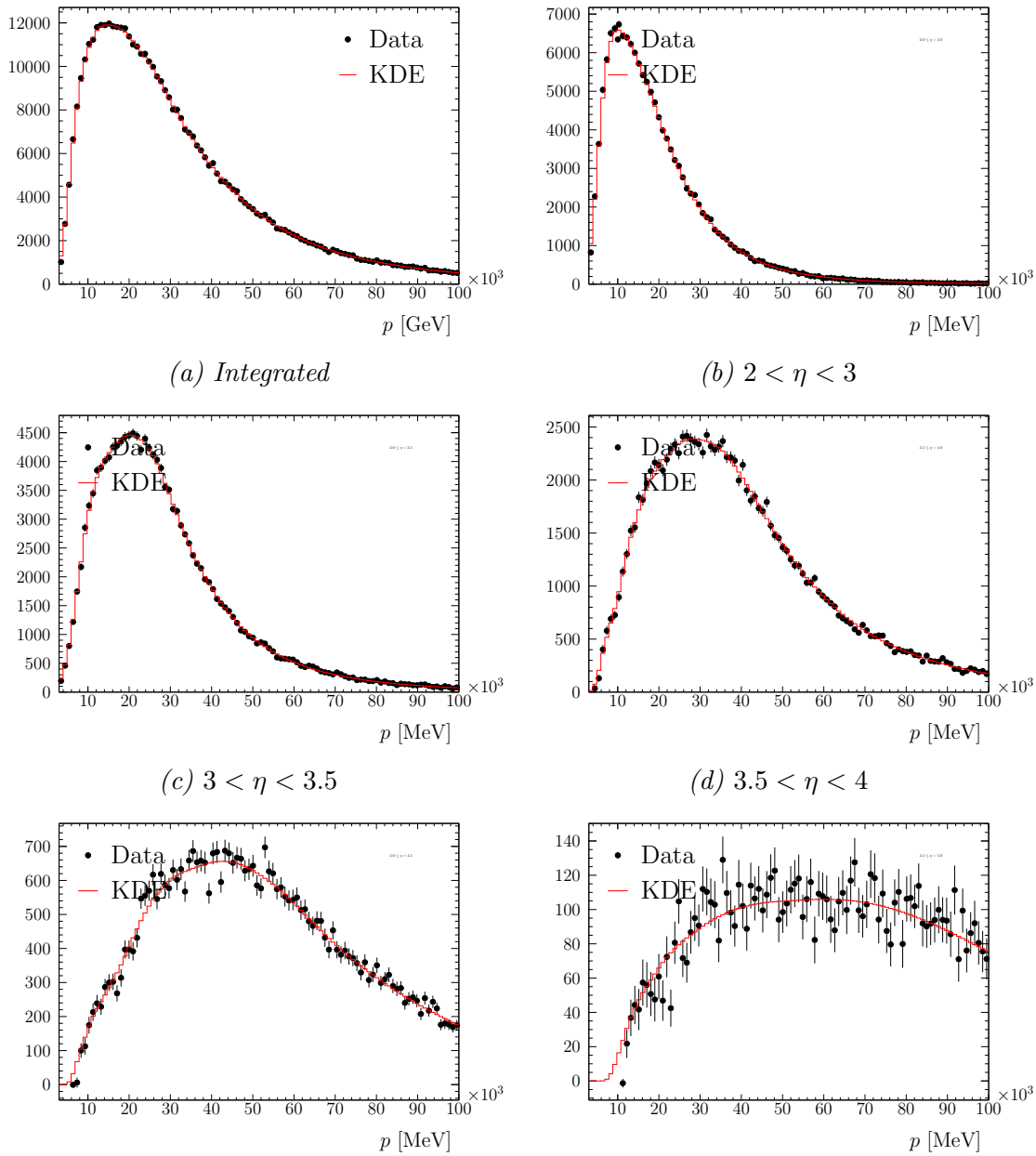

(a) Integrated

(b) $2 < \eta < 3$

(c) $3 < \eta < 3.5$

(d) $3.5 < \eta < 4$

(e) $4 < \eta < 4.5$

(f) $4.5 < \eta < 5$

Figure 7.1: Distributions in p for kaons in the calibration sample before applying the PID cut. The KDE result is the projection of $P_K(p, \eta)$ *onto p in the stated* η *range and integrated over the shown bins.*

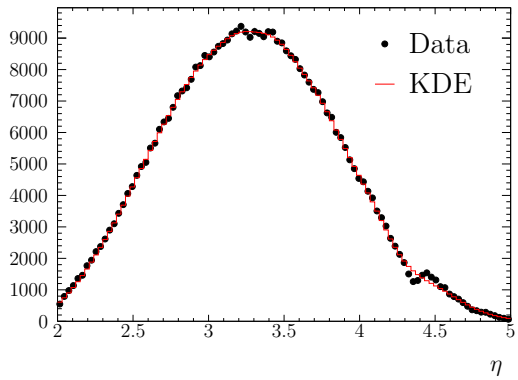

(a) Integrated

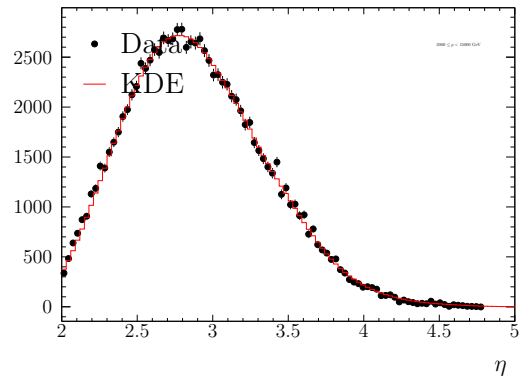

(b) $3 < p < 15\ GeV$

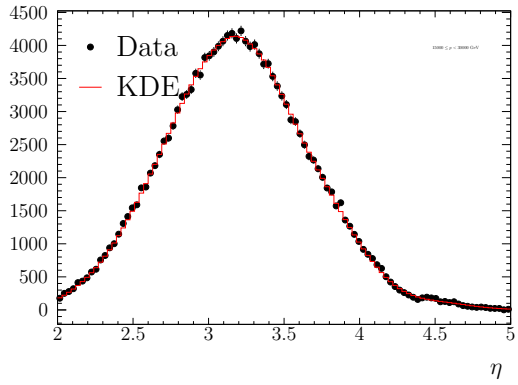

(c) $15 < p < 30\ GeV$

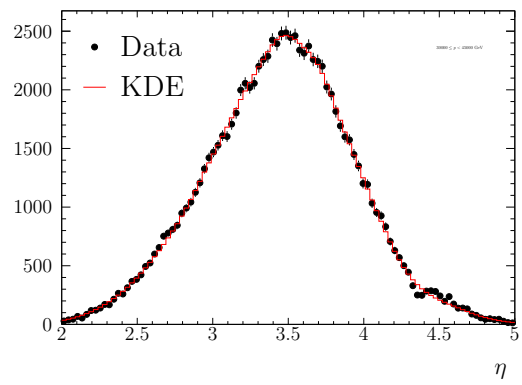

(d) $30 < p < 45\ GeV$

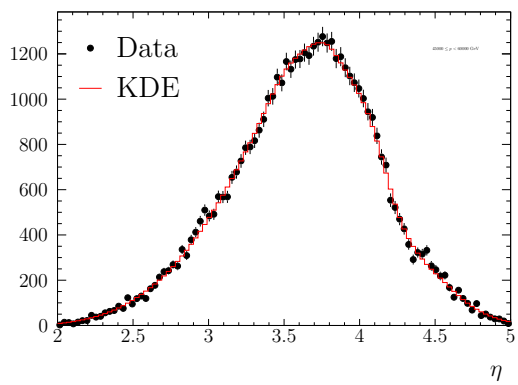

(e) $45 < p < 60\ GeV$

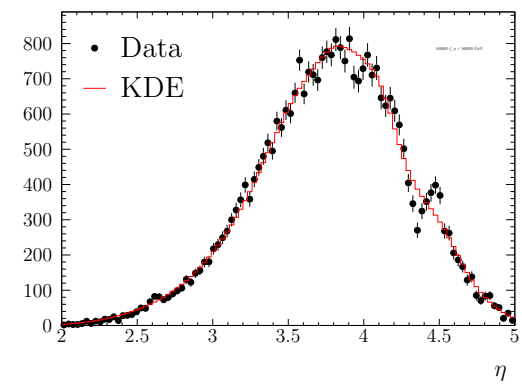

(f) $60 < p < 80\ GeV$

Figure 7.2: Distributions in η for kaons in the calibration sample before applying the PID cut. The KDE result is the projection of $P_K(p, \eta)$ onto η in the stated p range and integrated over the shown bins.

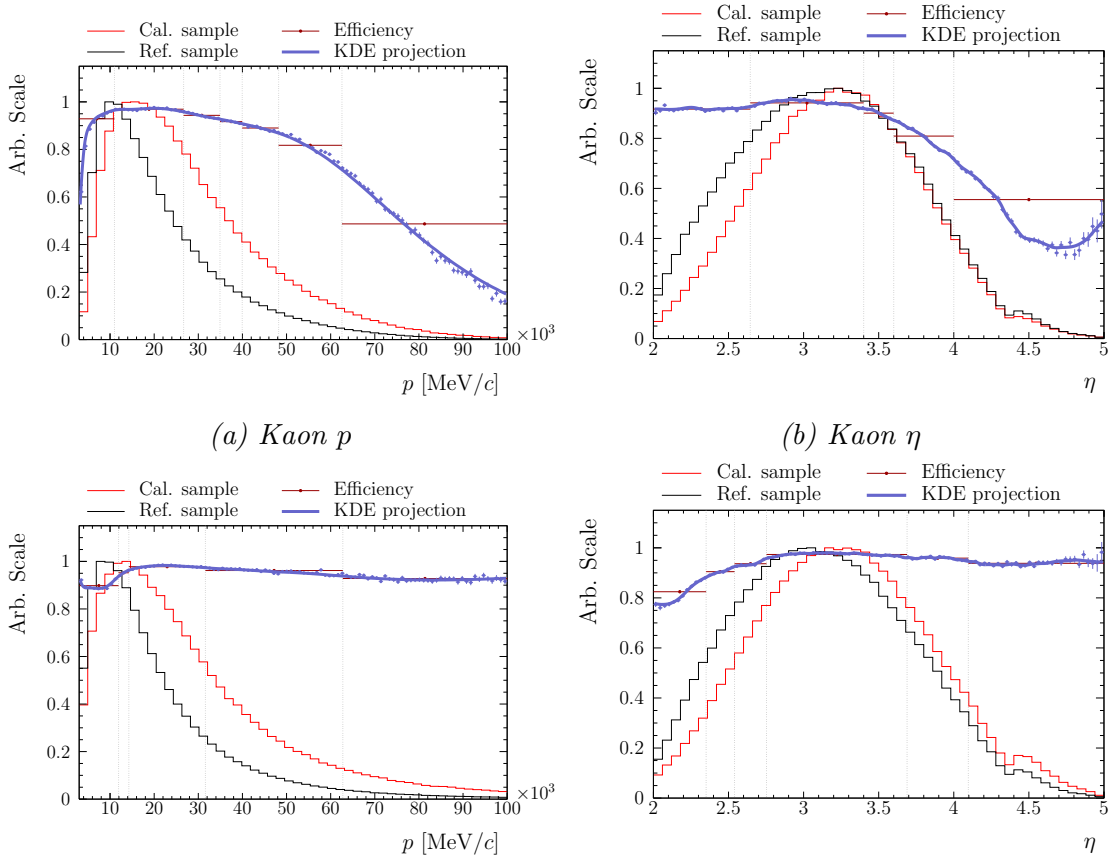

(a) Kaon p

(b) Kaon η

(c) Pion p

(d) Pion η

Figure 7.3: Binning plots for kaons and pions as in Section showing the projection of the efficiency onto p and η respectively.

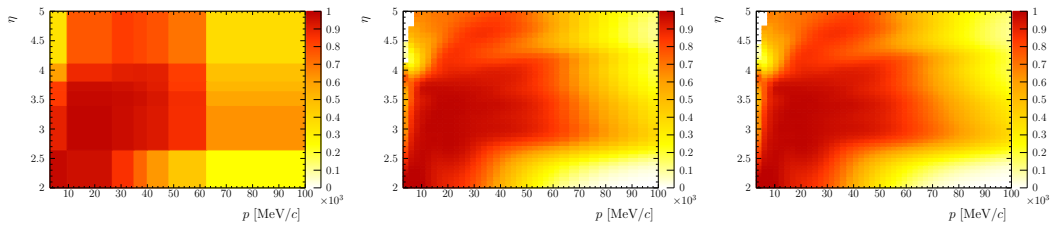

(a) Nominal

(b) 1221 bins

(c) 2256 bins

Figure 7.4: Example two-dimensional kaon calibration histograms with increasing granularity. The nominal binning scheme refers to the one used in the analysis.

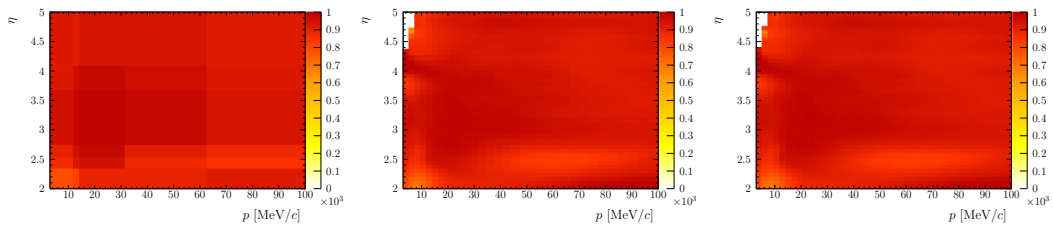

(a) Nominal *(b) 960 bins* *(c) 2162 bins*

Figure 7.5: Example two-dimensional pion calibration histograms with increasing granularity. The nominal binning scheme refers to the one used in the analysis.

Even if the distributions in the calibration and reference sample are identical for these toys, a variation with the number of bins is seen. This variation is dependent on the size of the reference sample and tends to zero in case of very large samples. To incorporate this dependence on the size of the reference sample, the reference sample is resampled 10000 times using bootstrapping and performing the procedure above in each of those samples. This yields a set of 10000 differences in the efficiencies between the nominal and finest binning studied. To avoid counting statistical uncertainty related to the size of the reference sample twice (it is already included as the statistical uncertainty on the signal yield extracted from the fit), quoted systematic uncertainties are obtained by quadratically subtracting the standard deviation from the mean of this set of differences. In case the mean of the differences agrees with zero within one standard deviation, no uncertainty is quoted.

As each bin and each mode shows a consecutive trend with increasing granularity in the binning scheme, the resulting uncertainties are assumed to be fully correlated.

The resulting relative uncertainty is given in Table B.15 for $D^0 \to K^-\pi^+$, in Table B.16 for $D^+ \to K^-\pi^+\pi^+$, in Table B.17 for $D^+ \to K^-K^+\pi^+$, in Table B.18 for $D_s^+ \to \phi\pi^+$, in Table B.19 for $D_s^+ \to K^-K^+\pi^+$, in Table B.20 for $D^{*+} \to D^0\pi^+$ with $D^0 \to K^-\pi^+$ and in Table B.21 for $D^{*+} \to D^0\pi^+$ with $D^0 \to K^-\pi^+\pi^-\pi^+$

7.4 Luminosity

There is an uncertainty on the luminosity measurement provided by the luminosity group, which we will propagate as a systematic uncertainty on our measurement. The relative uncertainty on the luminosity measurement is expected to be around 5%.

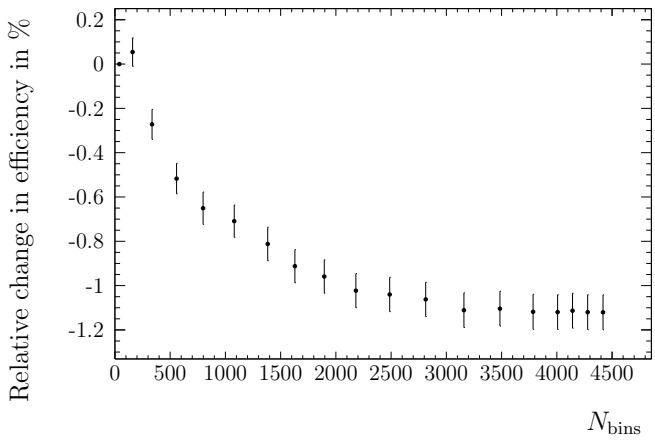

Figure 7.6: Integrated systematic uncertainty for $D^0 \to K^-\pi^+$ due to the binning scheme applied for kaons and pions. Displayed uncertainties indicate the statistical uncertainty from the reference sample size, estimated using bootstrapping. 2011 data as reference sample with mock-up PID samples.

7.5 Tracking efficiency correction

There is an uncertainty on the tracking correction, discussed in Section 5.2.1, provided by the tracking group, which we will propagate as a systematic uncertainty on our measurement. There are several potential sources for systematic uncertainties:

- The uncertainties given in Figure 5.1 which incorporate the statistical uncertainties from the calibration mode and differences between different methods used to extract these factors.

- The correction table provides numbers estimated using muons. An additional uncertainty of 1.1% (1.4%) is applied for kaons (pions) due to uncertainties in the hadronic interactions. This is dominated by the uncertainty on the material budget and hence full correlation between kaons and pions is assumed.

- An additional uncertainty of 0.4% is applied due to the reweighting procedure.

All of these sources are propagated using Monte Carlo error propagation and assuming Gaussian distributions with the above mentioned relative widths for the different contributions to the tracking systematic uncertainty. Even though different bins and modes have different final state kinematics and hence access the table of correction factors for each track differently, the obtained uncertainty is driven by the global

Table 7.2: Branching ratios for the different modes. Quoted uncertainties are propagated as systematic uncertainties in this measurement.

Mode	$\mathcal{B}$ [%]
$D^0 \to K^-\pi^+$	3.88 ± 0.05
$D^0 \to K^-\pi^+\pi^-\pi^+$	8.08 ± 0.21
$D^{*+} \to D^0\pi^+$	67.7 ± 0.5
$D^+ \to K^-\pi^+\pi^+$	9.13 ± 0.19
$D^+ \to K^-K^+\pi^+$	0.954 ± 0.026
$D_s^+ \to \phi\pi^+$	2.24 ± 0.12
$D_s^+ \to \pi^-\pi^+\pi^+$	1.09 ± 0.05

factors for the reweighting and the hadronic interaction uncertainty and the results are found to be highly correlated (at least 90%) between different bins and modes.

The resulting relative systematic uncertainties are given in Table B.22 for $D^0 \to K^-\pi^+$, in Table B.23 for $D^+ \to K^-\pi^+\pi^+$, in Table B.24 for $D^+ \to K^-K^+\pi^+$, in Table B.25 for $D_s^+ \to \phi\pi^+$, in Table B.26 for $D_s^+ \to \phi\pi^+$ no ϕ, in Table B.27 for $D^{*+} \to D^0\pi^+$ with $D^0 \to K^-\pi^+$ and in Table B.28 for $D^{*+} \to D^0\pi^+$ with $D^0 \to K^-\pi^+\pi^-\pi^+$.

The posteriori distribution obtained from the toy propagation of the uncertainties is then used as the distribution for the associated nuisance parameter after shifting it such that the most probable value coincides with zero.

7.6 Branching fractions

There is an uncertainty on the branching fractions, provided by the Particle Data Group [25], which we will propagate as a systematic uncertainty on our measurement. As this measurement does not determine the resonant $\phi \to K^+K^-$ contribution but selects events within a $\pm 20\,\text{MeV}$ window around the ϕ mass, a dedicated measurement by CLEO is used [26]. The numerical values used are listed in Table 7.2.

7.7 Fit model

Other fit models may describe the well but give different results. The magnitude of the difference between the cross sections computed with other fit models and our 'nominal' model, described in Section 6, will be assigned as a systematic uncertainty on the result. This corresponds to an uncertainty on what the true generating probability

density function is for the observed data.

7.8 Correlations and summary

The different sources of systematic uncertainty discussed in this section can be grouped into different categories: global uncertainties which are correlated between all bins and all modes, uncertainties which are are only correlated between the bins of one mode and those which are uncorrelated between bins and modes.

Global uncertainties

- Branching ratio for D^0 and $D^{*+} \to D^0\pi^+$ for the same D^0 final state.
- Luminosity
- Tracking correction
- PID binning

Correlated between different bins

- Branching ratio
- Fit model
- PID calibration sample size

Uncorrelated

- Monte Carlo sample size

An overview of the uncertainties is given in Table 7.3.

7.9 Correlations between 7 TeV and 13 TeV measurements

To make a comparison with the 7 TeV results and obtain cross-sections ratios between 13 TeV and 7 TeV, correlations between the different sources of systematic uncertainty have to be evaluated. Unfortunately, only the integrated uncertainty tables for the 7 TeV measurement are available which combine all but the globally correlated uncertainties from the tracking, the branching ratios and the luminosity. Therefore, all of the uncertainties entering this combined number have to be assumed to be uncorrelated between both centre-of-mass energies.

Table 7.3: Overview of systematic uncertainties and their values, expressed as relative fractions of the cross-section measurements in percent (%). Uncertainties that are computed bin-by-bin are expressed as ranges giving the minimum to maximum values of the bin uncertainties. Ranges for the correlations are also given seperately for bins and modes in %.

Sources	D^0	D^+		D_s^+		D^{*+}		Correlations		
	$K\pi$	$K\pi\pi$	$KK\pi$	$\phi\pi$	$KK\pi$	$K2\pi$	$K4\pi$	bins	modes	years
MC stat.	2-27	2-36	2-36	4-25	3-55	2-22	4-55	-	-	-
MC/data										-
Tracking	3-5	5-17	5-17	4-18	4-18	5-20	9-40	90-100	90-100	50
PID cal.	0-2	0-1	0-2	0-2	0-3	0-1	0-3	0-100	-	-
PID binning	0-44	0-10	0-33	0-20	0-17	0-15	0-18	100	100	
Fit										
$\mathcal{BR}$	1.2	2.1	2.7	4.5	4.6	1.5	2.7	100	0-95	100
Luminosity				3.9				100	100	37

- As both measurements use different Monte Carlo samples to evaluate the statistical uncertainty due to the finite size of the sample, those contributions are uncorrelated between both centre-of-mass energies.

- Both measurements used similar simulations of the physics and the detector and hence the systematic uncertainties due to disagreements between the data and the Monte Carlo simulations could be correlated. However, this uncertainty is included in the combined number and thus no correlation is assumed.

- The systematic uncertainty on the tracking correction applied in this analysis is dominated by the uncertainties on the hadronic interactions with the detector material. As those are correlated with the ones used in the 7 TeV analysis, a high correlation is expected. To account for potential differences in the estimation, a conservative 50% correlation is assumed.

- The 7 TeV only quotes a combined number for the PID systematic uncertainty while this analysis splits it into two categories. As different calibration samples are used in both measurements, the uncertainties due to the calibration sample sizes are uncorrelated. As the same insufficiencies due to a binned reweighting approach should affect both measurements, there might be correlations which would reduce the uncertainty on the ratio. However, the 7 TeV uses a Monte

Carlo sample as reference sample and evaluates the systematic uncertainty by applying the calibration procedure on Monte Carlo samples using Monte Carlo simulated calibration samples. Therefore, the estimation of the actual correlation is impossible without having access to the original data. Furthermore, the PID uncertainty is one of the dominant systematic uncertainties in both measurements and hence a wrongly estimated correlation could lead to a significant underestimation of the actual uncertainty. Hence, no correlation is assumed.

- The uncertainty from the fit model is included in the combined number and hence one assumes no correlation.

- As both measurements use the same external measurements (with the possible exception of the D_s^+ decays), the uncertainties on the branching fractions are fully correlated.

- The correlation between the luminosity measurements at 7 TeV and 8 TeV has been estimated to $\rho = 55 \pm 6\%$ by the luminosity group[8]. The final result was measured using both vDM and BGI results, each contributing equally to the final result. As this measurement only uses a luminosity measurement from BGI which decreases the correlation.

[8] https://indico.cern.ch/event/387165/contribution/1/material/slides/0.pdf

Decay mode	1	2	3	4	> 5
$D^0 \to K^-\pi^+$	99.89	0.11			
$D^+ \to K^-\pi^+\pi^+$	99.41	0.58	0.01		
$D^+ \to K^-K^+\pi^+$	98.57	1.38	0.05		
$D_s^+ \to \phi\pi^+$	98.81	1.17	0.02		
$D_s^+ \to K^-K^+\pi^+$	95.00	4.52	0.39	0.07	0.02
$D_s^+ \to K^-K^+\pi^+$ no ϕ	98.37	1.58	0.04	0.01	
$D^{*+} \to D^0\pi^+$, $D^0 \to K^-\pi^+$	88.03	10.24	1.43	0.24	0.05
$D^{*+} \to D^0\pi^+$, $D^0 \to K^-\pi^+\pi^-\pi^+$	91.11	7.80	0.84	0.21	0.04

Table 8.1: Relative number of events in % split into different candidate multiplicities. Each event is identified by a unique `runNumber-eventNumber` *combination.*

8 Validation

Several cross-checks and studies have been performed as part of the validation procedure for the analysis on the data taken in 2015. This section describes each of these checks.

8.1 Dependence of background $\ln \chi^2_{\mathrm{IP}}$ on mass

The background template PDFs used in the $\ln \chi^2_{\mathrm{IP}}$ fit, described in Section 6.2, assume that the background shape is independent of the charm hadron mass. Figure 8.1 shows the $\ln \chi^2_{\mathrm{IP}}$ distributions in the lower and upper sidebands for $D^0 \to K^-\pi^+$, $D^+ \to K^-\pi^+\pi^+$, and $D_s^+ \to \phi\pi^+$. The two distributions are similar for each mode, which we interpret to mean that the background $\ln \chi^2_{\mathrm{IP}}$ shapes are independent of the mass.

8.2 Number of candidates per event

The number of candidates per event in the selected data sample (with signal window cut applied) is studied by counting how often each `runNumber-eventNumber` pair is found in the sample. Table 8.1 shows the obtained fractions of the different candidate multiplicities in the selected data sample for the different modes.

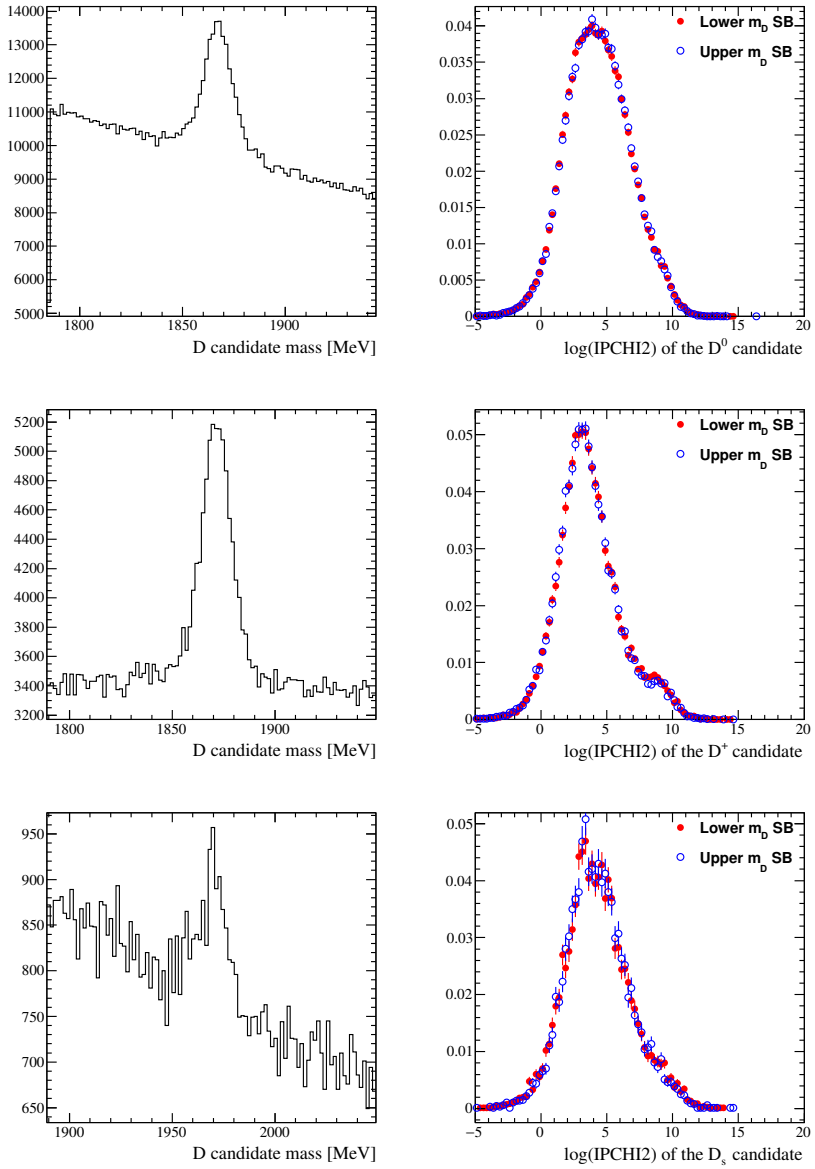

Figure 8.1: PDF factorization plots for the $D^0 \to K^-\pi^+$, $D^+ \to K^-\pi^+\pi^+$, and $D_s^+ \to \phi\pi^+$ decay modes (top to bottom). The left panel in each plot shows the D candidate mass distribution to give an idea of the sample purity; the right panel shows the D candidate $\ln \chi^2_{\mathrm{IP}}$ distribution in the lower and upper sidebands of the D mass.

8.3 Checks for fitter biases

The fitter used to extract the number of promptly-produced charm hadron signal decays, described in Section 6, should not be biased in the fitted signal yields and should correctly compute the uncertainties on those yields. We test this by performing many pseudo-experiments, where for each experiment we generate toy Monte Carlo data from a model, described in Section 6, and then fit the model to the toy data. The fitted values v_{Fitted}, uncertainties σ_{Fitted}, and the true (generated) values v_{True} are recorded for each pseudo-experiment, and the distribution of these quantities is used to determine the validity of the fitter.

The *pull* distributions are the most interesting object produced by these studies, where a single pull value p for a given parameter and pseudo-experiment is computed as

$$p = \frac{v_{\text{True}} - v_{\text{Fitted}}}{\sigma_{\text{Fitted}}} \tag{8.1}$$

The distribution of p for all toys should be a Gaussian with a mean μ of zero and a width σ of unity. If the mean of a pull distribution is not zero, the fitter is said to be biased in that parameter. If the width of the pull distribution if different from unity, the fitter is not correctly computing the uncertainty on the parameter.

The model used is the total, simultaneous PDF, described in Section 6, after having been fitted to the total data sample, described in Section 3. The events are generated independently within each p_{T}-y by sampling from the prompt, secondary, and background PDF, and then the same model is fitted to the toy data. The parameters of the 'generating' PDF are fixed between toys. The number of events sampled from each generating PDF is itself sampled from a Poisson distribution with an expectation value as the fitted value of the yield parameter of that PDF. The mean value of the each of the Gaussian background constraints is also sampled from the background constraint PDF itself [27].

This is repeated 300 times for the PDFs used to fit the $D^0 \to K^-\pi^+$, $D^+ \to K^-\pi^+\pi^+$, $D_s^+ \to \phi\pi^+$, and $D^{*+} \to D^0\pi^+$ with $D^0 \to K^-\pi^+$ samples, in order to cover the different sets of fixed and split shape parameters and the different purities.

Figures 8.5–8.4 shows the distribution of the mean and widths of the pull distributions for each fitter configuration, where the each pull mean and width was computed with a Gaussian fit to the respective pull distribution. There are no signs of bias in the fitter on either the central values or the uncertainties of the signal yields.

TODO: Add toy studies for modes other than $D^+ \to K^-\pi^+\pi^+$ and $D_s^+ \to \phi\pi^+$.

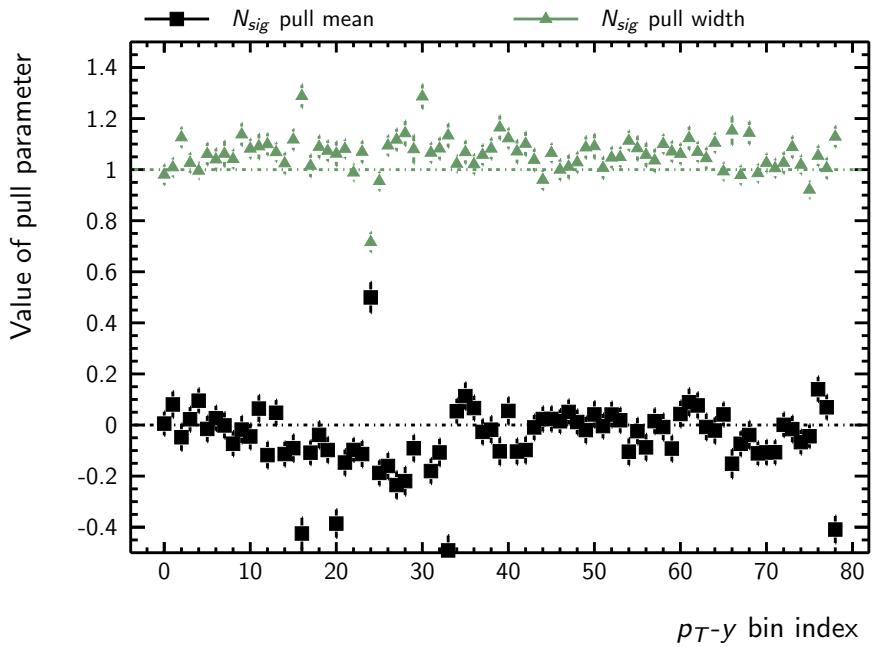

Figure 8.2: Distribution of prompt signal yield pull parameters for the PDF used in the $D^0 \to K^-\pi^+$ yield extraction. One pull distribution is computed for each per p_{T}-y bin, and the mean and width of each pull distribution is shown in black and green points, respectively. The bin index N_{Bin} runs first with increasing rapidity and then with increasing transverse momentum.

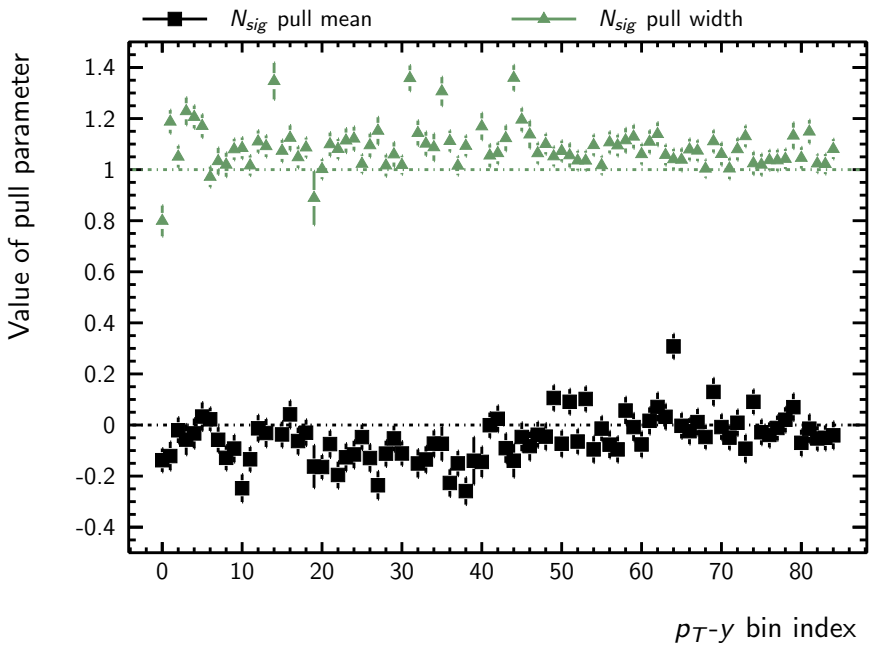

Figure 8.3: Distribution of prompt signal yield pull parameters for the PDF used in the $D^+ \to K^-\pi^+\pi^+$ yield extraction. One pull distribution is computed for each per p_{T}-y bin, and the mean and width of each pull distribution is shown in black and green points, respectively. The bin index N_{Bin} runs first with increasing rapidity and then with increasing transverse momentum.

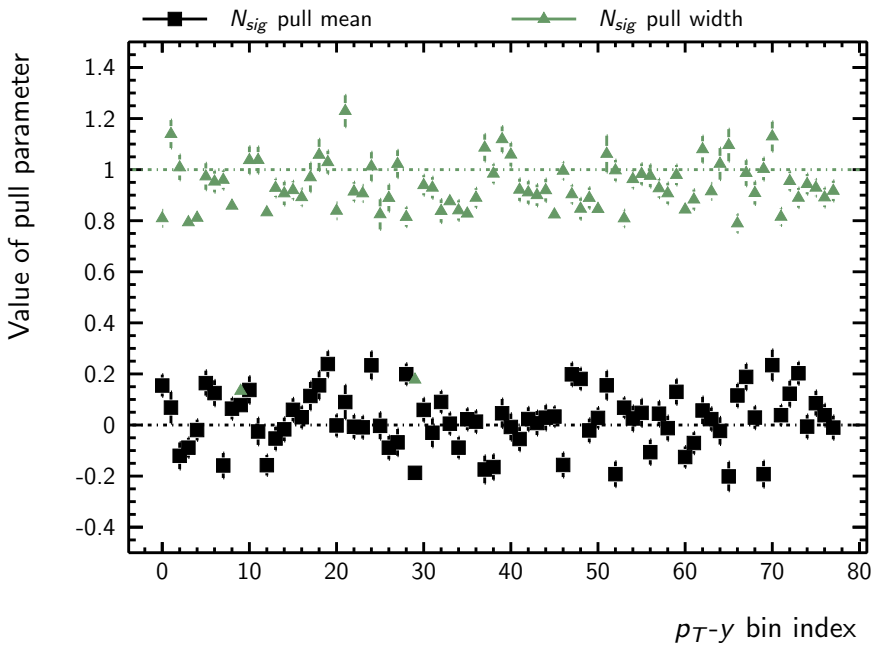

Figure 8.4: Distribution of prompt signal yield pull parameters for the PDF used in the $D_s^+ \to \phi\pi^+$ yield extraction. One pull distribution is computed for each per p_{T}-y bin, and the mean and width of each pull distribution is shown in black and green points, respectively. The bin index N_{Bin} runs first with increasing rapidity and then with increasing transverse momentum.

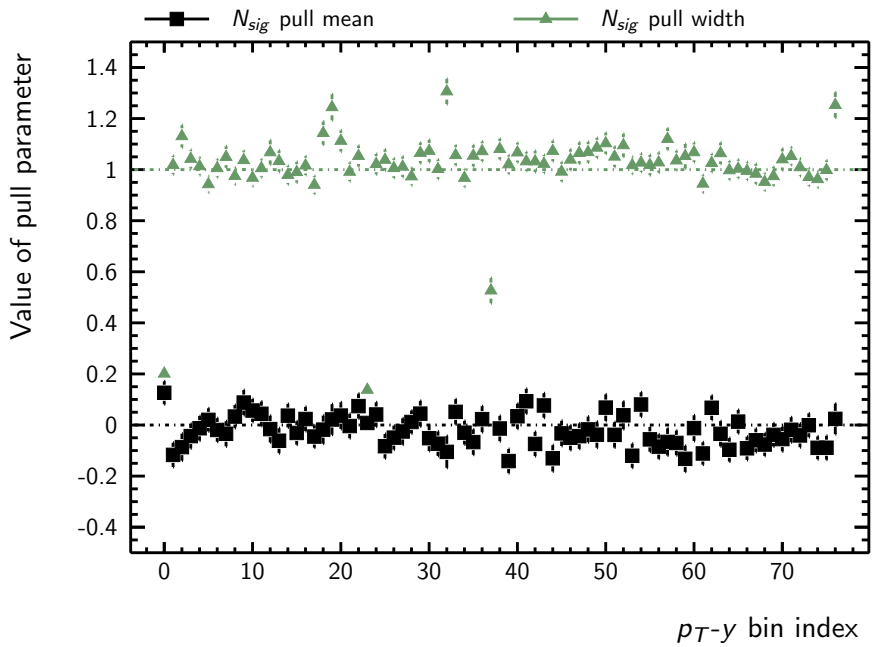

Figure 8.5: Distribution of prompt signal yield pull parameters for the PDF used in the $D^{*+} \to D^0\pi^+$ with $D^0 \to K^-\pi^+$ yield extraction. One pull distribution is computed for each per p_{T}-y bin, and the mean and width of each pull distribution is shown in black and green points, respectively. The bin index N_{Bin} runs first with increasing rapidity and then with increasing transverse momentum.

8.4 Relative cross-sections using 2011 $\sqrt{s} = 7\,\text{TeV}$ data

The entire analysis described in this note was applied to minimum bias data collected in 2011 at a centre-of-mass energy of $\sqrt{s} = 7\,\text{TeV}$ [28]. This section details that cross-check, describing the differences between the validation and the analysis proper. Unless explicitly stated otherwise, it should be assumed that the analysis procedure is identical to that described in the previous sections of this note.

The main difference is the dataset used. The data were selected by a minimum bias trigger at L0, which ran at a very low rate throughout 2011, corresponding to an as-yet undetermined amount integrated luminosity, and were processed during the Stripping 21 campaign. Not knowing the integrated luminosity prevents an absolute cross section measurement, but still permits relative measurements; either relative between open charm hadrons ($\sigma(D^0)/\sigma(D^{*+})$ for example) or normalised to a given p_{T}-y bin. The published results using the 2010 dataset [5] can be manipulated into these relative measurements, and as they were taken at the same centre-of-mass energy of $\sqrt{s} = 7\,\text{TeV}$ the two results can be directly compared. Any differences between the two results would be assumed to be due to problems in the newer analysis, and further investigation performed.

The same set of event types listed in Table 3.2 is generated, except for minimum bias Monte Carlo, event type 30000000, which is not used as there are mass sidebands in the data already available to use for background studies. One million generated signal candidates were used per magnet polarity per event type. The aforementioned mass sidebands in data are used as a background sample for BDT trainings. The beam crossing angles, defined in Section 3.4, were symmetric during 2011 and there was no vertical crossing angle, giving $\theta_{h,1} = -\theta_{h,2}$ and $\theta_{v,1} = \theta_{v,2} = \theta_v = 0$. The horizontal crossing angle was 520 µrad during magnet down data-taking and 20 µrad during magnet up.[9]

There were no exclusive open charm hadron trigger lines written for cross section measurements running in 2011. Instead, the data were selected by a set of minimum bias lines in HLT1, all starting with `Hlt1MB` and ending with `NoBias`, `RZVelo`, `RZVeloRateLimited`, `TStation`, and `TStationRateLimited`. The HLT2 trigger was the pass-through `Hlt2PassThrough` line. This trigger chain is assumed to be 100% efficient for the signal decays of interest, with respect to the reconstruction. The stripping selection applied in Stripping 21 is generally looser than that described in Section 4, in particular having no BDT discriminant requirement. This allows us to tighten the cuts to match those used in the 2015 analysis.

[9] Taken from the "LHC plans" presentation given by Burkhard Schmidt on 17th June 2013 (https://indico.cern.ch/event/226068/contribution/1/0).

All efficiencies are computed and applied in an manner identical to that described in Section 5, and the fitter used is identical to that described in Section 6.

Before evaluating the systematic uncertainties as described in Section 7, it is already possible to compare the results of the 2015 analysis applied to the 2011 data with the results published using the 2010 data. Only the lowest multiplicity Cabibbo-favoured decay modes are analysed. Results of the yield extraction are shown in Figures 8.6–8.13 and Tables 8.2–8.5. The total efficiency of the analysis is then shown in Figures 8.14–8.17 which includes the acceptance, reconstruction, selection, BDT and PID efficiencies along with the tracking correction. The final result for the normalised cross-section is then shown in Figures 8.18–8.21. The deviation tables show the absolute value of the difference between the 2010 result and the 2011 result in units of the statistical error. This error is calculated by propagating the error of each cross-section using liner error propagation.

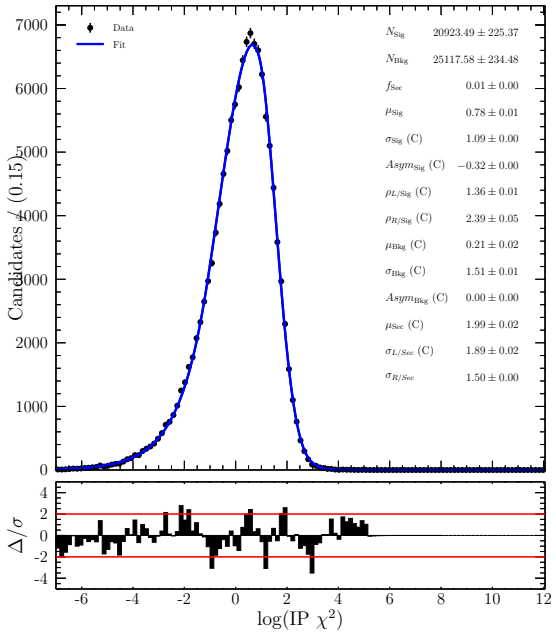

(a) Prompt signal

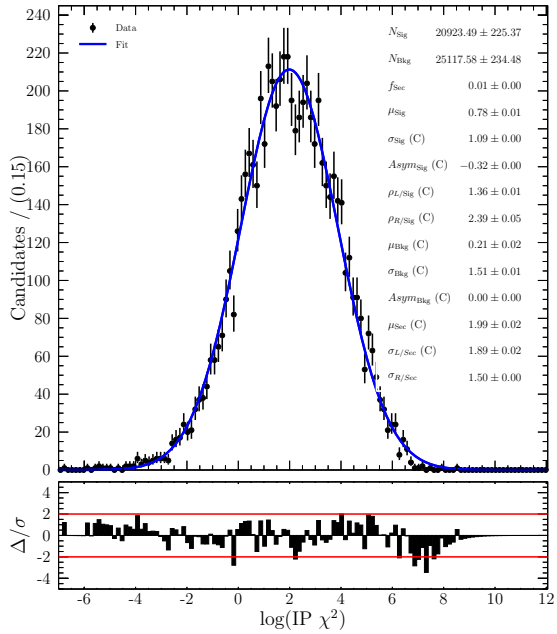

(b) Secondary signal

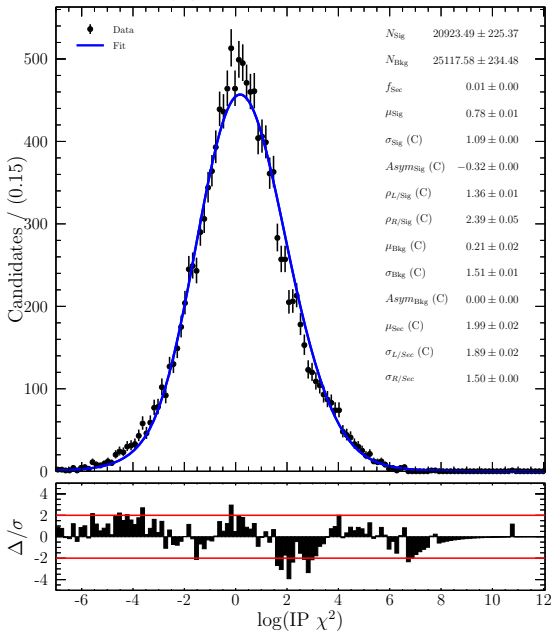

(c) Sidebands

Figure 8.6: Example $\ln \chi^2_{\rm IP}$ *prefits for* $D^0 \to K^-\pi^+$ *in the prompt signal sample, secondary signal sample, and data sidebands sample. The 2011 magnet down minimum bias and MC data are shown.*

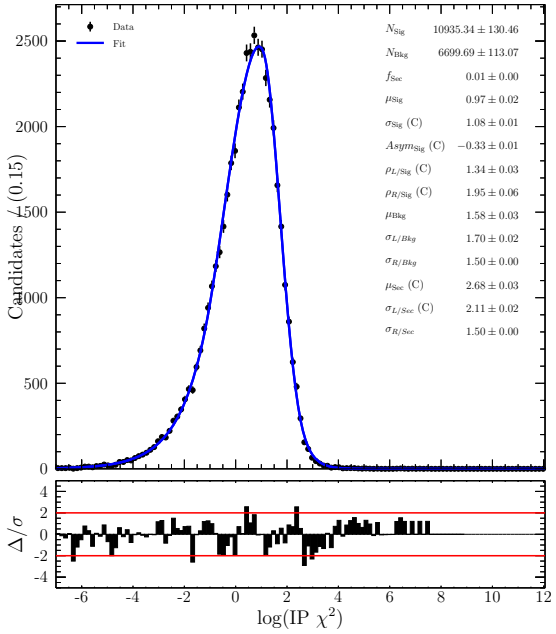

(a) Prompt signal

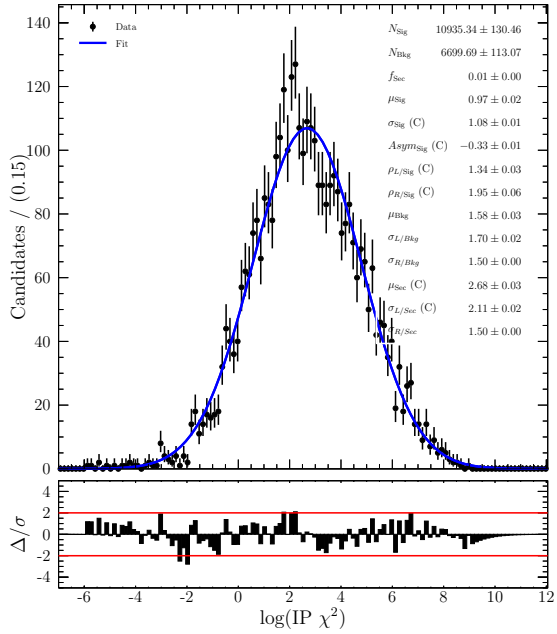

(b) Secondary signal

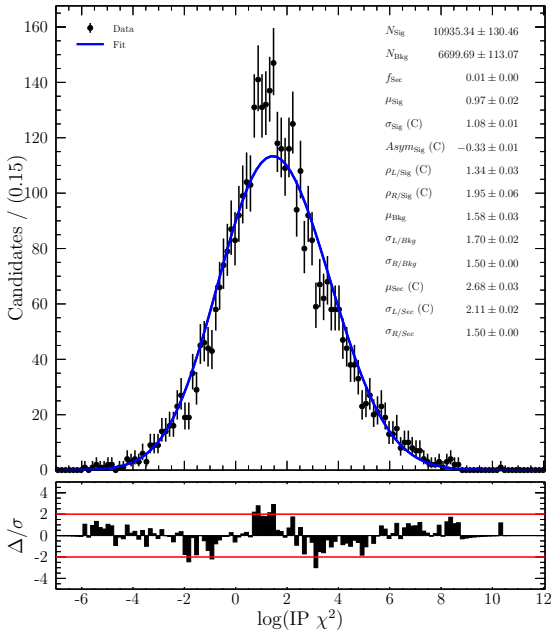

(c) Sidebands

Figure 8.7: Example $\ln\chi^2_{\rm IP}$ *prefits for* $D^+ \to K^-\pi^+\pi^+$ *in the prompt signal sample, secondary signal sample, and data sidebands sample. The 2011 magnet down minimum bias and MC data are shown.*

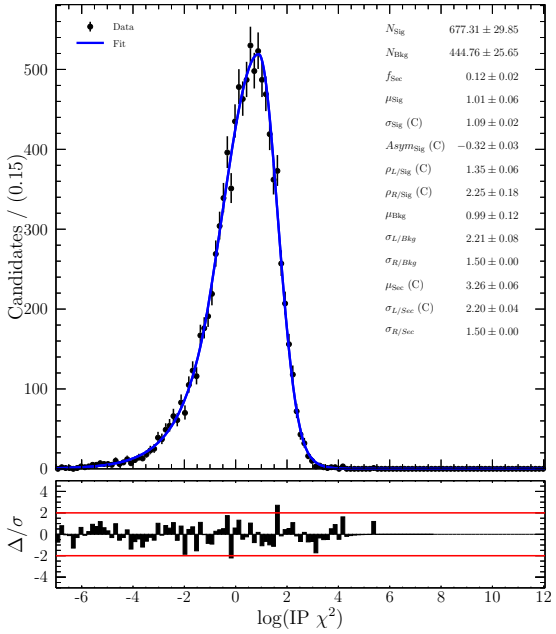

(a) Prompt signal

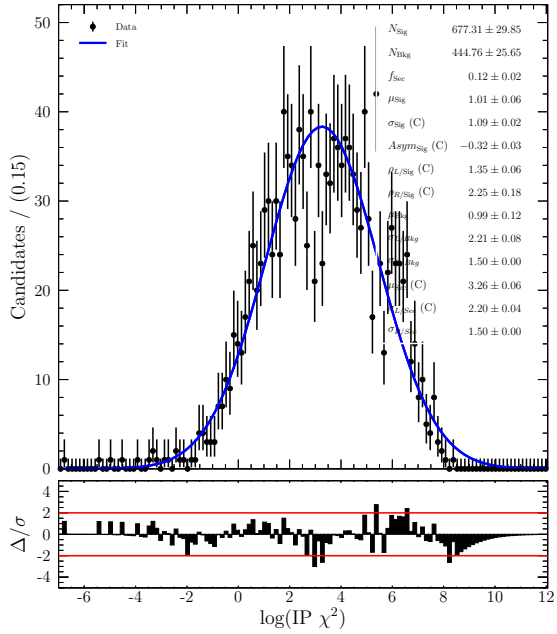

(b) Secondary signal

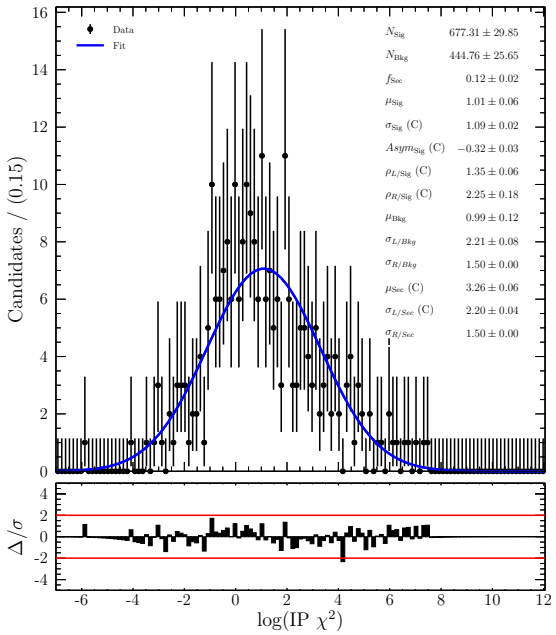

(c) Sidebands

Figure 8.8: Example $\ln \chi^2_{\rm IP}$ *prefits for* $D_s^+ \to \phi\pi^+$ *in the prompt signal sample, secondary signal sample, and data sidebands sample. The 2011 magnet down minimum bias and MC data are shown.*

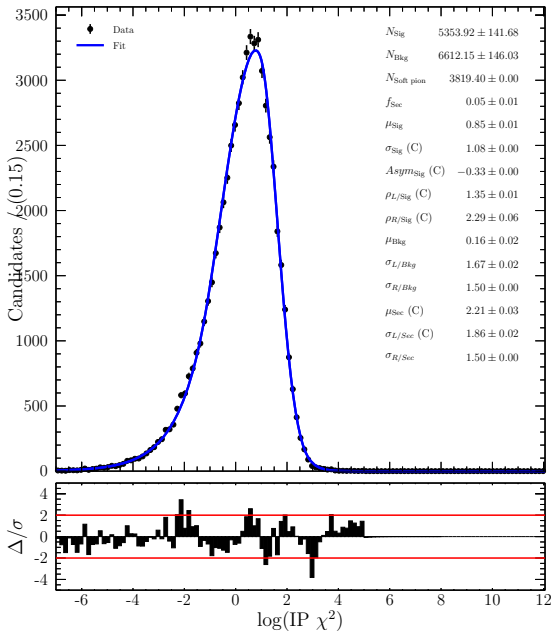

(a) Prompt signal

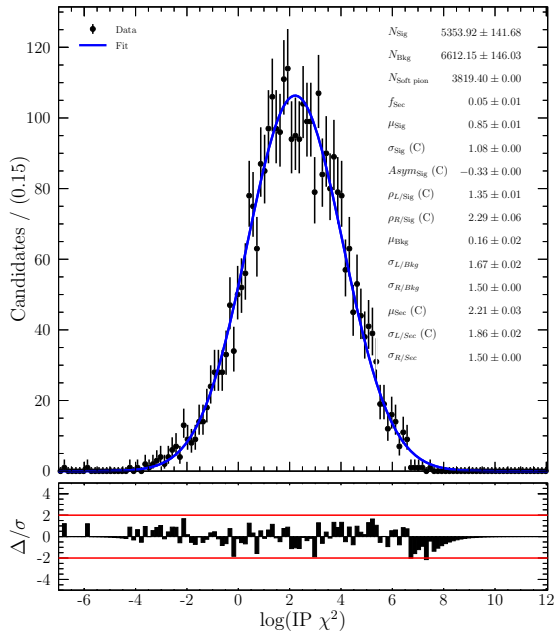

(b) Secondary signal

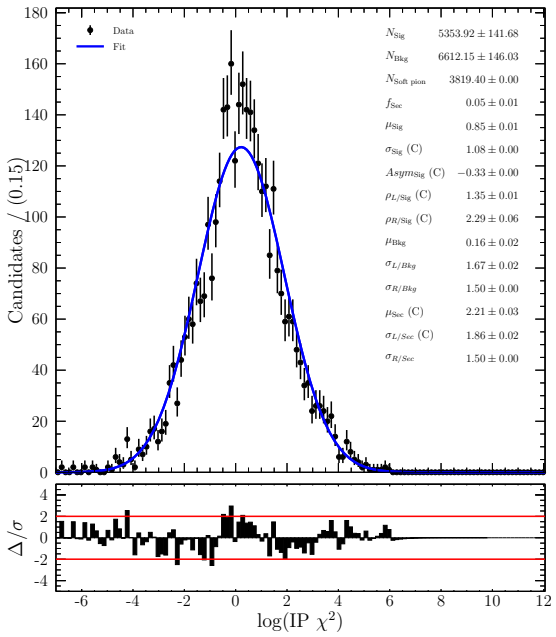

(c) Sidebands

Figure 8.9: Example $\ln \chi^2_{\rm IP}$ prefits for $D^{*+} \to D^0\pi^+$, with $D^0 \to K^-\pi^+$, in the prompt signal sample, secondary signal sample, and data sidebands sample. The 2011 magnet down minimum bias and MC data are shown.

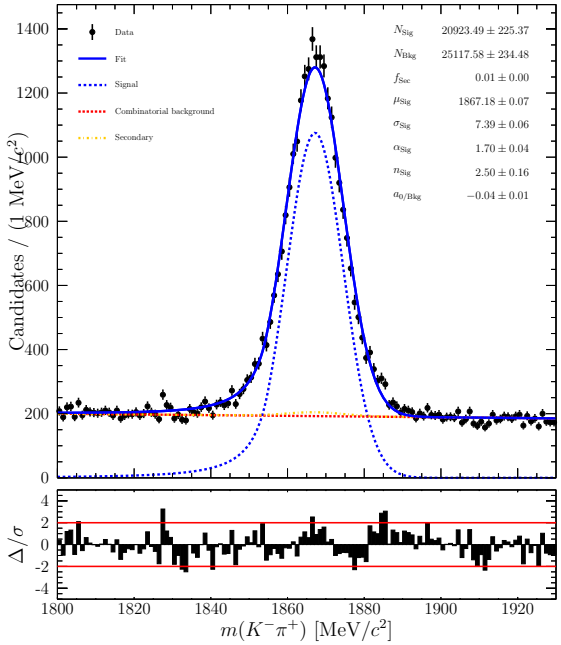

(a) Mass

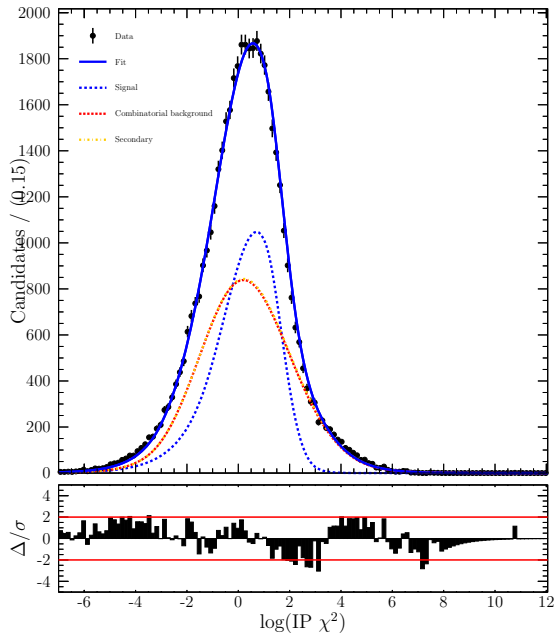

(b) $\ln\chi^2_{\rm IP}$

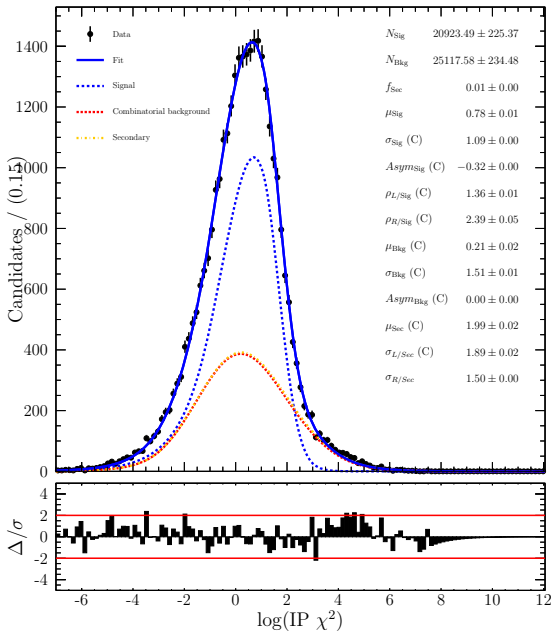

(c) $\ln\chi^2_{\rm IP}$ *in signal window*

Figure 8.10: Example fit projections for $D^0 \to K^-\pi^+$*, integrated across all* $p_{\rm T}$*-*y *bins, in mass,* $\ln\chi^2_{\rm IP}$*, and* $\ln\chi^2_{\rm IP}$ *within the* $m(K^-\pi^+)$ *signal region. The 2011 magnet down minimum bias data are shown.*

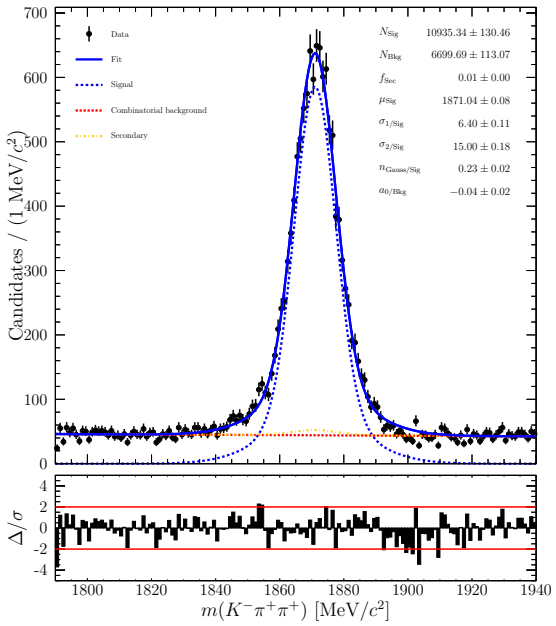

(a) Mass

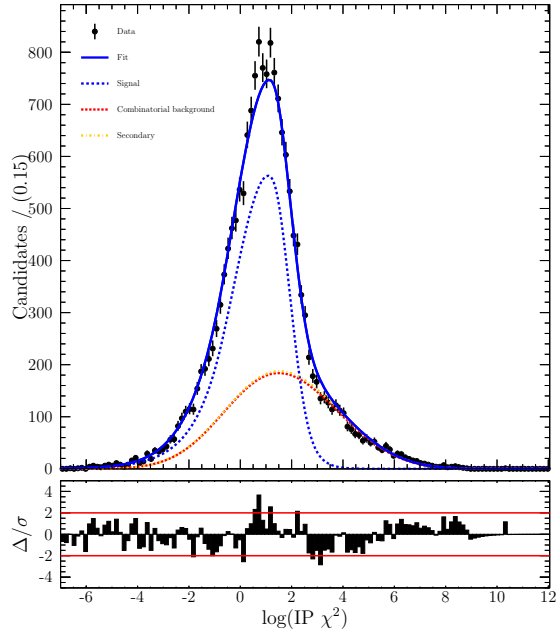

(b) $\ln \chi^2_{\rm IP}$

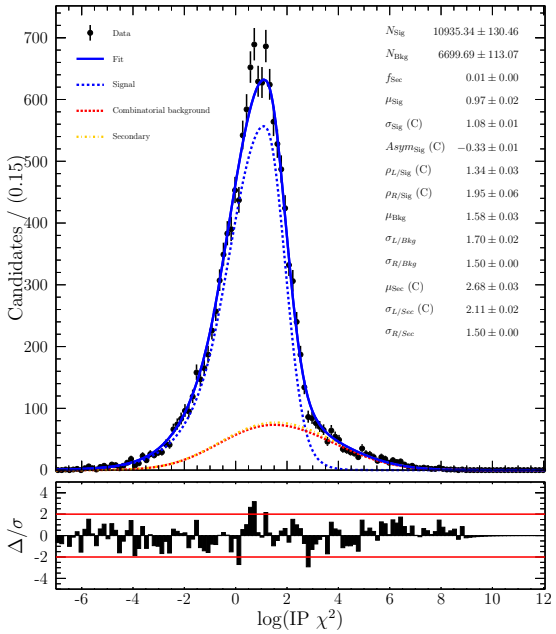

(c) $\ln \chi^2_{\rm IP}$ *in signal window*

Figure 8.11: Example fit projections for $D^+ \to K^-\pi^+\pi^+$*, integrated across all* $p_{\rm T}$*-y bins, in mass,* $\ln \chi^2_{\rm IP}$*, and* $\ln \chi^2_{\rm IP}$ *within the* $m(K^-\pi^+\pi^+)$ *signal region. The 2011 magnet down minimum bias data are shown.*

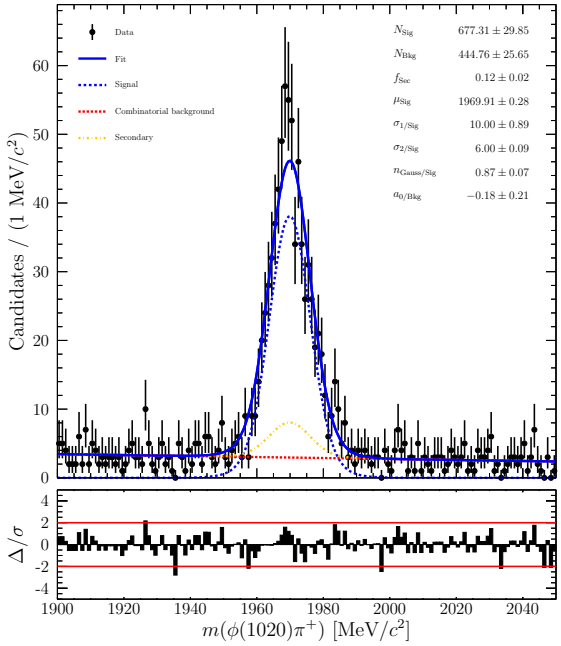

(a) Mass

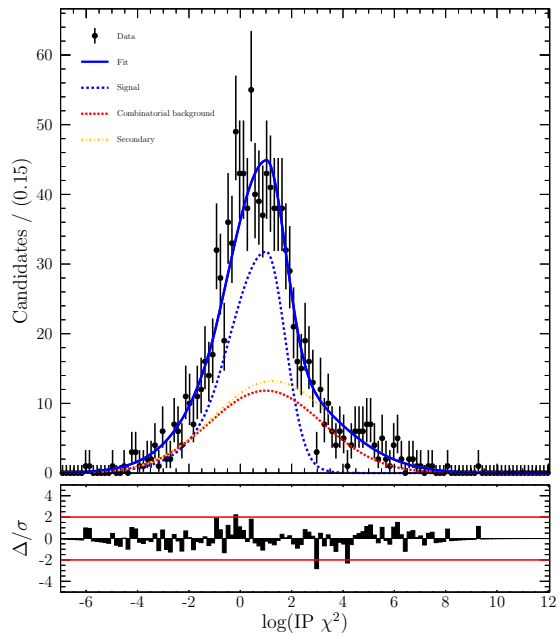

(b) $\ln\chi^2_{\rm IP}$

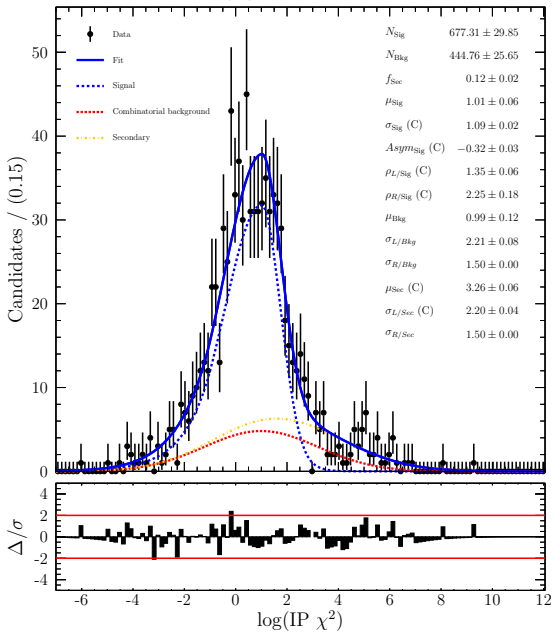

(c) $\ln\chi^2_{\rm IP}$ *in signal window*

Figure 8.12: Example fit projections for $D_s^+ \to \phi\pi^+$*, integrated across all* $p_{\rm T}$*-*y *bins, in mass,* $\ln\chi^2_{\rm IP}$*, and* $\ln\chi^2_{\rm IP}$ *within the* $m(\phi\pi^+)$ *signal region. The 2011 magnet down minimum bias data are shown.*

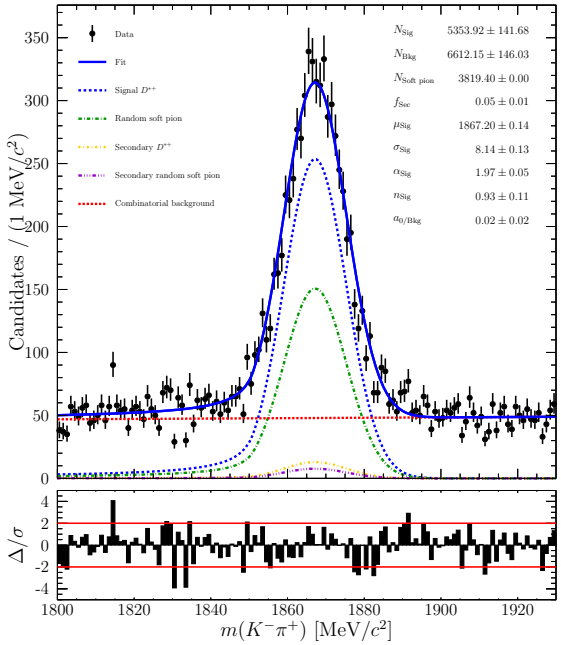

(a) Mass

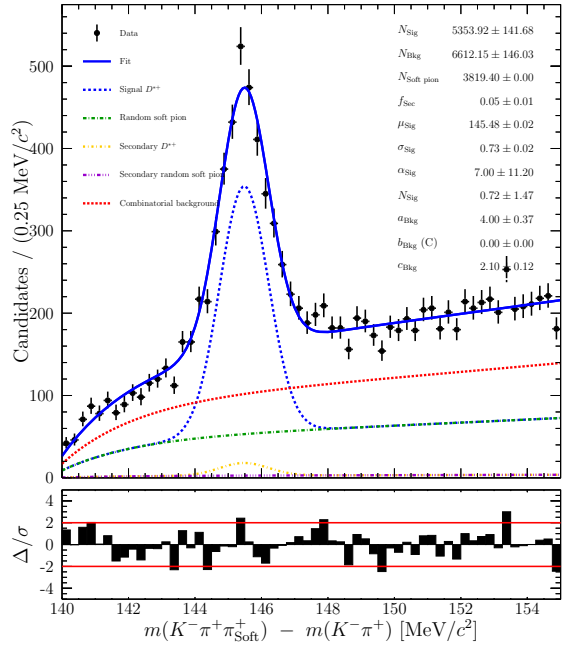

(b) δm

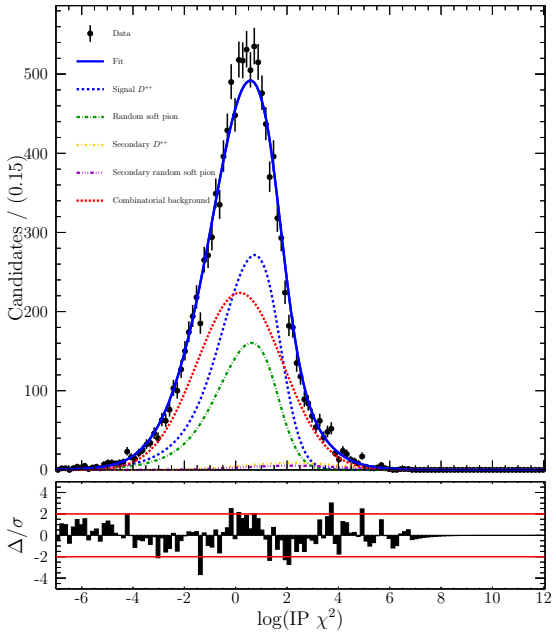

(c) $\ln \chi^2_{\rm IP}$

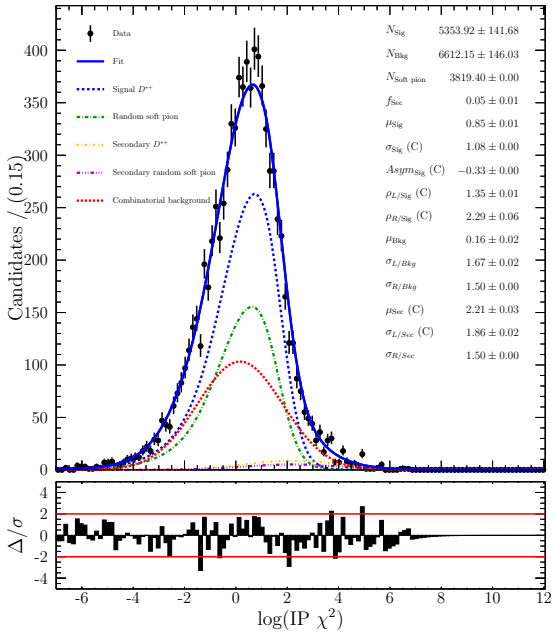

(d) $\ln \chi^2_{\rm IP}$ in signal window

Figure 8.13: Example fit projections for $D^{*+} \to D^0\pi^+$, with $D^0 \to K^-\pi^+$,, integrated across all $p_{\rm T}$-y bins, in mass, δm, $\ln \chi^2_{\rm IP}$, and $\ln \chi^2_{\rm IP}$ within the $m(K^-\pi^+)$ signal region. The 2011 magnet down minimum bias data are shown.

Table 8.2: Prompt signal yields for $D^0 \to K^-\pi^+$ in D^0 p_{T}-y bins. The yields are for the full 2011 dataset.

p_{T} [MeV]	y $[2, 2.5[$	$[2.5, 3[$	$[3, 3.5[$	$[3.5, 4[$	$[4, 4.5[$
$[0, 1000[$	283.3 ± 21.6	597.2 ± 31.4	568.4 ± 30.8	331.4 ± 23.9	60.0 ± 9.9
$[1000, 2000[$	579.5 ± 28.3	1405.7 ± 45.4	1229.5 ± 43.0	766.7 ± 34.0	182.4 ± 16.5
$[2000, 3000[$	588.1 ± 27.5	1426.9 ± 45.5	1292.9 ± 43.5	822.8 ± 33.7	198.1 ± 16.1
$[3000, 4000[$	472.2 ± 24.7	1043.4 ± 38.1	909.2 ± 35.3	465.2 ± 24.5	88.5 ± 10.5
$[4000, 5000[$	284.7 ± 19.3	484.2 ± 25.5	430.0 ± 23.7	227.3 ± 16.4	24.8 ± 5.5
$[5000, 6000[$	204.8 ± 16.3	237.2 ± 18.0	222.3 ± 16.8	94.8 ± 10.8	5.0 ± 2.2
$[6000, 7000[$	126.6 ± 12.7	133.9 ± 13.4	87.6 ± 10.7	29.5 ± 6.0	0.0 ± 0.0
$[7000, 8000[$	54.7 ± 8.5	82.4 ± 10.1	58.8 ± 8.4	6.6 ± 2.7	0.0 ± 0.0

Table 8.3: Prompt signal yields for $D^+ \to K^-\pi^+\pi^+$ in D^+ p_{T}-y bins. The yields are for the full 2011 dataset.

p_{T} [MeV]	y $[2, 2.5[$	$[2.5, 3[$	$[3, 3.5[$	$[3.5, 4[$	$[4, 4.5[$
$[0, 1000[$	283.3 ± 21.6	597.2 ± 31.4	568.4 ± 30.8	331.4 ± 23.9	60.0 ± 9.9
$[1000, 2000[$	579.5 ± 28.3	1405.7 ± 45.4	1229.5 ± 43.0	766.7 ± 34.0	182.4 ± 16.5
$[2000, 3000[$	588.1 ± 27.5	1426.9 ± 45.5	1292.9 ± 43.5	822.8 ± 33.7	198.1 ± 16.1
$[3000, 4000[$	472.2 ± 24.7	1043.4 ± 38.1	909.2 ± 35.3	465.2 ± 24.5	88.5 ± 10.5
$[4000, 5000[$	284.7 ± 19.3	484.2 ± 25.5	430.0 ± 23.7	227.3 ± 16.4	24.8 ± 5.5
$[5000, 6000[$	204.8 ± 16.3	237.2 ± 18.0	222.3 ± 16.8	94.8 ± 10.8	5.0 ± 2.2
$[6000, 7000[$	126.6 ± 12.7	133.9 ± 13.4	87.6 ± 10.7	29.5 ± 6.0	0.0 ± 0.0
$[7000, 8000[$	54.7 ± 8.5	82.4 ± 10.1	58.8 ± 8.4	6.6 ± 2.7	0.0 ± 0.0

Table 8.4: Prompt signal yields for $D_s^+ \to \phi\pi^+$ in D_s^+ p_{T}-y bins. The yields are for the full 2011 dataset.

p_{T} [MeV]	y $[2, 2.5[$	$[2.5, 3[$	$[3, 3.5[$	$[3.5, 4[$	$[4, 4.5[$
$[0, 1000[$	283.3 ± 21.6	597.2 ± 31.4	568.4 ± 30.8	331.4 ± 23.9	60.0 ± 9.9
$[1000, 2000[$	579.5 ± 28.3	1405.7 ± 45.4	1229.5 ± 43.0	766.7 ± 34.0	182.4 ± 16.5
$[2000, 3000[$	588.1 ± 27.5	1426.9 ± 45.5	1292.9 ± 43.5	822.8 ± 33.7	198.1 ± 16.1
$[3000, 4000[$	472.2 ± 24.7	1043.4 ± 38.1	909.2 ± 35.3	465.2 ± 24.5	88.5 ± 10.5
$[4000, 5000[$	284.7 ± 19.3	484.2 ± 25.5	430.0 ± 23.7	227.3 ± 16.4	24.8 ± 5.5
$[5000, 6000[$	204.8 ± 16.3	237.2 ± 18.0	222.3 ± 16.8	94.8 ± 10.8	5.0 ± 2.2
$[6000, 7000[$	126.6 ± 12.7	133.9 ± 13.4	87.6 ± 10.7	29.5 ± 6.0	0.0 ± 0.0
$[7000, 8000[$	54.7 ± 8.5	82.4 ± 10.1	58.8 ± 8.4	6.6 ± 2.7	0.0 ± 0.0

Table 8.5: Prompt signal yields for $D^{*+} \to D^0\pi^+$, with $D^0 \to K^-\pi^+$, in D^{*+} p_{T}-y bins. The yields are for the full 2011 dataset.

p_{T} [MeV]	y $[2, 2.5[$	$[2.5, 3[$	$[3, 3.5[$	$[3.5, 4[$	$[4, 4.5[$
$[0, 1000[$	283.3 ± 21.6	597.2 ± 31.4	568.4 ± 30.8	331.4 ± 23.9	60.0 ± 9.9
$[1000, 2000[$	579.5 ± 28.3	1405.7 ± 45.4	1229.5 ± 43.0	766.7 ± 34.0	182.4 ± 16.5
$[2000, 3000[$	588.1 ± 27.5	1426.9 ± 45.5	1292.9 ± 43.5	822.8 ± 33.7	198.1 ± 16.1
$[3000, 4000[$	472.2 ± 24.7	1043.4 ± 38.1	909.2 ± 35.3	465.2 ± 24.5	88.5 ± 10.5
$[4000, 5000[$	284.7 ± 19.3	484.2 ± 25.5	430.0 ± 23.7	227.3 ± 16.4	24.8 ± 5.5
$[5000, 6000[$	204.8 ± 16.3	237.2 ± 18.0	222.3 ± 16.8	94.8 ± 10.8	5.0 ± 2.2
$[6000, 7000[$	126.6 ± 12.7	133.9 ± 13.4	87.6 ± 10.7	29.5 ± 6.0	0.0 ± 0.0
$[7000, 8000[$	54.7 ± 8.5	82.4 ± 10.1	58.8 ± 8.4	6.6 ± 2.7	0.0 ± 0.0

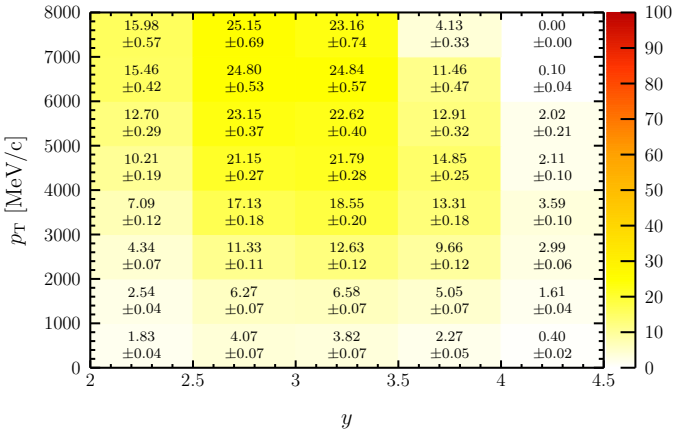

(a) MagDown

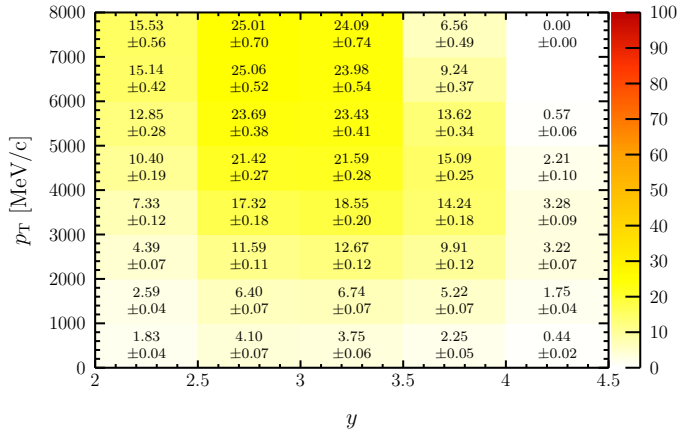

(b) MagUp

Figure 8.14: Total efficiency tables of $D^0 \to K^-\pi^+$ for the 2011 cross-check including the acceptance, reconstruction, tracking correction, selection and PID. The errors shown are purely statistical in nature.

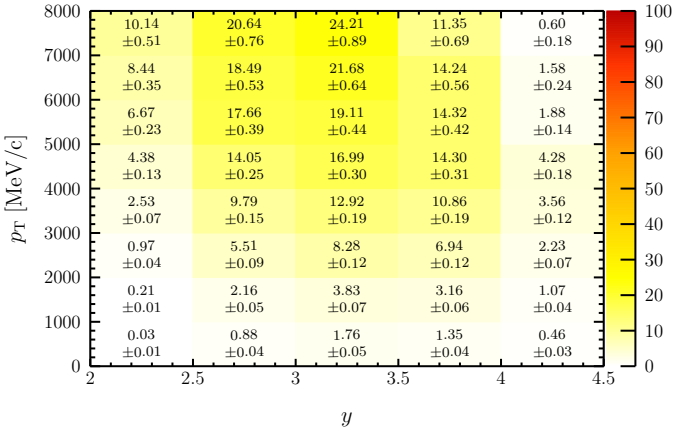

(a) MagDown

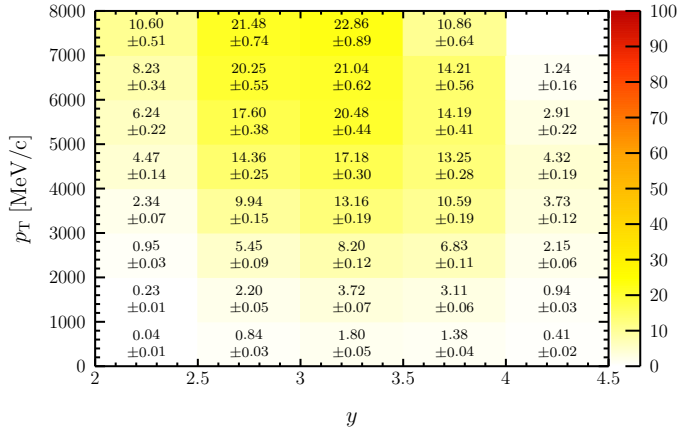

(b) MagUp

Figure 8.15: Total efficiency tables of $D^+ \to K^-\pi^+\pi^+$ for the 2011 cross-check including the acceptance, reconstruction, tracking correction, selection and PID. The errors shown are purely statistical in nature.

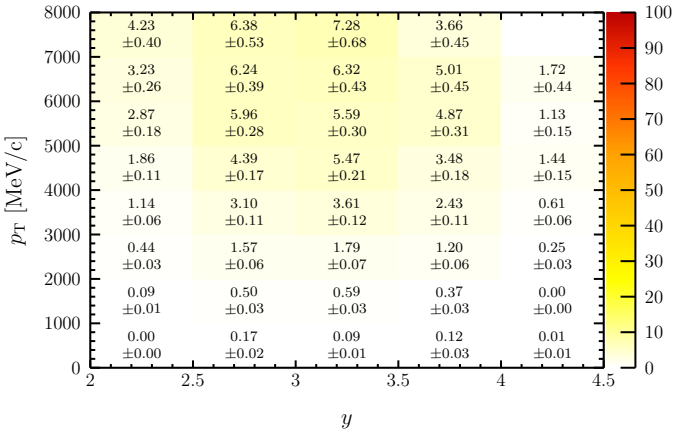

(a) MagDown

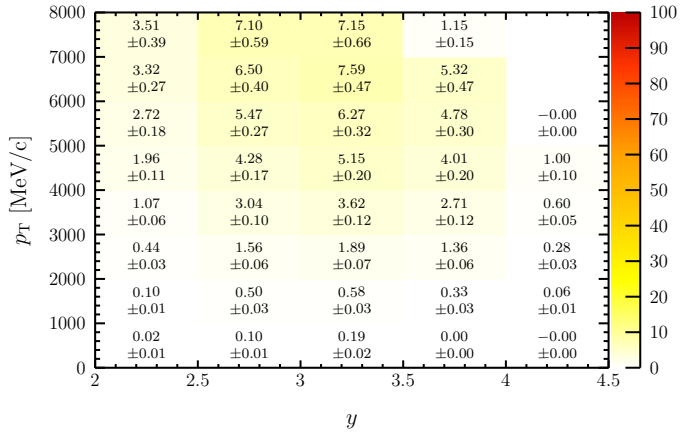

(b) MagUp

Figure 8.16: Total efficiency tables of $D_s^+ \to \phi\pi^+$ for the 2011 cross-check including the acceptance, reconstruction, tracking correction, selection and PID. The errors shown are purely statistical in nature.

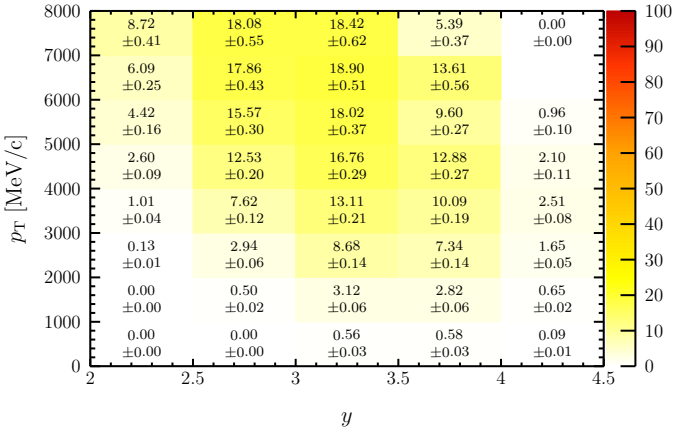

(a) MagDown

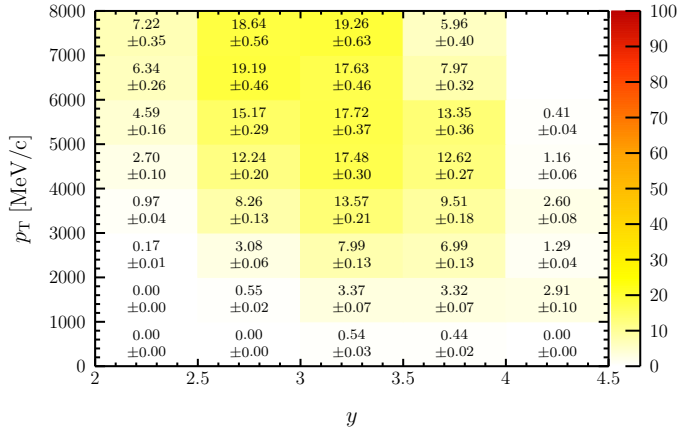

(b) MagUp

Figure 8.17: Total efficiency tables of $D^{*+} \to D^0\pi^+$, with $D^0 \to K^-\pi^+$, for the 2011 cross-check including the acceptance, reconstruction, tracking correction, selection and PID. The errors shown are purely statistical in nature.

p_T [MeV]	y [2.0, 2.5[	[2.5, 3.0[	[3.0, 3.5[	[3.5, 4.0[	[4.0, 4.5[
[0.0, 1000.0[	1.49 ± 0.12	1.67 ± 0.09	1.56 ± 0.09	1.46 ± 0.11	1.83 ± 0.27
[1000.0, 2000.0[	2.32 ± 0.13	2.35 ± 0.10	1.97 ± 0.09	1.66 ± 0.08	1.38 ± 0.11
[2000.0, 3000.0[	1.44 ± 0.07	1.28 ± 0.05	-	0.85 ± 0.04	0.78 ± 0.06
[3000.0, 4000.0[	0.71 ± 0.04	0.55 ± 0.03	0.47 ± 0.02	0.40 ± 0.02	0.25 ± 0.03
[4000.0, 5000.0[	0.30 ± 0.02	0.24 ± 0.01	0.21 ± 0.01	0.16 ± 0.01	0.10 ± 0.02
[5000.0, 6000.0[	0.16 ± 0.01	0.11 ± 0.01	0.09 ± 0.01	0.08 ± 0.01	0.01 ± 0.01
[6000.0, 7000.0[	0.09 ± 0.01	0.06 ± 0.01	0.05 ± 0.00	0.02 ± 0.00	-
[7000.0, 8000.0[	0.04 ± 0.01	0.04 ± 0.00	0.02 ± 0.00	0.01 ± 0.01	-

(a) 2011 MagDown normalised cross-section

p_T [MeV]	y [2.0, 2.5[	[2.5, 3.0[	[3.0, 3.5[	[3.5, 4.0[	[4.0, 4.5[
[0.0, 1000.0[	1.65 ± 0.14	1.52 ± 0.10	1.47 ± 0.10	1.51 ± 0.12	1.37 ± 0.26
[1000.0, 2000.0[	2.26 ± 0.14	2.19 ± 0.11	1.77 ± 0.09	1.47 ± 0.08	1.07 ± 0.11
[2000.0, 3000.0[	1.34 ± 0.08	1.17 ± 0.06	-	0.82 ± 0.04	0.65 ± 0.06
[3000.0, 4000.0[	0.61 ± 0.04	0.57 ± 0.03	0.47 ± 0.02	0.31 ± 0.02	0.26 ± 0.03
[4000.0, 5000.0[	0.28 ± 0.02	0.22 ± 0.01	0.19 ± 0.01	0.15 ± 0.01	0.11 ± 0.03
[5000.0, 6000.0[	0.16 ± 0.01	0.10 ± 0.01	0.10 ± 0.01	0.07 ± 0.01	0.09 ± 0.04
[6000.0, 7000.0[	0.08 ± 0.01	0.05 ± 0.01	0.03 ± 0.00	0.03 ± 0.01	-
[7000.0, 8000.0[	0.03 ± 0.01	0.03 ± 0.00	0.02 ± 0.00	0.01 ± 0.00	-

(b) 2011 MagUp normalised cross-section

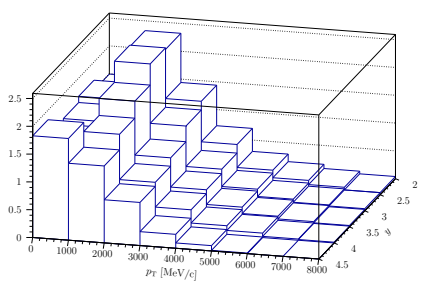

(c) 2011 MagDown

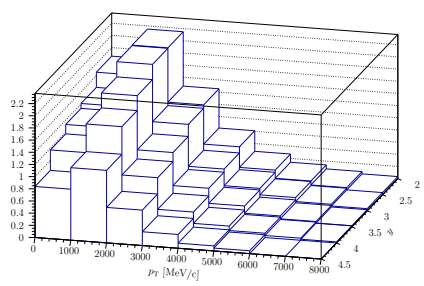

(d) 2010

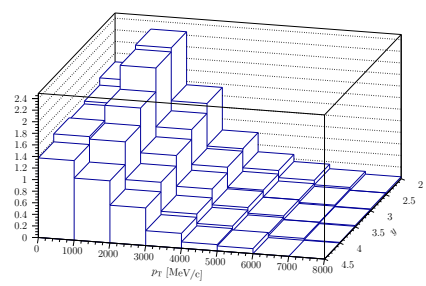

(e) 2011 MagUp

	[2.0, 2.5[	[2.5, 3.0[	[3.0, 3.5[	[3.5, 4.0[	[4.0, 4.5[
[0.0, 1000.0[	1.1σ	2.1σ	1.9σ	2.0σ	3.0σ
[1000.0, 2000.0[	1.0σ	1.5σ	0.7σ	0.2σ	1.3σ
[2000.0, 3000.0[	1.8σ	1.1σ	–	0.0σ	2.4σ
[3000.0, 4000.0[	1.8σ	1.3σ	0.5σ	2.3σ	0.7σ
[4000.0, 5000.0[	0.9σ	0.4σ	0.0σ	1.2σ	0.5σ
[5000.0, 6000.0[	1.4σ	1.6σ	0.4σ	0.8σ	5.3σ
[6000.0, 7000.0[	1.1σ	0.8σ	0.3σ	2.2σ	–
[7000.0, 8000.0[	0.5σ	0.4σ	1.0σ	0.4σ	–

(f) 2011 MagDown deviations

	[2.0, 2.5[	[2.5, 3.0[	[3.0, 3.5[	[3.5, 4.0[	[4.0, 4.5[
[0.0, 1000.0[	0.1σ	0.9σ	1.2σ	2.2σ	1.8σ
[1000.0, 2000.0[	0.6σ	0.3σ	1.0σ	1.6σ	0.9σ
[2000.0, 3000.0[	0.8σ	0.4σ	–	0.6σ	0.9σ
[3000.0, 4000.0[	0.0σ	1.5σ	0.3σ	0.6σ	0.8σ
[4000.0, 5000.0[	0.2σ	1.0σ	0.9σ	0.4σ	0.9σ
[5000.0, 6000.0[	1.1σ	3.0σ	0.5σ	0.4σ	0.8σ
[6000.0, 7000.0[	0.6σ	1.6σ	1.6σ	0.3σ	–
[7000.0, 8000.0[	0.3σ	0.7σ	0.8σ	1.3σ	–

(g) 2011 MagUp deviations

Figure 8.18: Cross-check results of the $D^0 \to K^-\pi^+$ cross-section normalised to $2\,\mathrm{GeV} < p_T < 3\,\mathrm{GeV}$ and $3.0 < \eta < 3.5$. Calculated using 2011 data for comparison with the published 2010 result. Only statistical errors are included in the comparison between 2010 and 2011 and these are assumed to be fully uncorrelated.

p_{T} [MeV]	y [2.0, 2.5[	[2.5, 3.0[	[3.0, 3.5[	[3.5, 4.0[	[4.0, 4.5[
[0.0, 1000.0[	1.51 ± 0.34	1.36 ± 0.06	1.36 ± 0.05	1.15 ± 0.04	0.88 ± 0.06
[1000.0, 2000.0[	2.13 ± 0.15	2.12 ± 0.06	2.39 ± 0.066	1.49 ± 0.04	1.18 ± 0.05
[2000.0, 3000.0[	1.33 ± 0.05	1.16 ± 0.03	-	0.72 ± 0.02	0.65 ± 0.02
[3000.0, 4000.0[	0.66 ± 0.02	0.57 ± 0.01	0.48 ± 0.01	0.32 ± 0.01	0.24 ± 0.01
[4000.0, 5000.0[	0.27 ± 0.01	0.26 ± 0.01	0.21 ± 0.00	0.15 ± 0.00	0.11 ± 0.01
[5000.0, 6000.0[	0.14 ± 0.01	0.12 ± 0.00	0.10 ± 0.00	0.07 ± 0.00	0.05 ± 0.00
[6000.0, 7000.0[	0.07 ± 0.00	0.07 ± 0.00	0.04 ± 0.00	0.03 ± 0.00	0.02 ± 0.00
[7000.0, 8000.0[	0.03 ± 0.00	0.03 ± 0.00	0.02 ± 0.00	0.02 ± 0.00	-

(a) 2011 MagDown normalised cross-section

p_{T} [MeV]	y [2.0, 2.5[	[2.5, 3.0[	[3.0, 3.5[	[3.5, 4.0[	[4.0, 4.5[
[0.0, 1000.0[	1.60 ± 0.74	1.28 ± 0.15	1.14 ± 0.11	0.94 ± 0.11	1.18 ± 0.22
[1000.0, 2000.0[	2.37 ± 0.36	1.77 ± 0.12	1.76 ± 0.11	1.44 ± 0.10	1.42 ± 0.15
[2000.0, 3000.0[	1.11 ± 0.12	1.14 ± 0.07	-	0.73 ± 0.05	0.60 ± 0.06
[3000.0, 4000.0[	0.73 ± 0.07	0.54 ± 0.03	0.42 ± 0.03	0.32 ± 0.02	0.27 ± 0.03
[4000.0, 5000.0[	0.31 ± 0.03	0.22 ± 0.02	0.19 ± 0.01	0.12 ± 0.01	0.09 ± 0.02
[5000.0, 6000.0[	0.12 ± 0.02	0.12 ± 0.01	0.08 ± 0.01	0.07 ± 0.01	0.04 ± 0.01
[6000.0, 7000.0[	0.07 ± 0.01	0.05 ± 0.01	0.06 ± 0.01	0.03 ± 0.00	0.02 ± 0.01
[7000.0, 8000.0[	0.03 ± 0.01	0.03 ± 0.00	0.02 ± 0.00	0.01 ± 0.00	-

(b) 2011 MagUp normalised cross-section

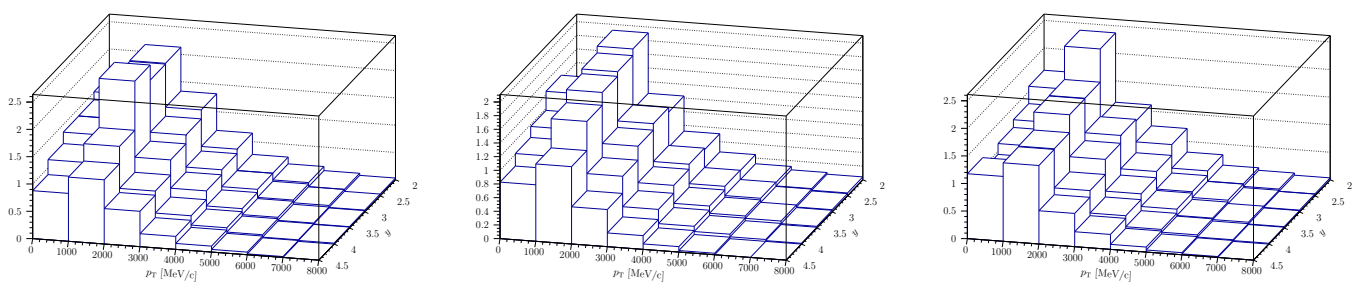

(c) 2011 MagDown *(d) 2010* *(e) 2011 MagUp*

	[2.0, 2.5[	[2.5, 3.0[	[3.0, 3.5[	[3.5, 4.0[	[4.0, 4.5[
[0.0, 1000.0[	–	0.7σ	1.9σ	1.4σ	0.4σ
[1000.0, 2000.0[	0.7σ	2.2σ	4.6σ	0.7σ	0.4σ
[2000.0, 3000.0[	2.3σ	1.0σ	–	1.7σ	1.7σ
[3000.0, 4000.0[	2.5σ	1.0σ	0.6σ	1.4σ	1.4σ
[4000.0, 5000.0[	0.7σ	0.5σ	0.2σ	0.7σ	1.8σ
[5000.0, 6000.0[	1.8σ	0.2σ	0.0σ	0.9σ	1.8σ
[6000.0, 7000.0[	0.3σ	1.4σ	5.5σ	0.1σ	–
[7000.0, 8000.0[	2.2σ	0.1σ	0.0σ	1.5σ	–

(f) 2011 MagDown deviations

	[2.0, 2.5[	[2.5, 3.0[	[3.0, 3.5[	[3.5, 4.0[	[4.0, 4.5[
[0.0, 1000.0[	–	0.9σ	0.2σ	0.5σ	1.3σ
[1000.0, 2000.0[	1.0σ	0.3σ	0.1σ	1.0σ	1.5σ
[2000.0, 3000.0[	0.5σ	0.5σ	–	1.1σ	0.7σ
[3000.0, 4000.0[	2.5σ	0.1σ	1.2σ	1.0σ	1.7σ
[4000.0, 5000.0[	1.4σ	1.8σ	0.4σ	1.6σ	0.6σ
[5000.0, 6000.0[	0.2σ	0.5σ	1.6σ	0.3σ	1.0σ
[6000.0, 7000.0[	0.5σ	1.0σ	0.9σ	0.3σ	–
[7000.0, 8000.0[	1.0σ	0.0σ	0.1σ	0.7σ	–

(g) 2011 MagUp deviations

Figure 8.19: Cross-check results of the $D^+ \to K^-\pi^+\pi^+$ cross-section normalised to $2\,\mathrm{GeV} < p_{\mathrm{T}} < 3\,\mathrm{GeV}$ and $3.0 < \eta < 3.5$. Calculated using 2011 data for comparison with the published 2010 result. Only statistical errors are included in the comparison between 2010 and 2011 and these are assumed to be fully uncorrelated.

p_{T} [MeV]	y [2.0, 2.5[	[2.5, 3.0[	[3.0, 3.5[	[3.5, 4.0[	[4.0, 4.5[
[0.0, 1000.0[	-	0.49 ± 0.42	1.89 ± 1.29	-	5.35 ± 6.02
[1000.0, 2000.0[	2.57 ± 1.14	1.40 ± 0.42	1.65 ± 0.44	1.23 ± 0.46	-
[2000.0, 3000.0[	0.67 ± 0.26	1.16 ± 0.25	-	1.07 ± 0.26	1.04 ± 0.45
[3000.0, 4000.0[	0.76 ± 0.20	0.59 ± 0.13	0.74 ± 0.14	0.39 ± 0.10	0.51 ± 0.20
[4000.0, 5000.0[	0.38 ± 0.10	0.21 ± 0.05	0.22 ± 0.05	0.10 ± 0.04	0.10 ± 0.06
[5000.0, 6000.0[	0.12 ± 0.04	0.11 ± 0.03	0.09 ± 0.03	0.08 ± 0.03	-
[6000.0, 7000.0[	0.09 ± 0.03	0.07 ± 0.02	0.09 ± 0.03	0.02 ± 0.01	-
[7000.0, 8000.0[	0.08 ± 0.03	0.04 ± 0.02	0.03 ± 0.02	0.04 ± 0.02	-

(a) 2011 MagDown normalised cross-section

p_{T} [MeV]	y [2.0, 2.5[	[2.5, 3.0[	[3.0, 3.5[	[3.5, 4.0[	[4.0, 4.5[
[0.0, 1000.0[	-	0.48 ± 0.63	0.57 ± 0.60	-	-
[1000.0, 2000.0[	2.53 ± 1.17	1.29 ± 0.44	2.54 ± 0.69	1.21 ± 0.54	-
[2000.0, 3000.0[	1.57 ± 0.48	1.25 ± 0.30	-	0.50 ± 0.17	0.85 ± 0.43
[3000.0, 4000.0[	0.65 ± 0.20	0.50 ± 0.13	0.45 ± 0.11	0.28 ± 0.09	0.28 ± 0.17
[4000.0, 5000.0[	0.41 ± 0.12	0.28 ± 0.07	0.31 ± 0.08	0.20 ± 0.06	0.14 ± 0.09
[5000.0, 6000.0[	0.18 ± 0.06	0.17 ± 0.05	0.14 ± 0.04	0.08 ± 0.03	-
[6000.0, 7000.0[	0.12 ± 0.05	0.13 ± 0.04	0.05 ± 0.02	0.05 ± 0.02	-
[7000.0, 8000.0[	0.05 ± 0.03	0.02 ± 0.02	0.03 ± 0.02	0.07 ± 0.05	-

(b) 2011 MagUp normalised cross-section

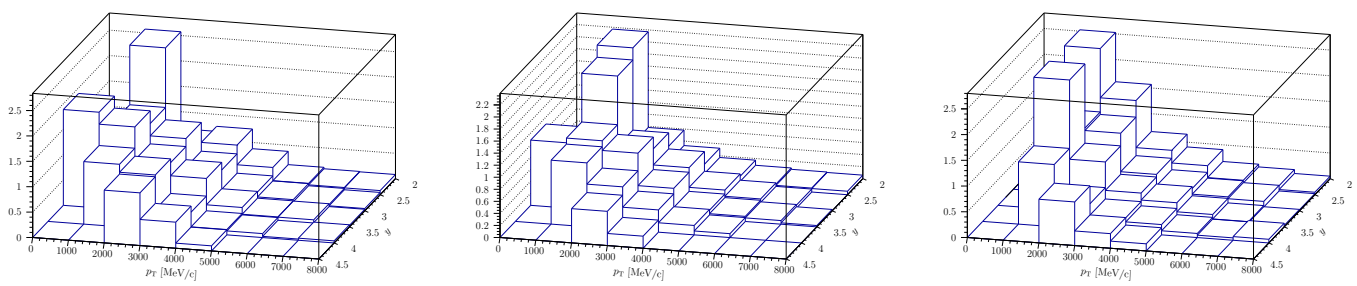

(c) 2011 MagDown *(d) 2010* *(e) 2011 MagUp*

	[2.0, 2.5[	[2.5, 3.0[	[3.0, 3.5[	[3.5, 4.0[	[4.0, 4.5[
[0.0, 1000.0[	–	–	0.6σ	–	–
[1000.0, 2000.0[	0.3σ	1.1σ	0.9σ	0.3σ	–
[2000.0, 3000.0[	0.2σ	1.1σ	–	1.0σ	0.8σ
[3000.0, 4000.0[	1.4σ	0.3σ	1.4σ	0.2σ	1.0σ
[4000.0, 5000.0[	1.3σ	0.0σ	1.1σ	1.1σ	–
[5000.0, 6000.0[	0.5σ	0.2σ	0.1σ	0.3σ	–
[6000.0, 7000.0[	0.5σ	0.6σ	0.7σ	–	–
[7000.0, 8000.0[	0.6σ	–	0.4σ	–	–

(f) 2011 MagDown deviations

	[2.0, 2.5[	[2.5, 3.0[	[3.0, 3.5[	[3.5, 4.0[	[4.0, 4.5[
[0.0, 1000.0[	–	–	0.8σ	–	–
[1000.0, 2000.0[	0.2σ	1.3σ	1.6σ	0.2σ	–
[2000.0, 3000.0[	1.4σ	1.2σ	–	1.0σ	0.5σ
[3000.0, 4000.0[	1.2σ	0.3σ	0.1σ	0.8σ	0.4σ
[4000.0, 5000.0[	1.3σ	0.7σ	1.6σ	0.5σ	–
[5000.0, 6000.0[	0.9σ	0.9σ	0.9σ	0.4σ	–
[6000.0, 7000.0[	0.9σ	1.4σ	0.4σ	–	–
[7000.0, 8000.0[	0.3σ	–	0.3σ	–	–

(g) 2011 MagUp deviations

Figure 8.20: Cross-check results of the $D_s^+ \to \phi\pi^+$ cross-section normalised to $2\,\mathrm{GeV} < p_{\mathrm{T}} < 3\,\mathrm{GeV}$ and $3.0 < \eta < 3.5$. Calculated using 2011 data for comparison with the published 2010 result. Only statistical errors are included in the comparison between 2010 and 2011 and these are assumed to be fully uncorrelated.

p_{T} [MeV]	y [2.0, 2.5[	[2.5, 3.0[	[3.0, 3.5[	[3.5, 4.0[	[4.0, 4.5[
[0.0, 1000.0[	-	-	0.99 ± 0.45	0.71 ± 0.37	0.99 ± 0.87
[1000.0, 2000.0[	-	1.92 ± 0.52	-	0.98 ± 0.17	0.96 ± 0.33
[2000.0, 3000.0[	1.53 ± 0.72	1.20 ± 0.15	-	0.81 ± 0.10	0.88 ± 0.18
[3000.0, 4000.0[	0.60 ± 0.16	0.60 ± 0.07	0.56 ± 0.06	0.36 ± 0.05	0.42 ± 0.09
[4000.0, 5000.0[	0.32 ± 0.07	0.32 ± 0.04	0.24 ± 0.03	0.15 ± 0.02	0.11 ± 0.05
[5000.0, 6000.0[	0.19 ± 0.04	0.14 ± 0.02	0.14 ± 0.02	0.13 ± 0.03	0.08 ± 0.05
[6000.0, 7000.0[	0.07 ± 0.02	0.08 ± 0.01	0.07 ± 0.01	0.03 ± 0.01	-
[7000.0, 8000.0[	0.03 ± 0.01	0.06 ± 0.01	0.02 ± 0.01	0.04 ± 0.02	-

(a) 2011 MagDown normalised cross-section

p_{T} [MeV]	y [2.0, 2.5[	[2.5, 3.0[	[3.0, 3.5[	[3.5, 4.0[	[4.0, 4.5[
[0.0, 1000.0[	-	-	2.02 ± 0.73	0.48 ± 0.75	-
[1000.0, 2000.0[	-	1.60 ± 0.45	1.00 ± 0.18	1.20 ± 0.19	0.36 ± 0.11
[2000.0, 3000.0[	-	1.16 ± 0.17	-	0.62 ± 0.09	1.05 ± 0.23
[3000.0, 4000.0[	0.50 ± 0.16	0.48 ± 0.07	0.49 ± 0.06	0.41 ± 0.06	0.28 ± 0.08
[4000.0, 5000.0[	0.28 ± 0.07	0.29 ± 0.04	0.22 ± 0.03	0.16 ± 0.03	0.12 ± 0.09
[5000.0, 6000.0[	0.21 ± 0.05	0.15 ± 0.02	0.10 ± 0.02	0.05 ± 0.01	-
[6000.0, 7000.0[	0.13 ± 0.03	0.04 ± 0.01	0.06 ± 0.01	0.03 ± 0.01	-
[7000.0, 8000.0[	0.08 ± 0.02	0.05 ± 0.01	0.02 ± 0.01	0.02 ± 0.01	-

(b) 2011 MagUp normalised cross-section

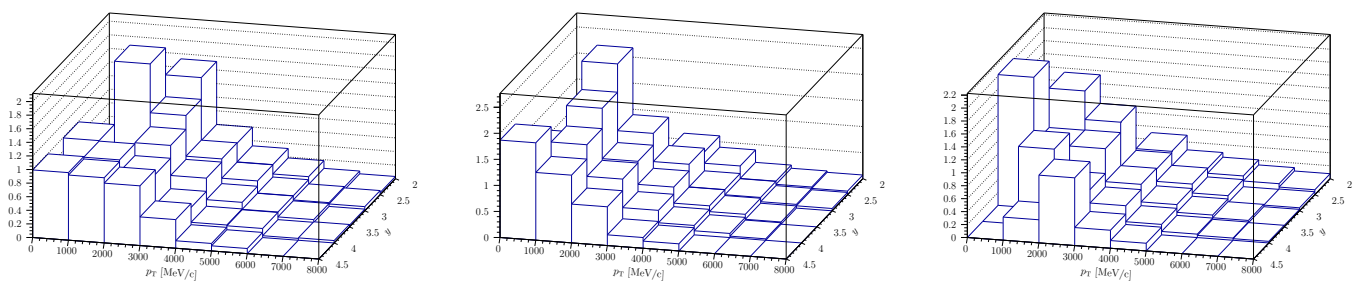

(c) 2011 MagDown *(d) 2010* *(e) 2011 MagUp*

	[2.0, 2.5[	[2.5, 3.0[	[3.0, 3.5[	[3.5, 4.0[	[4.0, 4.5[
[0.0, 1000.0[	–	–	0.1σ	2.0σ	1.0σ
[1000.0, 2000.0[	–	1.0σ	29.6σ	3.0σ	1.0σ
[2000.0, 3000.0[	–	0.1σ	–	1.3σ	0.6σ
[3000.0, 4000.0[	0.1σ	0.8σ	0.0σ	0.9σ	1.7σ
[4000.0, 5000.0[	0.8σ	1.2σ	0.2σ	1.1σ	0.5σ
[5000.0, 6000.0[	0.5σ	0.4σ	0.1σ	1.5σ	–
[6000.0, 7000.0[	0.8σ	0.4σ	1.2σ	0.0σ	–
[7000.0, 8000.0[	2.4σ	0.8σ	–	–	–

(f) 2011 MagDown deviations

	[2.0, 2.5[	[2.5, 3.0[	[3.0, 3.5[	[3.5, 4.0[	[4.0, 4.5[
[0.0, 1000.0[	–	–	1.2σ	1.3σ	–
[1000.0, 2000.0[	–	1.8σ	4.7σ	1.6σ	8.0σ
[2000.0, 3000.0[	–	0.3σ	–	3.2σ	1.1σ
[3000.0, 4000.0[	0.6σ	2.5σ	0.9σ	0.1σ	0.7σ
[4000.0, 5000.0[	1.4σ	0.7σ	0.8σ	0.5σ	0.2σ
[5000.0, 6000.0[	0.8σ	0.1σ	1.7σ	1.5σ	–
[6000.0, 7000.0[	0.7σ	2.3σ	0.8σ	0.3σ	–
[7000.0, 8000.0[	0.2σ	0.1σ	–	–	–

(g) 2011 MagUp deviations

Figure 8.21: Cross-check results of the $D^{*+} \to D^0\pi^+$, with $D^0 \to K^-\pi^+$, cross-section normalised to $2\,\mathrm{GeV} < p_{\mathrm{T}} < 3\,\mathrm{GeV}$ and $3.0 < \eta < 3.5$. Calculated using 2011 data for comparison with the published 2010 result. Only statistical errors are included in the comparison between 2010 and 2011 and these are assumed to be fully uncorrelated.

9 Results

The cross-sections for prompt D^0, D^+, D_s^+, and D^{*+} hadrons in pp collisions at $\sqrt{s} = 13\,\text{TeV}$ are given in Tables 9.3–9.6, in bins of charm hadron p_T and y as measured in the proton-proton collision rest frame. Those results are obtained from the high statistic modes only. The control modes have been evaluated separately and show a good agreement. The differential cross-sections have been computed as

$$\sigma_i(H_c) = \frac{1}{\Delta p_\text{T} \Delta y} \cdot \frac{N_i(H_c \to f)}{\epsilon_i(H_c \to f) \cdot \mathcal{B}(H_c \to f) \cdot \mathcal{L}}, \tag{9.1}$$

in units of $\mu\text{b}\,\text{GeV}^{-1}$. Figures 9.2–9.5 show the results for the high statistic modes in y bins as a function of p_T, compared with the three theory predictions described in Section 2. Shown is one set of results per hadron species using the measured cross-sections of the higher statistic mode respectively. The respective other mode serves as cross-check and shows a good agreement between both reconstructed final states. In all cases, as throughout this note, the inclusion of the charge conjugate meson is implied.

9.1 Integrated cross-sections

We provide integrated cross-section per mode by summing the per-bin measurements within the fiducial p_T-y volume $0 < p_\text{T} < 8$ and $2 < y < 4.5$. Although we measure absolute cross-sections in higher p_T regions, the fiducial volume for the integrated measurement is limited by the lack of data in high y, high p_T bins.

To correct the integrated cross-sections for bins without a measurement, a multiplicative extrapolation factor is calculated using the POWHEG+NNPDF3.0L predictions for D^0 and D^+, the FONLL predictions for D^{*+}, and the GMVFNS predictions for D_s^+. This is computed as the ratio between the sum of all per-bin cross-sections within the measurement volume and the sum of all per-bin cross-sections within the measurement volume that have a corresponding measurement. The uncertainty on the extrapolation factor is taken as the difference between factors computed using the upper and lower bounds of the theory predictions, and this uncertainty is propagated to the integrated cross-sections as a systematic uncertainty. The obtained integrated cross-sections are given in Table 9.1.

9.2 Total $c\bar{c}$ cross-section

For each measurement presented in Section 9.1, we compute the total $c\bar{c}$ cross-section within the respective fiducial p_T-y volume by scaling the measurement by the

Table 9.1: Prompt charm production cross-sections in the kinematic ranges given. The computation of the extrapolation factors is described in the text. The first uncertainty on the cross-section is statistical, and the second is systematic and includes the contribution from the extrapolation factor. No extrapolation factor is given for D_s^+ as a measurement is available in every bin of the integrated kinematic volume.

			Extrapolation factor	Cross-section (µb)
D^0	$0 < p_{\mathrm{T}} < 8\,\mathrm{GeV}/c$	$2 < y < 4.5$	1.0004 ± 0.0009	$3368 \pm 4 \pm 196$
D^+	$0 < p_{\mathrm{T}} < 8\,\mathrm{GeV}/c$	$2 < y < 4.5$	-	$1290 \pm 8 \pm 185$
D^0	$1 < p_{\mathrm{T}} < 8\,\mathrm{GeV}/c$	$2 < y < 4.5$	1.0005 ± 0.0009	$2457 \pm 3 \pm 126$
D^+	$1 < p_{\mathrm{T}} < 8\,\mathrm{GeV}/c$	$2 < y < 4.5$	-	$1004 \pm 3 \pm 108$
D_s^+	$1 < p_{\mathrm{T}} < 8\,\mathrm{GeV}/c$	$2 < y < 4.5$	-	$455 \pm 13 \pm 100$
D^{*+}	$1 < p_{\mathrm{T}} < 8\,\mathrm{GeV}/c$	$2 < y < 4.5$	1.0004 ± 0.0023	$879 \pm 5 \pm 140$

Table 9.2: Charm hadron fragmentation fractions, taken from [29]. Here, H_c refers to a single charge of charm meson.

H_c	$f(c \to H_c)$
D^0	0.565 ± 0.032
D^+	0.246 ± 0.020
D_s^+	0.224 ± 0.028
D^{*+}	0.080 ± 0.017

reciprocal of the respective *fragmentation fraction*. These are taken from the 2008 edition of the Particle Data Group booklet [29], and are given in Table 9.2.

For each integrated cross-section from Section 9.1, the total $c\bar{c}$ cross-section is computed from the fragmentation fractions as $\sigma(c\bar{c}) = \sigma(H_c + \bar{H}_c)/2f(c \to H_c)$, where here H_c is a charm meson and $\bar{H}_c$ is its charge conjugate. The factor 1/2 comes from the fragmentation fractions measuring the charm quark fragmentation to a single charge, whereas we measure the integrated cross-sections combined for both mesons and anti-mesons.

Figure 9.1 shows the results for the total $c\bar{c}$ cross-section obtained from the D^0 and D^+ measurements respectively as well as their weighted average. This average is computed using the BLUE method [30] to be:

$$\sigma(pp \to c\bar{c}X)_{p_{\mathrm{T}} < 8\,\mathrm{GeV}/c,\, 2.0 < y < 4.5} = 2940 \pm 3 \pm 180 \pm 160\,\mu\mathrm{b}.$$

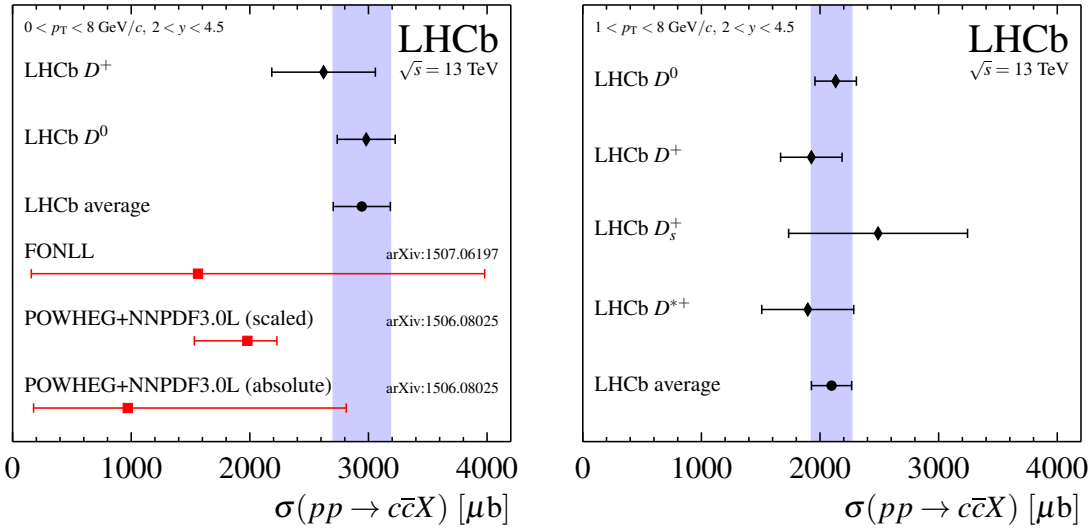

Figure 9.1: Integrated cross-section measurements (black diamonds) as well as their average (black circle and blue band) shown (left) based on the D^0 and D^+ cross-sections and theory predictions (red squares) [1, 2] for $0 < p_{\mathrm{T}} < 8\,\mathrm{GeV}/c$ and (right) for all four mesons for $1 < p_{\mathrm{T}} < 8\,\mathrm{GeV}/c$. The "absolute" predictions are based on calculations of the 13 TeV cross-section, while the "scaled" predictions are based on calculations of the 13 to 7 TeV ratio multiplied with the LHCb measurement.

9.3 Relative cross-sections

The absolute cross-sections measurements given above allows for several relative measurements to be made.

Relative measurements between our 13 TeV measurements and those made on data taken in 2010 at a centre-of-mass energy of 7 TeV are of particular interest to the theory community, as they can predict these ratios with considerably higher precision than absolute quantities due to cancellations in parton density function uncertainties. As we make our absolute measurements in a binning compatible with the 7 TeV measurement, that is with exactly aligned bin boundaries, the relative measurement is quite straightforward. For cases where the bin boundaries are identical, the measurement in those bins in simply the ratio. For cases where we have a finer binning than in 2010, we sum the sub-bins for a given 2010 bin and compute the ratio between the sum and the 2010 measurement. In all cases, the uncertainties on the ratio are computed by taking in to account the correlations between the two measurements, as described in Section 7.9.

The ratios between cross-sections at7 TeV and 13 TeV centre-of-mass energy are given for D^0 in Figure 9.6, for D^+ in Figure 9.7, for D_s^+ in Figure 9.8 and for D^{*+} in Figure 9.9. The corresponding numerical values are given in Tables 9.7–9.10.

Besides computing the ratios between the differential cross-section measurements at different energies, one can also obtain production ratios between different charm mesons. These ratios also benefit from a large reduction in the systematic uncertainties as correlated sources cancel. The expected value of this ratio is given by the ratio of the corresponding fragmentation fractions. Ratios with respect to D^0 are shown in Figure 9.10 while the remaining combinations are given in Figure 9.11. All numerical values are found in Tables 9.11–9.16

Table 9.3: Differential cross-sections for prompt D^0, estimated using $D^0 \to K^-\pi^+$, in $\mu b\, GeV^{-1}$.

	y				
p_{T} [MeV/c]	$[2, 2.5[$	$[2.5, 3[$	$[3, 3.5[$	$[3.5, 4[$	$[4, 4.5[$
$[0, 1000[$	$365.08 \pm 2.59^{+30.25}_{-25.43}$	$345.70 \pm 1.19^{+24.65}_{-20.38}$	$341.00 \pm 1.06^{+22.77}_{-18.38}$	$385.64 \pm 1.59^{+25.55}_{-23.06}$	$386.35 \pm 3.28^{+30.90}_{-26.25}$
$[1000, 1500[$	$580.74 \pm 3.85^{+49.29}_{-40.24}$	$528.12 \pm 1.79^{+38.08}_{-32.04}$	$482.75 \pm 1.52^{+31.45}_{-28.11}$	$459.67 \pm 1.92^{+32.51}_{-25.89}$	$385.45 \pm 3.30^{+28.98}_{-26.58}$
$[1500, 2000[$	$542.44 \pm 3.21^{+43.15}_{-38.85}$	$468.60 \pm 1.48^{+32.27}_{-28.40}$	$411.73 \pm 1.25^{+25.31}_{-23.70}$	$393.28 \pm 1.58^{+26.83}_{-21.00}$	$331.74 \pm 3.03^{+25.14}_{-22.56}$
$[2000, 2500[$	$408.66 \pm 2.31^{+28.37}_{-30.10}$	$374.67 \pm 1.15^{+24.40}_{-21.98}$	$328.04 \pm 0.99^{+19.40}_{-18.82}$	$283.17 \pm 1.15^{+18.91}_{-15.02}$	$217.80 \pm 1.85^{+15.18}_{-13.29}$
$[2500, 3000[$	$298.75 \pm 1.64^{+24.08}_{-17.49}$	$272.93 \pm 0.86^{+17.13}_{-15.32}$	$222.49 \pm 0.71^{+13.02}_{-12.02}$	$195.90 \pm 0.84^{+12.57}_{-11.26}$	$151.06 \pm 1.40^{+10.47}_{-10.11}$
$[3000, 3500[$	$219.19 \pm 1.23^{+15.55}_{-13.80}$	$187.76 \pm 0.63^{+11.35}_{-10.25}$	$154.74 \pm 0.54^{+9.25}_{-8.18}$	$132.45 \pm 0.63^{+9.03}_{-8.12}$	$90.94 \pm 0.98^{+6.95}_{-6.62}$
$[3500, 4000[$	$151.46 \pm 0.89^{+10.07}_{-9.01}$	$128.57 \pm 0.47^{+7.65}_{-6.89}$	$106.40 \pm 0.42^{+6.62}_{-5.36}$	$89.48 \pm 0.48^{+5.96}_{-5.38}$	$57.83 \pm 0.79^{+6.04}_{-5.28}$
$[4000, 5000[$	$92.92 \pm 0.43^{+6.26}_{-4.99}$	$76.38 \pm 0.24^{+4.51}_{-3.97}$	$62.19 \pm 0.21^{+3.94}_{-3.07}$	$48.63 \pm 0.24^{+2.88}_{-2.67}$	$33.14 \pm 0.52^{+4.70}_{-3.90}$
$[5000, 6000[$	$49.74 \pm 0.28^{+3.25}_{-2.88}$	$39.82 \pm 0.17^{+2.37}_{-2.03}$	$29.39 \pm 0.13^{+1.72}_{-1.68}$	$22.66 \pm 0.16^{+1.36}_{-1.32}$	$11.61 \pm 0.45^{+2.74}_{-1.95}$
$[6000, 7000[$	$25.69 \pm 0.18^{+1.70}_{-1.52}$	$20.60 \pm 0.11^{+1.23}_{-1.09}$	$15.62 \pm 0.10^{+0.97}_{-0.87}$	$10.87 \pm 0.12^{+0.91}_{-0.84}$	$3.46 \pm 0.52^{+2.44}_{-1.19}$
$[7000, 8000[$	$14.27 \pm 0.13^{+1.00}_{-0.91}$	$11.48 \pm 0.08^{+0.69}_{-0.65}$	$8.74 \pm 0.07^{+0.57}_{-0.47}$	$4.98 \pm 0.10^{+0.70}_{-0.57}$	-
$[8000, 9000[$	$9.50 \pm 0.11^{+0.76}_{-0.65}$	$6.53 \pm 0.06^{+0.42}_{-0.38}$	$5.02 \pm 0.06^{+0.35}_{-0.28}$	$3.27 \pm 0.12^{+0.64}_{-0.50}$	-
$[9000, 10000[$	$5.78 \pm 0.08^{+0.38}_{-0.34}$	$4.22 \pm 0.05^{+0.26}_{-0.19}$	$3.05 \pm 0.05^{+0.18}_{-0.14}$	$1.71 \pm 0.13^{+0.55}_{-0.32}$	-
$[10000, 11000[$	$3.76 \pm 0.07^{+0.27}_{-0.25}$	$2.65 \pm 0.04^{+0.17}_{-0.12}$	$1.84 \pm 0.04^{+0.14}_{-0.11}$	$0.78 \pm 0.14^{+0.33}_{-0.17}$	-
$[11000, 12000[$	$2.22 \pm 0.05^{+0.17}_{-0.16}$	$1.82 \pm 0.04^{+0.12}_{-0.08}$	$1.18 \pm 0.04^{+0.09}_{-0.07}$	-	-
$[12000, 13000[$	$1.54 \pm 0.04^{+0.16}_{-0.14}$	$1.28 \pm 0.03^{+0.09}_{-0.06}$	$0.81 \pm 0.04^{+0.07}_{-0.06}$	-	-
$[13000, 14000[$	$1.12 \pm 0.04^{+0.12}_{-0.10}$	$0.90 \pm 0.03^{+0.07}_{-0.04}$	$0.50 \pm 0.04^{+0.08}_{-0.06}$	-	-
$[14000, 15000[$	$0.75 \pm 0.03^{+0.08}_{-0.06}$	$0.60 \pm 0.02^{+0.05}_{-0.03}$	$0.30 \pm 0.03^{+0.06}_{-0.04}$	-	-

Table 9.4: Differential cross-sections for prompt D^+, estimated using $D^+ \to K^-\pi^+\pi^+$, in $\mu b\, GeV^{-1}$.

	y				
p_T [MeV/c]	$[2, 2.5[$	$[2.5, 3[$	$[3, 3.5[$	$[3.5, 4[$	$[4, 4.5[$
$[0, 1000[$	$109.34 \pm 9.41^{+43.51}_{-76.52}$	$115.80 \pm 4.41^{+27.98}_{-26.15}$	$128.82 \pm 3.17^{+28.65}_{-26.58}$	$100.56 \pm 3.17^{+19.24}_{-17.72}$	$118.18 \pm 7.78^{+29.53}_{-29.26}$
$[1000, 1500[$	$191.13 \pm 7.21^{+44.20}_{-42.23}$	$225.08 \pm 2.35^{+44.35}_{-37.62}$	$202.28 \pm 1.59^{+34.81}_{-32.44}$	$180.75 \pm 1.74^{+26.49}_{-24.45}$	$153.41 \pm 3.07^{+21.03}_{-20.38}$
$[1500, 2000[$	$248.43 \pm 4.06^{+39.80}_{-34.74}$	$185.58 \pm 1.01^{+30.17}_{-24.57}$	$168.85 \pm 0.75^{+24.58}_{-22.56}$	$146.26 \pm 0.80^{+17.72}_{-17.47}$	$139.88 \pm 1.59^{+16.16}_{-15.33}$
$[2000, 2500[$	$169.78 \pm 1.73^{+21.63}_{-17.86}$	$146.76 \pm 0.59^{+18.60}_{-16.08}$	$129.47 \pm 0.45^{+16.56}_{-14.25}$	$108.93 \pm 0.47^{+11.38}_{-11.34}$	$87.67 \pm 0.77^{+8.76}_{-8.55}$
$[2500, 3000[$	$131.44 \pm 1.11^{+15.22}_{-12.25}$	$105.48 \pm 0.38^{+11.08}_{-9.96}$	$90.62 \pm 0.30^{+9.94}_{-8.81}$	$74.32 \pm 0.30^{+7.21}_{-6.79}$	$60.58 \pm 0.50^{+5.86}_{-5.63}$
$[3000, 3500[$	$92.31 \pm 0.72^{+9.19}_{-8.30}$	$78.19 \pm 0.29^{+7.43}_{-6.54}$	$64.81 \pm 0.23^{+6.29}_{-5.80}$	$52.62 \pm 0.23^{+4.66}_{-4.52}$	$40.68 \pm 0.36^{+3.63}_{-3.55}$
$[3500, 4000[$	$60.95 \pm 0.47^{+5.50}_{-5.20}$	$54.00 \pm 0.21^{+4.57}_{-4.32}$	$43.55 \pm 0.17^{+3.58}_{-3.74}$	$35.20 \pm 0.17^{+3.14}_{-2.72}$	$27.80 \pm 0.27^{+2.41}_{-2.36}$
$[4000, 5000[$	$39.56 \pm 0.23^{+3.39}_{-2.95}$	$32.04 \pm 0.11^{+2.58}_{-2.25}$	$25.79 \pm 0.08^{+2.33}_{-1.77}$	$21.13 \pm 0.09^{+1.89}_{-1.53}$	$15.20 \pm 0.14^{+1.29}_{-1.14}$
$[5000, 6000[$	$21.17 \pm 0.14^{+1.84}_{-1.47}$	$16.42 \pm 0.07^{+1.27}_{-1.08}$	$13.35 \pm 0.06^{+1.04}_{-0.98}$	$10.04 \pm 0.06^{+0.83}_{-0.72}$	$7.79 \pm 0.12^{+0.75}_{-0.72}$
$[6000, 7000[$	$11.92 \pm 0.10^{+0.98}_{-0.88}$	$8.37 \pm 0.05^{+0.65}_{-0.53}$	$6.95 \pm 0.04^{+0.54}_{-0.50}$	$5.54 \pm 0.04^{+0.44}_{-0.39}$	$3.49 \pm 0.10^{+0.36}_{-0.35}$
$[7000, 8000[$	$6.41 \pm 0.06^{+0.53}_{-0.48}$	$4.80 \pm 0.03^{+0.38}_{-0.31}$	$3.85 \pm 0.03^{+0.29}_{-0.28}$	$2.79 \pm 0.03^{+0.22}_{-0.22}$	$1.97 \pm 0.11^{+0.42}_{-0.36}$
$[8000, 9000[$	$4.31 \pm 0.05^{+0.36}_{-0.35}$	$2.89 \pm 0.03^{+0.23}_{-0.19}$	$2.29 \pm 0.02^{+0.17}_{-0.17}$	$1.48 \pm 0.03^{+0.14}_{-0.13}$	$0.98 \pm 0.08^{+0.34}_{-0.34}$
$[9000, 10000[$	$2.29 \pm 0.03^{+0.18}_{-0.19}$	$1.75 \pm 0.02^{+0.14}_{-0.12}$	$1.38 \pm 0.02^{+0.10}_{-0.10}$	$1.02 \pm 0.03^{+0.12}_{-0.10}$	-
$[10000, 11000[$	$1.71 \pm 0.03^{+0.12}_{-0.12}$	$1.15 \pm 0.02^{+0.09}_{-0.07}$	$0.88 \pm 0.01^{+0.06}_{-0.06}$	$0.51 \pm 0.02^{+0.06}_{-0.05}$	-
$[11000, 12000[$	$1.13 \pm 0.02^{+0.09}_{-0.08}$	$0.76 \pm 0.01^{+0.06}_{-0.04}$	$0.59 \pm 0.01^{+0.05}_{-0.03}$	$0.35 \pm 0.02^{+0.04}_{-0.03}$	-
$[12000, 13000[$	$0.78 \pm 0.02^{+0.07}_{-0.05}$	$0.54 \pm 0.01^{+0.04}_{-0.03}$	$0.37 \pm 0.01^{+0.03}_{-0.02}$	$0.18 \pm 0.01^{+0.03}_{-0.02}$	-
$[13000, 14000[$	$0.55 \pm 0.02^{+0.05}_{-0.03}$	$0.37 \pm 0.01^{+0.03}_{-0.02}$	$0.27 \pm 0.01^{+0.03}_{-0.01}$	$0.12 \pm 0.01^{+0.02}_{-0.01}$	-
$[14000, 15000[$	$0.40 \pm 0.01^{+0.04}_{-0.02}$	$0.26 \pm 0.01^{+0.03}_{-0.01}$	$0.18 \pm 0.01^{+0.02}_{-0.01}$	-	-

Table 9.5: Differential cross-sections for prompt D_s^+, estimated using $D_s^+ \to \phi\pi^+$, in $\mu b\, GeV^{-1}$.

	y				
p_{T} [MeV/c]	$[2, 2.5[$	$[2.5, 3[$	$[3, 3.5[$	$[3.5, 4[$	$[4, 4.5[$
$[1000, 1500[$	$86.34 \pm 21.25^{+44.22}_{-48.55}$	$67.78 \pm 4.80^{+22.29}_{-17.68}$	$73.43 \pm 4.41^{+19.32}_{-16.35}$	$83.62 \pm 8.27^{+22.34}_{-19.68}$	$147.62 \pm 47.78^{+47.00}_{-97.36}$
$[1500, 2000[$	$67.94 \pm 4.26^{+16.67}_{-14.32}$	$74.48 \pm 1.93^{+16.09}_{-13.40}$	$79.23 \pm 1.98^{+13.98}_{-12.66}$	$73.55 \pm 2.63^{+10.11}_{-10.34}$	$43.46 \pm 4.48^{+9.55}_{-8.25}$
$[2000, 2500[$	$80.64 \pm 2.90^{+16.85}_{-12.61}$	$68.42 \pm 1.17^{+10.55}_{-9.10}$	$57.23 \pm 0.96^{+8.15}_{-7.25}$	$49.86 \pm 1.16^{+5.39}_{-5.45}$	$34.25 \pm 2.24^{+5.62}_{-4.57}$
$[2500, 3000[$	$61.38 \pm 1.75^{+10.31}_{-8.70}$	$52.40 \pm 0.76^{+6.28}_{-5.73}$	$47.65 \pm 0.68^{+5.61}_{-5.32}$	$36.13 \pm 0.71^{+4.00}_{-3.32}$	$22.85 \pm 1.11^{+3.04}_{-2.47}$
$[3000, 3500[$	$42.44 \pm 1.12^{+6.03}_{-5.08}$	$38.74 \pm 0.56^{+4.32}_{-3.67}$	$31.94 \pm 0.47^{+3.47}_{-3.12}$	$23.62 \pm 0.46^{+2.45}_{-2.04}$	$18.43 \pm 0.89^{+2.34}_{-2.06}$
$[3500, 4000[$	$34.39 \pm 0.89^{+4.37}_{-3.67}$	$25.97 \pm 0.40^{+2.78}_{-2.24}$	$21.28 \pm 0.34^{+2.38}_{-1.81}$	$18.60 \pm 0.39^{+1.95}_{-1.65}$	$11.83 \pm 0.64^{+1.44}_{-1.39}$
$[4000, 5000[$	$17.75 \pm 0.34^{+1.95}_{-1.68}$	$16.08 \pm 0.20^{+1.69}_{-1.27}$	$11.73 \pm 0.15^{+1.19}_{-0.94}$	$9.98 \pm 0.17^{+0.94}_{-0.89}$	$6.80 \pm 0.29^{+0.71}_{-0.67}$
$[5000, 6000[$	$9.90 \pm 0.21^{+1.11}_{-0.91}$	$8.32 \pm 0.13^{+0.89}_{-0.65}$	$6.76 \pm 0.11^{+0.67}_{-0.55}$	$5.33 \pm 0.12^{+0.58}_{-0.50}$	$3.89 \pm 0.25^{+0.55}_{-0.49}$
$[6000, 7000[$	$5.61 \pm 0.15^{+0.64}_{-0.55}$	$4.40 \pm 0.09^{+0.48}_{-0.36}$	$3.13 \pm 0.07^{+0.32}_{-0.27}$	$2.66 \pm 0.08^{+0.31}_{-0.27}$	$1.78 \pm 0.21^{+0.30}_{-0.29}$
$[7000, 8000[$	$3.64 \pm 0.12^{+0.45}_{-0.40}$	$2.54 \pm 0.07^{+0.28}_{-0.22}$	$1.73 \pm 0.05^{+0.18}_{-0.16}$	$1.54 \pm 0.07^{+0.19}_{-0.16}$	$0.51 \pm 0.13^{+0.12}_{-0.11}$
$[8000, 9000[$	$2.11 \pm 0.08^{+0.28}_{-0.25}$	$1.37 \pm 0.04^{+0.16}_{-0.12}$	$1.05 \pm 0.04^{+0.12}_{-0.10}$	$0.80 \pm 0.05^{+0.11}_{-0.09}$	-
$[9000, 10000[$	$1.18 \pm 0.06^{+0.16}_{-0.14}$	$0.72 \pm 0.03^{+0.09}_{-0.06}$	$0.74 \pm 0.03^{+0.09}_{-0.07}$	$0.38 \pm 0.04^{+0.05}_{-0.04}$	-
$[10000, 11000[$	$0.90 \pm 0.05^{+0.09}_{-0.07}$	$0.57 \pm 0.03^{+0.06}_{-0.04}$	$0.41 \pm 0.03^{+0.05}_{-0.03}$	$0.20 \pm 0.03^{+0.03}_{-0.01}$	-
$[11000, 12000[$	$0.53 \pm 0.04^{+0.06}_{-0.03}$	$0.36 \pm 0.02^{+0.04}_{-0.02}$	$0.29 \pm 0.02^{+0.03}_{-0.01}$	-	-
$[12000, 13000[$	$0.42 \pm 0.04^{+0.06}_{-0.02}$	$0.22 \pm 0.02^{+0.03}_{-0.01}$	$0.20 \pm 0.02^{+0.03}_{-0.01}$	-	-
$[13000, 14000[$	$0.22 \pm 0.03^{+0.04}_{-0.01}$	$0.20 \pm 0.02^{+0.03}_{-0.01}$	-	-	-
$[14000, 15000[$	-	-	-	-	-

Table 9.6: Differential cross-sections for prompt D^{*+}, estimated using $D^{*+} \to D^0\pi^+$ with $D^0 \to K^-\pi^+$, in $\mu b\, GeV^{-1}$.

	y				
p_{T} [MeV/c]	$[2, 2.5[$	$[2.5, 3[$	$[3, 3.5[$	$[3.5, 4[$	$[4, 4.5[$
$[0, 1000[$	-	-	-	-	$67.70 \pm 9.29^{+25.42}_{-20.50}$
$[1000, 1500[$	-	$160.49 \pm 6.60^{+38.33}_{-32.88}$	$176.68 \pm 2.22^{+41.71}_{-33.15}$	$143.81 \pm 2.26^{+34.93}_{-27.85}$	$157.94 \pm 4.85^{+43.45}_{-32.87}$
$[1500, 2000[$	-	$182.30 \pm 3.07^{+27.47}_{-27.74}$	$166.75 \pm 1.31^{+38.93}_{-31.00}$	$150.65 \pm 1.50^{+35.91}_{-28.93}$	$129.39 \pm 2.78^{+31.17}_{-24.48}$
$[2000, 2500[$	$123.64 \pm 11.23^{+30.88}_{-29.15}$	$154.64 \pm 1.70^{+18.22}_{-16.48}$	$143.84 \pm 0.92^{+31.76}_{-25.81}$	$115.24 \pm 0.98^{+26.91}_{-21.03}$	$95.14 \pm 1.80^{+21.35}_{-17.15}$
$[2500, 3000[$	$123.84 \pm 4.27^{+17.86}_{-16.39}$	$114.54 \pm 1.01^{+10.96}_{-9.97}$	$101.19 \pm 0.64^{+20.83}_{-17.60}$	$83.68 \pm 0.72^{+19.44}_{-15.31}$	$65.09 \pm 1.24^{+12.30}_{-10.42}$
$[3000, 3500[$	$95.97 \pm 2.40^{+11.22}_{-10.18}$	$80.26 \pm 0.65^{+6.85}_{-5.93}$	$68.73 \pm 0.44^{+12.82}_{-11.35}$	$55.65 \pm 0.51^{+12.57}_{-9.91}$	$43.62 \pm 0.91^{+7.70}_{-6.90}$
$[3500, 4000[$	$64.86 \pm 1.33^{+6.88}_{-6.06}$	$57.74 \pm 0.46^{+4.77}_{-3.92}$	$51.69 \pm 0.36^{+9.13}_{-8.24}$	$40.53 \pm 0.40^{+9.08}_{-7.08}$	$26.37 \pm 0.68^{+3.16}_{-3.12}$
$[4000, 5000[$	$41.68 \pm 0.55^{+3.83}_{-3.15}$	$33.48 \pm 0.20^{+2.60}_{-2.18}$	$28.85 \pm 0.17^{+4.60}_{-4.37}$	$22.49 \pm 0.19^{+4.58}_{-3.71}$	$15.40 \pm 0.41^{+2.24}_{-1.79}$
$[5000, 6000[$	$22.79 \pm 0.32^{+2.08}_{-1.68}$	$17.58 \pm 0.13^{+1.32}_{-1.14}$	$14.52 \pm 0.11^{+2.20}_{-2.06}$	$11.35 \pm 0.13^{+1.83}_{-1.59}$	$6.28 \pm 0.33^{+1.30}_{-0.96}$
$[6000, 7000[$	$11.18 \pm 0.18^{+1.02}_{-0.83}$	$9.56 \pm 0.09^{+0.72}_{-0.64}$	$7.45 \pm 0.08^{+1.06}_{-0.99}$	$5.22 \pm 0.09^{+0.61}_{-0.57}$	$2.24 \pm 0.37^{+0.45}_{-0.42}$
$[7000, 8000[$	$7.61 \pm 0.14^{+0.67}_{-0.64}$	$5.41 \pm 0.06^{+0.45}_{-0.37}$	$4.47 \pm 0.06^{+0.59}_{-0.56}$	$2.83 \pm 0.08^{+0.35}_{-0.30}$	-
$[8000, 9000[$	$4.47 \pm 0.09^{+0.41}_{-0.39}$	$3.33 \pm 0.05^{+0.28}_{-0.23}$	$2.54 \pm 0.04^{+0.29}_{-0.29}$	$1.46 \pm 0.07^{+0.25}_{-0.19}$	-
$[9000, 10000[$	$2.25 \pm 0.06^{+0.20}_{-0.19}$	$2.01 \pm 0.04^{+0.16}_{-0.15}$	$1.52 \pm 0.03^{+0.15}_{-0.14}$	$0.85 \pm 0.07^{+0.15}_{-0.12}$	-
$[10000, 11000[$	$1.87 \pm 0.06^{+0.14}_{-0.13}$	$1.33 \pm 0.03^{+0.09}_{-0.08}$	$0.97 \pm 0.03^{+0.08}_{-0.06}$	$0.43 \pm 0.07^{+0.09}_{-0.08}$	-
$[11000, 12000[$	$1.17 \pm 0.04^{+0.09}_{-0.09}$	$0.83 \pm 0.02^{+0.06}_{-0.05}$	$0.57 \pm 0.03^{+0.05}_{-0.05}$	$0.23 \pm 0.03^{+0.12}_{-0.11}$	-
$[12000, 13000[$	$0.77 \pm 0.04^{+0.06}_{-0.06}$	$0.63 \pm 0.02^{+0.05}_{-0.04}$	$0.41 \pm 0.02^{+0.04}_{-0.02}$	-	-
$[13000, 14000[$	$0.62 \pm 0.03^{+0.06}_{-0.05}$	$0.39 \pm 0.02^{+0.03}_{-0.03}$	$0.32 \pm 0.03^{+0.04}_{-0.02}$	-	-
$[14000, 15000[$	$0.37 \pm 0.03^{+0.05}_{-0.04}$	$0.32 \pm 0.02^{+0.03}_{-0.02}$	$0.14 \pm 0.02^{+0.03}_{-0.02}$	-	-

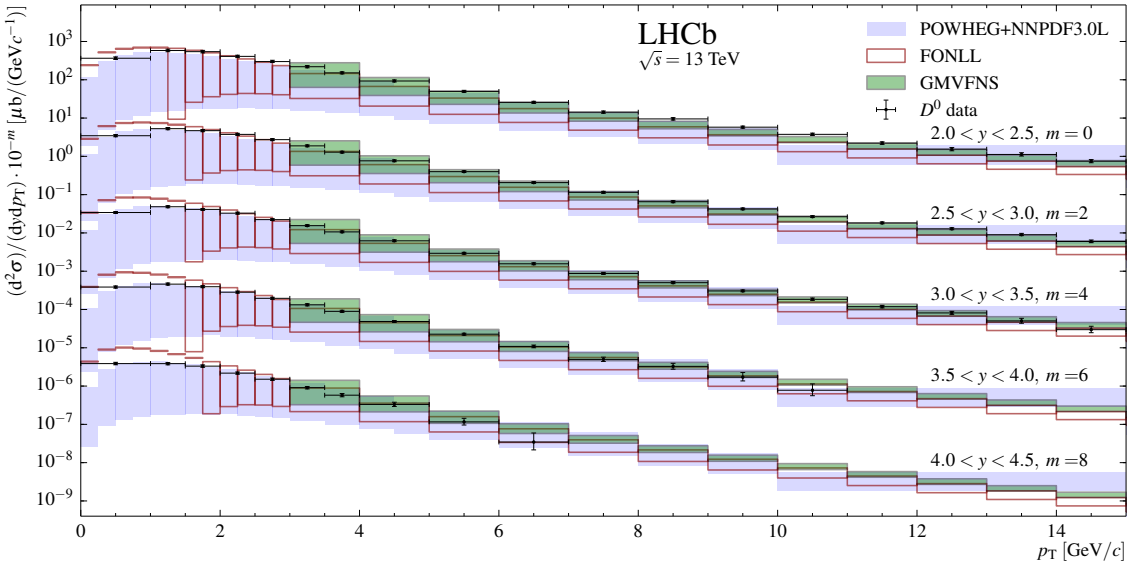

Figure 9.2: Differential cross-sections for prompt D^0, estimated using $D^0 \to K^-\pi^+$, in $\mu b\, GeV^{-1}$.

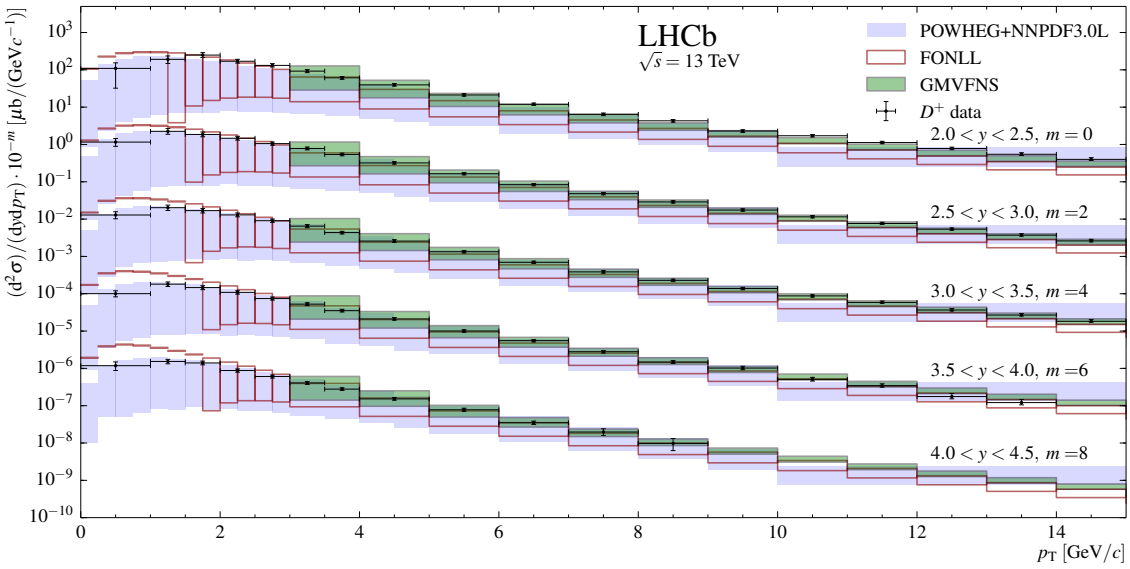

Figure 9.3: Differential cross-sections for prompt D^+, estimated using $D^+ \to K^-\pi^+\pi^+$, in $\mu b\, GeV^{-1}$.

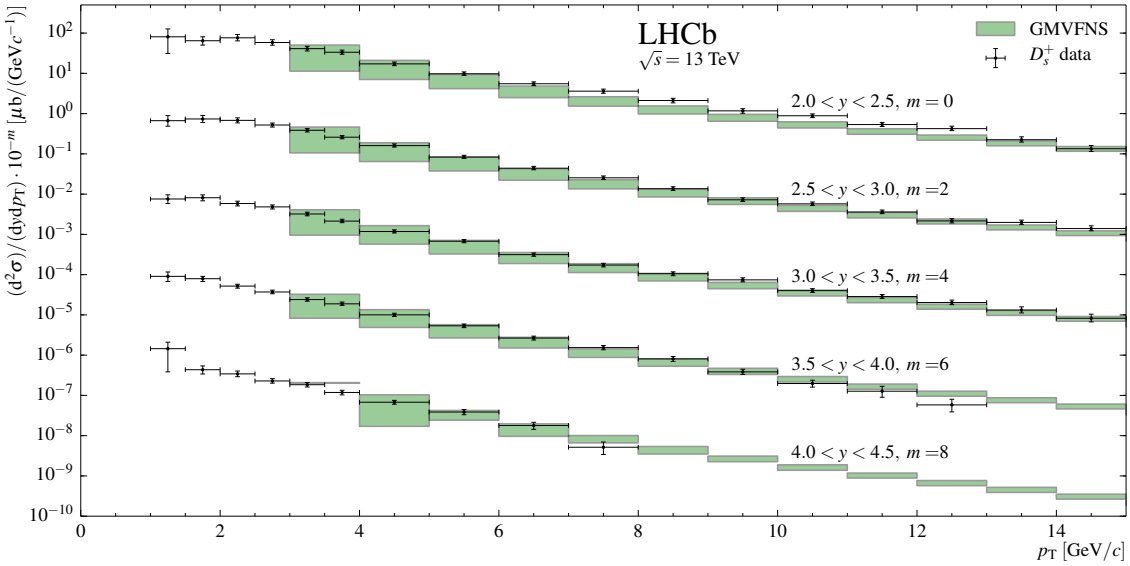

Figure 9.4: Differential cross-sections for prompt D_s^+, estimated using $D_s^+ \to \phi\pi^+$, in $\mu b\, GeV^{-1}$.

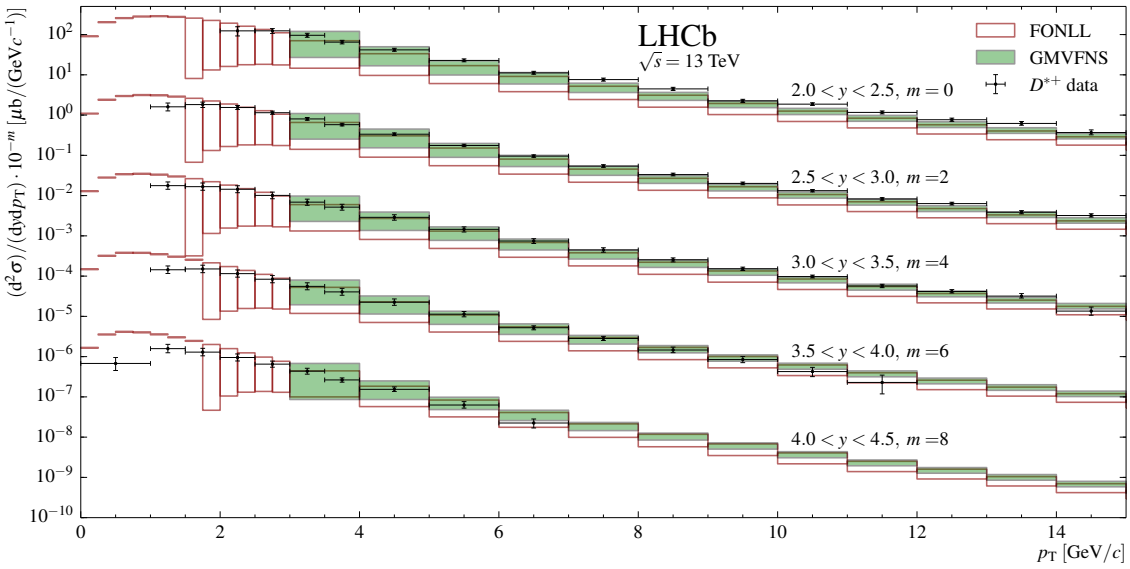

Figure 9.5: Differential cross-sections for prompt D^{*+}, estimated using $D^{*+} \to D^0\pi^+$ with $D^0 \to K^-\pi^+$, in $\mu b\, GeV^{-1}$.

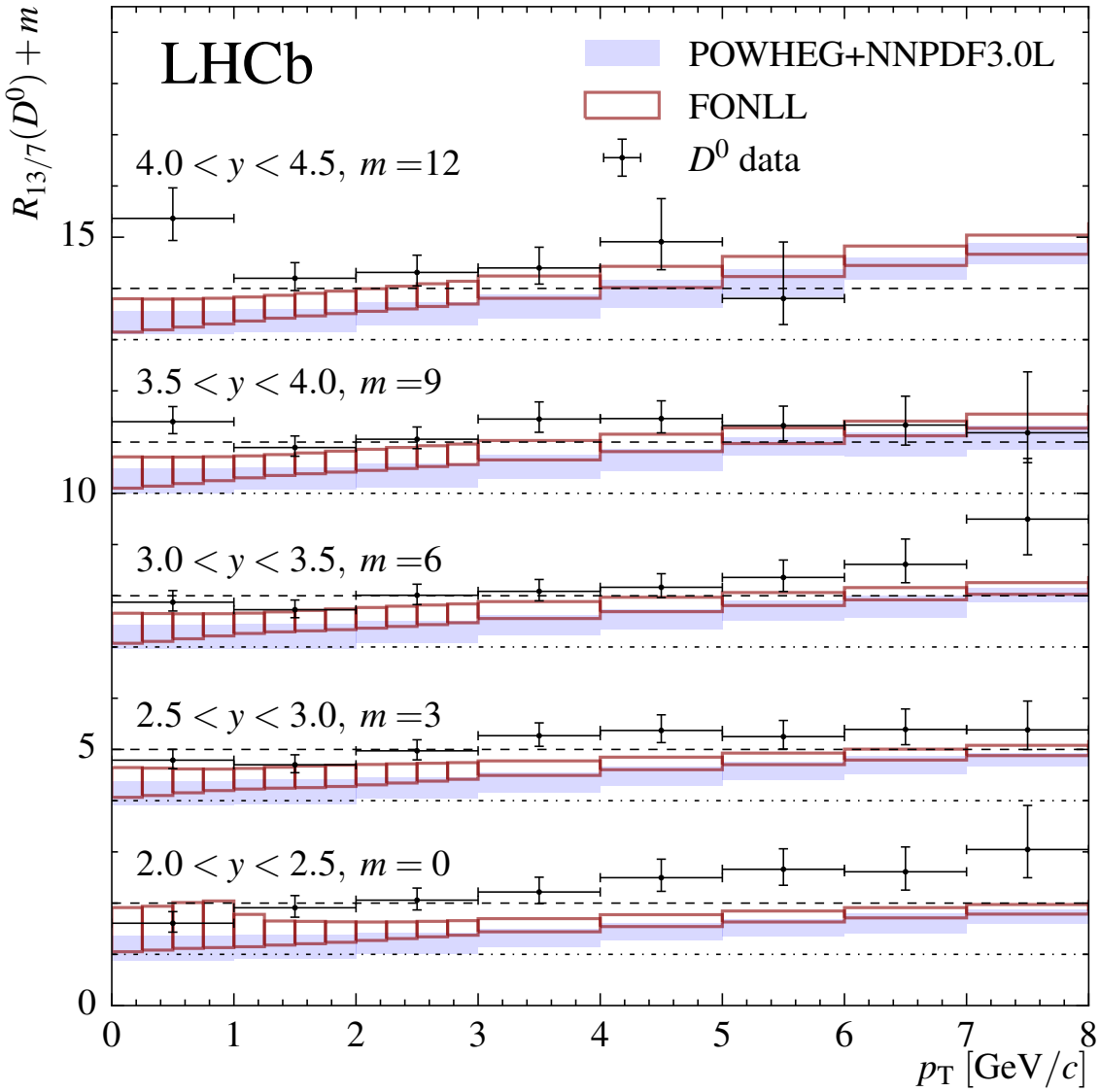

Figure 9.6: Cross-sections relative between 13 TeV and 7 TeV for D^0 estimated using the $D^0 \to K^-\pi^+$ cross-section results.

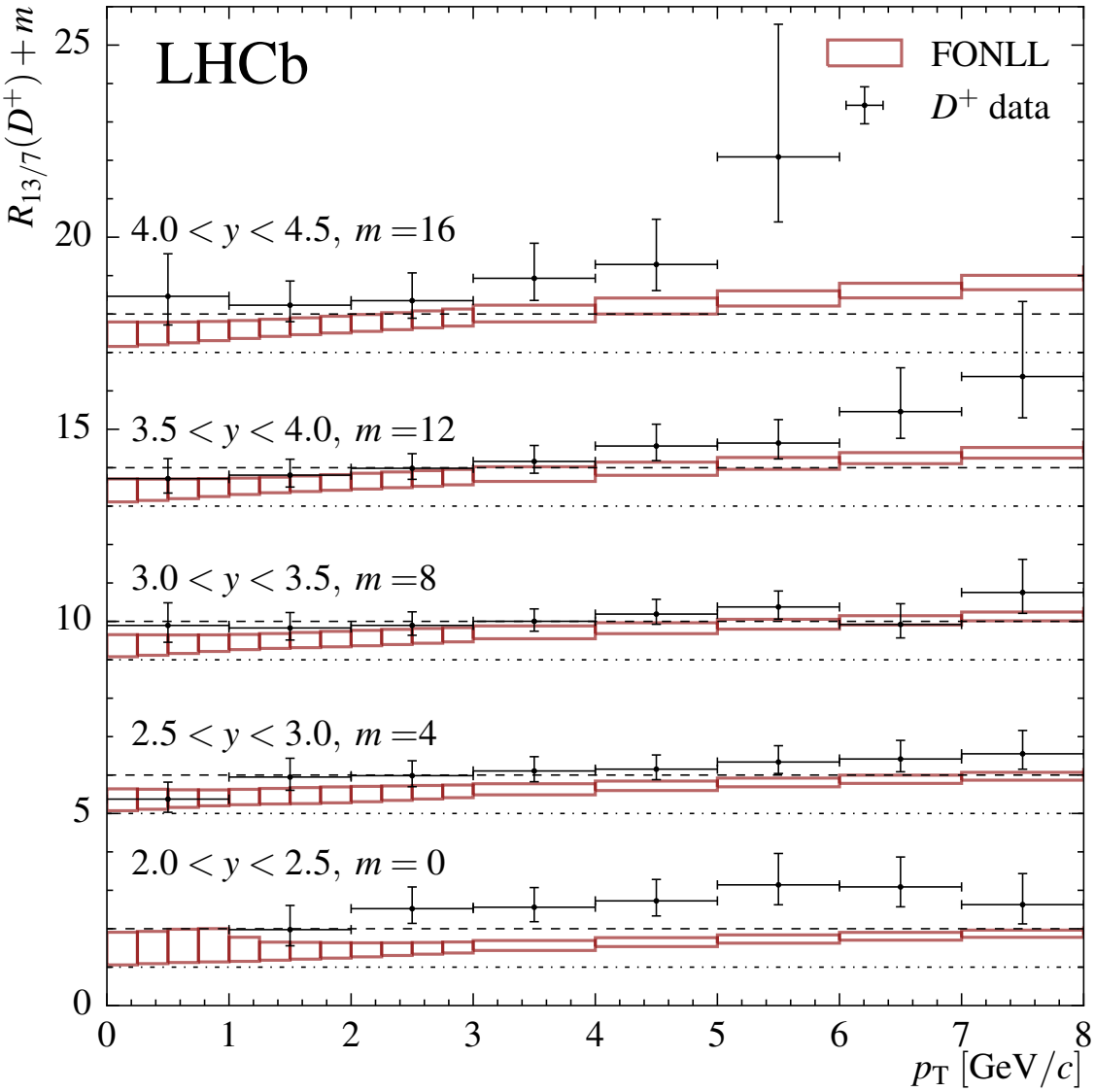

Figure 9.7: Cross-sections relative between 13 TeV and 7 TeV for D^+ estimated using the $D^+ \to K^-\pi^+\pi^+$ cross-section results.

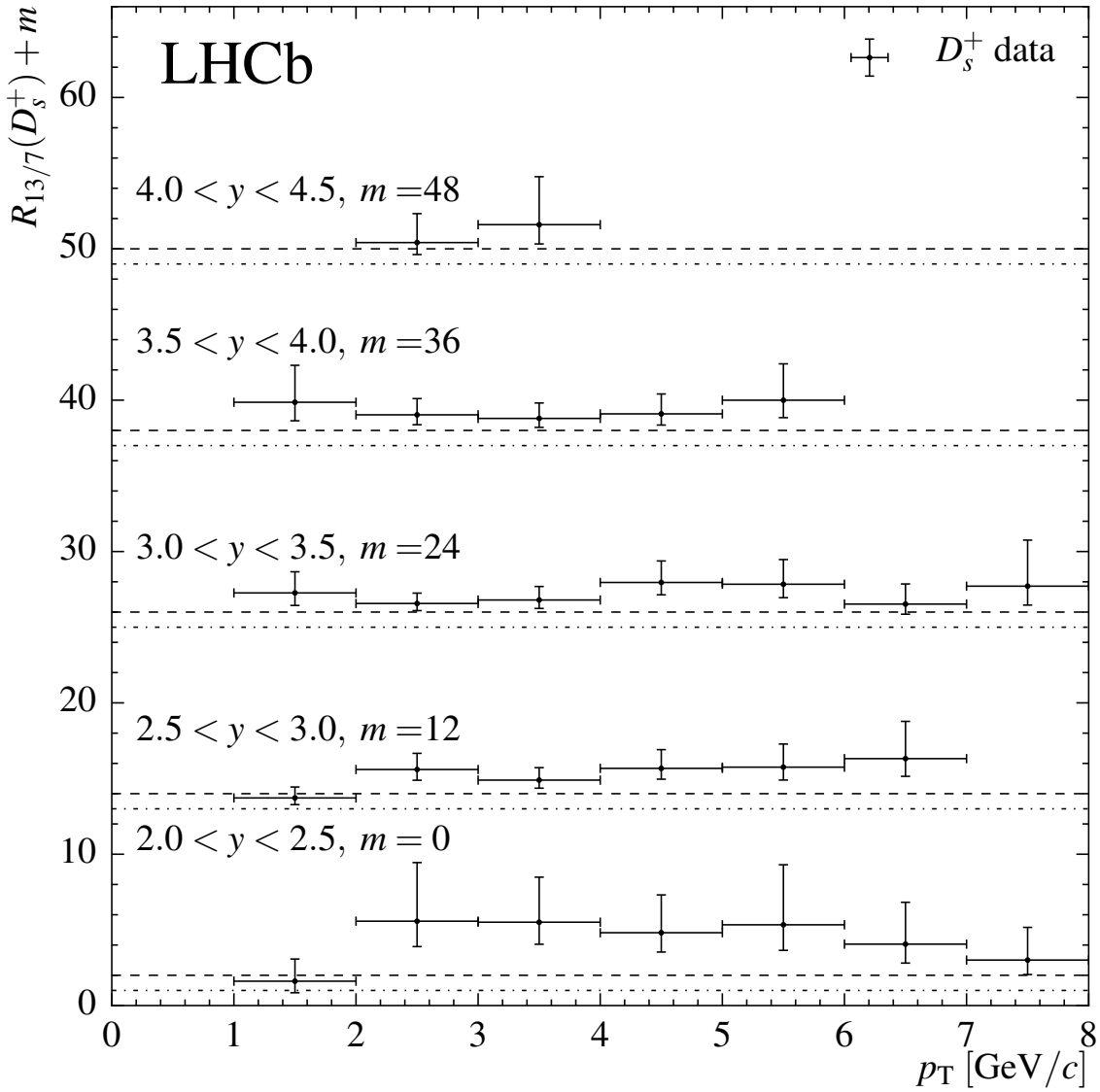

Figure 9.8: Cross-sections relative between 13 TeV and 7 TeV for D_s^+ estimated using the $D_s^+ \to \phi\pi^+$ cross-section results.

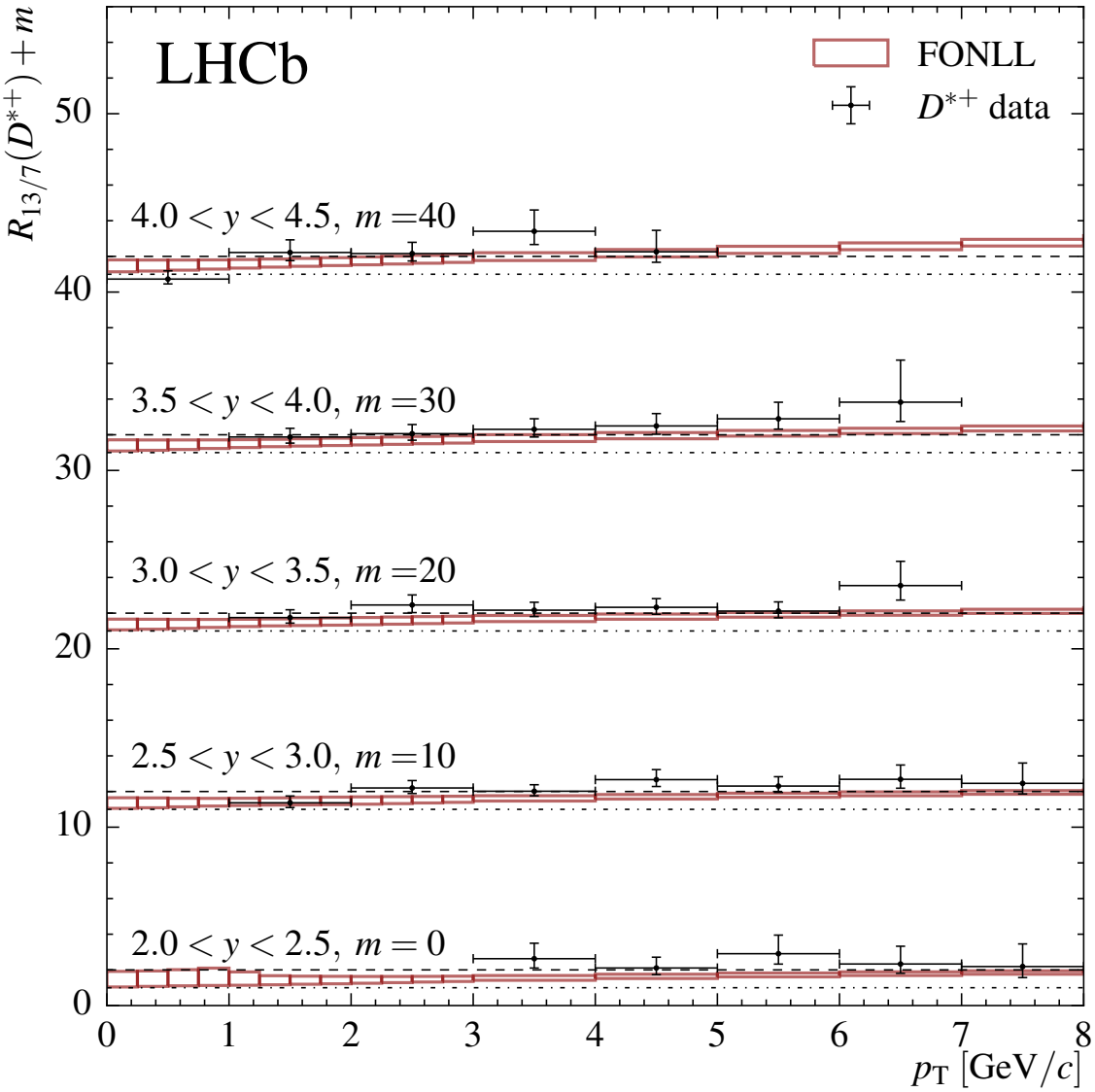

Figure 9.9: Cross-sections relative between 13 TeV and 7 TeV for D^{*+} estimated using the $D^{*+} \to D^0\pi^+$ with $D^0 \to K^-\pi^+$ cross-section results.

Table 9.7: Relative cross-sections for prompt $D^0 \to K^-\pi^+$ in $\mu b\, GeV^{-1}$.

p_T [MeV/c]	y [2, 2.5[	[2.5, 3[	[3, 3.5[	[3.5, 4[	[4, 4.5[
[0, 1000[	$1.61^{+0.08+0.21}_{-0.07-0.16}$	$1.79^{+0.07+0.20}_{-0.06-0.15}$	$1.87^{+0.08+0.21}_{-0.07-0.16}$	$2.40^{+0.13+0.26}_{-0.12-0.20}$	$3.37^{+0.35+0.48}_{-0.29-0.32}$
[1000, 2000[	$1.91^{+0.08+0.22}_{-0.07-0.17}$	$1.70^{+0.05+0.19}_{-0.05-0.15}$	$1.73^{+0.05+0.18}_{-0.05-0.15}$	$1.89^{+0.08+0.21}_{-0.07-0.15}$	$2.20^{+0.15+0.27}_{-0.13-0.20}$
[2000, 3000[	$2.06^{+0.08+0.22}_{-0.07-0.18}$	$1.97^{+0.05+0.21}_{-0.05-0.17}$	$2.01^{+0.06+0.21}_{-0.05-0.17}$	$2.06^{+0.07+0.23}_{-0.07-0.17}$	$2.31^{+0.16+0.30}_{-0.14-0.22}$
[3000, 4000[	$2.22^{+0.10+0.27}_{-0.09-0.21}$	$2.27^{+0.07+0.24}_{-0.07-0.20}$	$2.09^{+0.07+0.22}_{-0.07-0.17}$	$2.45^{+0.11+0.32}_{-0.10-0.24}$	$2.40^{+0.22+0.34}_{-0.19-0.25}$
[4000, 5000[	$2.50^{+0.14+0.33}_{-0.13-0.24}$	$2.37^{+0.10+0.29}_{-0.09-0.22}$	$2.17^{+0.10+0.24}_{-0.10-0.18}$	$2.46^{+0.16+0.31}_{-0.14-0.24}$	$2.91^{+0.53+0.65}_{-0.39-0.39}$
[5000, 6000[	$2.66^{+0.20+0.35}_{-0.18-0.26}$	$2.25^{+0.13+0.29}_{-0.12-0.21}$	$2.36^{+0.17+0.30}_{-0.15-0.23}$	$2.32^{+0.22+0.31}_{-0.19-0.23}$	$1.80^{+0.79+0.77}_{-0.43-0.27}$
[6000, 7000[	$2.61^{+0.30+0.38}_{-0.25-0.26}$	$2.39^{+0.23+0.33}_{-0.20-0.23}$	$2.61^{+0.32+0.38}_{-0.26-0.25}$	$2.33^{+0.40+0.40}_{-0.30-0.25}$	-
[7000, 8000[	$3.05^{+0.67+0.54}_{-0.46-0.30}$	$2.38^{+0.42+0.38}_{-0.31-0.23}$	$3.50^{+0.96+0.69}_{-0.62-0.31}$	$2.18^{+0.97+0.68}_{-0.51-0.28}$	-

Table 9.8: Relative cross-sections for prompt $D^+ \to K^-\pi^+\pi^+$ in $\mu b\, GeV^{-1}$.

p_{T} [MeV/c]	y [2, 2.5[	[2.5, 3[	[3, 3.5[	[3.5, 4[	[4, 4.5[
[0, 1000[	-	$1.37^{+0.12+0.43}_{-0.10-0.33}$	$1.89^{+0.12+0.58}_{-0.10-0.43}$	$1.72^{+0.13+0.50}_{-0.12-0.36}$	$2.46^{+0.38+1.04}_{-0.31-0.68}$
[1000, 2000[	$1.98^{+0.28+0.56}_{-0.22-0.36}$	$1.95^{+0.09+0.48}_{-0.08-0.34}$	$1.83^{+0.06+0.40}_{-0.06-0.31}$	$1.81^{+0.07+0.41}_{-0.07-0.30}$	$2.23^{+0.18+0.60}_{-0.16-0.40}$
[2000, 3000[	$2.52^{+0.22+0.52}_{-0.19-0.33}$	$1.98^{+0.07+0.38}_{-0.07-0.28}$	$1.90^{+0.06+0.35}_{-0.06-0.25}$	$1.98^{+0.07+0.37}_{-0.07-0.28}$	$2.35^{+0.19+0.70}_{-0.16-0.43}$
[3000, 4000[	$2.56^{+0.19+0.47}_{-0.16-0.34}$	$2.11^{+0.08+0.36}_{-0.07-0.27}$	$2.00^{+0.07+0.31}_{-0.07-0.25}$	$2.16^{+0.10+0.40}_{-0.09-0.29}$	$2.93^{+0.31+0.86}_{-0.25-0.52}$
[4000, 5000[	$2.72^{+0.22+0.51}_{-0.19-0.34}$	$2.15^{+0.10+0.36}_{-0.09-0.26}$	$2.19^{+0.10+0.37}_{-0.10-0.25}$	$2.56^{+0.17+0.54}_{-0.15-0.35}$	$3.29^{+0.53+1.05}_{-0.40-0.55}$
[5000, 6000[	$3.14^{+0.32+0.75}_{-0.27-0.44}$	$2.34^{+0.15+0.40}_{-0.13-0.27}$	$2.38^{+0.16+0.38}_{-0.14-0.28}$	$2.64^{+0.24+0.56}_{-0.20-0.36}$	$6.09^{+2.37+2.51}_{-1.34-1.03}$
[6000, 7000[	$3.09^{+0.38+0.68}_{-0.30-0.42}$	$2.42^{+0.21+0.44}_{-0.18-0.28}$	$1.92^{+0.16+0.51}_{-0.14-0.32}$	$3.46^{+0.49+1.03}_{-0.39-0.58}$	-
[7000, 8000[	$2.63^{+0.42+0.69}_{-0.32-0.38}$	$2.55^{+0.34+0.50}_{-0.27-0.30}$	$2.75^{+0.41+0.76}_{-0.31-0.44}$	$4.37^{+1.22+1.52}_{-0.79-0.73}$	-

Table 9.9: Relative cross-sections for prompt $D_s^+ \to \phi\pi^+$ in $\mu b\, GeV^{-1}$.

p_{T} [MeV/c]	y [2, 2.5[	[2.5, 3[	[3, 3.5[	[3.5, 4[	[4, 4.5[
[0, 1000[	-	-	-	-	-
[1000, 2000[	$1.61^{+0.90+1.16}_{-0.46-0.61}$	$1.72^{+0.31+0.65}_{-0.23-0.38}$	$3.26^{+0.68+1.22}_{-0.50-0.66}$	$3.86^{+1.52+1.91}_{-0.87-0.86}$	-
[2000, 3000[	$5.58^{+2.52+2.93}_{-1.32-1.04}$	$3.60^{+0.58+0.89}_{-0.44-0.55}$	$2.57^{+0.33+0.60}_{-0.26-0.39}$	$3.03^{+0.66+0.85}_{-0.46-0.47}$	$2.41^{+1.44+1.25}_{-0.67-0.42}$
[3000, 4000[	$5.51^{+2.07+2.14}_{-1.17-0.86}$	$2.90^{+0.44+0.70}_{-0.34-0.41}$	$2.80^{+0.47+0.76}_{-0.36-0.43}$	$2.79^{+0.60+0.82}_{-0.42-0.42}$	$3.60^{+2.63+1.76}_{-1.10-0.64}$
[4000, 5000[	$4.81^{+1.86+1.67}_{-1.05-0.72}$	$3.67^{+0.76+0.98}_{-0.53-0.48}$	$3.96^{+0.96+1.05}_{-0.65-0.50}$	$3.09^{+0.99+0.87}_{-0.60-0.43}$	-
[5000, 6000[	$5.34^{+3.14+2.42}_{-1.45-0.87}$	$3.75^{+1.03+1.13}_{-0.67-0.52}$	$3.84^{+1.20+1.10}_{-0.74-0.49}$	$4.00^{+1.81+1.58}_{-0.96-0.64}$	-
[6000, 7000[	$4.06^{+2.05+1.86}_{-1.04-0.70}$	$4.31^{+1.96+1.49}_{-1.03-0.56}$	$2.53^{+1.04+0.82}_{-0.57-0.35}$	-	-
[7000, 8000[	$3.01^{+1.60+1.45}_{-0.78-0.54}$	-	$3.71^{+2.73+1.35}_{-1.12-0.55}$	-	-

Table 9.10: Relative cross-sections for prompt $D^{*+} \to D^0\pi^+$ with $D^0 \to K^-\pi^+$ in $\mu b\, GeV^{-1}$.

p_{T} [MeV/c]	y [2, 2.5[	[2.5, 3[	[3, 3.5[	[3.5, 4[	[4, 4.5[
[0, 1000[	-	-	-	-	$0.73^{+0.30+0.36}_{-0.18-0.20}$
[1000, 2000[	-	$1.37^{+0.22+0.31}_{-0.16-0.21}$	$1.75^{+0.12+0.42}_{-0.11-0.29}$	$1.87^{+0.16+0.46}_{-0.14-0.31}$	$2.22^{+0.35+0.62}_{-0.27-0.37}$
[2000, 3000[	-	$2.20^{+0.23+0.35}_{-0.19-0.25}$	$2.46^{+0.16+0.54}_{-0.14-0.40}$	$2.06^{+0.16+0.48}_{-0.14-0.34}$	$2.16^{+0.32+0.54}_{-0.25-0.33}$
[3000, 4000[	$2.63^{+0.67+0.56}_{-0.44-0.28}$	$2.02^{+0.18+0.32}_{-0.15-0.21}$	$2.17^{+0.16+0.42}_{-0.14-0.33}$	$2.30^{+0.22+0.55}_{-0.19-0.39}$	$3.41^{+0.89+0.80}_{-0.58-0.46}$
[4000, 5000[	$2.11^{+0.41+0.44}_{-0.30-0.23}$	$2.67^{+0.31+0.47}_{-0.25-0.29}$	$2.33^{+0.24+0.42}_{-0.20-0.33}$	$2.49^{+0.33+0.61}_{-0.27-0.38}$	$2.26^{+0.97+0.71}_{-0.52-0.27}$
[5000, 6000[	$2.91^{+0.79+0.68}_{-0.51-0.28}$	$2.31^{+0.32+0.41}_{-0.25-0.25}$	$2.12^{+0.30+0.42}_{-0.23-0.30}$	$2.90^{+0.63+0.68}_{-0.44-0.37}$	-
[6000, 7000[	$2.33^{+0.76+0.65}_{-0.46-0.24}$	$2.68^{+0.59+0.54}_{-0.41-0.29}$	$3.54^{+1.11+0.79}_{-0.68-0.44}$	$3.83^{+2.08+1.12}_{-1.00-0.41}$	-
[7000, 8000[	$2.19^{+1.09+0.65}_{-0.55-0.29}$	$2.46^{+0.96+0.62}_{-0.54-0.25}$	-	-	-

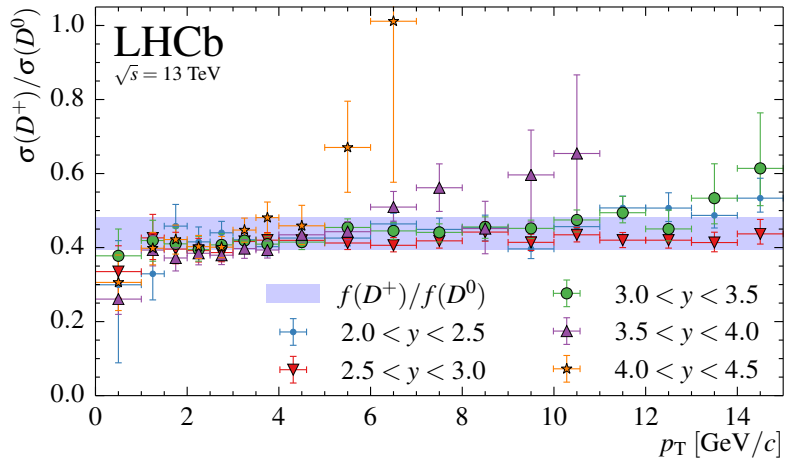
LHCb
$\sqrt{s} = 13$ TeV
$\sigma(D^+)/\sigma(D^0)$
$f(D^+)/f(D^0)$
$2.0 < y < 2.5$
$2.5 < y < 3.0$
$3.0 < y < 3.5$
$3.5 < y < 4.0$
$4.0 < y < 4.5$
p_T [GeV/c]

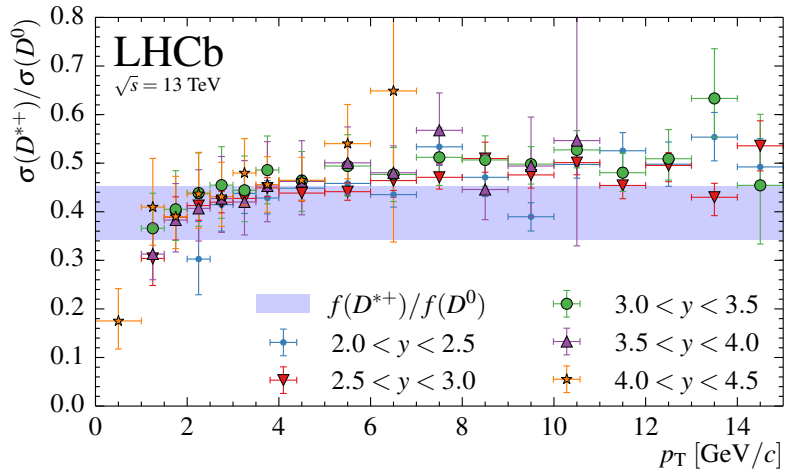
LHCb
$\sqrt{s} = 13$ TeV
$\sigma(D^{*+})/\sigma(D^0)$
$f(D^{*+})/f(D^0)$
$2.0 < y < 2.5$
$2.5 < y < 3.0$
$3.0 < y < 3.5$
$3.5 < y < 4.0$
$4.0 < y < 4.5$
p_T [GeV/c]

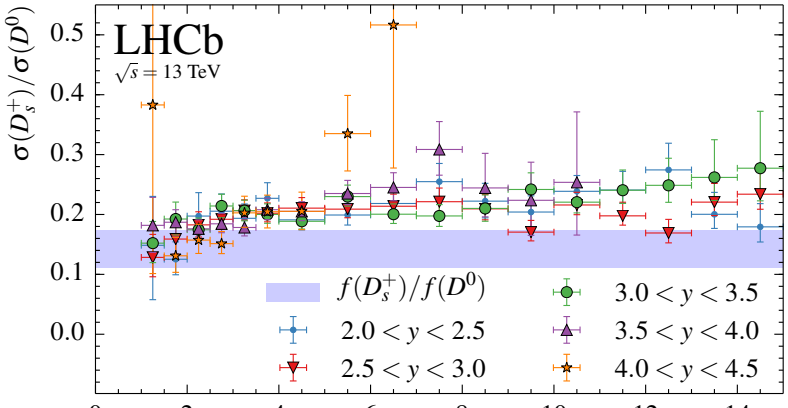
LHCb
$\sqrt{s} = 13$ TeV
$\sigma(D_s^+)/\sigma(D^0)$
$f(D_s^+)/f(D^0)$
$2.0 < y < 2.5$
$2.5 < y < 3.0$
$3.0 < y < 3.5$
$3.5 < y < 4.0$
$4.0 < y < 4.5$

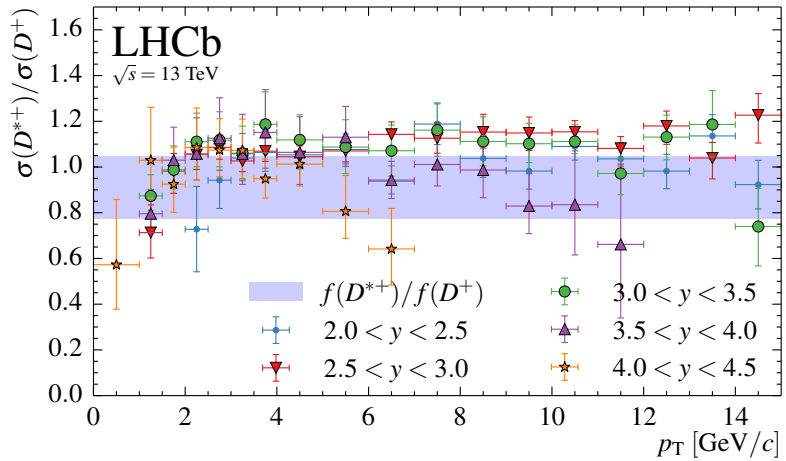
LHCb
$\sqrt{s} = 13$ TeV
$\sigma(D^{*+})/\sigma(D^+)$
$f(D^{*+})/f(D^+)$
$2.0 < y < 2.5$
$2.5 < y < 3.0$
$3.0 < y < 3.5$
$3.5 < y < 4.0$
$4.0 < y < 4.5$
p_T [GeV/c]

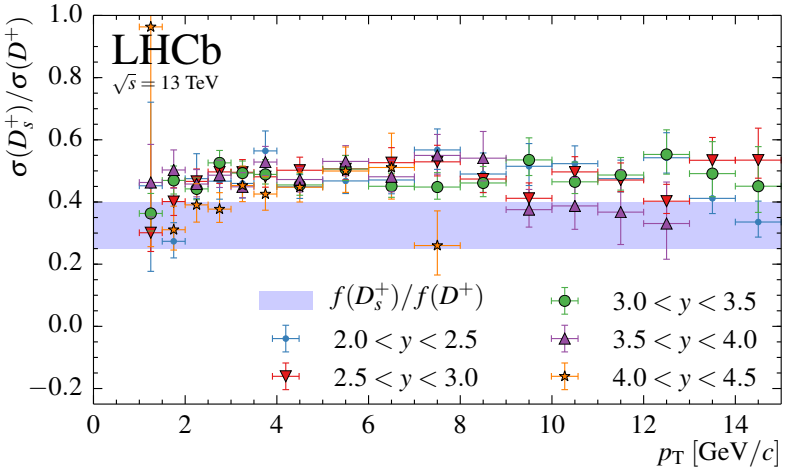
LHCb
$\sqrt{s} = 13$ TeV
$\sigma(D_s^+)/\sigma(D^+)$
$f(D_s^+)/f(D^+)$
$2.0 < y < 2.5$
$2.5 < y < 3.0$
$3.0 < y < 3.5$
$3.5 < y < 4.0$
$4.0 < y < 4.5$
p_T [GeV/c]

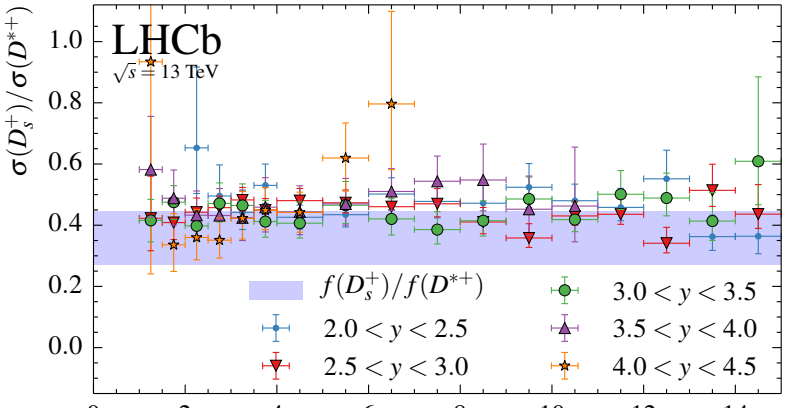
LHCb
$\sqrt{s} = 13$ TeV
$\sigma(D_s^+)/\sigma(D^{*+})$
$f(D_s^+)/f(D^{*+})$
$2.0 < y < 2.5$
$2.5 < y < 3.0$
$3.0 < y < 3.5$
$3.5 < y < 4.0$
$4.0 < y < 4.5$

Table 9.11: The ratios of differential production cross-sections in 10^{-2} for prompt D^+ and D^0 mesons in bins of (y, p_T). The first uncertainty is statistical, and the second is the total systematic.

	y				
p_{T} [MeV/c]	$[2, 2.5[$	$[2.5, 3[$	$[3, 3.5[$	$[3.5, 4[$	$[4, 4.5[$
$[0, 1000[$	$29.95^{+2.59+11.65}_{-2.57-20.93}$	$33.51^{+1.28+6.86}_{-1.29-7.09}$	$37.77^{+0.95+7.18}_{-0.93-7.16}$	$26.08^{+0.83+4.09}_{-0.83-4.05}$	$30.59^{+2.01+7.13}_{-2.02-7.32}$
$[1000, 1500[$	$32.91^{+1.27+6.71}_{-1.26-6.94}$	$42.62^{+0.46+6.33}_{-0.47-5.84}$	$41.90^{+0.36+5.46}_{-0.35-5.57}$	$39.32^{+0.42+3.86}_{-0.42-4.25}$	$39.81^{+0.87+4.20}_{-0.88-4.39}$
$[1500, 2000[$	$45.80^{+0.80+5.80}_{-0.79-5.36}$	$39.60^{+0.25+4.52}_{-0.24-3.96}$	$41.01^{+0.23+4.33}_{-0.22-4.29}$	$37.19^{+0.25+2.76}_{-0.25-3.50}$	$42.17^{+0.62+3.85}_{-0.61-3.88}$
$[2000, 2500[$	$41.54^{+0.48+4.00}_{-0.47-2.92}$	$39.17^{+0.19+3.31}_{-0.20-3.06}$	$39.47^{+0.18+3.58}_{-0.18-3.14}$	$38.46^{+0.23+2.48}_{-0.23-3.12}$	$40.25^{+0.49+2.98}_{-0.49-3.15}$
$[2500, 3000[$	$43.99^{+0.45+3.06}_{-0.44-3.12}$	$38.65^{+0.19+2.53}_{-0.18-2.47}$	$40.73^{+0.18+3.01}_{-0.19-2.82}$	$37.94^{+0.22+2.49}_{-0.23-2.53}$	$40.11^{+0.50+2.86}_{-0.50-2.80}$
$[3000, 3500[$	$42.12^{+0.40+2.81}_{-0.40-2.69}$	$41.64^{+0.21+2.38}_{-0.21-2.22}$	$41.88^{+0.20+2.70}_{-0.21-2.67}$	$39.73^{+0.26+2.39}_{-0.25-2.63}$	$44.73^{+0.63+3.17}_{-0.61-3.23}$
$[3500, 4000[$	$40.24^{+0.39+2.44}_{-0.39-2.46}$	$42.00^{+0.23+2.04}_{-0.22-2.20}$	$40.93^{+0.22+1.99}_{-0.22-2.65}$	$39.34^{+0.29+2.44}_{-0.28-2.14}$	$48.09^{+0.80+4.14}_{-0.81-4.16}$
$[4000, 5000[$	$42.58^{+0.31+2.27}_{-0.32-2.22}$	$41.95^{+0.19+1.92}_{-0.19-1.75}$	$41.48^{+0.20+2.23}_{-0.19-2.00}$	$43.45^{+0.29+2.56}_{-0.28-1.96}$	$45.88^{+0.86+5.46}_{-0.81-5.01}$
$[5000, 6000[$	$42.57^{+0.38+2.57}_{-0.38-2.06}$	$41.24^{+0.24+1.92}_{-0.24-1.75}$	$45.44^{+0.28+2.30}_{-0.28-2.18}$	$44.29^{+0.41+2.68}_{-0.42-2.13}$	$67.05^{+2.93+12.15}_{-2.63-11.82}$
$[6000, 7000[$	$46.39^{+0.50+2.84}_{-0.50-2.63}$	$40.61^{+0.31+2.07}_{-0.31-1.74}$	$44.50^{+0.37+2.16}_{-0.37-2.25}$	$50.94^{+0.72+4.16}_{-0.70-3.75}$	$101.15^{+18.34+58.42}_{-13.63-41.31}$
$[7000, 8000[$	$44.91^{+0.61+2.99}_{-0.60-2.77}$	$41.82^{+0.42+2.38}_{-0.41-1.92}$	$44.10^{+0.49+2.26}_{-0.51-2.54}$	$56.16^{+1.29+6.32}_{-1.30-6.26}$	-
$[8000, 9000[$	$45.37^{+0.75+3.30}_{-0.72-3.46}$	$44.19^{+0.58+2.71}_{-0.57-2.39}$	$45.57^{+0.69+2.64}_{-0.68-3.00}$	$45.14^{+1.97+7.10}_{-1.83-6.56}$	-
$[9000, 10000[$	$39.64^{+0.83+2.27}_{-0.78-2.49}$	$41.41^{+0.70+2.09}_{-0.67-2.09}$	$45.19^{+0.92+2.03}_{-0.90-2.60}$	$59.63^{+5.11+10.98}_{-4.47-11.88}$	-
$[10000, 11000[$	$45.66^{+1.15+2.08}_{-1.13-2.19}$	$43.45^{+0.92+1.78}_{-0.90-1.70}$	$47.46^{+1.34+2.35}_{-1.30-2.97}$	$65.42^{+14.22+15.77}_{-10.08-14.82}$	-
$[11000, 12000[$	$50.71^{+1.58+2.77}_{-1.52-2.51}$	$42.00^{+1.10+1.75}_{-1.07-1.70}$	$49.42^{+2.03+3.92}_{-1.84-2.02}$	-	-
$[12000, 13000[$	$50.68^{+1.94+3.64}_{-1.90-3.09}$	$41.99^{+1.39+1.85}_{-1.33-1.68}$	$45.04^{+2.56+4.38}_{-2.44-2.12}$	-	-
$[13000, 14000[$	$48.69^{+2.24+3.75}_{-2.14-2.65}$	$41.36^{+1.69+2.22}_{-1.64-1.88}$	$53.34^{+4.37+8.20}_{-3.96-5.69}$	-	-
$[14000, 15000[$	$53.35^{+3.12+4.39}_{-2.83-2.50}$	$43.70^{+2.25+3.19}_{-2.13-1.74}$	$61.40^{+8.46+12.39}_{-6.83-7.40}$	-	-

Table 9.12: The ratios of differential production cross-sections in 10^{-2} for prompt D_s^+ and D^0 mesons in bins of (y, p_T). The first uncertainty is statistical, and the second is the total systematic.

	y				
p_{T} [MeV/c]	$[2, 2.5[$	$[2.5, 3[$	$[3, 3.5[$	$[3.5, 4[$	$[4, 4.5[$
$[1000, 1500[$	$14.85^{+3.67+7.29}_{-3.65-8.31}$	$12.84^{+0.91+3.73}_{-0.91-3.11}$	$15.21^{+0.91+3.50}_{-0.91-3.12}$	$18.19^{+1.80+4.31}_{-1.80-4.15}$	$38.29^{+12.41+12.12}_{-12.38-25.29}$
$[1500, 2000[$	$12.52^{+0.79+2.79}_{-0.79-2.47}$	$15.89^{+0.42+2.81}_{-0.42-2.47}$	$19.24^{+0.48+2.79}_{-0.48-2.63}$	$18.70^{+0.67+1.98}_{-0.68-2.39}$	$13.10^{+1.37+2.75}_{-1.35-2.41}$
$[2000, 2500[$	$19.73^{+0.72+3.84}_{-0.72-2.72}$	$18.26^{+0.32+2.16}_{-0.32-2.00}$	$17.45^{+0.30+1.93}_{-0.30-1.76}$	$17.61^{+0.41+1.44}_{-0.42-1.68}$	$15.72^{+1.04+2.42}_{-1.03-1.98}$
$[2500, 3000[$	$20.55^{+0.60+2.82}_{-0.60-2.77}$	$19.20^{+0.28+1.75}_{-0.28-1.67}$	$21.42^{+0.31+1.94}_{-0.31-1.93}$	$18.44^{+0.37+1.70}_{-0.37-1.44}$	$15.13^{+0.76+1.88}_{-0.75-1.49}$
$[3000, 3500[$	$19.36^{+0.53+2.33}_{-0.53-2.05}$	$20.63^{+0.30+1.78}_{-0.31-1.54}$	$20.65^{+0.31+1.72}_{-0.31-1.67}$	$17.83^{+0.36+1.62}_{-0.36-1.36}$	$20.27^{+1.00+2.59}_{-0.99-2.20}$
$[3500, 4000[$	$22.70^{+0.60+2.53}_{-0.59-2.15}$	$20.20^{+0.32+1.70}_{-0.32-1.40}$	$20.00^{+0.33+1.74}_{-0.32-1.44}$	$20.80^{+0.45+1.87}_{-0.45-1.60}$	$20.46^{+1.16+2.51}_{-1.13-2.46}$
$[4000, 5000[$	$19.10^{+0.38+1.68}_{-0.38-1.64}$	$21.06^{+0.27+1.74}_{-0.26-1.34}$	$18.86^{+0.26+1.44}_{-0.25-1.26}$	$20.52^{+0.37+1.58}_{-0.37-1.50}$	$20.53^{+0.96+3.05}_{-0.92-2.92}$
$[5000, 6000[$	$19.91^{+0.44+1.90}_{-0.44-1.61}$	$20.89^{+0.34+1.78}_{-0.33-1.40}$	$22.99^{+0.40+1.88}_{-0.39-1.53}$	$23.50^{+0.54+2.13}_{-0.54-1.76}$	$33.50^{+2.53+5.85}_{-2.47-5.72}$
$[6000, 7000[$	$21.83^{+0.60+2.16}_{-0.60-1.95}$	$21.38^{+0.44+1.97}_{-0.44-1.48}$	$20.04^{+0.46+1.65}_{-0.45-1.48}$	$24.52^{+0.82+2.31}_{-0.81-2.07}$	$51.65^{+11.15+30.87}_{-8.75\ -22.23}$
$[7000, 8000[$	$25.48^{+0.88+2.91}_{-0.86-2.64}$	$22.13^{+0.59+2.20}_{-0.60-1.65}$	$19.75^{+0.59+1.80}_{-0.58-1.65}$	$30.86^{+1.55+4.39}_{-1.51-4.02}$	-
$[8000, 9000[$	$22.23^{+0.92+2.83}_{-0.94-2.63}$	$20.94^{+0.71+2.29}_{-0.71-1.69}$	$21.01^{+0.79+2.10}_{-0.78-1.99}$	$24.43^{+1.84+5.47}_{-1.79-4.49}$	-
$[9000, 10000[$	$20.41^{+1.03+2.50}_{-1.00-2.25}$	$17.05^{+0.73+1.81}_{-0.73-1.27}$	$24.17^{+1.20+2.51}_{-1.16-1.92}$	$22.37^{+2.83+5.70}_{-2.58-5.25}$	-
$[10000, 11000[$	$23.87^{+1.49+2.18}_{-1.45-1.48}$	$21.59^{+1.14+1.78}_{-1.15-1.15}$	$22.06^{+1.47+2.20}_{-1.47-1.03}$	$25.37^{+7.20+9.30}_{-5.61-6.79}$	-
$[11000, 12000[$	$24.08^{+1.89+2.48}_{-1.87-1.17}$	$19.77^{+1.30+1.87}_{-1.31-0.84}$	$24.05^{+2.01+2.71}_{-1.90-1.11}$	-	-
$[12000, 13000[$	$27.44^{+2.43+3.73}_{-2.35-1.12}$	$16.91^{+1.49+1.71}_{-1.48-0.73}$	$24.87^{+2.77+3.57}_{-2.55-1.25}$	-	-
$[13000, 14000[$	$20.03^{+2.39+2.77}_{-2.33-0.37}$	$22.06^{+2.06+2.35}_{-1.95-1.11}$	$26.19^{+4.10+4.78}_{-3.79-0.68}$	-	-
$[14000, 15000[$	-	-	-	-	-

Table 9.13: The ratios of differential production cross-sections in 10^{-2} for prompt D^{*+} and D^0 mesons in bins of (y, p_T). The first uncertainty is statistical, and the second is the total systematic.

	y				
p_{T} [MeV/c]	$[2, 2.5[$	$[2.5, 3[$	$[3, 3.5[$	$[3.5, 4[$	$[4, 4.5[$
$[0, 1000[$	-	-	-	-	$17.52^{+2.41+6.21}_{-2.41-5.25}$
$[1000, 1500[$	-	$30.39^{+1.26+5.86}_{-1.26-5.42}$	$36.60^{+0.47+7.21}_{-0.47-5.97}$	$31.28^{+0.51+6.17}_{-0.50-5.25}$	$40.97^{+1.32+9.92}_{-1.33-7.75}$
$[1500, 2000[$	-	$38.90^{+0.67+4.13}_{-0.66-4.67}$	$40.50^{+0.34+7.95}_{-0.34-6.40}$	$38.30^{+0.42+7.48}_{-0.40-6.57}$	$39.00^{+0.91+8.24}_{-0.91-6.53}$
$[2000, 2500[$	$30.26^{+2.75+7.23}_{-2.75-6.81}$	$41.27^{+0.47+3.07}_{-0.47-2.98}$	$43.85^{+0.31+8.25}_{-0.31-6.84}$	$40.70^{+0.38+7.94}_{-0.38-6.71}$	$43.69^{+0.89+8.49}_{-0.90-7.03}$
$[2500, 3000[$	$41.46^{+1.44+4.65}_{-1.47-5.24}$	$41.97^{+0.40+2.21}_{-0.39-2.16}$	$45.48^{+0.32+7.90}_{-0.32-6.84}$	$42.72^{+0.41+8.64}_{-0.42-6.95}$	$43.09^{+0.92+7.04}_{-0.92-6.04}$
$[3000, 3500[$	$43.78^{+1.15+4.05}_{-1.11-3.97}$	$42.74^{+0.37+2.04}_{-0.37-1.75}$	$44.42^{+0.33+7.04}_{-0.33-6.47}$	$42.01^{+0.44+8.50}_{-0.43-6.77}$	$47.98^{+1.12+7.00}_{-1.13-6.49}$
$[3500, 4000[$	$42.83^{+0.91+3.45}_{-0.91-3.15}$	$44.91^{+0.40+2.06}_{-0.39-1.76}$	$48.58^{+0.39+7.01}_{-0.39-6.93}$	$45.30^{+0.51+9.11}_{-0.49-7.34}$	$45.60^{+1.34+5.59}_{-1.31-5.56}$
$[4000, 5000[$	$44.85^{+0.64+2.57}_{-0.63-2.39}$	$43.84^{+0.31+1.83}_{-0.30-1.62}$	$46.40^{+0.31+6.00}_{-0.31-6.33}$	$46.24^{+0.45+8.37}_{-0.45-6.86}$	$46.48^{+1.45+4.50}_{-1.44-3.88}$
$[5000, 6000[$	$45.83^{+0.70+2.99}_{-0.69-2.41}$	$44.13^{+0.37+1.77}_{-0.37-1.73}$	$49.41^{+0.43+6.44}_{-0.43-6.11}$	$50.07^{+0.68+7.36}_{-0.71-6.36}$	$54.02^{+3.64+7.19}_{-3.39-6.37}$
$[6000, 7000[$	$43.53^{+0.77+2.99}_{-0.76-2.44}$	$46.42^{+0.49+2.04}_{-0.50-1.98}$	$47.68^{+0.57+5.51}_{-0.57-5.55}$	$48.03^{+1.02+5.43}_{-1.04-4.94}$	$64.87^{+16.52+38.32}_{-12.90-28.31}$
$[7000, 8000[$	$53.37^{+1.09+3.74}_{-1.09-3.68}$	$47.09^{+0.65+2.88}_{-0.65-2.34}$	$51.20^{+0.81+5.56}_{-0.79-5.73}$	$56.77^{+1.93+7.44}_{-1.85-6.77}$	-
$[8000, 9000[$	$47.09^{+1.14+3.72}_{-1.13-3.79}$	$50.95^{+0.91+3.25}_{-0.87-2.69}$	$50.66^{+1.09+4.84}_{-1.06-5.30}$	$44.58^{+2.81+6.59}_{-2.65-5.61}$	-
$[9000, 10000[$	$38.97^{+1.21+2.62}_{-1.22-2.68}$	$47.58^{+1.06+1.94}_{-1.03-2.51}$	$49.80^{+1.39+3.33}_{-1.38-3.87}$	$49.41^{+5.86+8.20}_{-5.27-9.03}$	-
$[10000, 11000[$	$49.74^{+1.81+2.21}_{-1.79-2.18}$	$50.12^{+1.46+1.25}_{-1.41-2.06}$	$52.73^{+2.07+3.39}_{-1.96-3.13}$	$54.65^{+15.70+21.56}_{-12.17-17.93}$	-
$[11000, 12000[$	$52.56^{+2.29+2.95}_{-2.31-2.62}$	$45.41^{+1.62+1.21}_{-1.61-2.21}$	$48.04^{+2.71+2.94}_{-2.58-2.86}$	-	-
$[12000, 13000[$	$49.79^{+2.74+3.67}_{-2.68-3.67}$	$49.53^{+2.22+1.43}_{-2.10-2.60}$	$50.91^{+3.95+4.53}_{-3.72-2.33}$	-	-
$[13000, 14000[$	$55.36^{+3.50+3.69}_{-3.43-3.47}$	$42.98^{+2.53+1.37}_{-2.47-2.86}$	$63.32^{+7.17+7.31}_{-6.63-4.41}$	-	-
$[14000, 15000[$	$49.23^{+4.19+4.03}_{-3.92-2.52}$	$53.58^{+3.90+3.34}_{-3.61-3.71}$	$45.44^{+9.12+11.45}_{-7.92-9.12}$	-	-

Table 9.14: The ratios of differential production cross-sections in 10^{-2} for prompt D_s^+ and D^+ mesons in bins of (y, p_T). The first uncertainty is statistical, and the second is the total systematic.

	y				
p_{T} [MeV/c]	$[2, 2.5[$	$[2.5, 3[$	$[3, 3.5[$	$[3.5, 4[$	$[4, 4.5[$
$[1000, 1500[$	$45.21^{+11.39+24.35}_{-11.24-25.13}$	$30.11^{+2.17+6.50}_{-2.15-5.63}$	$36.31^{+2.21+6.04}_{-2.20-5.19}$	$46.27^{+4.59+11.35}_{-4.59-10.11}$	$96.32^{+31.21+32.99}_{-31.22-63.42}$
$[1500, 2000[$	$27.35^{+1.78+5.73}_{-1.76-5.04}$	$40.14^{+1.07+4.32}_{-1.07-4.34}$	$46.93^{+1.18+4.48}_{-1.20-4.21}$	$50.29^{+1.82+6.19}_{-1.82-5.57}$	$31.07^{+3.22+6.87}_{-3.20-5.69}$
$[2000, 2500[$	$47.50^{+1.75+7.83}_{-1.76-6.18}$	$46.62^{+0.81+3.91}_{-0.82-3.64}$	$44.21^{+0.75+3.43}_{-0.77-3.39}$	$45.78^{+1.07+4.52}_{-1.08-3.97}$	$39.07^{+2.54+6.32}_{-2.57-4.91}$
$[2500, 3000[$	$46.69^{+1.39+6.00}_{-1.40-5.62}$	$49.68^{+0.75+3.79}_{-0.75-3.63}$	$52.58^{+0.78+3.91}_{-0.77-3.98}$	$48.61^{+0.97+4.75}_{-0.99-3.82}$	$37.70^{+1.89+4.95}_{-1.85-3.85}$
$[3000, 3500[$	$45.96^{+1.28+5.34}_{-1.24-4.52}$	$49.55^{+0.74+4.02}_{-0.74-3.60}$	$49.29^{+0.73+3.82}_{-0.73-3.58}$	$44.88^{+0.90+4.46}_{-0.90-3.39}$	$45.30^{+2.23+5.82}_{-2.22-4.69}$
$[3500, 4000[$	$56.43^{+1.51+6.23}_{-1.53-5.15}$	$48.10^{+0.75+4.19}_{-0.75-3.25}$	$48.87^{+0.80+4.70}_{-0.78-2.99}$	$52.85^{+1.16+4.89}_{-1.13-4.25}$	$42.56^{+2.34+5.01}_{-2.32-4.66}$
$[4000, 5000[$	$44.88^{+0.91+3.81}_{-0.90-3.62}$	$50.21^{+0.64+4.16}_{-0.65-3.23}$	$45.48^{+0.61+3.53}_{-0.61-3.26}$	$47.22^{+0.84+3.72}_{-0.84-3.93}$	$44.75^{+1.99+4.38}_{-1.97-4.33}$
$[5000, 6000[$	$46.77^{+1.08+4.09}_{-1.07-3.91}$	$50.67^{+0.81+4.24}_{-0.80-3.47}$	$50.59^{+0.87+4.27}_{-0.85-3.58}$	$53.06^{+1.24+4.91}_{-1.20-4.51}$	$49.96^{+3.30+6.98}_{-3.32-6.03}$
$[6000, 7000[$	$47.08^{+1.30+4.76}_{-1.31-4.24}$	$52.64^{+1.07+4.71}_{-1.09-3.88}$	$45.05^{+1.01+4.06}_{-1.02-3.40}$	$48.11^{+1.56+5.09}_{-1.52-4.60}$	$51.09^{+6.10+9.19}_{-6.06-8.16}$
$[7000, 8000[$	$56.74^{+1.96+6.46}_{-1.96-5.95}$	$52.91^{+1.42+5.14}_{-1.39-4.31}$	$44.80^{+1.31+4.43}_{-1.32-3.68}$	$54.98^{+2.57+6.24}_{-2.59-5.44}$	$25.99^{+7.03+8.66}_{-6.82-6.57}$
$[8000, 9000[$	$49.00^{+2.01+6.46}_{-2.05-5.55}$	$47.38^{+1.61+5.17}_{-1.60-4.07}$	$46.11^{+1.71+5.01}_{-1.68-4.07}$	$54.09^{+3.66+7.77}_{-3.57-6.38}$	-
$[9000, 10000[$	$51.48^{+2.57+6.84}_{-2.57-5.63}$	$41.18^{+1.75+4.64}_{-1.78-3.23}$	$53.53^{+2.56+6.63}_{-2.56-4.31}$	$37.53^{+3.67+5.36}_{-3.70-4.22}$	-
$[10000, 11000[$	$52.33^{+3.18+4.75}_{-3.18-2.97}$	$49.68^{+2.59+4.16}_{-2.66-2.73}$	$46.48^{+3.02+5.59}_{-3.02-2.25}$	$38.73^{+6.96+5.93}_{-6.78-3.26}$	-
$[11000, 12000[$	$47.50^{+3.65+4.71}_{-3.65-2.28}$	$47.06^{+3.10+4.54}_{-3.02-2.20}$	$48.67^{+3.87+4.10}_{-3.77-3.07}$	-	-
$[12000, 13000[$	$54.23^{+4.77+6.49}_{-4.70-1.50}$	$40.25^{+3.52+4.13}_{-3.46-1.91}$	$55.29^{+5.55+5.64}_{-5.53-3.08}$	$33.07^{+11.06+7.46}_{-10.81-3.89}$	-
$[13000, 14000[$	$41.16^{+4.83+5.20}_{-4.80-0.93}$	$53.41^{+4.79+5.56}_{-4.69-3.08}$	$49.13^{+6.90+7.62}_{-6.77-3.03}$	-	-
$[14000, 15000[$	$33.56^{+4.98+4.51}_{-4.82-0.56}$	-	$45.07^{+8.56+9.43}_{-8.41-0.50}$	-	-

Table 9.15: The ratios of differential production cross-sections in 10^{-2} for prompt D^{*+} and D^{+} mesons in bins of (y, p_T). The first uncertainty is statistical, and the second is the total systematic.

	y				
p_{T} [MeV/c]	$[2, 2.5[$	$[2.5, 3[$	$[3, 3.5[$	$[3.5, 4[$	$[4, 4.5[$
$[0, 1000[$	-	-	-	-	$57.26^{+9.02+27.07}_{-8.54-17.48}$
$[1000, 1500[$	-	$71.31^{+3.02+11.76}_{-3.04-10.70}$	$87.36^{+1.27+9.16}_{-1.31-6.17}$	$79.58^{+1.48+10.49}_{-1.48-8.15}$	$102.95^{+3.84+22.83}_{-3.75-16.20}$
$[1500, 2000[$	-	$98.22^{+1.75+7.52}_{-1.73-9.56}$	$98.76^{+0.88+10.46}_{-0.88-8.22}$	$103.00^{+1.18+14.36}_{-1.16-10.84}$	$92.48^{+2.30+16.05}_{-2.19-12.11}$
$[2000, 2500[$	$72.76^{+6.76+17.49}_{-6.58-17.38}$	$105.36^{+1.23+6.29}_{-1.23-6.31}$	$111.09^{+0.82+12.45}_{-0.79-10.92}$	$105.81^{+1.00+15.69}_{-1.02-11.45}$	$108.51^{+2.26+17.14}_{-2.24-13.99}$
$[2500, 3000[$	$94.24^{+3.33+11.70}_{-3.39-11.92}$	$108.60^{+1.03+5.39}_{-1.04-5.08}$	$111.67^{+0.79+12.49}_{-0.79-11.53}$	$112.58^{+1.08+17.67}_{-1.05-13.96}$	$107.41^{+2.29+13.54}_{-2.22-11.44}$
$[3000, 3500[$	$103.94^{+2.80+10.38}_{-2.70-9.60}$	$102.65^{+0.90+5.05}_{-0.92-4.58}$	$106.06^{+0.76+11.79}_{-0.78-11.12}$	$105.76^{+1.06+17.25}_{-1.07-13.32}$	$107.23^{+2.45+13.50}_{-2.45-12.50}$
$[3500, 4000[$	$106.38^{+2.38+9.25}_{-2.28-7.95}$	$106.92^{+0.95+5.73}_{-0.95-4.35}$	$118.68^{+0.95+14.19}_{-0.92-12.44}$	$115.16^{+1.24+18.67}_{-1.27-15.64}$	$94.87^{+2.61+8.22}_{-2.59-8.03}$
$[4000, 5000[$	$105.34^{+1.52+6.47}_{-1.50-5.66}$	$104.51^{+0.72+4.67}_{-0.73-4.32}$	$111.86^{+0.74+11.01}_{-0.76-12.70}$	$106.42^{+1.00+15.58}_{-1.01-14.03}$	$101.28^{+2.89+11.16}_{-2.85-9.24}$
$[5000, 6000[$	$107.65^{+1.72+6.61}_{-1.65-6.10}$	$107.03^{+0.91+4.56}_{-0.89-4.66}$	$108.74^{+0.95+11.90}_{-0.95-11.61}$	$113.03^{+1.46+13.41}_{-1.45-12.65}$	$80.62^{+4.42+15.02}_{-4.40-10.95}$
$[6000, 7000[$	$93.82^{+1.70+6.50}_{-1.68-5.38}$	$114.29^{+1.21+5.30}_{-1.20-5.67}$	$107.12^{+1.27+11.11}_{-1.22-11.04}$	$94.27^{+1.85+8.01}_{-1.88-7.81}$	$64.16^{+10.65+14.16}_{-10.46-11.78}$
$[7000, 8000[$	$118.80^{+2.52+8.46}_{-2.39-8.63}$	$112.59^{+1.53+6.66}_{-1.50-6.37}$	$116.13^{+1.78+11.85}_{-1.77-11.29}$	$101.12^{+2.99+10.31}_{-2.94-8.94}$	-
$[8000, 9000[$	$103.79^{+2.52+8.85}_{-2.52-7.93}$	$115.30^{+2.00+7.50}_{-1.93-6.75}$	$111.18^{+2.26+10.52}_{-2.20-10.41}$	$98.69^{+5.00+14.24}_{-4.86-11.08}$	-
$[9000, 10000[$	$98.25^{+3.12+8.41}_{-2.99-7.33}$	$114.89^{+2.46+6.53}_{-2.36-7.18}$	$110.20^{+2.88+8.41}_{-2.83-7.79}$	$82.93^{+7.46+12.01}_{-7.22-9.67}$	-
$[10000, 11000[$	$108.99^{+3.86+5.24}_{-3.78-4.61}$	$115.39^{+3.18+3.72}_{-3.10-5.44}$	$111.14^{+3.90+6.23}_{-3.82-3.71}$	$83.51^{+15.13+18.08}_{-14.87-16.16}$	-
$[11000, 12000[$	$103.58^{+4.47+5.50}_{-4.42-5.09}$	$108.15^{+3.72+3.65}_{-3.71-5.79}$	$97.20^{+4.77+4.52}_{-4.76-7.99}$	$66.15^{+9.23+32.96}_{-8.91-30.95}$	-
$[12000, 13000[$	$98.21^{+5.13+5.23}_{-4.98-5.87}$	$117.96^{+4.91+4.30}_{-4.73-6.50}$	$113.08^{+7.61+5.87}_{-7.51-6.48}$	-	-
$[13000, 14000[$	$113.59^{+6.92+6.22}_{-6.67-7.80}$	$103.93^{+5.77+3.63}_{-5.56-7.27}$	$118.61^{+10.82+10.15}_{-10.26-9.84}$	-	-
$[14000, 15000[$	$92.30^{+7.31+7.69}_{-7.14-7.88}$	$122.67^{+7.96+5.13}_{-7.62-9.51}$	$73.97^{+11.38+12.16}_{-10.85-13.37}$	-	-

Table 9.16: The ratios of differential production cross-sections in 10^{-2} for prompt D_s^+ and D^{*+} mesons in bins of (y, p_T). The first uncertainty is statistical, and the second is the total systematic.

	y				
p_{T} [MeV/c]	$[2, 2.5[$	$[2.5, 3[$	$[3, 3.5[$	$[3.5, 4[$	$[4, 4.5[$
$[1000, 1500[$	-	$42.27^{+3.50+13.30}_{-3.42-10.03}$	$41.57^{+2.55+6.37}_{-2.55-6.51}$	$58.18^{+5.89+16.35}_{-5.84-14.49}$	$93.41^{+30.23+33.94}_{-30.15-62.40}$
$[1500, 2000[$	-	$40.86^{+1.27+7.10}_{-1.25-5.41}$	$47.52^{+1.23+5.28}_{-1.26-5.48}$	$48.82^{+1.82+9.03}_{-1.81-8.60}$	$33.59^{+3.55+9.58}_{-3.49-7.97}$
$[2000, 2500[$	$65.28^{+6.87+25.52}_{-5.89-13.70}$	$44.25^{+0.89+4.55}_{-0.91-4.01}$	$39.78^{+0.72+5.17}_{-0.70-4.80}$	$43.27^{+1.06+7.85}_{-1.07-7.36}$	$35.99^{+2.49+8.78}_{-2.41-6.89}$
$[2500, 3000[$	$49.56^{+2.28+9.89}_{-2.17-7.61}$	$45.74^{+0.78+3.66}_{-0.75-3.58}$	$47.10^{+0.73+6.69}_{-0.74-5.98}$	$43.17^{+0.92+8.77}_{-0.91-7.37}$	$35.11^{+1.86+7.04}_{-1.82-5.55}$
$[3000, 3500[$	$44.21^{+1.65+6.73}_{-1.59-5.38}$	$48.26^{+0.81+4.00}_{-0.79-3.59}$	$46.47^{+0.74+7.00}_{-0.75-5.86}$	$42.44^{+0.91+9.03}_{-0.91-7.40}$	$42.23^{+2.25+8.51}_{-2.17-6.39}$
$[3500, 4000[$	$53.02^{+1.75+6.73}_{-1.72-5.63}$	$44.99^{+0.78+3.67}_{-0.78-3.26}$	$41.19^{+0.70+6.91}_{-0.72-5.05}$	$45.89^{+1.07+9.60}_{-1.04-8.03}$	$44.86^{+2.73+6.90}_{-2.66-5.70}$
$[4000, 5000[$	$42.60^{+1.00+3.84}_{-0.99-3.76}$	$48.03^{+0.67+3.94}_{-0.66-3.08}$	$40.66^{+0.57+6.88}_{-0.59-4.82}$	$44.38^{+0.87+8.46}_{-0.85-7.41}$	$44.18^{+2.28+6.22}_{-2.18-6.07}$
$[5000, 6000[$	$43.44^{+1.13+4.09}_{-1.10-3.82}$	$47.34^{+0.82+4.10}_{-0.81-3.21}$	$46.54^{+0.85+7.72}_{-0.86-5.88}$	$46.96^{+1.18+8.25}_{-1.18-6.80}$	$61.96^{+5.44+10.07}_{-5.02-9.58}$
$[6000, 7000[$	$50.19^{+1.56+5.07}_{-1.58-4.82}$	$46.05^{+1.00+4.30}_{-0.99-3.33}$	$42.05^{+1.00+6.56}_{-0.98-5.15}$	$51.04^{+1.91+7.20}_{-1.81-5.91}$	$79.63^{+18.36+24.05}_{-14.39-15.93}$
$[7000, 8000[$	$47.78^{+1.79+5.83}_{-1.81-5.06}$	$47.00^{+1.35+4.80}_{-1.33-4.05}$	$38.57^{+1.23+5.74}_{-1.18-4.53}$	$54.36^{+2.93+7.69}_{-2.85-6.75}$	-
$[8000, 9000[$	$47.19^{+2.12+6.43}_{-2.09-5.58}$	$41.06^{+1.51+4.49}_{-1.43-3.58}$	$41.46^{+1.68+6.23}_{-1.62-4.73}$	$54.78^{+4.49+10.84}_{-4.23-9.16}$	-
$[9000, 10000[$	$52.40^{+2.91+7.19}_{-2.89-5.99}$	$35.83^{+1.61+4.38}_{-1.61-2.63}$	$48.57^{+2.52+6.69}_{-2.51-4.46}$	$45.23^{+6.13+8.95}_{-5.40-6.64}$	-
$[10000, 11000[$	$48.00^{+3.26+4.34}_{-3.15-2.75}$	$43.03^{+2.45+4.10}_{-2.39-1.87}$	$41.85^{+2.90+4.88}_{-2.91-2.69}$	$46.26^{+13.39+13.85}_{-10.15-5.75}$	-
$[11000, 12000[$	$45.83^{+3.93+4.82}_{-3.70-2.36}$	$43.57^{+2.99+4.84}_{-3.02-1.28}$	$50.11^{+4.47+6.34}_{-4.30-2.53}$	-	-
$[12000, 13000[$	$55.16^{+5.31+7.69}_{-4.89-1.80}$	$34.11^{+3.16+4.12}_{-3.06-0.77}$	$48.88^{+5.68+5.81}_{-5.25-2.51}$	-	-
$[13000, 14000[$	-	$51.40^{+5.14+6.80}_{-4.94-1.75}$	$41.36^{+6.96+6.19}_{-6.27-0.88}$	-	-
$[14000, 15000[$	$36.39^{+5.90+6.35}_{-5.54-1.40}$	-	$60.90^{+15.41+22.88}_{-12.96-5.77}$	-	-

A Efficiency tables for modes other than $D^0 \to K^-\pi^+$

A.1 Tracking correction

Table A.1: Tracking efficiency correction for $D^+ \to K^-\pi^+\pi^+$. Shown uncertainties are due to the size of the simulated sample.

p_{T} [MeV/c]	y $[2, 2.5[$	$[2.5, 3[$	$[3, 3.5[$	$[3.5, 4[$	$[4, 4.5[$
$[14000, 15000[$	107.06 ± 0.09	104.36 ± 0.09	101.02 ± 0.08	101.00 ± 0.06	102.75 ± 0.09
$[13000, 14000[$	107.55 ± 0.07	104.51 ± 0.07	101.04 ± 0.07	100.78 ± 0.07	102.35 ± 0.09
$[12000, 13000[$	108.15 ± 0.06	104.80 ± 0.06	100.87 ± 0.06	100.44 ± 0.04	102.17 ± 0.06
$[11000, 12000[$	108.84 ± 0.05	105.15 ± 0.05	100.83 ± 0.05	100.10 ± 0.04	102.02 ± 0.05
$[10000, 11000[$	109.69 ± 0.04	105.61 ± 0.04	100.89 ± 0.04	99.70 ± 0.03	101.63 ± 0.04
$[9000, 10000[$	110.58 ± 0.12	106.29 ± 0.12	100.87 ± 0.12	99.55 ± 0.09	101.50 ± 0.09
$[8000, 9000[$	111.98 ± 0.11	106.99 ± 0.12	101.48 ± 0.12	99.15 ± 0.11	100.99 ± 0.11
$[7000, 8000[$	113.16 ± 0.10	107.64 ± 0.12	101.61 ± 0.10	98.85 ± 0.08	100.17 ± 0.09
$[6000, 7000[$	114.75 ± 0.10	108.75 ± 0.09	101.97 ± 0.10	98.79 ± 0.06	99.68 ± 0.07
$[5000, 6000[$	116.02 ± 0.08	109.79 ± 0.07	102.75 ± 0.07	98.93 ± 0.05	99.09 ± 0.06
$[4000, 5000[$	117.63 ± 0.08	111.11 ± 0.07	103.62 ± 0.05	99.30 ± 0.05	98.61 ± 0.04
$[3500, 4000[$	118.45 ± 0.11	111.94 ± 0.09	104.11 ± 0.07	99.81 ± 0.05	98.41 ± 0.05
$[3000, 3500[$	119.16 ± 0.12	112.43 ± 0.08	104.64 ± 0.06	100.10 ± 0.05	98.32 ± 0.04
$[2500, 3000[$	118.99 ± 0.13	112.73 ± 0.09	105.01 ± 0.06	100.49 ± 0.05	98.43 ± 0.04
$[2000, 2500[$	119.05 ± 0.14	112.89 ± 0.08	105.43 ± 0.06	100.88 ± 0.05	98.64 ± 0.05
$[1500, 2000[$	118.95 ± 0.14	112.56 ± 0.08	105.48 ± 0.06	101.09 ± 0.05	98.89 ± 0.05
$[1000, 1500[$	118.68 ± 0.16	112.12 ± 0.09	105.18 ± 0.06	101.09 ± 0.06	99.04 ± 0.05
$[0, 1000[$	118.73 ± 0.15	111.54 ± 0.08	104.83 ± 0.06	101.04 ± 0.05	99.38 ± 0.06

Table A.2: Tracking efficiency correction for $D^+ \to K^-K^+\pi^+$. Shown uncertainties are due to the size of the simulated sample.

p_{T} [MeV/c]	y [2, 2.5[	[2.5, 3[	[3, 3.5[	[3.5, 4[	[4, 4.5[
[14000, 15000[	105.95 ± 0.07	103.11 ± 0.06	100.40 ± 0.07	100.89 ± 0.06	103.07 ± 0.09
[13000, 14000[	106.64 ± 0.06	103.50 ± 0.08	100.27 ± 0.06	100.42 ± 0.05	103.02 ± 0.08
[12000, 13000[	107.48 ± 0.05	103.81 ± 0.04	100.10 ± 0.07	100.04 ± 0.04	102.49 ± 0.06
[11000, 12000[	108.20 ± 0.04	104.22 ± 0.04	100.10 ± 0.04	99.66 ± 0.04	102.24 ± 0.05
[10000, 11000[	109.11 ± 0.04	104.86 ± 0.03	100.14 ± 0.04	99.26 ± 0.03	101.62 ± 0.05
[9000, 10000[	110.16 ± 0.14	105.33 ± 0.10	100.15 ± 0.10	98.97 ± 0.07	101.38 ± 0.08
[8000, 9000[	111.75 ± 0.12	106.46 ± 0.11	100.66 ± 0.12	98.56 ± 0.08	100.59 ± 0.13
[7000, 8000[	112.94 ± 0.12	107.39 ± 0.09	100.97 ± 0.08	98.47 ± 0.07	99.85 ± 0.09
[6000, 7000[	114.88 ± 0.09	108.49 ± 0.08	101.63 ± 0.07	98.38 ± 0.05	99.32 ± 0.07
[5000, 6000[	116.72 ± 0.07	110.06 ± 0.07	102.37 ± 0.06	98.66 ± 0.03	98.63 ± 0.05
[4000, 5000[	118.64 ± 0.07	111.65 ± 0.06	103.17 ± 0.05	99.20 ± 0.03	98.37 ± 0.03
[3500, 4000[	119.74 ± 0.09	112.67 ± 0.09	103.81 ± 0.06	99.73 ± 0.04	98.22 ± 0.04
[3000, 3500[	120.33 ± 0.10	113.17 ± 0.09	104.23 ± 0.06	100.08 ± 0.04	98.31 ± 0.03
[2500, 3000[	120.04 ± 0.10	113.26 ± 0.09	104.64 ± 0.06	100.51 ± 0.04	98.55 ± 0.04
[2000, 2500[	119.71 ± 0.11	112.58 ± 0.09	104.47 ± 0.06	100.78 ± 0.04	98.94 ± 0.04
[1500, 2000[	118.70 ± 0.14	111.59 ± 0.09	103.75 ± 0.06	100.88 ± 0.05	99.32 ± 0.06
[1000, 1500[	117.68 ± 0.17	110.09 ± 0.09	102.71 ± 0.06	100.70 ± 0.05	99.60 ± 0.06

Table A.3: Tracking efficiency correction for $D_s^+ \to \phi\pi^+$. Shown uncertainties are due to the size of the simulated sample.

p_{T} [MeV/c]	y [2, 2.5[	[2.5, 3[	[3, 3.5[	[3.5, 4[	[4, 4.5[
[14000, 15000[	105.62 ± 0.13	102.53 ± 0.10	100.15 ± 0.10	100.76 ± 0.10	103.09 ± 0.17
[13000, 14000[	106.19 ± 0.12	103.05 ± 0.08	100.03 ± 0.09	100.30 ± 0.10	102.93 ± 0.13
[12000, 13000[	107.21 ± 0.09	103.36 ± 0.06	99.99 ± 0.07	99.95 ± 0.06	102.64 ± 0.10
[11000, 12000[	107.94 ± 0.08	103.81 ± 0.06	99.84 ± 0.06	99.57 ± 0.06	102.18 ± 0.09
[10000, 11000[	108.92 ± 0.07	104.40 ± 0.05	100.01 ± 0.06	99.18 ± 0.05	101.75 ± 0.08
[9000, 10000[	109.92 ± 0.21	105.30 ± 0.15	100.12 ± 0.19	98.77 ± 0.11	101.38 ± 0.15
[8000, 9000[	111.19 ± 0.22	105.75 ± 0.16	100.45 ± 0.14	98.33 ± 0.14	100.31 ± 0.16
[7000, 8000[	112.63 ± 0.19	107.11 ± 0.16	100.87 ± 0.14	98.42 ± 0.10	100.00 ± 0.14
[6000, 7000[	114.60 ± 0.17	108.39 ± 0.12	101.36 ± 0.09	98.53 ± 0.08	99.21 ± 0.14
[5000, 6000[	116.52 ± 0.13	110.15 ± 0.11	102.32 ± 0.09	98.80 ± 0.06	98.57 ± 0.07
[4000, 5000[	118.75 ± 0.12	111.65 ± 0.10	103.34 ± 0.08	99.43 ± 0.05	98.24 ± 0.06
[3500, 4000[	119.83 ± 0.15	112.67 ± 0.13	103.84 ± 0.10	100.00 ± 0.06	98.18 ± 0.06
[3000, 3500[	119.98 ± 0.21	113.18 ± 0.14	104.24 ± 0.11	100.57 ± 0.05	98.37 ± 0.07
[2500, 3000[	120.08 ± 0.18	112.90 ± 0.15	104.47 ± 0.11	100.84 ± 0.06	98.66 ± 0.06
[2000, 2500[	119.12 ± 0.20	112.28 ± 0.17	104.24 ± 0.11	101.16 ± 0.07	99.22 ± 0.08
[1500, 2000[	118.11 ± 0.24	111.91 ± 0.18	103.71 ± 0.11	101.28 ± 0.09	99.75 ± 0.07
[1000, 1500[	117.62 ± 0.29	110.77 ± 0.19	102.36 ± 0.11	101.40 ± 0.09	100.02 ± 0.12

Table A.4: Tracking efficiency correction for $D_s^+ \to K^-K^+\pi^+$ no ϕ. Shown uncertainties are due to the size of the simulated sample.

p_{T} [MeV/c]	y [2, 2.5[	[2.5, 3[	[3, 3.5[	[3.5, 4[	[4, 4.5[
[14000, 15000[	107.00 ± 0.12	104.17 ± 0.10	101.16 ± 0.10	100.95 ± 0.07	102.94 ± 0.14
[13000, 14000[	107.67 ± 0.09	104.61 ± 0.07	101.19 ± 0.09	100.54 ± 0.06	102.34 ± 0.09
[12000, 13000[	108.31 ± 0.08	105.00 ± 0.07	100.91 ± 0.07	100.30 ± 0.05	102.11 ± 0.08
[11000, 12000[	109.06 ± 0.07	105.34 ± 0.06	100.85 ± 0.06	100.09 ± 0.04	101.84 ± 0.07
[10000, 11000[	109.98 ± 0.05	105.98 ± 0.05	100.82 ± 0.05	99.80 ± 0.04	101.48 ± 0.05
[9000, 10000[	110.94 ± 0.18	106.72 ± 0.17	100.73 ± 0.17	99.58 ± 0.10	101.24 ± 0.12
[8000, 9000[	112.07 ± 0.15	107.23 ± 0.15	101.26 ± 0.18	99.08 ± 0.10	100.63 ± 0.14
[7000, 8000[	113.17 ± 0.12	108.35 ± 0.13	101.25 ± 0.13	98.97 ± 0.10	100.36 ± 0.12
[6000, 7000[	114.79 ± 0.11	109.09 ± 0.11	101.68 ± 0.11	98.74 ± 0.07	99.96 ± 0.09
[5000, 6000[	116.53 ± 0.09	110.28 ± 0.10	102.31 ± 0.09	98.72 ± 0.05	99.22 ± 0.07
[4000, 5000[	117.91 ± 0.10	111.34 ± 0.09	102.98 ± 0.08	98.97 ± 0.05	98.78 ± 0.05
[3500, 4000[	118.68 ± 0.15	112.07 ± 0.12	103.33 ± 0.10	99.34 ± 0.06	98.56 ± 0.06
[3000, 3500[	118.88 ± 0.15	112.42 ± 0.11	103.73 ± 0.09	99.32 ± 0.05	98.62 ± 0.06
[2500, 3000[	119.31 ± 0.16	112.33 ± 0.12	103.98 ± 0.08	99.74 ± 0.06	98.60 ± 0.05
[2000, 2500[	119.11 ± 0.16	112.09 ± 0.11	103.75 ± 0.09	99.82 ± 0.07	98.70 ± 0.06
[1500, 2000[	118.21 ± 0.22	111.29 ± 0.12	103.47 ± 0.08	99.71 ± 0.06	98.71 ± 0.07
[1000, 1500[	117.63 ± 0.26	110.13 ± 0.12	103.06 ± 0.08	99.66 ± 0.07	98.69 ± 0.08

Table A.5: Tracking efficiency correction for $D^{*+} \to D^0\pi^+$ with $D^0 \to K^-\pi^+$. Shown uncertainties are due to the size of the simulated sample.

	y				
p_{T} [MeV/c]	$[2, 2.5[$	$[2.5, 3[$	$[3, 3.5[$	$[3.5, 4[$	$[4, 4.5[$
$[14000, 15000[$	110.29 ± 0.05	108.67 ± 0.05	103.97 ± 0.06	101.93 ± 0.04	101.87 ± 0.05
$[13000, 14000[$	110.51 ± 0.04	108.88 ± 0.04	103.93 ± 0.05	102.00 ± 0.03	101.83 ± 0.04
$[12000, 13000[$	110.88 ± 0.04	109.16 ± 0.03	103.78 ± 0.05	102.06 ± 0.02	101.84 ± 0.03
$[11000, 12000[$	111.16 ± 0.03	109.47 ± 0.02	103.51 ± 0.04	102.10 ± 0.02	101.79 ± 0.03
$[10000, 11000[$	111.60 ± 0.03	109.69 ± 0.02	103.13 ± 0.04	102.10 ± 0.02	101.85 ± 0.02
$[9000, 10000[$	112.02 ± 0.08	109.81 ± 0.06	102.69 ± 0.12	101.88 ± 0.05	101.89 ± 0.06
$[8000, 9000[$	112.57 ± 0.08	110.32 ± 0.06	101.86 ± 0.13	101.22 ± 0.07	101.97 ± 0.06
$[7000, 8000[$	113.22 ± 0.07	110.55 ± 0.05	101.17 ± 0.11	100.28 ± 0.06	102.09 ± 0.04
$[6000, 7000[$	114.06 ± 0.06	110.92 ± 0.04	100.82 ± 0.09	99.04 ± 0.05	101.99 ± 0.04
$[5000, 6000[$	114.98 ± 0.06	111.37 ± 0.04	100.78 ± 0.06	97.63 ± 0.04	101.44 ± 0.04
$[4000, 5000[$	115.97 ± 0.07	111.97 ± 0.03	100.80 ± 0.05	96.79 ± 0.02	100.36 ± 0.04
$[3500, 4000[$	116.61 ± 0.12	112.30 ± 0.05	100.75 ± 0.05	96.68 ± 0.02	99.20 ± 0.05
$[3000, 3500[$	117.09 ± 0.14	112.36 ± 0.06	100.80 ± 0.04	96.87 ± 0.02	98.16 ± 0.04
$[2500, 3000[$	117.32 ± 0.20	111.69 ± 0.07	100.66 ± 0.04	97.25 ± 0.02	97.42 ± 0.04
$[2000, 2500[$	117.02 ± 0.43	110.65 ± 0.09	100.72 ± 0.03	97.58 ± 0.02	96.69 ± 0.03
$[1500, 2000[$	117.13 ± 2.19	108.56 ± 0.12	100.87 ± 0.03	97.93 ± 0.02	96.41 ± 0.03
$[1000, 1500[$	117.38 ± 3.33	105.49 ± 0.14	101.29 ± 0.03	98.09 ± 0.03	96.38 ± 0.03
$[0, 1000[$	116.23 ± 2.83	106.26 ± 0.31	102.07 ± 0.04	98.40 ± 0.03	96.65 ± 0.04

Table A.6: Tracking efficiency correction for $D^{*+} \to D^0\pi^+$ with $D^0 \to K^-\pi^+\pi^-\pi^+$. Shown uncertainties are due to the size of the simulated sample.

	y				
p_{T} [MeV/c]	$[2, 2.5[$	$[2.5, 3[$	$[3, 3.5[$	$[3.5, 4[$	$[4, 4.5[$
$[14000, 15000[$	122.21 ± 0.13	116.32 ± 0.12	103.96 ± 0.15	99.76 ± 0.07	101.05 ± 0.11
$[13000, 14000[$	123.59 ± 0.11	117.36 ± 0.10	104.30 ± 0.13	99.78 ± 0.06	100.90 ± 0.09
$[12000, 13000[$	124.62 ± 0.09	118.32 ± 0.08	104.43 ± 0.11	99.68 ± 0.05	100.59 ± 0.07
$[11000, 12000[$	125.72 ± 0.07	119.30 ± 0.06	104.66 ± 0.10	99.69 ± 0.04	100.35 ± 0.06
$[10000, 11000[$	127.11 ± 0.06	120.47 ± 0.06	105.01 ± 0.09	99.55 ± 0.04	100.10 ± 0.05
$[9000, 10000[$	128.54 ± 0.19	120.98 ± 0.17	104.78 ± 0.25	99.36 ± 0.09	99.80 ± 0.12
$[8000, 9000[$	130.36 ± 0.20	122.50 ± 0.18	104.64 ± 0.27	99.06 ± 0.11	99.84 ± 0.15
$[7000, 8000[$	132.33 ± 0.16	123.99 ± 0.15	104.54 ± 0.23	98.50 ± 0.09	99.61 ± 0.11
$[6000, 7000[$	134.19 ± 0.16	125.07 ± 0.14	104.75 ± 0.18	97.82 ± 0.08	99.40 ± 0.09
$[5000, 6000[$	136.05 ± 0.15	126.25 ± 0.12	105.10 ± 0.14	97.06 ± 0.06	98.89 ± 0.07
$[4000, 5000[$	137.14 ± 0.21	127.21 ± 0.12	105.13 ± 0.11	96.63 ± 0.05	98.02 ± 0.07
$[3500, 4000[$	136.75 ± 0.44	126.60 ± 0.18	105.06 ± 0.12	96.80 ± 0.06	97.05 ± 0.09
$[3000, 3500[$	136.29 ± 0.55	125.79 ± 0.20	104.72 ± 0.11	96.84 ± 0.06	96.20 ± 0.08
$[2500, 3000[$	137.14 ± 0.86	122.68 ± 0.24	103.77 ± 0.10	96.82 ± 0.06	95.71 ± 0.08
$[2000, 2500[$	136.08 ± 1.42	119.75 ± 0.29	102.69 ± 0.10	96.53 ± 0.06	95.12 ± 0.08
$[1500, 2000[$	-	114.24 ± 0.38	101.50 ± 0.10	96.36 ± 0.07	95.11 ± 0.09
$[1000, 1500[$	-	110.52 ± 0.63	99.83 ± 0.12	95.60 ± 0.08	94.82 ± 0.12
$[0, 1000[$	-	108.81 ± 1.30	98.16 ± 0.17	94.90 ± 0.11	95.10 ± 0.21

Table A.7: Total MC selection efficiency for $D^+ \to K^-\pi^+\pi^+$ in bins of D^0 p_{T} and y.

p_{T} [MeV/c]	y $[2, 2.5[$	$[2.5, 3[$	$[3, 3.5[$	$[3.5, 4[$	$[4, 4.5[$
$[14000, 15000[$	$11.65^{+0.35}_{-0.34}$	$22.02^{+0.49}_{-0.49}$	$13.11^{+0.47}_{-0.46}$	$0.67^{+0.15}_{-0.12}$	$0.00^{+0.06}_{-0.00}$
$[13000, 14000[$	$11.56^{+0.29}_{-0.29}$	$22.59^{+0.42}_{-0.42}$	$15.76^{+0.42}_{-0.41}$	$0.87^{+0.14}_{-0.12}$	$0.00^{+0.04}_{-0.00}$
$[12000, 13000[$	$11.60^{+0.25}_{-0.24}$	$23.15^{+0.35}_{-0.35}$	$18.65^{+0.37}_{-0.37}$	$2.38^{+0.18}_{-0.17}$	$0.00^{+0.03}_{-0.00}$
$[11000, 12000[$	$11.49^{+0.20}_{-0.20}$	$22.97^{+0.29}_{-0.29}$	$20.84^{+0.32}_{-0.31}$	$3.75^{+0.18}_{-0.17}$	$0.00^{+0.02}_{-0.00}$
$[10000, 11000[$	$10.42^{+0.16}_{-0.16}$	$22.99^{+0.24}_{-0.24}$	$23.07^{+0.27}_{-0.27}$	$6.53^{+0.19}_{-0.19}$	$0.00^{+0.01}_{-0.00}$
$[9000, 10000[$	$11.28^{+0.61}_{-0.58}$	$22.47^{+0.79}_{-0.77}$	$24.61^{+0.86}_{-0.84}$	$8.49^{+0.59}_{-0.55}$	$0.05^{+0.09}_{-0.04}$
$[8000, 9000[$	$9.36^{+0.49}_{-0.47}$	$21.71^{+0.72}_{-0.70}$	$24.76^{+0.85}_{-0.83}$	$13.51^{+0.77}_{-0.74}$	$0.44^{+0.22}_{-0.15}$
$[7000, 8000[$	$8.04^{+0.36}_{-0.34}$	$20.60^{+0.56}_{-0.55}$	$23.94^{+0.64}_{-0.63}$	$16.43^{+0.62}_{-0.60}$	$1.33^{+0.26}_{-0.22}$
$[6000, 7000[$	$7.39^{+0.26}_{-0.26}$	$18.62^{+0.41}_{-0.40}$	$22.38^{+0.48}_{-0.47}$	$16.95^{+0.49}_{-0.47}$	$2.77^{+0.26}_{-0.24}$
$[5000, 6000[$	$5.40^{+0.18}_{-0.17}$	$16.44^{+0.29}_{-0.29}$	$20.03^{+0.34}_{-0.34}$	$18.63^{+0.37}_{-0.36}$	$4.89^{+0.24}_{-0.23}$
$[4000, 5000[$	$4.26^{+0.12}_{-0.12}$	$13.60^{+0.20}_{-0.20}$	$18.01^{+0.24}_{-0.24}$	$16.14^{+0.26}_{-0.25}$	$6.44^{+0.20}_{-0.19}$
$[3500, 4000[$	$3.22^{+0.12}_{-0.12}$	$11.60^{+0.22}_{-0.21}$	$15.91^{+0.26}_{-0.26}$	$14.29^{+0.27}_{-0.27}$	$5.86^{+0.21}_{-0.20}$
$[3000, 3500[$	$2.12^{+0.09}_{-0.08}$	$9.48^{+0.17}_{-0.17}$	$13.09^{+0.21}_{-0.21}$	$11.92^{+0.22}_{-0.21}$	$5.26^{+0.17}_{-0.17}$
$[2500, 3000[$	$1.35^{+0.06}_{-0.06}$	$7.49^{+0.14}_{-0.13}$	$11.14^{+0.17}_{-0.17}$	$9.91^{+0.18}_{-0.17}$	$4.10^{+0.13}_{-0.13}$
$[2000, 2500[$	$0.76^{+0.04}_{-0.04}$	$4.77^{+0.10}_{-0.10}$	$7.34^{+0.13}_{-0.12}$	$6.59^{+0.13}_{-0.13}$	$2.60^{+0.10}_{-0.09}$
$[1500, 2000[$	$0.21^{+0.02}_{-0.02}$	$2.20^{+0.06}_{-0.06}$	$3.64^{+0.08}_{-0.08}$	$3.39^{+0.09}_{-0.08}$	$1.17^{+0.06}_{-0.06}$
$[1000, 1500[$	$0.04^{+0.01}_{-0.01}$	$0.51^{+0.03}_{-0.03}$	$1.12^{+0.04}_{-0.04}$	$1.06^{+0.05}_{-0.04}$	$0.42^{+0.04}_{-0.03}$
$[0, 1000[$	$0.00^{+0.00}_{-0.00}$	$0.04^{+0.01}_{-0.01}$	$0.11^{+0.01}_{-0.01}$	$0.13^{+0.01}_{-0.01}$	$0.04^{+0.01}_{-0.01}$

A.2 MC selection efficiency

Table A.8: Total MC selection efficiency for $D^+ \to K^-K^+\pi^+$ in bins of D^0 p_{T} and y.

p_{T} [MeV/c]	y [2, 2.5[	[2.5, 3[	[3, 3.5[	[3.5, 4[	[4, 4.5[
[14000, 15000[	$10.84^{+0.34}_{-0.33}$	$21.52^{+0.49}_{-0.48}$	$14.49^{+0.48}_{-0.47}$	$0.68^{+0.15}_{-0.12}$	$0.00^{+0.06}_{-0.00}$
[13000, 14000[	$11.49^{+0.29}_{-0.29}$	$21.06^{+0.41}_{-0.40}$	$17.42^{+0.44}_{-0.43}$	$1.74^{+0.19}_{-0.17}$	$0.00^{+0.04}_{-0.00}$
[12000, 13000[	$11.21^{+0.24}_{-0.24}$	$21.66^{+0.34}_{-0.34}$	$19.99^{+0.38}_{-0.38}$	$2.81^{+0.19}_{-0.18}$	$0.00^{+0.02}_{-0.00}$
[11000, 12000[	$11.27^{+0.20}_{-0.20}$	$21.15^{+0.28}_{-0.28}$	$21.66^{+0.32}_{-0.32}$	$5.35^{+0.21}_{-0.20}$	$0.00^{+0.02}_{-0.00}$
[10000, 11000[	$10.71^{+0.16}_{-0.16}$	$21.43^{+0.23}_{-0.23}$	$22.30^{+0.27}_{-0.26}$	$8.30^{+0.21}_{-0.21}$	$0.00^{+0.01}_{-0.00}$
[9000, 10000[	$10.68^{+0.61}_{-0.58}$	$22.29^{+0.83}_{-0.81}$	$23.09^{+0.86}_{-0.84}$	$11.68^{+0.70}_{-0.67}$	$0.16^{+0.12}_{-0.07}$
[8000, 9000[	$10.38^{+0.53}_{-0.51}$	$19.57^{+0.75}_{-0.73}$	$22.46^{+0.88}_{-0.85}$	$15.82^{+0.87}_{-0.83}$	$0.63^{+0.27}_{-0.19}$
[7000, 8000[	$9.57^{+0.40}_{-0.39}$	$20.03^{+0.58}_{-0.57}$	$23.03^{+0.66}_{-0.65}$	$18.98^{+0.72}_{-0.70}$	$1.82^{+0.31}_{-0.26}$
[6000, 7000[	$8.05^{+0.29}_{-0.28}$	$17.96^{+0.42}_{-0.42}$	$22.50^{+0.51}_{-0.50}$	$19.14^{+0.53}_{-0.52}$	$3.96^{+0.32}_{-0.30}$
[5000, 6000[	$6.99^{+0.21}_{-0.20}$	$16.25^{+0.31}_{-0.30}$	$20.81^{+0.37}_{-0.36}$	$18.50^{+0.39}_{-0.38}$	$6.31^{+0.28}_{-0.27}$
[4000, 5000[	$5.06^{+0.13}_{-0.13}$	$14.47^{+0.22}_{-0.22}$	$17.74^{+0.25}_{-0.25}$	$16.40^{+0.27}_{-0.27}$	$6.68^{+0.21}_{-0.20}$
[3500, 4000[	$3.89^{+0.14}_{-0.13}$	$12.65^{+0.24}_{-0.23}$	$15.56^{+0.27}_{-0.27}$	$13.81^{+0.28}_{-0.28}$	$5.75^{+0.22}_{-0.21}$
[3000, 3500[	$2.86^{+0.10}_{-0.10}$	$10.34^{+0.19}_{-0.18}$	$13.41^{+0.22}_{-0.22}$	$11.60^{+0.23}_{-0.22}$	$4.71^{+0.17}_{-0.16}$
[2500, 3000[	$1.94^{+0.08}_{-0.07}$	$8.24^{+0.15}_{-0.15}$	$10.76^{+0.18}_{-0.17}$	$8.74^{+0.17}_{-0.17}$	$3.25^{+0.13}_{-0.12}$
[2000, 2500[	$0.91^{+0.05}_{-0.04}$	$4.75^{+0.10}_{-0.10}$	$6.33^{+0.12}_{-0.12}$	$5.25^{+0.12}_{-0.12}$	$1.86^{+0.09}_{-0.08}$
[1500, 2000[	$0.21^{+0.02}_{-0.02}$	$1.50^{+0.05}_{-0.05}$	$2.37^{+0.07}_{-0.07}$	$1.94^{+0.07}_{-0.07}$	$0.52^{+0.04}_{-0.04}$
[1000, 1500[	$0.01^{+0.01}_{-0.00}$	$0.17^{+0.02}_{-0.02}$	$0.37^{+0.03}_{-0.03}$	$0.29^{+0.03}_{-0.02}$	$0.12^{+0.02}_{-0.02}$

Table A.9: Total MC selection efficiency for $D_s^+ \to \phi\pi^+$ in bins of D^0 p_{T} and y.

p_{T} [MeV/c]	y [2, 2.5[	[2.5, 3[	[3, 3.5[	[3.5, 4[	[4, 4.5[
[14000, 15000[	$8.43^{+0.50}_{-0.47}$	$13.87^{+0.67}_{-0.64}$	$10.56^{+0.71}_{-0.67}$	$0.94^{+0.30}_{-0.23}$	$0.00^{+0.14}_{-0.00}$
[13000, 14000[	$7.44^{+0.40}_{-0.38}$	$13.98^{+0.57}_{-0.55}$	$11.80^{+0.60}_{-0.57}$	$1.78^{+0.31}_{-0.27}$	$0.00^{+0.10}_{-0.00}$
[12000, 13000[	$7.30^{+0.33}_{-0.32}$	$13.44^{+0.47}_{-0.45}$	$12.90^{+0.52}_{-0.50}$	$2.78^{+0.32}_{-0.29}$	$0.00^{+0.07}_{-0.00}$
[11000, 12000[	$6.80^{+0.26}_{-0.25}$	$13.60^{+0.39}_{-0.38}$	$14.03^{+0.44}_{-0.43}$	$4.61^{+0.32}_{-0.30}$	$0.00^{+0.04}_{-0.00}$
[10000, 11000[	$6.56^{+0.21}_{-0.21}$	$13.13^{+0.31}_{-0.31}$	$13.78^{+0.36}_{-0.35}$	$6.04^{+0.30}_{-0.29}$	$0.00^{+0.03}_{-0.00}$
[9000, 10000[	$7.41^{+0.83}_{-0.75}$	$16.05^{+1.17}_{-1.10}$	$14.38^{+1.14}_{-1.07}$	$9.16^{+1.00}_{-0.91}$	$0.00^{+0.17}_{-0.00}$
[8000, 9000[	$5.67^{+0.63}_{-0.57}$	$12.95^{+0.97}_{-0.91}$	$15.04^{+1.14}_{-1.08}$	$9.33^{+1.06}_{-0.96}$	$0.20^{+0.34}_{-0.14}$
[7000, 8000[	$4.89^{+0.47}_{-0.43}$	$10.61^{+0.69}_{-0.66}$	$13.82^{+0.86}_{-0.81}$	$9.48^{+0.82}_{-0.76}$	$1.47^{+0.45}_{-0.34}$
[6000, 7000[	$5.12^{+0.37}_{-0.35}$	$10.65^{+0.53}_{-0.51}$	$12.93^{+0.63}_{-0.60}$	$9.85^{+0.63}_{-0.60}$	$2.25^{+0.39}_{-0.33}$
[5000, 6000[	$4.44^{+0.26}_{-0.25}$	$9.33^{+0.37}_{-0.36}$	$10.47^{+0.43}_{-0.42}$	$9.63^{+0.45}_{-0.44}$	$2.71^{+0.30}_{-0.27}$
[4000, 5000[	$3.25^{+0.17}_{-0.16}$	$7.97^{+0.26}_{-0.25}$	$9.45^{+0.31}_{-0.30}$	$7.57^{+0.30}_{-0.29}$	$3.01^{+0.22}_{-0.21}$
[3500, 4000[	$1.97^{+0.16}_{-0.15}$	$6.46^{+0.27}_{-0.26}$	$7.35^{+0.31}_{-0.30}$	$5.53^{+0.29}_{-0.28}$	$2.08^{+0.21}_{-0.19}$
[3000, 3500[	$1.40^{+0.12}_{-0.11}$	$5.12^{+0.22}_{-0.21}$	$5.93^{+0.24}_{-0.23}$	$5.11^{+0.24}_{-0.23}$	$1.64^{+0.17}_{-0.15}$
[2500, 3000[	$0.83^{+0.08}_{-0.07}$	$3.78^{+0.17}_{-0.16}$	$4.31^{+0.18}_{-0.18}$	$3.45^{+0.18}_{-0.17}$	$1.28^{+0.13}_{-0.12}$
[2000, 2500[	$0.45^{+0.06}_{-0.05}$	$2.25^{+0.12}_{-0.11}$	$2.84^{+0.14}_{-0.13}$	$2.00^{+0.12}_{-0.12}$	$0.56^{+0.08}_{-0.07}$
[1500, 2000[	$0.18^{+0.03}_{-0.03}$	$0.95^{+0.07}_{-0.07}$	$1.07^{+0.08}_{-0.07}$	$0.60^{+0.07}_{-0.06}$	$0.19^{+0.05}_{-0.04}$
[1000, 1500[	$0.01^{+0.01}_{-0.01}$	$0.17^{+0.03}_{-0.03}$	$0.21^{+0.03}_{-0.03}$	$0.10^{+0.03}_{-0.02}$	$0.00^{+0.01}_{-0.00}$

Table A.10: Total MC selection efficiency for $D_s^+ \to K^-K^+\pi^+$ in bins of D^0 p_{T} and y.

p_{T} [MeV/c]	y [2, 2.5[	[2.5, 3[	[3, 3.5[	[3.5, 4[	[4, 4.5[
[14000, 15000[	$8.20^{+0.40}_{-0.38}$	$15.18^{+0.57}_{-0.55}$	$8.10^{+0.50}_{-0.48}$	$0.05^{+0.09}_{-0.04}$	$0.00^{+0.10}_{-0.00}$
[13000, 14000[	$7.59^{+0.33}_{-0.32}$	$14.79^{+0.47}_{-0.46}$	$9.43^{+0.46}_{-0.44}$	$0.88^{+0.19}_{-0.16}$	$0.00^{+0.07}_{-0.00}$
[12000, 13000[	$6.89^{+0.26}_{-0.25}$	$14.44^{+0.39}_{-0.38}$	$11.59^{+0.41}_{-0.40}$	$1.28^{+0.18}_{-0.16}$	$0.00^{+0.04}_{-0.00}$
[11000, 12000[	$7.06^{+0.22}_{-0.21}$	$14.28^{+0.32}_{-0.32}$	$12.61^{+0.35}_{-0.34}$	$2.44^{+0.20}_{-0.18}$	$0.00^{+0.03}_{-0.00}$
[10000, 11000[	$6.46^{+0.17}_{-0.17}$	$13.40^{+0.26}_{-0.25}$	$14.13^{+0.30}_{-0.30}$	$3.67^{+0.20}_{-0.19}$	$0.00^{+0.02}_{-0.00}$
[9000, 10000[	$5.91^{+0.60}_{-0.55}$	$14.12^{+0.92}_{-0.87}$	$14.49^{+0.95}_{-0.91}$	$5.49^{+0.66}_{-0.60}$	$0.00^{+0.11}_{-0.00}$
[8000, 9000[	$5.15^{+0.50}_{-0.46}$	$13.61^{+0.82}_{-0.78}$	$13.73^{+0.91}_{-0.87}$	$7.36^{+0.83}_{-0.75}$	$0.13^{+0.23}_{-0.10}$
[7000, 8000[	$4.84^{+0.38}_{-0.36}$	$11.11^{+0.59}_{-0.57}$	$13.78^{+0.71}_{-0.68}$	$8.06^{+0.63}_{-0.59}$	$0.81^{+0.28}_{-0.21}$
[6000, 7000[	$3.73^{+0.26}_{-0.24}$	$10.17^{+0.42}_{-0.41}$	$11.95^{+0.50}_{-0.48}$	$9.95^{+0.52}_{-0.50}$	$1.83^{+0.29}_{-0.25}$
[5000, 6000[	$2.83^{+0.17}_{-0.16}$	$8.96^{+0.31}_{-0.30}$	$9.78^{+0.35}_{-0.34}$	$7.94^{+0.35}_{-0.34}$	$1.82^{+0.21}_{-0.19}$
[4000, 5000[	$1.87^{+0.11}_{-0.10}$	$6.61^{+0.20}_{-0.20}$	$8.42^{+0.24}_{-0.23}$	$7.20^{+0.24}_{-0.24}$	$2.58^{+0.17}_{-0.16}$
[3500, 4000[	$1.20^{+0.10}_{-0.09}$	$5.65^{+0.21}_{-0.21}$	$6.60^{+0.24}_{-0.24}$	$5.76^{+0.25}_{-0.24}$	$1.85^{+0.17}_{-0.16}$
[3000, 3500[	$0.90^{+0.08}_{-0.07}$	$4.03^{+0.16}_{-0.15}$	$5.16^{+0.19}_{-0.18}$	$4.42^{+0.19}_{-0.18}$	$1.26^{+0.12}_{-0.11}$
[2500, 3000[	$0.46^{+0.05}_{-0.04}$	$2.70^{+0.12}_{-0.11}$	$3.96^{+0.15}_{-0.14}$	$2.90^{+0.14}_{-0.13}$	$1.10^{+0.10}_{-0.09}$
[2000, 2500[	$0.26^{+0.03}_{-0.03}$	$1.42^{+0.08}_{-0.07}$	$2.15^{+0.10}_{-0.10}$	$1.60^{+0.09}_{-0.09}$	$0.59^{+0.07}_{-0.06}$
[1500, 2000[	$0.07^{+0.02}_{-0.01}$	$0.54^{+0.04}_{-0.04}$	$0.81^{+0.06}_{-0.05}$	$0.73^{+0.06}_{-0.05}$	$0.32^{+0.05}_{-0.04}$
[1000, 1500[	$0.02^{+0.01}_{-0.01}$	$0.11^{+0.02}_{-0.02}$	$0.19^{+0.03}_{-0.02}$	$0.15^{+0.03}_{-0.02}$	$0.04^{+0.02}_{-0.01}$

Table A.11: Total MC selection efficiency for $D^{*+} \to D^0\pi^+$ with $D^0 \to K^-\pi^+$ in bins of D^0 p_{T} and y.

	y				
p_{T} [MeV/c]	$[2, 2.5[$	$[2.5, 3[$	$[3, 3.5[$	$[3.5, 4[$	$[4, 4.5[$
$[14000, 15000[$	$7.06^{+0.27}_{-0.26}$	$13.39^{+0.40}_{-0.39}$	$4.44^{+0.28}_{-0.26}$	$0.00^{+0.03}_{-0.00}$	$0.00^{+0.05}_{-0.00}$
$[13000, 14000[$	$7.13^{+0.23}_{-0.22}$	$13.97^{+0.34}_{-0.34}$	$6.21^{+0.27}_{-0.26}$	$0.00^{+0.02}_{-0.00}$	$0.00^{+0.04}_{-0.00}$
$[12000, 13000[$	$7.18^{+0.19}_{-0.19}$	$14.89^{+0.29}_{-0.29}$	$8.31^{+0.26}_{-0.25}$	$0.04^{+0.03}_{-0.02}$	$0.00^{+0.02}_{-0.00}$
$[11000, 12000[$	$6.29^{+0.15}_{-0.15}$	$14.91^{+0.24}_{-0.24}$	$10.56^{+0.24}_{-0.23}$	$0.46^{+0.06}_{-0.06}$	$0.00^{+0.02}_{-0.00}$
$[10000, 11000[$	$5.90^{+0.12}_{-0.12}$	$14.10^{+0.20}_{-0.19}$	$12.26^{+0.21}_{-0.21}$	$1.27^{+0.09}_{-0.08}$	$0.00^{+0.01}_{-0.00}$
$[9000, 10000[$	$5.83^{+0.41}_{-0.38}$	$15.05^{+0.62}_{-0.60}$	$14.56^{+0.66}_{-0.63}$	$2.78^{+0.34}_{-0.30}$	$0.00^{+0.05}_{-0.00}$
$[8000, 9000[$	$4.86^{+0.33}_{-0.31}$	$13.52^{+0.55}_{-0.53}$	$14.05^{+0.61}_{-0.59}$	$4.62^{+0.43}_{-0.40}$	$0.00^{+0.07}_{-0.00}$
$[7000, 8000[$	$3.90^{+0.23}_{-0.22}$	$12.32^{+0.41}_{-0.40}$	$14.06^{+0.47}_{-0.46}$	$7.05^{+0.40}_{-0.38}$	$0.03^{+0.06}_{-0.02}$
$[6000, 7000[$	$3.35^{+0.17}_{-0.16}$	$11.44^{+0.31}_{-0.30}$	$13.84^{+0.36}_{-0.36}$	$8.15^{+0.32}_{-0.31}$	$0.46^{+0.10}_{-0.08}$
$[5000, 6000[$	$2.26^{+0.11}_{-0.10}$	$9.27^{+0.21}_{-0.21}$	$12.42^{+0.26}_{-0.26}$	$8.83^{+0.25}_{-0.24}$	$1.18^{+0.11}_{-0.10}$
$[4000, 5000[$	$1.34^{+0.06}_{-0.06}$	$7.15^{+0.14}_{-0.14}$	$10.52^{+0.18}_{-0.18}$	$8.40^{+0.18}_{-0.18}$	$1.80^{+0.10}_{-0.10}$
$[3500, 4000[$	$0.78^{+0.06}_{-0.05}$	$5.23^{+0.14}_{-0.14}$	$8.45^{+0.19}_{-0.18}$	$6.94^{+0.19}_{-0.18}$	$2.34^{+0.13}_{-0.12}$
$[3000, 3500[$	$0.38^{+0.04}_{-0.03}$	$3.81^{+0.11}_{-0.11}$	$7.60^{+0.16}_{-0.15}$	$5.91^{+0.15}_{-0.15}$	$2.08^{+0.11}_{-0.10}$
$[2500, 3000[$	$0.15^{+0.02}_{-0.02}$	$2.29^{+0.08}_{-0.07}$	$5.72^{+0.12}_{-0.12}$	$4.49^{+0.12}_{-0.11}$	$1.80^{+0.09}_{-0.08}$
$[2000, 2500[$	$0.03^{+0.01}_{-0.01}$	$1.23^{+0.05}_{-0.05}$	$4.04^{+0.09}_{-0.09}$	$3.39^{+0.09}_{-0.09}$	$1.27^{+0.07}_{-0.06}$
$[1500, 2000[$	$0.00^{+0.00}_{-0.00}$	$0.48^{+0.03}_{-0.03}$	$2.44^{+0.07}_{-0.07}$	$1.95^{+0.07}_{-0.06}$	$0.74^{+0.05}_{-0.04}$
$[1000, 1500[$	$0.00^{+0.00}_{-0.00}$	$0.12^{+0.02}_{-0.01}$	$1.03^{+0.04}_{-0.04}$	$0.90^{+0.04}_{-0.04}$	$0.37^{+0.03}_{-0.03}$
$[0, 1000[$	$0.00^{+0.00}_{-0.00}$	$0.00^{+0.00}_{-0.00}$	$0.06^{+0.01}_{-0.01}$	$0.09^{+0.01}_{-0.01}$	$0.08^{+0.02}_{-0.02}$

Table A.12: Total MC selection efficiency for $D^{*+} \to D^0\pi^+$ with $D^0 \to K^-\pi^+\pi^-\pi^+$ in bins of D^0 p_{T} and y.

	y				
p_{T} [MeV/c]	$[2, 2.5[$	$[2.5, 3[$	$[3, 3.5[$	$[3.5, 4[$	$[4, 4.5[$
$[14000, 15000[$	$2.58^{+0.17}_{-0.16}$	$7.16^{+0.30}_{-0.29}$	$6.10^{+0.32}_{-0.31}$	$1.37^{+0.20}_{-0.17}$	$0.00^{+0.05}_{-0.00}$
$[13000, 14000[$	$2.47^{+0.14}_{-0.13}$	$7.43^{+0.26}_{-0.25}$	$6.94^{+0.28}_{-0.27}$	$1.75^{+0.18}_{-0.16}$	$0.00^{+0.04}_{-0.00}$
$[12000, 13000[$	$2.16^{+0.11}_{-0.10}$	$6.53^{+0.20}_{-0.20}$	$7.26^{+0.24}_{-0.23}$	$2.61^{+0.18}_{-0.17}$	$0.07^{+0.05}_{-0.03}$
$[11000, 12000[$	$2.17^{+0.09}_{-0.09}$	$6.73^{+0.17}_{-0.16}$	$7.29^{+0.20}_{-0.19}$	$3.38^{+0.16}_{-0.16}$	$0.15^{+0.05}_{-0.04}$
$[10000, 11000[$	$1.72^{+0.07}_{-0.06}$	$5.90^{+0.13}_{-0.13}$	$7.15^{+0.16}_{-0.16}$	$3.97^{+0.15}_{-0.14}$	$0.18^{+0.04}_{-0.04}$
$[9000, 10000[$	$1.45^{+0.21}_{-0.19}$	$6.88^{+0.44}_{-0.42}$	$7.47^{+0.48}_{-0.45}$	$4.35^{+0.40}_{-0.37}$	$0.23^{+0.13}_{-0.08}$
$[8000, 9000[$	$0.84^{+0.14}_{-0.12}$	$4.54^{+0.33}_{-0.31}$	$5.59^{+0.40}_{-0.37}$	$4.28^{+0.41}_{-0.38}$	$0.38^{+0.18}_{-0.12}$
$[7000, 8000[$	$0.90^{+0.11}_{-0.10}$	$4.07^{+0.24}_{-0.23}$	$5.15^{+0.30}_{-0.29}$	$3.97^{+0.30}_{-0.28}$	$0.44^{+0.14}_{-0.10}$
$[6000, 7000[$	$0.65^{+0.07}_{-0.07}$	$2.91^{+0.16}_{-0.15}$	$4.01^{+0.20}_{-0.19}$	$3.05^{+0.20}_{-0.19}$	$0.45^{+0.10}_{-0.08}$
$[5000, 6000[$	$0.29^{+0.04}_{-0.03}$	$1.98^{+0.10}_{-0.09}$	$3.20^{+0.14}_{-0.13}$	$2.33^{+0.13}_{-0.12}$	$0.36^{+0.06}_{-0.05}$
$[4000, 5000[$	$0.09^{+0.02}_{-0.01}$	$1.13^{+0.06}_{-0.06}$	$2.05^{+0.08}_{-0.08}$	$1.15^{+0.07}_{-0.07}$	$0.24^{+0.04}_{-0.03}$
$[3500, 4000[$	$0.03^{+0.01}_{-0.01}$	$0.53^{+0.05}_{-0.04}$	$1.33^{+0.08}_{-0.07}$	$0.69^{+0.06}_{-0.06}$	$0.14^{+0.03}_{-0.03}$
$[3000, 3500[$	$0.01^{+0.01}_{-0.00}$	$0.25^{+0.03}_{-0.03}$	$0.85^{+0.05}_{-0.05}$	$0.41^{+0.04}_{-0.04}$	$0.06^{+0.02}_{-0.02}$
$[2500, 3000[$	$0.00^{+0.00}_{-0.00}$	$0.09^{+0.02}_{-0.01}$	$0.35^{+0.03}_{-0.03}$	$0.19^{+0.03}_{-0.02}$	$0.04^{+0.02}_{-0.01}$
$[2000, 2500[$	$0.00^{+0.00}_{-0.00}$	$0.02^{+0.01}_{-0.01}$	$0.09^{+0.02}_{-0.01}$	$0.10^{+0.02}_{-0.01}$	$0.02^{+0.01}_{-0.01}$
$[1500, 2000[$	$0.00^{+0.00}_{-0.00}$	$0.00^{+0.00}_{-0.00}$	$0.02^{+0.01}_{-0.01}$	$0.02^{+0.01}_{-0.00}$	$0.00^{+0.01}_{-0.00}$
$[1000, 1500[$	$0.00^{+0.00}_{-0.00}$	$0.00^{+0.00}_{-0.00}$	$0.00^{+0.00}_{-0.00}$	$0.00^{+0.00}_{-0.00}$	$0.00^{+0.00}_{-0.00}$
$[0, 1000[$	$0.00^{+0.00}_{-0.00}$	$0.00^{+0.00}_{-0.00}$	$0.00^{+0.00}_{-0.00}$	$0.00^{+0.00}_{-0.00}$	$0.00^{+0.01}_{-0.00}$

Table A.13: Total PID selection efficiency for $D^+ \to K^-\pi^+\pi^+$ in bins of D^+ p_{T} and y. Shown uncertainties are due to the size of the calibration sample.

p_{T} [MeV/c]	y $[2, 2.5[$	$[2.5, 3[$	$[3, 3.5[$	$[3.5, 4[$	$[4, 4.5[$
$[14000, 15000[$	65.37 ± 0.39	72.67 ± 0.38	72.73 ± 0.26	50.17 ± 0.49	-
$[13000, 14000[$	66.37 ± 0.32	74.52 ± 0.23	74.11 ± 0.24	46.65 ± 0.85	-
$[12000, 13000[$	68.72 ± 0.26	75.62 ± 0.26	75.50 ± 0.21	58.87 ± 0.30	-
$[11000, 12000[$	69.77 ± 0.24	78.22 ± 0.25	77.70 ± 0.18	58.45 ± 0.26	-
$[10000, 11000[$	71.45 ± 0.22	80.95 ± 0.14	79.38 ± 0.16	62.09 ± 0.24	-
$[9000, 10000[$	73.17 ± 0.21	83.46 ± 0.11	82.02 ± 0.13	65.63 ± 0.21	45.24 ± 0.54
$[8000, 9000[$	73.54 ± 0.20	85.38 ± 0.09	83.82 ± 0.12	67.07 ± 0.19	43.05 ± 0.36
$[7000, 8000[$	74.18 ± 0.20	86.88 ± 0.08	86.31 ± 0.09	69.73 ± 0.17	45.92 ± 0.28
$[6000, 7000[$	73.76 ± 0.21	87.11 ± 0.09	88.73 ± 0.08	73.01 ± 0.15	50.27 ± 0.27
$[5000, 6000[$	72.97 ± 0.21	86.41 ± 0.10	90.30 ± 0.07	76.63 ± 0.13	54.53 ± 0.26
$[4000, 5000[$	71.94 ± 0.23	85.05 ± 0.11	90.73 ± 0.08	79.71 ± 0.12	60.12 ± 0.23
$[3500, 4000[$	71.49 ± 0.24	83.42 ± 0.13	89.98 ± 0.10	82.03 ± 0.12	63.79 ± 0.22
$[3000, 3500[$	70.97 ± 0.25	82.07 ± 0.15	89.00 ± 0.12	83.17 ± 0.14	66.77 ± 0.21
$[2500, 3000[$	71.29 ± 0.25	80.86 ± 0.17	87.58 ± 0.15	83.47 ± 0.16	69.54 ± 0.21
$[2000, 2500[$	71.40 ± 0.24	80.30 ± 0.19	85.90 ± 0.21	83.30 ± 0.20	72.11 ± 0.24
$[1500, 2000[$	73.38 ± 0.23	80.41 ± 0.23	84.58 ± 0.32	82.45 ± 0.28	74.12 ± 0.28
$[1000, 1500[$	75.26 ± 0.21	81.44 ± 0.24	83.71 ± 0.39	81.74 ± 0.36	75.05 ± 0.36
$[0, 1000[$	80.52 ± 0.25	82.48 ± 0.26	85.69 ± 0.32	84.12 ± 0.42	73.66 ± 0.56

A.3 PID selection efficiency

Table A.14: Total PID selection efficiency for $D^+ \to K^-K^+\pi^+$ in bins of D^+ p_{T} and y. Shown uncertainties are due to the size of the calibration sample.

	y				
p_{T} [MeV/c]	$[2, 2.5[$	$[2.5, 3[$	$[3, 3.5[$	$[3.5, 4[$	$[4, 4.5[$
$[14000, 15000[$	65.40 ± 0.37	69.83 ± 0.41	62.76 ± 0.32	26.52 ± 0.54	-
$[13000, 14000[$	63.32 ± 0.41	67.06 ± 0.49	62.91 ± 0.31	42.80 ± 0.51	-
$[12000, 13000[$	73.33 ± 0.27	74.63 ± 0.48	66.06 ± 0.26	37.36 ± 0.47	-
$[11000, 12000[$	76.27 ± 0.26	75.01 ± 0.29	70.04 ± 0.25	37.21 ± 0.38	-
$[10000, 11000[$	77.07 ± 0.21	79.21 ± 0.21	71.04 ± 0.21	46.12 ± 0.30	-
$[9000, 10000[$	79.05 ± 0.19	85.36 ± 0.12	78.05 ± 0.16	49.03 ± 0.29	-
$[8000, 9000[$	80.74 ± 0.18	87.64 ± 0.10	80.25 ± 0.14	53.08 ± 0.26	24.44 ± 0.39
$[7000, 8000[$	81.57 ± 0.17	90.27 ± 0.08	86.00 ± 0.11	58.12 ± 0.22	22.33 ± 0.30
$[6000, 7000[$	81.22 ± 0.19	89.56 ± 0.09	88.86 ± 0.08	63.35 ± 0.19	31.35 ± 0.29
$[5000, 6000[$	80.86 ± 0.20	89.14 ± 0.11	91.30 ± 0.08	69.58 ± 0.16	35.65 ± 0.30
$[4000, 5000[$	79.97 ± 0.23	87.66 ± 0.15	92.04 ± 0.11	76.47 ± 0.17	44.33 ± 0.27
$[3500, 4000[$	80.10 ± 0.25	85.86 ± 0.19	91.07 ± 0.15	79.08 ± 0.22	51.13 ± 0.27
$[3000, 3500[$	80.70 ± 0.25	83.92 ± 0.24	89.04 ± 0.16	80.58 ± 0.24	55.08 ± 0.27
$[2500, 3000[$	80.06 ± 0.26	82.33 ± 0.26	86.62 ± 0.22	80.34 ± 0.25	60.27 ± 0.30
$[2000, 2500[$	80.29 ± 0.28	81.03 ± 0.32	83.37 ± 0.42	79.18 ± 0.40	65.87 ± 0.55
$[1500, 2000[$	82.44 ± 0.28	78.57 ± 0.49	78.43 ± 0.87	75.50 ± 0.53	66.37 ± 0.42
$[1000, 1500[$	79.47 ± 0.34	77.17 ± 0.72	71.75 ± 2.06	68.18 ± 1.19	69.10 ± 1.75

Table A.15: Total PID selection efficiency for $D_s^+ \to \phi\pi^+$ in bins of D_s^+ p_{T} and y. Shown uncertainties are due to the size of the calibration sample.

	y				
p_{T} [MeV/c]	$[2, 2.5[$	$[2.5, 3[$	$[3, 3.5[$	$[3.5, 4[$	$[4, 4.5[$
$[14000, 15000[$	74.63 ± 0.36	73.00 ± 0.42	55.72 ± 0.40	-	-
$[13000, 14000[$	77.35 ± 0.26	80.39 ± 0.19	61.06 ± 0.31	65.11 ± 1.11	-
$[12000, 13000[$	78.93 ± 0.23	81.92 ± 0.18	69.47 ± 0.24	39.45 ± 0.43	-
$[11000, 12000[$	80.68 ± 0.21	85.36 ± 0.13	75.74 ± 0.20	31.73 ± 0.38	-
$[10000, 11000[$	80.96 ± 0.20	87.51 ± 0.11	77.90 ± 0.17	48.88 ± 0.32	-
$[9000, 10000[$	82.76 ± 0.20	88.41 ± 0.10	81.54 ± 0.14	52.70 ± 0.27	-
$[8000, 9000[$	82.81 ± 0.20	89.85 ± 0.09	85.73 ± 0.11	58.25 ± 0.24	-
$[7000, 8000[$	83.03 ± 0.19	90.62 ± 0.09	89.14 ± 0.09	62.67 ± 0.20	25.44 ± 0.28
$[6000, 7000[$	82.86 ± 0.21	90.67 ± 0.10	91.44 ± 0.08	69.55 ± 0.17	34.82 ± 0.31
$[5000, 6000[$	81.95 ± 0.22	89.18 ± 0.12	92.66 ± 0.08	75.32 ± 0.15	39.57 ± 0.29
$[4000, 5000[$	81.05 ± 0.25	87.13 ± 0.17	92.29 ± 0.10	80.57 ± 0.15	49.00 ± 0.27
$[3500, 4000[$	80.45 ± 0.26	85.20 ± 0.22	90.96 ± 0.13	81.96 ± 0.18	56.14 ± 0.28
$[3000, 3500[$	80.14 ± 0.26	83.00 ± 0.26	88.97 ± 0.25	82.04 ± 0.22	60.29 ± 0.28
$[2500, 3000[$	80.53 ± 0.27	81.68 ± 0.30	87.27 ± 0.22	81.40 ± 0.26	64.44 ± 0.32
$[2000, 2500[$	81.30 ± 0.26	80.17 ± 0.35	84.69 ± 0.34	80.06 ± 0.31	65.80 ± 0.42
$[1500, 2000[$	83.55 ± 0.29	81.54 ± 1.01	81.50 ± 0.59	77.20 ± 0.42	66.00 ± 0.48
$[1000, 1500[$	84.49 ± 0.31	78.58 ± 0.49	75.55 ± 1.01	68.49 ± 3.53	61.04 ± 0.62

Table A.16: Total PID selection efficiency for $D_s^+ \to K^-K^+\pi^+$ in bins of D_s^+ p_{T} and y. Shown uncertainties are due to the size of the calibration sample.

	y				
p_{T} [MeV/c]	$[2, 2.5[$	$[2.5, 3[$	$[3, 3.5[$	$[3.5, 4[$	$[4, 4.5[$
$[14000, 15000[$	47.30 ± 0.68	52.73 ± 1.02	60.71 ± 0.43	-	-
$[13000, 14000[$	55.97 ± 0.54	58.32 ± 1.60	58.50 ± 0.32	20.68 ± 0.44	-
$[12000, 13000[$	61.12 ± 0.46	59.50 ± 1.12	60.25 ± 0.34	48.75 ± 0.64	-
$[11000, 12000[$	64.55 ± 0.34	67.50 ± 0.34	62.57 ± 0.29	40.62 ± 0.35	-
$[10000, 11000[$	71.64 ± 0.25	74.93 ± 0.25	65.70 ± 0.27	50.75 ± 0.32	-
$[9000, 10000[$	76.11 ± 0.23	79.38 ± 0.19	69.47 ± 0.23	45.05 ± 0.29	-
$[8000, 9000[$	76.75 ± 0.20	85.70 ± 0.13	73.07 ± 0.18	49.08 ± 0.28	22.98 ± 0.34
$[7000, 8000[$	79.44 ± 0.17	86.69 ± 0.10	80.49 ± 0.13	54.77 ± 0.26	22.12 ± 0.37
$[6000, 7000[$	80.42 ± 0.18	88.03 ± 0.09	85.09 ± 0.11	53.99 ± 0.24	34.54 ± 0.45
$[5000, 6000[$	79.76 ± 0.19	87.69 ± 0.11	88.34 ± 0.08	61.54 ± 0.19	51.69 ± 0.72
$[4000, 5000[$	79.14 ± 0.21	87.31 ± 0.13	90.07 ± 0.11	70.38 ± 0.20	38.02 ± 0.28
$[3500, 4000[$	80.49 ± 0.25	85.81 ± 0.17	89.90 ± 0.14	73.33 ± 0.19	43.22 ± 0.29
$[3000, 3500[$	79.24 ± 0.27	85.97 ± 0.35	88.84 ± 0.14	77.88 ± 0.30	48.47 ± 0.52
$[2500, 3000[$	81.21 ± 0.34	83.87 ± 0.33	86.69 ± 0.20	79.39 ± 0.41	51.54 ± 0.43
$[2000, 2500[$	86.38 ± 0.66	81.67 ± 0.60	82.56 ± 0.51	77.51 ± 0.33	62.67 ± 0.69
$[1500, 2000[$	78.06 ± 1.72	74.12 ± 4.53	77.82 ± 1.17	75.67 ± 0.46	73.02 ± 1.11
$[1000, 1500[$	82.82 ± 2.53	65.73 ± 2.94	66.79 ± 3.79	73.95 ± 3.68	57.51 ± 110.16

Table A.17: Total PID selection efficiency for $D^{*+} \to D^0\pi^+$, with $D^0 \to K^-\pi^+$, in bins of D^{*+} p_{T} and y. Shown uncertainties are due to the size of the calibration sample.

	y				
p_{T} [MeV/c]	$[2, 2.5[$	$[2.5, 3[$	$[3, 3.5[$	$[3.5, 4[$	$[4, 4.5[$
$[14000, 15000[$	65.01 ± 0.65	59.74 ± 0.68	69.01 ± 0.44	-	-
$[13000, 14000[$	68.85 ± 0.46	66.43 ± 0.77	66.67 ± 0.35	-	-
$[12000, 13000[$	68.57 ± 0.41	70.79 ± 0.40	67.30 ± 0.30	-	-
$[11000, 12000[$	77.38 ± 0.33	76.44 ± 0.35	71.62 ± 0.25	61.23 ± 0.69	-
$[10000, 11000[$	78.32 ± 0.24	76.83 ± 0.23	74.55 ± 0.22	51.13 ± 0.38	-
$[9000, 10000[$	78.98 ± 0.26	80.18 ± 0.23	74.90 ± 0.20	56.43 ± 0.30	-
$[8000, 9000[$	82.10 ± 0.18	86.12 ± 0.12	80.31 ± 0.17	57.71 ± 0.24	-
$[7000, 8000[$	84.59 ± 0.15	89.75 ± 0.09	82.58 ± 0.12	63.85 ± 0.21	-
$[6000, 7000[$	86.33 ± 0.14	90.85 ± 0.06	86.64 ± 0.09	66.38 ± 0.18	37.39 ± 0.35
$[5000, 6000[$	86.21 ± 0.14	92.91 ± 0.06	90.11 ± 0.07	69.91 ± 0.16	47.45 ± 0.25
$[4000, 5000[$	85.84 ± 0.13	92.80 ± 0.06	93.28 ± 0.17	76.38 ± 0.12	53.63 ± 0.24
$[3500, 4000[$	84.14 ± 0.14	91.98 ± 0.06	93.38 ± 0.05	81.44 ± 0.11	57.76 ± 0.26
$[3000, 3500[$	82.96 ± 0.16	92.00 ± 0.07	93.50 ± 0.09	84.95 ± 0.11	62.28 ± 0.24
$[2500, 3000[$	84.14 ± 0.18	91.49 ± 0.08	93.88 ± 0.06	85.96 ± 0.10	63.37 ± 0.23
$[2000, 2500[$	80.91 ± 0.22	90.23 ± 0.10	93.42 ± 0.08	88.50 ± 0.11	67.67 ± 0.27
$[1500, 2000[$	97.43 ± 3.98	91.63 ± 0.18	94.29 ± 0.17	92.29 ± 0.49	72.97 ± 0.30
$[1000, 1500[$	-	92.54 ± 0.22	94.42 ± 0.13	95.11 ± 0.55	76.66 ± 1.12
$[0, 1000[$	-	-0.01 ± 0.83	111.33 ± 1.00	103.35 ± 0.62	81.07 ± 0.38

Table A.18: Total PID selection efficiency for $D^{*+} \to D^0\pi^+$, with $D^0 \to K^-\pi^+\pi^-\pi^+$, in bins of D^{*+} p_{T} and y. Shown uncertainties are due to the size of the calibration sample.

	y				
p_{T} [MeV/c]	$[2, 2.5[$	$[2.5, 3[$	$[3, 3.5[$	$[3.5, 4[$	$[4, 4.5[$
$[14000, 15000[$	56.69 ± 0.32	76.10 ± 0.28	72.75 ± 0.24	34.81 ± 0.64	-
$[13000, 14000[$	58.00 ± 0.32	74.54 ± 0.37	79.88 ± 0.16	54.62 ± 0.31	-
$[12000, 13000[$	61.93 ± 0.29	81.71 ± 0.15	75.33 ± 0.20	56.09 ± 0.27	-
$[11000, 12000[$	63.10 ± 0.28	80.05 ± 0.14	81.37 ± 0.15	63.05 ± 0.23	35.97 ± 0.49
$[10000, 11000[$	62.03 ± 0.28	82.21 ± 0.13	84.60 ± 0.12	64.62 ± 0.23	35.41 ± 0.41
$[9000, 10000[$	61.45 ± 0.27	82.85 ± 0.12	84.44 ± 0.12	70.04 ± 0.21	34.43 ± 0.37
$[8000, 9000[$	61.40 ± 0.28	82.40 ± 0.13	86.20 ± 0.11	72.26 ± 0.18	46.59 ± 0.29
$[7000, 8000[$	60.36 ± 0.29	81.91 ± 0.14	87.63 ± 0.11	73.44 ± 0.16	54.49 ± 0.26
$[6000, 7000[$	60.74 ± 0.29	80.77 ± 0.15	89.45 ± 0.11	79.80 ± 0.15	59.12 ± 0.25
$[5000, 6000[$	61.31 ± 0.30	79.52 ± 0.17	88.49 ± 0.13	79.79 ± 0.17	58.57 ± 0.43
$[4000, 5000[$	62.84 ± 0.29	76.97 ± 0.19	87.04 ± 0.15	81.83 ± 0.16	61.86 ± 0.27
$[3500, 4000[$	62.08 ± 0.30	76.54 ± 0.21	84.91 ± 0.19	82.20 ± 0.30	59.73 ± 0.68
$[3000, 3500[$	66.59 ± 0.35	76.18 ± 0.23	83.85 ± 0.25	81.57 ± 0.35	72.08 ± 0.47
$[2500, 3000[$	59.75 ± 0.56	77.13 ± 0.42	82.19 ± 0.26	82.28 ± 0.42	75.35 ± 1.06
$[2000, 2500[$	64.01 ± 0.48	70.87 ± 0.35	82.33 ± 0.38	91.34 ± 1.47	70.42 ± 0.60
$[1500, 2000[$	-	81.25 ± 0.44	83.80 ± 1.30	78.19 ± 1.05	0.00 ± 0.00
$[1000, 1500[$	-	88.13 ± 0.46	89.29 ± 0.72	72.01 ± 2.23	-0.00 ± 0.00
$[0, 1000[$	-	-	86.39 ± 1.96	89.82 ± 2.62	-

Table A.19: Signal window requirement efficiencies, in percent, for $D^+ \to K^-\pi^+\pi^+$.

p_{T} [MeV/c]	y [2, 2.5[	[2.5, 3[	[3, 3.5[	[3.5, 4[	[4, 4.5[
[14000, 15000[	96.74 ± 0.15	96.14 ± 0.22	96.17 ± 0.35	96.58 ± 1.32	97.30 ± 0.04
[13000, 14000[	96.96 ± 0.10	96.69 ± 0.12	96.11 ± 0.26	97.09 ± 0.65	97.30 ± 0.04
[12000, 13000[	96.97 ± 0.09	96.63 ± 0.11	95.89 ± 0.23	96.34 ± 0.72	97.30 ± 0.04
[11000, 12000[	97.05 ± 0.06	96.90 ± 0.07	96.11 ± 0.15	96.01 ± 0.57	97.30 ± 0.04
[10000, 11000[	97.21 ± 0.05	96.97 ± 0.06	96.31 ± 0.11	95.67 ± 0.36	97.30 ± 0.04
[9000, 10000[	97.18 ± 0.05	97.01 ± 0.05	96.35 ± 0.09	95.78 ± 0.24	92.94 ± 2.08
[8000, 9000[	97.22 ± 0.04	97.10 ± 0.04	96.43 ± 0.07	95.58 ± 0.17	96.33 ± 1.07
[7000, 8000[	97.25 ± 0.04	97.19 ± 0.04	96.65 ± 0.05	95.31 ± 0.13	94.03 ± 0.38
[6000, 7000[	97.29 ± 0.04	97.22 ± 0.04	96.77 ± 0.05	95.43 ± 0.09	93.75 ± 0.12
[5000, 6000[	97.30 ± 0.04	97.25 ± 0.04	96.89 ± 0.04	95.76 ± 0.06	93.78 ± 1.62
[4000, 5000[	97.31 ± 0.04	97.28 ± 0.04	96.99 ± 0.04	95.94 ± 0.05	93.78 ± 0.07
[3500, 4000[	97.31 ± 0.04	97.29 ± 0.04	97.04 ± 0.04	96.16 ± 0.05	93.86 ± 0.13
[3000, 3500[	97.32 ± 0.04	97.30 ± 0.04	97.08 ± 0.04	96.28 ± 0.05	93.89 ± 0.12
[2500, 3000[	97.32 ± 0.04	97.31 ± 0.04	97.12 ± 0.04	96.28 ± 0.05	94.09 ± 0.12
[2000, 2500[	97.32 ± 0.04	97.31 ± 0.04	97.13 ± 0.04	96.26 ± 0.05	94.63 ± 0.14
[1500, 2000[	97.32 ± 0.04	97.30 ± 0.04	97.08 ± 0.04	96.34 ± 0.06	93.75 ± 0.08
[1000, 1500[	97.33 ± 0.04	97.30 ± 0.04	97.06 ± 0.04	96.14 ± 0.09	93.61 ± 0.09
[0, 1000[	97.15 ± 0.50	97.28 ± 0.05	97.03 ± 0.08	96.29 ± 0.23	94.67 ± 0.88

A.4 Signal window efficiency

Table A.20: Signal window requirement efficiencies, in percent, for $D^+ \to K^-K^+\pi^+$.

p_{T} [MeV/c]	y [2, 2.5[	[2.5, 3[	[3, 3.5[	[3.5, 4[	[4, 4.5[
[14000, 15000[	98.61 ± 0.30	98.61 ± 0.30	98.61 ± 0.34	98.61 ± 0.71	98.61 ± 0.27
[13000, 14000[	98.59 ± 0.30	98.59 ± 0.29	98.59 ± 0.32	98.61 ± 1.52	98.61 ± 0.27
[12000, 13000[	98.60 ± 0.30	98.58 ± 0.28	98.58 ± 0.30	98.61 ± 0.52	98.61 ± 0.27
[11000, 12000[	98.57 ± 0.29	98.61 ± 0.28	98.58 ± 0.29	98.61 ± 0.63	98.61 ± 0.27
[10000, 11000[	98.60 ± 0.28	98.60 ± 0.28	98.59 ± 0.28	98.60 ± 0.38	98.61 ± 0.27
[9000, 10000[	98.64 ± 0.27	98.64 ± 0.27	98.56 ± 0.28	98.60 ± 0.33	98.61 ± 0.27
[8000, 9000[	98.64 ± 0.27	98.64 ± 0.27	98.58 ± 0.28	98.56 ± 0.29	98.61 ± 0.72
[7000, 8000[	98.67 ± 0.27	98.67 ± 0.27	98.61 ± 0.27	98.54 ± 0.28	98.60 ± 0.41
[6000, 7000[	98.68 ± 0.27	98.68 ± 0.27	98.65 ± 0.27	98.55 ± 0.28	98.58 ± 0.32
[5000, 6000[	98.68 ± 0.27	98.68 ± 0.27	98.65 ± 0.27	98.56 ± 0.27	98.50 ± 0.30
[4000, 5000[	98.68 ± 0.27	98.68 ± 0.27	98.65 ± 0.27	98.52 ± 0.27	98.37 ± 0.31
[3500, 4000[	98.68 ± 0.27	98.68 ± 0.27	98.65 ± 0.27	98.60 ± 0.27	98.45 ± 0.30
[3000, 3500[	98.68 ± 0.27	98.68 ± 0.27	98.66 ± 0.27	98.57 ± 0.27	98.41 ± 0.30
[2500, 3000[	98.68 ± 0.27	98.68 ± 0.27	98.65 ± 0.27	98.64 ± 0.27	98.36 ± 0.31
[2000, 2500[	98.68 ± 0.27	98.68 ± 0.27	98.66 ± 0.27	98.64 ± 0.27	98.50 ± 0.31
[1500, 2000[	98.62 ± 0.28	98.68 ± 0.27	98.67 ± 0.27	98.62 ± 0.28	98.38 ± 0.40
[1000, 1500[	98.60 ± 1.16	98.54 ± 0.37	98.50 ± 0.34	98.46 ± 0.67	98.45 ± 0.67

Table A.21: Signal window requirement efficiencies, in percent, for $D_s^+ \to \phi\pi^+$.

p_{T} [MeV/c]	y [2, 2.5[	[2.5, 3[	[3, 3.5[	[3.5, 4[	[4, 4.5[
[14000, 15000[	98.68 ± 0.06	98.59 ± 0.08	96.25 ± 1.36	98.61 ± 0.06	98.61 ± 0.06
[13000, 14000[	98.52 ± 0.14	98.47 ± 0.12	97.51 ± 0.61	98.56 ± 0.52	98.61 ± 0.06
[12000, 13000[	98.45 ± 0.14	98.59 ± 0.07	98.50 ± 0.14	97.19 ± 0.49	98.61 ± 0.06
[11000, 12000[	98.63 ± 0.06	98.62 ± 0.06	98.49 ± 0.12	98.58 ± 0.11	98.61 ± 0.06
[10000, 11000[	98.63 ± 0.06	98.58 ± 0.07	98.50 ± 0.09	96.33 ± 1.21	98.61 ± 0.06
[9000, 10000[	98.55 ± 0.07	98.58 ± 0.06	98.34 ± 0.11	98.33 ± 0.20	98.61 ± 0.06
[8000, 9000[	98.65 ± 0.06	98.63 ± 0.06	98.54 ± 0.06	97.90 ± 0.24	93.52 ± 3.97
[7000, 8000[	98.65 ± 0.06	98.62 ± 0.06	98.57 ± 0.06	98.39 ± 0.10	98.68 ± 0.06
[6000, 7000[	98.65 ± 0.06	98.64 ± 0.06	98.47 ± 0.06	97.92 ± 0.12	97.59 ± 0.77
[5000, 6000[	98.66 ± 0.06	98.66 ± 0.06	98.56 ± 0.06	98.07 ± 0.09	96.28 ± 0.53
[4000, 5000[	98.66 ± 0.06	98.67 ± 0.06	98.59 ± 0.06	98.26 ± 0.07	97.60 ± 0.23
[3500, 4000[	98.66 ± 0.06	98.66 ± 0.06	98.58 ± 0.06	98.06 ± 0.09	96.37 ± 0.43
[3000, 3500[	98.65 ± 0.06	98.66 ± 0.06	98.58 ± 0.06	98.28 ± 0.07	96.14 ± 0.47
[2500, 3000[	98.65 ± 0.06	98.66 ± 0.06	98.61 ± 0.06	98.37 ± 0.07	97.75 ± 0.22
[2000, 2500[	98.65 ± 0.06	98.66 ± 0.06	98.57 ± 0.06	98.20 ± 0.08	97.50 ± 0.33
[1500, 2000[	98.63 ± 0.06	98.63 ± 0.06	98.53 ± 0.06	98.08 ± 0.14	95.88 ± 0.90
[1000, 1500[	98.63 ± 0.06	98.65 ± 0.06	98.57 ± 0.07	98.13 ± 0.33	98.63 ± 1.29

Table A.22: Signal window requirement efficiencies, in percent, for $D_s^+ \to K^-K^+\pi^+$.

	y				
p_{T} [MeV/c]	$[2, 2.5[$	$[2.5, 3[$	$[3, 3.5[$	$[3.5, 4[$	$[4, 4.5[$
$[14000, 15000[$	98.09 ± 1.12	98.23 ± 0.49	98.45 ± 0.72	98.64 ± 0.18	98.64 ± 0.18
$[13000, 14000[$	98.19 ± 0.57	98.57 ± 0.26	98.31 ± 0.80	98.63 ± 2.79	98.64 ± 0.18
$[12000, 13000[$	98.41 ± 0.38	98.22 ± 0.38	97.05 ± 1.19	98.45 ± 1.67	98.64 ± 0.18
$[11000, 12000[$	98.66 ± 0.19	98.32 ± 0.28	98.12 ± 0.42	98.42 ± 1.13	98.64 ± 0.18
$[10000, 11000[$	98.67 ± 0.19	97.89 ± 0.40	97.94 ± 0.42	97.62 ± 1.97	98.64 ± 0.18
$[9000, 10000[$	98.66 ± 0.19	98.57 ± 0.19	98.02 ± 0.35	98.27 ± 0.65	98.64 ± 0.18
$[8000, 9000[$	98.65 ± 0.18	98.47 ± 0.20	98.38 ± 0.21	96.95 ± 0.84	98.58 ± 1.69
$[7000, 8000[$	98.67 ± 0.18	98.65 ± 0.18	98.37 ± 0.20	97.48 ± 0.49	98.38 ± 2.07
$[6000, 7000[$	98.69 ± 0.18	98.66 ± 0.18	98.31 ± 0.20	97.38 ± 0.40	98.14 ± 1.49
$[5000, 6000[$	98.71 ± 0.18	98.67 ± 0.18	98.51 ± 0.18	97.44 ± 0.31	97.42 ± 0.95
$[4000, 5000[$	98.70 ± 0.18	98.68 ± 0.18	98.54 ± 0.18	97.91 ± 0.23	95.75 ± 0.95
$[3500, 4000[$	98.70 ± 0.18	98.70 ± 0.18	98.60 ± 0.18	98.13 ± 0.23	96.93 ± 0.83
$[3000, 3500[$	98.70 ± 0.18	98.69 ± 0.18	98.58 ± 0.18	97.57 ± 0.31	96.95 ± 0.78
$[2500, 3000[$	98.70 ± 0.18	98.71 ± 0.18	98.60 ± 0.18	97.96 ± 0.27	96.07 ± 0.97
$[2000, 2500[$	98.71 ± 0.18	98.70 ± 0.18	98.63 ± 0.18	98.27 ± 0.25	97.00 ± 1.20
$[1500, 2000[$	98.69 ± 0.27	98.66 ± 0.18	98.43 ± 0.23	96.44 ± 0.94	97.68 ± 1.05
$[1000, 1500[$	98.16 ± 5.83	98.62 ± 0.80	98.57 ± 0.32	98.18 ± 0.97	98.23 ± 2.75

Table A.23: Signal window requirement efficiencies, in percent, for $D^{*+} \to D^0\pi^+$, with $D^0 \to K^-\pi^+$.

p_{T} [MeV/c]	y [2, 2.5[	[2.5, 3[	[3, 3.5[	[3.5, 4[	[4, 4.5[
[14000, 15000[	89.17 ± 0.87	89.18 ± 0.78	89.73 ± 1.74	90.79 ± 0.16	90.79 ± 0.16
[13000, 14000[	85.55 ± 0.89	87.10 ± 0.86	87.76 ± 1.26	90.79 ± 0.16	90.79 ± 0.16
[12000, 13000[	89.83 ± 0.60	88.99 ± 0.53	92.75 ± 0.65	90.79 ± 0.16	90.79 ± 0.16
[11000, 12000[	89.19 ± 0.53	91.43 ± 0.37	90.33 ± 0.78	79.65 ± 4.65	90.79 ± 0.16
[10000, 11000[	89.75 ± 0.44	90.62 ± 0.33	91.71 ± 0.46	91.25 ± 1.65	90.79 ± 0.16
[9000, 10000[	91.17 ± 0.35	91.83 ± 0.26	92.01 ± 0.37	90.09 ± 1.17	90.79 ± 0.16
[8000, 9000[	90.74 ± 0.30	92.69 ± 0.22	93.13 ± 0.27	92.53 ± 0.62	90.79 ± 0.16
[7000, 8000[	92.70 ± 0.25	93.75 ± 0.19	92.97 ± 0.24	90.89 ± 0.50	90.79 ± 0.16
[6000, 7000[	93.74 ± 0.22	94.09 ± 0.18	93.65 ± 0.20	92.22 ± 0.33	85.07 ± 2.43
[5000, 6000[	93.78 ± 0.20	94.47 ± 0.17	94.32 ± 0.18	92.17 ± 0.24	88.72 ± 0.54
[4000, 5000[	95.17 ± 0.18	95.44 ± 0.16	94.76 ± 0.17	92.29 ± 0.20	87.72 ± 0.34
[3500, 4000[	96.36 ± 0.18	95.83 ± 0.16	94.93 ± 0.17	92.51 ± 0.21	87.83 ± 0.47
[3000, 3500[	97.06 ± 0.17	95.81 ± 0.16	94.83 ± 0.17	92.49 ± 0.20	87.78 ± 0.38
[2500, 3000[	97.01 ± 0.19	96.16 ± 0.16	94.81 ± 0.16	92.19 ± 0.19	88.35 ± 0.37
[2000, 2500[	97.65 ± 0.19	96.39 ± 0.16	94.12 ± 0.17	91.54 ± 0.19	88.29 ± 0.35
[1500, 2000[	$88.37 \pm nan$	96.90 ± 0.16	93.61 ± 0.17	90.52 ± 0.20	87.33 ± 0.29
[1000, 1500[	90.48 ± 3.78	97.38 ± 0.16	95.39 ± 0.17	92.79 ± 0.23	90.57 ± 0.46
[0, 1000[	90.79 ± 0.16	77.59 ± 5.09	$86.65 \pm nan$	74.94 ± 5.24	71.73 ± 4.89

Table A.24: Signal window requirement efficiencies, in percent, for $D^{*+} \to D^0\pi^+$, with $D^0 \to K^-\pi^+\pi^-\pi^+$.

	y				
p_{T} [MeV/c]	$[2, 2.5[$	$[2.5, 3[$	$[3, 3.5[$	$[3.5, 4[$	$[4, 4.5[$
$[14000, 15000[$	84.07 ± 0.96	83.94 ± 0.87	84.03 ± 0.92	82.25 ± 1.73	85.11 ± 0.75
$[13000, 14000[$	85.02 ± 0.80	84.01 ± 0.84	81.60 ± 1.88	81.22 ± 1.37	85.11 ± 0.75
$[12000, 13000[$	85.08 ± 0.79	84.16 ± 0.79	83.64 ± 0.85	83.42 ± 1.12	85.11 ± 0.75
$[11000, 12000[$	84.95 ± 0.77	84.83 ± 0.76	83.86 ± 0.82	84.13 ± 0.99	84.71 ± 1.38
$[10000, 11000[$	85.03 ± 0.77	84.69 ± 0.76	83.91 ± 0.78	81.66 ± 0.75	85.23 ± 1.11
$[9000, 10000[$	84.95 ± 0.77	84.92 ± 0.75	83.82 ± 0.77	81.66 ± 0.90	81.78 ± 1.92
$[8000, 9000[$	85.37 ± 0.75	84.81 ± 0.75	84.21 ± 0.76	82.31 ± 0.84	81.27 ± 1.03
$[7000, 8000[$	85.15 ± 0.76	85.03 ± 0.75	84.33 ± 0.75	82.87 ± 0.80	81.36 ± 1.06
$[6000, 7000[$	85.35 ± 0.75	85.07 ± 0.75	84.45 ± 0.75	83.32 ± 0.77	81.27 ± 0.82
$[5000, 6000[$	85.36 ± 0.75	85.15 ± 0.75	84.74 ± 0.75	83.54 ± 0.76	81.83 ± 0.81
$[4000, 5000[$	85.52 ± 0.75	85.27 ± 0.75	84.76 ± 0.75	83.95 ± 0.75	81.31 ± 0.80
$[3500, 4000[$	85.54 ± 0.76	85.39 ± 0.75	84.98 ± 0.75	84.09 ± 0.76	82.93 ± 1.09
$[3000, 3500[$	85.72 ± 0.76	85.44 ± 0.75	85.01 ± 0.75	83.42 ± 0.79	82.32 ± 1.08
$[2500, 3000[$	84.99 ± 1.03	85.35 ± 0.75	85.03 ± 0.75	84.67 ± 0.77	84.25 ± 1.13
$[2000, 2500[$	82.84 ± 2.24	85.51 ± 0.76	85.06 ± 0.76	84.12 ± 0.90	84.02 ± 1.39
$[1500, 2000[$	85.11 ± 0.75	84.09 ± 1.30	85.30 ± 0.79	85.27 ± 0.85	83.85 ± 1.49
$[1000, 1500[$	85.11 ± 0.75	85.51 ± 1.18	82.04 ± 1.61	85.52 ± 1.23	80.80 ± 3.57
$[0, 1000[$	85.11 ± 0.75	85.11 ± 0.75	81.92 ± 3.03	72.02 ± 1.67	78.82 ± 3.54

B Individual per systematic tables

B.1 Finite Monte Carlo statistic

Table B.1: Relative uncertainty in % due to the Monte Carlo sample size for $D^0 \to K^-\pi^+$.

	y				
p_{T} [MeV/c]	$[2, 2.5[$	$[2.5, 3[$	$[3, 3.5[$	$[3.5, 4[$	$[4, 4.5[$
$[0, 1000[$	4.36	2.01	1.78	2.30	5.13
$[1000, 1500[$	4.17	2.01	1.82	2.28	4.20
$[1500, 2000[$	3.75	1.89	1.72	2.19	4.01
$[2000, 2500[$	3.29	1.80	1.69	2.08	3.70
$[2500, 3000[$	3.12	1.74	1.63	2.07	3.81
$[3000, 3500[$	3.13	1.74	1.71	2.08	3.93
$[3500, 4000[$	3.10	1.82	1.83	2.24	4.56
$[4000, 5000[$	2.38	1.49	1.48	1.82	4.84
$[5000, 6000[$	2.82	1.87	1.82	2.49	8.94
$[6000, 7000[$	3.29	2.31	2.28	3.66	27.17
$[7000, 8000[$	3.95	2.92	3.05	5.71	-
$[8000, 9000[$	5.16	3.53	3.97	11.40	-
$[9000, 10000[$	1.71	1.26	1.56	5.92	-
$[10000, 11000[$	1.73	1.31	1.76	9.42	-
$[11000, 12000[$	1.99	1.62	2.55	-	-
$[12000, 13000[$	2.39	2.00	3.59	-	-
$[13000, 14000[$	2.86	2.51	5.18	-	-
$[14000, 15000[$	3.38	3.11	7.60	-	-

Table B.2: Relative uncertainty in % due to the Monte Carlo sample size for $D^+ \to K^-\pi^+\pi^+$.

p_{T} [MeV/c]	y [2, 2.5[	[2.5, 3[	[3, 3.5[	[3.5, 4[	[4, 4.5[
[0, 1000[	-	16.98	10.97	11.12	23.81
[1000, 1500[	21.47	5.61	3.88	4.31	8.20
[1500, 2000[	9.88	2.81	2.24	2.53	5.06
[2000, 2500[	5.56	2.05	1.69	1.96	3.72
[2500, 3000[	4.56	1.80	1.53	1.78	3.27
[3000, 3500[	4.05	1.79	1.60	1.84	3.29
[3500, 4000[	3.73	1.86	1.65	1.93	3.60
[4000, 5000[	2.74	1.48	1.33	1.59	3.01
[5000, 6000[	3.19	1.76	1.68	1.98	4.84
[6000, 7000[	3.51	2.16	2.11	2.82	8.89
[7000, 8000[	4.33	2.66	2.65	3.70	17.18
[8000, 9000[	5.06	3.25	3.37	5.59	36.44
[9000, 10000[	5.24	3.46	3.44	6.71	-
[10000, 11000[	1.54	1.06	1.19	2.93	-
[11000, 12000[	1.76	1.28	1.54	4.71	-
[12000, 13000[	2.13	1.54	2.04	7.24	-
[13000, 14000[	2.56	1.93	2.73	14.78	-
[14000, 15000[	3.01	2.33	3.67	-	-

Table B.3: Relative uncertainty in % due to the Monte Carlo sample size for $D^+ \to K^-K^+\pi^+$.

p_{T} [MeV/c]	y [2, 2.5[	[2.5, 3[	[3, 3.5[	[3.5, 4[	[4, 4.5[
[1000, 1500[	36.37	10.23	7.12	8.75	16.72
[1500, 2000[	9.73	3.54	2.93	3.55	8.03
[2000, 2500[	5.00	2.14	1.92	2.32	4.52
[2500, 3000[	3.82	1.79	1.63	1.97	3.78
[3000, 3500[	3.51	1.78	1.64	1.92	3.55
[3500, 4000[	3.44	1.85	1.74	2.03	3.72
[4000, 5000[	2.58	1.49	1.42	1.64	3.09
[5000, 6000[	2.88	1.87	1.74	2.08	4.37
[6000, 7000[	3.50	2.33	2.22	2.75	7.84
[7000, 8000[	4.12	2.84	2.84	3.73	15.33
[8000, 9000[	4.96	3.75	3.84	5.33	32.35
[9000, 10000[	5.53	3.66	3.68	5.83	-
[10000, 11000[	1.50	1.09	1.19	2.54	-
[11000, 12000[	1.76	1.32	1.47	3.83	-
[12000, 13000[	2.11	1.58	1.90	6.58	-
[13000, 14000[	2.53	1.93	2.51	-	-
[14000, 15000[	3.06	2.29	3.33	19.48	-

Table B.4: Relative uncertainty in % due to the Monte Carlo sample size for $D_s^+ \to \phi\pi^+$.

p_{T} [MeV/c]	y [2, 2.5[	[2.5, 3[	[3, 3.5[	[3.5, 4[	[4, 4.5[
[1000, 1500[	51.28	16.27	15.09	23.82	-
[1500, 2000[	16.68	7.26	7.04	10.15	20.60
[2000, 2500[	11.51	5.02	4.64	5.98	12.81
[2500, 3000[	9.37	4.30	4.19	5.03	9.50
[3000, 3500[	8.01	4.09	4.01	4.68	9.54
[3500, 4000[	7.63	4.14	4.11	5.17	9.69
[4000, 5000[	5.08	3.23	3.17	3.95	7.15
[5000, 6000[	5.72	3.91	4.01	4.62	10.26
[6000, 7000[	6.93	4.84	4.73	6.21	15.49
[7000, 8000[	9.14	6.33	6.01	8.30	25.30
[8000, 9000[	10.55	7.22	7.35	10.73	-
[9000, 10000[	10.61	7.05	7.67	10.38	-
[10000, 11000[	3.22	2.43	2.76	4.92	-
[11000, 12000[	3.81	2.87	3.20	6.90	-
[12000, 13000[	4.44	3.51	4.10	11.16	-
[13000, 14000[	5.26	4.15	5.22	-	-
[14000, 15000[	5.92	5.08	6.90	-	-

Table B.5: Relative uncertainty in % due to the Monte Carlo sample size for $D_s^+ \to K^-K^+\pi^+$.

p_{T} [MeV/c]	y [2, 2.5[	[2.5, 3[	[3, 3.5[	[3.5, 4[	[4, 4.5[
[1000, 1500[	39.04	16.97	13.33	16.28	36.30
[1500, 2000[	21.53	7.81	6.76	7.76	13.77
[2000, 2500[	12.27	5.26	4.52	5.67	10.98
[2500, 3000[	10.28	4.22	3.64	4.68	8.79
[3000, 3500[	8.16	3.87	3.60	4.25	9.24
[3500, 4000[	8.12	3.71	3.64	4.26	8.71
[4000, 5000[	5.56	2.99	2.79	3.31	6.41
[5000, 6000[	5.97	3.38	3.48	4.30	10.69
[6000, 7000[	6.67	4.08	4.11	5.14	14.41
[7000, 8000[	7.58	5.19	4.96	7.48	28.24
[8000, 9000[	9.28	5.87	6.45	10.65	55.27
[9000, 10000[	9.65	6.30	6.38	11.34	-
[10000, 11000[	2.66	1.94	2.13	5.24	-
[11000, 12000[	3.08	2.27	2.74	7.75	-
[12000, 13000[	3.74	2.77	3.57	13.07	-
[13000, 14000[	4.31	3.25	4.85	-	-
[14000, 15000[	4.82	3.85	6.37	-	-

Table B.6: Relative uncertainty in % due to the Monte Carlo sample size for $D^{*+} \to D^0\pi^+$ with $D^0 \to K^-\pi^+$.

p_{T} [MeV/c]	y [2, 2.5[	[2.5, 3[	[3, 3.5[	[3.5, 4[	[4, 4.5[
[0, 1000[	-	-	-	-	22.05
[1000, 1500[	-	11.51	4.04	4.61	8.81
[1500, 2000[	-	6.03	2.72	3.28	6.07
[2000, 2500[	25.33	4.03	2.28	2.69	5.08
[2500, 3000[	13.15	3.27	2.11	2.61	4.75
[3000, 3500[	9.07	2.80	2.05	2.58	4.99
[3500, 4000[	7.15	2.69	2.20	2.68	5.39
[4000, 5000[	4.62	1.98	1.70	2.11	5.43
[5000, 6000[	4.63	2.26	2.07	2.75	9.03
[6000, 7000[	4.88	2.62	2.58	3.84	19.37
[7000, 8000[	5.79	3.27	3.32	5.45	-
[8000, 9000[	6.60	3.99	4.28	8.91	-
[9000, 10000[	6.75	4.07	4.42	11.35	-
[10000, 11000[	2.07	1.39	1.70	6.60	-
[11000, 12000[	2.42	1.62	2.22	13.08	-
[12000, 13000[	2.70	1.97	3.10	-	-
[13000, 14000[	3.21	2.45	4.35	-	-
[14000, 15000[	3.81	3.01	6.20	-	-

Table B.7: Relative uncertainty in % due to the Monte Carlo sample size for $D^{*+} \to D^0\pi^+$ with $D^0 \to K^-\pi^+\pi^-\pi^+$.

	y				
p_{T} [MeV/c]	$[2, 2.5[$	$[2.5, 3[$	$[3, 3.5[$	$[3.5, 4[$	$[4, 4.5[$
$[0, 1000[$	-	-	-	-	-
$[1000, 1500[$	-	-	-	55.15	-
$[1500, 2000[$	-	51.25	27.18	34.18	-
$[2000, 2500[$	-	27.13	14.60	15.65	36.40
$[2500, 3000[$	-	16.05	8.52	12.48	30.84
$[3000, 3500[$	46.27	10.68	6.13	9.63	28.14
$[3500, 4000[$	32.36	8.37	5.61	8.55	21.47
$[4000, 5000[$	16.94	4.97	3.92	5.78	14.60
$[5000, 6000[$	12.46	4.87	4.13	5.40	16.07
$[6000, 7000[$	10.80	5.27	4.90	6.29	19.01
$[7000, 8000[$	11.63	5.75	5.68	7.28	25.35
$[8000, 9000[$	15.40	7.04	6.86	9.11	34.23
$[9000, 10000[$	13.38	6.20	6.19	8.77	39.11
$[10000, 11000[$	3.84	2.21	2.26	3.63	21.65
$[11000, 12000[$	4.07	2.47	2.67	4.80	-
$[12000, 13000[$	4.95	3.05	3.27	6.65	-
$[13000, 14000[$	5.51	3.41	4.05	9.79	-
$[14000, 15000[$	6.37	4.14	5.27	13.40	-

B.2 PID calibration sample size

Table B.8: Relative uncertainty $\sigma_C^{PID}/\varepsilon$ in % due to the calibration sample size for $D^0 \to K^-\pi^+$.

p_{T} [MeV/c]	y [2, 2.5[	[2.5, 3[	[3, 3.5[	[3.5, 4[	[4, 4.5[
[0, 1000[	0.22	0.19	0.11	0.16	0.29
[1000, 1500[	0.21	0.15	0.11	0.13	0.25
[1500, 2000[	0.21	0.12	0.09	0.11	0.27
[2000, 2500[	0.21	0.10	0.07	0.10	0.33
[2500, 3000[	0.20	0.08	0.06	0.11	0.37
[3000, 3500[	0.18	0.07	0.06	0.12	0.42
[3500, 4000[	0.17	0.07	0.05	0.14	0.45
[4000, 5000[	0.16	0.06	0.06	0.19	0.50
[5000, 6000[	0.15	0.06	0.08	0.24	0.58
[6000, 7000[	0.17	0.08	0.13	0.29	0.62
[7000, 8000[	0.19	0.12	0.19	0.36	-
[8000, 9000[	0.23	0.17	0.24	0.44	-
[9000, 10000[	0.28	0.31	0.29	0.51	-
[10000, 11000[	0.41	0.38	0.35	0.79	-
[11000, 12000[	0.50	0.64	0.44	-	-
[12000, 13000[	0.62	1.01	0.50	-	-
[13000, 14000[	0.76	1.57	0.56	-	-
[14000, 15000[	1.20	2.01	0.67	-	-

Table B.9: Relative uncertainty $\sigma_C^{PID}/\varepsilon$ in % due to the calibration sample size for $D^+ \to K^-\pi^+\pi^+$.

p_{T} [MeV/c]	y [2, 2.5[	[2.5, 3[	[3, 3.5[	[3.5, 4[	[4, 4.5[
[0, 1000[	-	0.31	0.37	0.50	0.74
[1000, 1500[	0.28	0.29	0.44	0.43	0.48
[1500, 2000[	0.31	0.28	0.35	0.33	0.37
[2000, 2500[	0.34	0.24	0.24	0.24	0.33
[2500, 3000[	0.35	0.20	0.17	0.18	0.30
[3000, 3500[	0.35	0.18	0.13	0.16	0.32
[3500, 4000[	0.34	0.15	0.11	0.15	0.34
[4000, 5000[	0.32	0.13	0.08	0.14	0.38
[5000, 6000[	0.29	0.11	0.08	0.16	0.47
[6000, 7000[	0.28	0.10	0.09	0.20	0.54
[7000, 8000[	0.27	0.09	0.11	0.24	0.60
[8000, 9000[	0.28	0.11	0.14	0.29	0.82
[9000, 10000[	0.28	0.13	0.16	0.32	-
[10000, 11000[	0.31	0.18	0.20	0.38	-
[11000, 12000[	0.35	0.30	0.23	0.44	-
[12000, 13000[	0.37	0.33	0.28	0.50	-
[13000, 14000[	0.47	0.30	0.32	1.81	-
[14000, 15000[	0.59	0.50	0.35	-	-

Table B.10: Relative uncertainty $\sigma_C^{PID}/\varepsilon$ in % due to the calibration sample size for $D^+ \to K^-K^+\pi^+$.

p_{T} [MeV/c]	y [2, 2.5[	[2.5, 3[	[3, 3.5[	[3.5, 4[	[4, 4.5[
[1000, 1500[	0.42	0.88	1.74	1.58	1.81
[1500, 2000[	0.34	0.61	0.89	0.67	0.63
[2000, 2500[	0.35	0.40	0.44	0.47	0.70
[2500, 3000[	0.33	0.31	0.25	0.30	0.48
[3000, 3500[	0.31	0.28	0.18	0.28	0.48
[3500, 4000[	0.30	0.21	0.15	0.26	0.52
[4000, 5000[	0.29	0.16	0.11	0.21	0.62
[5000, 6000[	0.25	0.12	0.08	0.22	0.83
[6000, 7000[	0.23	0.10	0.09	0.29	0.91
[7000, 8000[	0.21	0.09	0.12	0.38	1.34
[8000, 9000[	0.22	0.11	0.17	0.49	1.60
[9000, 10000[	0.24	0.14	0.21	0.59	-
[10000, 11000[	0.28	0.27	0.29	0.64	-
[11000, 12000[	0.34	0.38	0.35	1.01	-
[12000, 13000[	0.36	0.58	0.39	1.25	-
[13000, 14000[	0.63	0.73	0.49	-	-
[14000, 15000[	0.57	0.58	0.51	2.00	-

Table B.11: Relative uncertainty $\sigma_C^{PID}/\varepsilon$ in % due to the calibration sample size for $D_s^+ \to \phi\pi^+$.

p_{T} [MeV/c]	y [2, 2.5[	[2.5, 3[	[3, 3.5[	[3.5, 4[	[4, 4.5[
[1000, 1500[	0.36	0.62	1.31	2.73	-
[1500, 2000[	0.34	0.90	0.70	0.54	0.73
[2000, 2500[	0.32	0.43	0.40	0.38	0.63
[2500, 3000[	0.33	0.36	0.25	0.31	0.50
[3000, 3500[	0.33	0.31	0.23	0.26	0.47
[3500, 4000[	0.32	0.25	0.14	0.22	0.49
[4000, 5000[	0.30	0.20	0.11	0.19	0.55
[5000, 6000[	0.27	0.13	0.09	0.19	0.74
[6000, 7000[	0.25	0.10	0.09	0.24	0.89
[7000, 8000[	0.23	0.09	0.10	0.32	1.11
[8000, 9000[	0.24	0.10	0.13	0.41	-
[9000, 10000[	0.24	0.11	0.17	0.52	-
[10000, 11000[	0.25	0.13	0.22	0.65	-
[11000, 12000[	0.26	0.15	0.26	1.18	-
[12000, 13000[	0.29	0.22	0.35	1.09	-
[13000, 14000[	0.33	0.23	0.51	-	-
[14000, 15000[	0.48	0.58	0.72	-	-

Table B.12: Relative uncertainty $\sigma_C^{PID}/\varepsilon$ in % due to the calibration sample size for $D_s^+ \to K^-K^+\pi^+$.

p_{T} [MeV/c]	y [2, 2.5[	[2.5, 3[	[3, 3.5[	[3.5, 4[	[4, 4.5[
[1000, 1500[	3.02	2.62	2.75	2.71	2.24
[1500, 2000[	2.15	1.74	1.01	0.60	1.23
[2000, 2500[	0.75	0.58	0.48	0.41	0.92
[2500, 3000[	0.41	0.34	0.22	0.42	0.74
[3000, 3500[	0.34	0.33	0.16	0.32	0.84
[3500, 4000[	0.30	0.20	0.14	0.25	0.67
[4000, 5000[	0.27	0.15	0.12	0.26	0.74
[5000, 6000[	0.24	0.12	0.10	0.30	1.38
[6000, 7000[	0.22	0.10	0.12	0.45	1.31
[7000, 8000[	0.22	0.11	0.16	0.47	1.65
[8000, 9000[	0.27	0.15	0.24	0.57	1.46
[9000, 10000[	0.31	0.24	0.32	0.63	-
[10000, 11000[	0.35	0.34	0.41	0.64	-
[11000, 12000[	0.53	0.50	0.47	0.86	-
[12000, 13000[	0.74	1.64	0.55	1.31	-
[13000, 14000[	0.97	2.39	0.53	-	-
[14000, 15000[	1.43	1.87	0.71	-	-

Table B.13: Relative uncertainty $\sigma_C^{PID}/\varepsilon$ in % due to the calibration sample size for $D^{*+} \to D^0\pi^+$ with $D^0 \to K^-\pi^+$.

p_{T} [MeV/c]	y [2, 2.5[	[2.5, 3[	[3, 3.5[	[3.5, 4[	[4, 4.5[
[0, 1000[	-	-	-	-	0.47
[1000, 1500[	-	0.23	0.13	0.42	0.92
[1500, 2000[	-	0.19	0.15	0.37	0.34
[2000, 2500[	0.27	0.11	0.09	0.12	0.36
[2500, 3000[	0.21	0.09	0.06	0.12	0.36
[3000, 3500[	0.20	0.07	0.08	0.13	0.38
[3500, 4000[	0.17	0.07	0.06	0.14	0.45
[4000, 5000[	0.14	0.06	0.13	0.16	0.46
[5000, 6000[	0.16	0.06	0.07	0.22	0.53
[6000, 7000[	0.16	0.07	0.11	0.27	0.93
[7000, 8000[	0.17	0.10	0.15	0.33	-
[8000, 9000[	0.22	0.14	0.21	0.42	-
[9000, 10000[	0.33	0.28	0.26	0.53	-
[10000, 11000[	0.31	0.30	0.30	0.73	-
[11000, 12000[	0.42	0.42	0.35	1.12	-
[12000, 13000[	0.60	0.55	0.44	-	-
[13000, 14000[	0.66	1.12	0.52	-	-
[14000, 15000[	0.97	1.09	0.64	-	-

Table B.14: Relative uncertainty $\sigma_C^{PID}/\varepsilon$ in % due to the calibration sample size for $D^{*+} \to D^0\pi^+$ with $D^0 \to K^-\pi^+\pi^-\pi^+$.

	y				
p_{T} [MeV/c]	$[2, 2.5[$	$[2.5, 3[$	$[3, 3.5[$	$[3.5, 4[$	$[4, 4.5[$
$[0, 1000[$	-	-	-	-	-
$[1000, 1500[$	-	-	-	2.83	-
$[1500, 2000[$	-	0.54	1.26	1.30	-
$[2000, 2500[$	-	0.49	0.46	1.27	0.84
$[2500, 3000[$	-	0.44	0.30	0.47	1.00
$[3000, 3500[$	0.53	0.30	0.27	0.39	0.59
$[3500, 4000[$	0.48	0.28	0.22	0.32	1.13
$[4000, 5000[$	0.46	0.25	0.17	0.20	0.43
$[5000, 6000[$	0.49	0.21	0.14	0.21	0.73
$[6000, 7000[$	0.48	0.19	0.12	0.19	0.42
$[7000, 8000[$	0.47	0.17	0.13	0.21	0.48
$[8000, 9000[$	0.46	0.16	0.12	0.25	0.61
$[9000, 10000[$	0.44	0.15	0.14	0.30	1.06
$[10000, 11000[$	0.44	0.16	0.14	0.35	1.15
$[11000, 12000[$	0.44	0.18	0.18	0.36	-
$[12000, 13000[$	0.47	0.18	0.26	0.48	-
$[13000, 14000[$	0.54	0.48	0.20	0.56	-
$[14000, 15000[$	0.56	0.36	0.32	1.83	-

B.3 PID binning

Table B.15: Relative uncertainty in % due to the binning scheme for $D^0 \to K^-\pi^+$.

p_{T} [MeV/c]	y [2, 2.5[	[2.5, 3[	[3, 3.5[	[3.5, 4[	[4, 4.5[
[0, 1000[	1.16	0.09	0.23	0.73	2.09
[1000, 1500[	1.43	0.98	0.33	0.26	1.87
[1500, 2000[	0.80	0.44	0.11	0.34	0.00
[2000, 2500[	0.52	0.11	0.14	0.88	0.06
[2500, 3000[	0.56	0.39	0.32	2.00	2.29
[3000, 3500[	0.88	0.53	0.51	2.96	3.89
[3500, 4000[	1.26	0.51	0.73	2.80	7.20
[4000, 5000[	1.58	0.40	1.28	1.40	10.80
[5000, 6000[	1.90	0.15	2.10	1.65	17.42
[6000, 7000[	1.92	0.20	1.84	5.37	44.87
[7000, 8000[	2.27	0.48	0.67	10.52	-
[8000, 9000[	2.54	0.38	0.38	12.99	-
[9000, 10000[	3.22	0.05	0.70	24.18	-
[10000, 11000[	4.46	0.35	3.84	0.00	-
[11000, 12000[	4.99	0.30	3.89	-	-
[12000, 13000[	7.82	0.31	4.69	-	-
[13000, 14000[	7.50	0.00	11.38	-	-
[14000, 15000[	6.43	3.08	13.37	-	-

Table B.16: Relative uncertainty in % due to the binning scheme for $D^+ \to K^-\pi^+\pi^+$.

p_{T} [MeV/c]	y [2, 2.5[	[2.5, 3[	[3, 3.5[	[3.5, 4[	[4, 4.5[
[0, 1000[	-	4.23	1.33	1.77	4.77
[1000, 1500[	9.36	8.27	2.50	2.57	3.63
[1500, 2000[	6.70	5.48	2.21	1.63	2.86
[2000, 2500[	3.98	3.05	1.31	0.90	1.71
[2500, 3000[	2.80	1.03	0.56	0.04	1.84
[3000, 3500[	2.05	0.21	0.11	0.73	2.21
[3500, 4000[	1.69	0.32	0.06	1.42	2.18
[4000, 5000[	1.49	0.79	0.45	1.67	1.81
[5000, 6000[	1.33	1.01	0.98	0.99	2.21
[6000, 7000[	1.19	0.81	1.32	0.11	0.25
[7000, 8000[	1.31	0.57	1.20	1.50	7.99
[8000, 9000[	1.58	0.43	0.77	3.32	0.00
[9000, 10000[	1.72	0.32	0.25	5.33	-
[10000, 11000[	2.05	0.00	0.03	7.21	-
[11000, 12000[	2.62	0.00	0.00	3.46	-
[12000, 13000[	3.26	0.62	0.00	10.64	-
[13000, 14000[	3.72	0.70	0.00	0.00	-
[14000, 15000[	3.41	1.19	0.24	-	-

Table B.17: Relative uncertainty in % due to the binning scheme for $D^+ \to K^- K^+ \pi^+$.

p_{T} [MeV/c]	y [2, 2.5[	[2.5, 3[	[3, 3.5[	[3.5, 4[	[4, 4.5[
[1000, 1500[	32.28	12.82	4.87	5.36	1.28
[1500, 2000[	14.78	10.97	0.83	3.14	4.67
[2000, 2500[	11.10	4.16	0.95	1.38	2.52
[2500, 3000[	6.51	0.45	0.01	0.21	3.95
[3000, 3500[	3.55	0.41	0.30	0.44	3.65
[3500, 4000[	0.59	1.39	0.63	1.98	0.92
[4000, 5000[	0.05	1.87	0.86	3.93	0.00
[5000, 6000[	0.72	1.64	1.40	3.83	1.18
[6000, 7000[	0.58	1.43	1.92	3.88	0.00
[7000, 8000[	0.00	0.73	2.69	0.00	0.00
[8000, 9000[	0.58	0.23	2.00	6.19	0.00
[9000, 10000[	1.32	0.00	1.51	4.15	-
[10000, 11000[	1.31	0.57	0.82	0.00	-
[11000, 12000[	2.29	0.00	0.00	0.00	-
[12000, 13000[	4.25	0.37	0.00	0.00	-
[13000, 14000[	2.48	0.00	0.60	-	-
[14000, 15000[	6.50	0.00	0.00	0.00	-

Table B.18: Relative uncertainty in % due to the binning scheme for $D_s^+ \to \phi\pi^+$.

p_{T} [MeV/c]	y [2, 2.5[	[2.5, 3[	[3, 3.5[	[3.5, 4[	[4, 4.5[
[1000, 1500[	18.19	18.43	3.63	3.72	-
[1500, 2000[	13.30	11.10	1.07	2.81	2.22
[2000, 2500[	10.35	4.38	0.83	0.40	2.02
[2500, 3000[	8.85	1.44	0.00	0.00	2.77
[3000, 3500[	5.62	0.00	0.56	0.34	0.56
[3500, 4000[	1.06	0.97	0.64	0.72	2.61
[4000, 5000[	0.00	1.76	1.01	1.82	0.00
[5000, 6000[	0.72	2.09	1.08	4.01	6.07
[6000, 7000[	1.14	1.71	1.42	4.41	0.00
[7000, 8000[	1.08	1.33	1.84	2.52	0.00
[8000, 9000[	0.31	0.87	2.48	0.00	-
[9000, 10000[	0.00	0.00	2.59	1.36	-
[10000, 11000[	1.57	0.36	3.22	0.00	-
[11000, 12000[	2.40	0.67	0.51	0.00	-
[12000, 13000[	3.46	0.00	0.19	0.00	-
[13000, 14000[	4.35	0.68	6.56	-	-
[14000, 15000[	3.25	0.00	6.84	-	-

Table B.19: Relative uncertainty in % due to the binning scheme for $D_s^+ \to K^- K^+ \pi^+$.

p_{T} [MeV/c]	y [2, 2.5[	[2.5, 3[	[3, 3.5[	[3.5, 4[	[4, 4.5[
[1000, 1500[	0.00	0.00	0.00	1.56	0.00
[1500, 2000[	0.00	0.40	4.42	1.04	0.00
[2000, 2500[	0.00	0.00	2.07	0.00	0.47
[2500, 3000[	1.52	2.23	1.29	0.00	3.43
[3000, 3500[	0.00	3.88	0.73	1.13	3.22
[3500, 4000[	0.98	3.71	0.54	3.32	2.39
[4000, 5000[	1.00	2.31	0.95	5.14	4.26
[5000, 6000[	0.93	1.07	1.88	3.17	0.00
[6000, 7000[	0.00	1.01	1.69	0.00	0.00
[7000, 8000[	0.00	0.24	3.02	0.00	0.00
[8000, 9000[	0.00	0.39	2.06	5.84	0.00
[9000, 10000[	1.34	0.00	0.00	16.67	-
[10000, 11000[	3.80	0.00	3.56	0.00	-
[11000, 12000[	5.08	0.00	2.90	0.00	-
[12000, 13000[	6.03	0.00	6.02	0.00	-
[13000, 14000[	7.44	0.00	12.67	-	-
[14000, 15000[	8.88	0.00	0.00	-	-

Table B.20: Relative uncertainty in % due to the binning scheme for $D^{*+} \to D^0\pi^+$ with $D^0 \to K^-\pi^+$.

p_{T} [MeV/c]	y [2, 2.5[	[2.5, 3[	[3, 3.5[	[3.5, 4[	[4, 4.5[
[0, 1000[	-	-	-	-	0.00
[1000, 1500[	-	0.00	0.00	0.00	1.27
[1500, 2000[	-	0.00	0.06	0.00	0.00
[2000, 2500[	0.00	0.06	0.58	0.81	0.00
[2500, 3000[	0.00	0.24	0.50	1.09	1.71
[3000, 3500[	0.00	0.16	0.49	0.38	5.72
[3500, 4000[	0.52	0.28	0.69	0.71	1.17
[4000, 5000[	0.82	0.35	0.31	2.06	8.65
[5000, 6000[	1.42	0.19	1.99	0.00	14.37
[6000, 7000[	1.67	0.00	1.36	0.83	7.63
[7000, 8000[	1.57	0.91	2.17	3.57	-
[8000, 9000[	1.82	0.00	0.00	10.77	-
[9000, 10000[	1.50	0.00	0.00	10.05	-
[10000, 11000[	2.53	0.00	0.00	7.41	-
[11000, 12000[	2.33	1.28	3.04	0.00	-
[12000, 13000[	2.83	0.40	1.03	-	-
[13000, 14000[	4.82	1.83	5.73	-	-
[14000, 15000[	9.06	0.00	0.00	-	-

Table B.21: Relative uncertainty in % due to the binning scheme for $D^{*+} \to D^0\pi^+$ with $D^0 \to K^-\pi^+\pi^-\pi^+$.

p_{T} [MeV/c]	y [2, 2.5[	[2.5, 3[	[3, 3.5[	[3.5, 4[	[4, 4.5[
[0, 1000[	-	-	-	-	-
[1000, 1500[	-	-	-	0.00	-
[1500, 2000[	-	0.00	1.90	0.00	-
[2000, 2500[	-	0.00	0.00	0.00	0.00
[2500, 3000[	-	0.35	0.47	1.31	0.00
[3000, 3500[	0.00	0.00	0.00	0.16	1.04
[3500, 4000[	0.09	0.07	0.08	0.00	0.00
[4000, 5000[	1.14	0.73	0.14	0.31	0.00
[5000, 6000[	2.62	1.58	0.33	0.87	0.00
[6000, 7000[	1.19	1.28	0.27	1.78	1.57
[7000, 8000[	0.96	1.09	0.57	0.43	2.48
[8000, 9000[	0.00	0.51	1.48	1.32	3.95
[9000, 10000[	0.00	0.42	0.58	0.00	0.00
[10000, 11000[	0.00	0.00	0.06	0.00	0.00
[11000, 12000[	0.67	0.02	1.72	0.07	-
[12000, 13000[	0.00	0.00	0.00	10.23	-
[13000, 14000[	2.67	0.79	0.00	17.83	-
[14000, 15000[	0.67	0.00	0.53	0.00	-

B.4 Tracking correction

Table B.22: Relative uncertainty in % due to the tracking correction for $D^0 \to K^-\pi^+$.

p_{T} [MeV/c]	y [2, 2.5[	[2.5, 3[	[3, 3.5[	[3.5, 4[	[4, 4.5[
[0, 1000[	4.61	3.91	3.49	3.41	3.06
[1000, 1500[	4.57	3.77	3.42	3.40	3.16
[1500, 2000[	4.47	3.58	3.25	3.22	3.14
[2000, 2500[	4.25	3.43	3.16	3.10	3.10
[2500, 3000[	3.80	3.25	3.04	3.03	2.99
[3000, 3500[	3.57	3.11	2.94	2.99	2.91
[3500, 4000[	3.34	3.00	2.91	2.93	2.87
[4000, 5000[	3.16	2.93	2.87	2.88	2.87
[5000, 6000[	2.95	2.88	2.85	2.84	2.90
[6000, 7000[	2.85	2.84	2.87	2.80	2.98
[7000, 8000[	2.81	2.88	2.80	2.83	-
[8000, 9000[	2.80	2.91	2.81	2.88	-
[9000, 10000[	2.80	2.96	2.79	2.90	-
[10000, 11000[	2.81	2.99	2.77	2.94	-
[11000, 12000[	2.84	3.04	2.76	-	-
[12000, 13000[	2.86	3.04	2.77	-	-
[13000, 14000[	2.89	3.05	2.79	-	-
[14000, 15000[	2.93	3.04	2.81	-	-

Table B.23: Relative uncertainty in % due to the tracking correction for $D^+ \to K^-\pi^+\pi^+$.

p_{T} [MeV/c]	y [2, 2.5[	[2.5, 3[	[3, 3.5[	[3.5, 4[	[4, 4.5[
[0, 1000[	-	10.31	10.99	9.01	6.80
[1000, 1500[	7.48	9.32	9.73	8.13	6.61
[1500, 2000[	7.32	8.24	8.36	7.30	6.19
[2000, 2500[	7.08	7.00	7.14	6.50	5.80
[2500, 3000[	6.76	6.24	6.37	5.90	5.46
[3000, 3500[	6.44	5.66	5.81	5.49	5.15
[3500, 4000[	6.10	5.34	5.38	5.14	4.93
[4000, 5000[	5.70	4.87	5.01	4.96	4.74
[5000, 6000[	5.33	4.61	4.74	4.74	4.62
[6000, 7000[	5.06	4.44	4.59	4.63	4.49
[7000, 8000[	4.69	4.37	4.44	4.52	4.51
[8000, 9000[	4.56	4.32	4.40	4.46	4.46
[9000, 10000[	4.47	4.36	4.44	4.42	-
[10000, 11000[	4.40	4.35	4.41	4.40	-
[11000, 12000[	4.35	4.46	4.38	4.42	-
[12000, 13000[	4.33	4.47	4.35	4.42	-
[13000, 14000[	4.34	4.51	4.34	4.42	-
[14000, 15000[	4.35	4.54	4.33	-	-

Table B.24: Relative uncertainty in % due to the tracking correction for $D^+ \to K^- K^+ \pi^+$.

p_{T} [MeV/c]	y [2, 2.5[	[2.5, 3[	[3, 3.5[	[3.5, 4[	[4, 4.5[
[1000, 1500[	7.69	10.75	11.38	7.77	5.37
[1500, 2000[	7.31	8.98	9.26	6.63	5.02
[2000, 2500[	6.85	7.32	7.50	5.76	4.70
[2500, 3000[	6.59	5.95	6.04	5.15	4.51
[3000, 3500[	6.35	5.31	5.39	4.80	4.37
[3500, 4000[	6.07	4.92	5.04	4.45	4.23
[4000, 5000[	5.64	4.54	4.62	4.29	4.15
[5000, 6000[	5.15	4.27	4.21	4.23	4.11
[6000, 7000[	4.83	4.12	4.11	4.15	4.11
[7000, 8000[	4.40	4.06	4.07	4.12	4.17
[8000, 9000[	4.29	4.04	4.05	4.11	4.19
[9000, 10000[	4.17	4.07	4.04	4.10	-
[10000, 11000[	4.11	4.07	4.04	4.12	-
[11000, 12000[	4.07	4.12	4.06	4.13	-
[12000, 13000[	4.05	4.16	4.05	4.17	-
[13000, 14000[	4.05	4.17	4.09	-	-
[14000, 15000[	4.05	4.23	4.07	4.21	-

Table B.25: Relative uncertainty in % due to the tracking correction for $D_s^+ \to \phi\pi^+$.

p_{T} [MeV/c]	y [2, 2.5[	[2.5, 3[	[3, 3.5[	[3.5, 4[	[4, 4.5[
[1000, 1500[	7.68	10.07	11.29	6.91	-
[1500, 2000[	7.48	8.62	8.98	6.04	4.67
[2000, 2500[	6.87	7.39	7.25	5.30	4.55
[2500, 3000[	6.59	6.07	6.01	4.87	4.35
[3000, 3500[	6.32	5.28	5.32	4.54	4.29
[3500, 4000[	6.11	4.84	4.91	4.34	4.16
[4000, 5000[	5.71	4.52	4.42	4.21	4.13
[5000, 6000[	5.17	4.22	4.17	4.15	4.11
[6000, 7000[	4.79	4.10	4.07	4.18	4.21
[7000, 8000[	4.40	4.04	4.02	4.14	4.19
[8000, 9000[	4.25	4.05	4.00	4.14	-
[9000, 10000[	4.16	4.05	4.02	4.10	-
[10000, 11000[	4.11	4.09	4.04	4.10	-
[11000, 12000[	4.07	4.11	4.05	4.13	-
[12000, 13000[	4.04	4.15	4.08	4.17	-
[13000, 14000[	4.04	4.18	4.06	-	-
[14000, 15000[	4.02	4.25	4.07	-	-

Table B.26: Relative uncertainty in % due to the tracking correction for $D_s^+ \to K^- K^+ \pi^+$.

p_{T} [MeV/c]	y [2, 2.5[	[2.5, 3[	[3, 3.5[	[3.5, 4[	[4, 4.5[
[1000, 1500[	7.71	10.15	10.76	8.87	6.60
[1500, 2000[	7.40	8.60	9.44	8.09	6.10
[2000, 2500[	6.82	7.15	8.17	7.02	5.30
[2500, 3000[	6.50	6.16	6.83	6.15	4.87
[3000, 3500[	6.19	5.42	6.14	5.70	4.60
[3500, 4000[	5.85	5.10	5.71	5.17	4.48
[4000, 5000[	5.50	4.66	5.08	4.78	4.30
[5000, 6000[	5.15	4.34	4.69	4.52	4.23
[6000, 7000[	4.85	4.21	4.44	4.39	4.12
[7000, 8000[	4.44	4.13	4.20	4.28	4.14
[8000, 9000[	4.36	4.09	4.23	4.18	4.14
[9000, 10000[	4.27	4.10	4.10	4.13	-
[10000, 11000[	4.19	4.10	4.08	4.10	-
[11000, 12000[	4.12	4.15	4.08	4.13	-
[12000, 13000[	4.09	4.19	4.06	4.12	-
[13000, 14000[	4.10	4.22	4.06	-	-
[14000, 15000[	4.09	4.25	4.05	-	-

Table B.27: Relative uncertainty in % due to the tracking correction for $D^{*+} \to D^0\pi^+$ with $D^0 \to K^-\pi^+$.

p_{T} [MeV/c]	y [2, 2.5[	[2.5, 3[	[3, 3.5[	[3.5, 4[	[4, 4.5[
[0, 1000[	-	-	-	-	11.33
[1000, 1500[	-	11.27	11.72	11.95	11.74
[1500, 2000[	-	8.74	11.65	11.78	11.59
[2000, 2500[	6.29	6.68	11.29	11.67	10.95
[2500, 3000[	5.99	5.68	10.77	11.47	9.64
[3000, 3500[	5.74	5.27	10.17	11.37	8.23
[3500, 4000[	5.58	5.08	9.77	11.19	6.71
[4000, 5000[	5.45	4.93	9.24	10.48	5.44
[5000, 6000[	5.23	4.84	8.67	8.82	4.94
[6000, 7000[	5.02	4.78	8.21	6.62	4.73
[7000, 8000[	4.87	4.71	7.42	5.36	-
[8000, 9000[	4.82	4.73	6.44	4.97	-
[9000, 10000[	4.77	4.71	5.37	4.81	-
[10000, 11000[	4.72	4.75	4.94	4.71	-
[11000, 12000[	4.69	4.75	4.64	4.66	-
[12000, 13000[	4.71	4.74	4.42	-	-
[13000, 14000[	4.70	4.70	4.38	-	-
[14000, 15000[	4.71	4.65	4.39	-	-

Table B.28: Relative uncertainty in % due to the tracking correction for $D^{*+} \to D^0\pi^+$ with $D^0 \to K^-\pi^+\pi^-\pi^+$.

p_{T} [MeV/c]	y [2, 2.5[	[2.5, 3[	[3, 3.5[	[3.5, 4[	[4, 4.5[
[0, 1000[	-	-	-	-	-
[1000, 1500[	-	-	-	25.98	-
[1500, 2000[	-	19.72	24.81	23.87	-
[2000, 2500[	-	16.03	22.48	22.34	19.38
[2500, 3000[	-	13.58	20.49	20.65	16.99
[3000, 3500[	11.33	11.12	18.56	19.42	15.19
[3500, 4000[	10.58	10.16	17.17	18.37	12.75
[4000, 5000[	10.34	9.64	15.78	17.02	9.98
[5000, 6000[	10.53	9.10	14.07	14.30	8.82
[6000, 7000[	10.08	8.65	12.97	11.58	8.18
[7000, 8000[	9.73	8.27	11.84	9.77	8.00
[8000, 9000[	9.44	8.09	10.60	9.07	7.68
[9000, 10000[	9.13	7.91	9.13	8.43	7.61
[10000, 11000[	8.84	7.84	8.56	8.22	7.56
[11000, 12000[	8.59	7.71	8.22	8.05	-
[12000, 13000[	8.36	7.61	7.89	7.92	-
[13000, 14000[	8.16	7.56	7.72	7.78	-
[14000, 15000[	7.95	7.54	7.59	7.64	-

C Stripping selections

As discussed in Section 3.2, the nominal analysis will use candidates produced within the exclusive HLT2 trigger lines, described in Section 4.2. The usual offline Brunel-DaVinci stripping processing will only be used if the HLT2 candidates are unavailable. This section described the set of stripping lines that have been created to select and reconstruct candidates offline.

Each stripping line is run over all events passing HLT2. Lines are grouped by hadron and topology into stripping modules. The selection code is kept in the `StrippingCharm` folder within the `StrippingSelections` package, in the `Stripping` project.

The general structure of a stripping line is to take as input a set of containers of particles, such as kaons and pions, and combine them into a composite 'parent' particle under a decay hypothesis, such as $D^+ \to K^-\pi^+\pi^+$. Each container defines the particles it provides with an ASCII string, such as `pi+` for a positively charged pion, or `D*(2010)+` for D^{*+}. The combination of the set of input containers can then be defined by a 'decay descriptor' string, which describes what particles should be used to form the parent. The decay descriptor `D+ -> K- pi+ pi+` can be read as "find all combinations of the particles provided by the input containers which match the set {`K-, pi+, pi+`} and call that combination `D+`".

The set of input containers used in all stripping lines for stable charged tracks are from the `StdAllLooseNoPIDsX` family, where `X` is one of `Pions` or `Kaons`. These differ from the `StdLooseNoPIDs` family in that the 'standard' $p_{\mathrm{T}} > 250\,\mathrm{MeV}$ and $\chi^2_{\mathrm{IP}} > 4$ are not applied.

There are many possible combinations of a given topology for a given set of input containers, and so to reduce the combinatorics the inputs can be preselected before being combined. Once the children are selected in this manner, the remaining input particles are combined by four vector addition, and further requirements can be imposed on the resulting combination. Finally, a vertex fit is performed on the passing inputs to construct a vertex, which defines the parent particle, upon which a final selection can be made. The set of resulting parent particles are then saved to disk to be used in offline analysis, and/or further combined as part of some longer decay chain.

We apply loose rectangular cuts to the input particles and the resulting composite parents. A cut is then made on the output of a boosted decision tree (BDT) discriminant, discussed in Section **??**, where the inputs to the training of the BDT, one per mode, are mode-dependent.

The following sections will describe the stripping modules used in the analysis and

define the respective selection requirements. Unless otherwise stated, each stripping line also selects the charge conjugate process.

`StrippingD02HHForXSec` module

The `D02HHForXSec` module reconstructs the two-body Cabibbo-favoured $D^0 \to K^-\pi^+$ decay, and then adds a charged pion to reconstruct the $D^{*+} \to D^0\pi^+$ decay. The flavour of the D^0 is always marked as D^0 in the stripping line. If the flavour of the D^0 is required, the charge of the soft pion in the D^{*+} line must be used, but the decay descriptors ignore this.

For each D^0 mode, one stripping line is made with untagged D^0 candidates, and another with tagged candidates. Table C.1 lists the stripping selection requirements made in the `D02HHForXSec` module.

`StrippingD02K3PiForXSec` module

The `D02K3PiForXSec` module reconstructs the four-body Cabibbo-favoured $D^0 \to K^-\pi^+\pi^-\pi^+$ decay, and then adds a charged pion to reconstruct the $D^{*+} \to D^0\pi^+$ decay, as in the `D02HHForXSec` module. The flavour of the D^0 is resolved in this stripping line, where the charge of the kaon determines the flavour of the D^0 (a negative charge for D^0, positive for $\overline{D}^0$). The doubly Cabibbo-suppressed $K^+\pi^-\pi^+\pi^-$ mode is assumed to be a negligible contribution in this way.

One stripping line is made with untagged D^0 candidates, and another with tagged candidates. Table C.2 lists the stripping selection requirements made in the `D02K3PiForXSec` module.

`StrippingD2HHHForXSec` module

The `D2HHHForXSec` module reconstructs the Cabibbo-favoured $D^+ \to K^-\pi^+\pi^+$ decay and the singly Cabibbo-suppressed $D^+ \to K^-K^+\pi^+$ and $D^+ \to \pi^-\pi^+\pi^+$ decays. The $h^-h^+h^-$ mass window is wide enough to also capture D_s^+ decays to the same final states and is labelled as `D+`. The combination is then split into two `Selection` instances: one centred 80 MeV around the nominal D^+ mass, and another 80 MeV around the nominal D_s^+ mass. The candidates centred on the D_s^+ mass are then relabelled as `D_s+` using the `SubstitutePID` algorithm. Table C.3 lists the stripping selection requirements made in the `D2HHHForXSec` module.

Table C.1: Selection requirements made in the `StrippingD02HHForXSec` *module.*

Particle	Variable	Cut value	LoKi functor
$\pi^\pm$, $K^\pm$	p_T	$> 250\,\mathrm{MeV}$	`PT`
	p	$3 < p < 100\,\mathrm{GeV}$	`P`
	η	$2 < \eta < 5$	`ETA`
	χ^2_IP	> 16	`BPVIPCHI2`
$\pi^\pm$	$\mathrm{DLL}_{K-\pi}$	< 3	`PIDK - PIDpi`
$K^\pm$	$\mathrm{DLL}_{K-\pi}$	> 5	`PIDK - PIDpi`
D^0	$m_\mathrm{PDG}(D^0) - m(K^-\pi^+)$	$< 80\,\mathrm{MeV}$	`ADAMASS('D0')`
	Vertex fit χ^2	< 10	`VFASPF(VCHI2/VDOF)`
	Direction angle	$< 17\,\mathrm{mrad}$	`BPVDIRA`
	Vertex displacement	$VD\chi^2 > 49$	`BPVVDCHI2`
	BDT discriminant	> -0.3	-
D^{*+}	$m(K^-\pi^+\pi^+_\mathrm{Soft}) - m(K^-\pi^+)$	$< 160\,\mathrm{MeV}$	`AM - AM1`
	Vertex fit χ^2	< 25	`VFASPF(VCHI2/VDOF)`

`StrippingD2PhiPiForXSec` module

The `D2PhiPiForXSec` module reconstructs the Cabibbo-favoured $D_s^+ \to \phi\pi^+$ decay by selecting $D_s^+ \to K^-K^+\pi^+$ with a $\phi(1020)$ mass window imposed on the reconstructed K^-K^+ mass. This requirement greatly reduces the size of the combinatorial background. The $\phi\pi^+$ mass window is wide enough to capture D^+ decays, but the candidates are labelled as `D_s+`. The combination is then split into two `Selection` instances: one centred 80 MeV around the nominal D^+ mass, and another 80 MeV around the nominal D_s^+ mass. The candidates centred on the D^+ mass are then relabelled as `D+` using the `SubstitutePID` algorithm. Table C.4 lists the stripping selection requirements made in the `D2PhiPiForXSec` module.

Table C.2: Selection requirements made in the `StrippingD02K3PiForXSec` *module. Cuts of the form $x > x_1$, x_2, x_3, x_4 require that all particles satisfy $x > x_1$, at least three satisfy $x > x_2$, at least two satisfy $x > x_3$, and at least one satisfies $x > x_4$.*

Particle	Variable	Cut value	LoKi functor
$\pi^\pm$, $K^\pm$	p_T	> 200, 300, 350, 400 MeV	`PT`
	p	$3 < p < 100$ GeV	`P`
	η	$2 < \eta < 5$	`ETA`
	χ^2_IP	> 4	`BPVIPCHI2`
$\pi^\pm$	$\mathrm{DLL}_{K-\pi}$	< 3	`PIDK - PIDpi`
$K^\pm$	$\mathrm{DLL}_{K-\pi}$	> 5	`PIDK - PIDpi`
D^0	$m_\mathrm{PDG}(D^0) - m(K^-\pi^+\pi^-\pi^+)$	< 80 MeV	`ADAMASS('D0')`
	DOCA	< 0.1 mm	`ACUTDOCA`
	Vertex fit χ^2	< 10	`VFASPF(VCHI2/VDOF)`
	Direction angle	< 17 mrad	`BPVDIRA`
	Vertex displacement	$VD\chi^2 > 16$ AND $\tau > 0.150$ ps	`BPVVDCHI2 & BPVLTIME()`
	BDT discriminant	> -0.3	-
D^{*+}	$m(K^-\pi^+\pi^-\pi^+\pi^+_\mathrm{Soft}) - m(K^-\pi^+\pi^-\pi^+)$	< 160 MeV	`AM - AM1`
	Vertex fit χ^2	< 25	`VFASPF(VCHI2/VDOF)`

Table C.3: Selection requirements made in the `StrippingD2HHHForXSec` *module. The window for the reconstructed $m(h^-h^+h^+)$ mass is wide enough to select both D^+ and D_s^+ decays; the $m_{PDG}(D^+_{(s)}) - m(h^-h^+h^+)$ requirement is a logical* `OR`*, asking that the three-body combination is within either of the D^+ or the D_s^+ windows.*

Particle	Variable	Cut value	LoKi functor
$\pi^\pm$, $K^\pm$	p_{T}	> 200, 400, 1000 MeV	`PT`
	p	$3 < p < 100$ GeV	`P`
	η	$2 < \eta < 5$	`ETA`
	χ^2_{IP}	> 4, 10, 50	`BPVIPCHI2`
$\pi^\pm$	$\mathrm{DLL}_{K-\pi}$	< 3	`PIDK - PIDpi`
$K^\pm$	$\mathrm{DLL}_{K-\pi}$	> 5	`PIDK - PIDpi`
D^+/D_s^+	$m_{\mathrm{PDG}}(D^+_{(s)}) - m(h^-h^+h^+)$	< 80 MeV	`AM`
	DOCA	< 0.5 mm	`ACUTDOCA`
	Vertex fit χ^2	< 25	`VFASPF(VCHI2/VDOF)`
	Direction angle	< 34 mrad	`BPVDIRA`
	Vertex displacement	$VD\chi^2 > 16$ AND $\tau > 0.150$ ps	`BPVVDCHI2 & BPVLTIME()`
	BDT discriminant	> -0.3	-

Table C.4: Selection requirements made in the `StrippingD2PhiPiForXSec` *module. The window for the reconstructed $m(\phi\pi^+)$ mass is wide enough to select both D^+ and D_s^+ decays; the $m_{PDG}(D^+_{(s)}) - m(\phi\pi^+)$ requirement is a logical* `OR`*, asking that the two-body combination is within either of the D^+ or the D_s^+ windows.*

Particle	Variable	Cut value	LoKi functor
$\pi^\pm$, $K^\pm$	p_{T}	$> 200\,\mathrm{MeV}$	`PT`
	p	$3 < p < 100\,\mathrm{GeV}$	`P`
	η	$2 < \eta < 5$	`ETA`
	χ^2_{IP}	> 4	`BPVIPCHI2`
$\pi^\pm$	$\mathrm{DLL}_{K-\pi}$	< 3	`PIDK - PIDpi`
$K^\pm$	$\mathrm{DLL}_{K-\pi}$	> 5	`PIDK - PIDpi`
ϕ	$m_{\mathrm{PDG}}(\phi) - m(K^-K^+)$	$< 20\,\mathrm{MeV}$	`ADAMASS('phi(1020)')`
D^+/D_s^+	$m_{\mathrm{PDG}}(D^+_{(s)}) - m(\phi\pi^+)$	$< 80\,\mathrm{MeV}$	`AM`
	Vertex fit χ^2	< 25	`VFASPF(VCHI2/VDOF)`
	Direction angle	$< 35\,\mathrm{mrad}$	`BPVDIRA`
	Vertex displacement	$VD\chi^2 > 25$ AND $\tau > 0.150\,\mathrm{ps}$	`BPVVDCHI2 & BPVLTIME()`
	BDT discriminant	> -0.3	-

D Probability density functions

The probability density functions (PDFs) used in the analysis are enumerated in this section. Which PDFs are used for each data species within each mode is discussed in Section 6.

The functional form of each one dimensional PDF will be given as $f(x; \alpha, \beta, \ldots)$ without a normalisation constant, where x is the dependent variable, the 'observable', and everything after the semicolon is the set of 'parameters'.

Gaussian SGS

The normal distribution; a bell-shaped curve centred on the mean μ with a width governed by σ

$$f_{\mathrm{SCS}}(x; \mu, \sigma) = e^{-\frac{(x-\mu)^2}{2\sigma^2}}. \tag{D.1}$$

Double Gaussian DGS

The sum of two Gaussian PDFs, sharing a common mean μ but with separate widths σ_1 and σ_2, with relative strengths κ

$$\begin{aligned} f_{DGS}(x; \mu, \sigma_1, \sigma_2, \kappa) &= (1-\kappa) \cdot e^{-\frac{(x-\mu)^2}{2\sigma_1^2}} + \kappa \cdot e^{-\frac{(x-\mu)^2}{2\sigma_2^2}}, \\ &= (1-\kappa) \cdot f_{SGS}(x; \mu, \sigma_1) + \kappa \cdot f_{SGS}(x; \mu, \sigma_2) \end{aligned} \tag{D.2}$$

Using two widths is useful for fitting distributions with a narrow core and wider tails.

Dimidated Gaussian BGS

A modified Gaussian PDF with differing widths σ_{L} and σ_{R} either side of the mean μ

$$f_{\mathrm{BGS}}(x; \mu, \sigma_{\mathrm{L}}, \sigma_{\mathrm{R}}) = \begin{cases} e^{-\frac{(x-\mu)^2}{2\sigma_{\mathrm{L}}^2}} & x < \mu, \\ e^{-\frac{(x-\mu)^2}{2\sigma_{\mathrm{R}}^2}} & x \geq \mu. \end{cases} \tag{D.3}$$

This is often called a 'bifurcated' Gaussian [31].

AsymGaussExp AGE

A modified Gaussian PDF with exponential tails of strength ρ_{L} and ρ_{R} either side of the mean μ and an asymmetrical width σ governed by ϵ

$$f_{\mathrm{AGE}}(x;\mu,\sigma,\epsilon,\rho_{\mathrm{L}},\rho_{\mathrm{R}}) = \begin{cases} e^{\frac{\rho_{\mathrm{L}}^2}{2}+\rho_{\mathrm{L}}\cdot\frac{x-\mu}{(1-\epsilon)\cdot\sigma}} & x < \mu - (\rho_{\mathrm{L}}\cdot\sigma\cdot(1-\epsilon)), \\ e^{-\left(\frac{x-\mu}{\sqrt{2}\cdot\sigma\cdot(1-\epsilon)}\right)^2} & \mu - (\rho_{\mathrm{L}}\cdot\sigma\cdot(1-\epsilon)) \leq x < \mu, \\ e^{-\left(\frac{x-\mu}{\sqrt{2}\cdot\sigma\cdot(1+\epsilon)}\right)^2} & \mu \leq x < \mu + (\rho_{\mathrm{R}}\cdot\sigma\cdot(1+\epsilon)), \\ e^{\frac{\rho_{\mathrm{R}}^2}{2}-\rho_{\mathrm{R}}\cdot\frac{x-\mu}{(1+\epsilon)\cdot\sigma}} & x \geq \mu + (\rho_{\mathrm{R}}\cdot\sigma\cdot(1+\epsilon)). \end{cases} \tag{D.4}$$

Crystal Ball SCB

A modified Gaussian PDF with a power-law tail on one side

$$f_{\mathrm{SCB}}(x;\mu,\sigma,\alpha,n) = \begin{cases} e^{-\frac{(x-\mu)^2}{2\sigma^2}} & \frac{x-\mu}{\sigma} > -\alpha, \\ \left(\frac{n}{|\alpha|}\right)^n \cdot e^{-\frac{|\alpha|^2}{2}} \cdot \left(\frac{n}{|\alpha|} - |\alpha| - \frac{x-\mu}{\sigma}\right)^{-n} & \frac{x-\mu}{\sigma} \leq -\alpha. \end{cases} \tag{D.5}$$

The α parameter defines how far away from the mean μ the power-law tail begins in units of the width of the core Gaussian σ, and n is the power law exponent.

Double Crystal Ball DCB

The sum of two Crystal Ball PDFs, sharing a common mean μ and tail parameters α and n, but with separate widths σ_1 and σ_2, with relative strengths κ

$$f_{\mathrm{DCB}}(x;\mu,\sigma_1,\sigma_2,\alpha,n,\kappa) = (1-\kappa)\cdot f_{\mathrm{SCB}}(x;\mu,\sigma_1,\alpha,n) + \kappa\cdot f_{\mathrm{SCB}}(x;\mu,\sigma_2,\alpha,n). \tag{D.6}$$

Gaussian Crystal Ball GCB

The sum of a Gaussian and a Crystal Ball PDF, sharing a common mean μ, but with separate widths σ_1 and σ_2

$$f_{\mathrm{GCB}}(x;\mu,\sigma_1,\sigma_2,\alpha,n,\kappa) = (1-\kappa)\cdot f_{\mathrm{SGS}}(x;\mu,\sigma_1) + \kappa\cdot f_{\mathrm{SCB}}(x;\mu,\sigma_2,\alpha,n). \tag{D.7}$$

Smeared $\log \chi^2$ SCS

The χ^2 distribution for n degrees of freedom is

$$f_{\chi^2}(x; n) = \frac{x^{\frac{n}{2}-1} \cdot e^{-\frac{x}{2}}}{2^{\frac{n}{2}} \cdot \Gamma(\frac{n}{2})}, \tag{D.8}$$

where $\Gamma(n)$ is the Gamma function for integer n defined as

$$\Gamma(n) = (n-1)!. \tag{D.9}$$

By substituting x for $\ln x$, allowing the observable to be 'smeared' by a factor α, and further allowing this smearing to be asymmetric about the mean μ [32], the χ^2 distribution above can be transformed into the so-called smeared $\log \chi^2$ PDF

$$f_{\mathrm{SCS}}(x, \mu, \alpha_{\mathrm{L}}, \alpha_{\mathrm{R}}) = \begin{cases} \exp(\alpha_{\mathrm{L}} x - \exp(\alpha_{\mathrm{L}}(x-\mu))) & x \leq \mu, \\ \exp(\alpha_{\mathrm{L}}\mu + \alpha_{\mathrm{R}}(x-\mu) - \exp(\alpha_{\mathrm{R}}(x-\mu))) & x > \mu. \end{cases} \tag{D.10}$$

Chebyshev polynomial FOP, SOP, TOP

The Chebyshev polynomials of the first kind can be defined recursively, where the ith power polynomial is defined by

$$\begin{aligned} T_0 &= 1, \\ T_1 &= x, \\ T_{n+1} &= 2x \cdot T_n(x) - T_{n-1}(x). \end{aligned}$$

As it is usually the shapes of background distributions that are described by such polynomials, and any non-trivial shape usually points to some structure that should be modelled with a PDF more 'meaningful' than a higher-order polynomial, we will explicitly define the Chebyshev polynomials for $n \leq 3$, as these are the most common

$$T_0 = 1, \tag{D.11}$$
$$T_1 = x, \tag{D.12}$$
$$T_2 = 2x^2 - 1 \tag{D.13}$$
$$T_3 = 4x^3 - 3x. \tag{D.14}$$

The fitted PDF for an ith order Chebyshev polynomial is then the sum of all polynomials up to the given order, each multiplied by a fitted parameter

$$f(x; \{a_1, \ldots, a_n\}) = 1 + \sum_{i=1}^{n} a_i T_i(x). \tag{D.15}$$

The first order polynomial is given the shorthand f_{FOP}, the second f_{SOP}, and the third f_{TOP}.

Chebyshev polynomials are often used rather than 'ordinary' polynomials, where each parameter a_i multiplies the ith power of x, as the correlation between parameters is much lower, and hence fits using Chebyshev polynomials are more stable.

Exponential EXP

The natural exponential function with strength parameter λ

$$f_{\mathrm{EXP}}(x;\lambda) = e^{\lambda x}. \tag{D.16}$$

Empirical δm background DST

An empirically derived shape commonly used for modelling the background components in distributions of δm, the mass difference between two decaying particles, usually D^{*+} and D^0, with a 'threshold' at δm_0 below which no physical events can occur, and shape parameters A, B, and C

$$f_{\mathrm{DST}}(x;\delta m_0, A, B, C) = \left(\frac{x}{\delta m_0}\right)^A \cdot (1 - e^{-\frac{x-\delta m_0}{C}}) + B \cdot \left(\frac{x}{\delta m_0} - 1\right). \tag{D.17}$$

E Factorization of the PDFs

The assumption that the PDFs factorize needs to be tested separately for signal and for background.

For signal, the assumption has been tested for the $D^0 \to K^-\pi^+$ decay mode using reconstructible truth-matched prompt signal simulated events. Figure E.1 shows the mean of the $\ln \chi^2_{\mathrm{IP}}$ distribution as a function of the signal D^0 mass, and shows a clear dependence. The effect of this on the fit is under study.

For background, the assumption is tested separately for each decay mode in question using data from the 2011 cross-section analysis. For the two-dimensional fit, the distribution of $\ln \chi^2_{\mathrm{IP}}$ is plotted in the upper and lower sidebands of the D candidate mass. For the three-dimensional fit, the distribution of $\ln \chi^2_{\mathrm{IP}}$ is plotted in the upper and lower sidebands of the D candidate mass and δm. In addition, the distribution of the δm variable is plotted in the upper and lower sidebands of the D candidate mass. These plots are shown for the two-dimensional fits in Figure E.2, and for the three-dimensional fits in Figure E.3, and no significant dependences are seen.

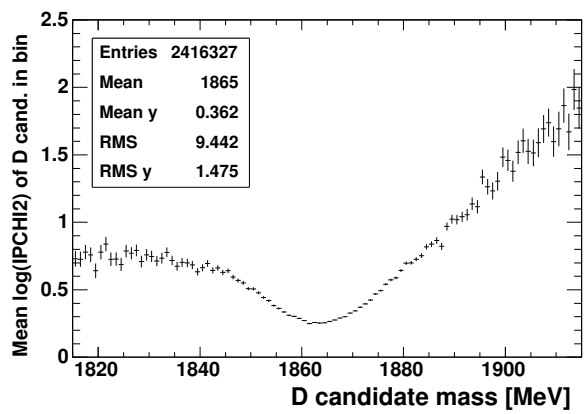

Figure E.1: The mean of the signal $\ln \chi^2_{\mathrm{IP}}$ *as a function of the* D^0 *mass for truth-matched prompt signal simulated events.*

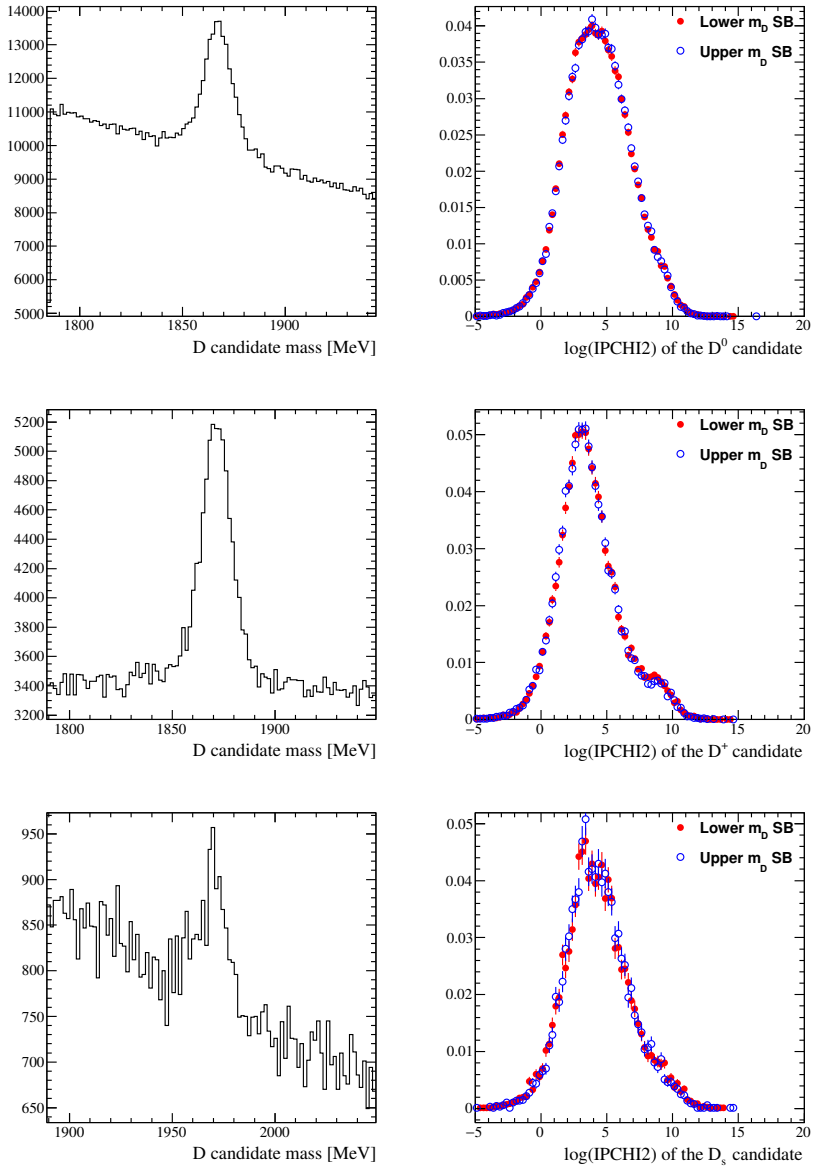

Figure E.2: PDF factorization plots for the $D^0 \to K^-\pi^+$, $D^+ \to K^-\pi^+\pi^+$, and $D_s^+ \to \phi\pi^+$ decay modes (top to bottom). The left panel in each plot shows the D candidate mass distribution to give an idea of the sample purity; the right panel shows the D candidate $\ln \chi^2_{\mathrm{IP}}$ distribution in the lower and upper sidebands of the D mass.

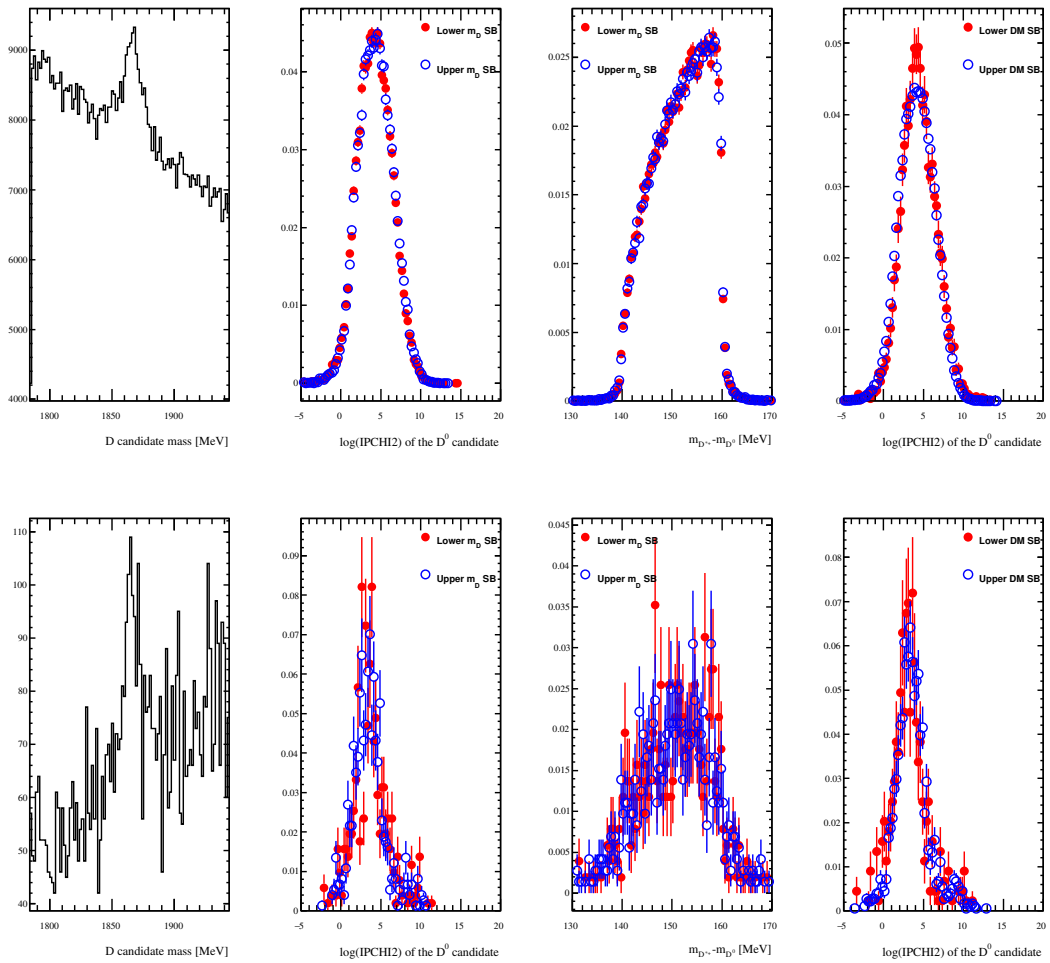

Figure E.3: PDF factorization plots for the tagged $D^0 \to K^-\pi^+$, and tagged $D^0 \to K^-\pi^+\pi^-\pi^+$ decay modes (top to bottom). The leftmost panel in each plot shows the D candidate mass distribution to give an idea of the sample purity. The next three panels show (left to right) the D candidate $\ln\chi^2_{\rm IP}$ distribution in the lower and upper sidebands of the D mass; the δm distribution in the lower and upper sidebands of the D mass; and the D candidate $\ln\chi^2_{\rm IP}$ distribution in the lower and upper sidebands of the δm.

F Fits in p_{T}-y bins

The final $\ln \chi^2_{\mathrm{IP}}$ fits for each mode within each p_{T}-y are given in this section. The integrated fits, which show the sum of the data and curves in the respective subsection here, are given in Section 6.5.

F.1 $D^0 \to K^-\pi^+$

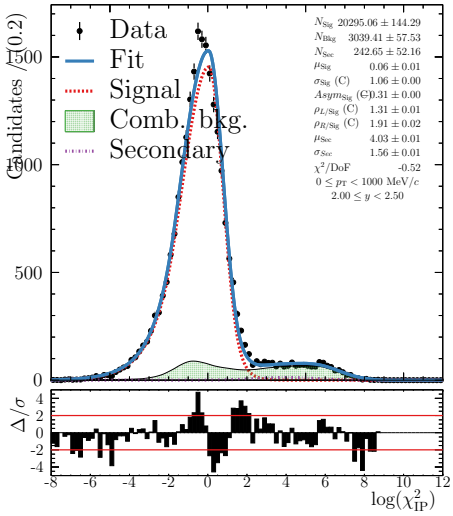

$0 \leq p_{\rm T} < 1\,{\rm GeV},\ 2.0 \leq y < 2.5$

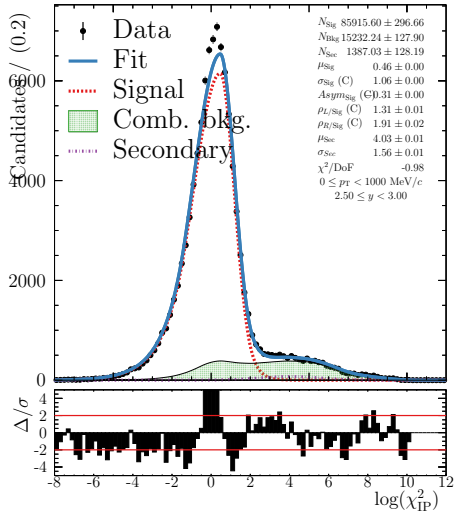

$0 \leq p_{\rm T} < 1\,{\rm GeV},\ 2.5 \leq y < 3.0$

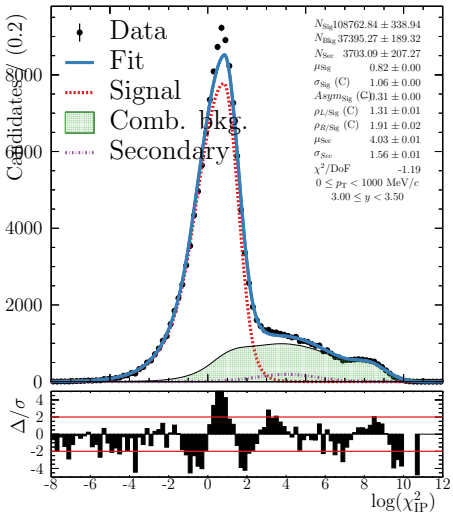

$0 \leq p_{\rm T} < 1\,{\rm GeV},\ 3.0 \leq y < 3.5$

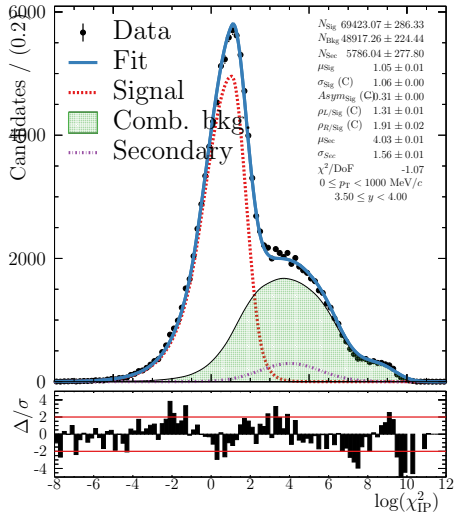

$0 \leq p_{\rm T} < 1\,{\rm GeV},\ 3.5 \leq y < 4.0$

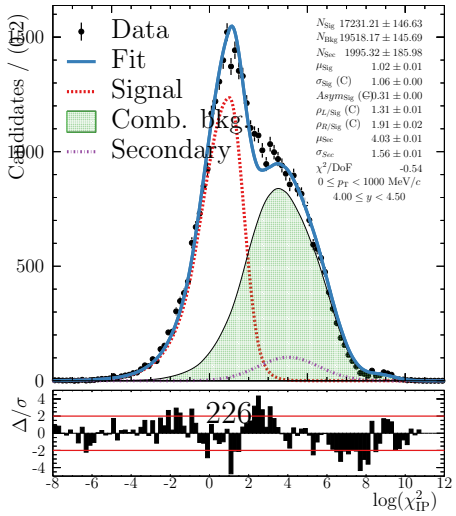

$0 \leq p_{\rm T} < 1\,{\rm GeV},\ 4.0 \leq y < 4.5$

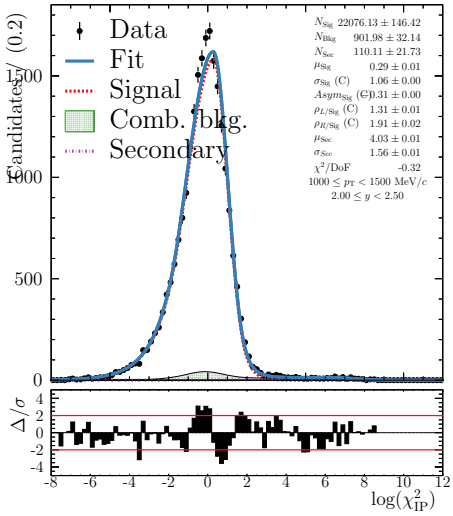

$1 \le p_{\rm T} < 1.5\,{\rm GeV},\ 2.0 \le y < 2.5$

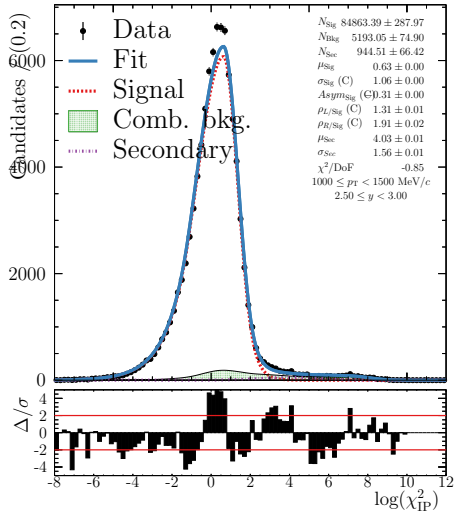

$1 \le p_{\rm T} < 1.5\,{\rm GeV},\ 2.5 \le y < 3.0$

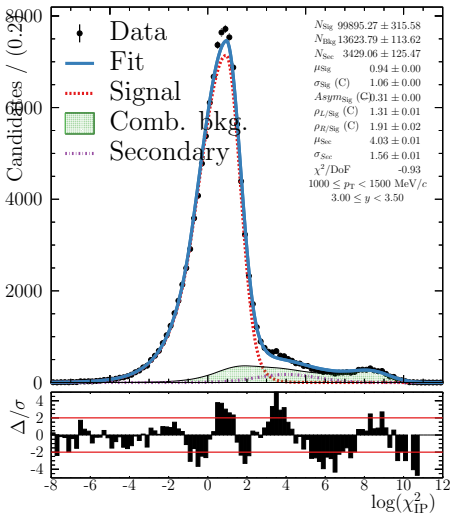

$1 \le p_{\rm T} < 1.5\,{\rm GeV},\ 3.0 \le y < 3.5$

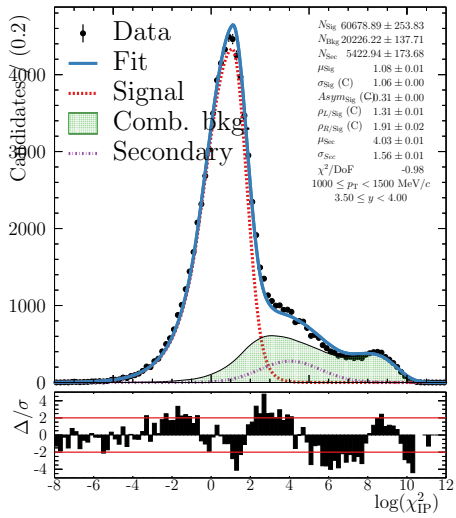

$1 \le p_{\rm T} < 1.5\,{\rm GeV},\ 3.5 \le y < 4.0$

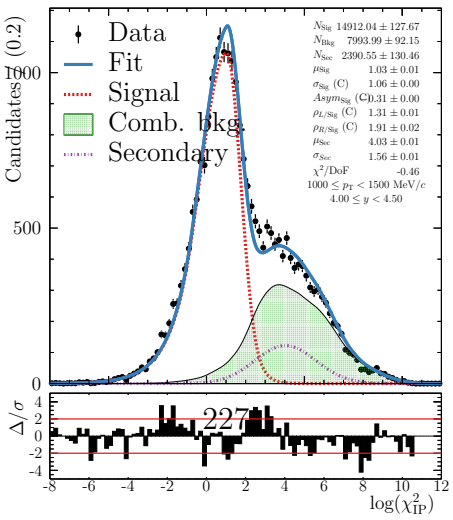

$1 \le p_{\rm T} < 1.5\,{\rm GeV},\ 4.0 \le y < 4.5$

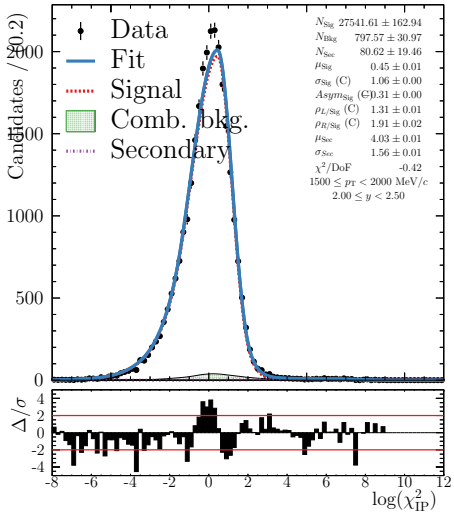

$1.5 \leq p_{\rm T} < 2\,{\rm GeV},\ 2.0 \leq y < 2.5$

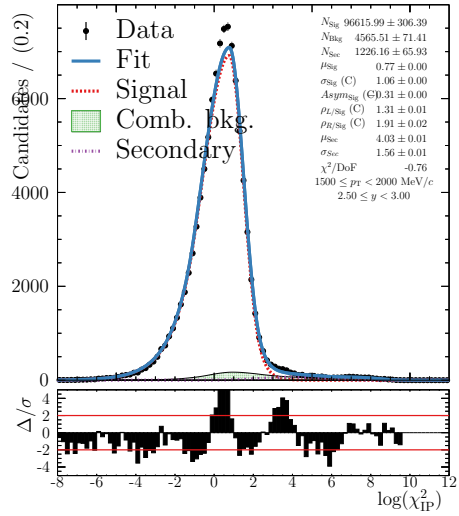

$1.5 \leq p_{\rm T} < 2\,{\rm GeV},\ 2.5 \leq y < 3.0$

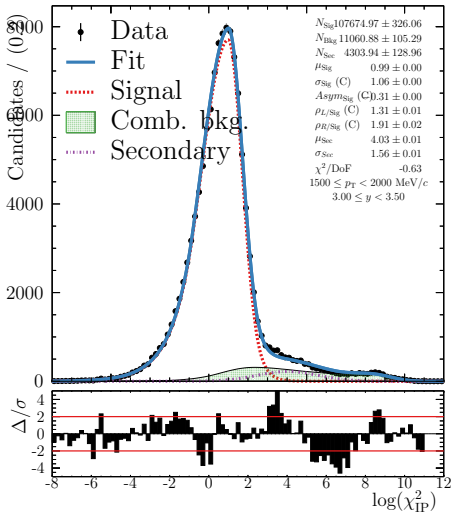

$1.5 \leq p_{\rm T} < 2\,{\rm GeV},\ 3.0 \leq y < 3.5$

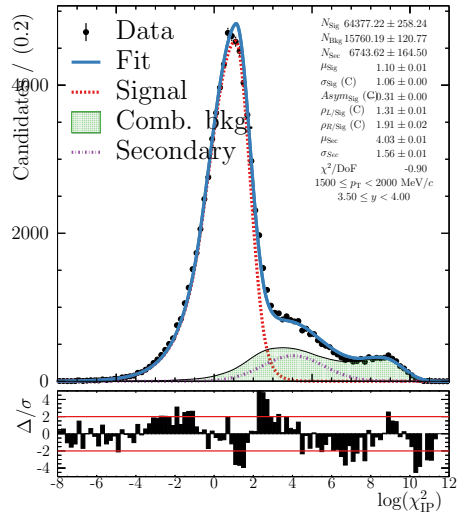

$1.5 \leq p_{\rm T} < 2\,{\rm GeV},\ 3.5 \leq y < 4.0$

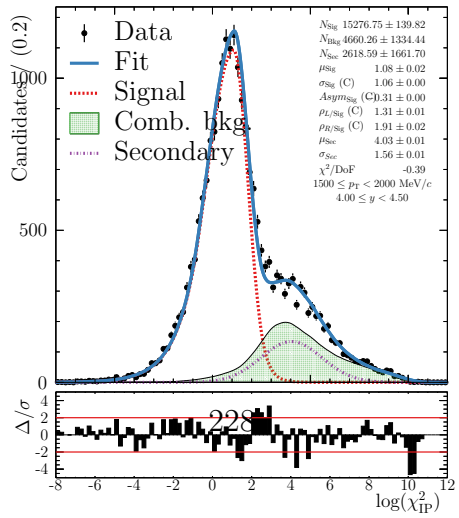

$1.5 \leq p_{\rm T} < 2\,{\rm GeV},\ 4.0 \leq y < 4.5$

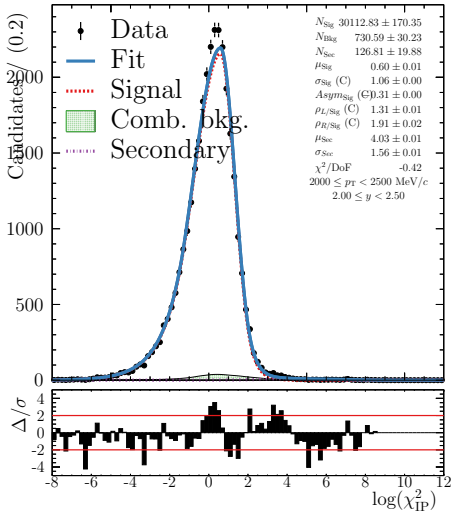

$2 \leq p_{\rm T} < 2.5\,{\rm GeV},\ 2.0 \leq y < 2.5$

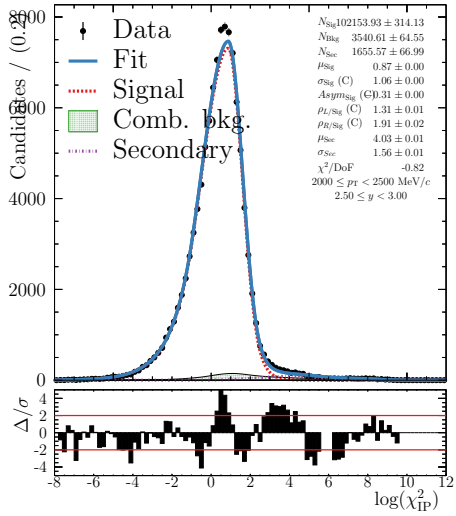

$2 \leq p_{\rm T} < 2.5\,{\rm GeV},\ 2.5 \leq y < 3.0$

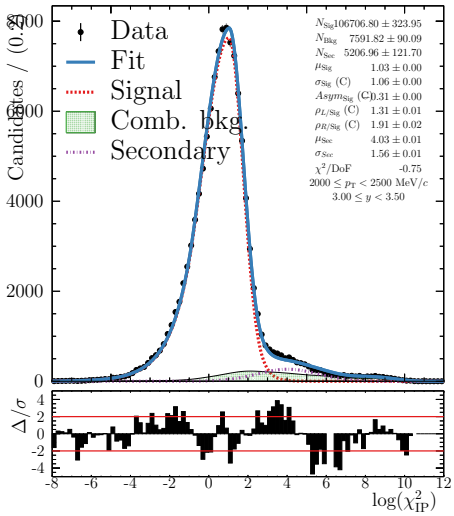

$2 \leq p_{\rm T} < 2.5\,{\rm GeV},\ 3.0 \leq y < 3.5$

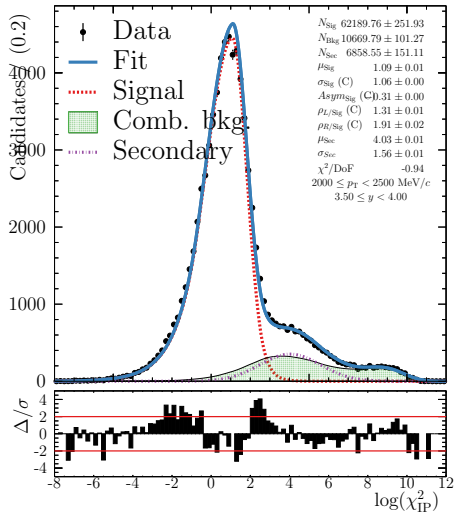

$2 \leq p_{\rm T} < 2.5\,{\rm GeV},\ 3.5 \leq y < 4.0$

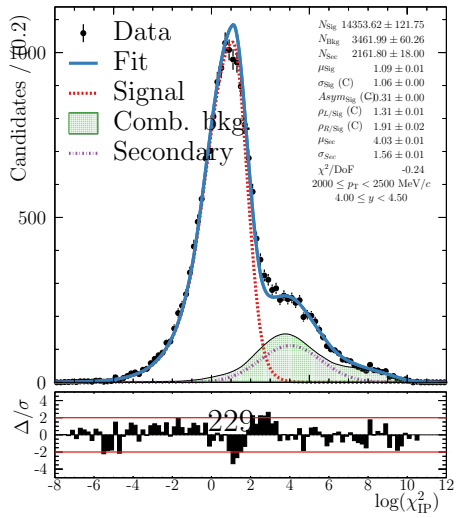

$2 \leq p_{\rm T} < 2.5\,{\rm GeV},\ 4.0 \leq y < 4.5$

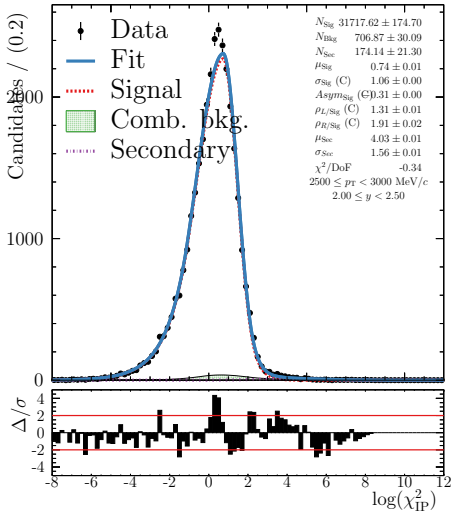

$2.5 \leq p_{\rm T} < 3\,{\rm GeV},\ 2.0 \leq y < 2.5$

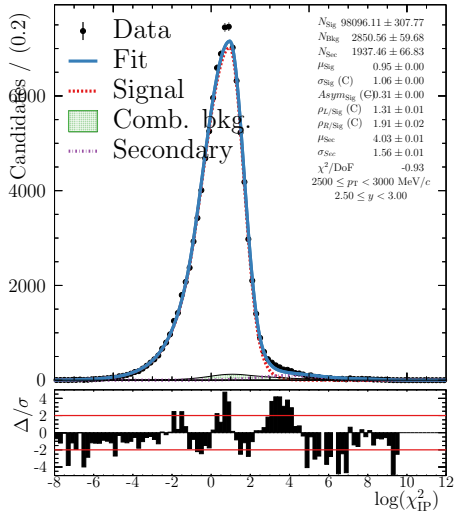

$2.5 \leq p_{\rm T} < 3\,{\rm GeV},\ 2.5 \leq y < 3.0$

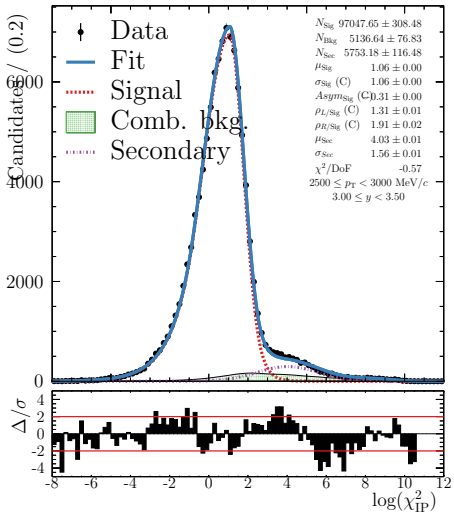

$2.5 \leq p_{\rm T} < 3\,{\rm GeV},\ 3.0 \leq y < 3.5$

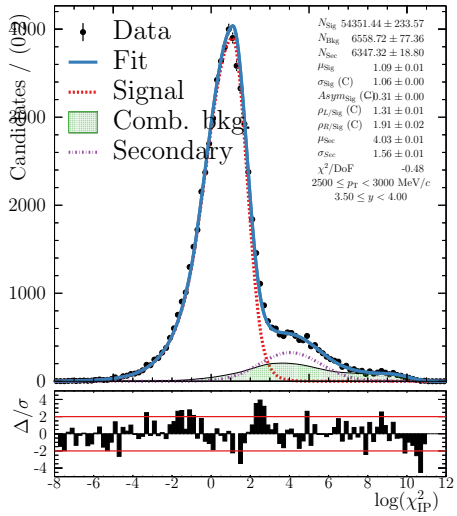

$2.5 \leq p_{\rm T} < 3\,{\rm GeV},\ 3.5 \leq y < 4.0$

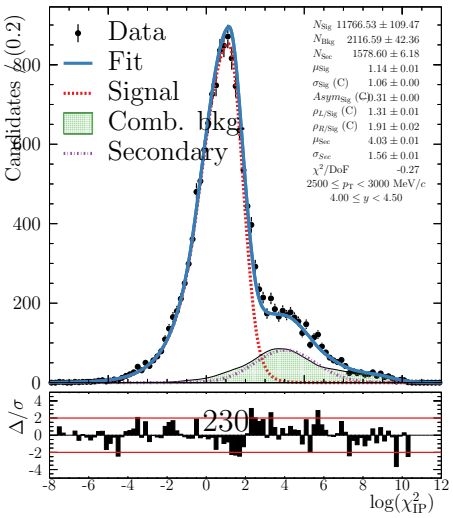

$2.5 \leq p_{\rm T} < 3\,{\rm GeV},\ 4.0 \leq y < 4.5$

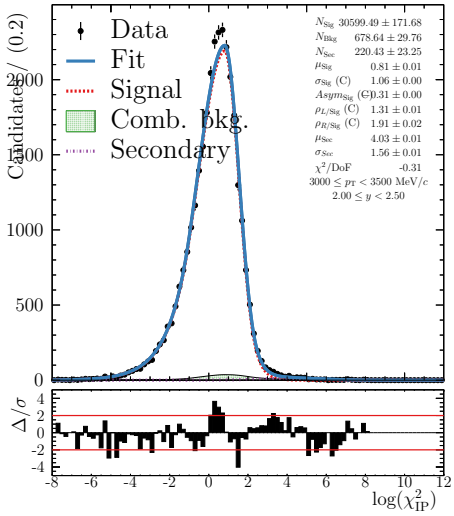

$3 \leq p_{\rm T} < 3.5\,{\rm GeV},\ 2.0 \leq y < 2.5$

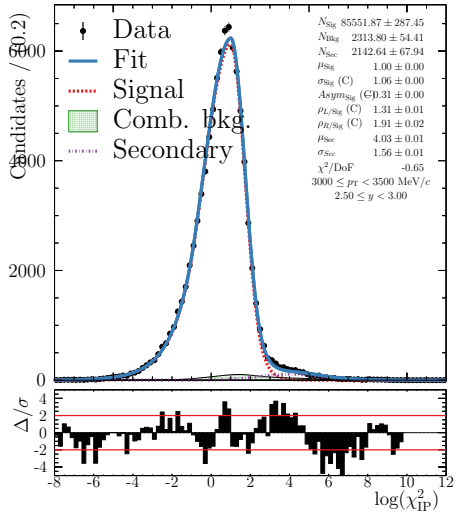

$3 \leq p_{\rm T} < 3.5\,{\rm GeV},\ 2.5 \leq y < 3.0$

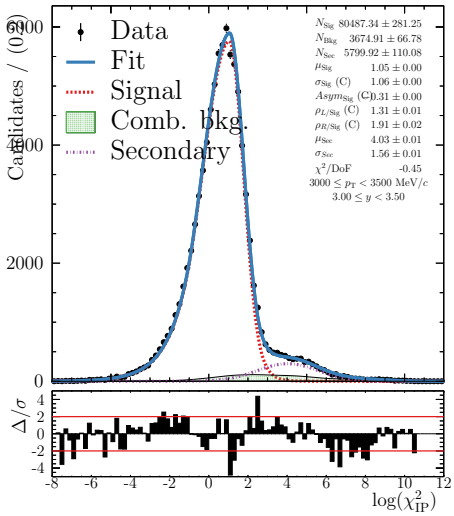

$3 \leq p_{\rm T} < 3.5\,{\rm GeV},\ 3.0 \leq y < 3.5$

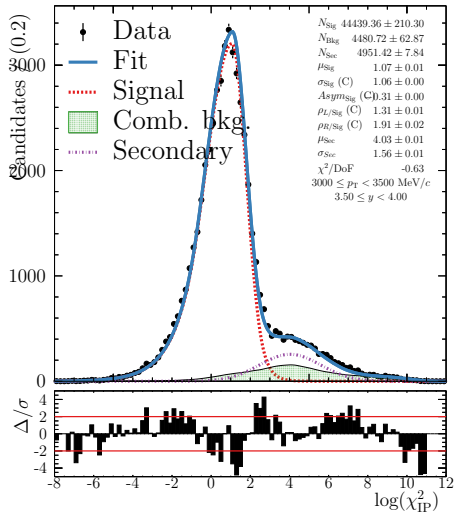

$3 \leq p_{\rm T} < 3.5\,{\rm GeV},\ 3.5 \leq y < 4.0$

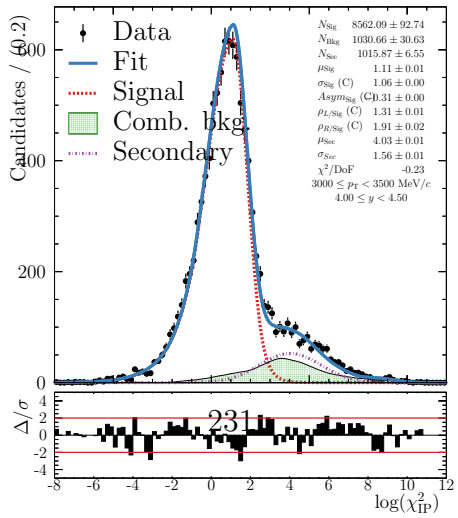

$3 \leq p_{\rm T} < 3.5\,{\rm GeV},\ 4.0 \leq y < 4.5$

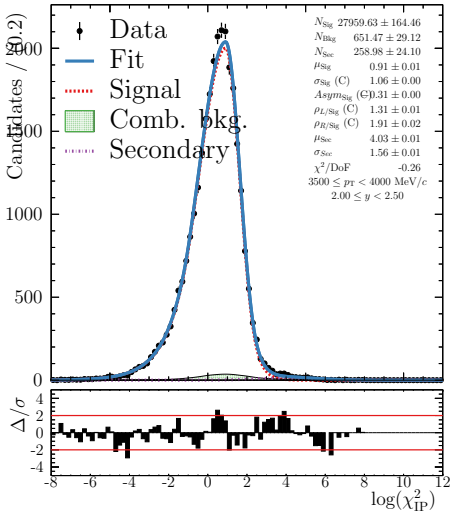

$3.5 \leq p_{\rm T} < 4\,{\rm GeV},\ 2.0 \leq y < 2.5$

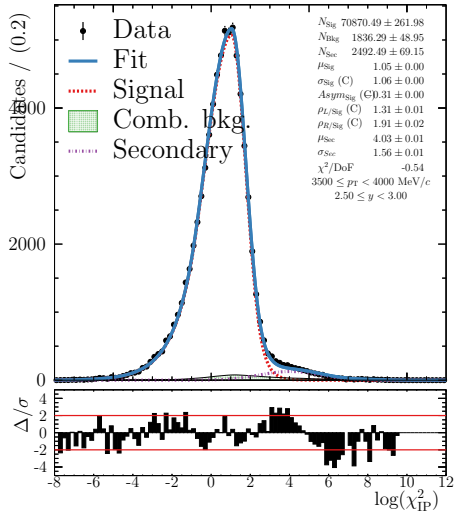

$3.5 \leq p_{\rm T} < 4\,{\rm GeV},\ 2.5 \leq y < 3.0$

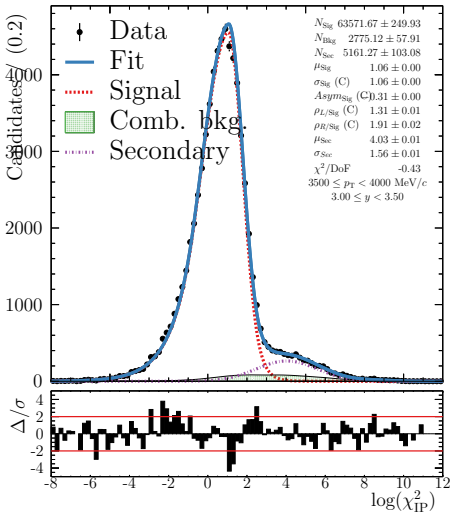

$3.5 \leq p_{\rm T} < 4\,{\rm GeV},\ 3.0 \leq y < 3.5$

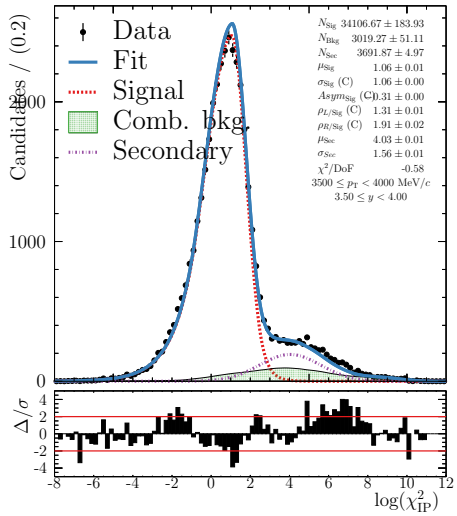

$3.5 \leq p_{\rm T} < 4\,{\rm GeV},\ 3.5 \leq y < 4.0$

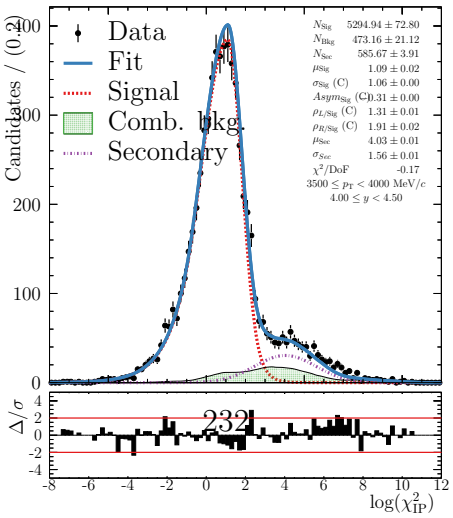

$3.5 \leq p_{\rm T} < 4\,{\rm GeV},\ 4.0 \leq y < 4.5$

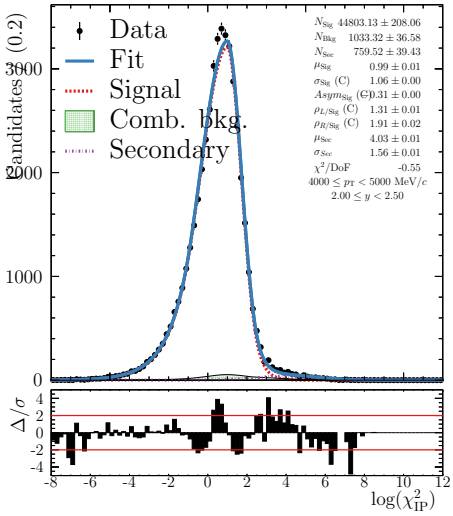

$4 \leq p_{\rm T} < 5\,{\rm GeV},\ 2.0 \leq y < 2.5$

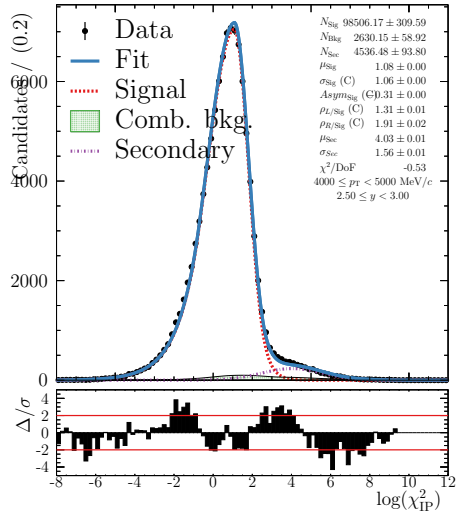

$4 \leq p_{\rm T} < 5\,{\rm GeV},\ 2.5 \leq y < 3.0$

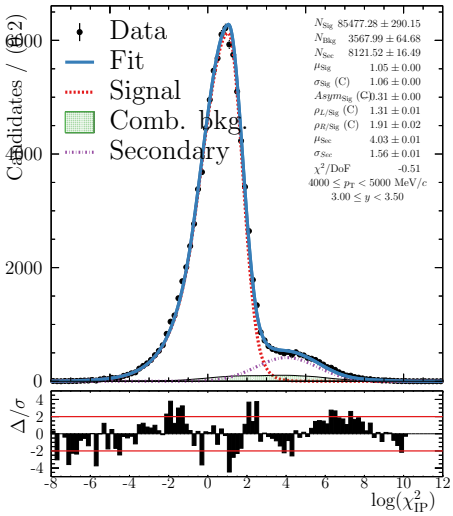

$4 \leq p_{\rm T} < 5\,{\rm GeV},\ 3.0 \leq y < 3.5$

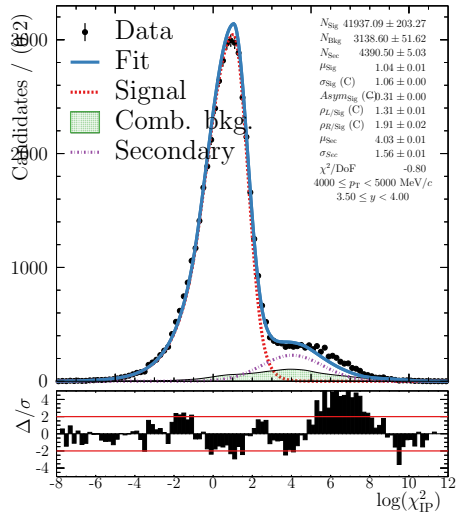

$4 \leq p_{\rm T} < 5\,{\rm GeV},\ 3.5 \leq y < 4.0$

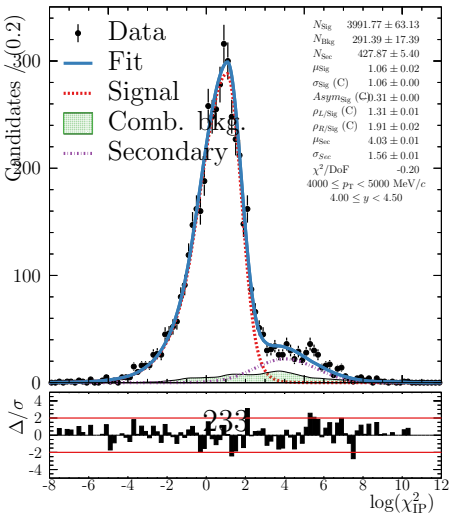

$4 \leq p_{\rm T} < 5\,{\rm GeV},\ 4.0 \leq y < 4.5$

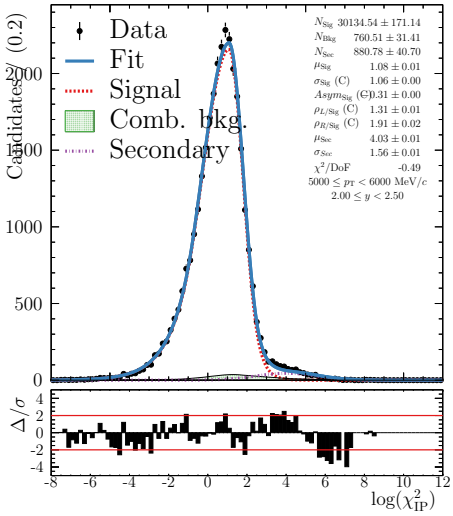

$5 \leq p_{\rm T} < 6\,{\rm GeV},\ 2.0 \leq y < 2.5$

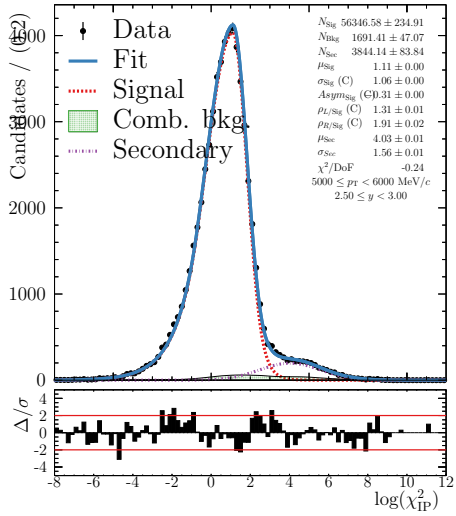

$5 \leq p_{\rm T} < 6\,{\rm GeV},\ 2.5 \leq y < 3.0$

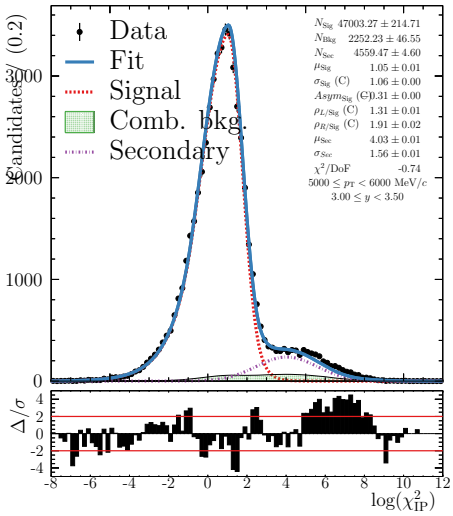

$5 \leq p_{\rm T} < 6\,{\rm GeV},\ 3.0 \leq y < 3.5$

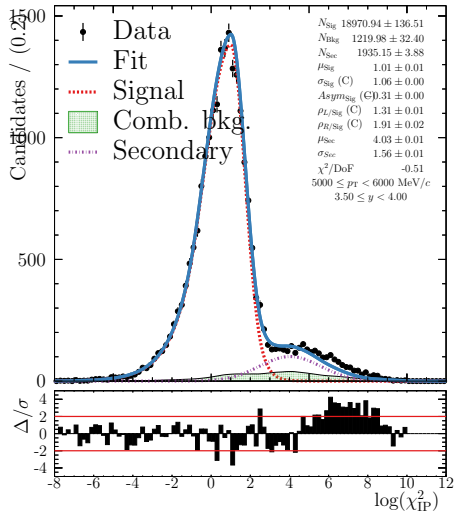

$5 \leq p_{\rm T} < 6\,{\rm GeV},\ 3.5 \leq y < 4.0$

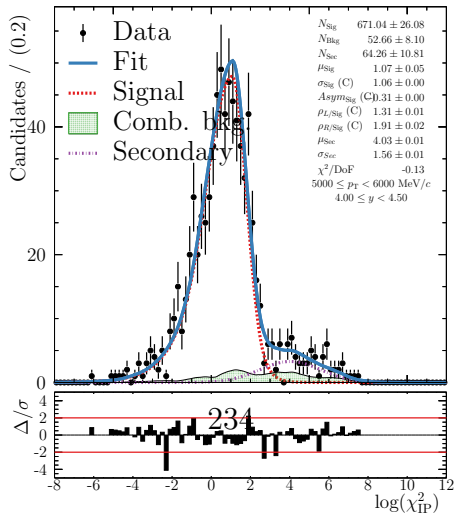

$5 \leq p_{\rm T} < 6\,{\rm GeV},\ 4.0 \leq y < 4.5$

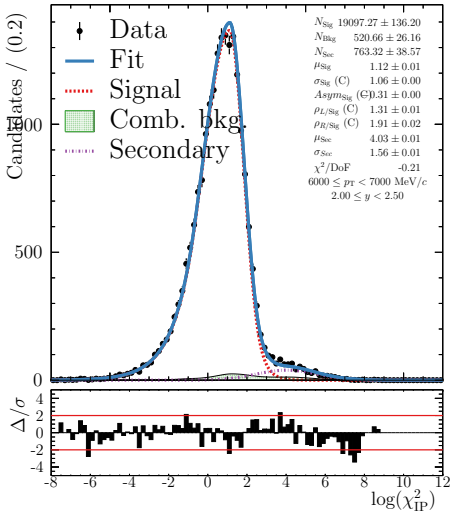

$6 \leq p_{\rm T} < 7\,{\rm GeV},\ 2.0 \leq y < 2.5$

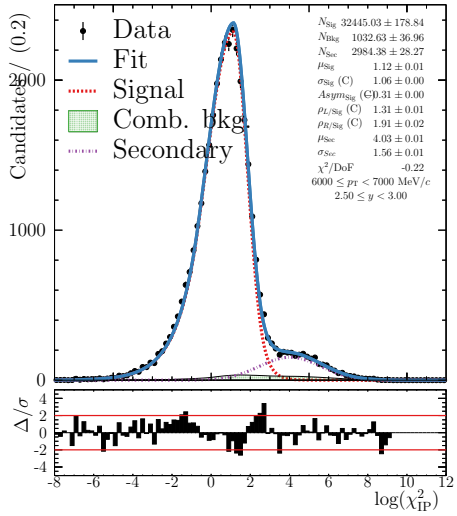

$6 \leq p_{\rm T} < 7\,{\rm GeV},\ 2.5 \leq y < 3.0$

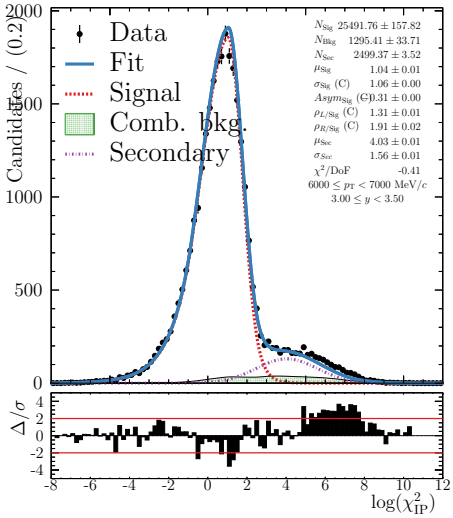

$6 \leq p_{\rm T} < 7\,{\rm GeV},\ 3.0 \leq y < 3.5$

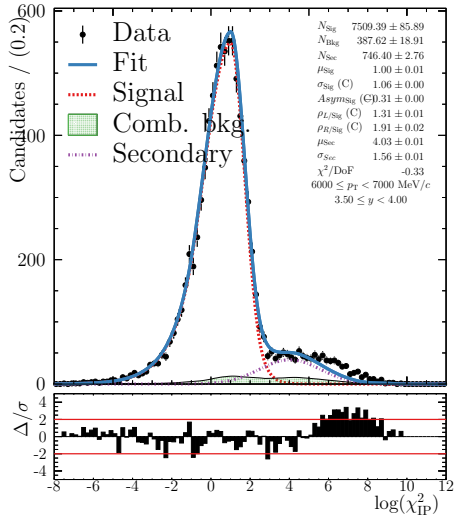

$6 \leq p_{\rm T} < 7\,{\rm GeV},\ 3.5 \leq y < 4.0$

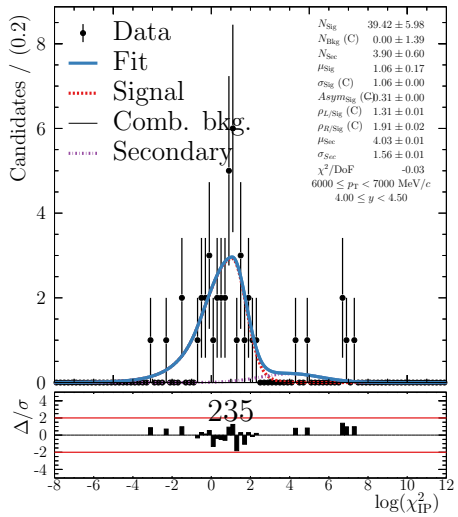

$6 \leq p_{\rm T} < 7\,{\rm GeV},\ 4.0 \leq y < 4.5$

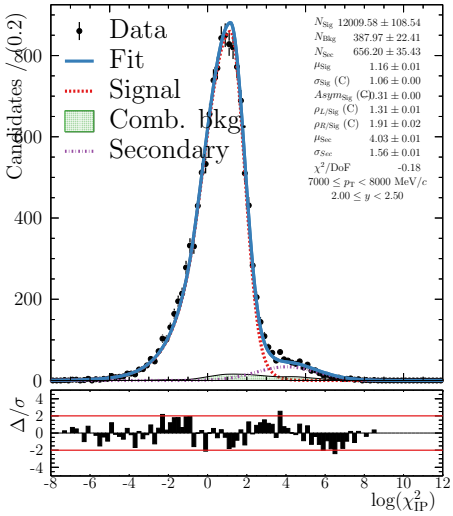

$7 \leq p_{\rm T} < 8\,{\rm GeV},\ 2.0 \leq y < 2.5$

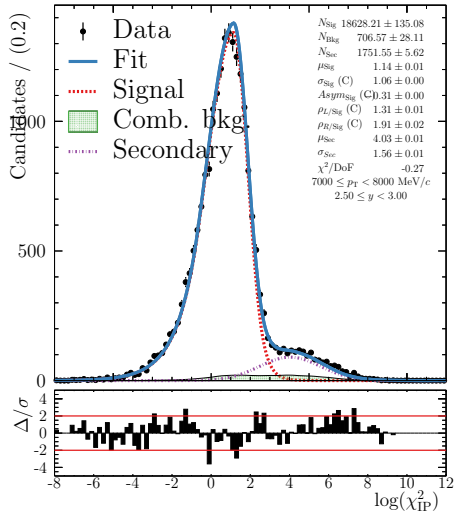

$7 \leq p_{\rm T} < 8\,{\rm GeV},\ 2.5 \leq y < 3.0$

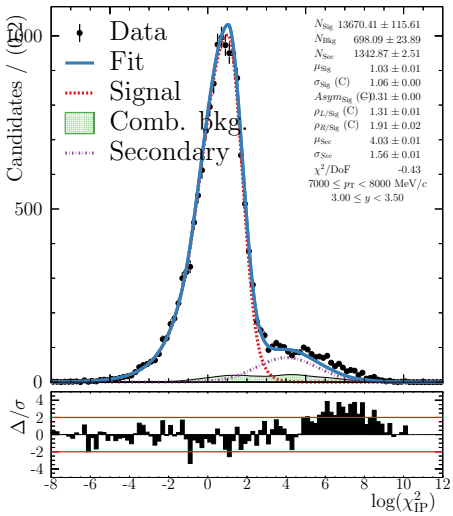

$7 \leq p_{\rm T} < 8\,{\rm GeV},\ 3.0 \leq y < 3.5$

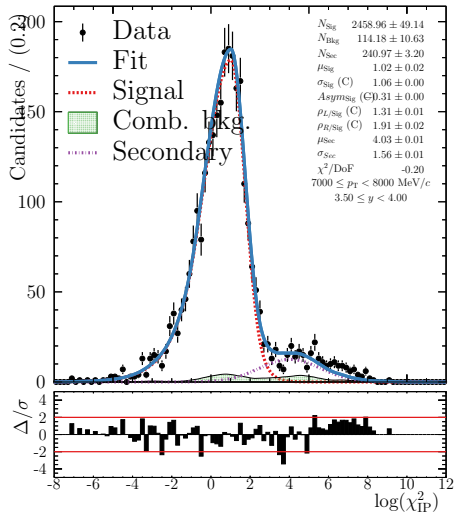

$7 \leq p_{\rm T} < 8\,{\rm GeV},\ 3.5 \leq y < 4.0$

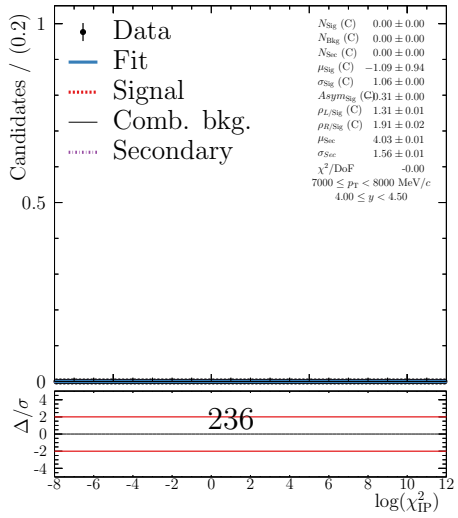

$7 \leq p_{\rm T} < 8\,{\rm GeV},\ 4.0 \leq y < 4.5$

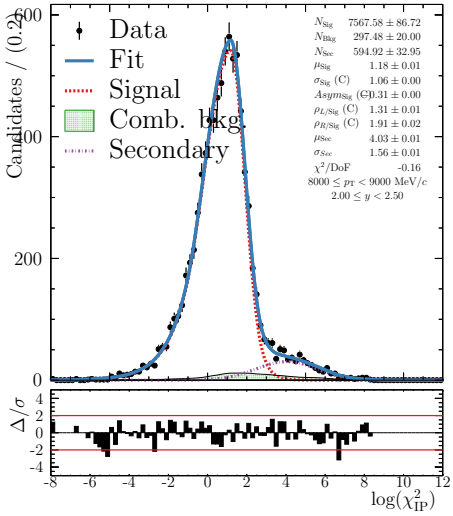

$8 \leq p_{\rm T} < 9\,{\rm GeV},\ 2.0 \leq y < 2.5$

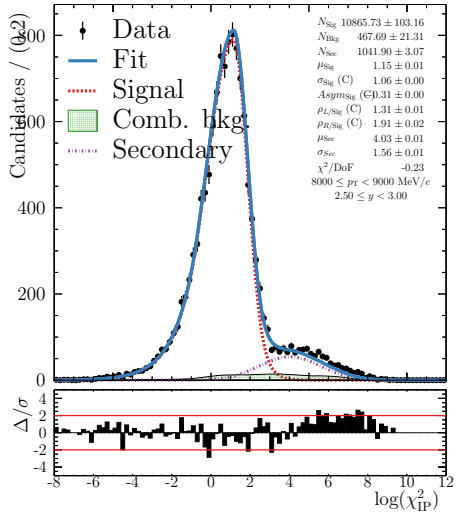

$8 \leq p_{\rm T} < 9\,{\rm GeV},\ 2.5 \leq y < 3.0$

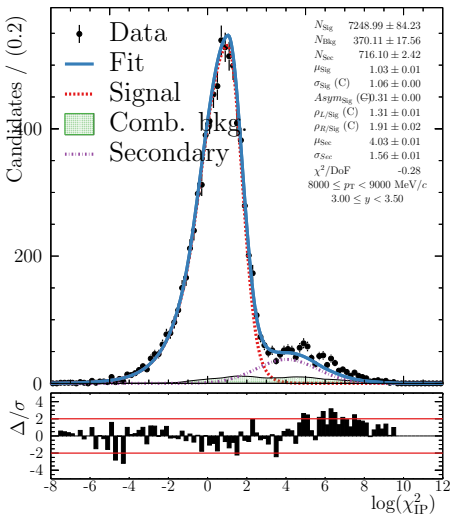

$8 \leq p_{\rm T} < 9\,{\rm GeV},\ 3.0 \leq y < 3.5$

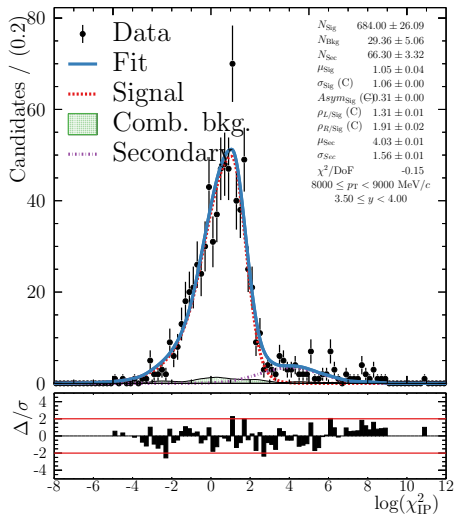

$8 \leq p_{\rm T} < 9\,{\rm GeV},\ 3.5 \leq y < 4.0$

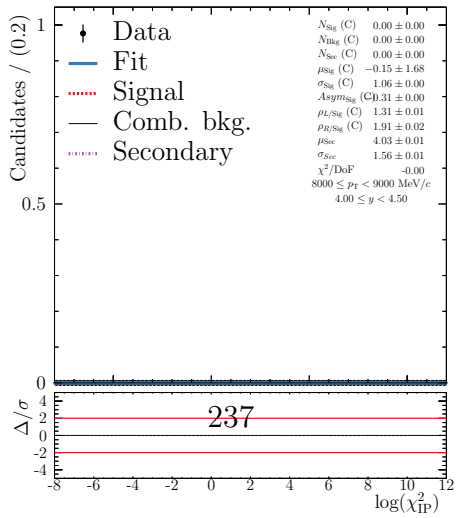

$8 \leq p_{\rm T} < 9\,{\rm GeV},\ 4.0 \leq y < 4.5$

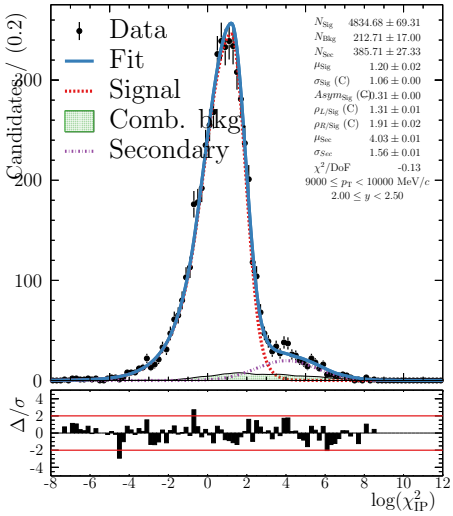

$9 \leq p_{\rm T} < 10\,{\rm GeV},\ 2.0 \leq y < 2.5$

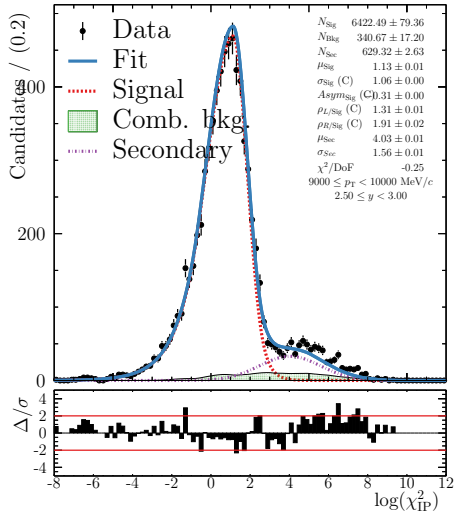

$9 \leq p_{\rm T} < 10\,{\rm GeV},\ 2.5 \leq y < 3.0$

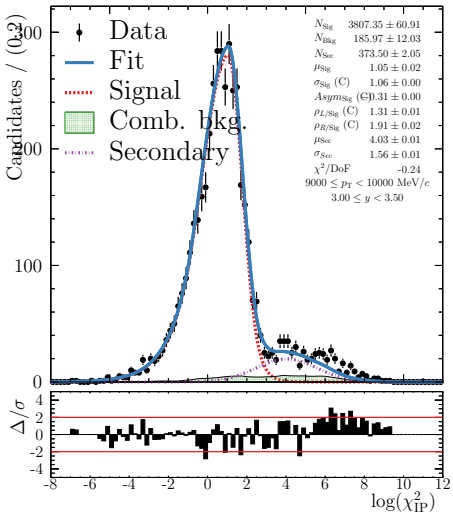

$9 \leq p_{\rm T} < 10\,{\rm GeV},\ 3.0 \leq y < 3.5$

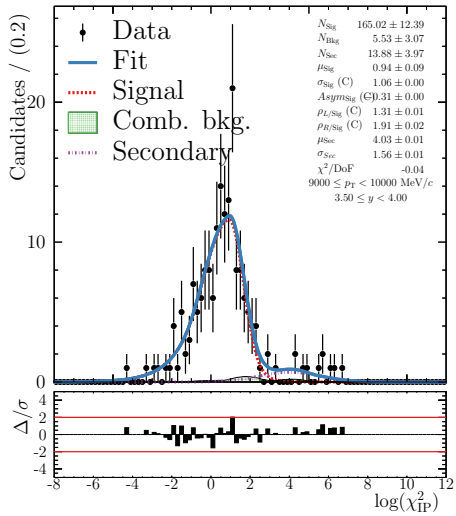

$9 \leq p_{\rm T} < 10\,{\rm GeV},\ 3.5 \leq y < 4.0$

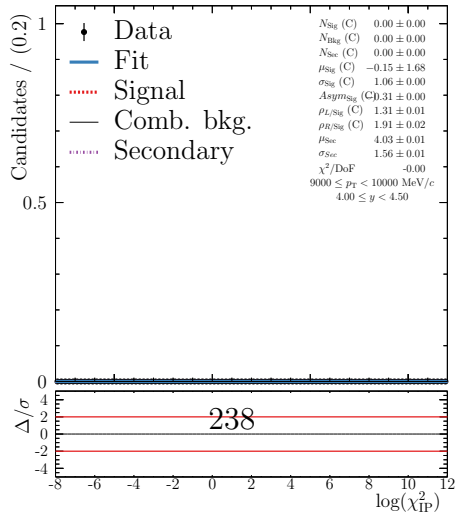

$9 \leq p_{\rm T} < 10\,{\rm GeV},\ 4.0 \leq y < 4.5$

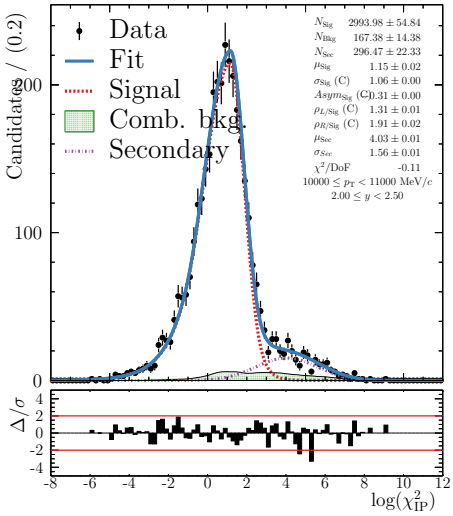

$10 \leq p_{\rm T} < 11\,{\rm GeV},\ 2.0 \leq y < 2.5$

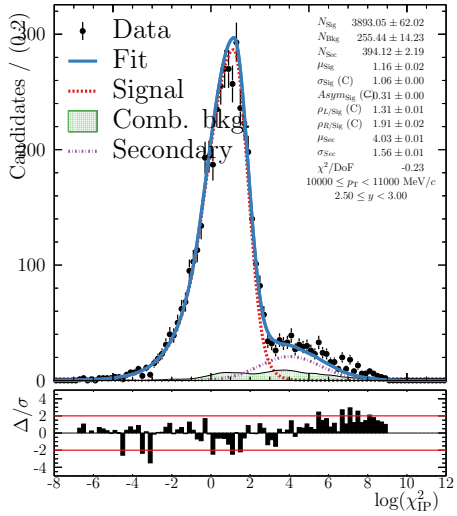

$10 \leq p_{\rm T} < 11\,{\rm GeV},\ 2.5 \leq y < 3.0$

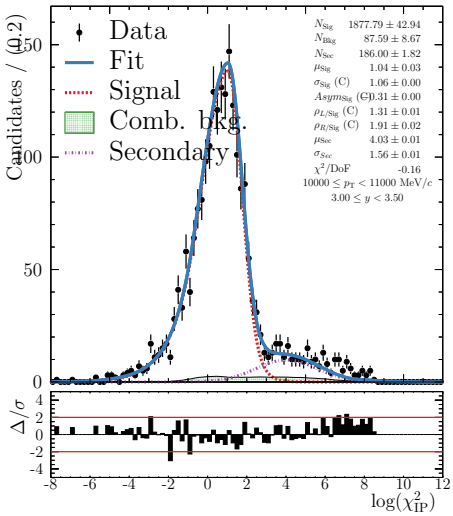

$10 \leq p_{\rm T} < 11\,{\rm GeV},\ 3.0 \leq y < 3.5$

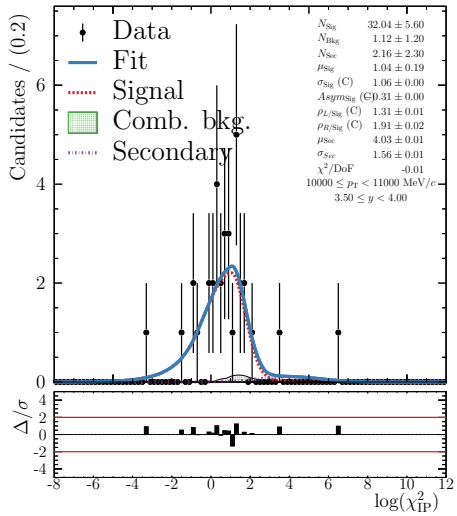

$10 \leq p_{\rm T} < 11\,{\rm GeV},\ 3.5 \leq y < 4.0$

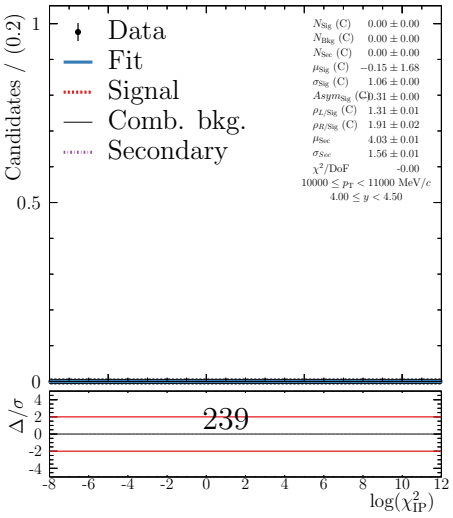

$10 \leq p_{\rm T} < 11\,{\rm GeV},\ 4.0 \leq y < 4.5$

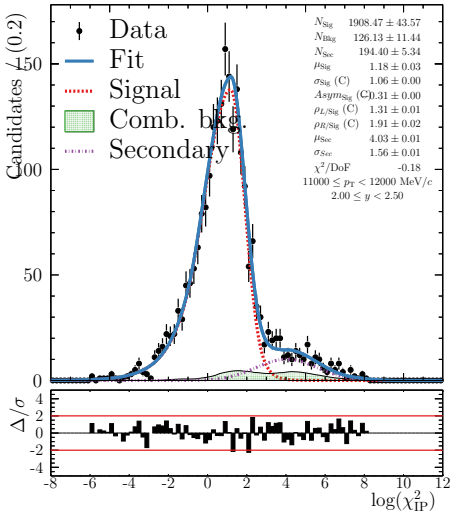

$11 \leq p_{\rm T} < 12\,{\rm GeV},\ 2.0 \leq y < 2.5$

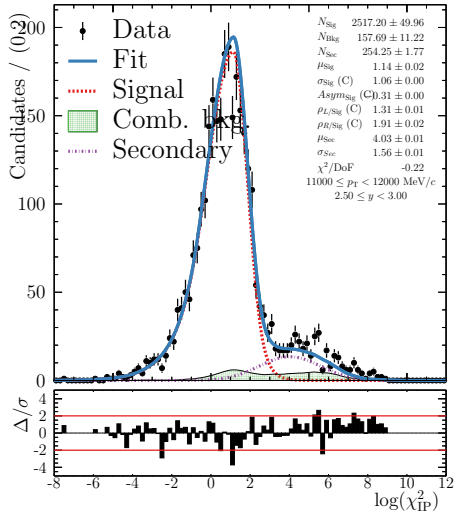

$11 \leq p_{\rm T} < 12\,{\rm GeV},\ 2.5 \leq y < 3.0$

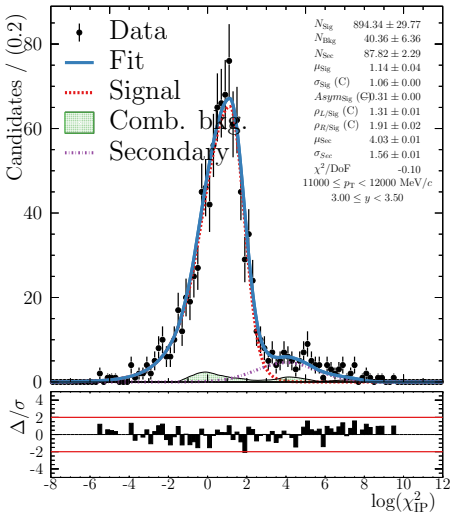

$11 \leq p_{\rm T} < 12\,{\rm GeV},\ 3.0 \leq y < 3.5$

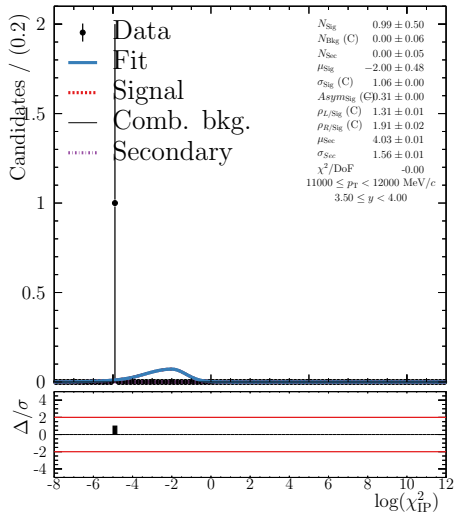

$11 \leq p_{\rm T} < 12\,{\rm GeV},\ 3.5 \leq y < 4.0$

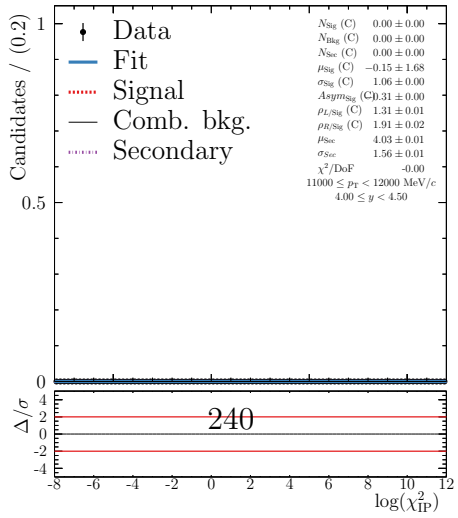

$6 \leq p_{\rm T} < 12\,{\rm GeV},\ 4.0 \leq y < 4.5$

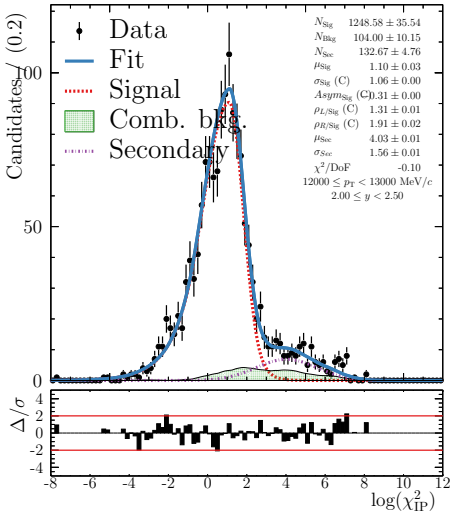

$12 \leq p_{\rm T} < 13\,{\rm GeV},\ 2.0 \leq y < 2.5$

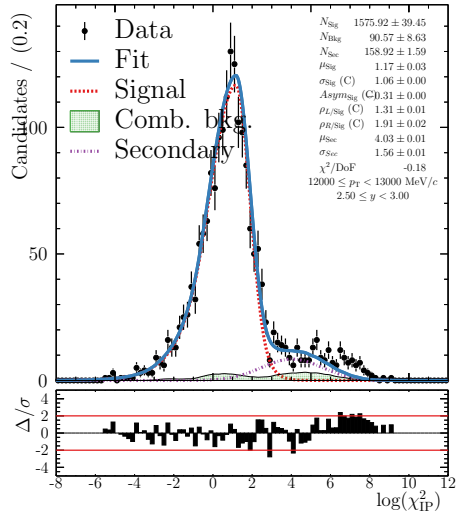

$12 \leq p_{\rm T} < 13\,{\rm GeV},\ 2.5 \leq y < 3.0$

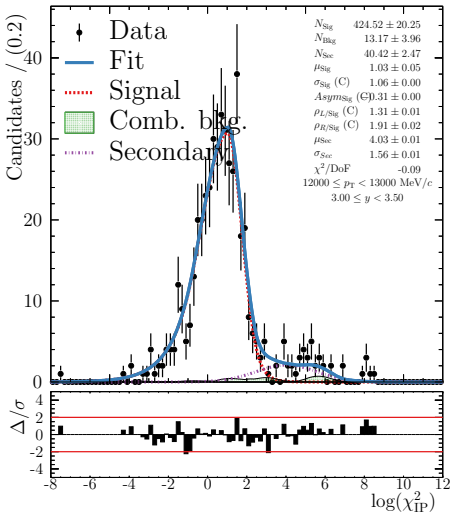

$12 \leq p_{\rm T} < 13\,{\rm GeV},\ 3.0 \leq y < 3.5$

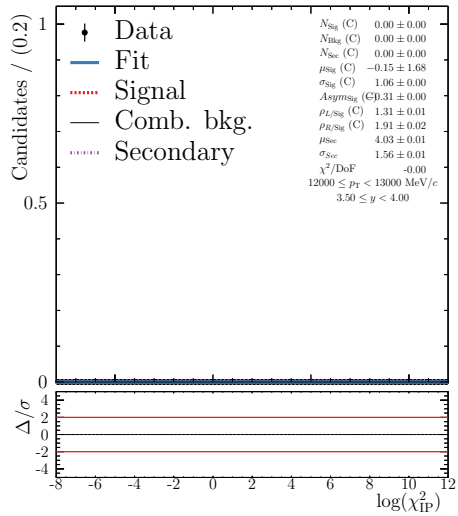

$12 \leq p_{\rm T} < 13\,{\rm GeV},\ 3.5 \leq y < 4.0$

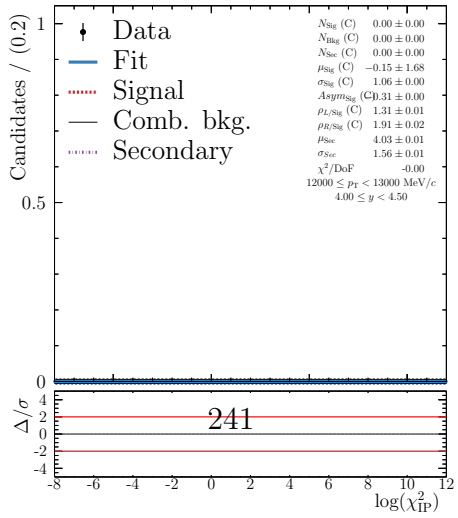

$12 \leq p_{\rm T} < 13\,{\rm GeV},\ 4.0 \leq y < 4.5$

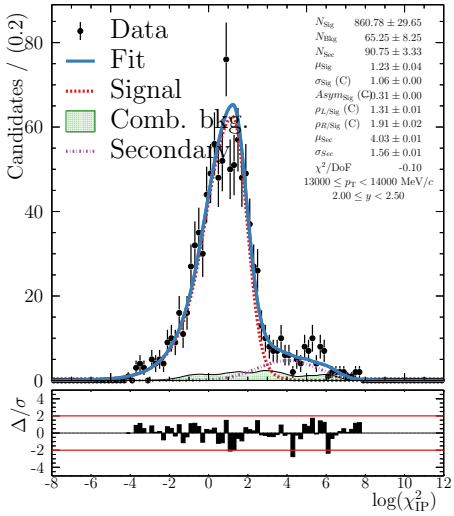

$13 \leq p_{\rm T} < 14\,{\rm GeV},\ 2.0 \leq y < 2.5$

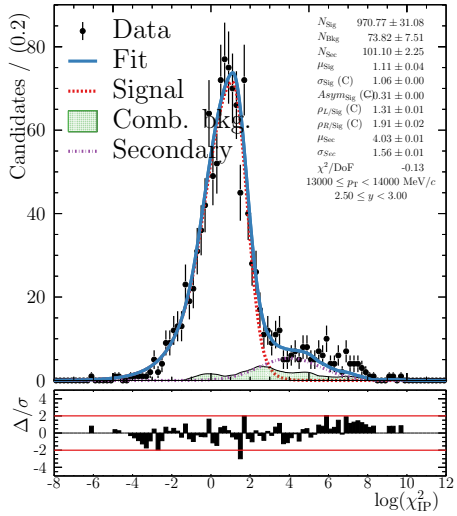

$13 \leq p_{\rm T} < 14\,{\rm GeV},\ 2.5 \leq y < 3.0$

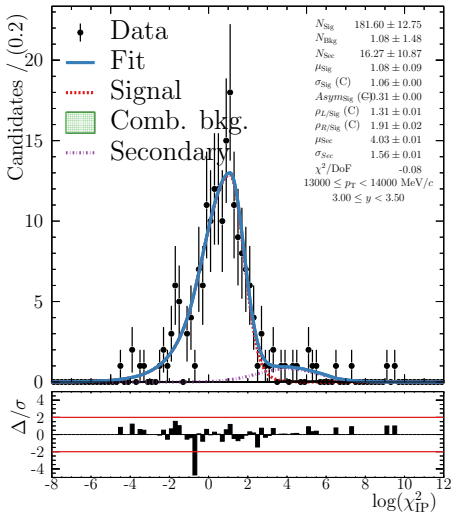

$13 \leq p_{\rm T} < 14\,{\rm GeV},\ 3.0 \leq y < 3.5$

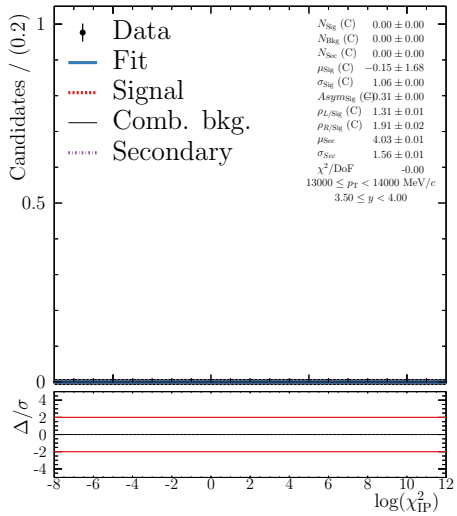

$13 \leq p_{\rm T} < 14\,{\rm GeV},\ 3.5 \leq y < 4.0$

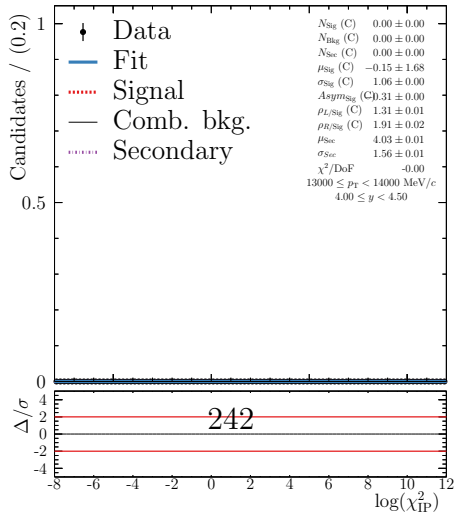

$13 \leq p_{\rm T} < 14\,{\rm GeV},\ 4.0 \leq y < 4.5$

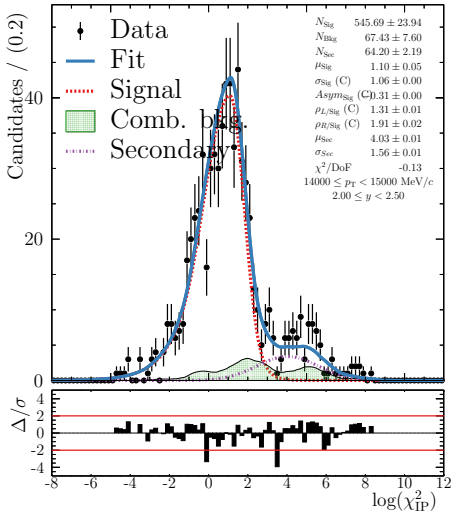

$14 \leq p_{\rm T} < 15\,{\rm GeV},\ 2.0 \leq y < 2.5$

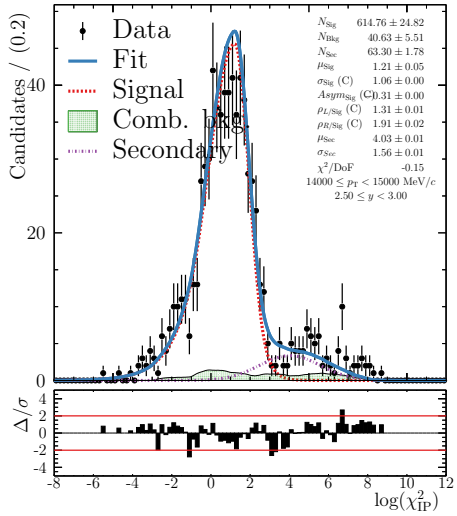

$14 \leq p_{\rm T} < 15\,{\rm GeV},\ 2.5 \leq y < 3.0$

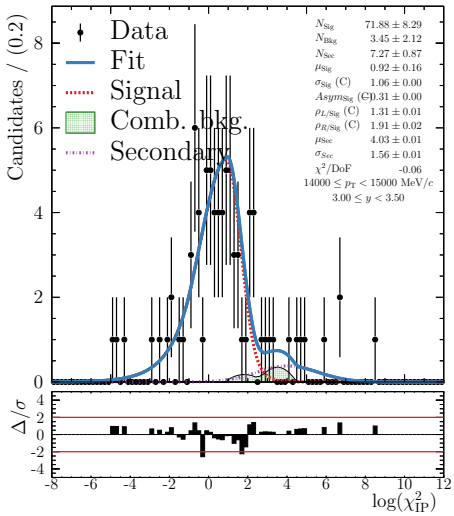

$14 \leq p_{\rm T} < 15\,{\rm GeV},\ 3.0 \leq y < 3.5$

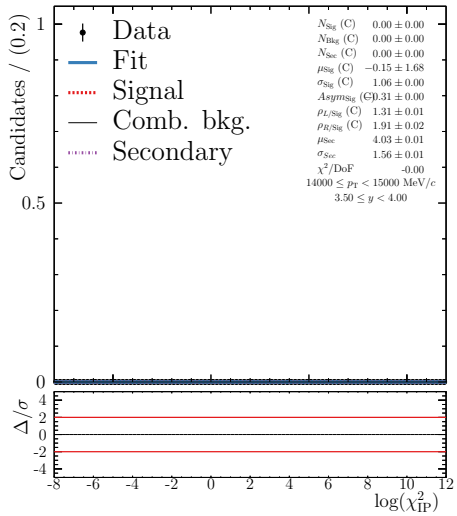

$14 \leq p_{\rm T} < 15\,{\rm GeV},\ 3.5 \leq y < 4.0$

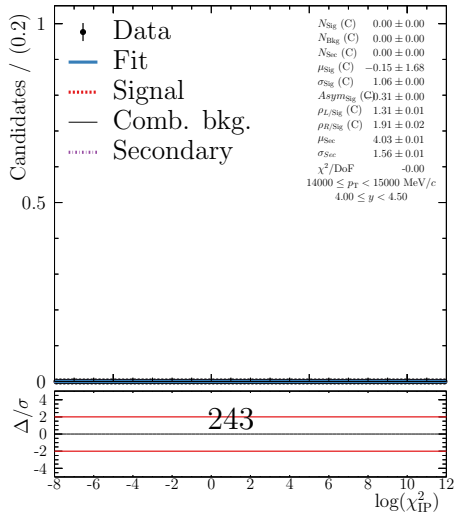

$14 \leq p_{\rm T} < 15\,{\rm GeV},\ 4.0 \leq y < 4.5$

Figure F.0: Fits to the fully selected $D^0 \to K^-\pi^+$ $\ln\chi^2_{\rm IP}$ distribution per $p_{\rm T}$-y bin.

F.2 $D^+ \to K^-\pi^+\pi^+$

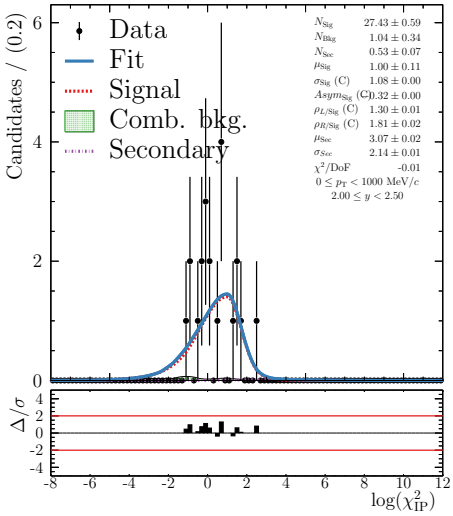

$0 \leq p_{\rm T} < 1\,{\rm GeV},\ 2.0 \leq y < 2.5$

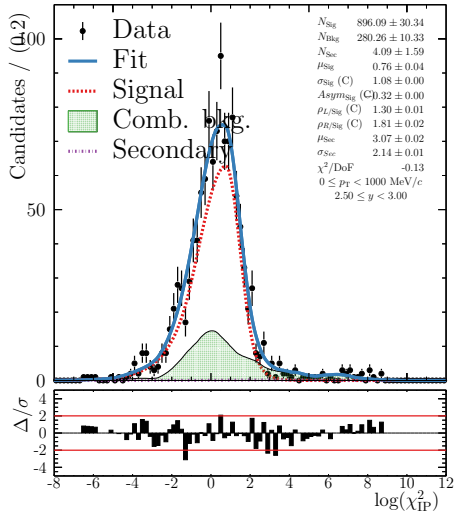

$0 \leq p_{\rm T} < 1\,{\rm GeV},\ 2.5 \leq y < 3.0$

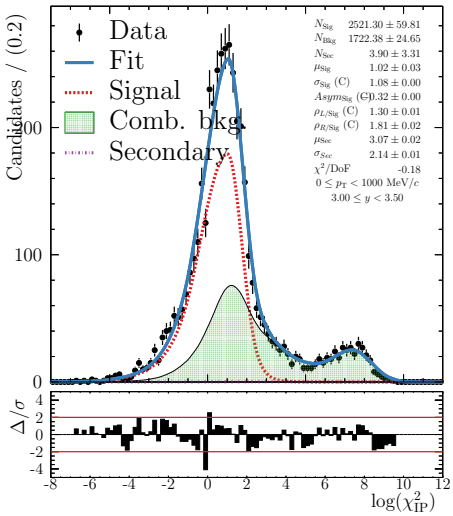

$0 \leq p_{\rm T} < 1\,{\rm GeV},\ 3.0 \leq y < 3.5$

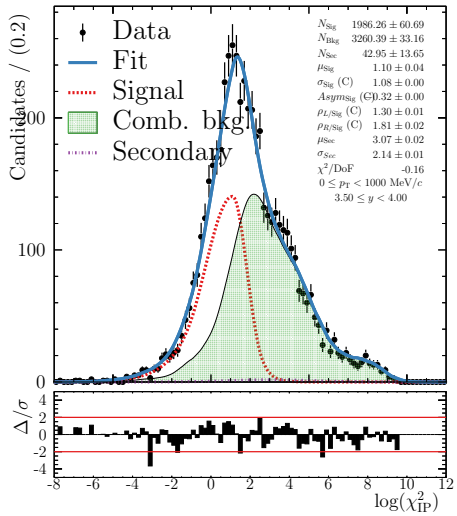

$0 \leq p_{\rm T} < 1\,{\rm GeV},\ 3.5 \leq y < 4.0$

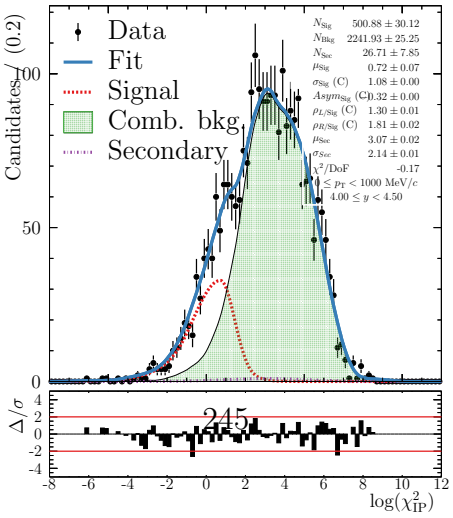

$0 \leq p_{\rm T} < 1\,{\rm GeV},\ 4.0 \leq y < 4.5$

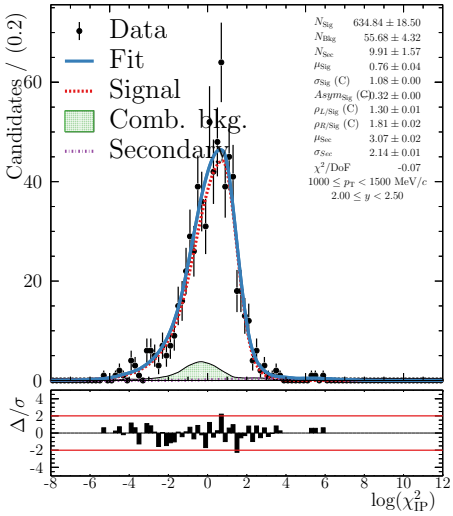

$1 \leq p_{\rm T} < 1.5\,\text{GeV},\ 2.0 \leq y < 2.5$

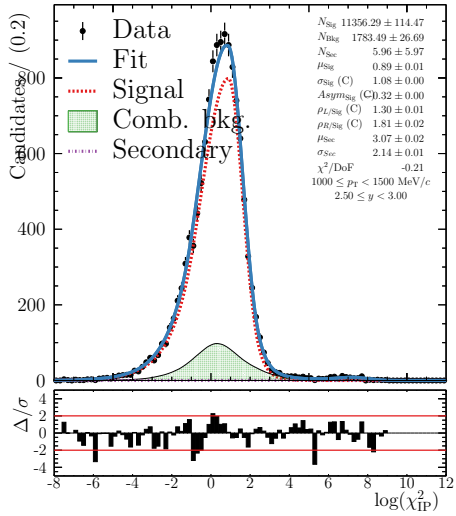

$1 \leq p_{\rm T} < 1.5\,\text{GeV},\ 2.5 \leq y < 3.0$

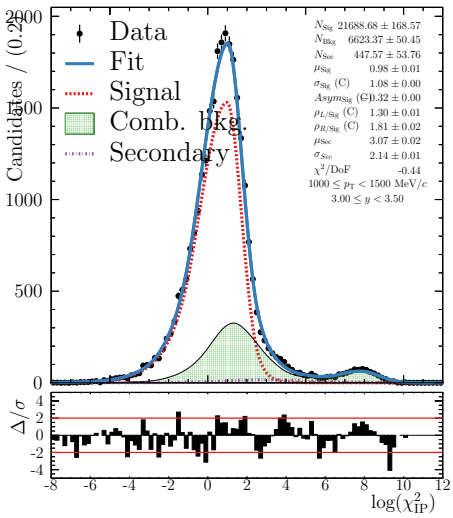

$1 \leq p_{\rm T} < 1.5\,\text{GeV},\ 3.0 \leq y < 3.5$

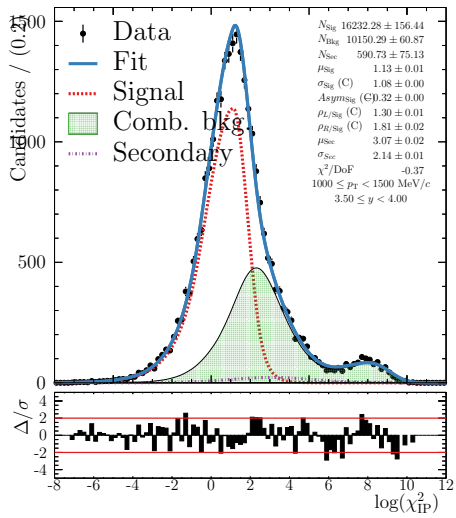

$1 \leq p_{\rm T} < 1.5\,\text{GeV},\ 3.5 \leq y < 4.0$

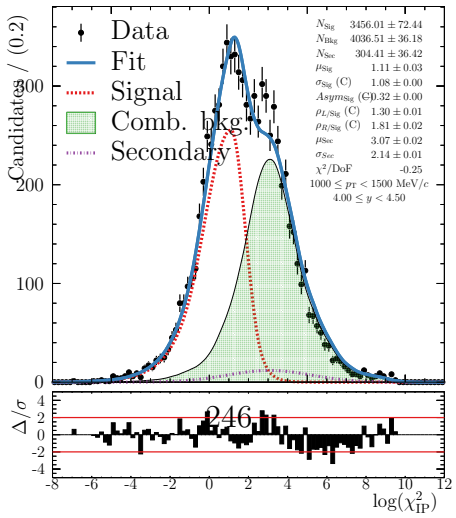

$1 \leq p_{\rm T} < 1.5\,\text{GeV},\ 4.0 \leq y < 4.5$

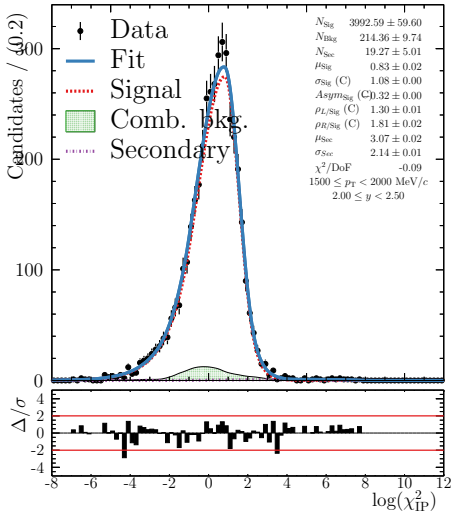

$1.5 \leq p_{\rm T} < 2\,{\rm GeV},\ 2.0 \leq y < 2.5$

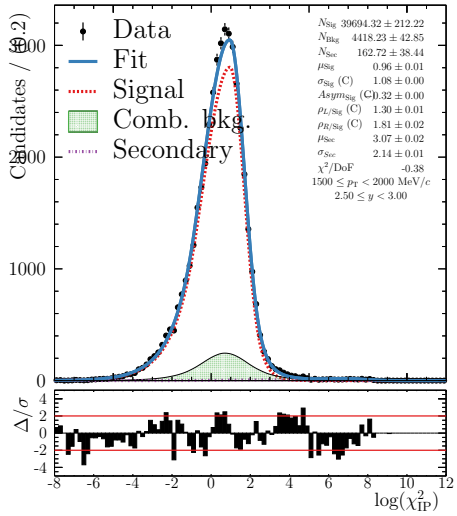

$1.5 \leq p_{\rm T} < 2\,{\rm GeV},\ 2.5 \leq y < 3.0$

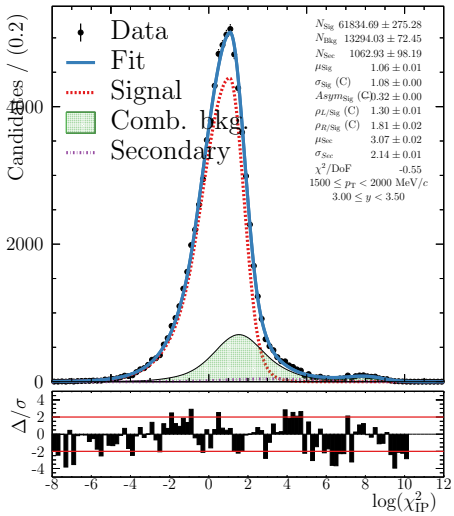

$1.5 \leq p_{\rm T} < 2\,{\rm GeV},\ 3.0 \leq y < 3.5$

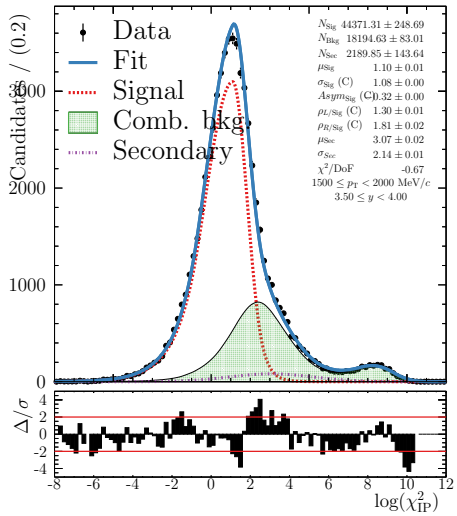

$1.5 \leq p_{\rm T} < 2\,{\rm GeV},\ 3.5 \leq y < 4.0$

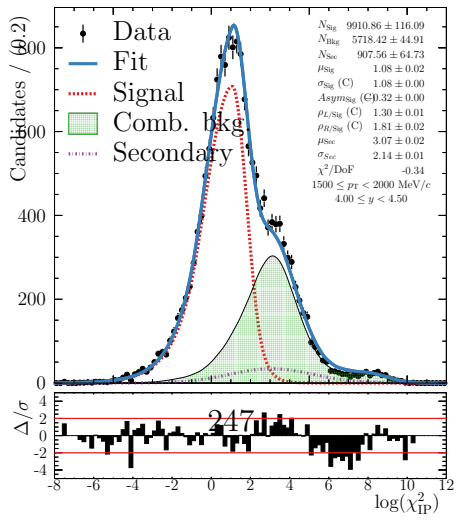

$1.5 \leq p_{\rm T} < 2\,{\rm GeV},\ 4.0 \leq y < 4.5$

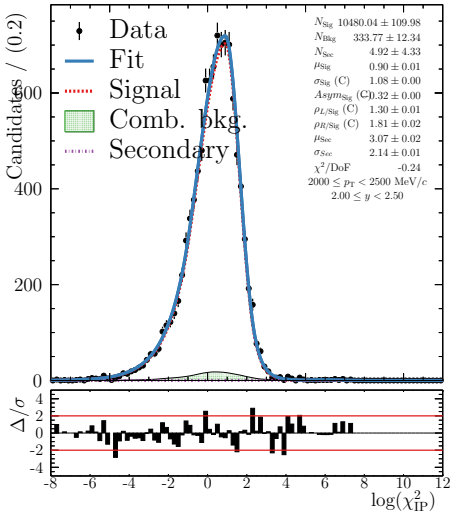

$2 \leq p_{\rm T} < 2.5\,{\rm GeV},\ 2.0 \leq y < 2.5$

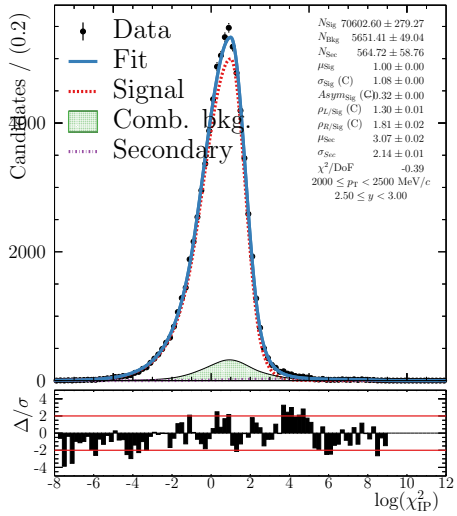

$2 \leq p_{\rm T} < 2.5\,{\rm GeV},\ 2.5 \leq y < 3.0$

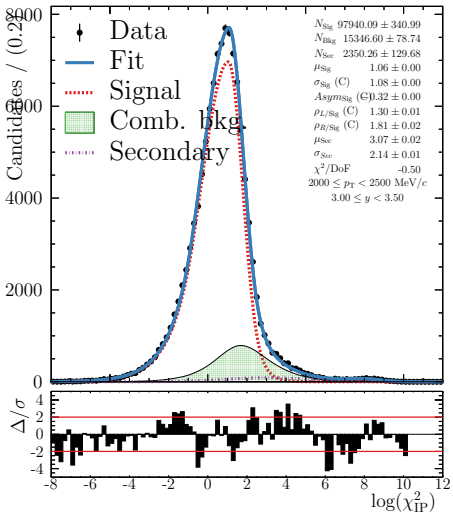

$2 \leq p_{\rm T} < 2.5\,{\rm GeV},\ 3.0 \leq y < 3.5$

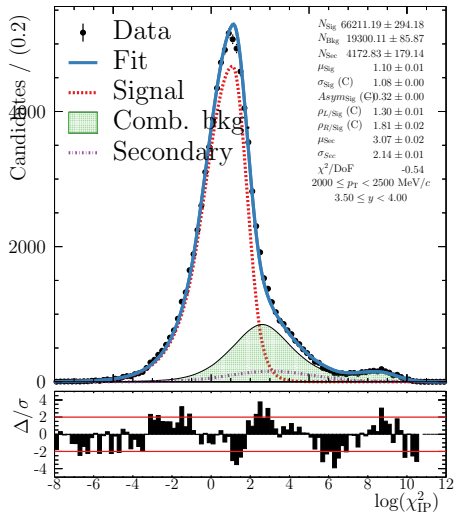

$2 \leq p_{\rm T} < 2.5\,{\rm GeV},\ 3.5 \leq y < 4.0$

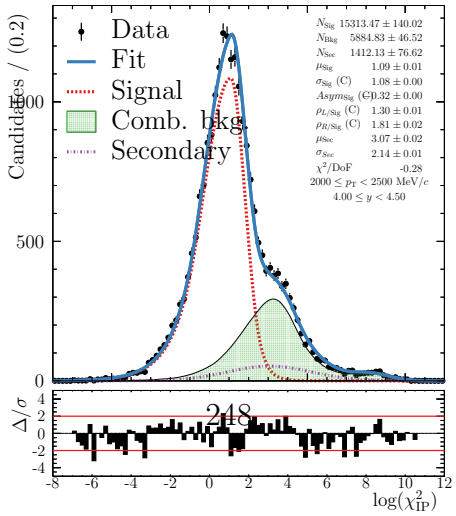

$2 \leq p_{\rm T} < 2.5\,{\rm GeV},\ 4.0 \leq y < 4.5$

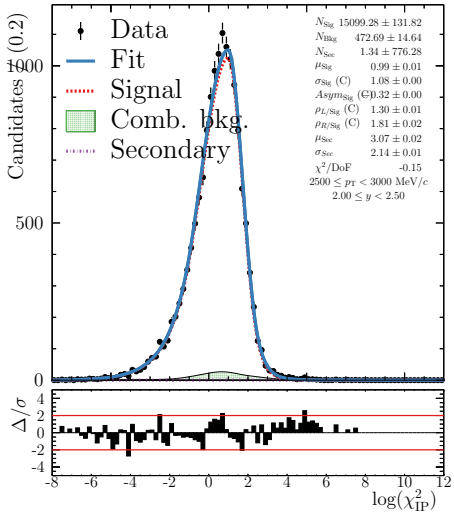

$2.5 \leq p_{\rm T} < 3\,{\rm GeV},\ 2.0 \leq y < 2.5$

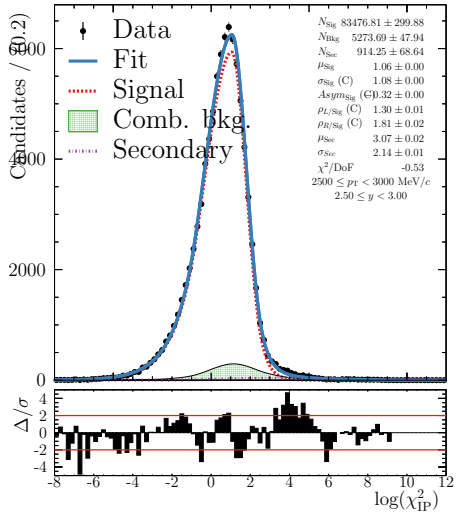

$2.5 \leq p_{\rm T} < 3\,{\rm GeV},\ 2.5 \leq y < 3.0$

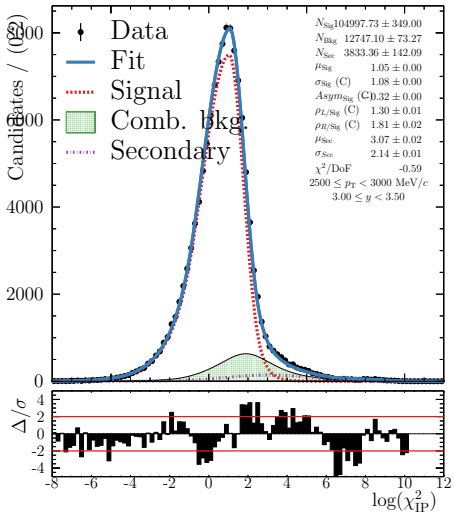

$2.5 \leq p_{\rm T} < 3\,{\rm GeV},\ 3.0 \leq y < 3.5$

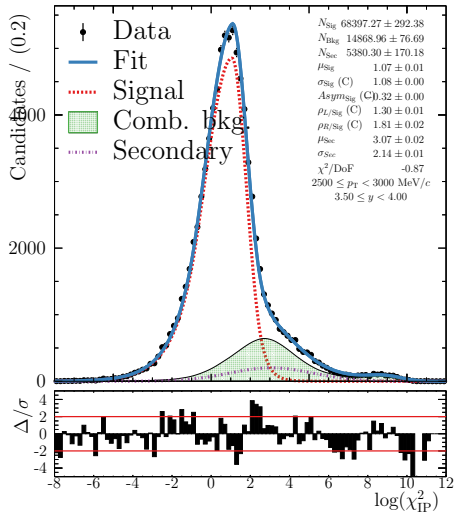

$2.5 \leq p_{\rm T} < 3\,{\rm GeV},\ 3.5 \leq y < 4.0$

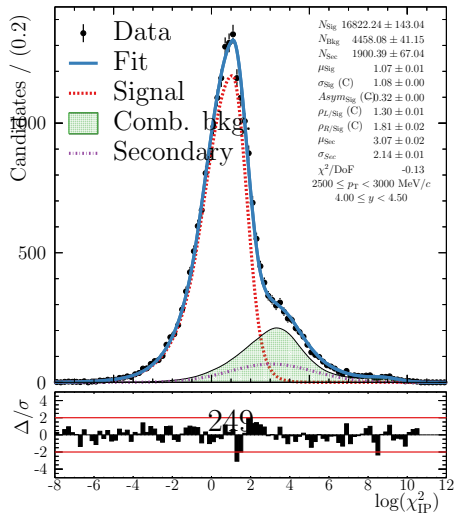

$2.5 \leq p_{\rm T} < 3\,{\rm GeV},\ 4.0 \leq y < 4.5$

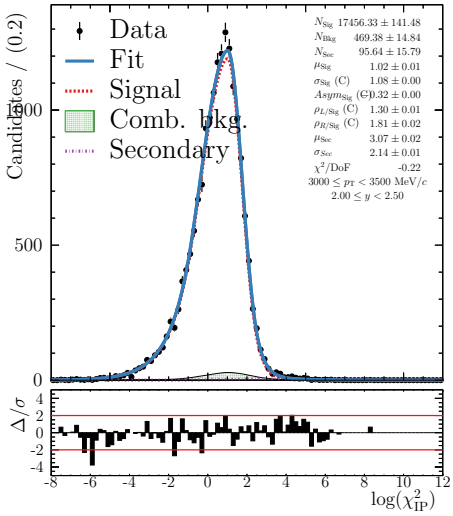

$3 \leq p_{\rm T} < 3.5\,\text{GeV},\ 2.0 \leq y < 2.5$

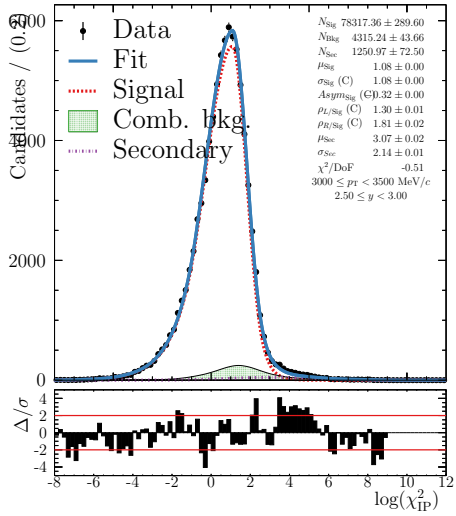

$3 \leq p_{\rm T} < 3.5\,\text{GeV},\ 2.5 \leq y < 3.0$

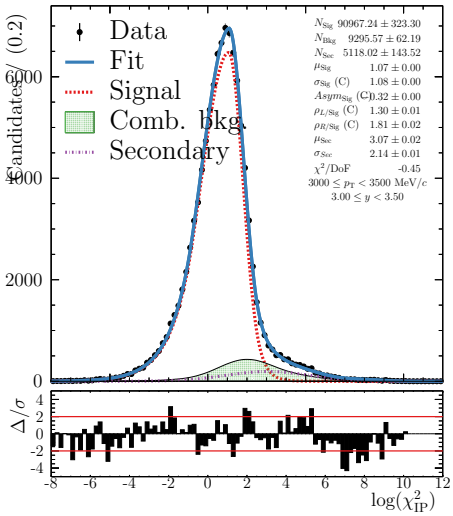

$3 \leq p_{\rm T} < 3.5\,\text{GeV},\ 3.0 \leq y < 3.5$

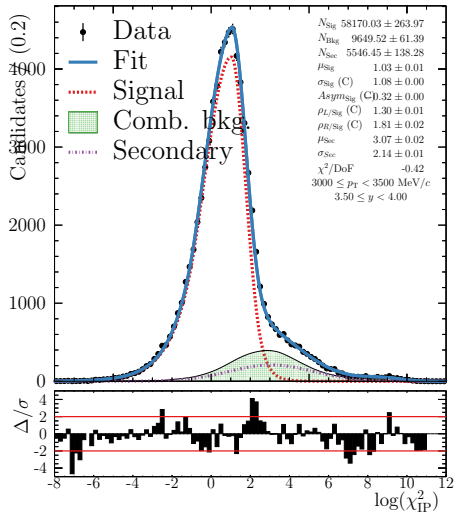

$3 \leq p_{\rm T} < 3.5\,\text{GeV},\ 3.5 \leq y < 4.0$

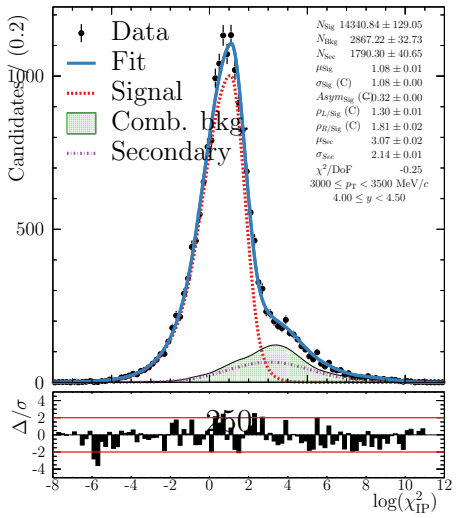

$3 \leq p_{\rm T} < 3.5\,\text{GeV},\ 4.0 \leq y < 4.5$

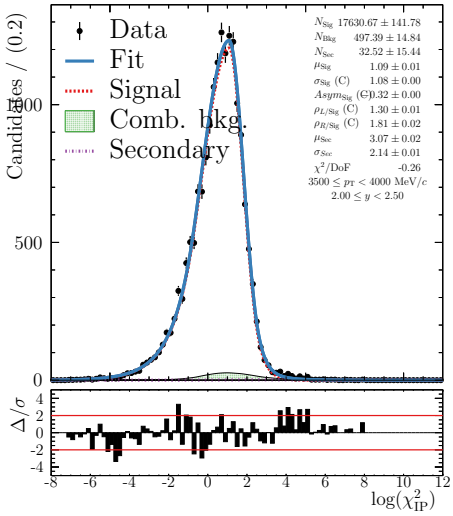

$3.5 \leq p_{\rm T} < 4\,{\rm GeV},\ 2.0 \leq y < 2.5$

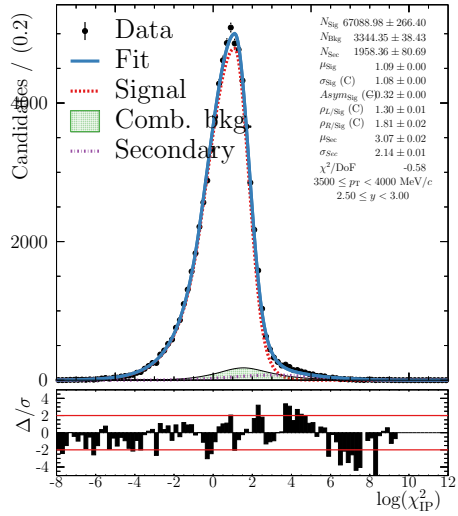

$3.5 \leq p_{\rm T} < 4\,{\rm GeV},\ 2.5 \leq y < 3.0$

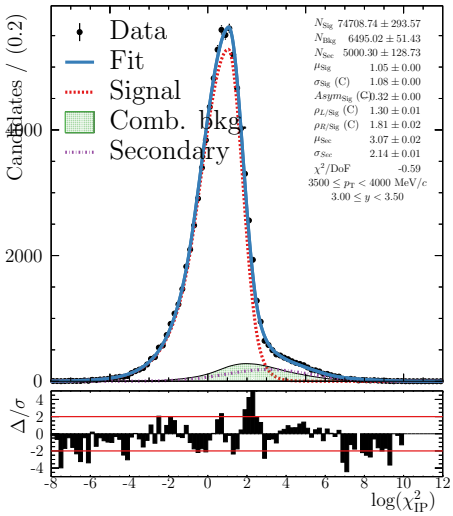

$3.5 \leq p_{\rm T} < 4\,{\rm GeV},\ 3.0 \leq y < 3.5$

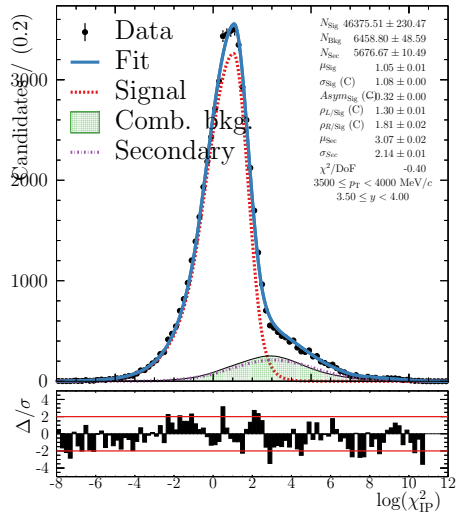

$3.5 \leq p_{\rm T} < 4\,{\rm GeV},\ 3.5 \leq y < 4.0$

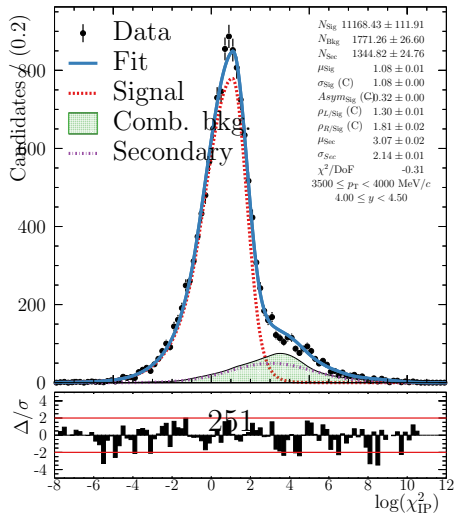

$3.5 \leq p_{\rm T} < 4\,{\rm GeV},\ 4.0 \leq y < 4.5$

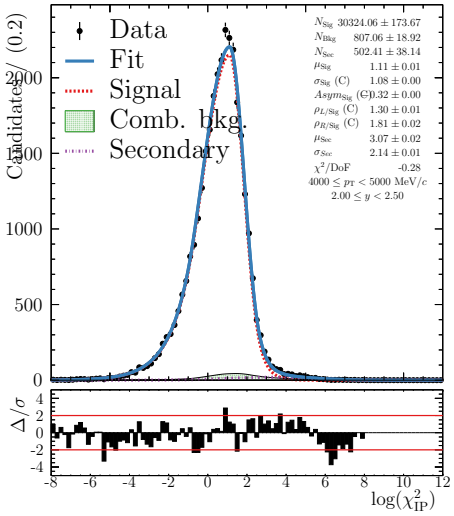

$4 \leq p_{\rm T} < 5\,{\rm GeV},\ 2.0 \leq y < 2.5$

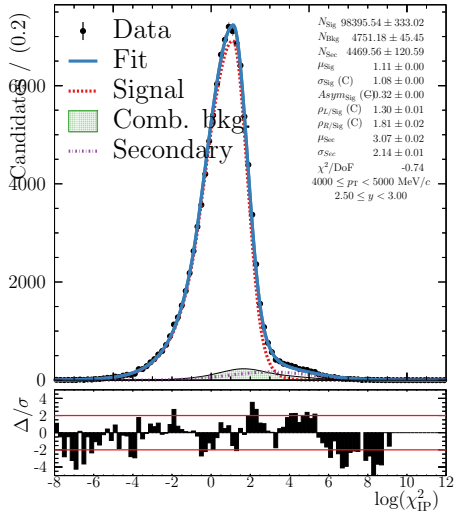

$4 \leq p_{\rm T} < 5\,{\rm GeV},\ 2.5 \leq y < 3.0$

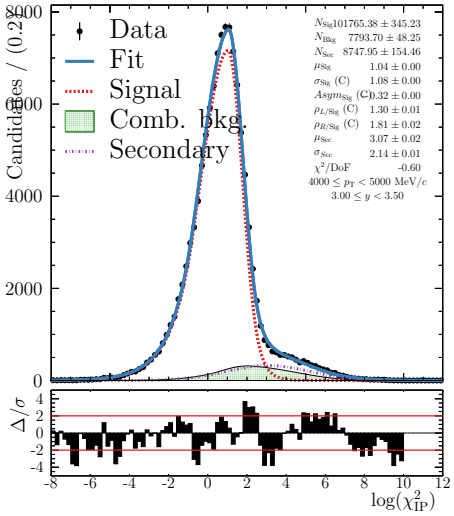

$4 \leq p_{\rm T} < 5\,{\rm GeV},\ 3.0 \leq y < 3.5$

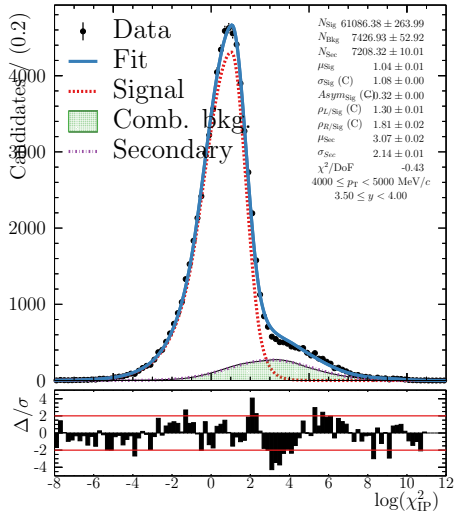

$4 \leq p_{\rm T} < 5\,{\rm GeV},\ 3.5 \leq y < 4.0$

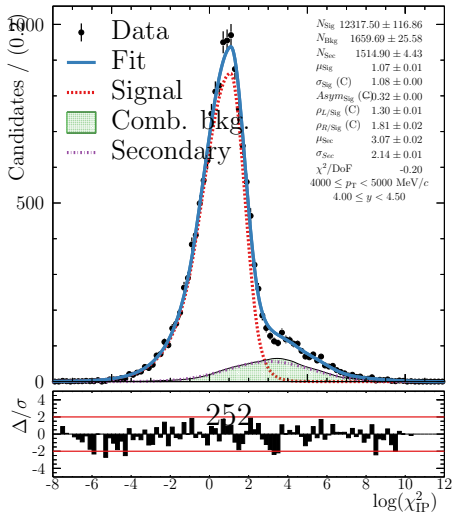

$4 \leq p_{\rm T} < 5\,{\rm GeV},\ 4.0 \leq y < 4.5$

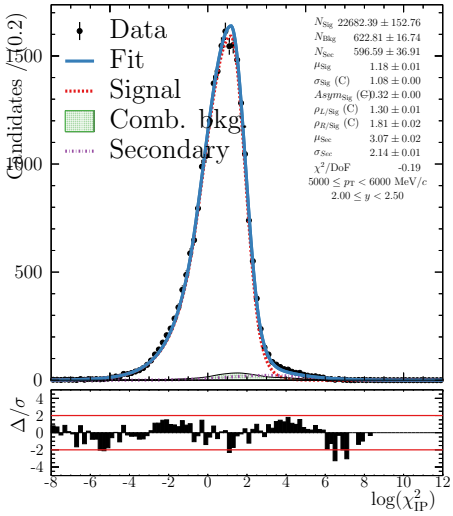

$5 \leq p_{\rm T} < 6\,{\rm GeV},\ 2.0 \leq y < 2.5$

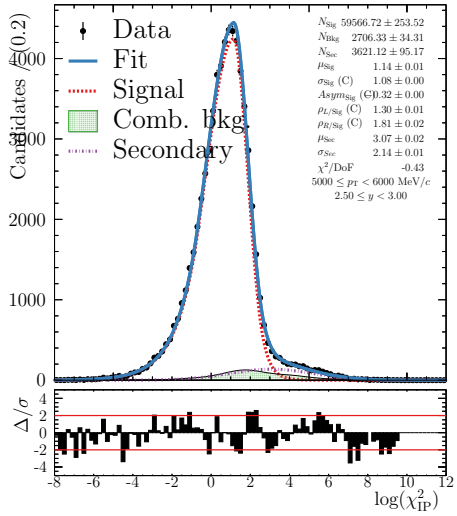

$5 \leq p_{\rm T} < 6\,{\rm GeV},\ 2.5 \leq y < 3.0$

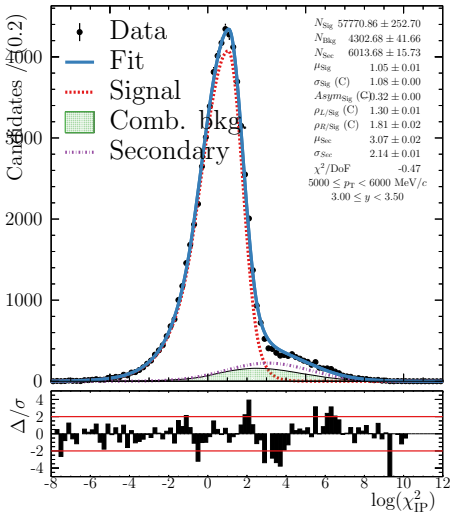

$5 \leq p_{\rm T} < 6\,{\rm GeV},\ 3.0 \leq y < 3.5$

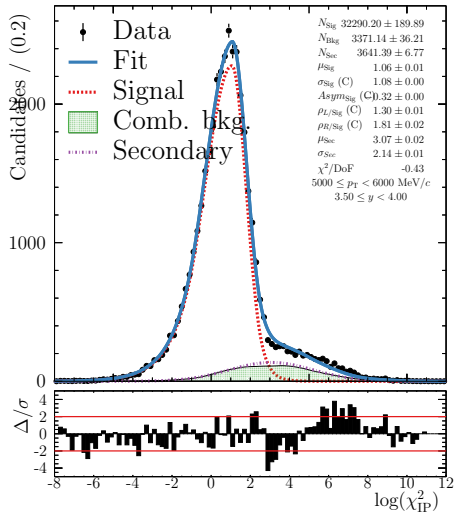

$5 \leq p_{\rm T} < 6\,{\rm GeV},\ 3.5 \leq y < 4.0$

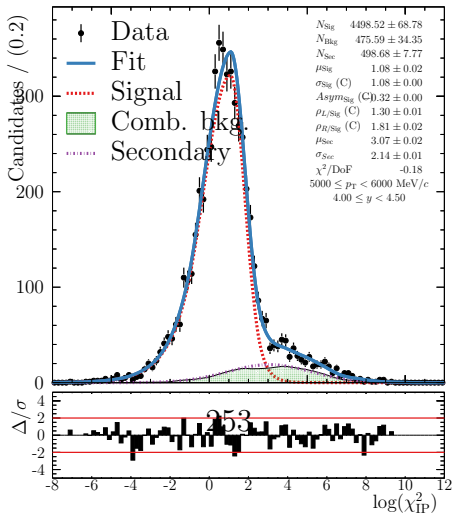

$5 \leq p_{\rm T} < 6\,{\rm GeV},\ 4.0 \leq y < 4.5$

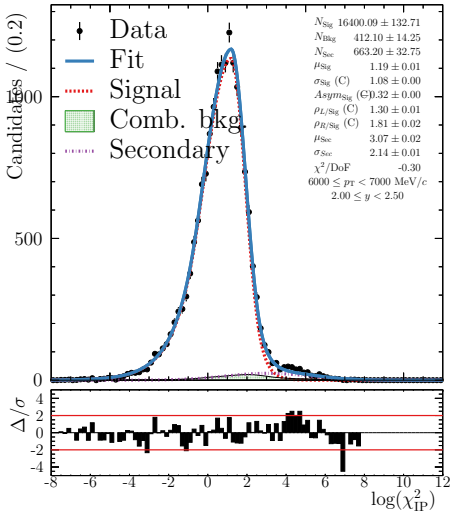

$6 \le p_{\rm T} < 7\,{\rm GeV},\ 2.0 \le y < 2.5$

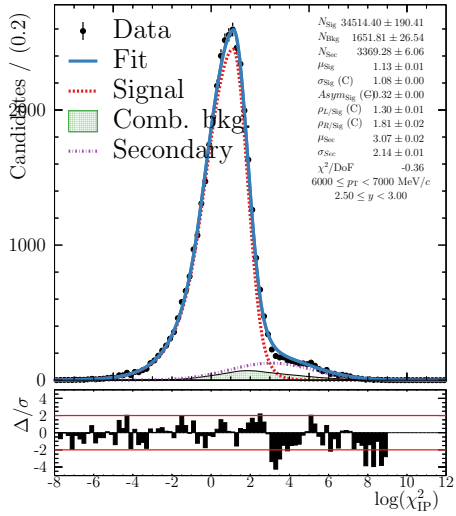

$6 \le p_{\rm T} < 7\,{\rm GeV},\ 2.5 \le y < 3.0$

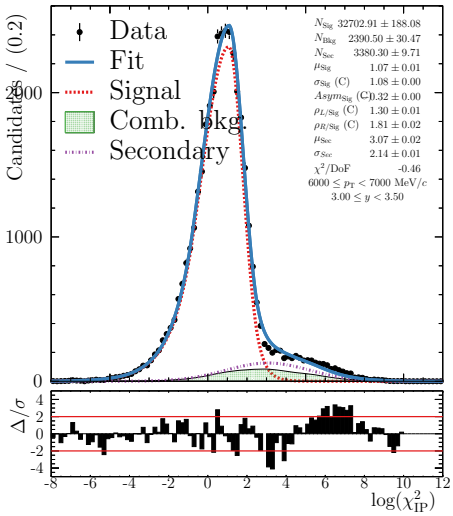

$6 \le p_{\rm T} < 7\,{\rm GeV},\ 3.0 \le y < 3.5$

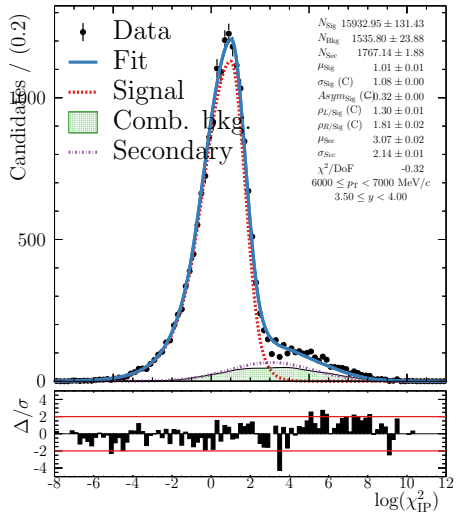

$6 \le p_{\rm T} < 7\,{\rm GeV},\ 3.5 \le y < 4.0$

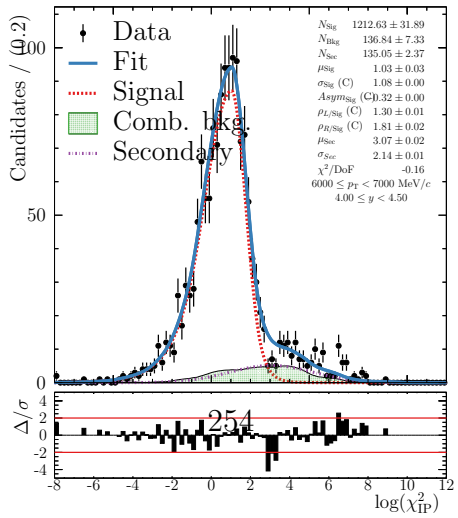

$6 \le p_{\rm T} < 7\,{\rm GeV},\ 4.0 \le y < 4.5$

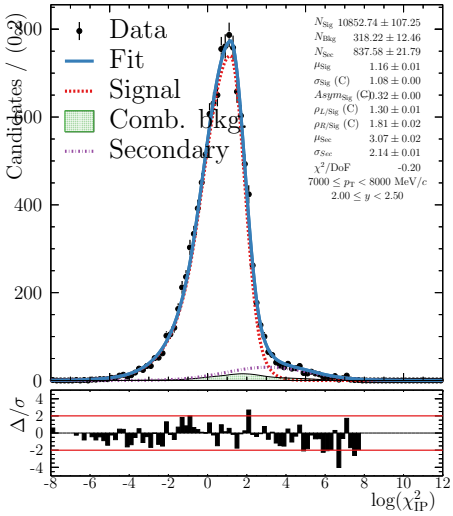

$7 \le p_{\rm T} < 8\,{\rm GeV},\ 2.0 \le y < 2.5$

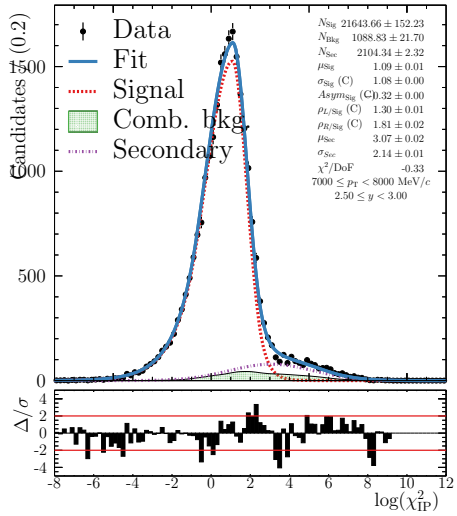

$7 \le p_{\rm T} < 8\,{\rm GeV},\ 2.5 \le y < 3.0$

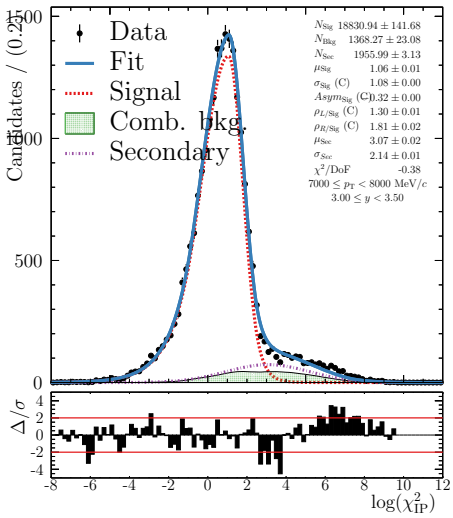

$7 \le p_{\rm T} < 8\,{\rm GeV},\ 3.0 \le y < 3.5$

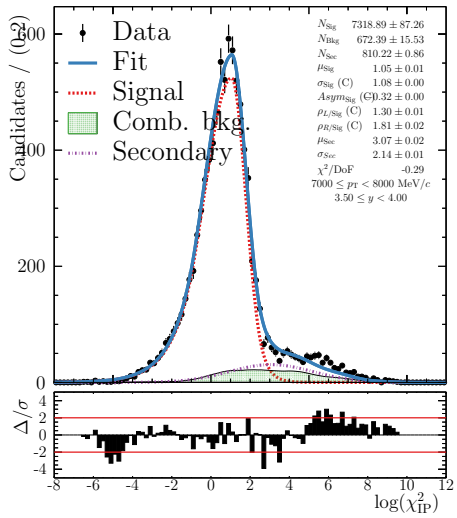

$7 \le p_{\rm T} < 8\,{\rm GeV},\ 3.5 \le y < 4.0$

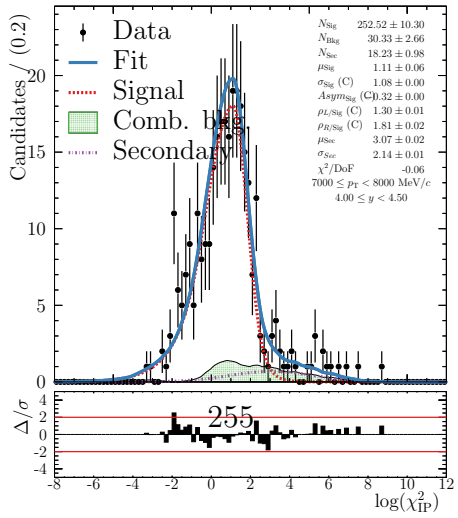

$7 \le p_{\rm T} < 8\,{\rm GeV},\ 4.0 \le y < 4.5$

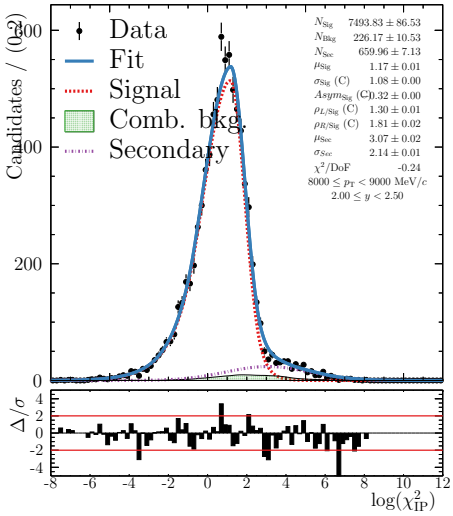

$8 \le p_{\rm T} < 9\,{\rm GeV},\ 2.0 \le y < 2.5$

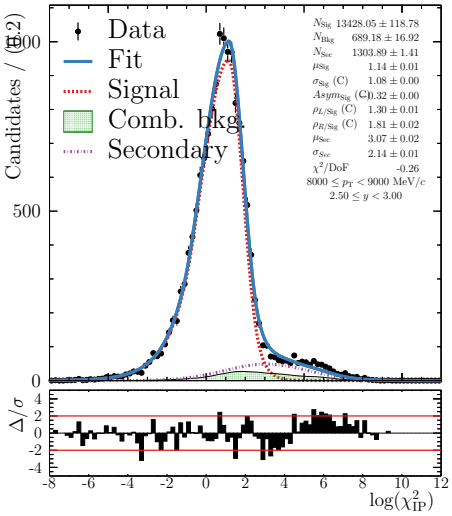

$8 \le p_{\rm T} < 9\,{\rm GeV},\ 2.5 \le y < 3.0$

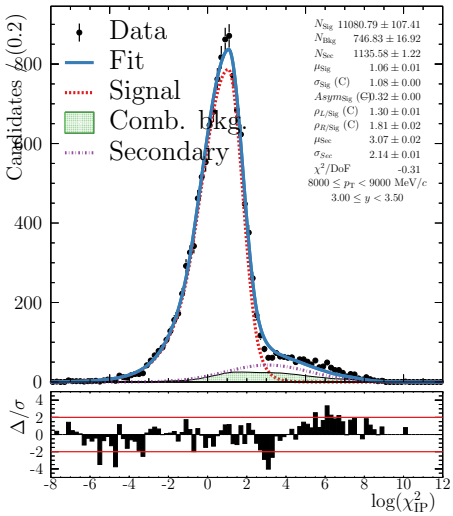

$8 \le p_{\rm T} < 9\,{\rm GeV},\ 3.0 \le y < 3.5$

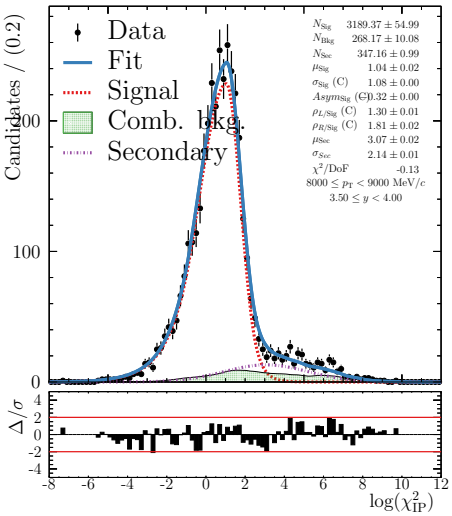

$8 \le p_{\rm T} < 9\,{\rm GeV},\ 3.5 \le y < 4.0$

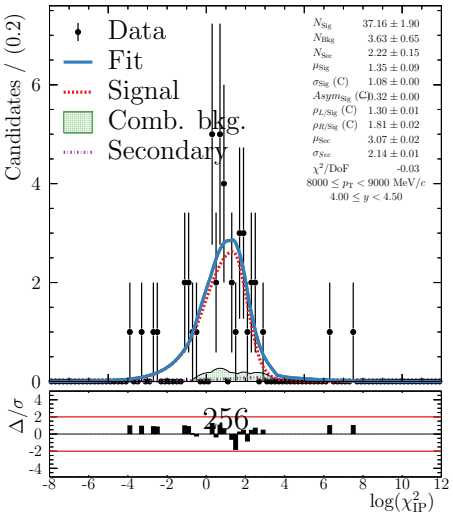

$8 \le p_{\rm T} < 9\,{\rm GeV},\ 4.0 \le y < 4.5$

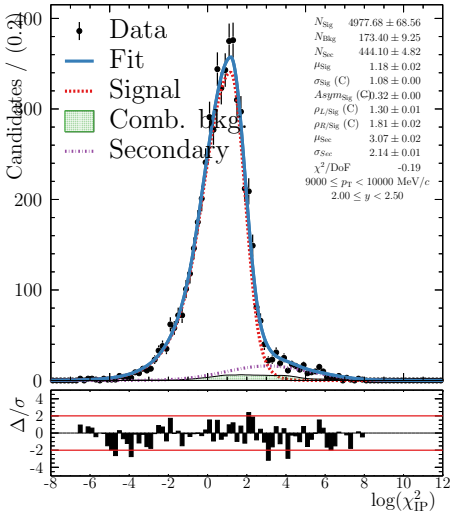

$9 \leq p_{\rm T} < 10\,{\rm GeV},\ 2.0 \leq y < 2.5$

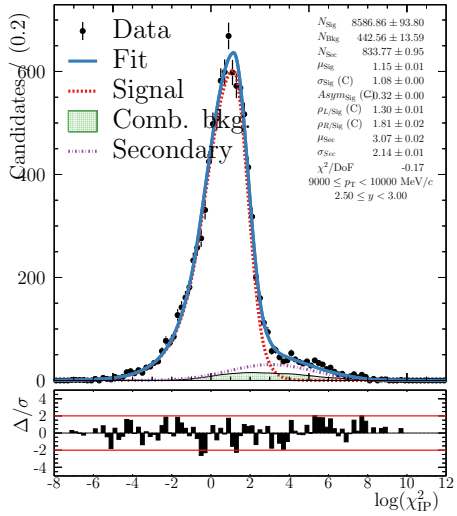

$9 \leq p_{\rm T} < 10\,{\rm GeV},\ 2.5 \leq y < 3.0$

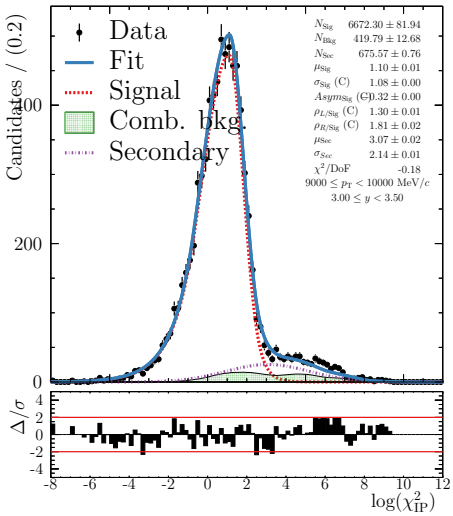

$9 \leq p_{\rm T} < 10\,{\rm GeV},\ 3.0 \leq y < 3.5$

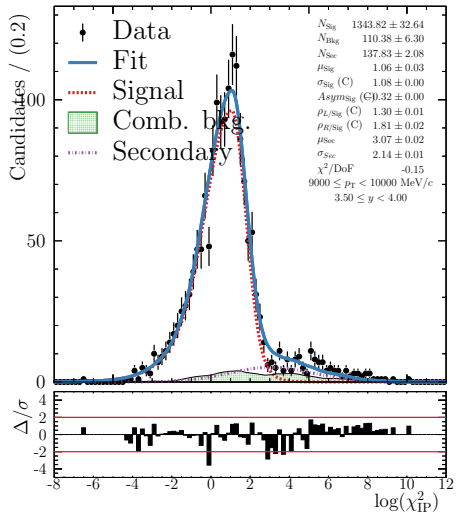

$9 \leq p_{\rm T} < 10\,{\rm GeV},\ 3.5 \leq y < 4.0$

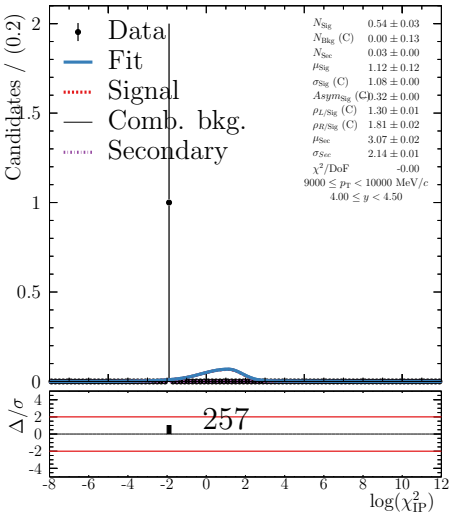

$9 \leq p_{\rm T} < 10\,{\rm GeV},\ 4.0 \leq y < 4.5$

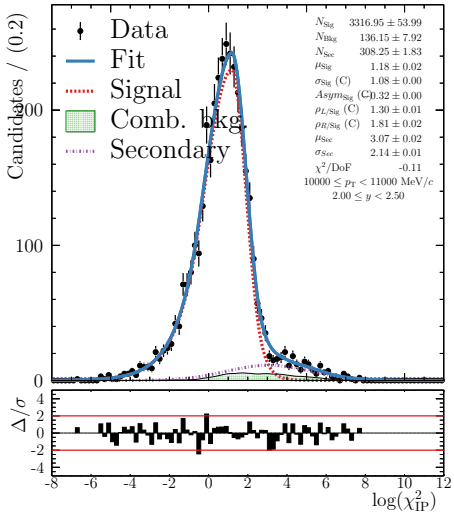

$10 \leq p_{\rm T} < 11\,{\rm GeV},\ 2.0 \leq y < 2.5$

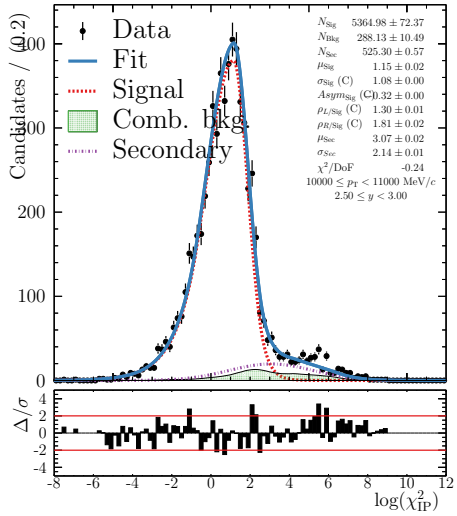

$10 \leq p_{\rm T} < 11\,{\rm GeV},\ 2.5 \leq y < 3.0$

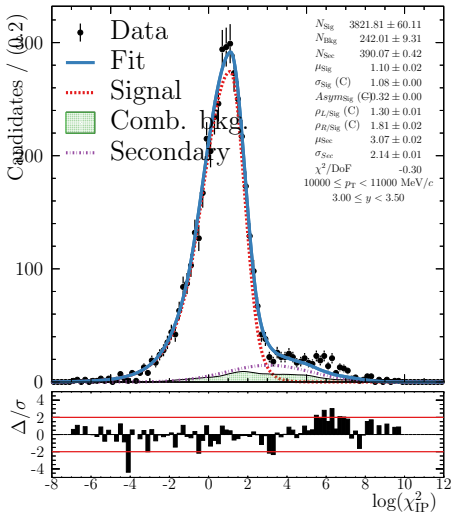

$10 \leq p_{\rm T} < 11\,{\rm GeV},\ 3.0 \leq y < 3.5$

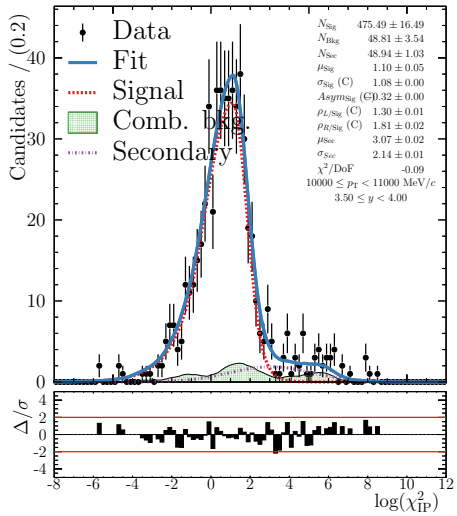

$10 \leq p_{\rm T} < 11\,{\rm GeV},\ 3.5 \leq y < 4.0$

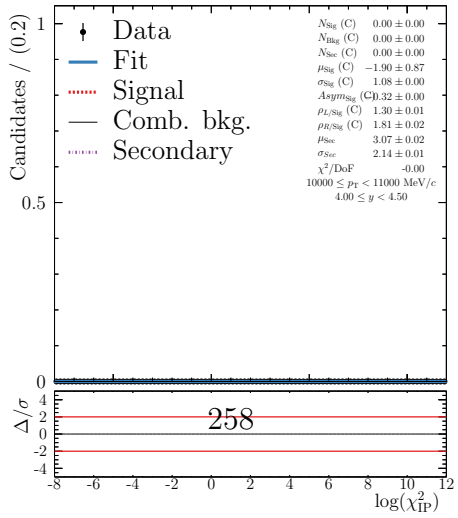

$10 \leq p_{\rm T} < 11\,{\rm GeV},\ 4.0 \leq y < 4.5$

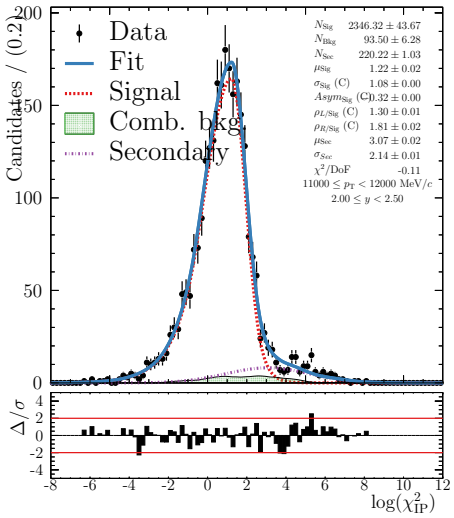

$11 \leq p_{\rm T} < 12\,{\rm GeV},\ 2.0 \leq y < 2.5$

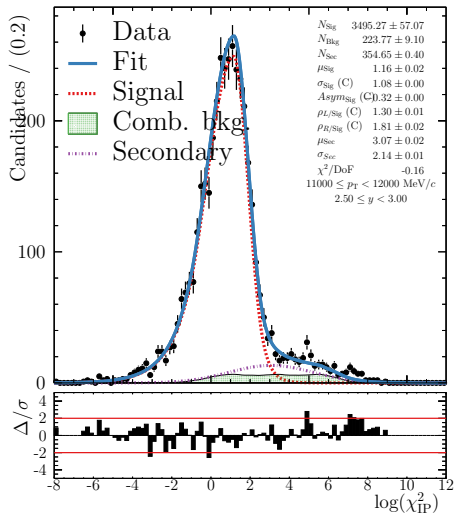

$11 \leq p_{\rm T} < 12\,{\rm GeV},\ 2.5 \leq y < 3.0$

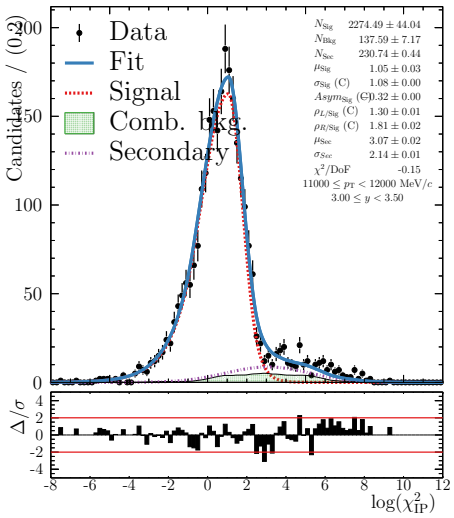

$11 \leq p_{\rm T} < 12\,{\rm GeV},\ 3.0 \leq y < 3.5$

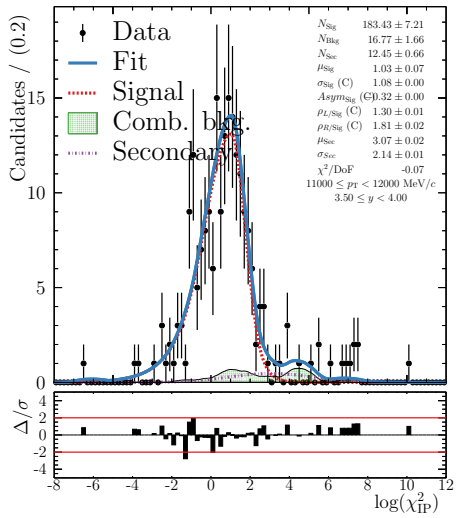

$11 \leq p_{\rm T} < 12\,{\rm GeV},\ 3.5 \leq y < 4.0$

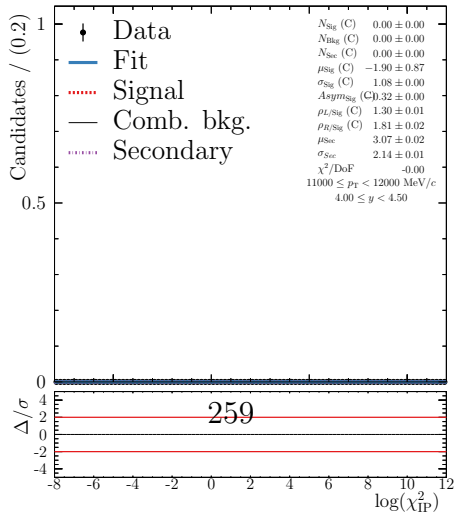

$11 \leq p_{\rm T} < 12\,{\rm GeV},\ 4.0 \leq y < 4.5$

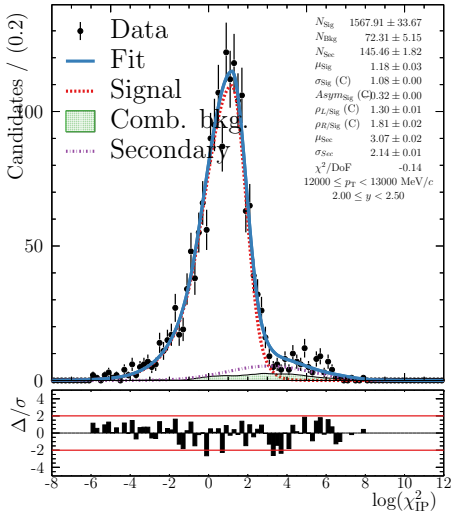

$12 \leq p_{\rm T} < 13\,{\rm GeV},\ 2.0 \leq y < 2.5$

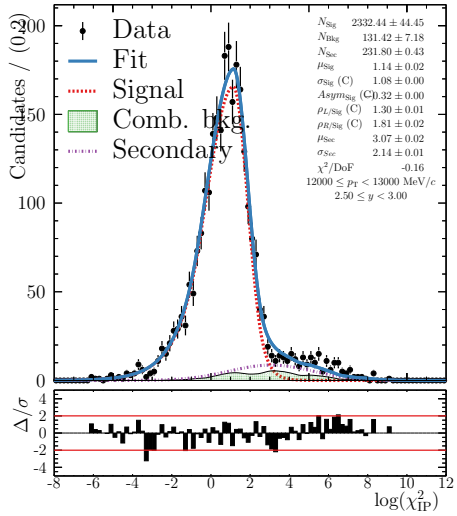

$12 \leq p_{\rm T} < 13\,{\rm GeV},\ 2.5 \leq y < 3.0$

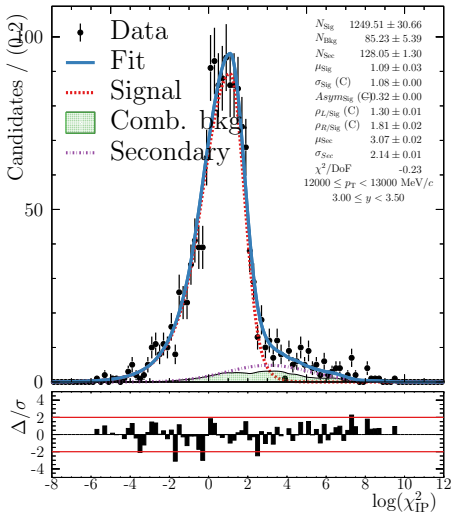

$12 \leq p_{\rm T} < 13\,{\rm GeV},\ 3.0 \leq y < 3.5$

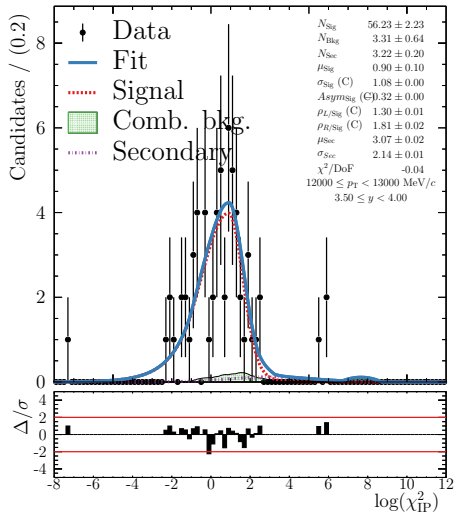

$12 \leq p_{\rm T} < 13\,{\rm GeV},\ 3.5 \leq y < 4.0$

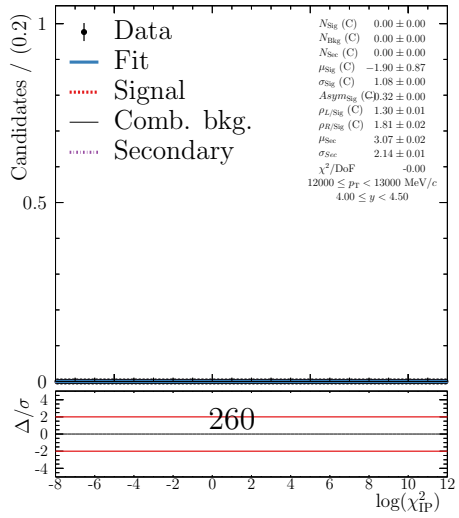

$12 \leq p_{\rm T} < 13\,{\rm GeV},\ 4.0 \leq y < 4.5$

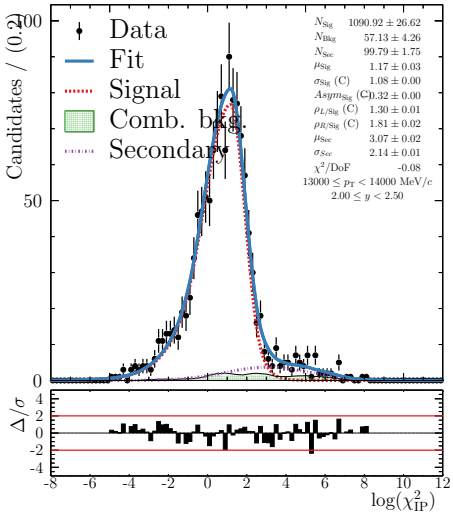

$13 \leq p_{\rm T} < 14\,{\rm GeV},\ 2.0 \leq y < 2.5$

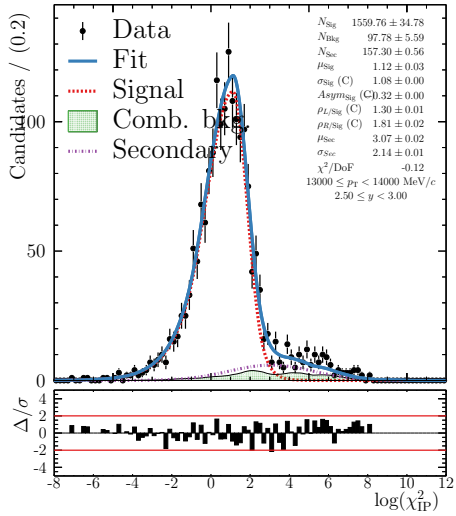

$13 \leq p_{\rm T} < 14\,{\rm GeV},\ 2.5 \leq y < 3.0$

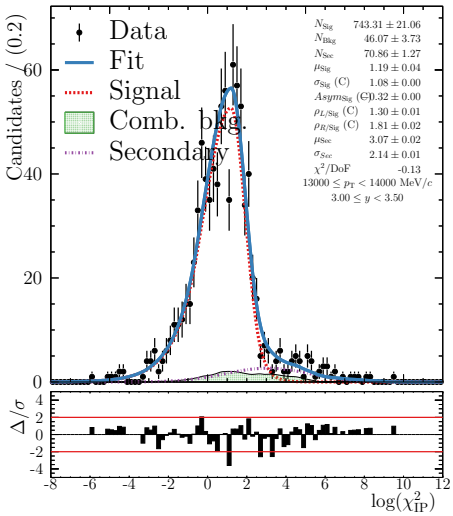

$13 \leq p_{\rm T} < 14\,{\rm GeV},\ 3.0 \leq y < 3.5$

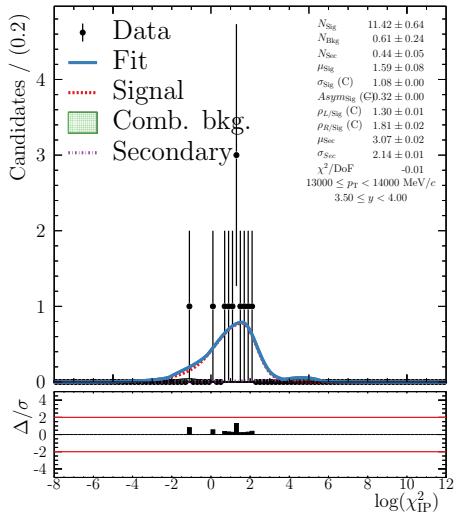

$13 \leq p_{\rm T} < 14\,{\rm GeV},\ 3.5 \leq y < 4.0$

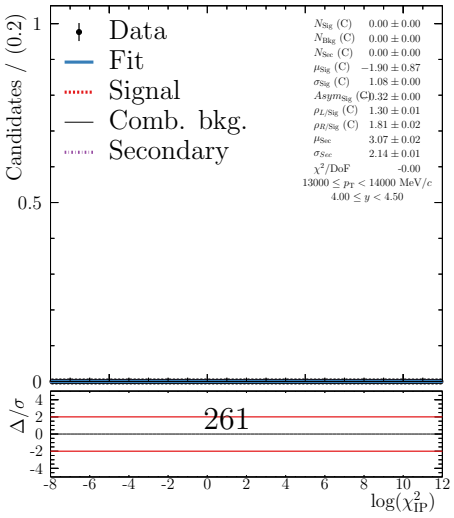

$13 \leq p_{\rm T} < 14\,{\rm GeV},\ 4.0 \leq y < 4.5$

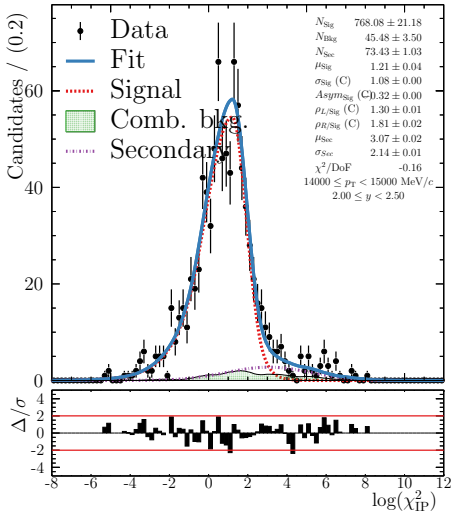

$14 \leq p_{\rm T} < 15\,{\rm GeV},\ 2.0 \leq y < 2.5$

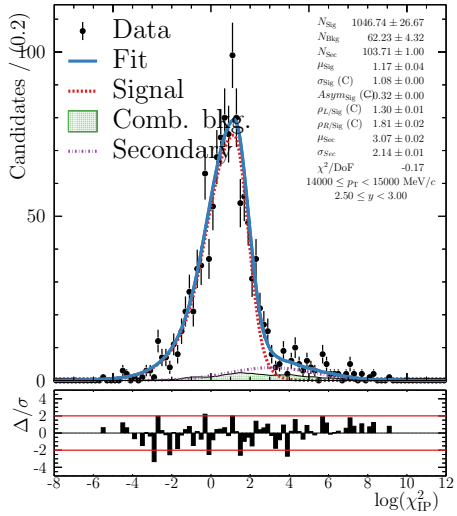

$14 \leq p_{\rm T} < 15\,{\rm GeV},\ 2.5 \leq y < 3.0$

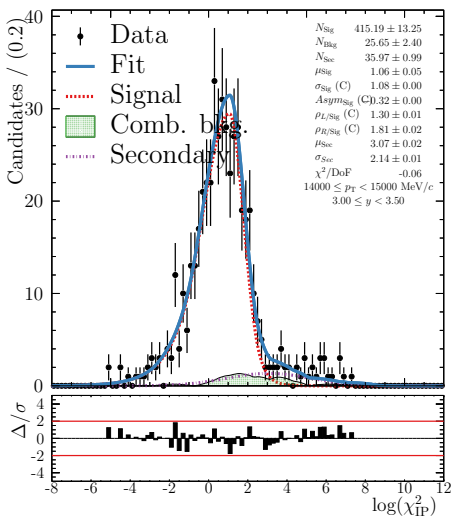

$14 \leq p_{\rm T} < 15\,{\rm GeV},\ 3.0 \leq y < 3.5$

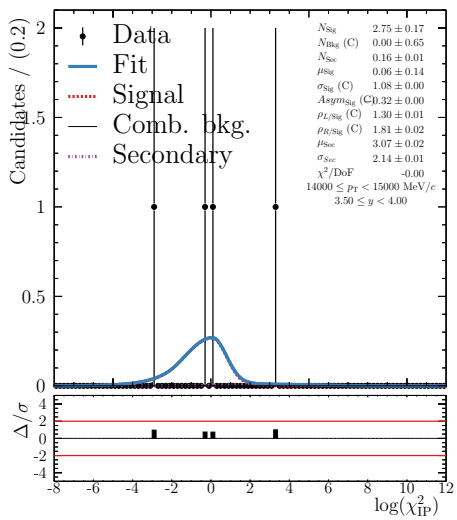

$14 \leq p_{\rm T} < 15\,{\rm GeV},\ 3.5 \leq y < 4.0$

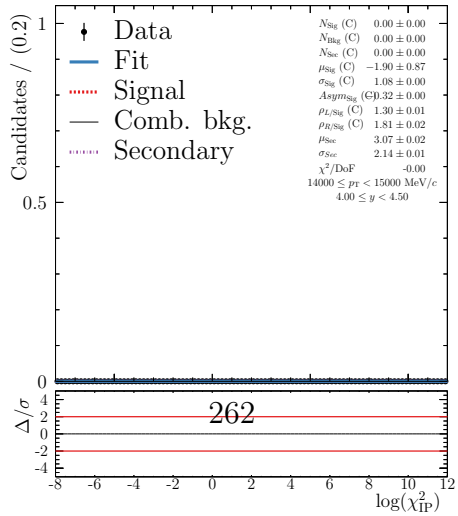

$14 \leq p_{\rm T} < 15\,{\rm GeV},\ 4.0 \leq y < 4.5$

Figure F.0: Fits to the fully selected $D^+ \to K^-\pi^+\pi^+$ $\ln\chi^2_{\rm IP}$ distribution per $p_{\rm T}$-y bin.

F.3 $D^+ \to K^- K^+ \pi^+$

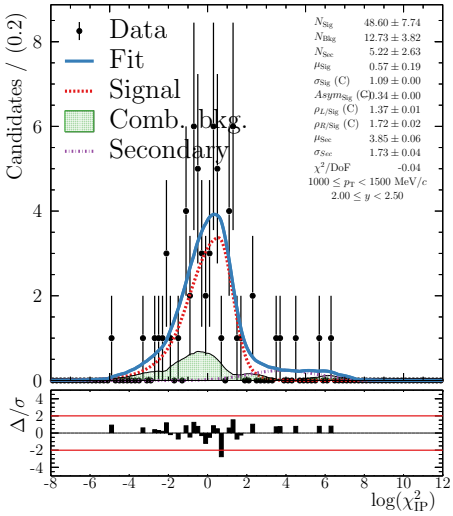

$1 \leq p_{\rm T} < 1.5\,\text{GeV},\ 2.0 \leq y < 2.5$

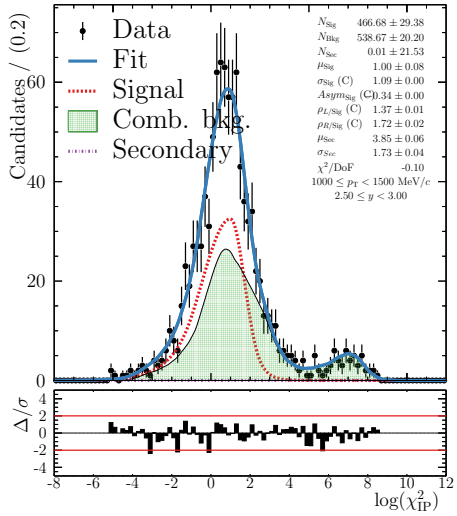

$1 \leq p_{\rm T} < 1.5\,\text{GeV},\ 2.5 \leq y < 3.0$

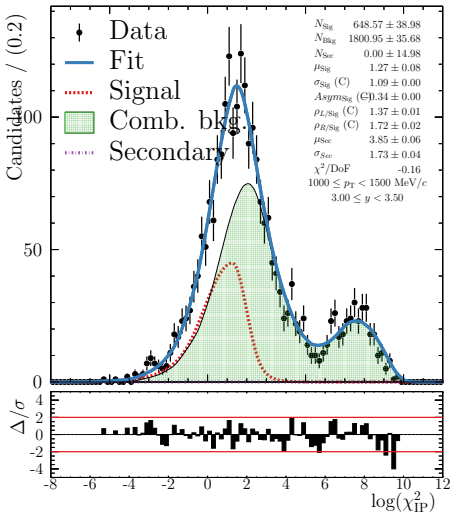

$1 \leq p_{\rm T} < 1.5\,\text{GeV},\ 3.0 \leq y < 3.5$

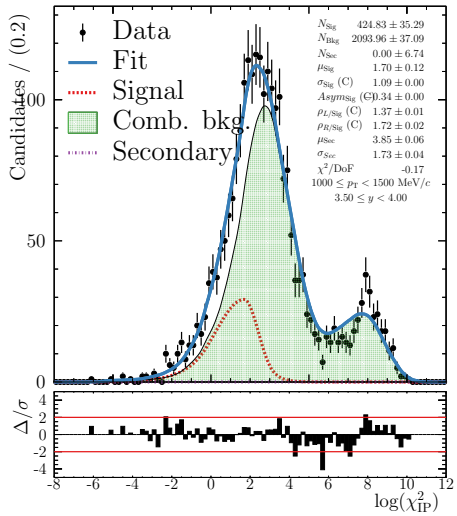

$1 \leq p_{\rm T} < 1.5\,\text{GeV},\ 3.5 \leq y < 4.0$

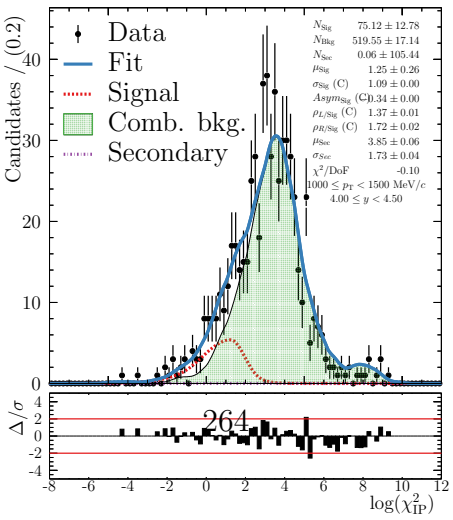

$1 \leq p_{\rm T} < 1.5\,\text{GeV},\ 4.0 \leq y < 4.5$

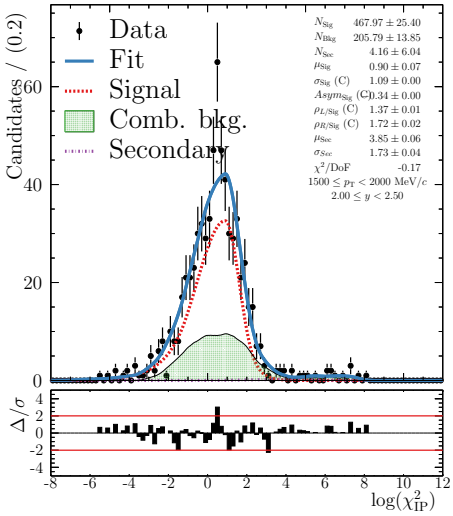

$1.5 \leq p_{\rm T} < 2\,{\rm GeV},\ 2.0 \leq y < 2.5$

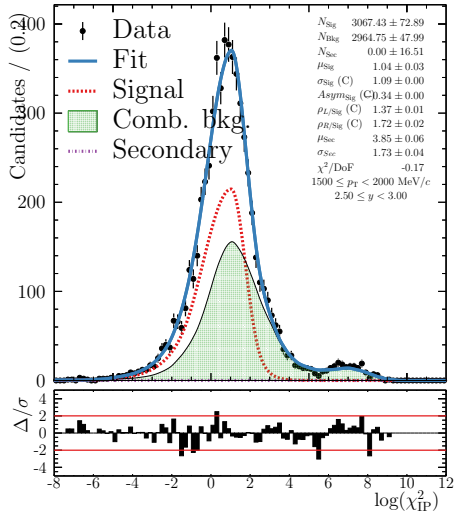

$1.5 \leq p_{\rm T} < 2\,{\rm GeV},\ 2.5 \leq y < 3.0$

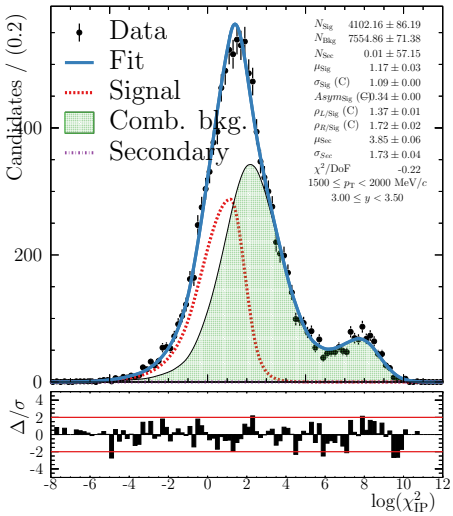

$1.5 \leq p_{\rm T} < 2\,{\rm GeV},\ 3.0 \leq y < 3.5$

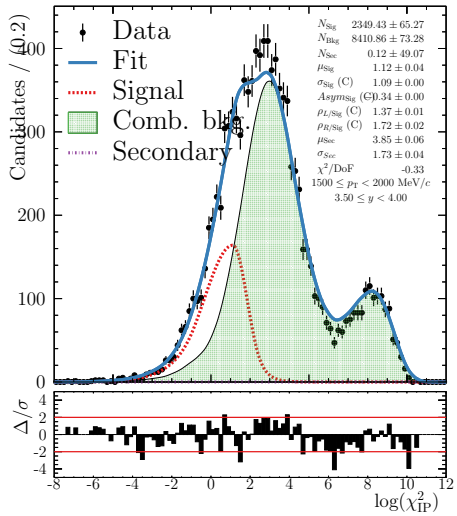

$1.5 \leq p_{\rm T} < 2\,{\rm GeV},\ 3.5 \leq y < 4.0$

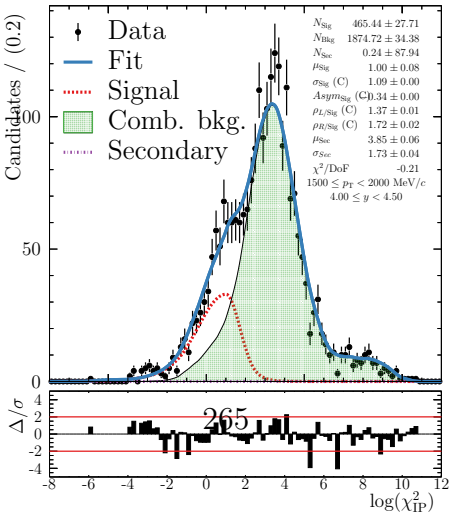

$1.5 \leq p_{\rm T} < 2\,{\rm GeV},\ 4.0 \leq y < 4.5$

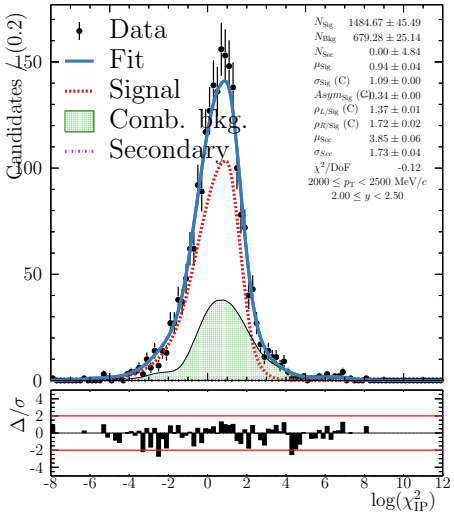

$2 \leq p_{\rm T} < 2.5\,{\rm GeV},\ 2.0 \leq y < 2.5$

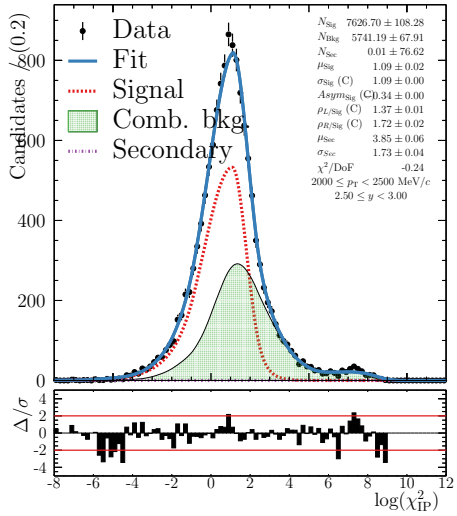

$2 \leq p_{\rm T} < 2.5\,{\rm GeV},\ 2.5 \leq y < 3.0$

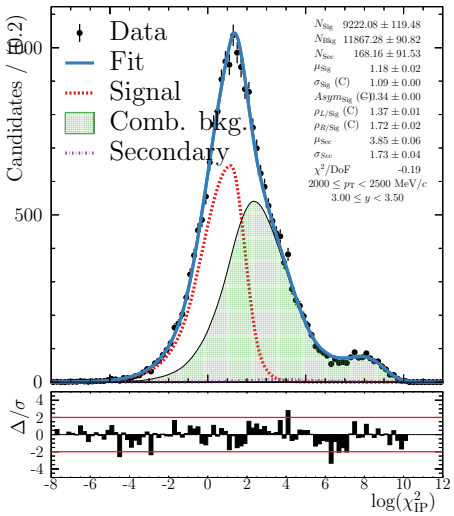

$2 \leq p_{\rm T} < 2.5\,{\rm GeV},\ 3.0 \leq y < 3.5$

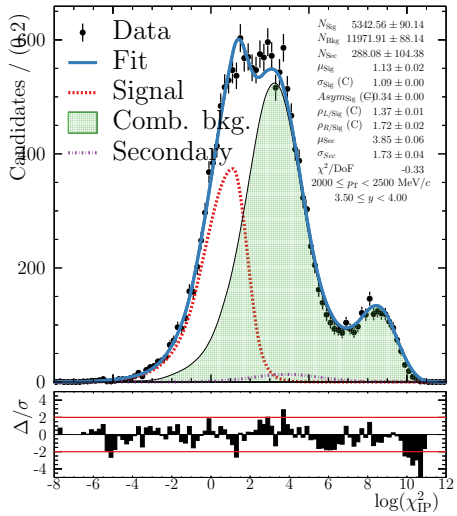

$2 \leq p_{\rm T} < 2.5\,{\rm GeV},\ 3.5 \leq y < 4.0$

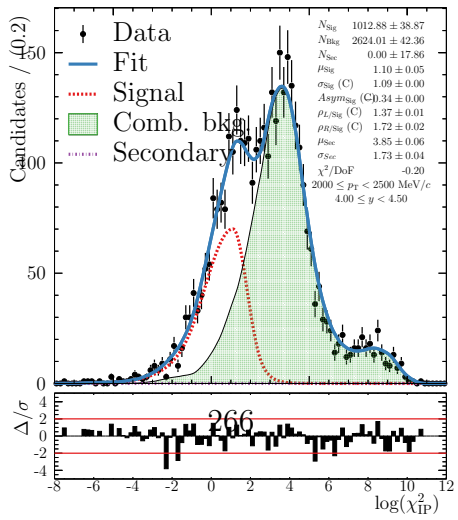

$2 \leq p_{\rm T} < 2.5\,{\rm GeV},\ 4.0 \leq y < 4.5$

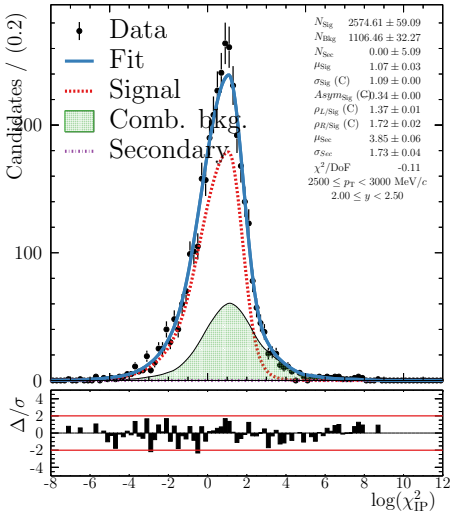

$2.5 \leq p_{\rm T} < 3\,{\rm GeV},\ 2.0 \leq y < 2.5$

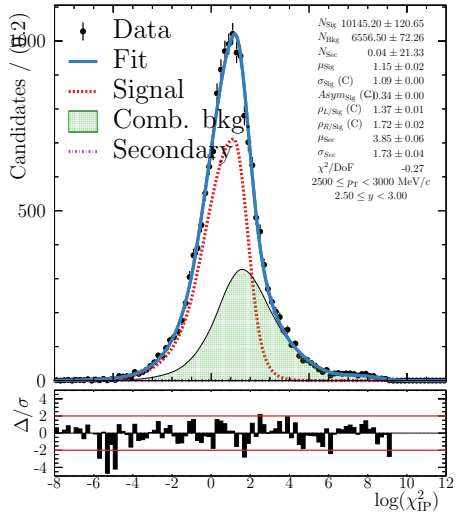

$2.5 \leq p_{\rm T} < 3\,{\rm GeV},\ 2.5 \leq y < 3.0$

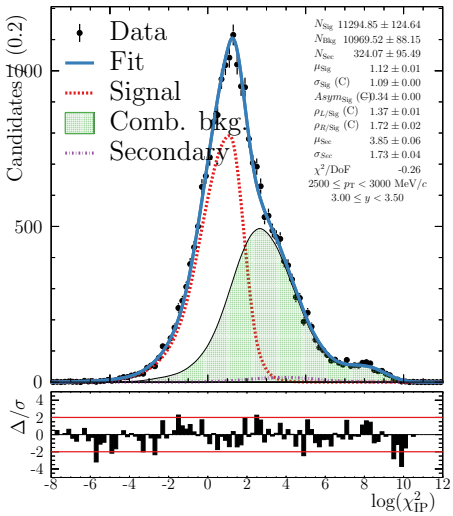

$2.5 \leq p_{\rm T} < 3\,{\rm GeV},\ 3.0 \leq y < 3.5$

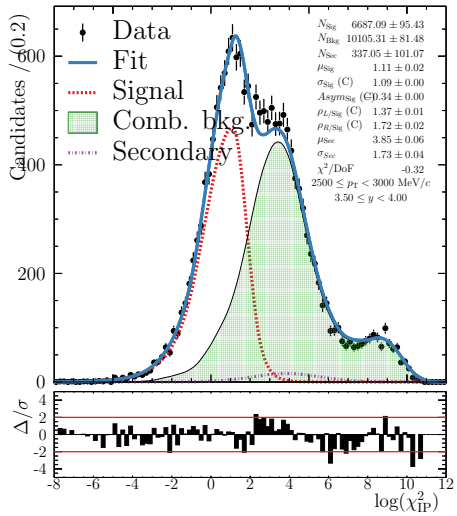

$2.5 \leq p_{\rm T} < 3\,{\rm GeV},\ 3.5 \leq y < 4.0$

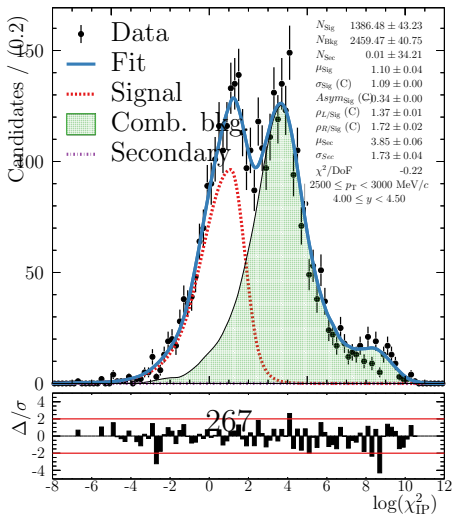

$2.5 \leq p_{\rm T} < 3\,{\rm GeV},\ 4.0 \leq y < 4.5$

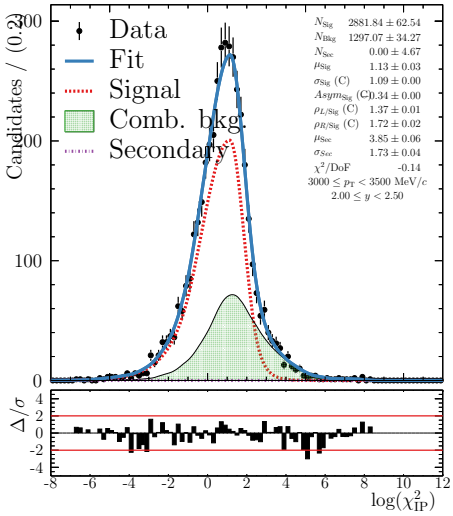

$3 \leq p_{\rm T} < 3.5\,{\rm GeV},\ 2.0 \leq y < 2.5$

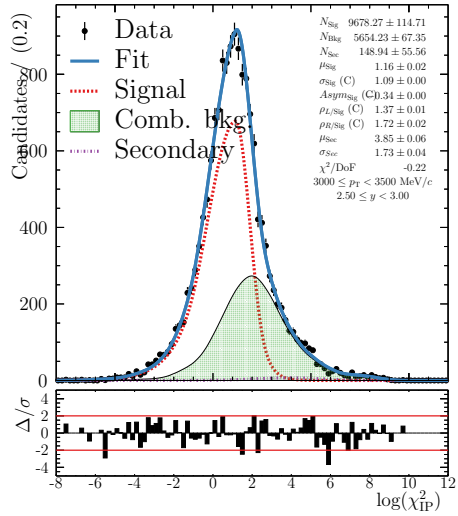

$3 \leq p_{\rm T} < 3.5\,{\rm GeV},\ 2.5 \leq y < 3.0$

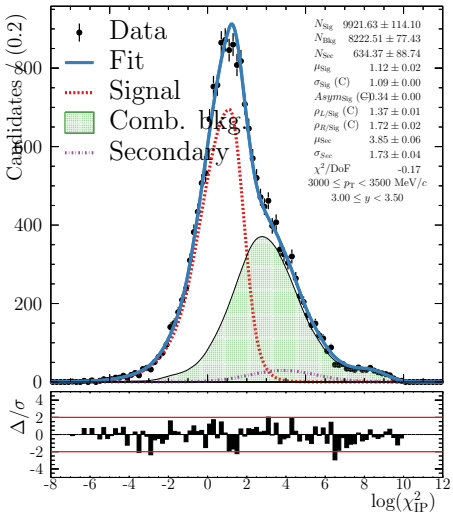

$3 \leq p_{\rm T} < 3.5\,{\rm GeV},\ 3.0 \leq y < 3.5$

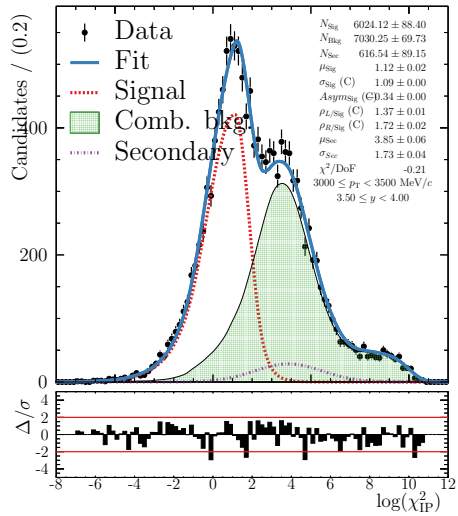

$3 \leq p_{\rm T} < 3.5\,{\rm GeV},\ 3.5 \leq y < 4.0$

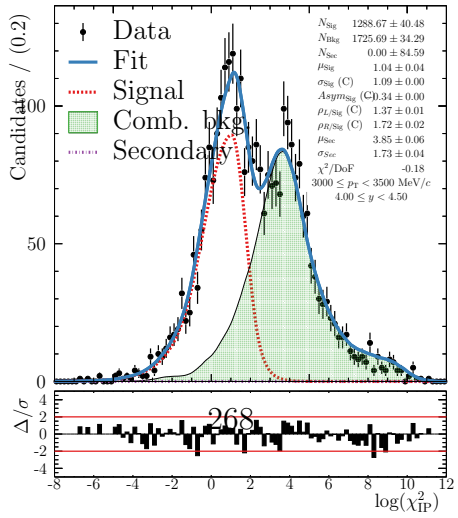

$3 \leq p_{\rm T} < 3.5\,{\rm GeV},\ 4.0 \leq y < 4.5$

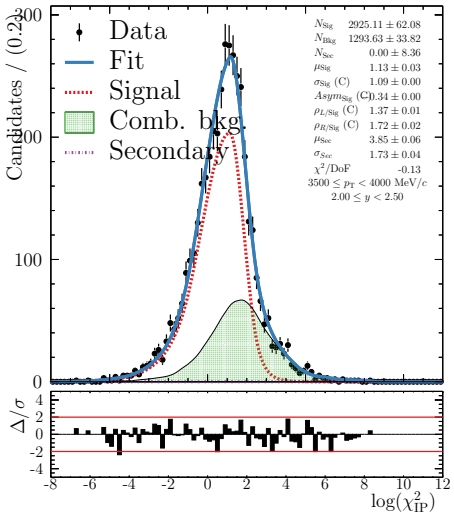

$3.5 \leq p_{\rm T} < 4\,{\rm GeV},\ 2.0 \leq y < 2.5$

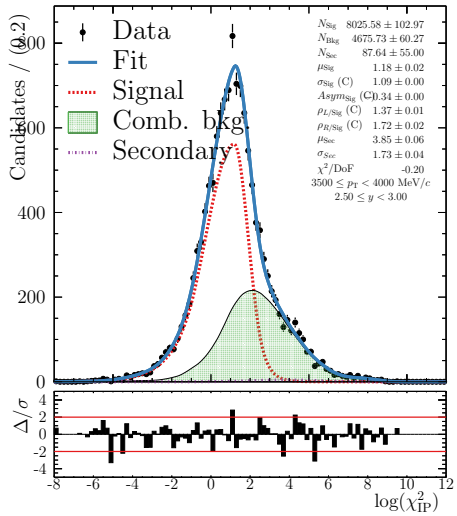

$3.5 \leq p_{\rm T} < 4\,{\rm GeV},\ 2.5 \leq y < 3.0$

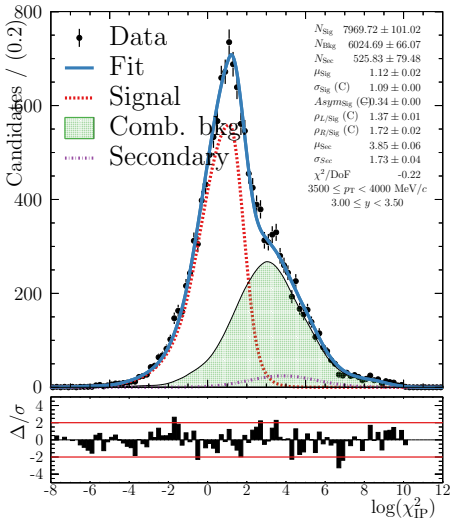

$3.5 \leq p_{\rm T} < 4\,{\rm GeV},\ 3.0 \leq y < 3.5$

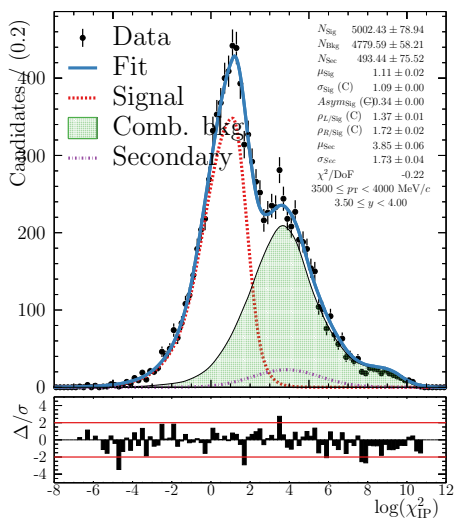

$3.5 \leq p_{\rm T} < 4\,{\rm GeV},\ 3.5 \leq y < 4.0$

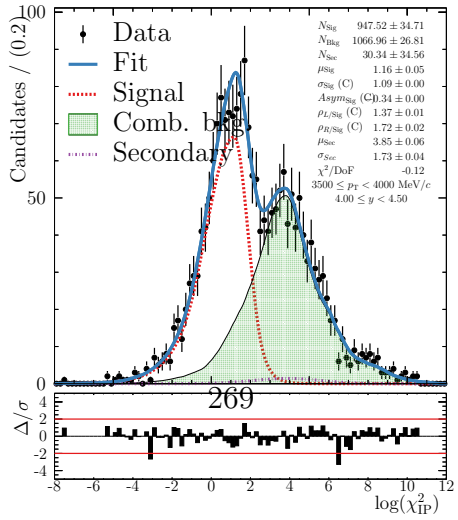

$3.5 \leq p_{\rm T} < 4\,{\rm GeV},\ 4.0 \leq y < 4.5$

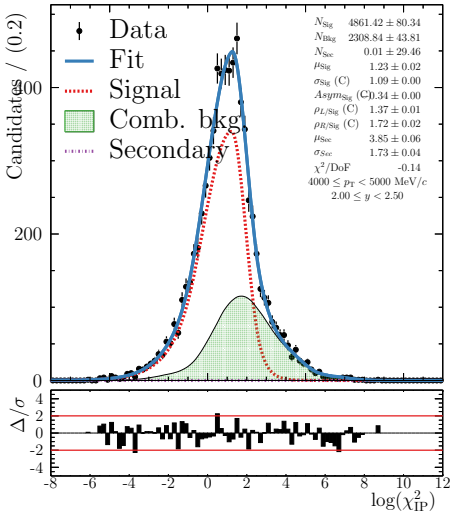

$4 \leq p_{\rm T} < 5\,{\rm GeV},\ 2.0 \leq y < 2.5$

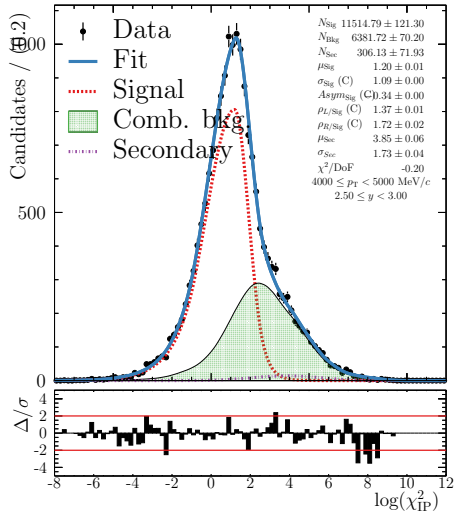

$4 \leq p_{\rm T} < 5\,{\rm GeV},\ 2.5 \leq y < 3.0$

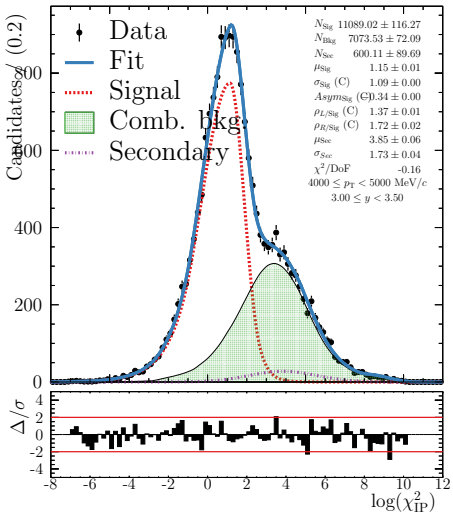

$4 \leq p_{\rm T} < 5\,{\rm GeV},\ 3.0 \leq y < 3.5$

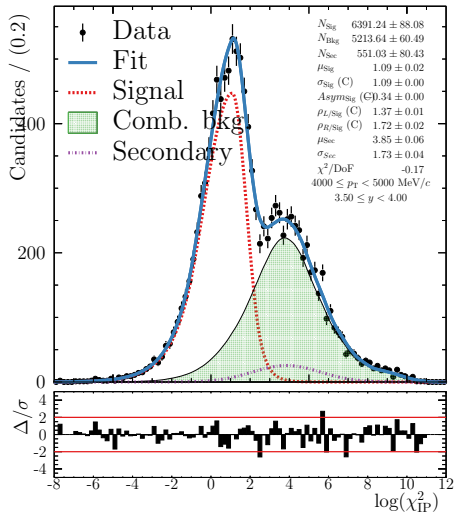

$4 \leq p_{\rm T} < 5\,{\rm GeV},\ 3.5 \leq y < 4.0$

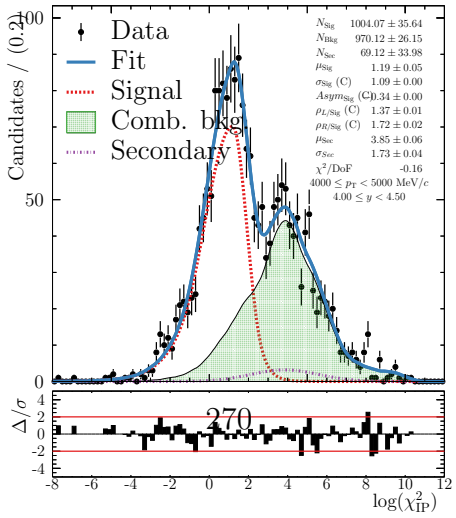

$4 \leq p_{\rm T} < 5\,{\rm GeV},\ 4.0 \leq y < 4.5$

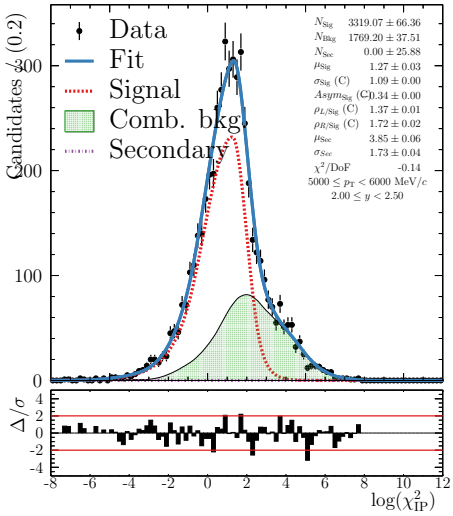

$5 \leq p_{\rm T} < 6\,{\rm GeV},\ 2.0 \leq y < 2.5$

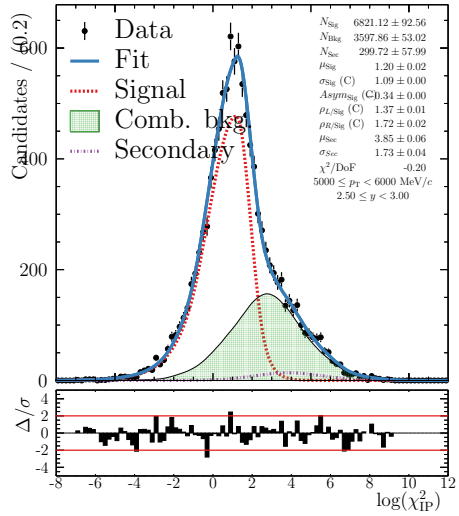

$5 \leq p_{\rm T} < 6\,{\rm GeV},\ 2.5 \leq y < 3.0$

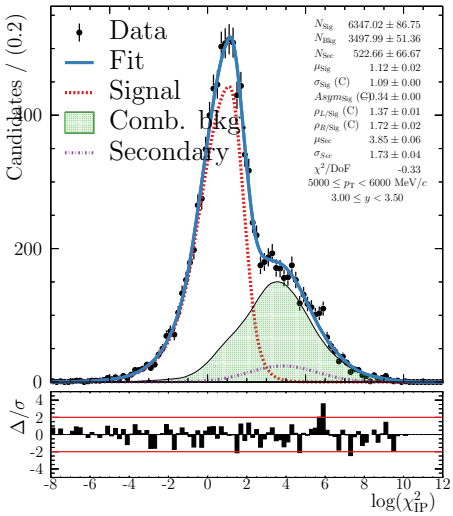

$5 \leq p_{\rm T} < 6\,{\rm GeV},\ 3.0 \leq y < 3.5$

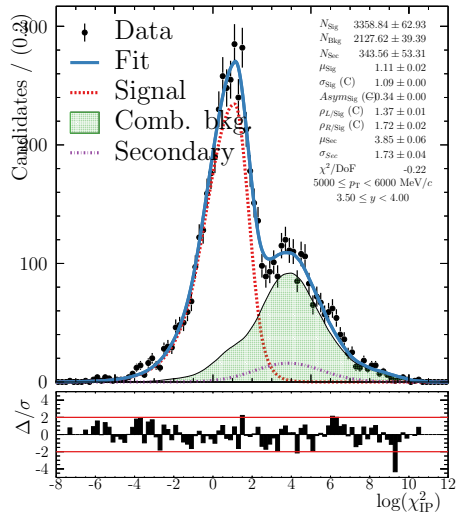

$5 \leq p_{\rm T} < 6\,{\rm GeV},\ 3.5 \leq y < 4.0$

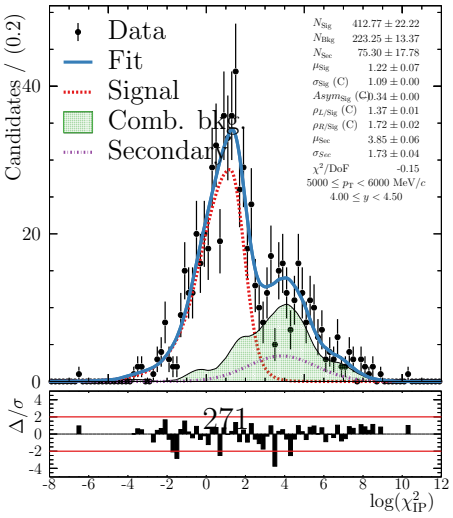

$5 \leq p_{\rm T} < 6\,{\rm GeV},\ 4.0 \leq y < 4.5$

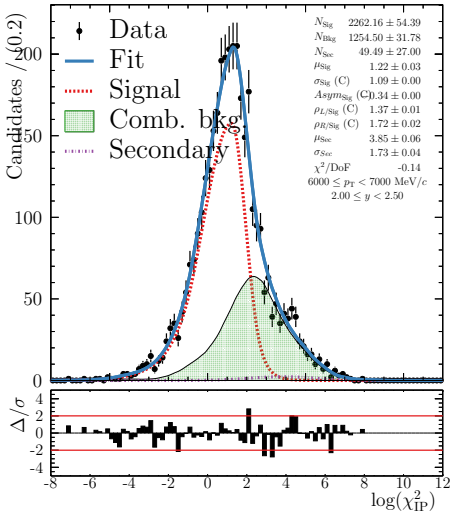

$6 \leq p_{\rm T} < 7\,{\rm GeV},\ 2.0 \leq y < 2.5$

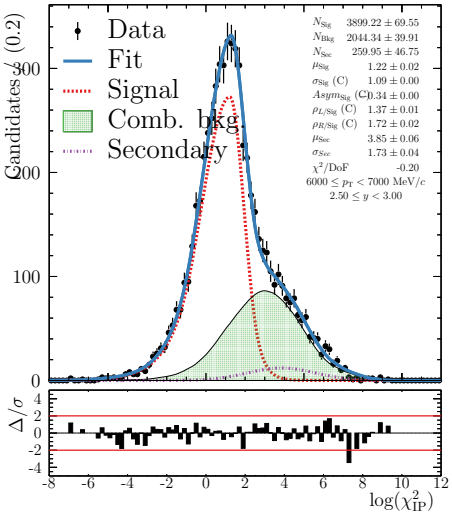

$6 \leq p_{\rm T} < 7\,{\rm GeV},\ 2.5 \leq y < 3.0$

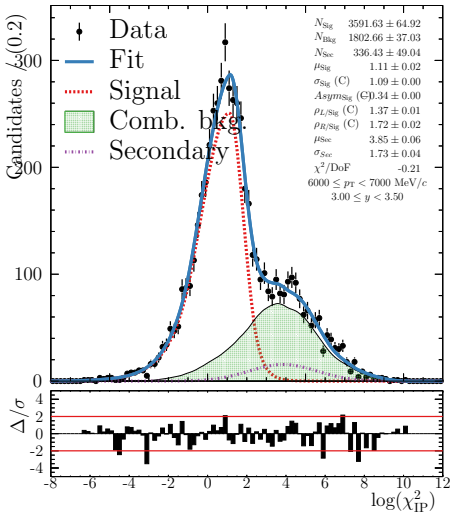

$6 \leq p_{\rm T} < 7\,{\rm GeV},\ 3.0 \leq y < 3.5$

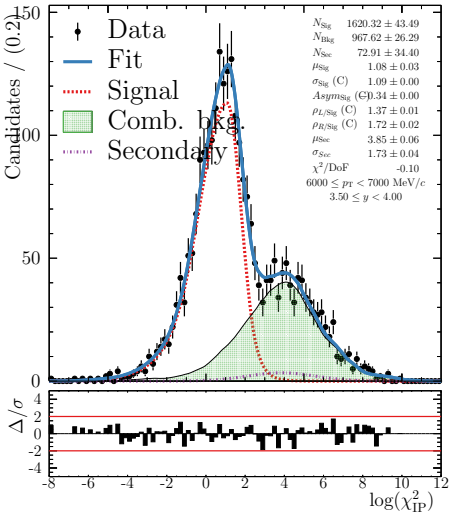

$6 \leq p_{\rm T} < 7\,{\rm GeV},\ 3.5 \leq y < 4.0$

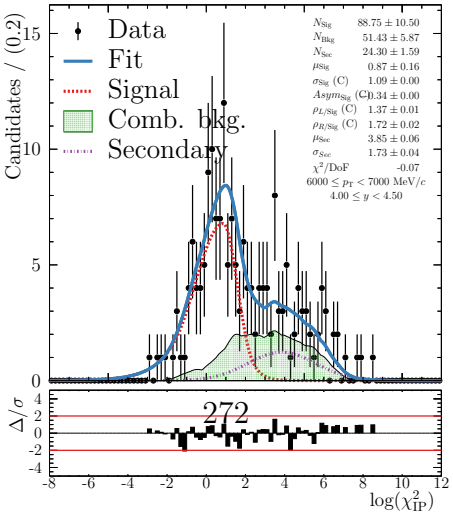

$6 \leq p_{\rm T} < 7\,{\rm GeV},\ 4.0 \leq y < 4.5$

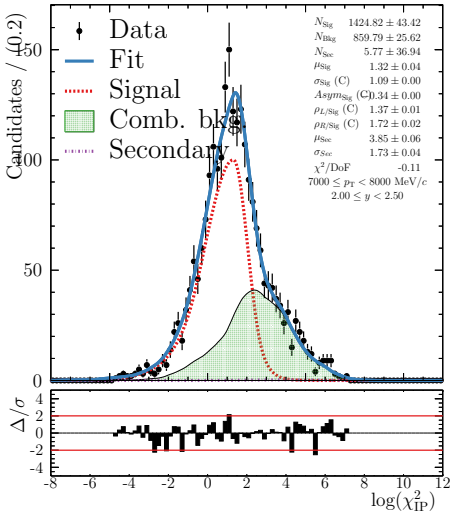

$7 \leq p_{\rm T} < 8\,{\rm GeV},\ 2.0 \leq y < 2.5$

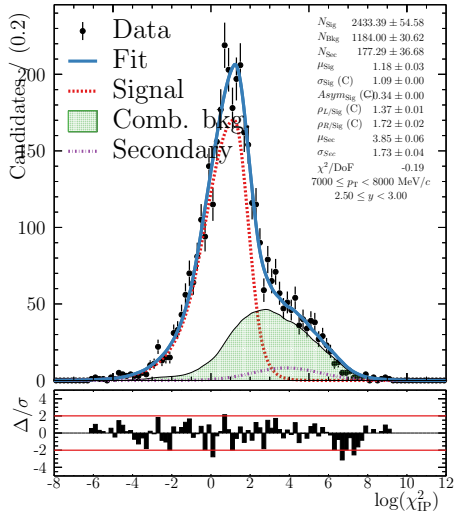

$7 \leq p_{\rm T} < 8\,{\rm GeV},\ 2.5 \leq y < 3.0$

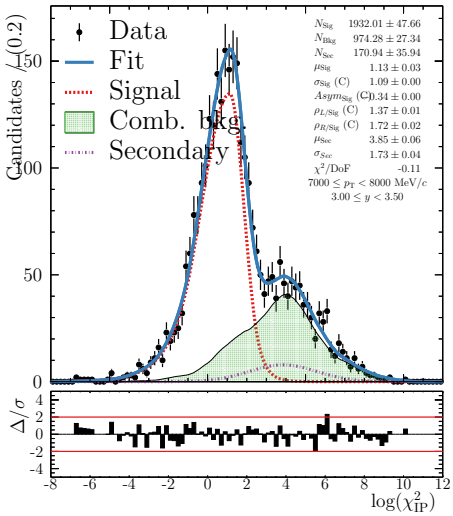

$7 \leq p_{\rm T} < 8\,{\rm GeV},\ 3.0 \leq y < 3.5$

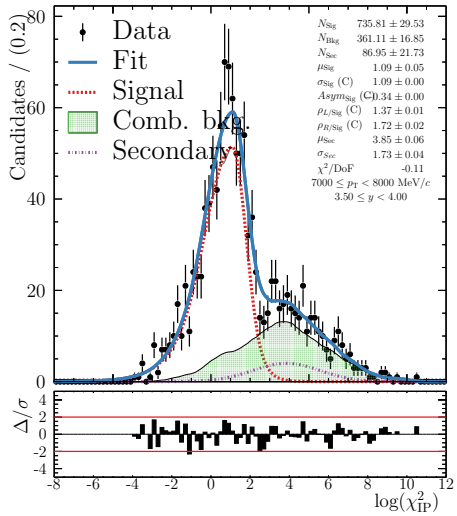

$7 \leq p_{\rm T} < 8\,{\rm GeV},\ 3.5 \leq y < 4.0$

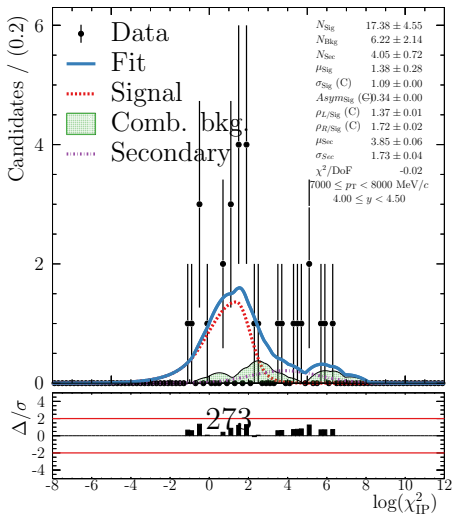

$7 \leq p_{\rm T} < 8\,{\rm GeV},\ 4.0 \leq y < 4.5$

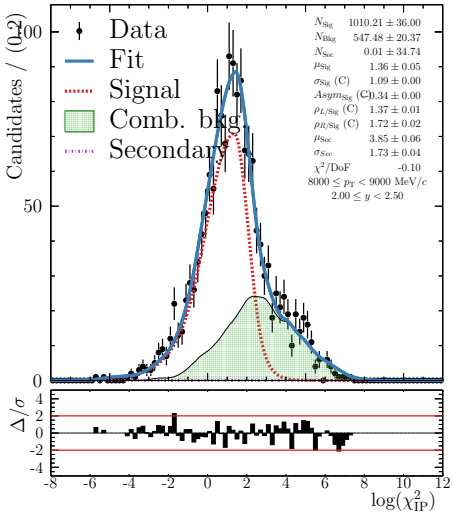

$8 \le p_{\rm T} < 9\,{\rm GeV},\ 2.0 \le y < 2.5$

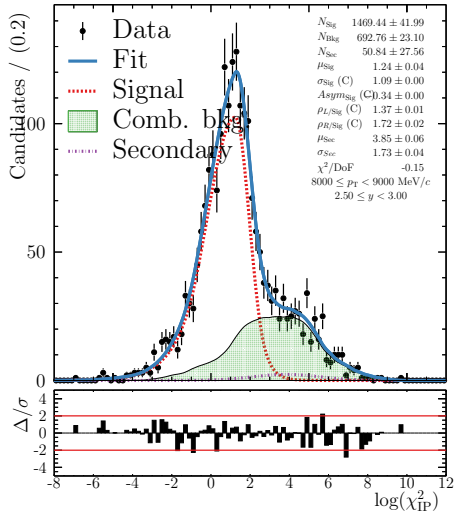

$8 \le p_{\rm T} < 9\,{\rm GeV},\ 2.5 \le y < 3.0$

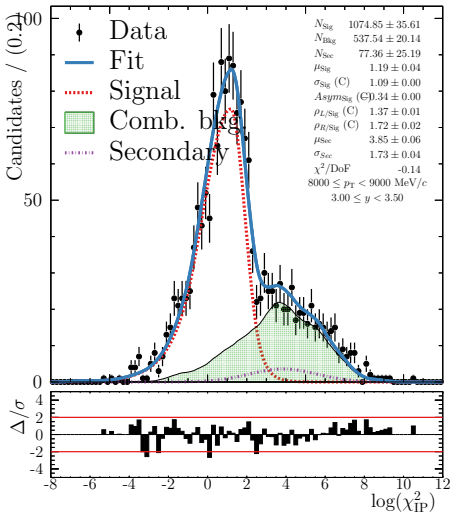

$8 \le p_{\rm T} < 9\,{\rm GeV},\ 3.0 \le y < 3.5$

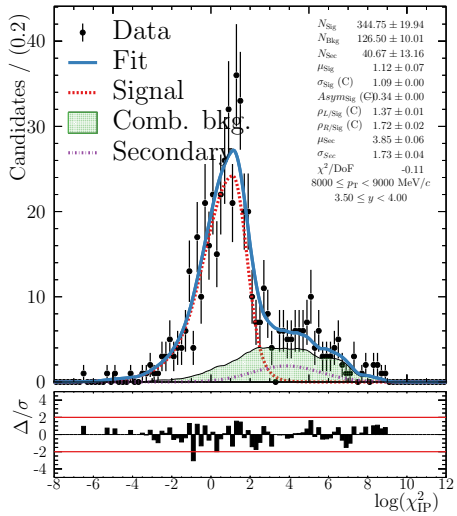

$8 \le p_{\rm T} < 9\,{\rm GeV},\ 3.5 \le y < 4.0$

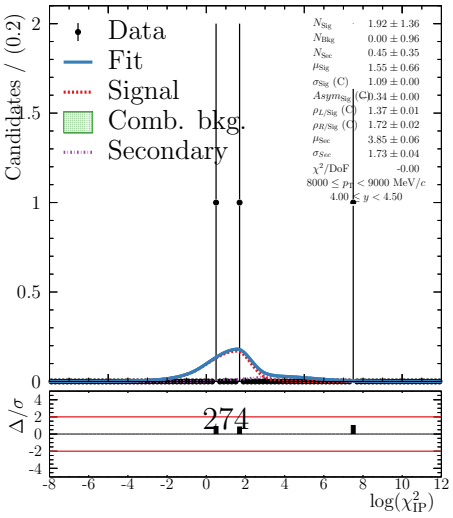

$8 \le p_{\rm T} < 9\,{\rm GeV},\ 4.0 \le y < 4.5$

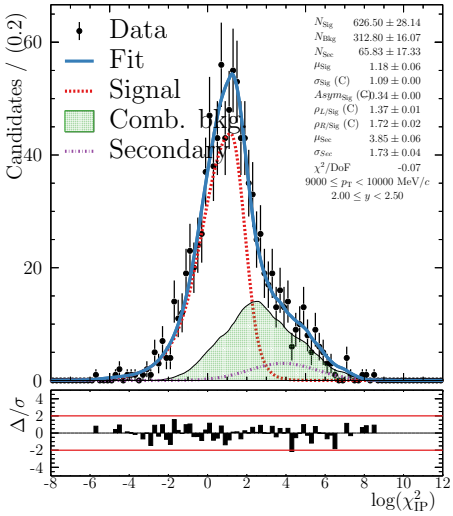

$9 \leq p_{\rm T} < 10\,{\rm GeV},\ 2.0 \leq y < 2.5$

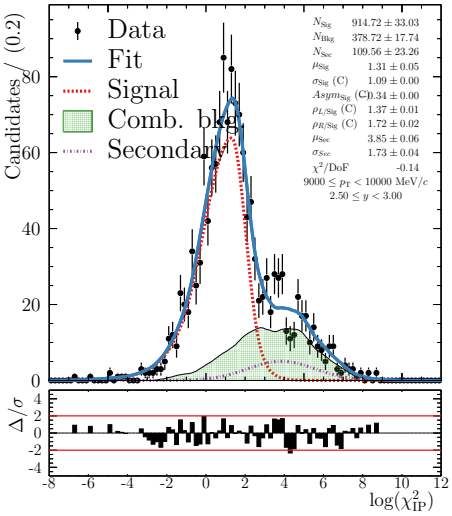

$9 \leq p_{\rm T} < 10\,{\rm GeV},\ 2.5 \leq y < 3.0$

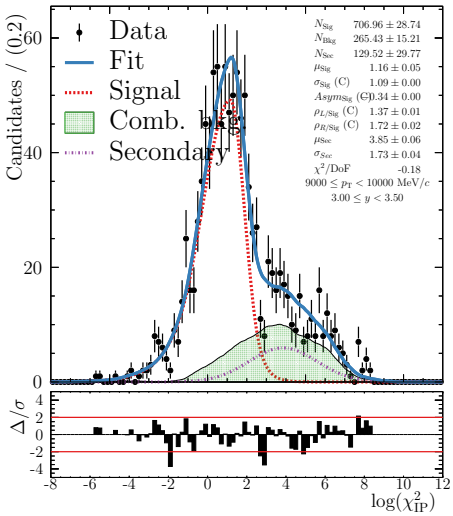

$9 \leq p_{\rm T} < 10\,{\rm GeV},\ 3.0 \leq y < 3.5$

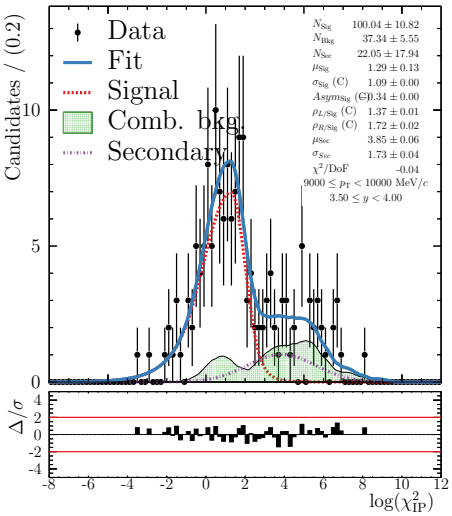

$9 \leq p_{\rm T} < 10\,{\rm GeV},\ 3.5 \leq y < 4.0$

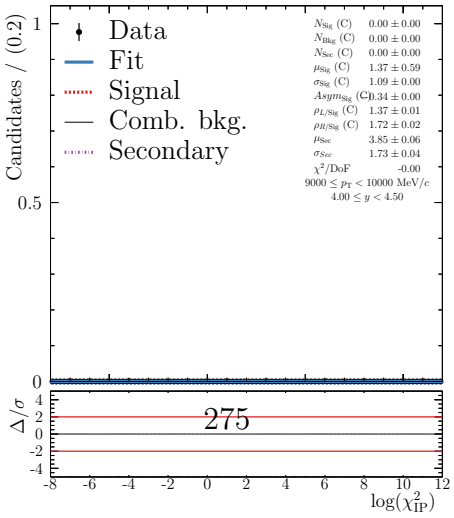

$9 \leq p_{\rm T} < 10\,{\rm GeV},\ 4.0 \leq y < 4.5$

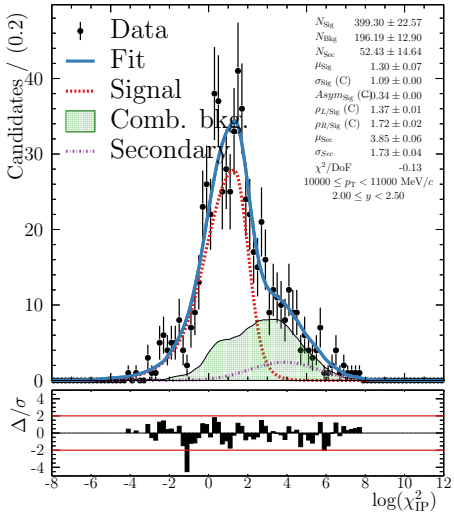

$10 \leq p_{\rm T} < 11\,{\rm GeV},\ 2.0 \leq y < 2.5$

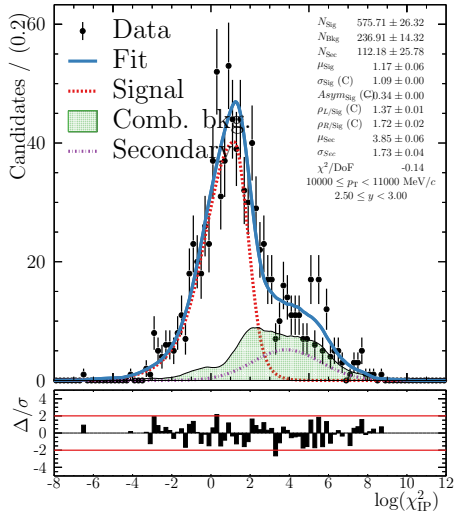

$10 \leq p_{\rm T} < 11\,{\rm GeV},\ 2.5 \leq y < 3.0$

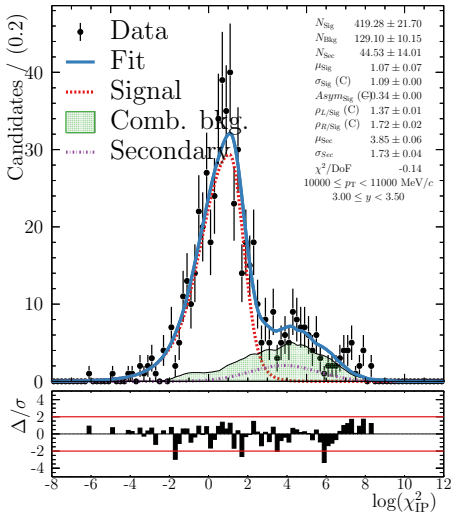

$10 \leq p_{\rm T} < 11\,{\rm GeV},\ 3.0 \leq y < 3.5$

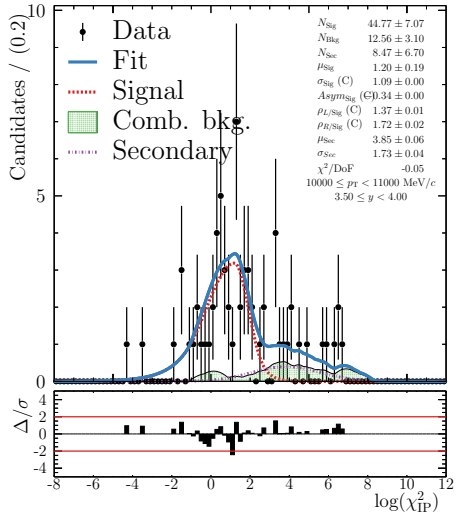

$10 \leq p_{\rm T} < 11\,{\rm GeV},\ 3.5 \leq y < 4.0$

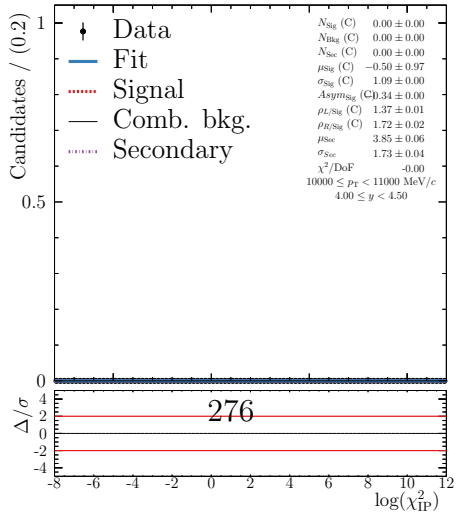

$10 \leq p_{\rm T} < 11\,{\rm GeV},\ 4.0 \leq y < 4.5$

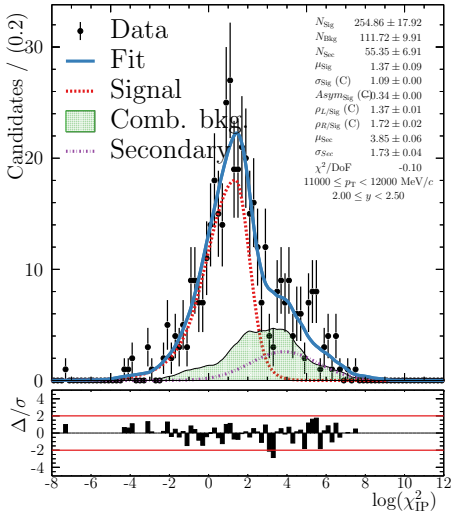

$11 \leq p_{\rm T} < 12\,{\rm GeV},\ 2.0 \leq y < 2.5$

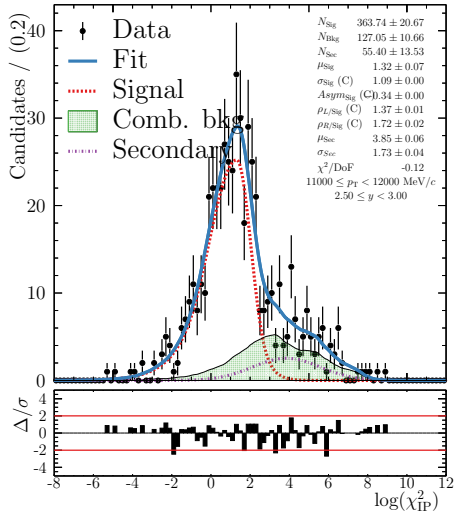

$11 \leq p_{\rm T} < 12\,{\rm GeV},\ 2.5 \leq y < 3.0$

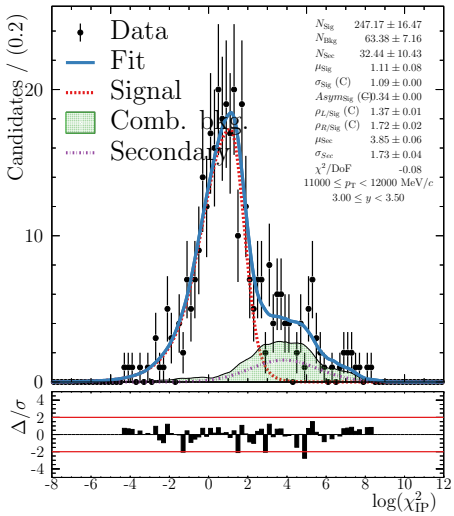

$11 \leq p_{\rm T} < 12\,{\rm GeV},\ 3.0 \leq y < 3.5$

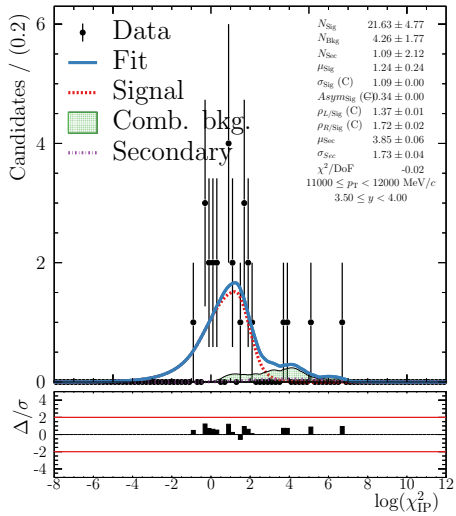

$11 \leq p_{\rm T} < 12\,{\rm GeV},\ 3.5 \leq y < 4.0$

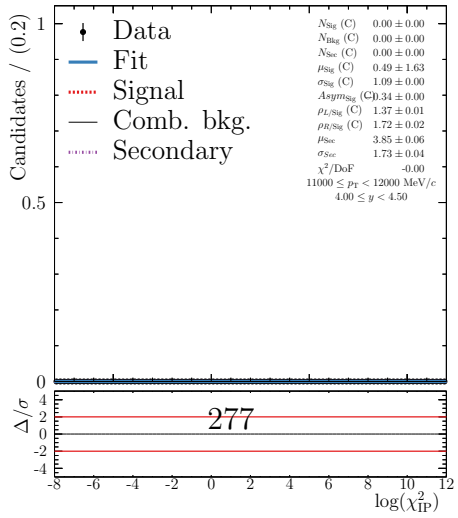

$11 \leq p_{\rm T} < 12\,{\rm GeV},\ 4.0 \leq y < 4.5$

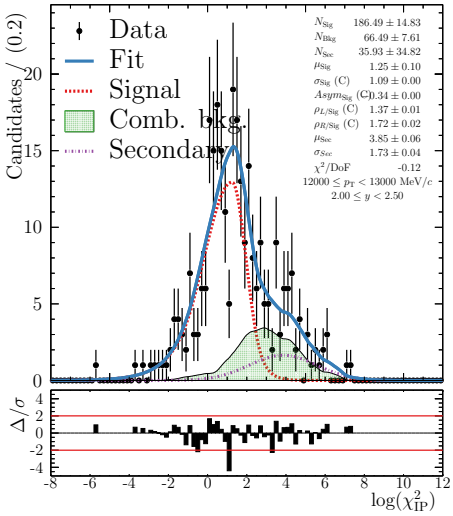

$12 \leq p_{\rm T} < 13\,{\rm GeV},\ 2.0 \leq y < 2.5$

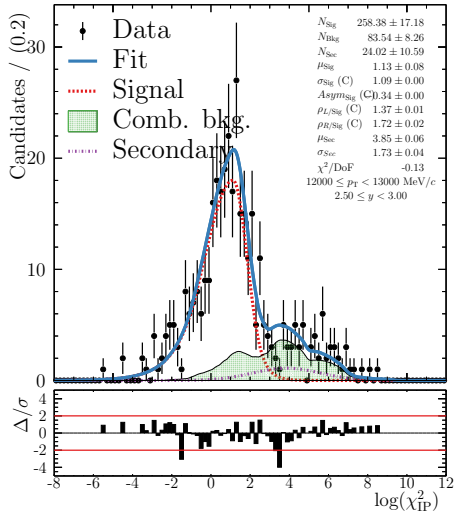

$12 \leq p_{\rm T} < 13\,{\rm GeV},\ 2.5 \leq y < 3.0$

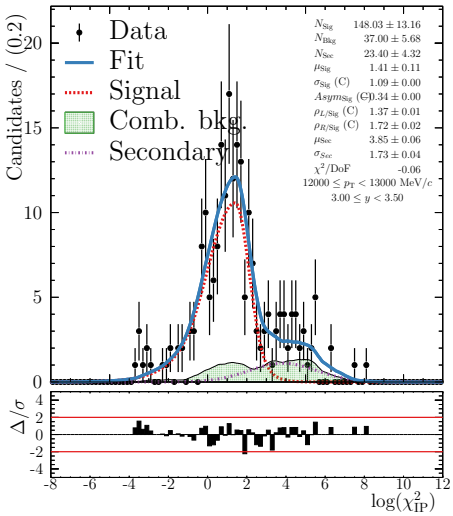

$12 \leq p_{\rm T} < 13\,{\rm GeV},\ 3.0 \leq y < 3.5$

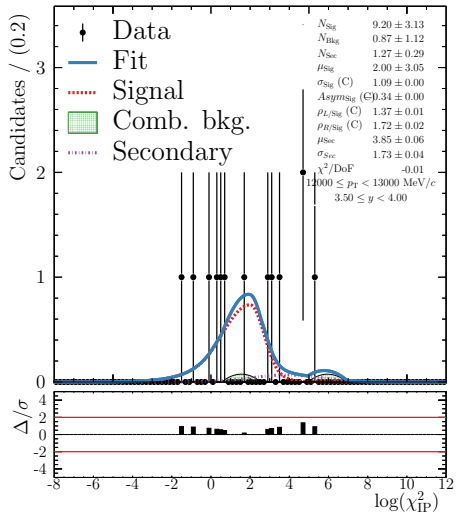

$12 \leq p_{\rm T} < 13\,{\rm GeV},\ 3.5 \leq y < 4.0$

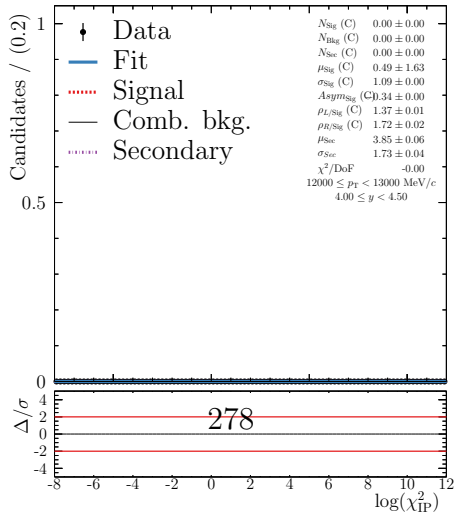

$12 \leq p_{\rm T} < 13\,{\rm GeV},\ 4.0 \leq y < 4.5$

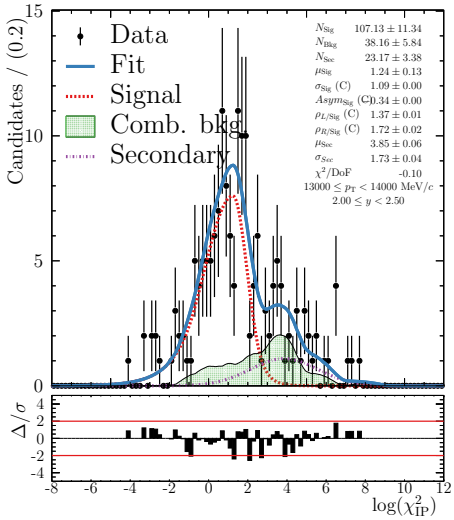

$13 \leq p_{\rm T} < 14\,{\rm GeV},\ 2.0 \leq y < 2.5$

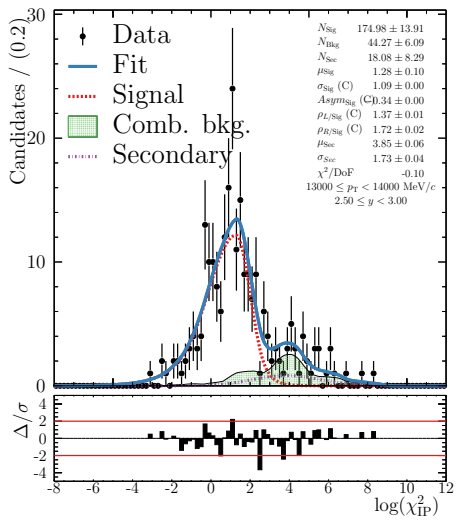

$13 \leq p_{\rm T} < 14\,{\rm GeV},\ 2.5 \leq y < 3.0$

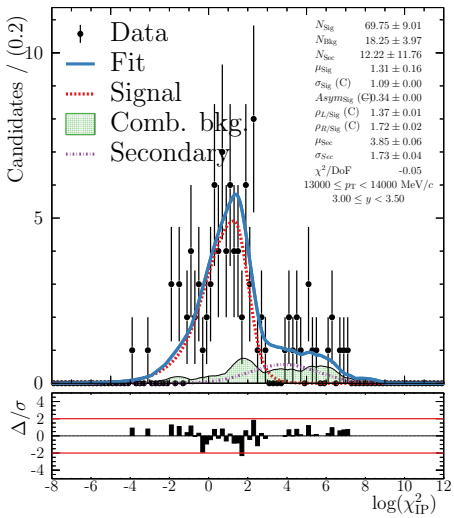

$13 \leq p_{\rm T} < 14\,{\rm GeV},\ 3.0 \leq y < 3.5$

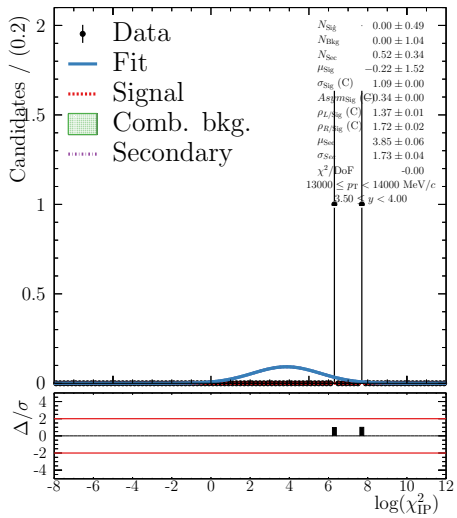

$13 \leq p_{\rm T} < 14\,{\rm GeV},\ 3.5 \leq y < 4.0$

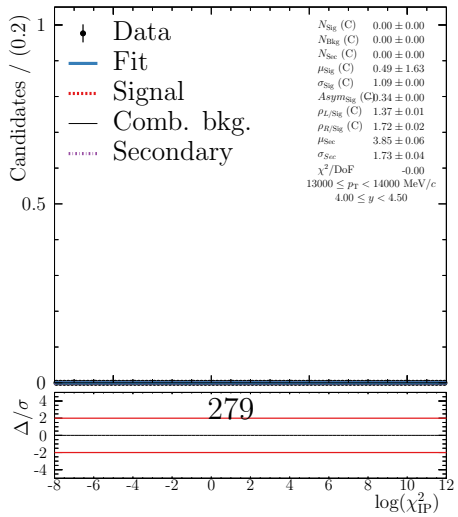

$13 \leq p_{\rm T} < 14\,{\rm GeV},\ 4.0 \leq y < 4.5$

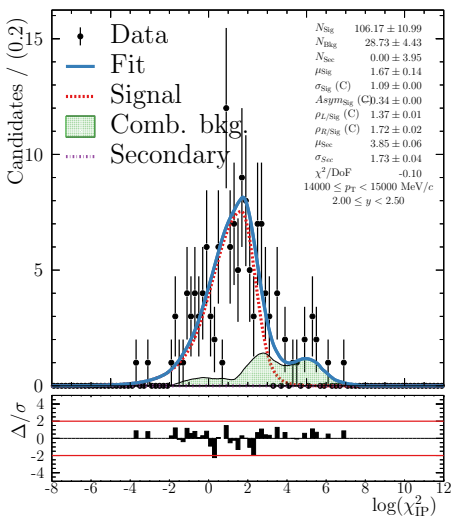

$14 \leq p_{\rm T} < 15\,{\rm GeV},\ 2.0 \leq y < 2.5$

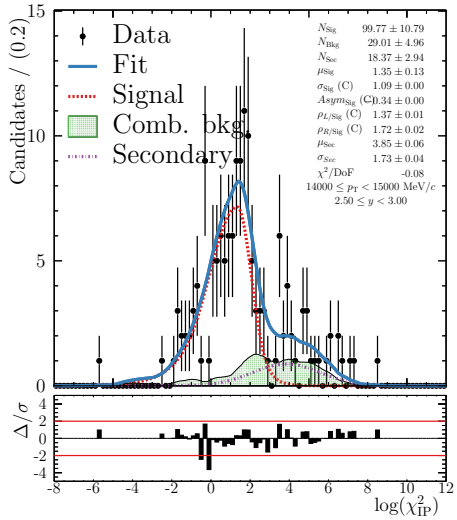

$14 \leq p_{\rm T} < 15\,{\rm GeV},\ 2.5 \leq y < 3.0$

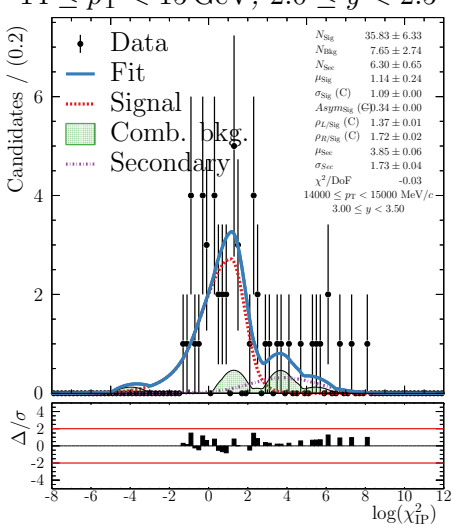

$14 \leq p_{\rm T} < 15\,{\rm GeV},\ 3.0 \leq y < 3.5$

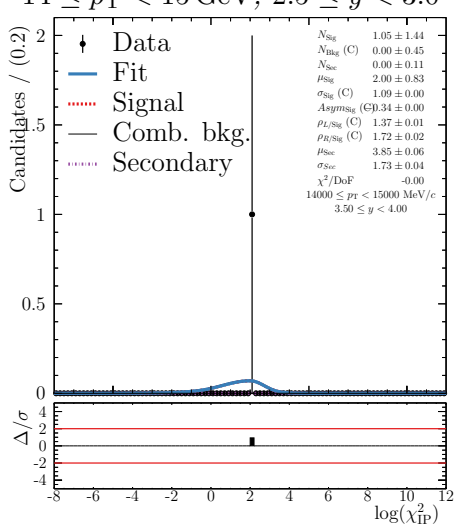

$14 \leq p_{\rm T} < 15\,{\rm GeV},\ 3.5 \leq y < 4.0$

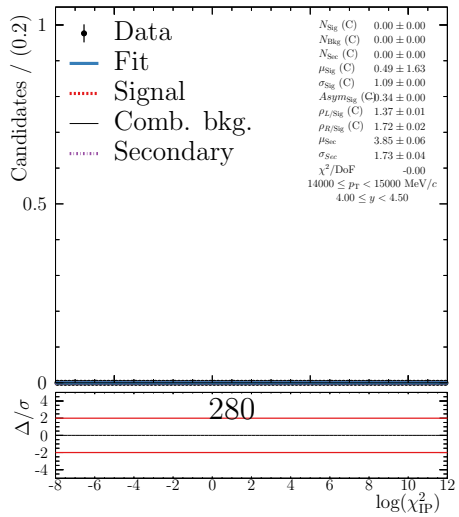

$14 \leq p_{\rm T} < 15\,{\rm GeV},\ 4.0 \leq y < 4.5$

Figure F.0: Fits to the fully selected $D^+ \to K^-K^+\pi^+$ $\ln\chi^2_{\rm IP}$ distribution per $p_{\rm T}$-y bin.

F.4 $D_s^+ \to \phi\pi^+$

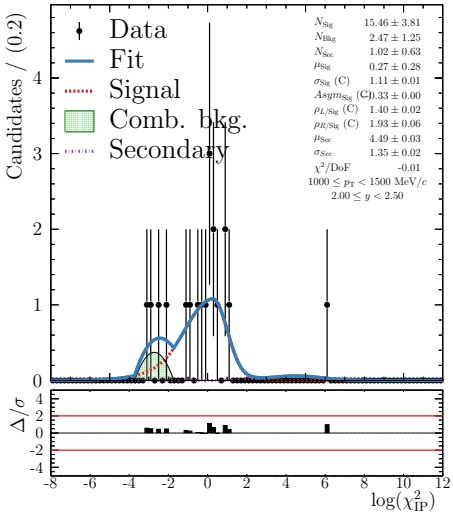

$1 \leq p_{\rm T} < 1.5\,{\rm GeV},\ 2.0 \leq y < 2.5$

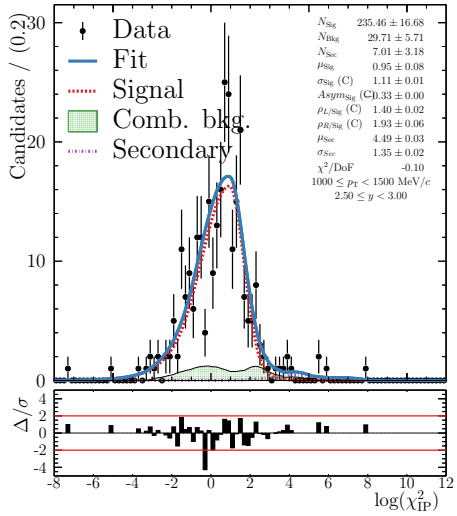

$1 \leq p_{\rm T} < 1.5\,{\rm GeV},\ 2.5 \leq y < 3.0$

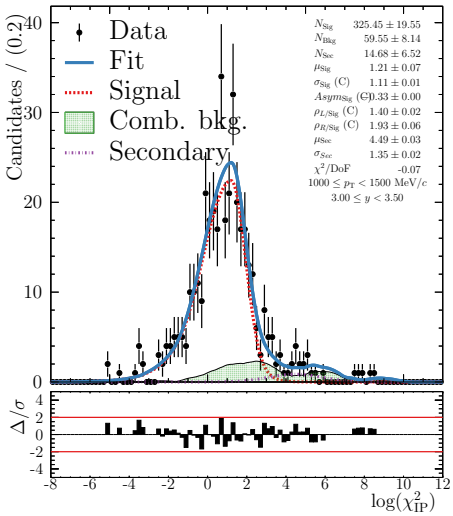

$1 \leq p_{\rm T} < 1.5\,{\rm GeV},\ 3.0 \leq y < 3.5$

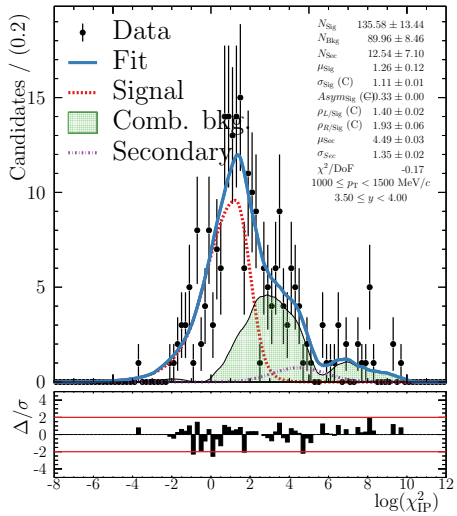

$1 \leq p_{\rm T} < 1.5\,{\rm GeV},\ 3.5 \leq y < 4.0$

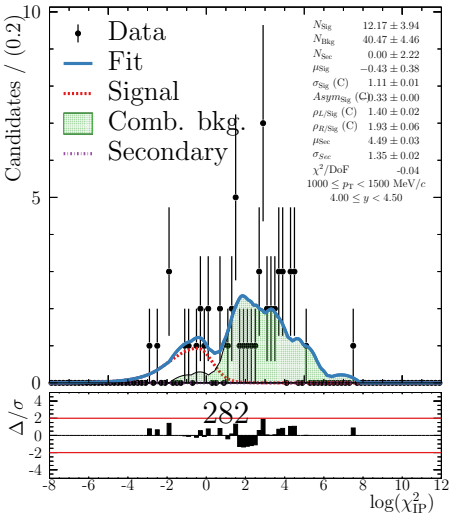

$1 \leq p_{\rm T} < 1.5\,{\rm GeV},\ 4.0 \leq y < 4.5$

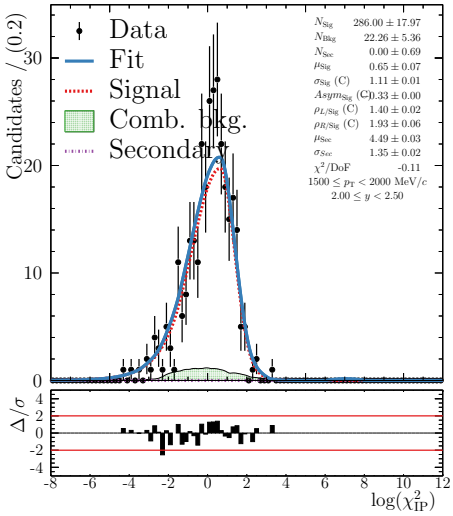

$1.5 \leq p_{\rm T} < 2\,{\rm GeV},\ 2.0 \leq y < 2.5$

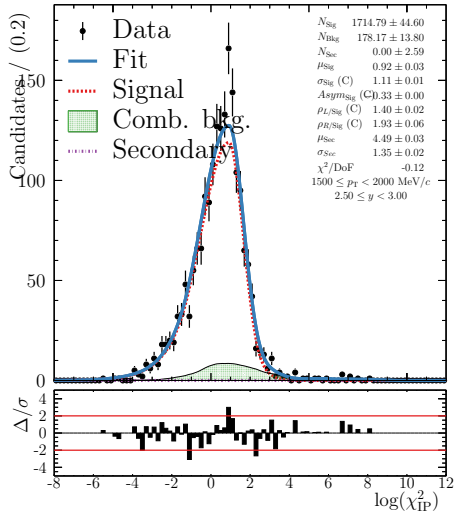

$1.5 \leq p_{\rm T} < 2\,{\rm GeV},\ 2.5 \leq y < 3.0$

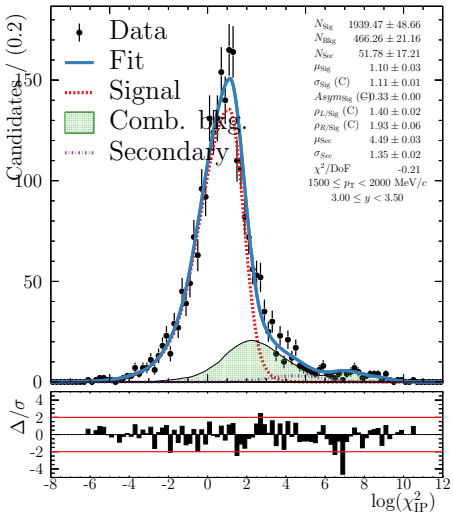

$1.5 \leq p_{\rm T} < 2\,{\rm GeV},\ 3.0 \leq y < 3.5$

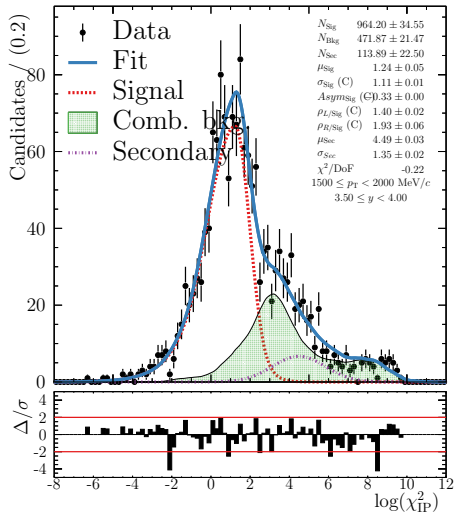

$1.5 \leq p_{\rm T} < 2\,{\rm GeV},\ 3.5 \leq y < 4.0$

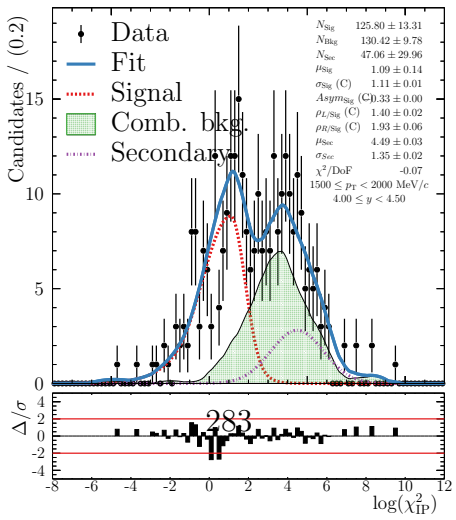

$1.5 \leq p_{\rm T} < 2\,{\rm GeV},\ 4.0 \leq y < 4.5$

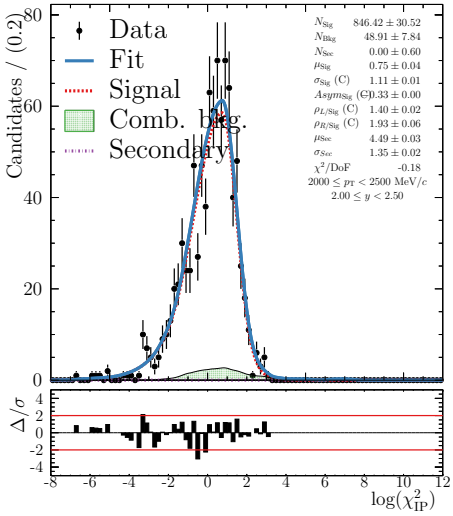

$2 \leq p_{\rm T} < 2.5\,{\rm GeV},\ 2.0 \leq y < 2.5$

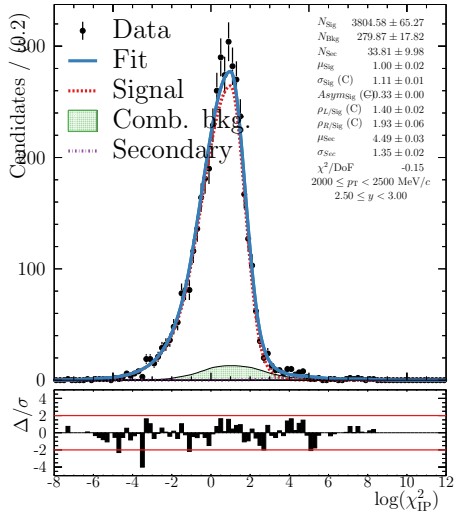

$2 \leq p_{\rm T} < 2.5\,{\rm GeV},\ 2.5 \leq y < 3.0$

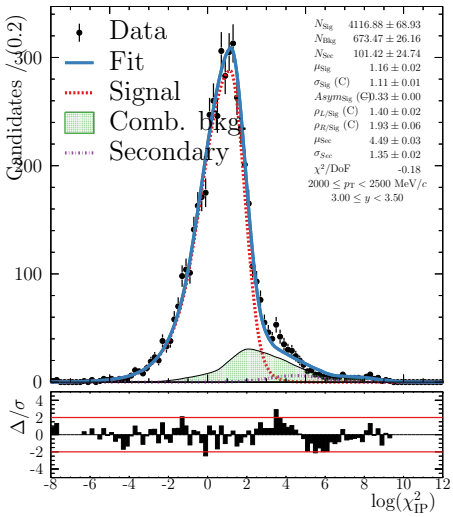

$2 \leq p_{\rm T} < 2.5\,{\rm GeV},\ 3.0 \leq y < 3.5$

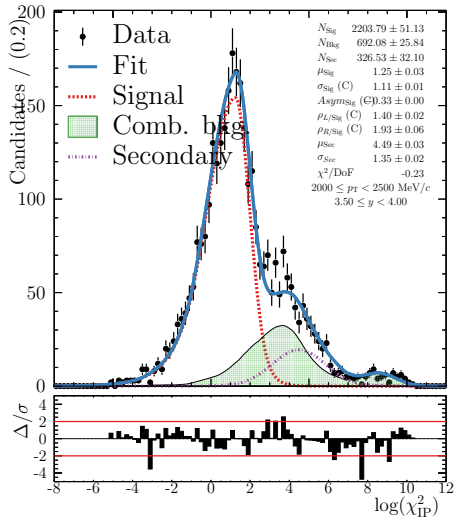

$2 \leq p_{\rm T} < 2.5\,{\rm GeV},\ 3.5 \leq y < 4.0$

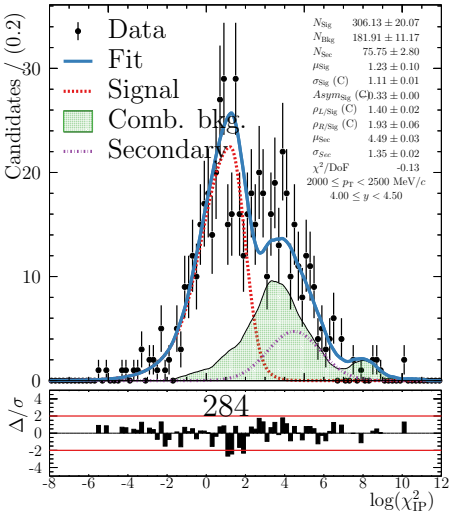

$2 \leq p_{\rm T} < 2.5\,{\rm GeV},\ 4.0 \leq y < 4.5$

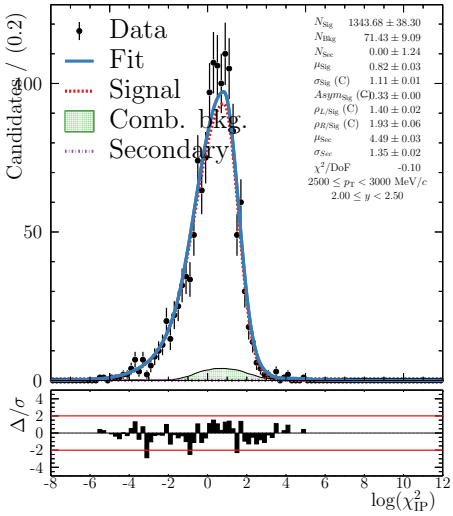

$2.5 \leq p_{\rm T} < 3\,{\rm GeV},\ 2.0 \leq y < 2.5$

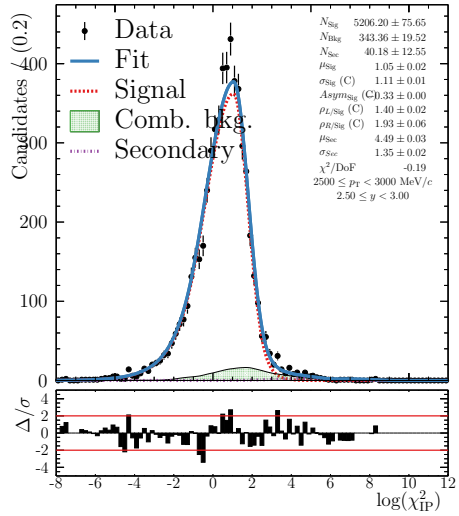

$2.5 \leq p_{\rm T} < 3\,{\rm GeV},\ 2.5 \leq y < 3.0$

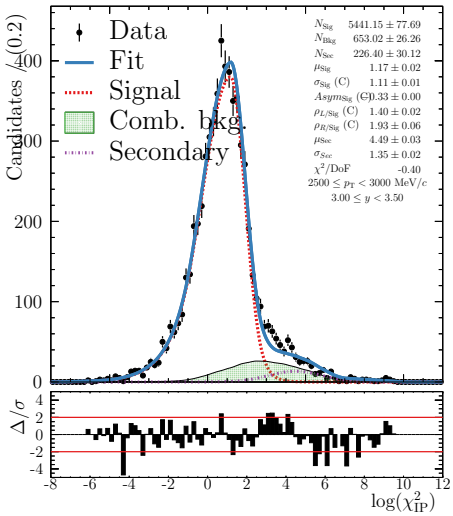

$2.5 \leq p_{\rm T} < 3\,{\rm GeV},\ 3.0 \leq y < 3.5$

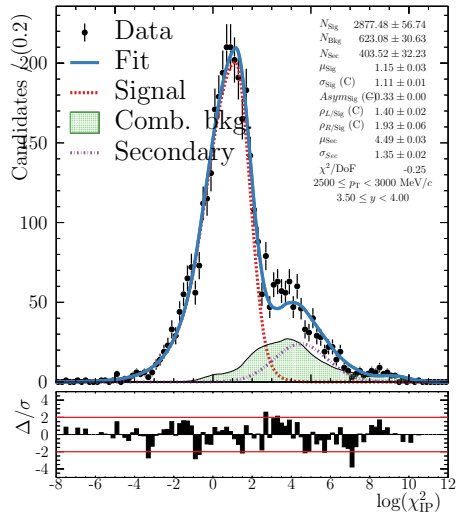

$2.5 \leq p_{\rm T} < 3\,{\rm GeV},\ 3.5 \leq y < 4.0$

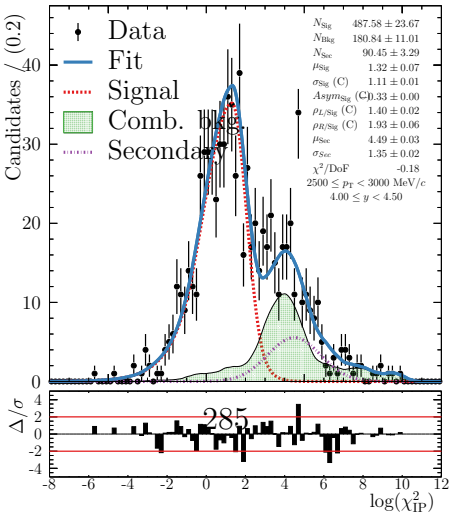

$2.5 \leq p_{\rm T} < 3\,{\rm GeV},\ 4.0 \leq y < 4.5$

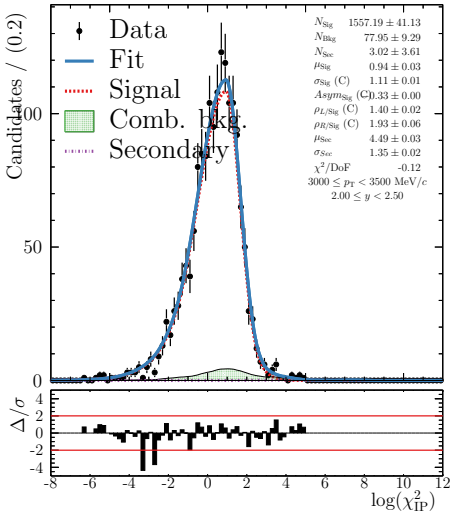

$3 \leq p_{\rm T} < 3.5\,\text{GeV},\ 2.0 \leq y < 2.5$

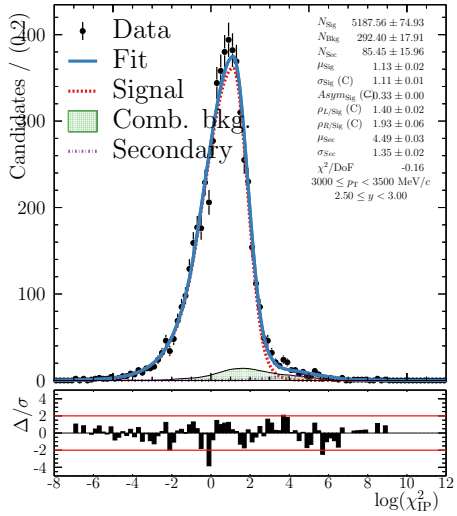

$3 \leq p_{\rm T} < 3.5\,\text{GeV},\ 2.5 \leq y < 3.0$

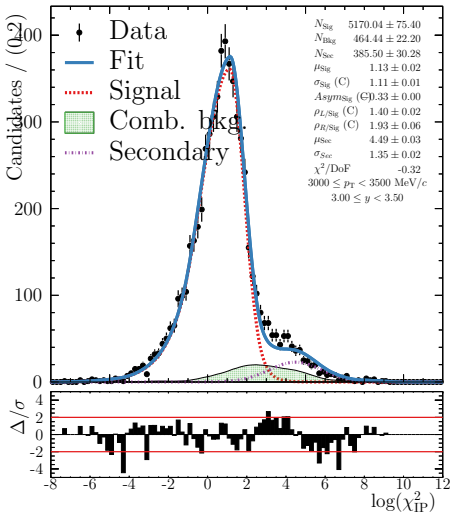

$3 \leq p_{\rm T} < 3.5\,\text{GeV},\ 3.0 \leq y < 3.5$

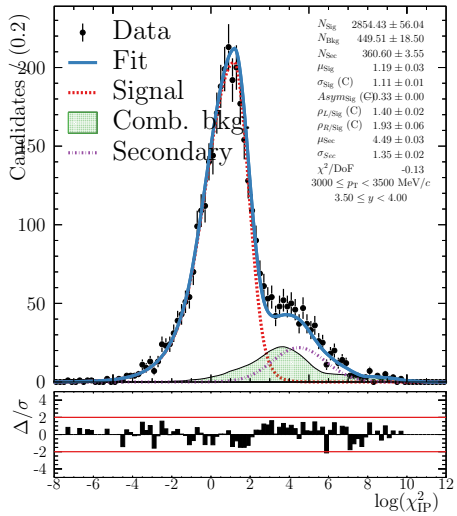

$3 \leq p_{\rm T} < 3.5\,\text{GeV},\ 3.5 \leq y < 4.0$

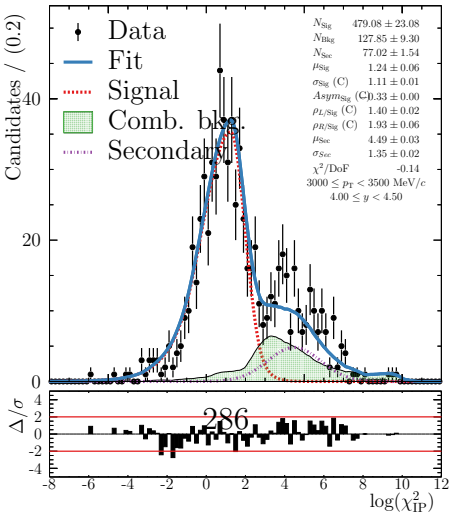

$3 \leq p_{\rm T} < 3.5\,\text{GeV},\ 4.0 \leq y < 4.5$

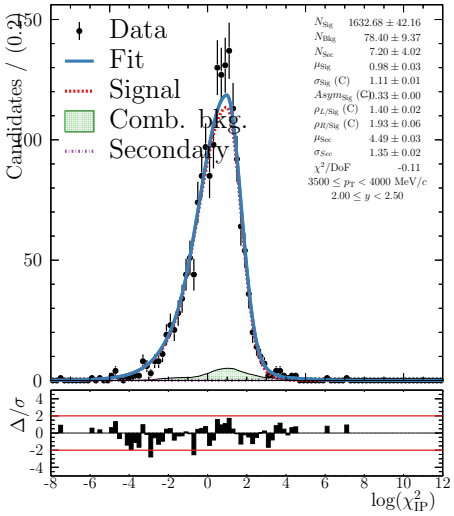

$3.5 \leq p_{\rm T} < 4\,{\rm GeV},\ 2.0 \leq y < 2.5$

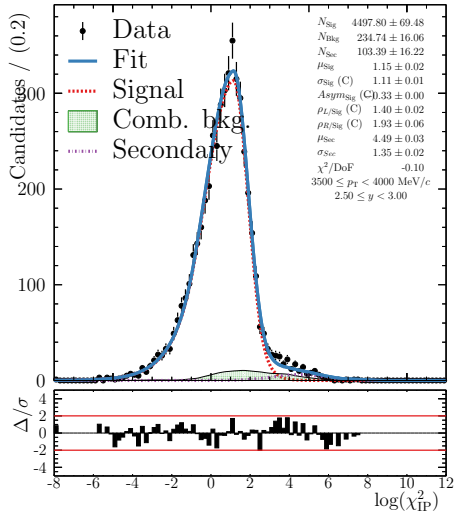

$3.5 \leq p_{\rm T} < 4\,{\rm GeV},\ 2.5 \leq y < 3.0$

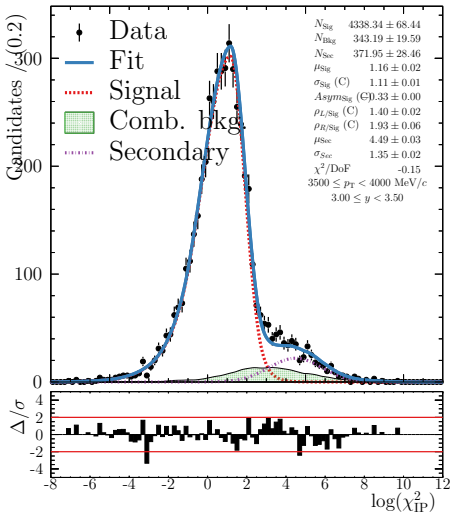

$3.5 \leq p_{\rm T} < 4\,{\rm GeV},\ 3.0 \leq y < 3.5$

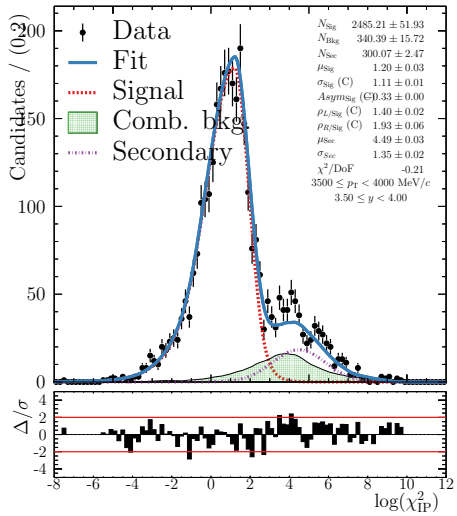

$3.5 \leq p_{\rm T} < 4\,{\rm GeV},\ 3.5 \leq y < 4.0$

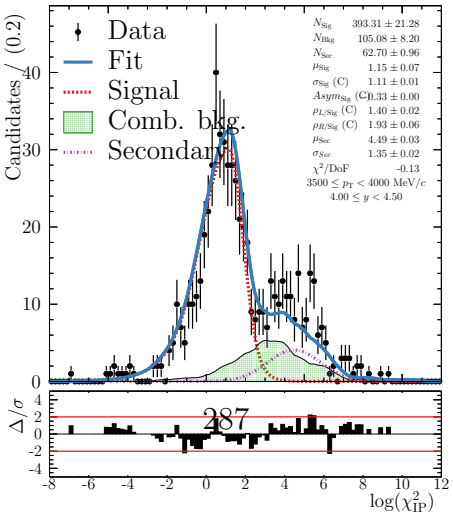

$3.5 \leq p_{\rm T} < 4\,{\rm GeV},\ 4.0 \leq y < 4.5$

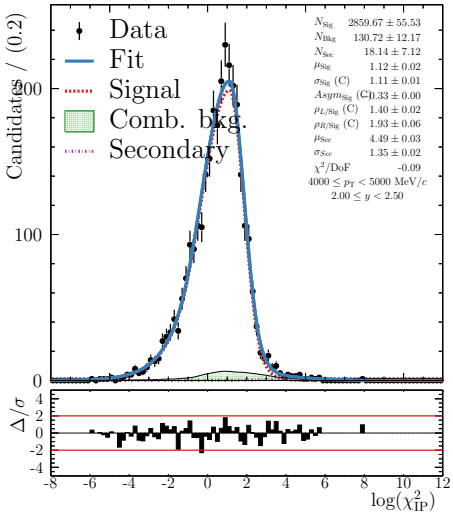

$4 \leq p_{\rm T} < 5\,{\rm GeV},\ 2.0 \leq y < 2.5$

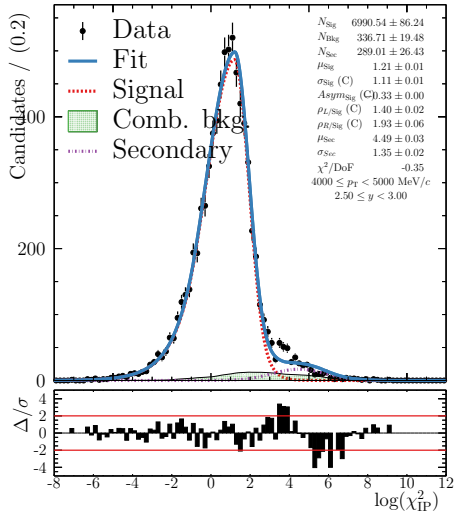

$4 \leq p_{\rm T} < 5\,{\rm GeV},\ 2.5 \leq y < 3.0$

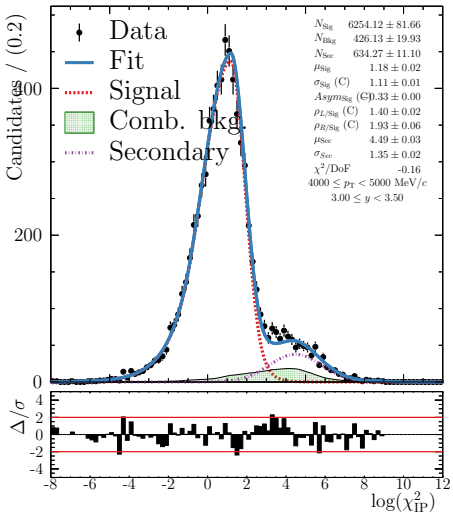

$4 \leq p_{\rm T} < 5\,{\rm GeV},\ 3.0 \leq y < 3.5$

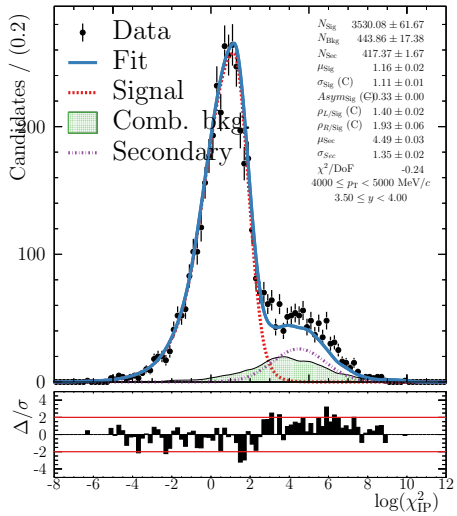

$4 \leq p_{\rm T} < 5\,{\rm GeV},\ 3.5 \leq y < 4.0$

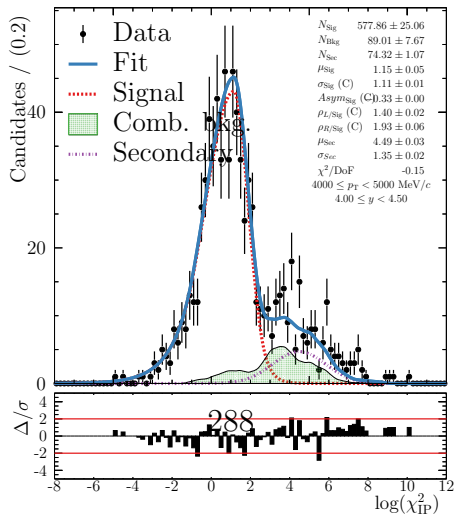

$4 \leq p_{\rm T} < 5\,{\rm GeV},\ 4.0 \leq y < 4.5$

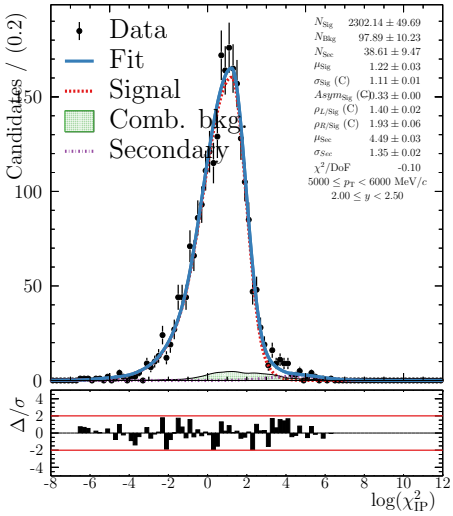

$5 \leq p_{\rm T} < 6\,{\rm GeV},\ 2.0 \leq y < 2.5$

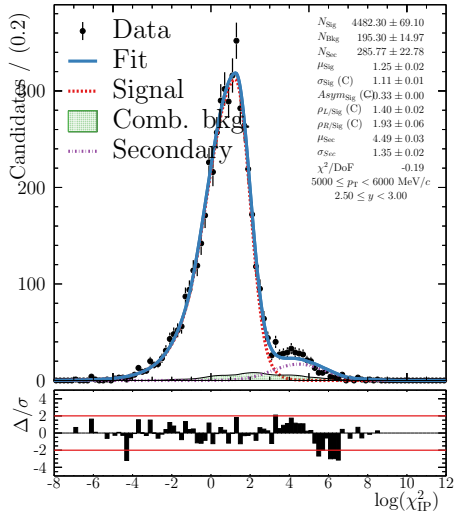

$5 \leq p_{\rm T} < 6\,{\rm GeV},\ 2.5 \leq y < 3.0$

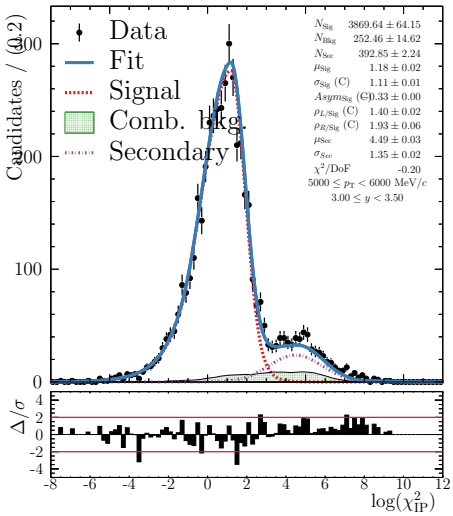

$5 \leq p_{\rm T} < 6\,{\rm GeV},\ 3.0 \leq y < 3.5$

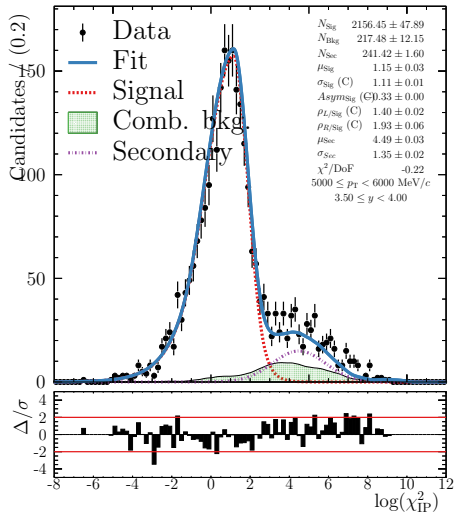

$5 \leq p_{\rm T} < 6\,{\rm GeV},\ 3.5 \leq y < 4.0$

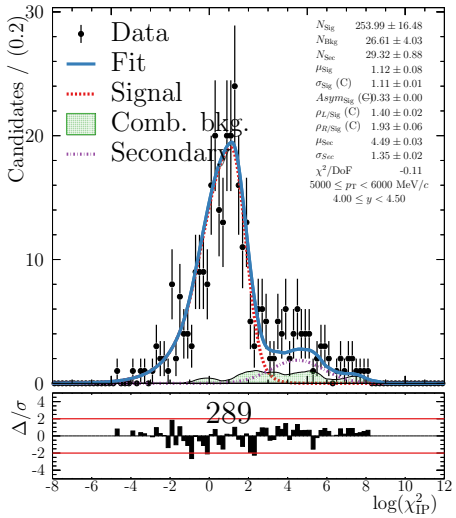

$5 \leq p_{\rm T} < 6\,{\rm GeV},\ 4.0 \leq y < 4.5$

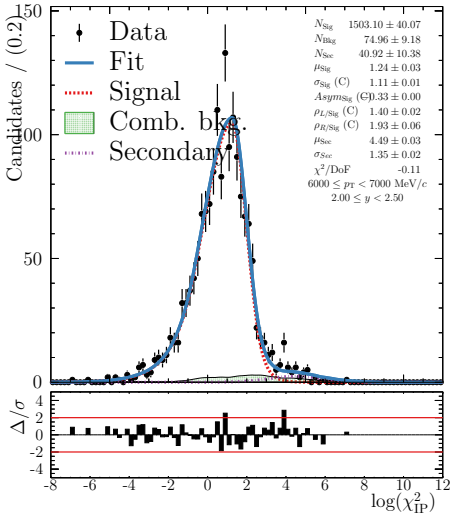

$6 \leq p_{\rm T} < 7\,{\rm GeV},\ 2.0 \leq y < 2.5$

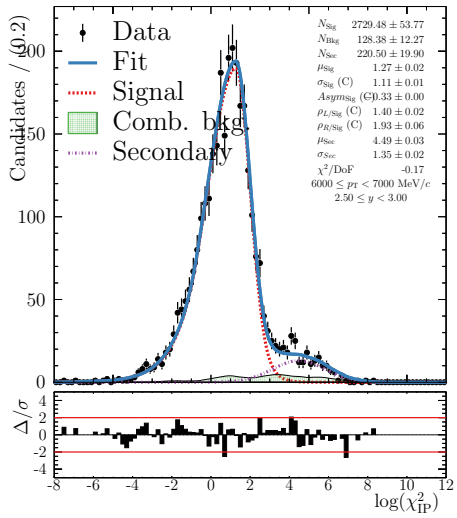

$6 \leq p_{\rm T} < 7\,{\rm GeV},\ 2.5 \leq y < 3.0$

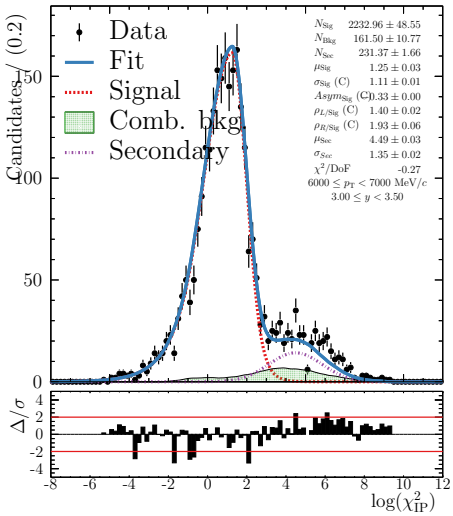

$6 \leq p_{\rm T} < 7\,{\rm GeV},\ 3.0 \leq y < 3.5$

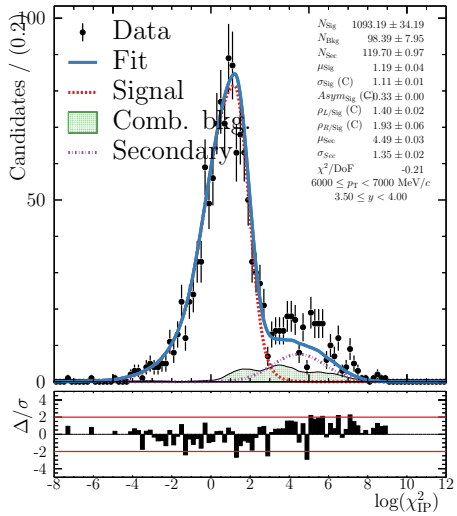

$6 \leq p_{\rm T} < 7\,{\rm GeV},\ 3.5 \leq y < 4.0$

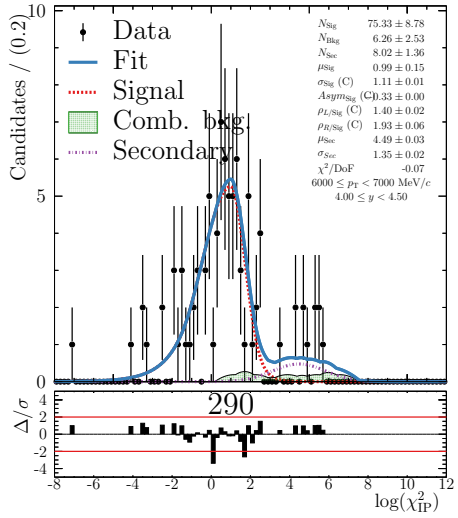

$6 \leq p_{\rm T} < 7\,{\rm GeV},\ 4.0 \leq y < 4.5$

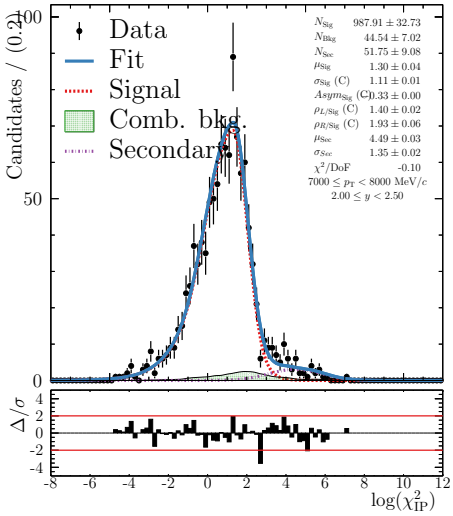

$7 \le p_{\rm T} < 8\,{\rm GeV},\ 2.0 \le y < 2.5$

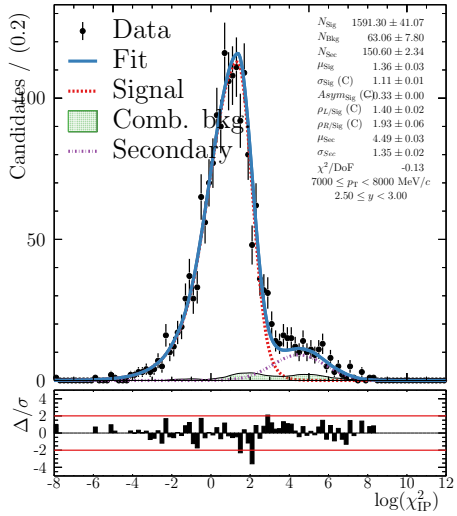

$7 \le p_{\rm T} < 8\,{\rm GeV},\ 2.5 \le y < 3.0$

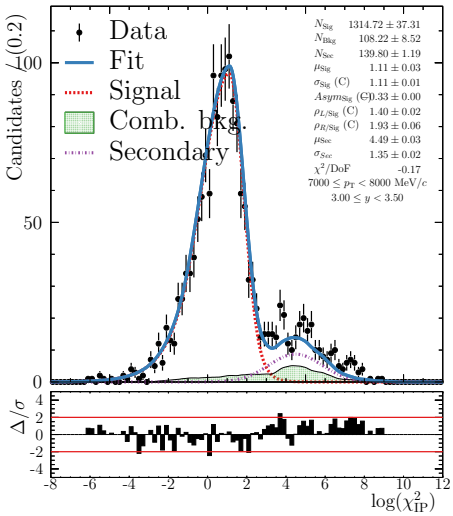

$7 \le p_{\rm T} < 8\,{\rm GeV},\ 3.0 \le y < 3.5$

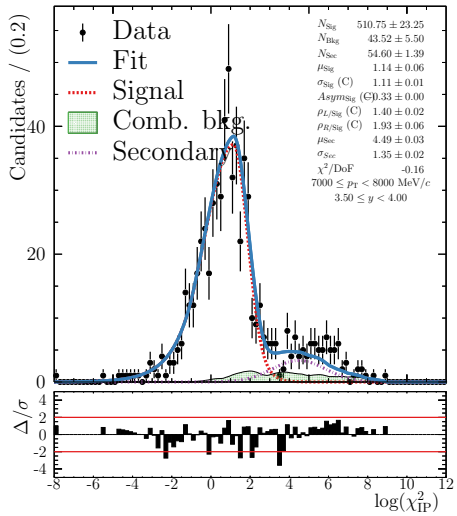

$7 \le p_{\rm T} < 8\,{\rm GeV},\ 3.5 \le y < 4.0$

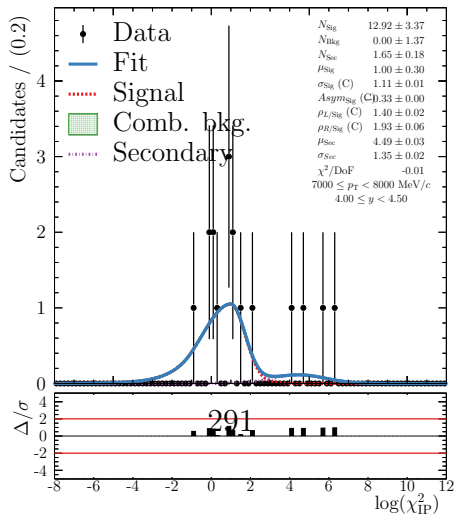

$7 \le p_{\rm T} < 8\,{\rm GeV},\ 4.0 \le y < 4.5$

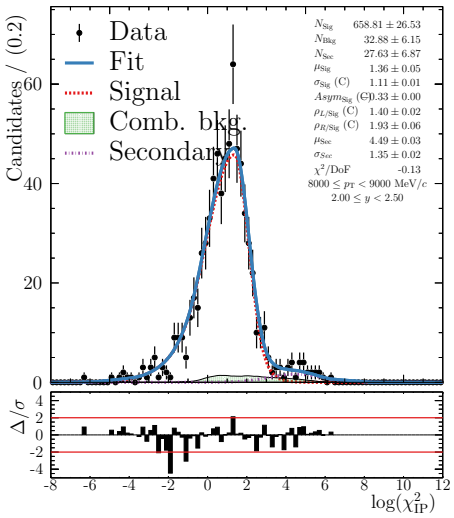

$8 \le p_{\rm T} < 9\,{\rm GeV},\ 2.0 \le y < 2.5$

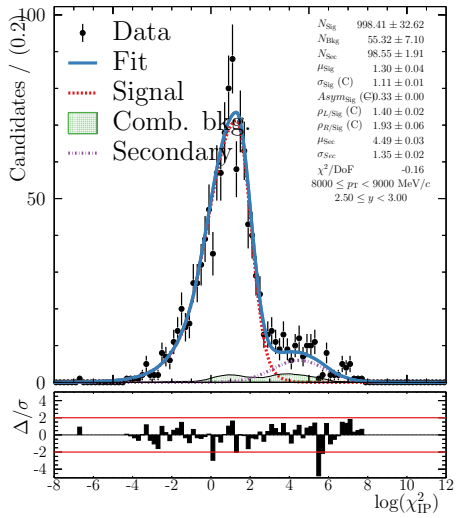

$8 \le p_{\rm T} < 9\,{\rm GeV},\ 2.5 \le y < 3.0$

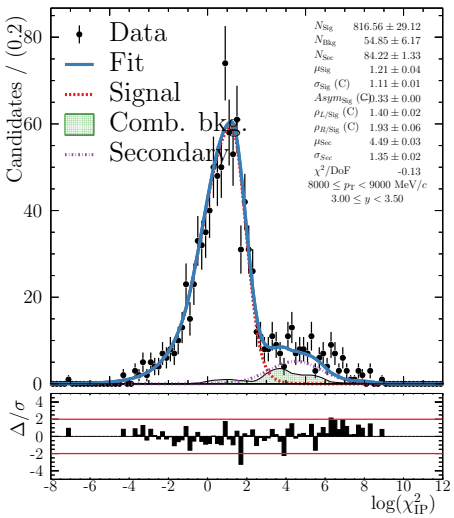

$8 \le p_{\rm T} < 9\,{\rm GeV},\ 3.0 \le y < 3.5$

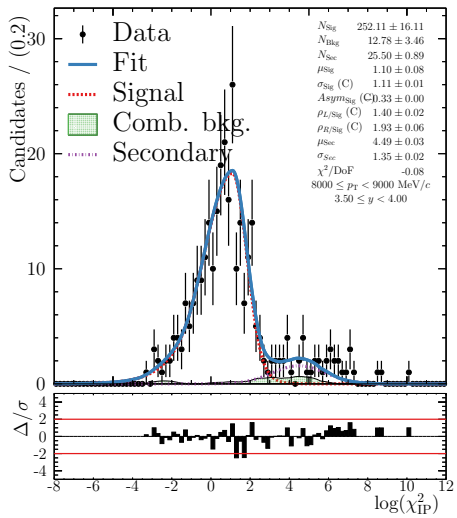

$8 \le p_{\rm T} < 9\,{\rm GeV},\ 3.5 \le y < 4.0$

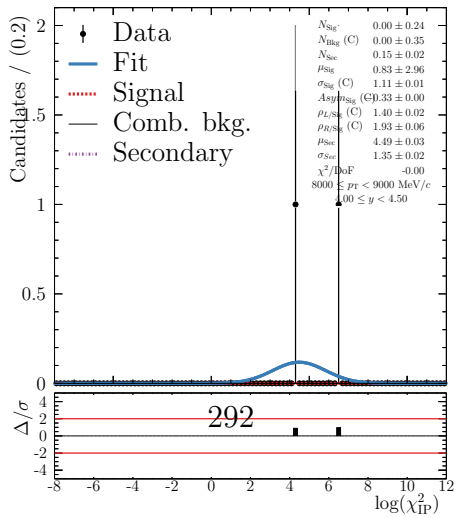

$8 \le p_{\rm T} < 9\,{\rm GeV},\ 4.0 \le y < 4.5$

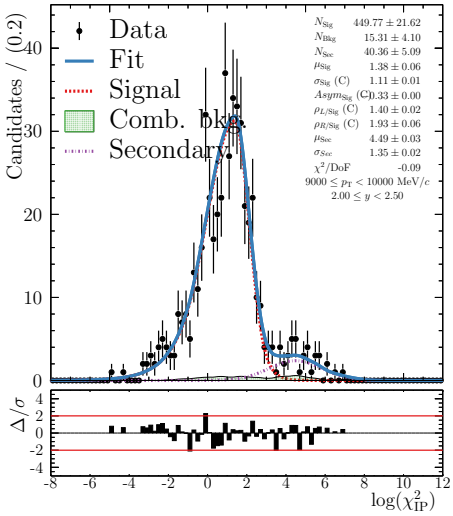

$9 \le p_{\rm T} < 10\,{\rm GeV},\ 2.0 \le y < 2.5$

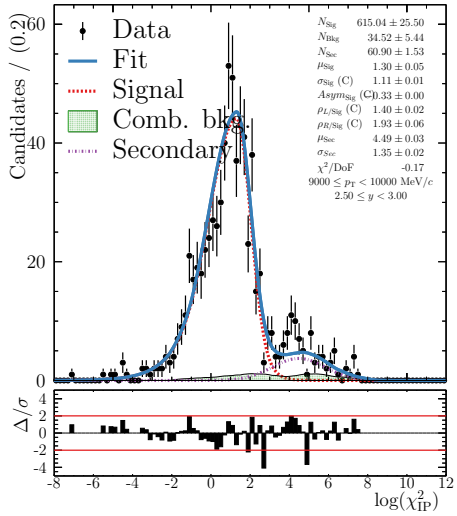

$9 \le p_{\rm T} < 10\,{\rm GeV},\ 2.5 \le y < 3.0$

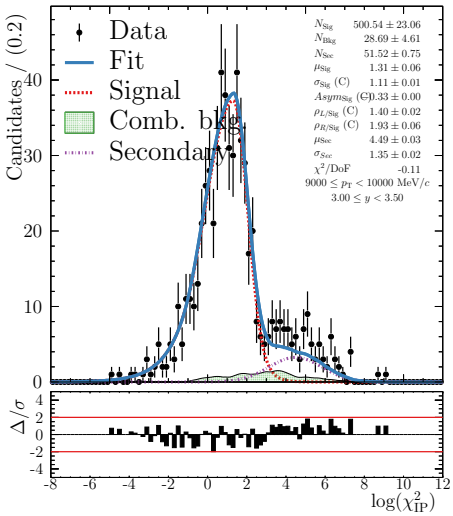

$9 \le p_{\rm T} < 10\,{\rm GeV},\ 3.0 \le y < 3.5$

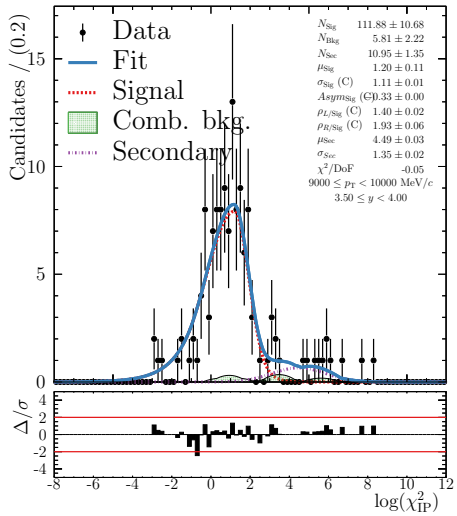

$9 \le p_{\rm T} < 10\,{\rm GeV},\ 3.5 \le y < 4.0$

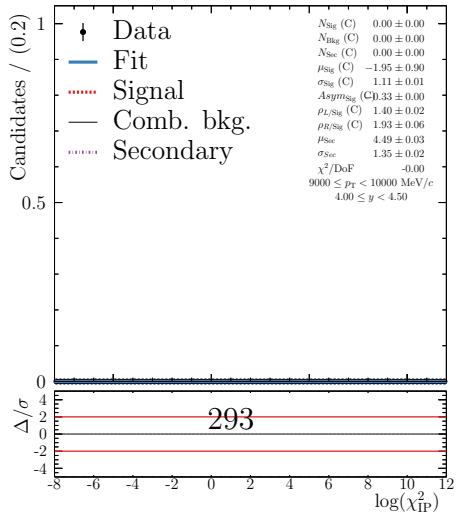

$9 \le p_{\rm T} < 10\,{\rm GeV},\ 4.0 \le y < 4.5$

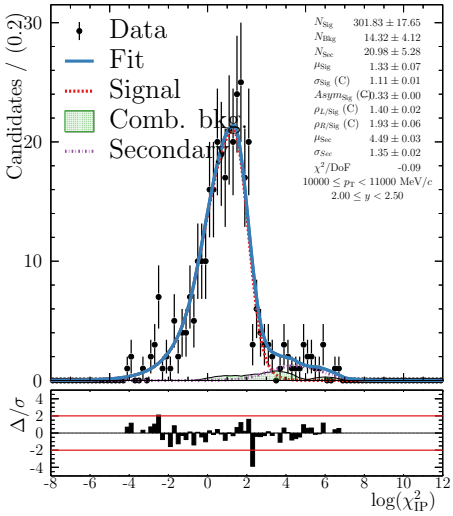

$10 \leq p_{\rm T} < 11\,{\rm GeV},\ 2.0 \leq y < 2.5$

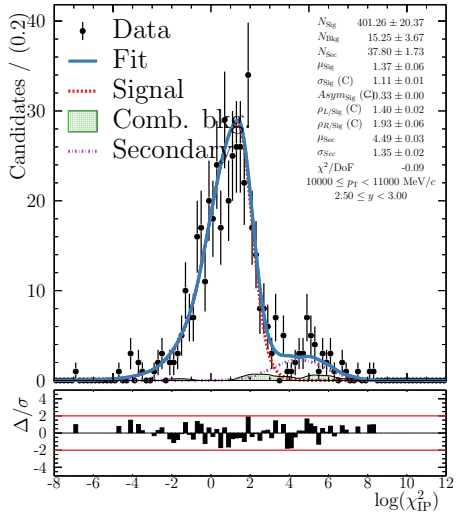

$10 \leq p_{\rm T} < 11\,{\rm GeV},\ 2.5 \leq y < 3.0$

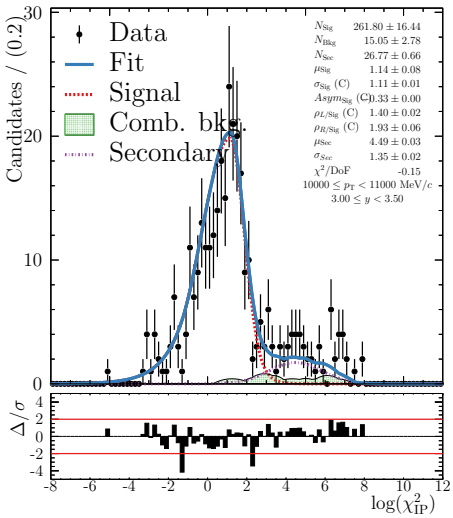

$10 \leq p_{\rm T} < 11\,{\rm GeV},\ 3.0 \leq y < 3.5$

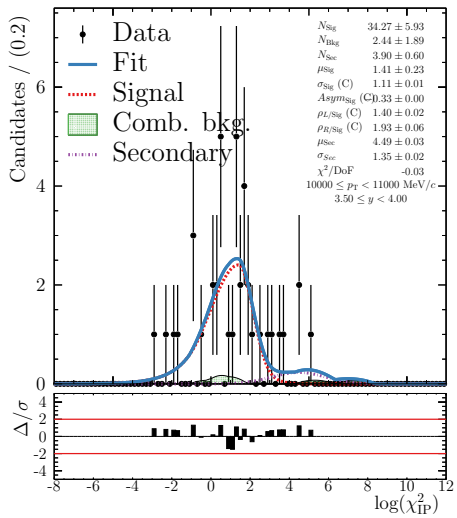

$10 \leq p_{\rm T} < 11\,{\rm GeV},\ 3.5 \leq y < 4.0$

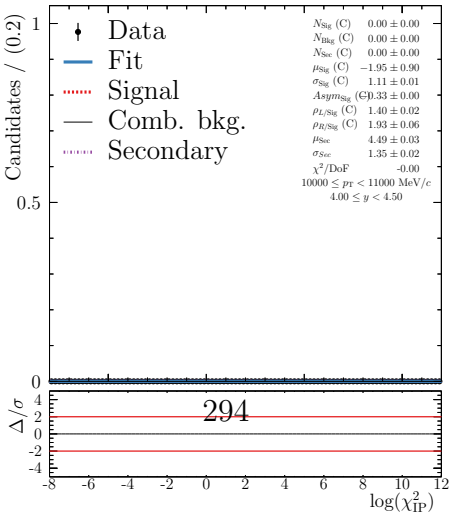

$10 \leq p_{\rm T} < 11\,{\rm GeV},\ 4.0 \leq y < 4.5$

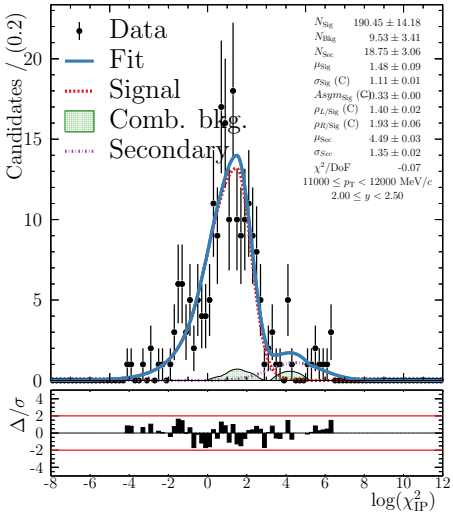

$11 \leq p_{\rm T} < 12\,{\rm GeV},\ 2.0 \leq y < 2.5$

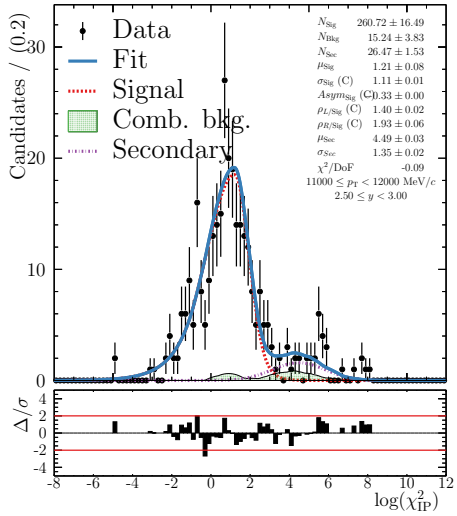

$11 \leq p_{\rm T} < 12\,{\rm GeV},\ 2.5 \leq y < 3.0$

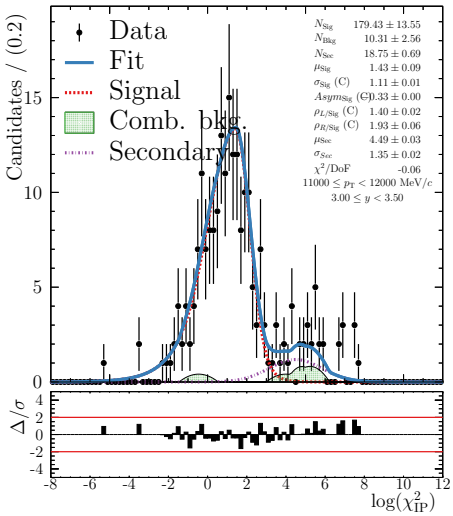

$11 \leq p_{\rm T} < 12\,{\rm GeV},\ 3.0 \leq y < 3.5$

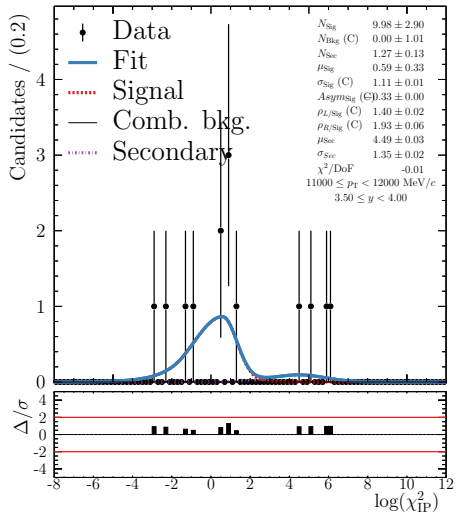

$11 \leq p_{\rm T} < 12\,{\rm GeV},\ 3.5 \leq y < 4.0$

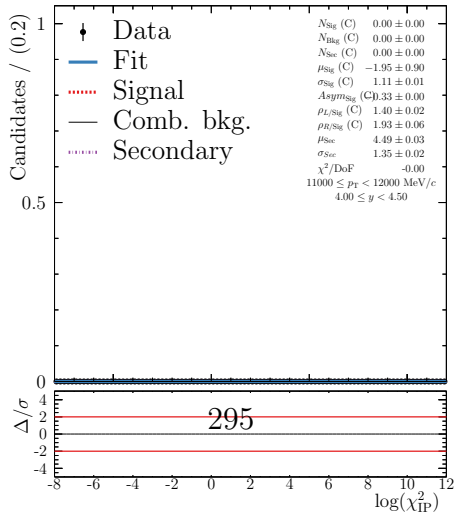

$11 \leq p_{\rm T} < 12\,{\rm GeV},\ 4.0 \leq y < 4.5$

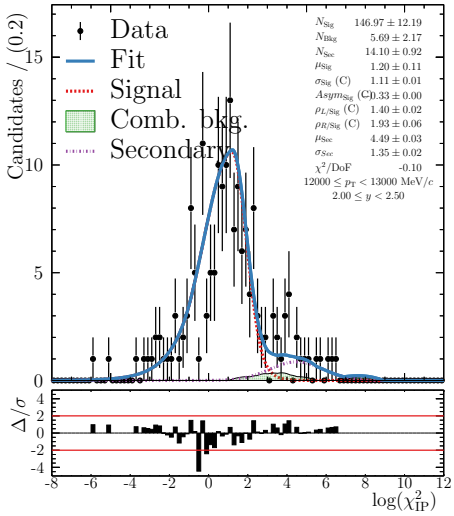

$12 \leq p_{\rm T} < 13\,{\rm GeV},\ 2.0 \leq y < 2.5$

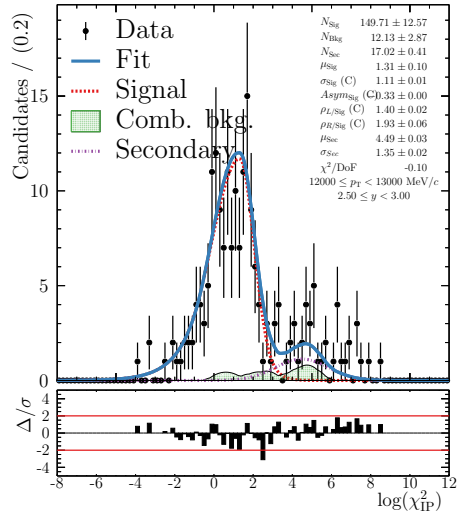

$12 \leq p_{\rm T} < 13\,{\rm GeV},\ 2.5 \leq y < 3.0$

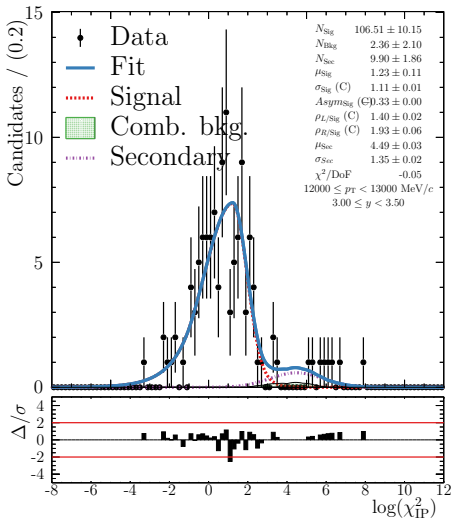

$12 \leq p_{\rm T} < 13\,{\rm GeV},\ 3.0 \leq y < 3.5$

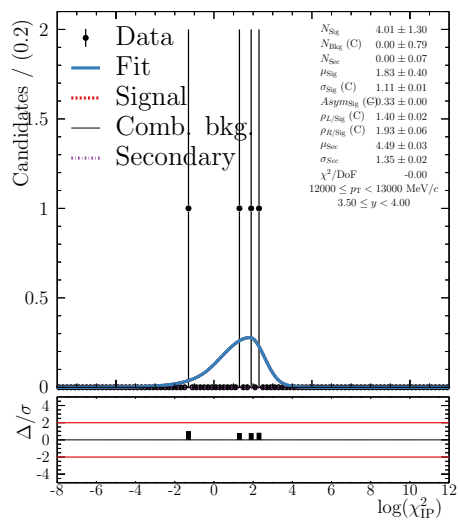

$12 \leq p_{\rm T} < 13\,{\rm GeV},\ 3.5 \leq y < 4.0$

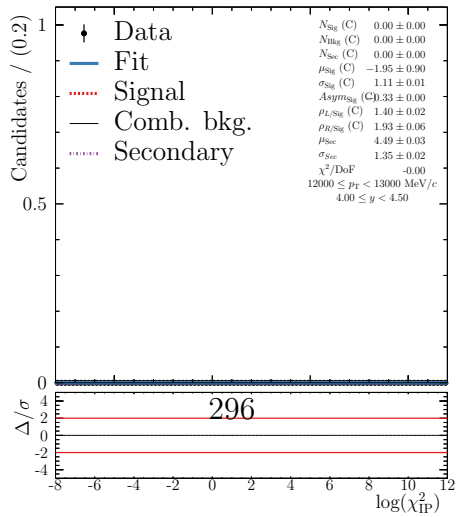

$12 \leq p_{\rm T} < 13\,{\rm GeV},\ 4.0 \leq y < 4.5$

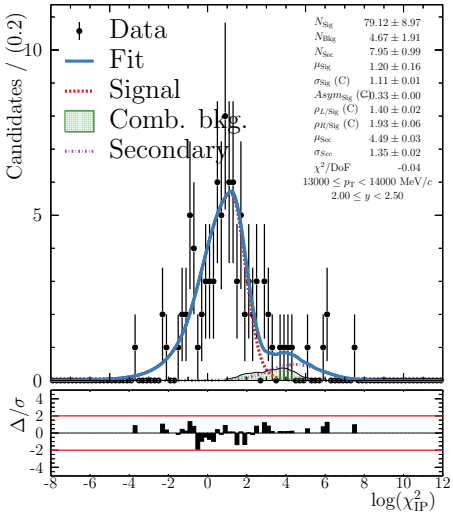

$13 \leq p_{\rm T} < 14\,{\rm GeV},\ 2.0 \leq y < 2.5$

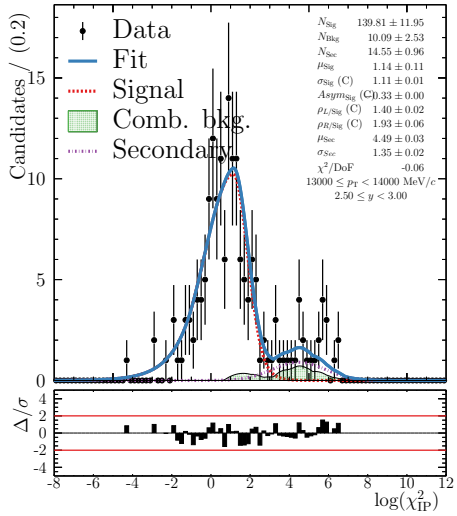

$13 \leq p_{\rm T} < 14\,{\rm GeV},\ 2.5 \leq y < 3.0$

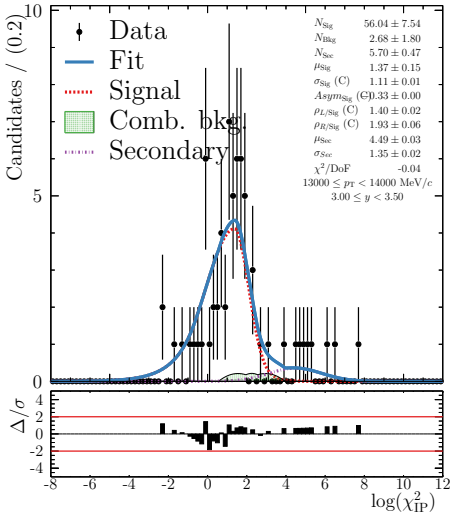

$13 \leq p_{\rm T} < 14\,{\rm GeV},\ 3.0 \leq y < 3.5$

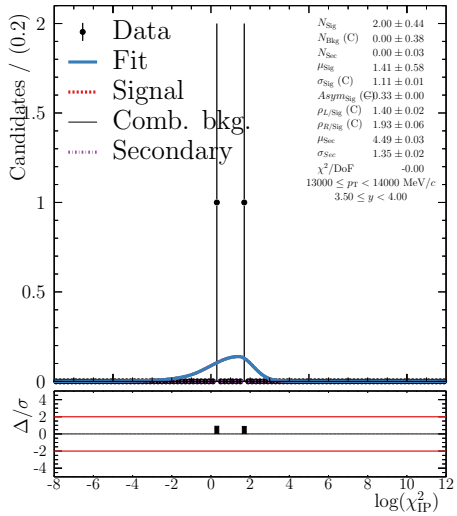

$13 \leq p_{\rm T} < 14\,{\rm GeV},\ 3.5 \leq y < 4.0$

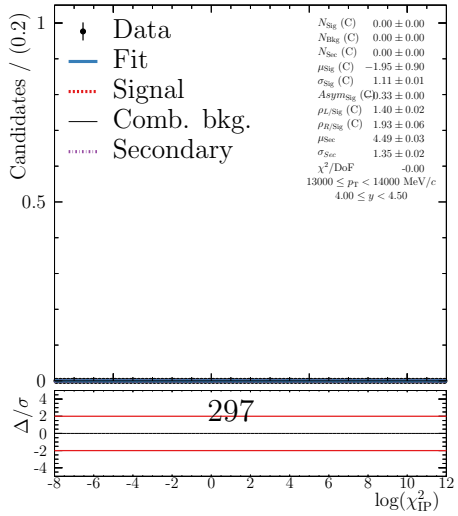

$13 \leq p_{\rm T} < 14\,{\rm GeV},\ 4.0 \leq y < 4.5$

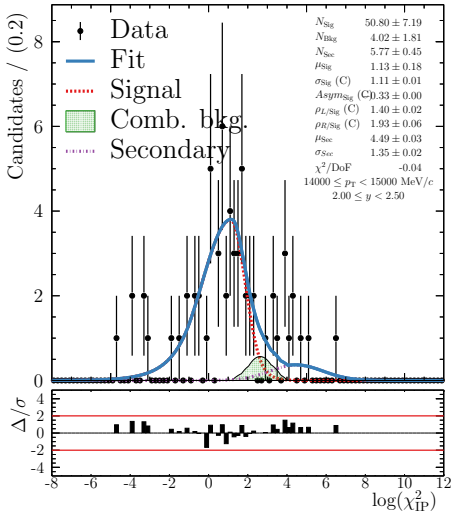

$14 \leq p_{\rm T} < 15\,{\rm GeV},\ 2.0 \leq y < 2.5$

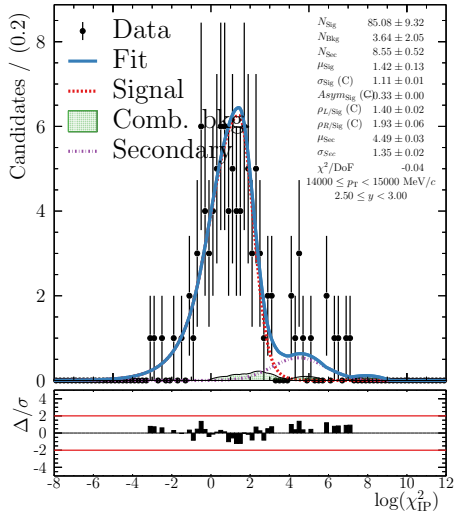

$14 \leq p_{\rm T} < 15\,{\rm GeV},\ 2.5 \leq y < 3.0$

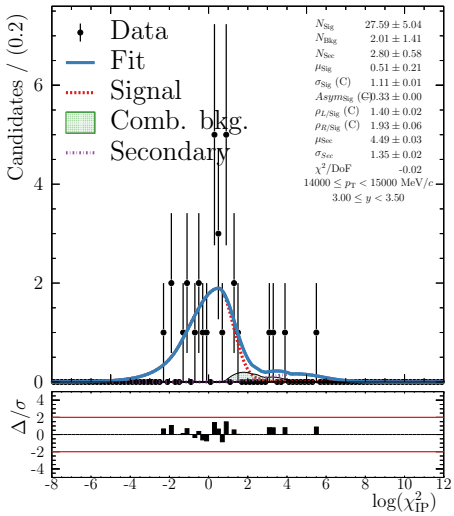

$14 \leq p_{\rm T} < 15\,{\rm GeV},\ 3.0 \leq y < 3.5$

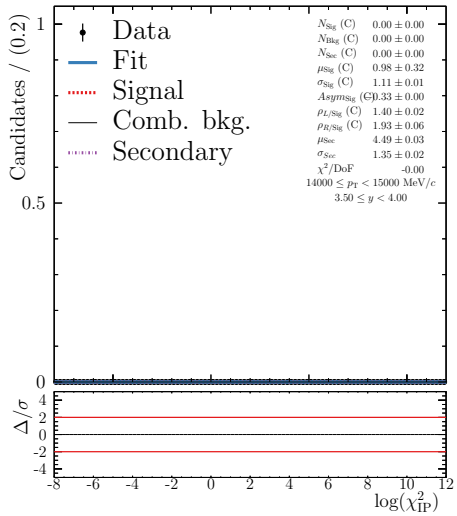

$14 \leq p_{\rm T} < 15\,{\rm GeV},\ 3.5 \leq y < 4.0$

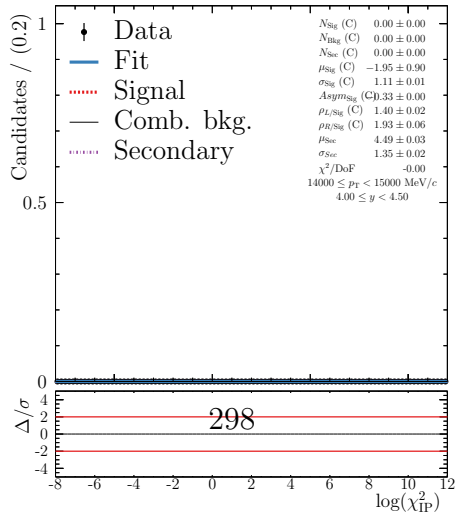

$14 \leq p_{\rm T} < 15\,{\rm GeV},\ 4.0 \leq y < 4.5$

Figure F.0: Fits to the fully selected $D_s^+ \to \phi\pi^+$ $\ln\chi^2_{\rm IP}$ distribution per $p_{\rm T}$-y bin.

F.5 $D_s^+ \to K^- K^+ \pi^+$

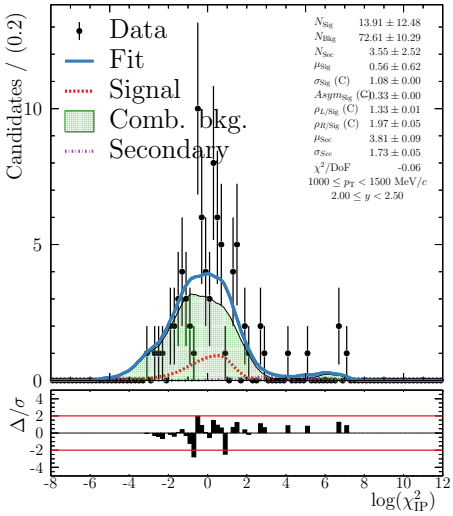

$1 \leq p_{\rm T} < 1.5\,{\rm GeV},\ 2.0 \leq y < 2.5$

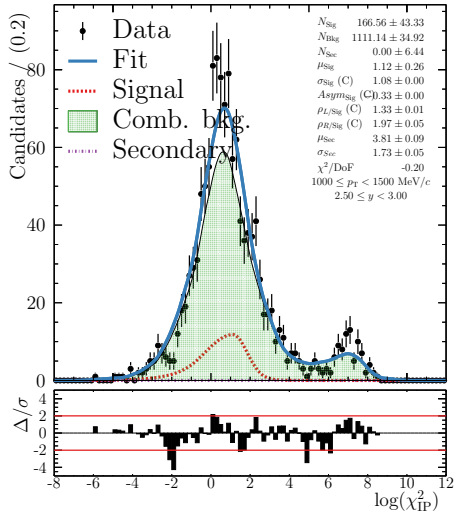

$1 \leq p_{\rm T} < 1.5\,{\rm GeV},\ 2.5 \leq y < 3.0$

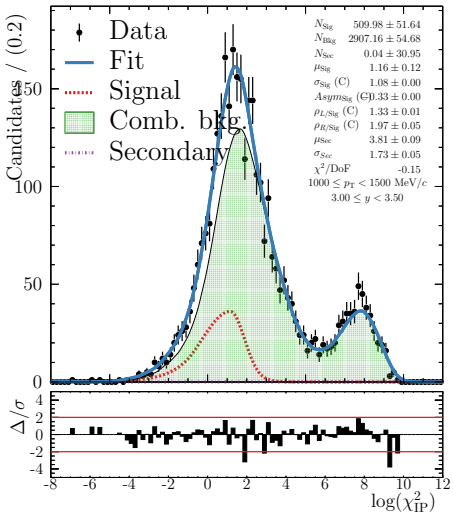

$1 \leq p_{\rm T} < 1.5\,{\rm GeV},\ 3.0 \leq y < 3.5$

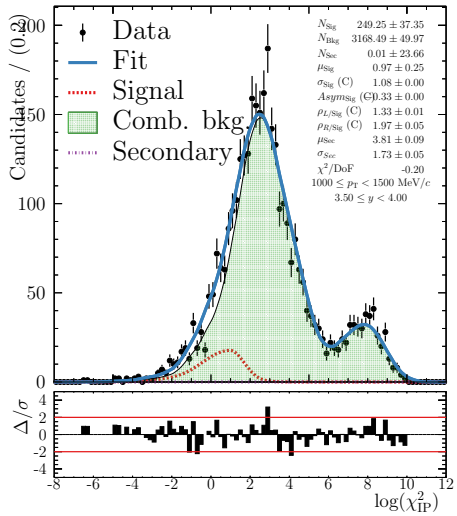

$1 \leq p_{\rm T} < 1.5\,{\rm GeV},\ 3.5 \leq y < 4.0$

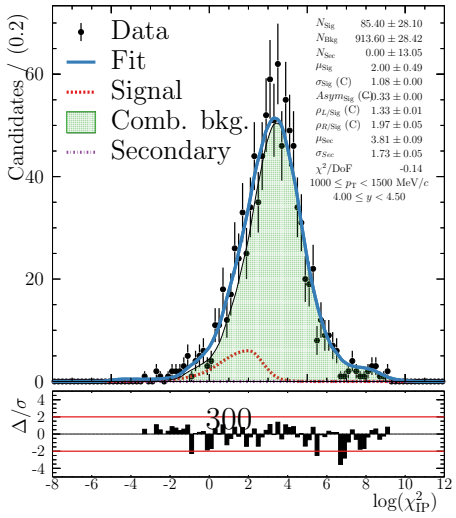

$1 \leq p_{\rm T} < 1.5\,{\rm GeV},\ 4.0 \leq y < 4.5$

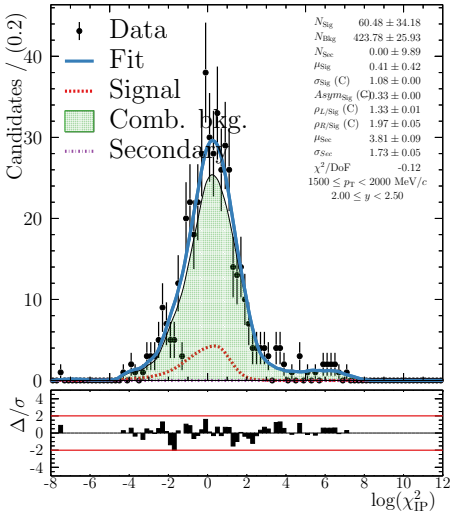

$1.5 \leq p_{\rm T} < 2\,{\rm GeV},\ 2.0 \leq y < 2.5$

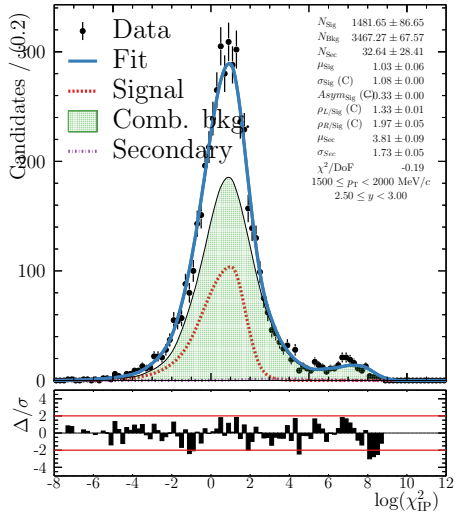

$1.5 \leq p_{\rm T} < 2\,{\rm GeV},\ 2.5 \leq y < 3.0$

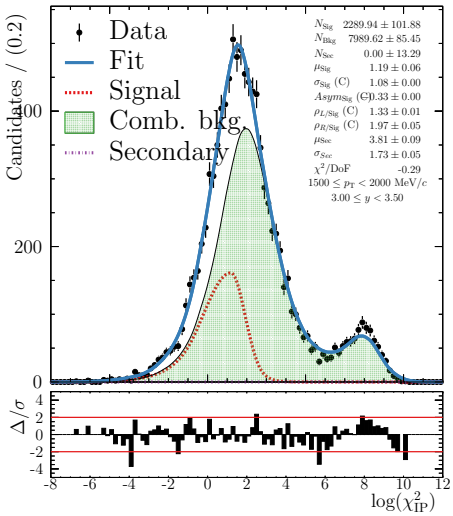

$1.5 \leq p_{\rm T} < 2\,{\rm GeV},\ 3.0 \leq y < 3.5$

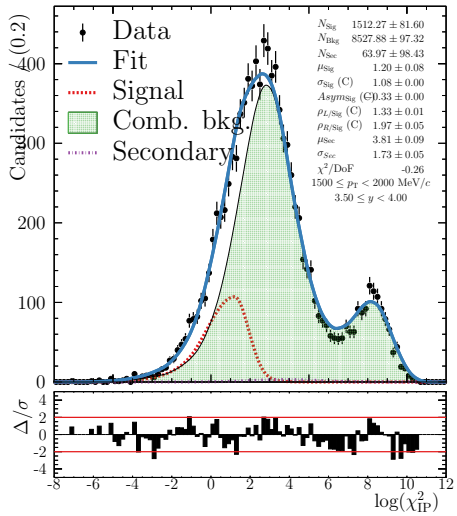

$1.5 \leq p_{\rm T} < 2\,{\rm GeV},\ 3.5 \leq y < 4.0$

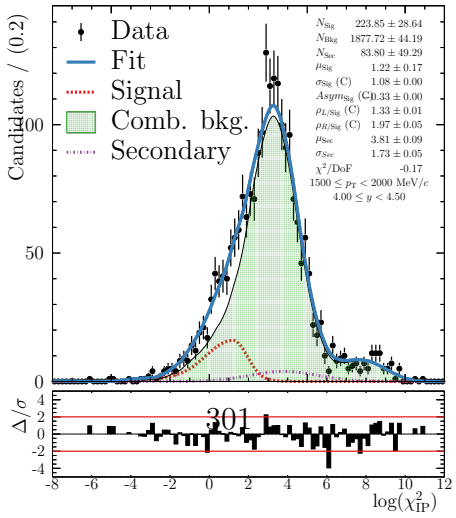

$1.5 \leq p_{\rm T} < 2\,{\rm GeV},\ 4.0 \leq y < 4.5$

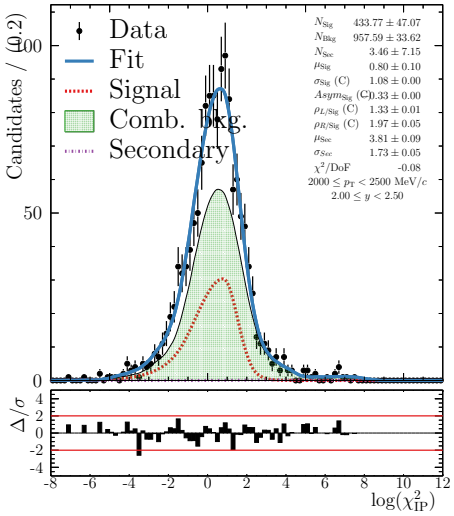

$2 \leq p_{\rm T} < 2.5\,{\rm GeV},\ 2.0 \leq y < 2.5$

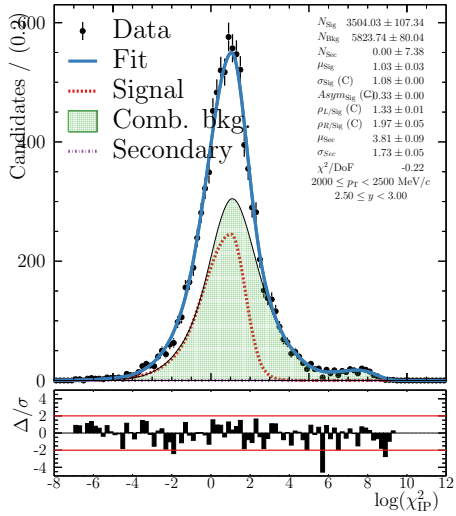

$2 \leq p_{\rm T} < 2.5\,{\rm GeV},\ 2.5 \leq y < 3.0$

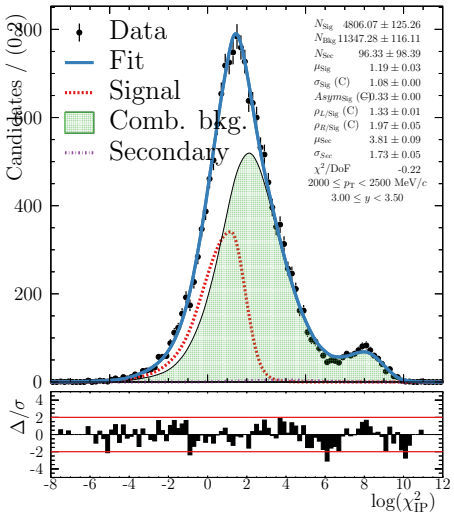

$2 \leq p_{\rm T} < 2.5\,{\rm GeV},\ 3.0 \leq y < 3.5$

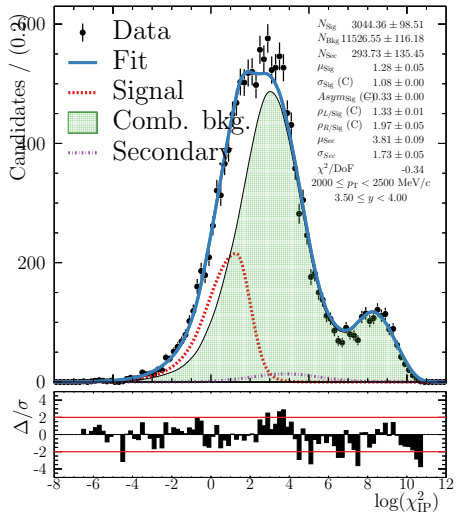

$2 \leq p_{\rm T} < 2.5\,{\rm GeV},\ 3.5 \leq y < 4.0$

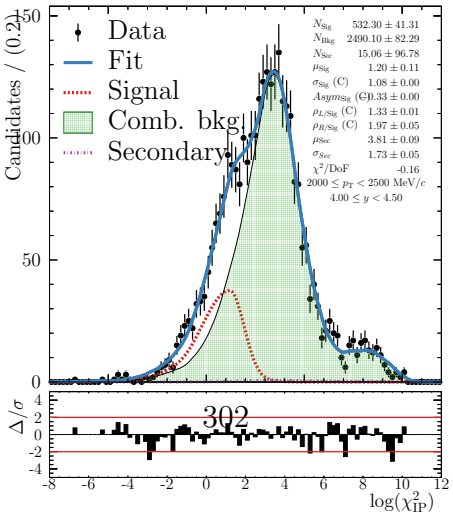

$2 \leq p_{\rm T} < 2.5\,{\rm GeV},\ 4.0 \leq y < 4.5$

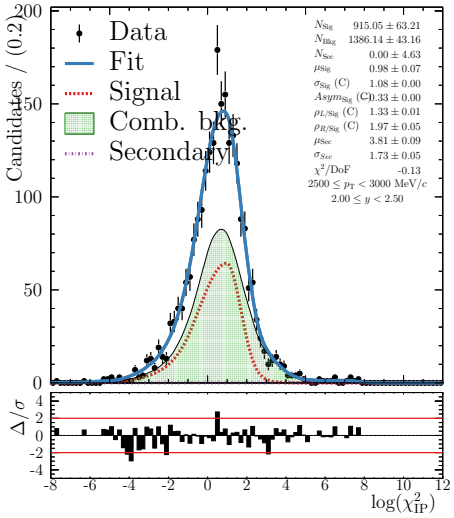

$2.5 \leq p_{\rm T} < 3\,{\rm GeV},\ 2.0 \leq y < 2.5$

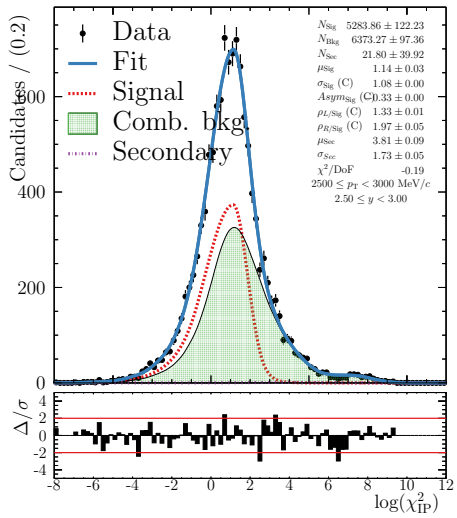

$2.5 \leq p_{\rm T} < 3\,{\rm GeV},\ 2.5 \leq y < 3.0$

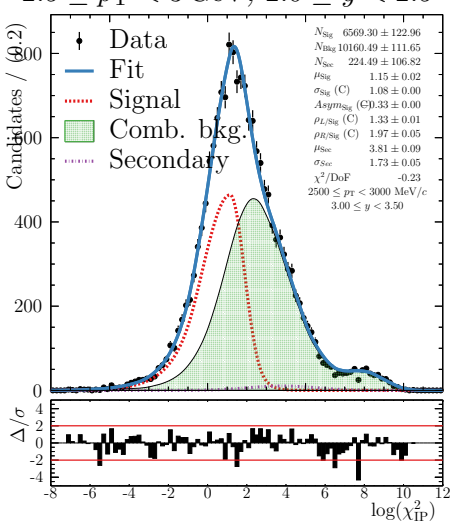

$2.5 \leq p_{\rm T} < 3\,{\rm GeV},\ 3.0 \leq y < 3.5$

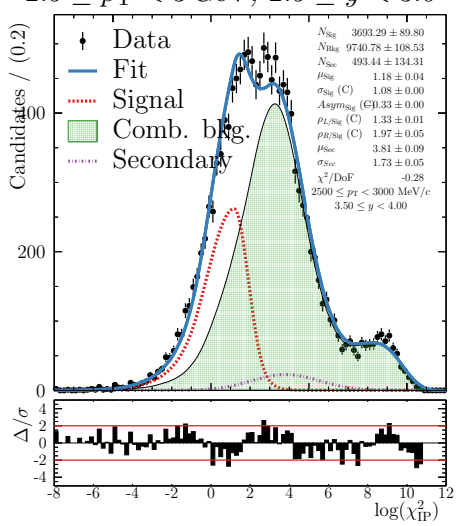

$2.5 \leq p_{\rm T} < 3\,{\rm GeV},\ 3.5 \leq y < 4.0$

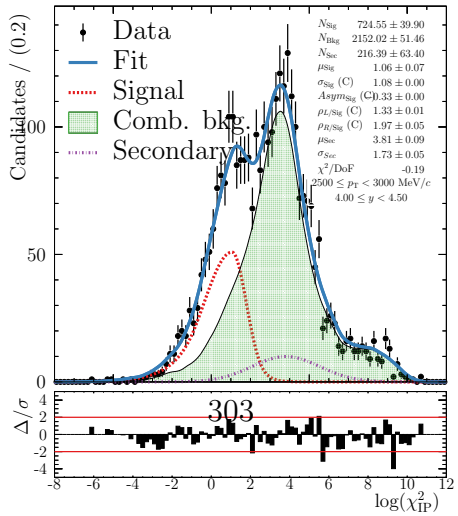

$2.5 \leq p_{\rm T} < 3\,{\rm GeV},\ 4.0 \leq y < 4.5$

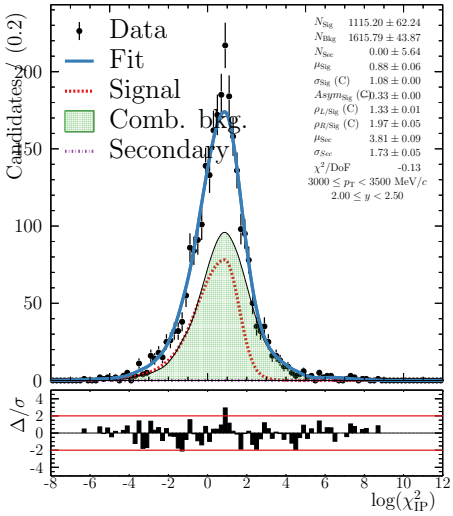

$3 \leq p_{\rm T} < 3.5\,\text{GeV},\ 2.0 \leq y < 2.5$

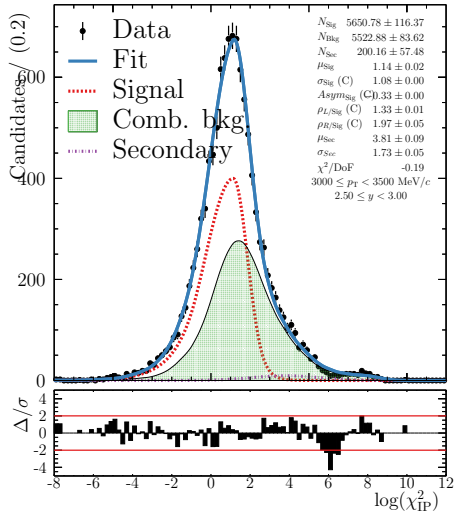

$3 \leq p_{\rm T} < 3.5\,\text{GeV},\ 2.5 \leq y < 3.0$

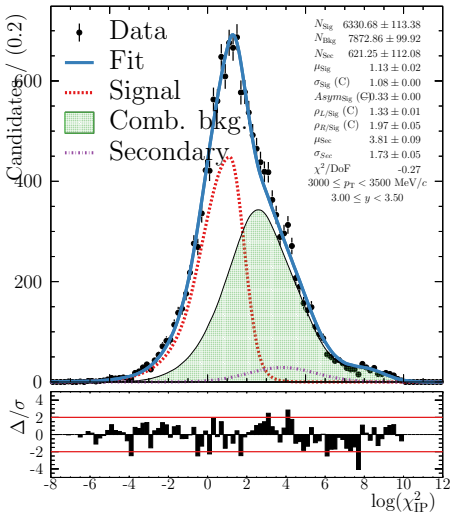

$3 \leq p_{\rm T} < 3.5\,\text{GeV},\ 3.0 \leq y < 3.5$

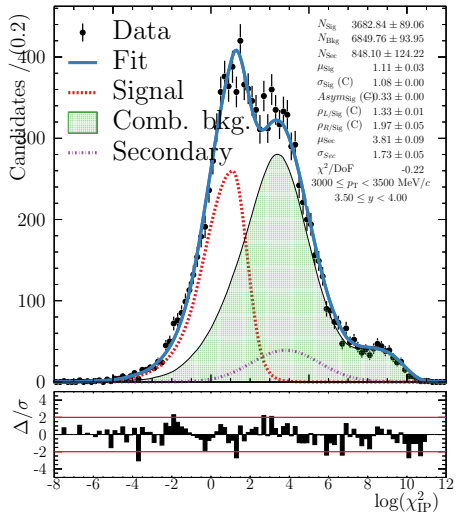

$3 \leq p_{\rm T} < 3.5\,\text{GeV},\ 3.5 \leq y < 4.0$

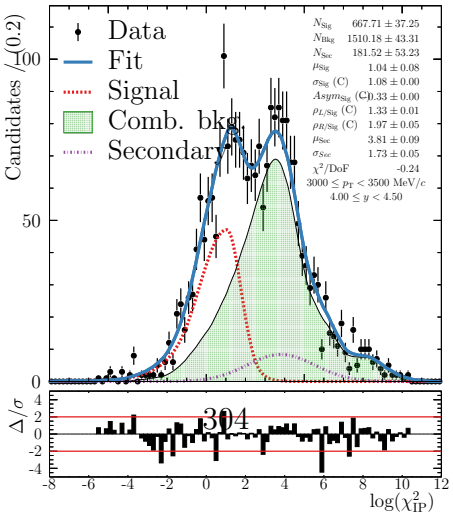

$3 \leq p_{\rm T} < 3.5\,\text{GeV},\ 4.0 \leq y < 4.5$

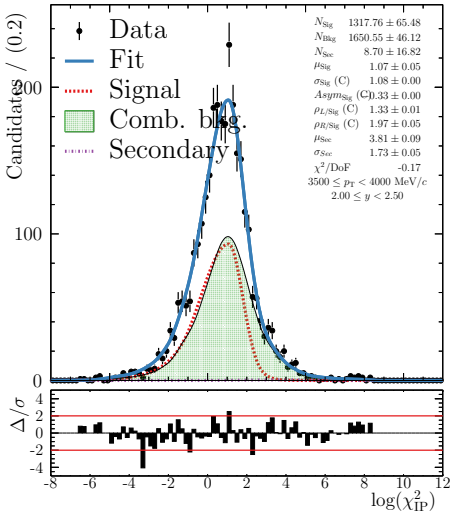

$3.5 \leq p_{\rm T} < 4\,{\rm GeV},\ 2.0 \leq y < 2.5$

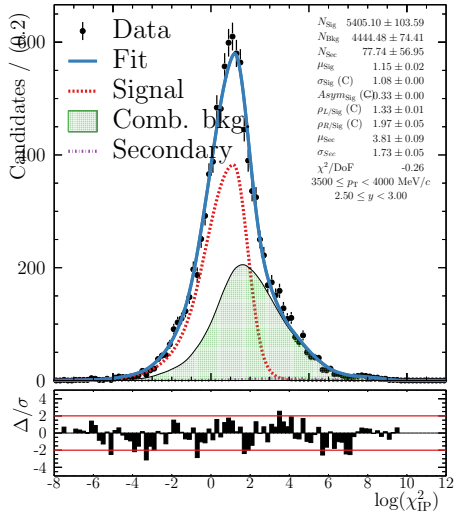

$3.5 \leq p_{\rm T} < 4\,{\rm GeV},\ 2.5 \leq y < 3.0$

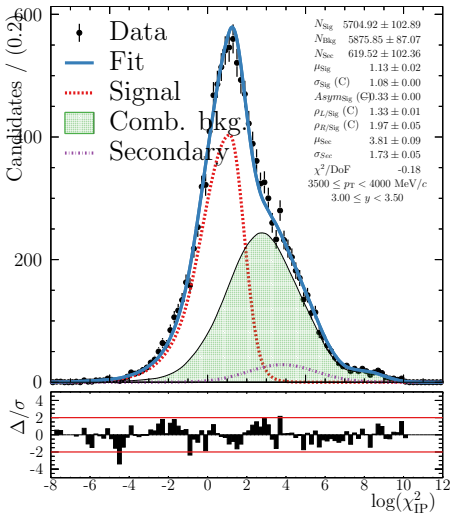

$3.5 \leq p_{\rm T} < 4\,{\rm GeV},\ 3.0 \leq y < 3.5$

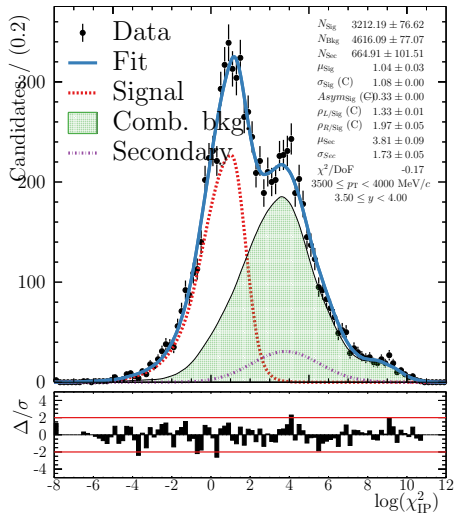

$3.5 \leq p_{\rm T} < 4\,{\rm GeV},\ 3.5 \leq y < 4.0$

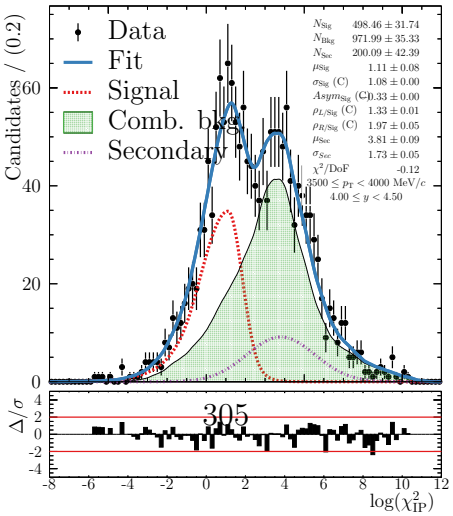

$3.5 \leq p_{\rm T} < 4\,{\rm GeV},\ 4.0 \leq y < 4.5$

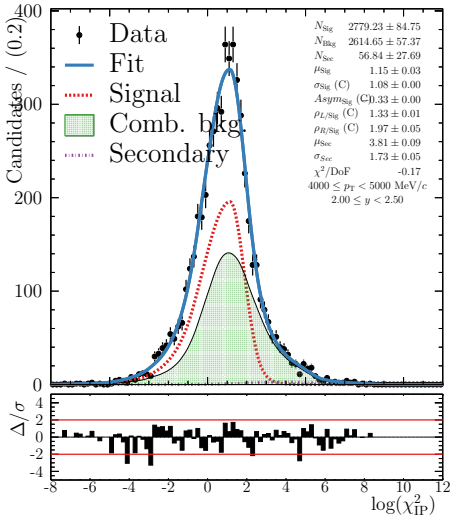

$4 \leq p_{\rm T} < 5\,{\rm GeV},\ 2.0 \leq y < 2.5$

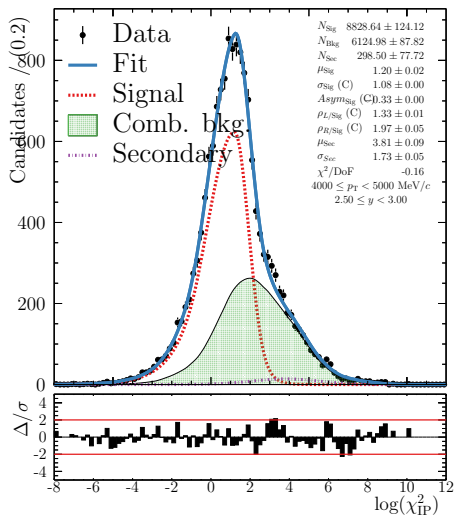

$4 \leq p_{\rm T} < 5\,{\rm GeV},\ 2.5 \leq y < 3.0$

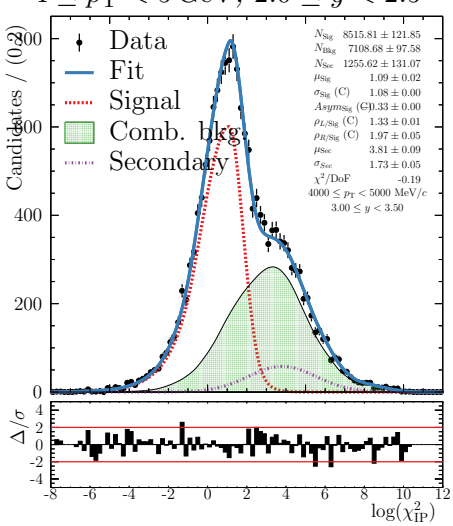

$4 \leq p_{\rm T} < 5\,{\rm GeV},\ 3.0 \leq y < 3.5$

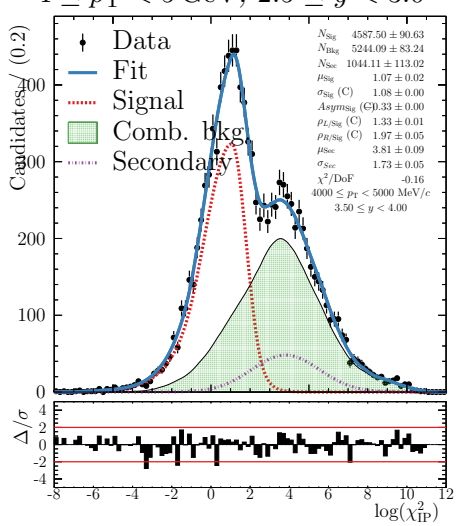

$4 \leq p_{\rm T} < 5\,{\rm GeV},\ 3.5 \leq y < 4.0$

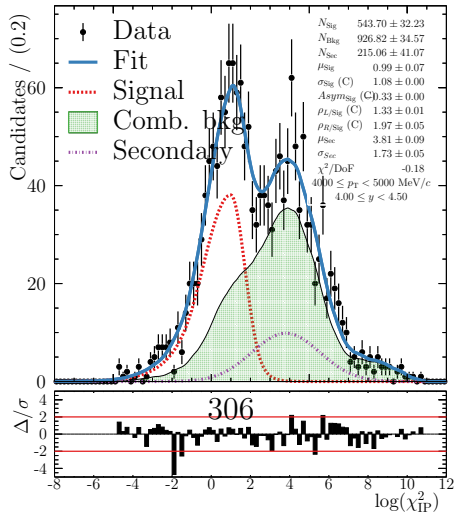

$4 \leq p_{\rm T} < 5\,{\rm GeV},\ 4.0 \leq y < 4.5$

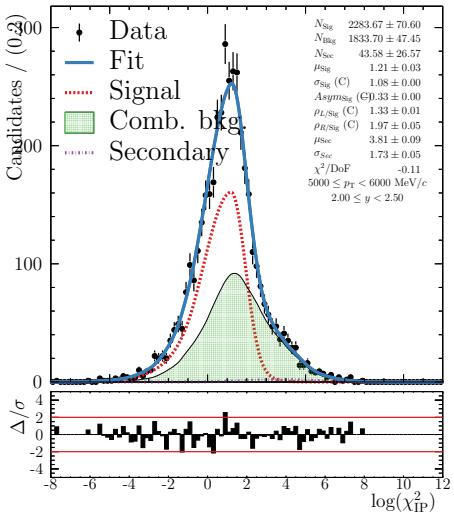

$5 \leq p_{\rm T} < 6\,{\rm GeV},\ 2.0 \leq y < 2.5$

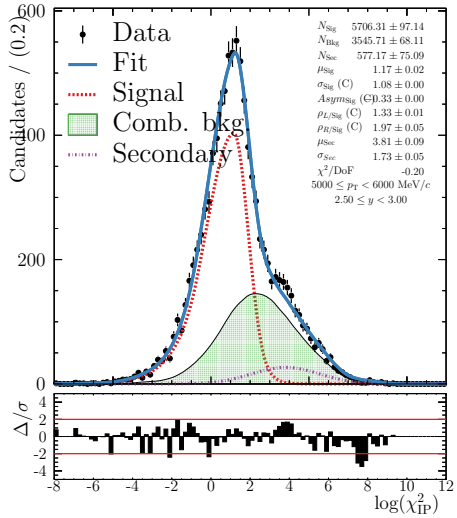

$5 \leq p_{\rm T} < 6\,{\rm GeV},\ 2.5 \leq y < 3.0$

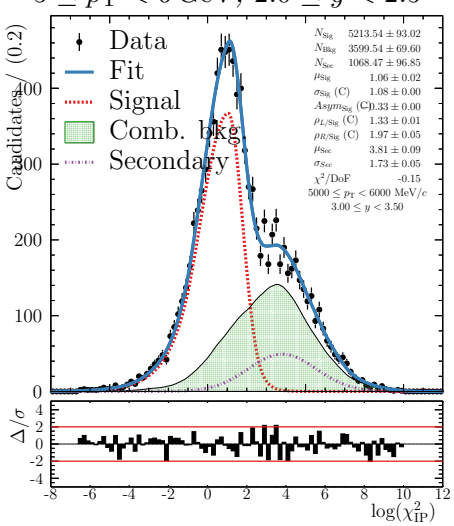

$5 \leq p_{\rm T} < 6\,{\rm GeV},\ 3.0 \leq y < 3.5$

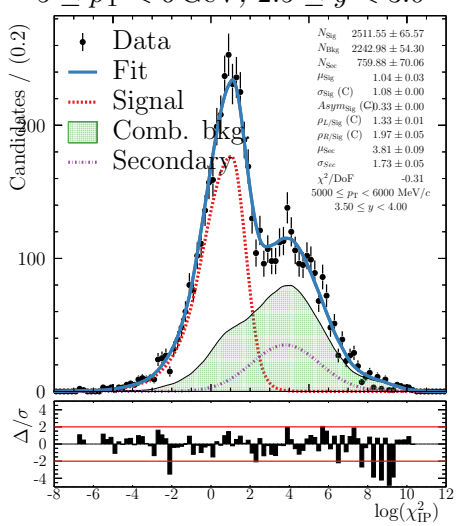

$5 \leq p_{\rm T} < 6\,{\rm GeV},\ 3.5 \leq y < 4.0$

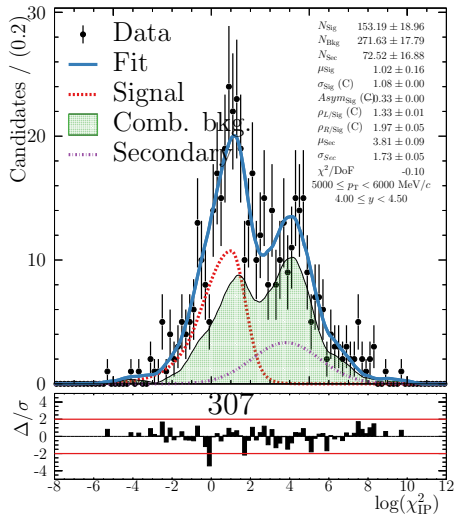

$5 \leq p_{\rm T} < 6\,{\rm GeV},\ 4.0 \leq y < 4.5$

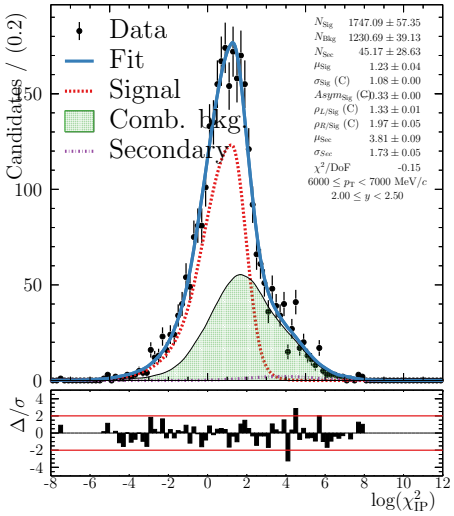

$6 \leq p_{\rm T} < 7\,{\rm GeV},\ 2.0 \leq y < 2.5$

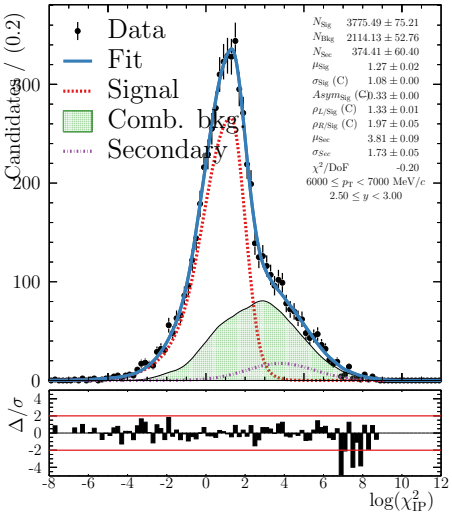

$6 \leq p_{\rm T} < 7\,{\rm GeV},\ 2.5 \leq y < 3.0$

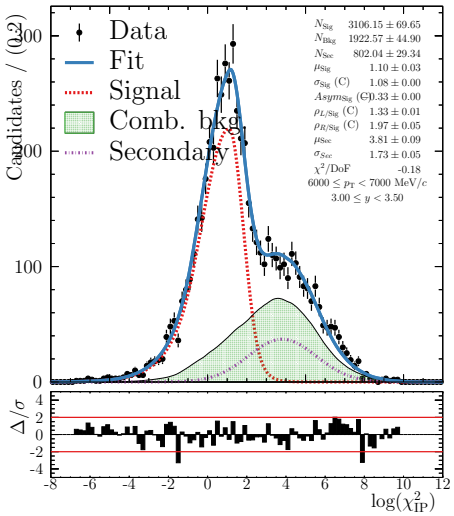

$6 \leq p_{\rm T} < 7\,{\rm GeV},\ 3.0 \leq y < 3.5$

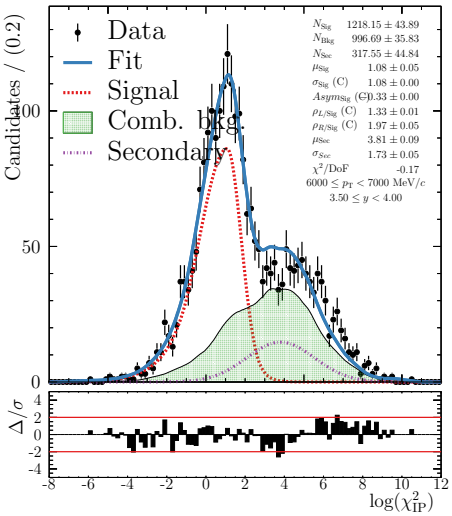

$6 \leq p_{\rm T} < 7\,{\rm GeV},\ 3.5 \leq y < 4.0$

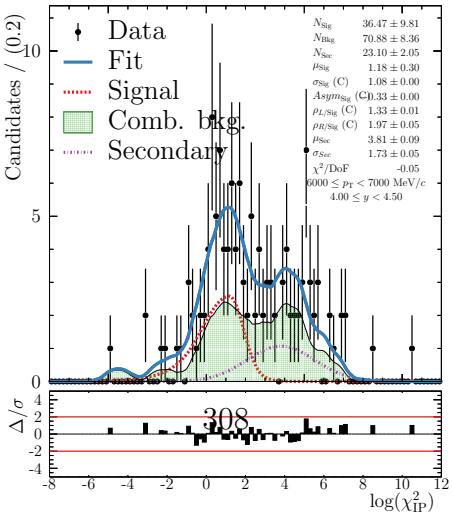

$6 \leq p_{\rm T} < 7\,{\rm GeV},\ 4.0 \leq y < 4.5$

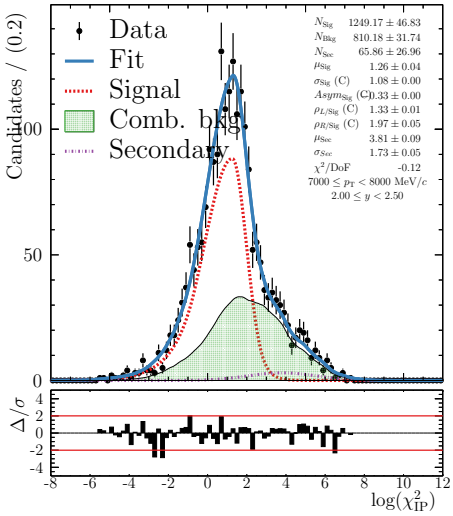

$7 \leq p_{\rm T} < 8\,{\rm GeV},\ 2.0 \leq y < 2.5$

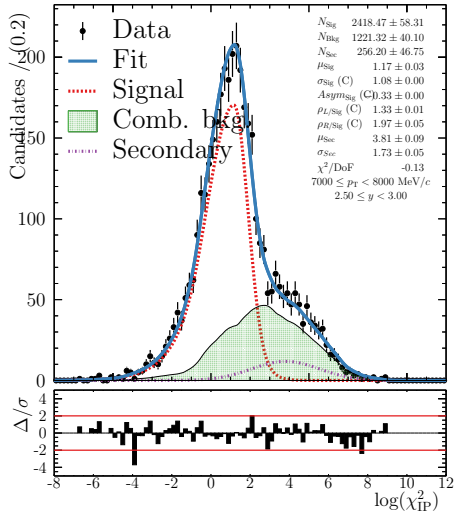

$7 \leq p_{\rm T} < 8\,{\rm GeV},\ 2.5 \leq y < 3.0$

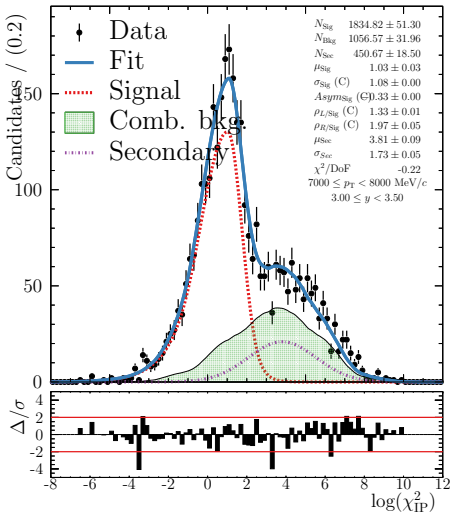

$7 \leq p_{\rm T} < 8\,{\rm GeV},\ 3.0 \leq y < 3.5$

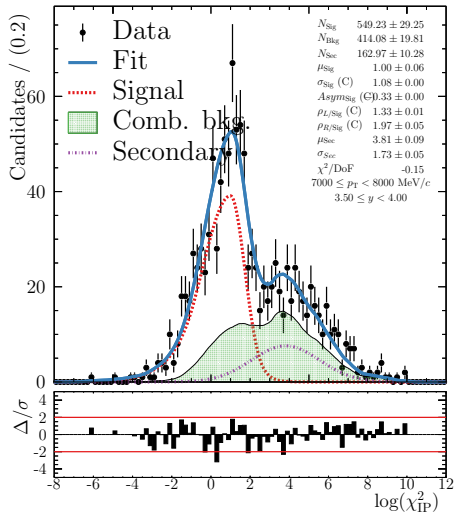

$7 \leq p_{\rm T} < 8\,{\rm GeV},\ 3.5 \leq y < 4.0$

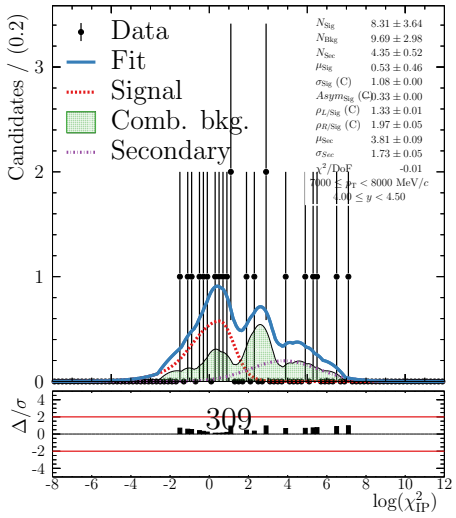

$7 \leq p_{\rm T} < 8\,{\rm GeV},\ 4.0 \leq y < 4.5$

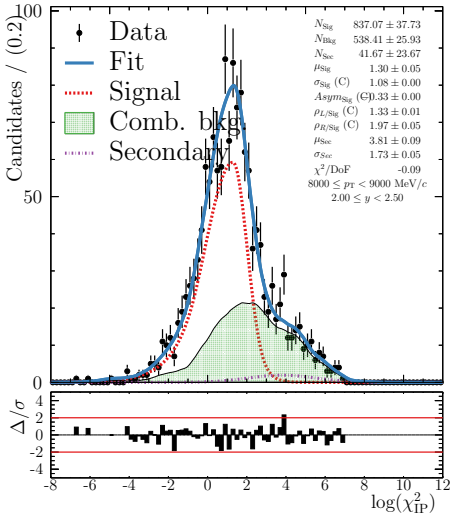

$8 \leq p_{\rm T} < 9\,{\rm GeV},\ 2.0 \leq y < 2.5$

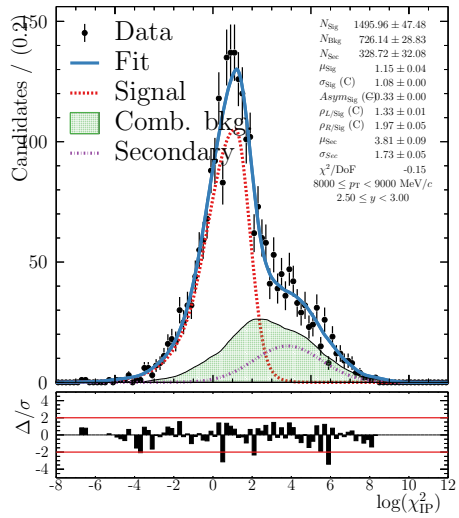

$8 \leq p_{\rm T} < 9\,{\rm GeV},\ 2.5 \leq y < 3.0$

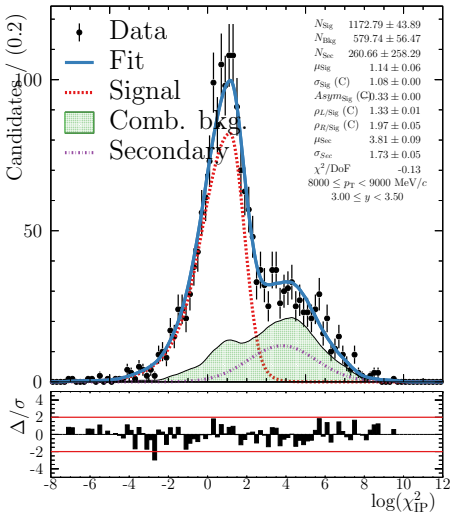

$8 \leq p_{\rm T} < 9\,{\rm GeV},\ 3.0 \leq y < 3.5$

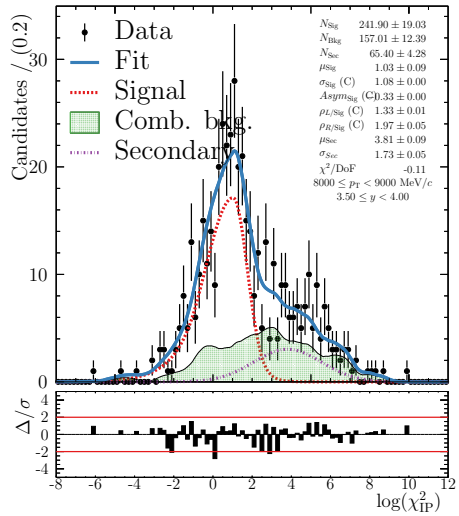

$8 \leq p_{\rm T} < 9\,{\rm GeV},\ 3.5 \leq y < 4.0$

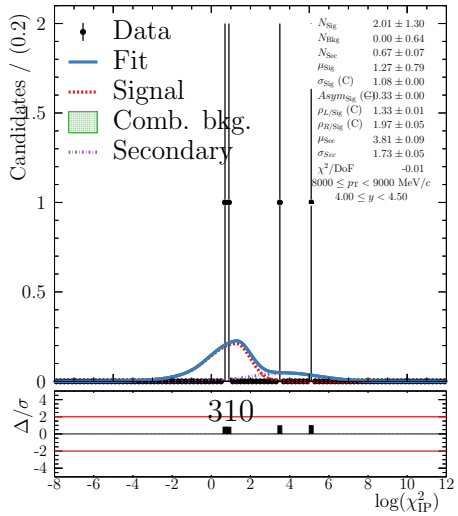

$8 \leq p_{\rm T} < 9\,{\rm GeV},\ 4.0 \leq y < 4.5$

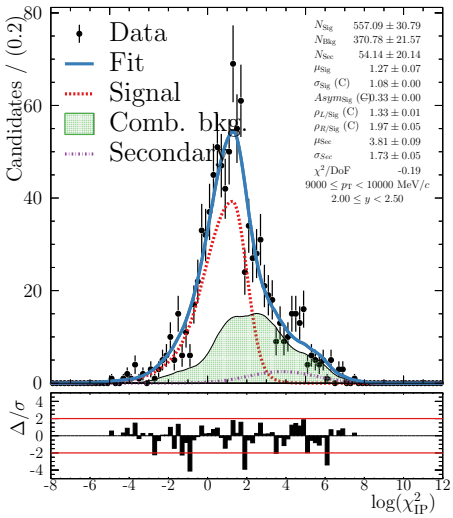

$9 \leq p_{\rm T} < 10\,{\rm GeV},\ 2.0 \leq y < 2.5$

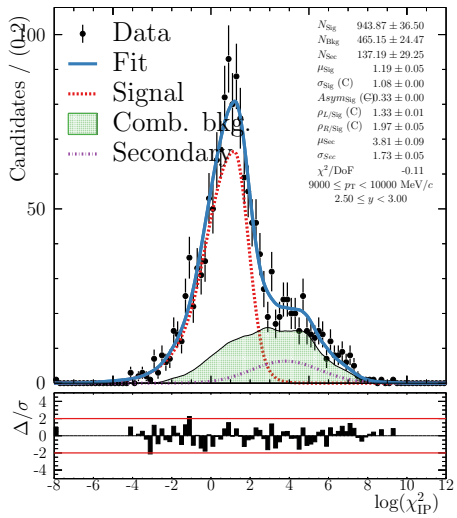

$9 \leq p_{\rm T} < 10\,{\rm GeV},\ 2.5 \leq y < 3.0$

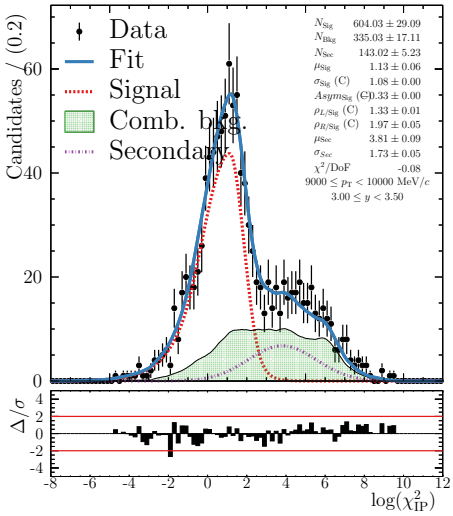

$9 \leq p_{\rm T} < 10\,{\rm GeV},\ 3.0 \leq y < 3.5$

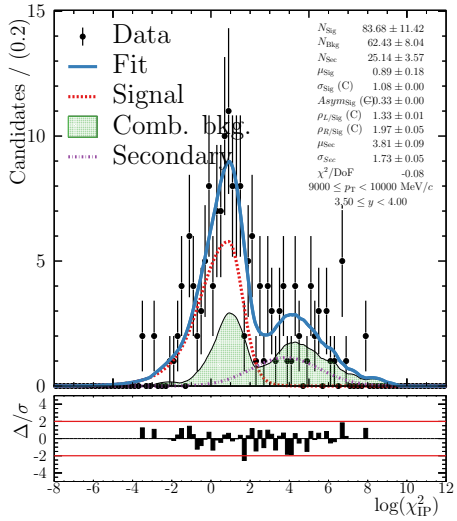

$9 \leq p_{\rm T} < 10\,{\rm GeV},\ 3.5 \leq y < 4.0$

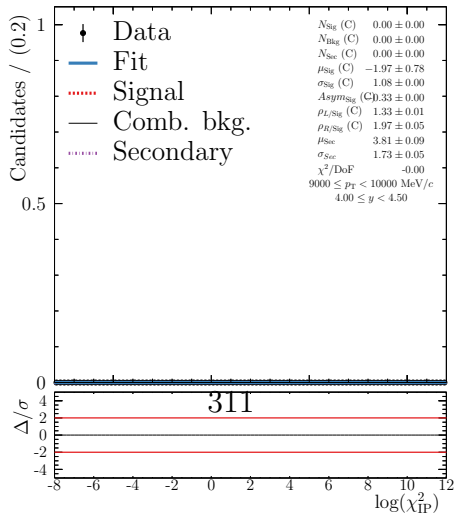

$9 \leq p_{\rm T} < 10\,{\rm GeV},\ 4.0 \leq y < 4.5$

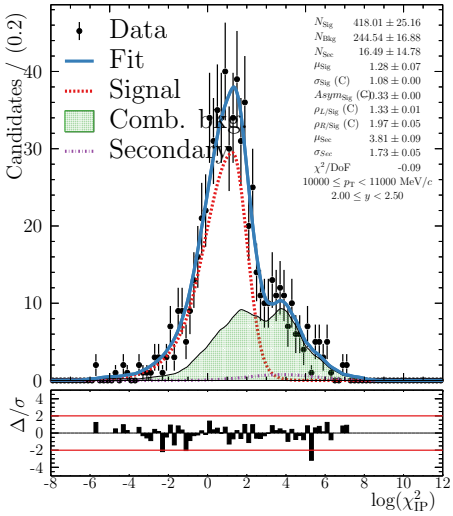

$10 \leq p_{\rm T} < 11\,{\rm GeV},\ 2.0 \leq y < 2.5$

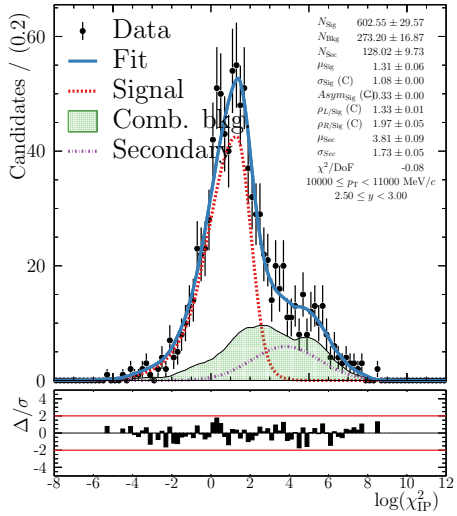

$10 \leq p_{\rm T} < 11\,{\rm GeV},\ 2.5 \leq y < 3.0$

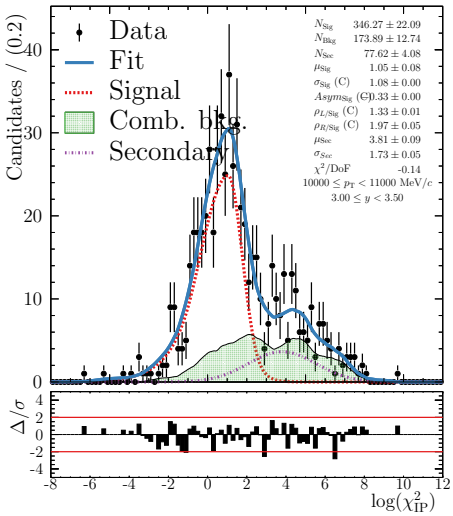

$10 \leq p_{\rm T} < 11\,{\rm GeV},\ 3.0 \leq y < 3.5$

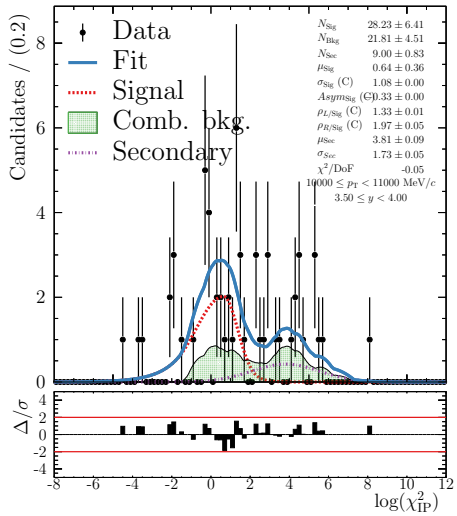

$10 \leq p_{\rm T} < 11\,{\rm GeV},\ 3.5 \leq y < 4.0$

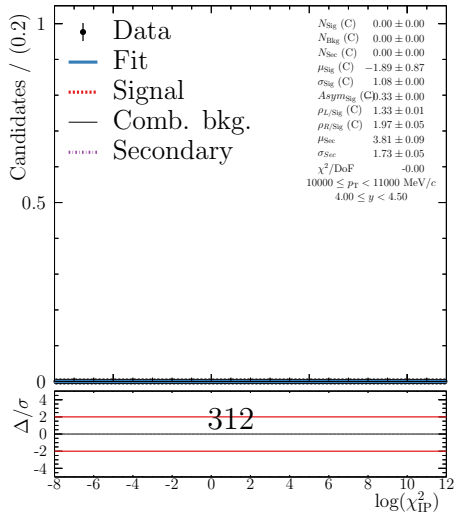

$10 \leq p_{\rm T} < 11\,{\rm GeV},\ 4.0 \leq y < 4.5$

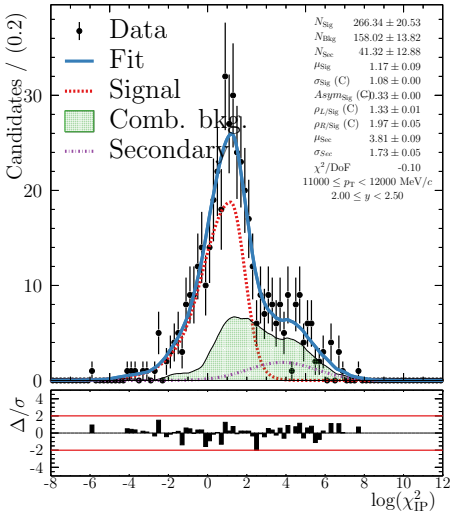

$11 \leq p_{\rm T} < 12\,{\rm GeV},\ 2.0 \leq y < 2.5$

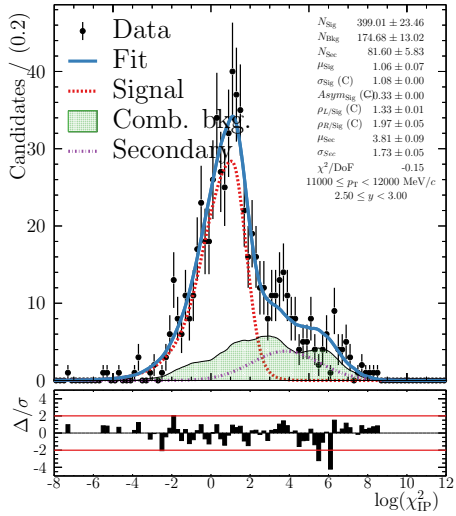

$11 \leq p_{\rm T} < 12\,{\rm GeV},\ 2.5 \leq y < 3.0$

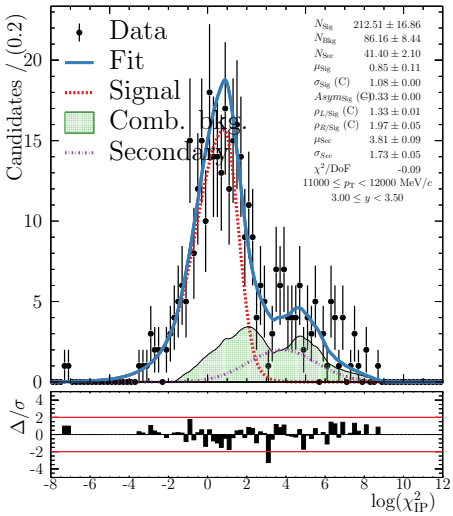

$11 \leq p_{\rm T} < 12\,{\rm GeV},\ 3.0 \leq y < 3.5$

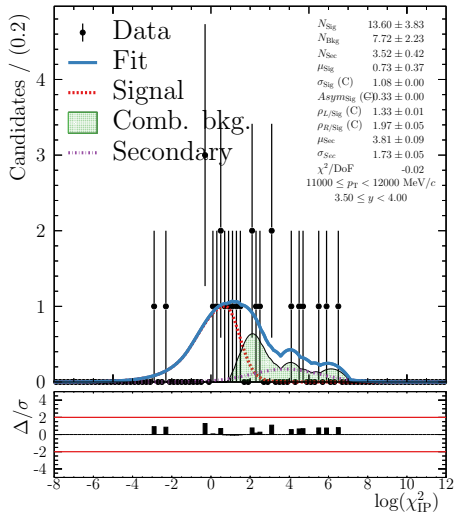

$11 \leq p_{\rm T} < 12\,{\rm GeV},\ 3.5 \leq y < 4.0$

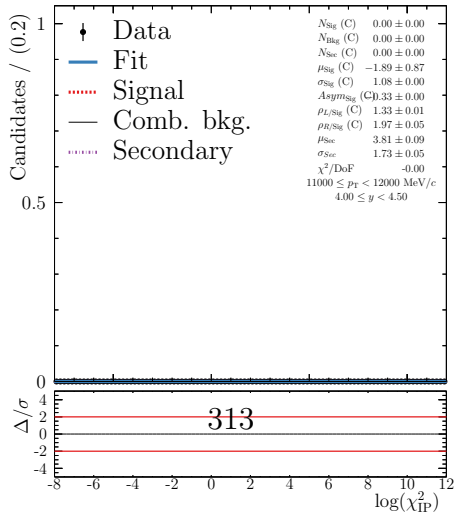

$11 \leq p_{\rm T} < 12\,{\rm GeV},\ 4.0 \leq y < 4.5$

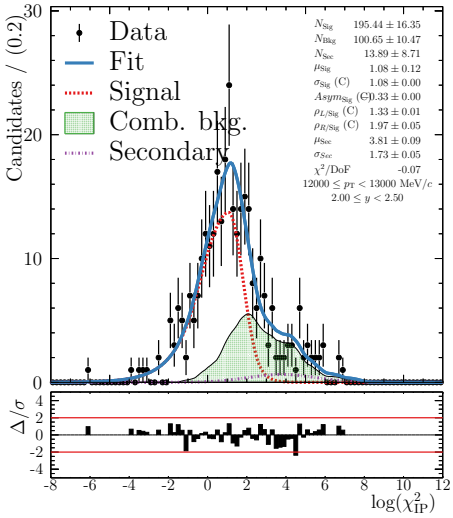

$12 \leq p_{\rm T} < 13\,{\rm GeV},\ 2.0 \leq y < 2.5$

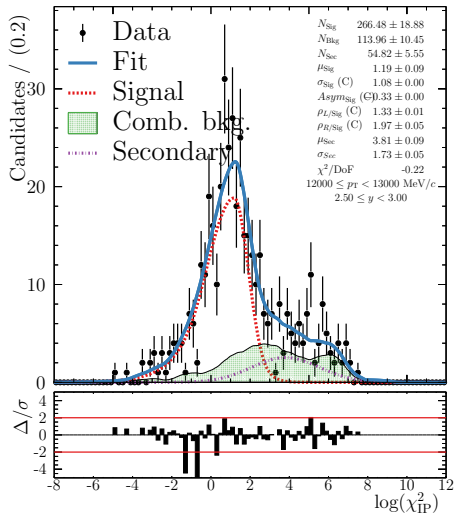

$12 \leq p_{\rm T} < 13\,{\rm GeV},\ 2.5 \leq y < 3.0$

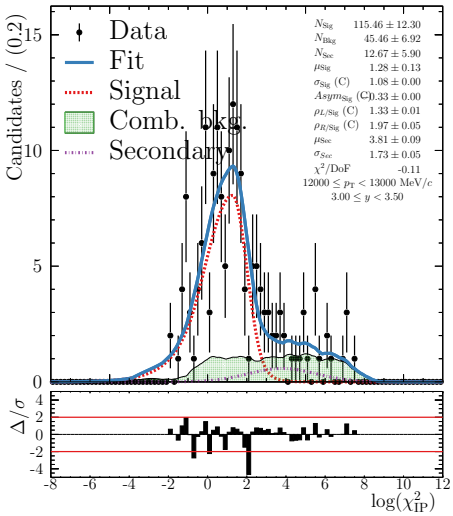

$12 \leq p_{\rm T} < 13\,{\rm GeV},\ 3.0 \leq y < 3.5$

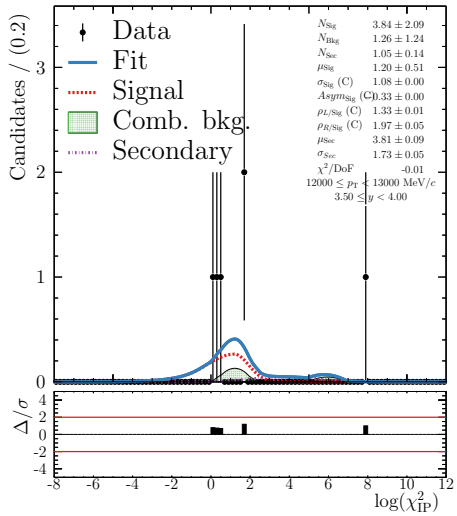

$12 \leq p_{\rm T} < 13\,{\rm GeV},\ 3.5 \leq y < 4.0$

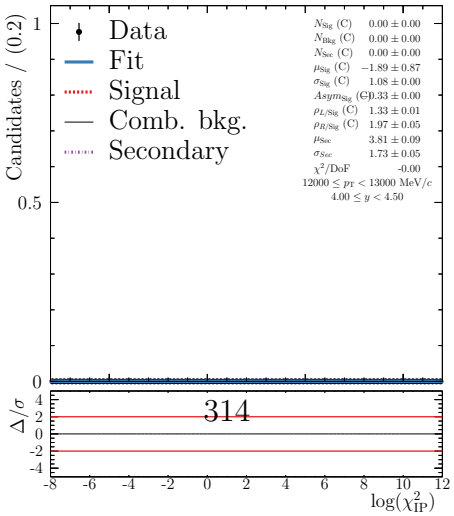

$12 \leq p_{\rm T} < 13\,{\rm GeV},\ 4.0 \leq y < 4.5$

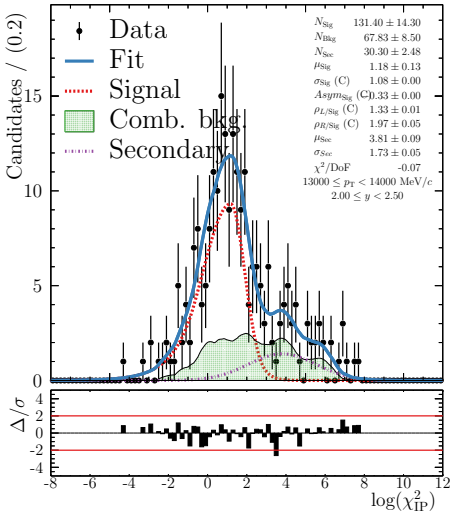

$13 \leq p_{\rm T} < 14\,{\rm GeV},\ 2.0 \leq y < 2.5$

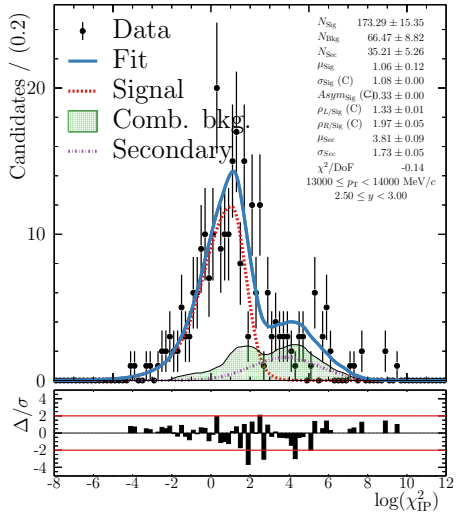

$13 \leq p_{\rm T} < 14\,{\rm GeV},\ 2.5 \leq y < 3.0$

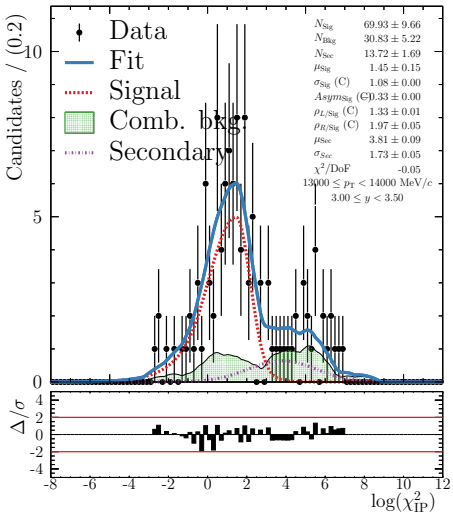

$13 \leq p_{\rm T} < 14\,{\rm GeV},\ 3.0 \leq y < 3.5$

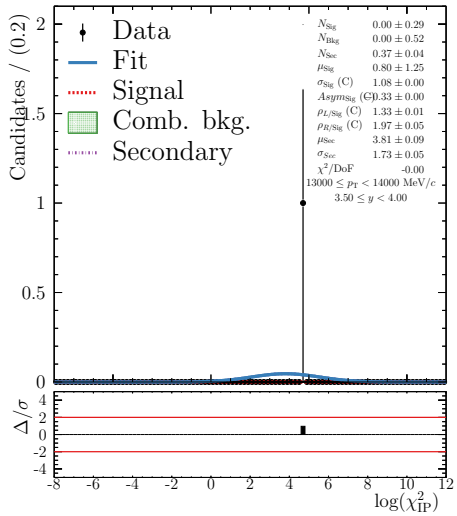

$13 \leq p_{\rm T} < 14\,{\rm GeV},\ 3.5 \leq y < 4.0$

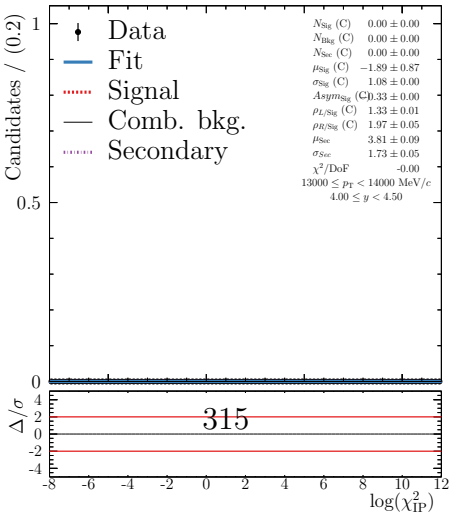

$13 \leq p_{\rm T} < 14\,{\rm GeV},\ 4.0 \leq y < 4.5$

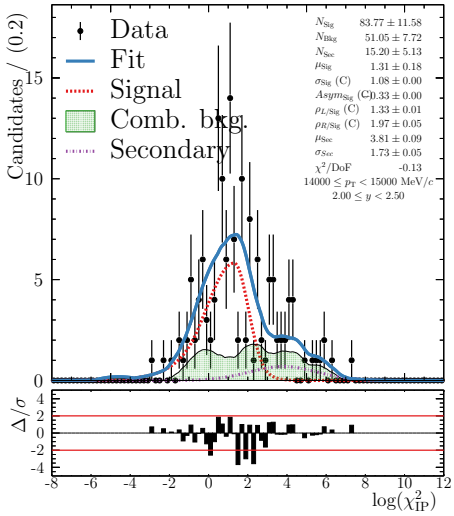

$14 \leq p_{\rm T} < 15\,{\rm GeV},\ 2.0 \leq y < 2.5$

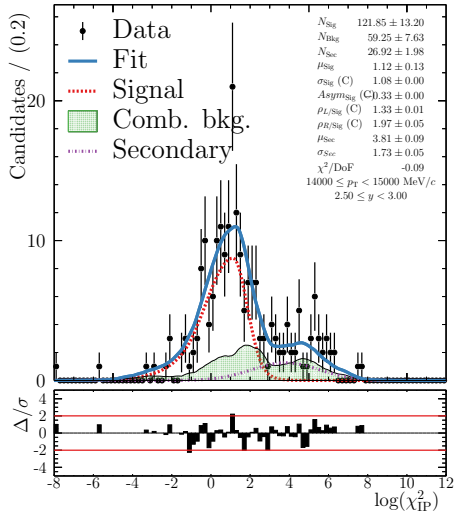

$14 \leq p_{\rm T} < 15\,{\rm GeV},\ 2.5 \leq y < 3.0$

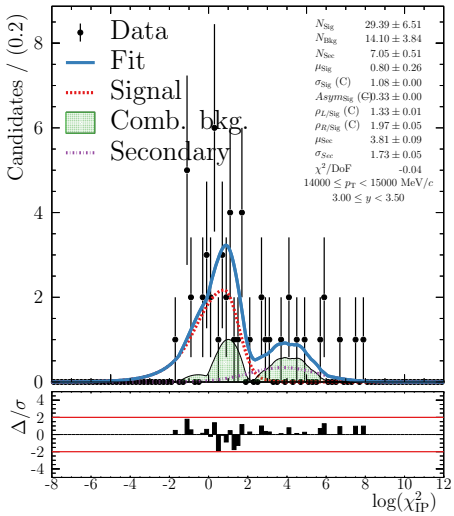

$14 \leq p_{\rm T} < 15\,{\rm GeV},\ 3.0 \leq y < 3.5$

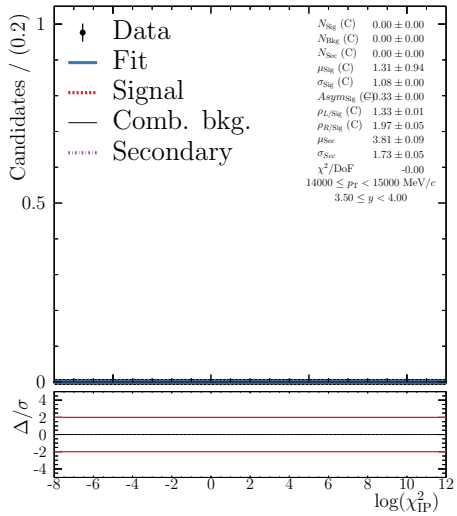

$14 \leq p_{\rm T} < 15\,{\rm GeV},\ 3.5 \leq y < 4.0$

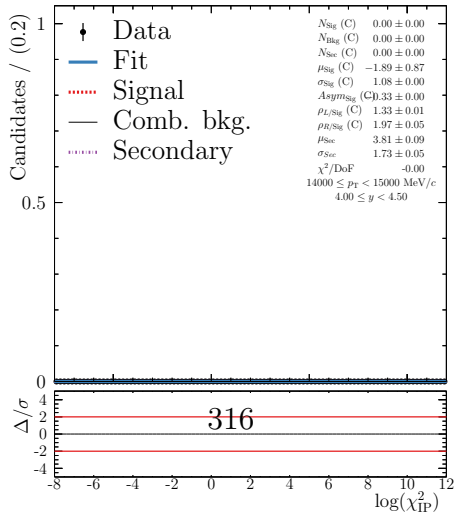

$14 \leq p_{\rm T} < 15\,{\rm GeV},\ 4.0 \leq y < 4.5$

Figure F.0: Fits to the fully selected $D_s^+ \to K^-K^+\pi^+$ $\ln\chi^2_{\rm IP}$ distribution per $p_{\rm T}$-y bin.

F.6 $D^{*+} \to D^0\pi^+$ with $D^0 \to K^-\pi^+$

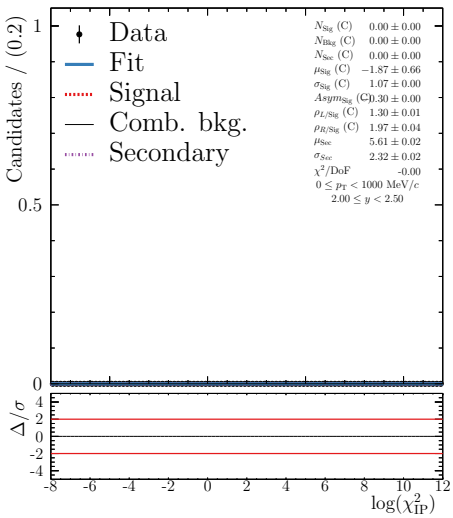

$0 \leq p_{\rm T} < 1\,\text{GeV},\ 2.0 \leq y < 2.5$

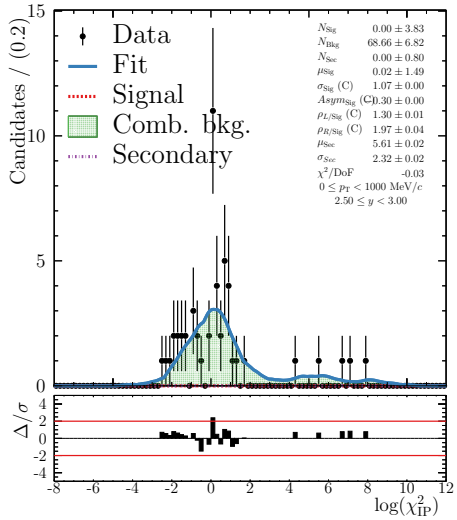

$0 \leq p_{\rm T} < 1\,\text{GeV},\ 2.5 \leq y < 3.0$

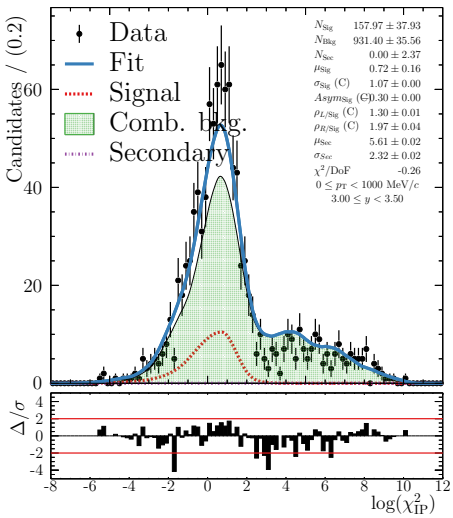

$0 \leq p_{\rm T} < 1\,\text{GeV},\ 3.0 \leq y < 3.5$

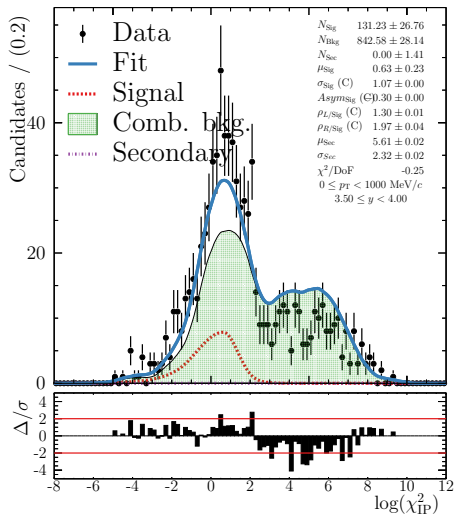

$0 \leq p_{\rm T} < 1\,\text{GeV},\ 3.5 \leq y < 4.0$

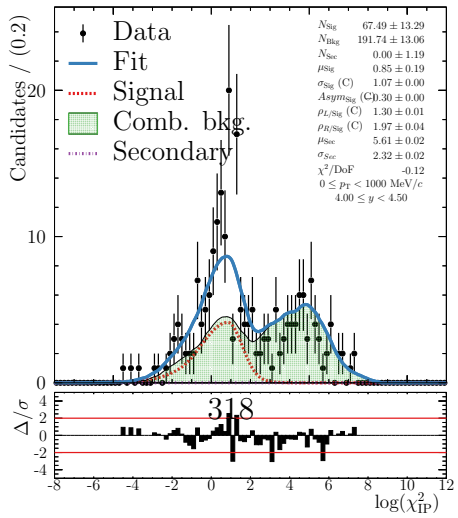

$0 \leq p_{\rm T} < 1\,\text{GeV},\ 4.0 \leq y < 4.5$

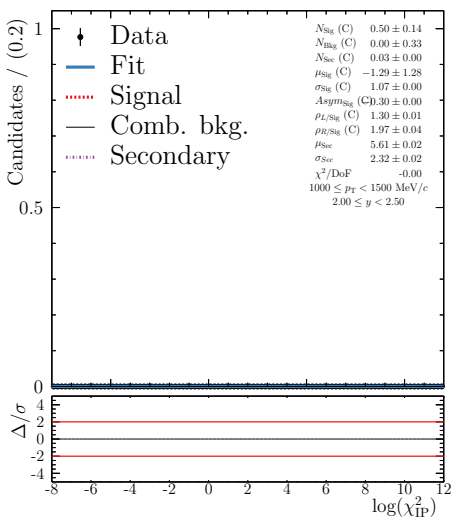

$1 \leq p_{\rm T} < 1.5\,{\rm GeV},\ 2.0 \leq y < 2.5$

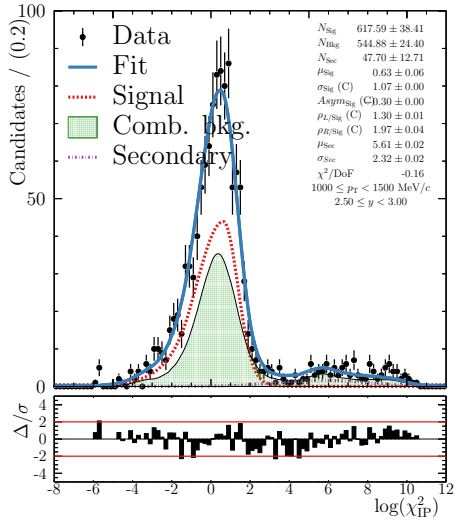

$1 \leq p_{\rm T} < 1.5\,{\rm GeV},\ 2.5 \leq y < 3.0$

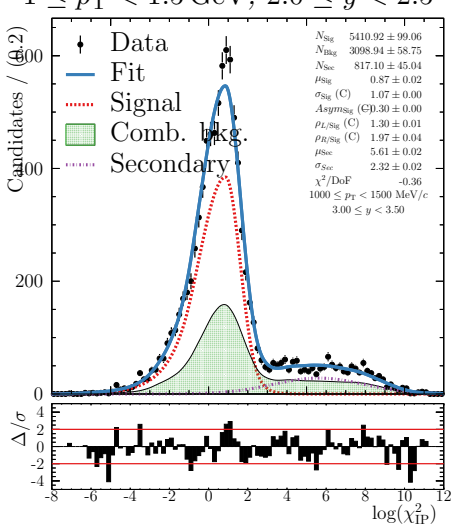

$1 \leq p_{\rm T} < 1.5\,{\rm GeV},\ 3.0 \leq y < 3.5$

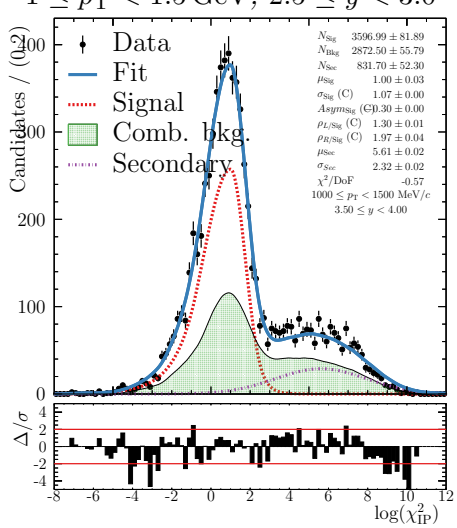

$1 \leq p_{\rm T} < 1.5\,{\rm GeV},\ 3.5 \leq y < 4.0$

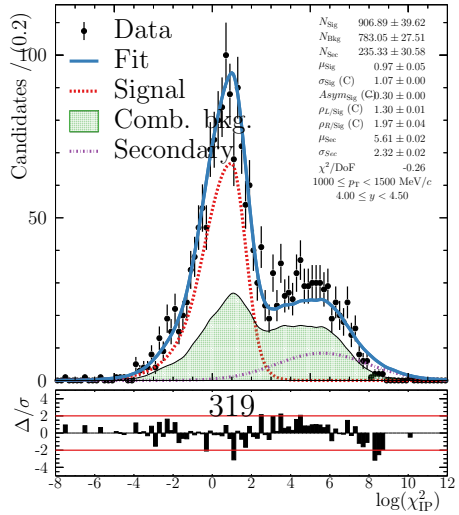

$1 \leq p_{\rm T} < 1.5\,{\rm GeV},\ 4.0 \leq y < 4.5$

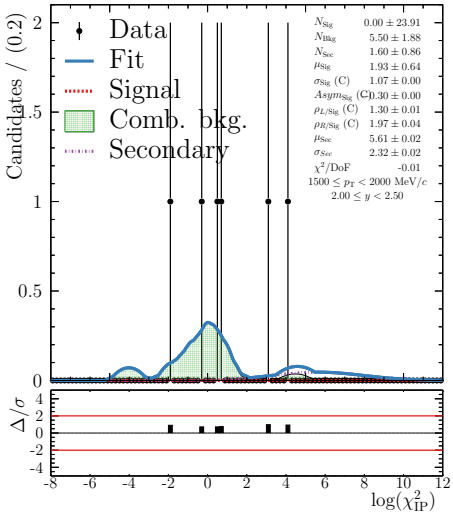

$1.5 \leq p_{\rm T} < 2\,{\rm GeV},\ 2.0 \leq y < 2.5$

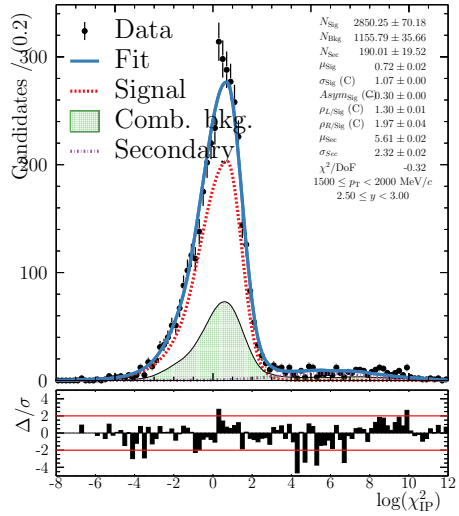

$1.5 \leq p_{\rm T} < 2\,{\rm GeV},\ 2.5 \leq y < 3.0$

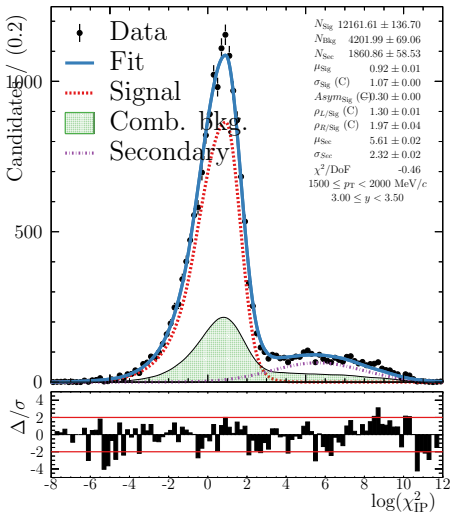

$1.5 \leq p_{\rm T} < 2\,{\rm GeV},\ 3.0 \leq y < 3.5$

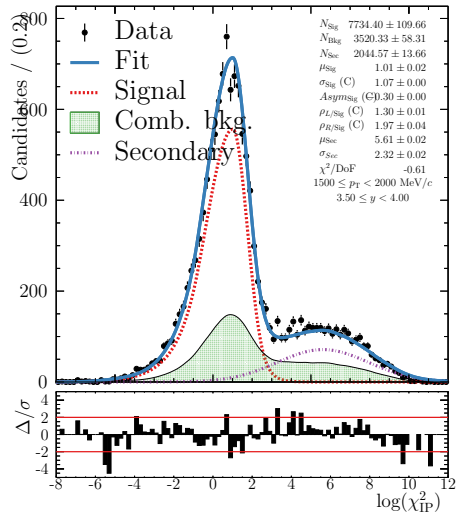

$1.5 \leq p_{\rm T} < 2\,{\rm GeV},\ 3.5 \leq y < 4.0$

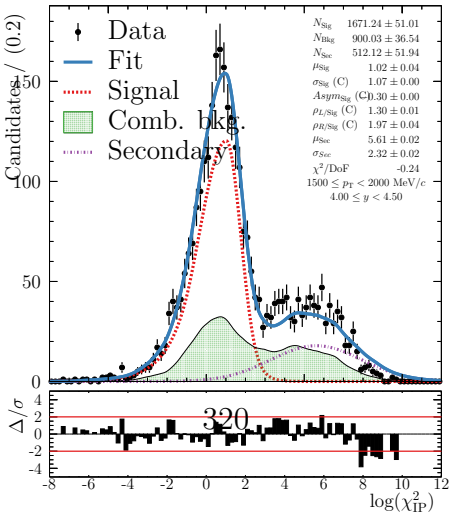

$1.5 \leq p_{\rm T} < 2\,{\rm GeV},\ 4.0 \leq y < 4.5$

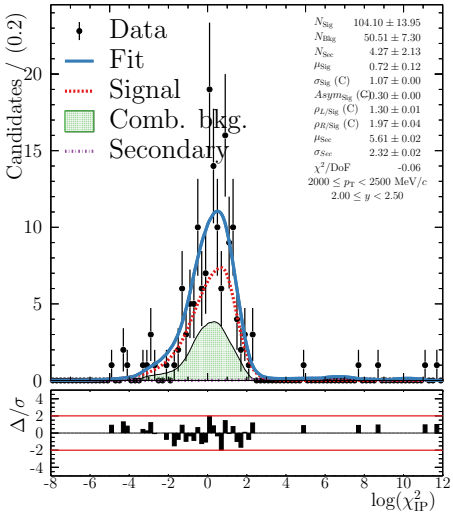

$2 \leq p_{\rm T} < 2.5\,{\rm GeV},\ 2.0 \leq y < 2.5$

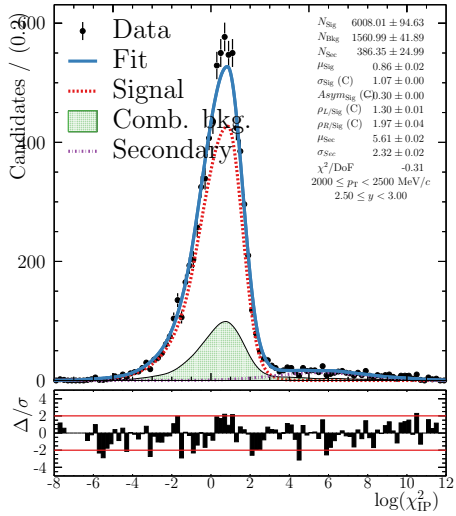

$2 \leq p_{\rm T} < 2.5\,{\rm GeV},\ 2.5 \leq y < 3.0$

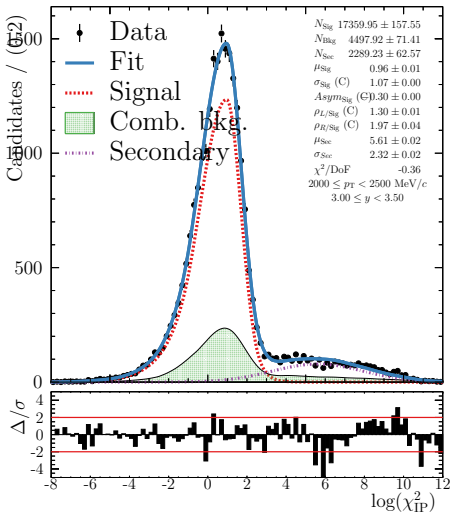

$2 \leq p_{\rm T} < 2.5\,{\rm GeV},\ 3.0 \leq y < 3.5$

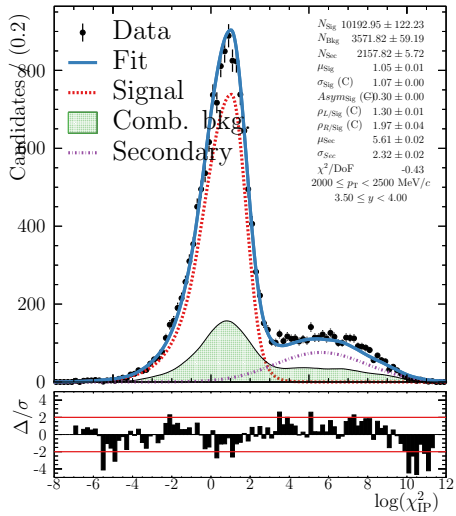

$2 \leq p_{\rm T} < 2.5\,{\rm GeV},\ 3.5 \leq y < 4.0$

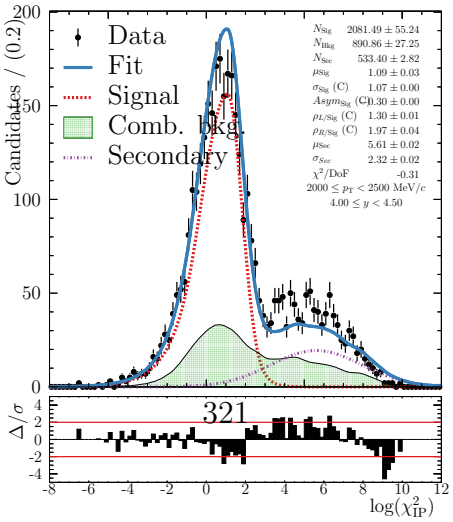

$2 \leq p_{\rm T} < 2.5\,{\rm GeV},\ 4.0 \leq y < 4.5$

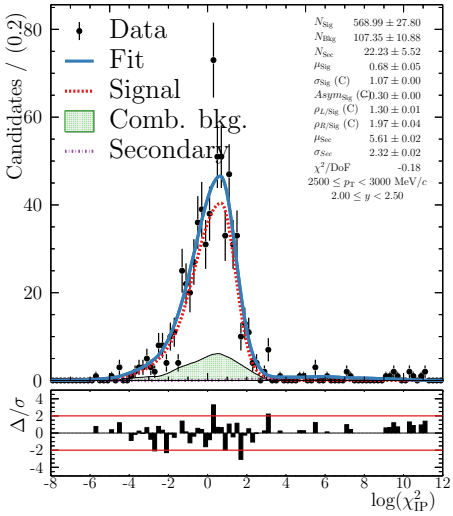

$2.5 \le p_{\rm T} < 3\,{\rm GeV},\ 2.0 \le y < 2.5$

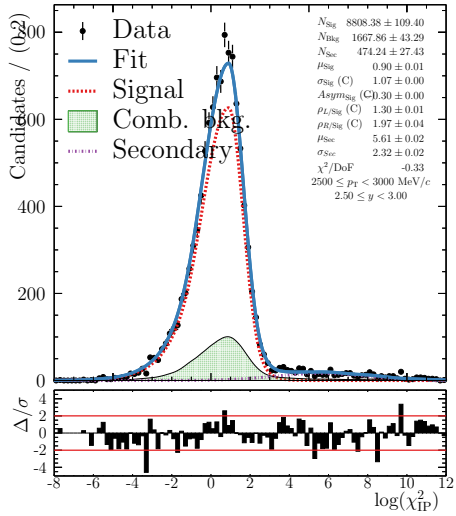

$2.5 \le p_{\rm T} < 3\,{\rm GeV},\ 2.5 \le y < 3.0$

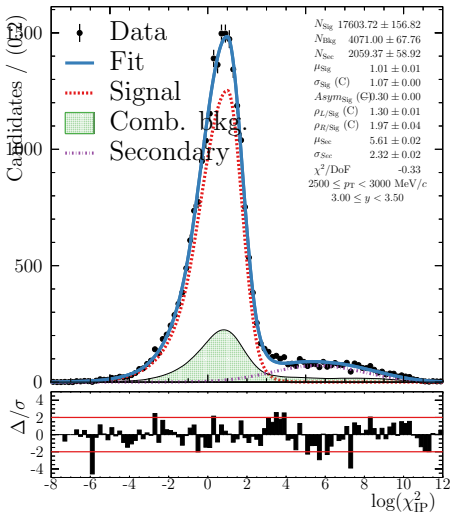

$2.5 \le p_{\rm T} < 3\,{\rm GeV},\ 3.0 \le y < 3.5$

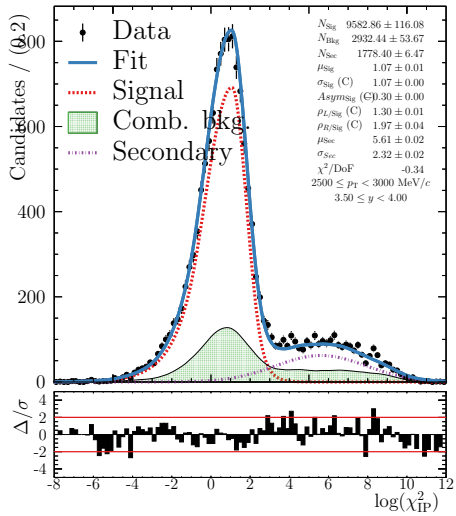

$2.5 \le p_{\rm T} < 3\,{\rm GeV},\ 3.5 \le y < 4.0$

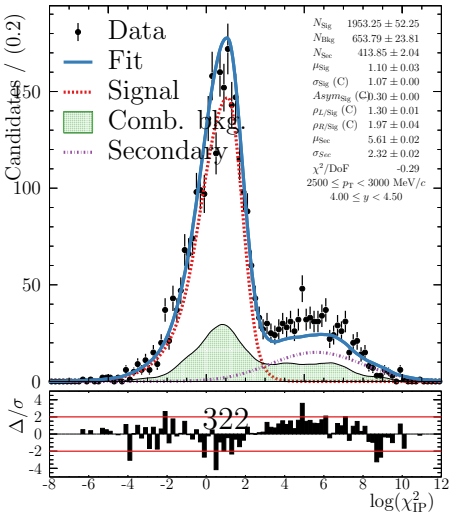

$2.5 \le p_{\rm T} < 3\,{\rm GeV},\ 4.0 \le y < 4.5$

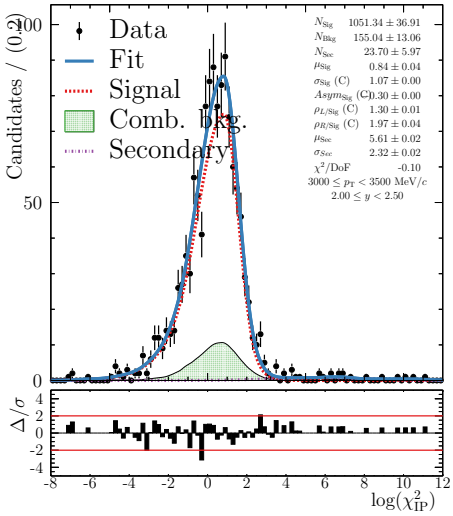

$3 \leq p_{\rm T} < 3.5\,{\rm GeV},\ 2.0 \leq y < 2.5$

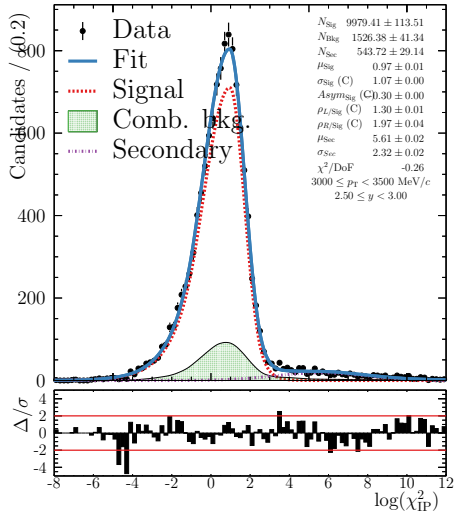

$3 \leq p_{\rm T} < 3.5\,{\rm GeV},\ 2.5 \leq y < 3.0$

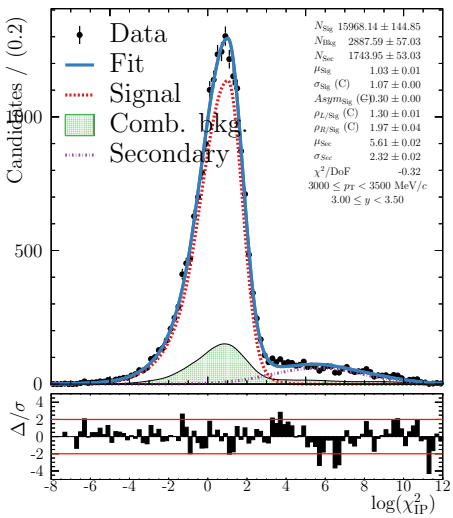

$3 \leq p_{\rm T} < 3.5\,{\rm GeV},\ 3.0 \leq y < 3.5$

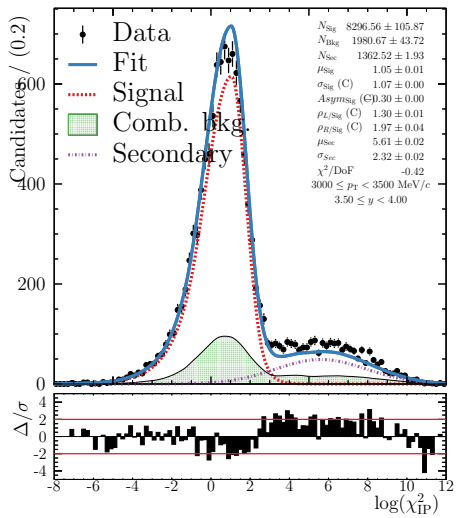

$3 \leq p_{\rm T} < 3.5\,{\rm GeV},\ 3.5 \leq y < 4.0$

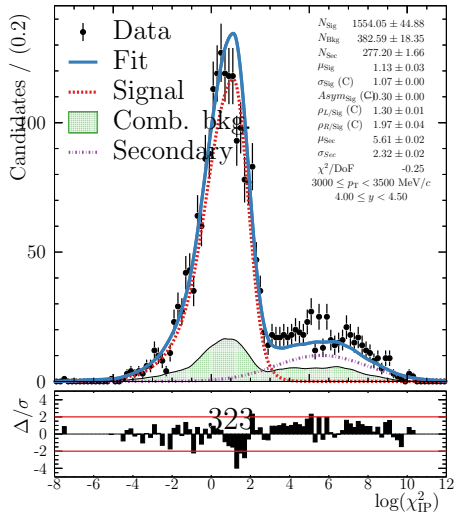

$3 \leq p_{\rm T} < 3.5\,{\rm GeV},\ 4.0 \leq y < 4.5$

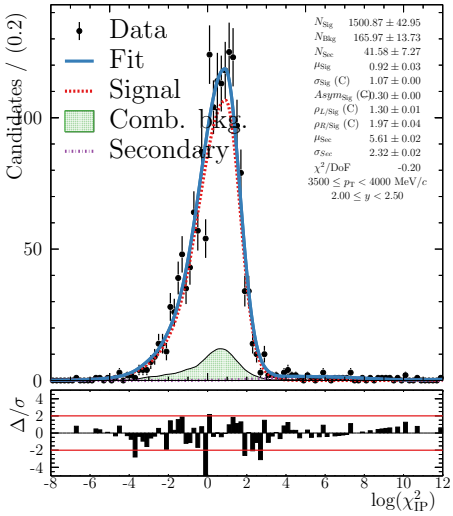

$3.5 \leq p_{\rm T} < 4\,{\rm GeV},\ 2.0 \leq y < 2.5$

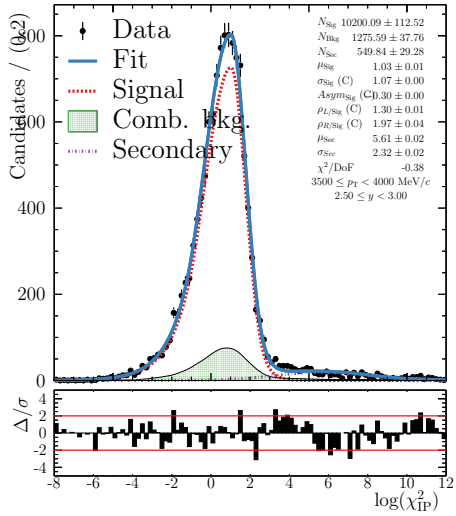

$3.5 \leq p_{\rm T} < 4\,{\rm GeV},\ 2.5 \leq y < 3.0$

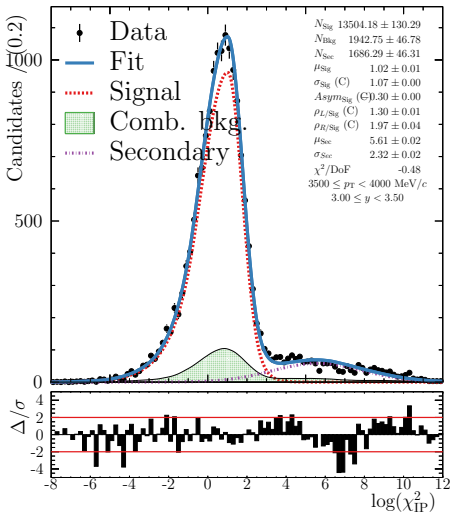

$3.5 \leq p_{\rm T} < 4\,{\rm GeV},\ 3.0 \leq y < 3.5$

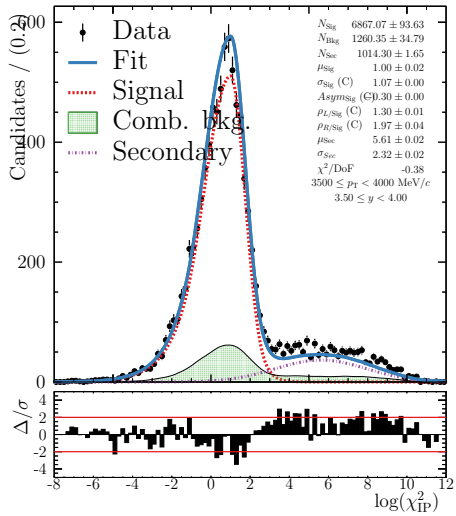

$3.5 \leq p_{\rm T} < 4\,{\rm GeV},\ 3.5 \leq y < 4.0$

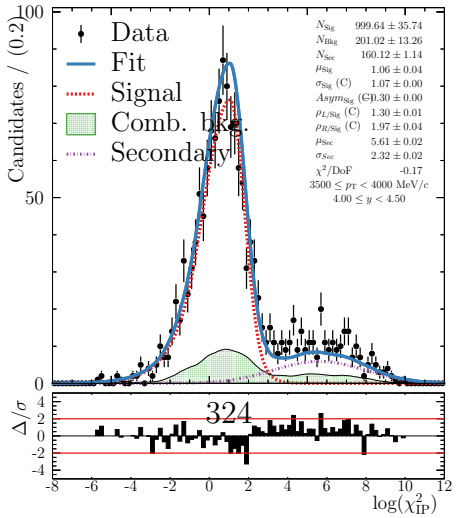

$3.5 \leq p_{\rm T} < 4\,{\rm GeV},\ 4.0 \leq y < 4.5$

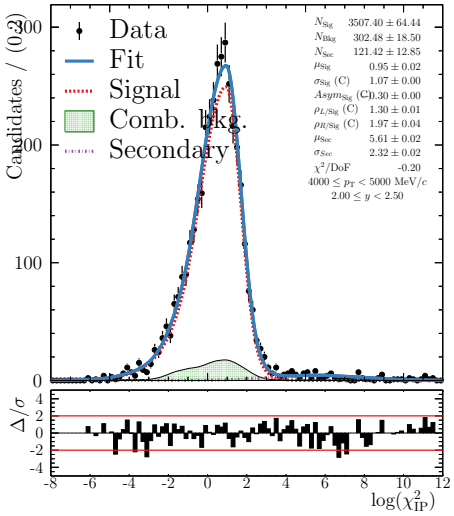

$4 \leq p_{\rm T} < 5\,{\rm GeV},\ 2.0 \leq y < 2.5$

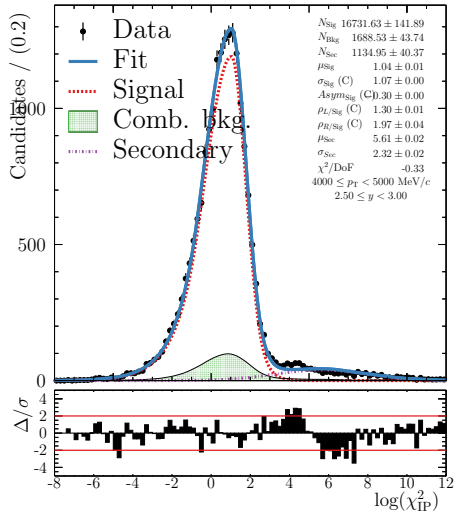

$4 \leq p_{\rm T} < 5\,{\rm GeV},\ 2.5 \leq y < 3.0$

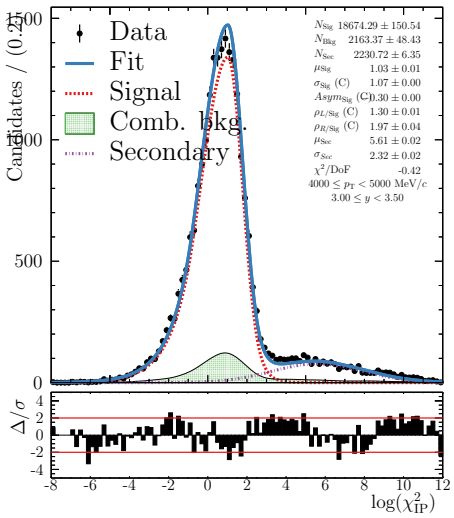

$4 \leq p_{\rm T} < 5\,{\rm GeV},\ 3.0 \leq y < 3.5$

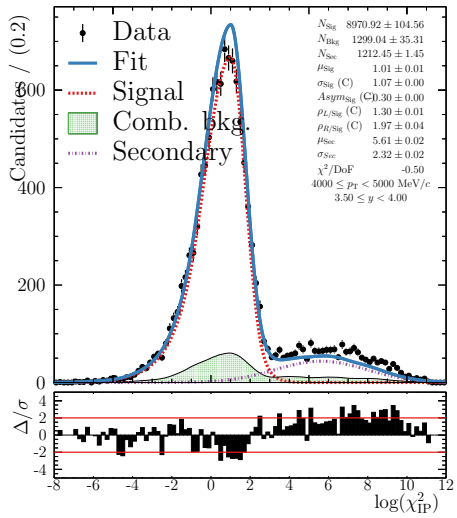

$4 \leq p_{\rm T} < 5\,{\rm GeV},\ 3.5 \leq y < 4.0$

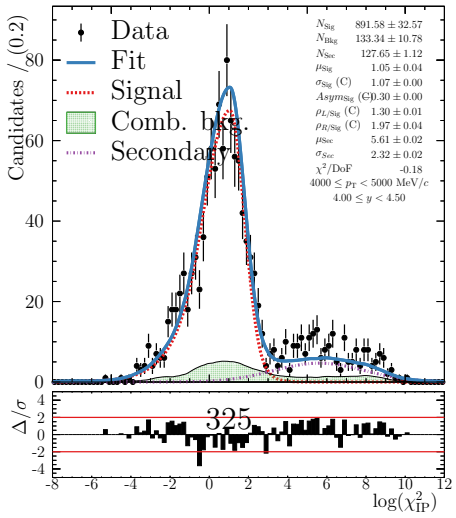

$4 \leq p_{\rm T} < 5\,{\rm GeV},\ 4.0 \leq y < 4.5$

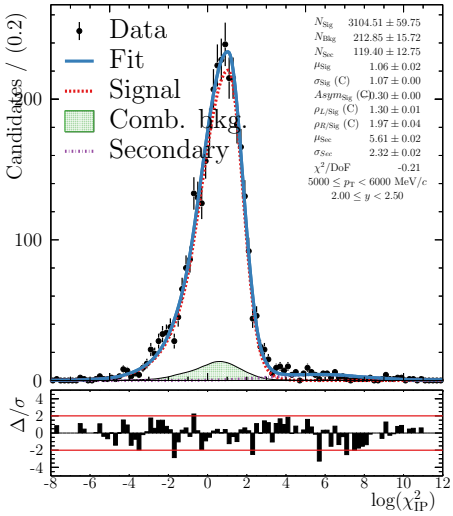

$5 \leq p_{\rm T} < 6\,{\rm GeV},\ 2.0 \leq y < 2.5$

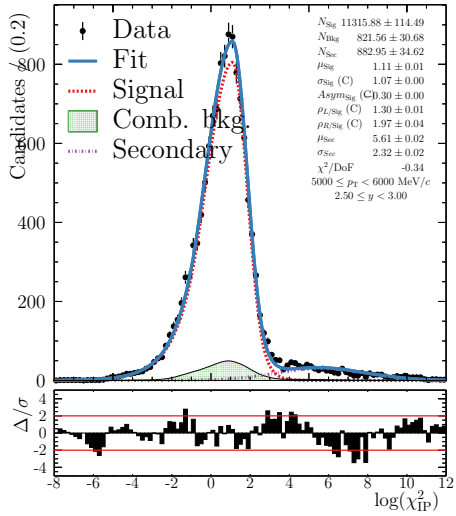

$5 \leq p_{\rm T} < 6\,{\rm GeV},\ 2.5 \leq y < 3.0$

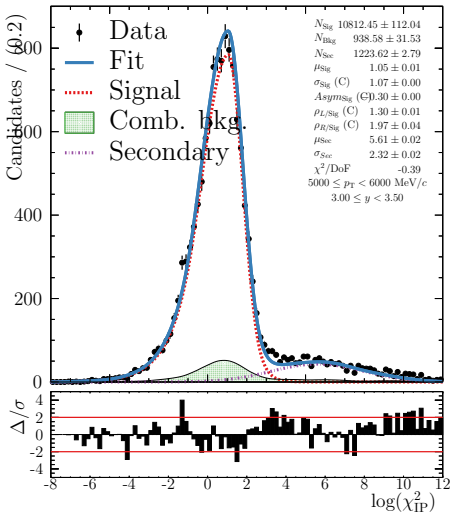

$5 \leq p_{\rm T} < 6\,{\rm GeV},\ 3.0 \leq y < 3.5$

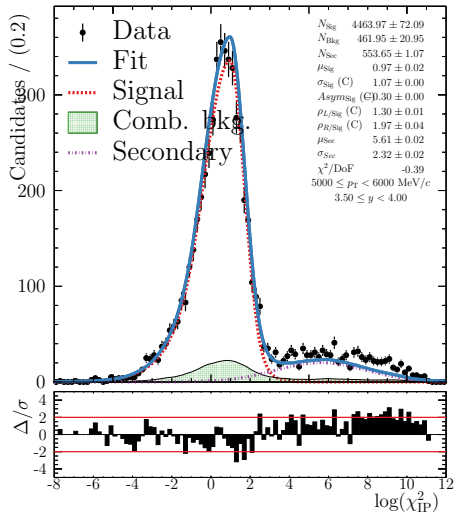

$5 \leq p_{\rm T} < 6\,{\rm GeV},\ 3.5 \leq y < 4.0$

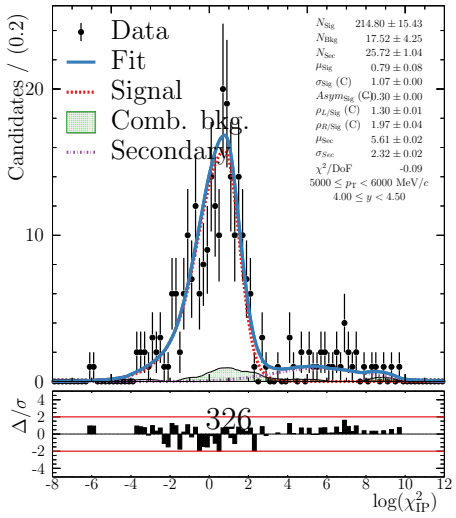

$5 \leq p_{\rm T} < 6\,{\rm GeV},\ 4.0 \leq y < 4.5$

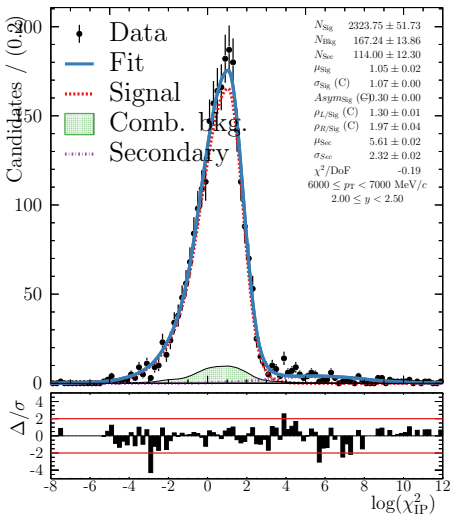

$6 \leq p_{\rm T} < 7\,{\rm GeV},\ 2.0 \leq y < 2.5$

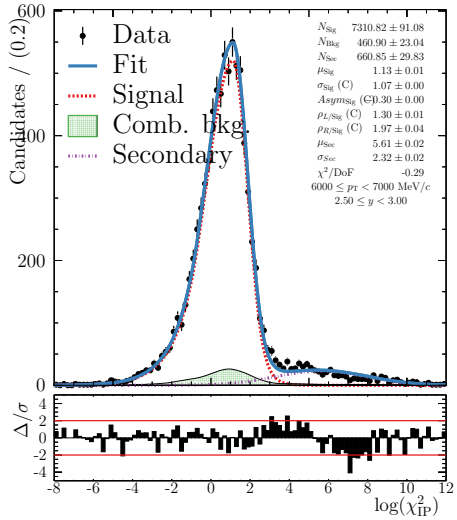

$6 \leq p_{\rm T} < 7\,{\rm GeV},\ 2.5 \leq y < 3.0$

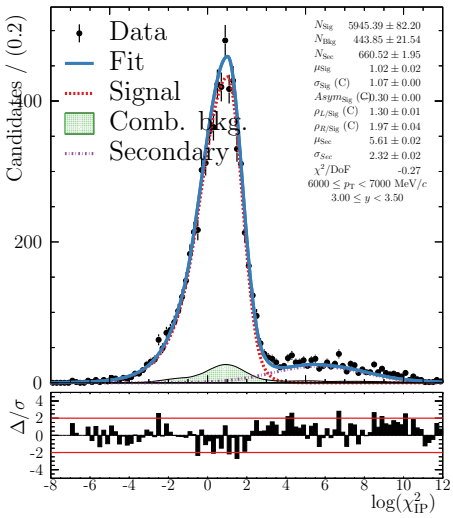

$6 \leq p_{\rm T} < 7\,{\rm GeV},\ 3.0 \leq y < 3.5$

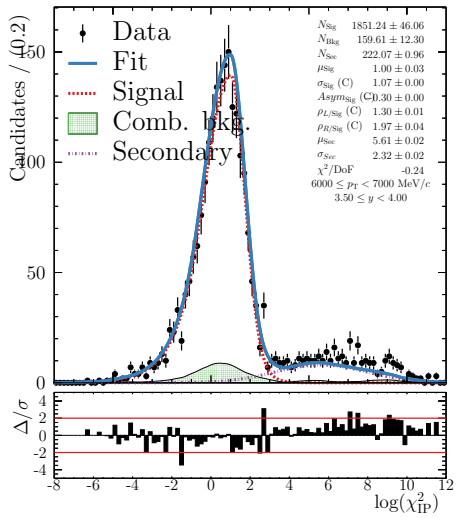

$6 \leq p_{\rm T} < 7\,{\rm GeV},\ 3.5 \leq y < 4.0$

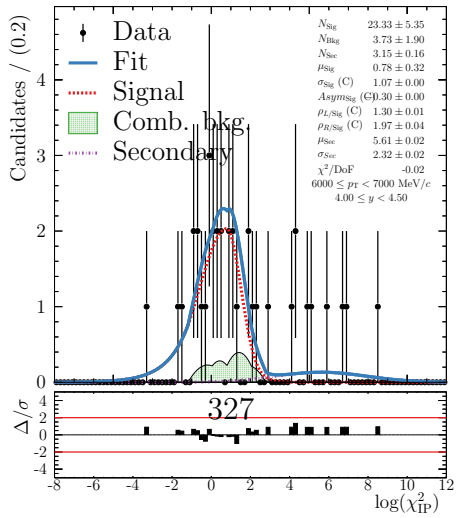

$6 \leq p_{\rm T} < 7\,{\rm GeV},\ 4.0 \leq y < 4.5$

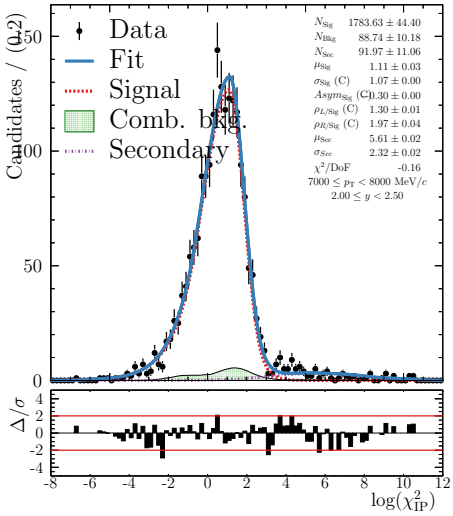

$7 \le p_{\rm T} < 8\,{\rm GeV},\ 2.0 \le y < 2.5$

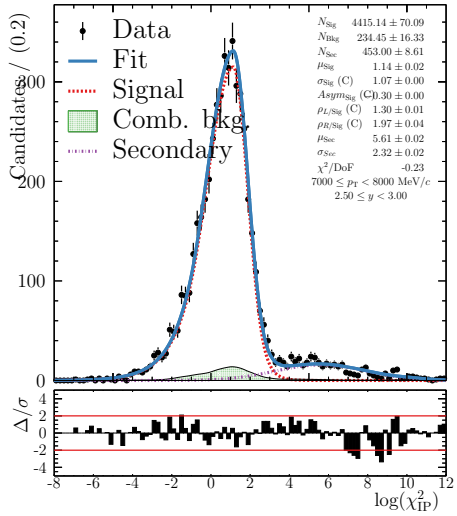

$7 \le p_{\rm T} < 8\,{\rm GeV},\ 2.5 \le y < 3.0$

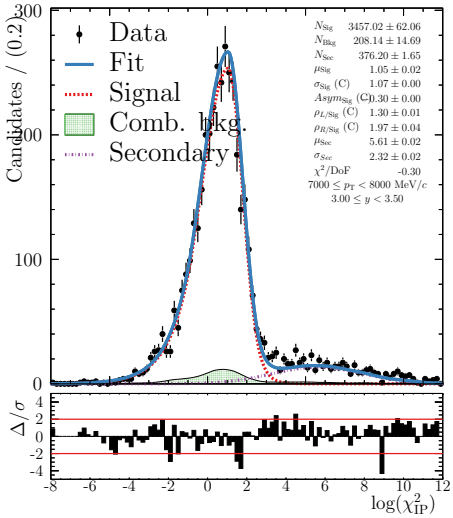

$7 \le p_{\rm T} < 8\,{\rm GeV},\ 3.0 \le y < 3.5$

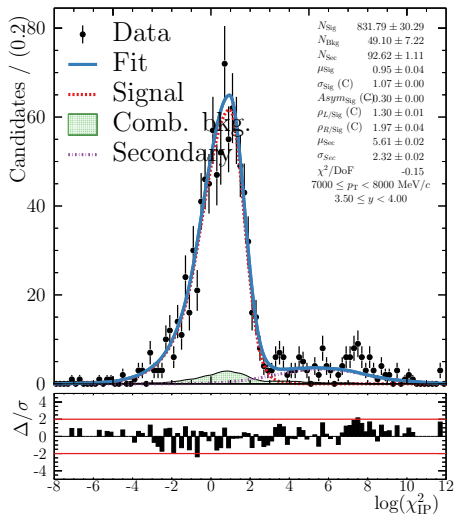

$7 \le p_{\rm T} < 8\,{\rm GeV},\ 3.5 \le y < 4.0$

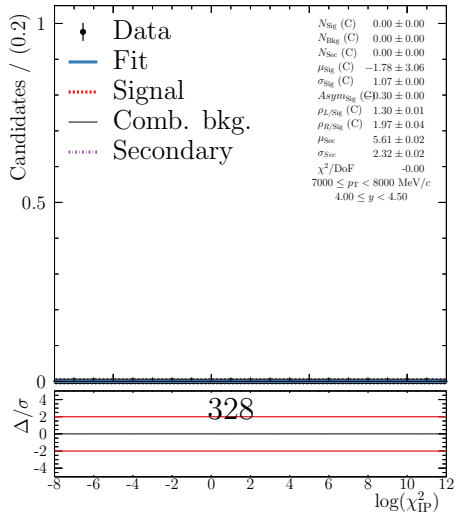

$7 \le p_{\rm T} < 8\,{\rm GeV},\ 4.0 \le y < 4.5$

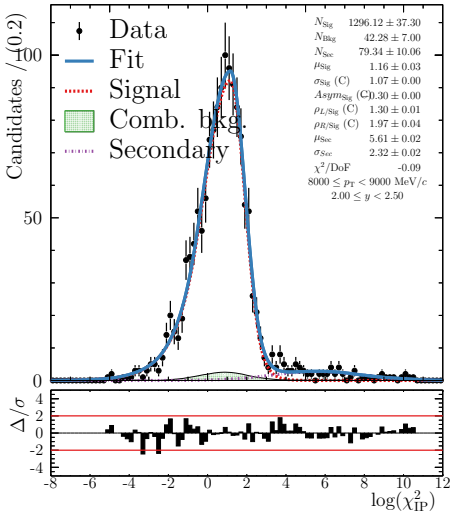

$8 \le p_{\rm T} < 9\,{\rm GeV},\ 2.0 \le y < 2.5$

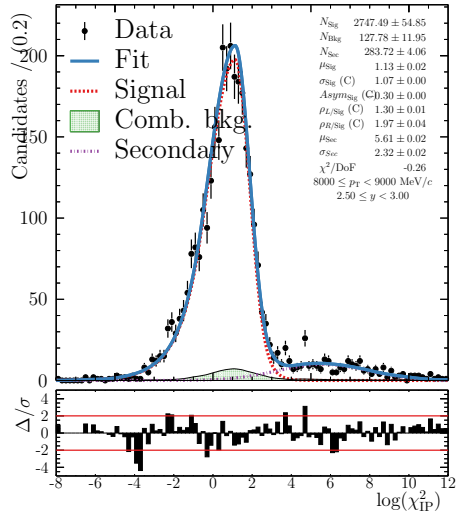

$8 \le p_{\rm T} < 9\,{\rm GeV},\ 2.5 \le y < 3.0$

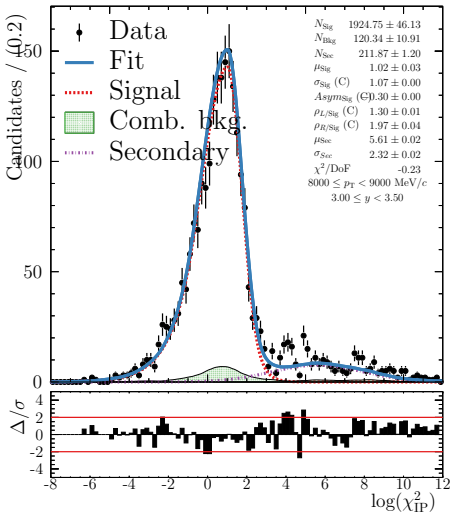

$8 \le p_{\rm T} < 9\,{\rm GeV},\ 3.0 \le y < 3.5$

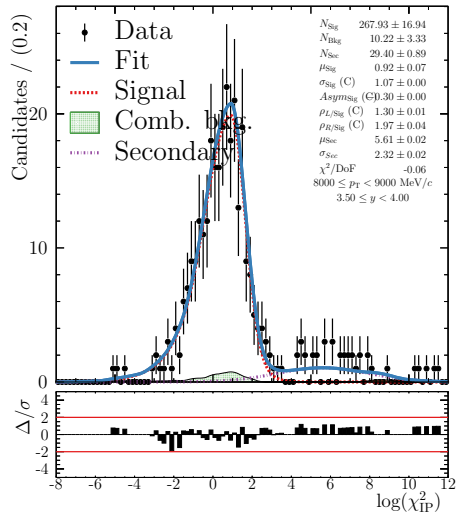

$8 \le p_{\rm T} < 9\,{\rm GeV},\ 3.5 \le y < 4.0$

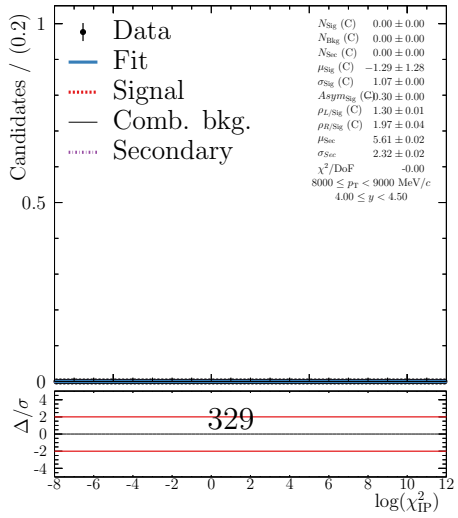

$8 \le p_{\rm T} < 9\,{\rm GeV},\ 4.0 \le y < 4.5$

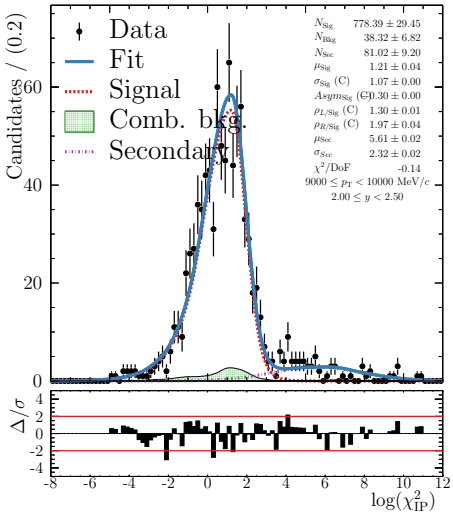

$9 \le p_{\rm T} < 10\,{\rm GeV},\ 2.0 \le y < 2.5$

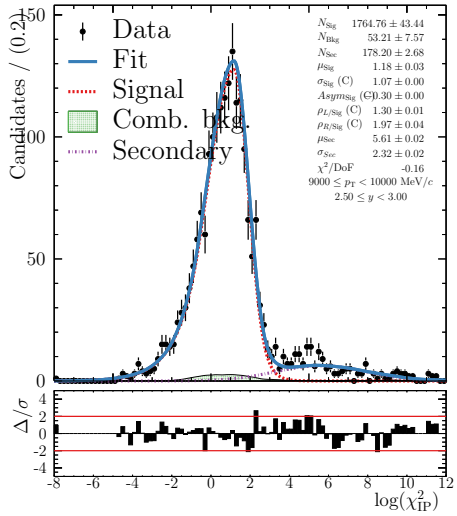

$9 \le p_{\rm T} < 10\,{\rm GeV},\ 2.5 \le y < 3.0$

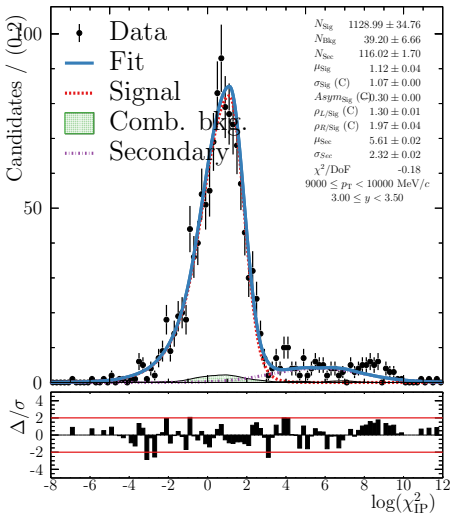

$9 \le p_{\rm T} < 10\,{\rm GeV},\ 3.0 \le y < 3.5$

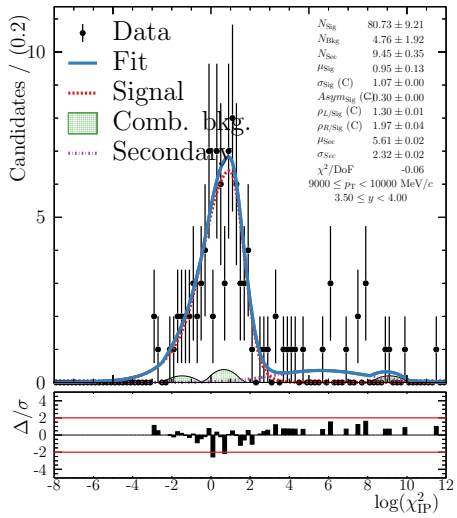

$9 \le p_{\rm T} < 10\,{\rm GeV},\ 3.5 \le y < 4.0$

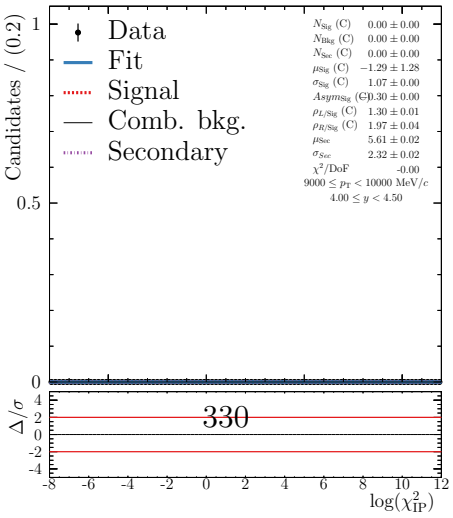

$9 \le p_{\rm T} < 10\,{\rm GeV},\ 4.0 \le y < 4.5$

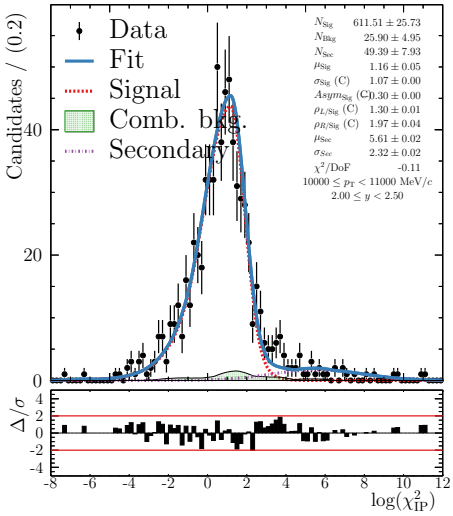

$10 \leq p_{\rm T} < 11\,{\rm GeV},\ 2.0 \leq y < 2.5$

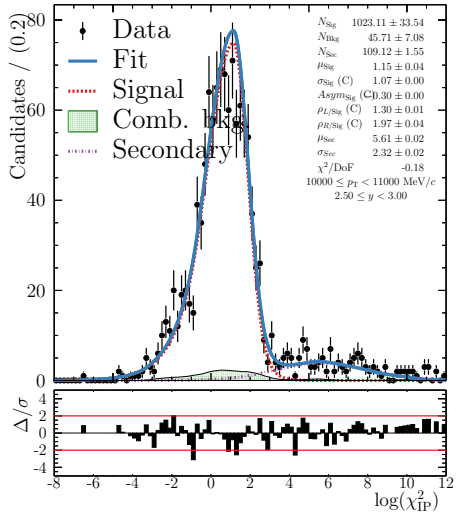

$10 \leq p_{\rm T} < 11\,{\rm GeV},\ 2.5 \leq y < 3.0$

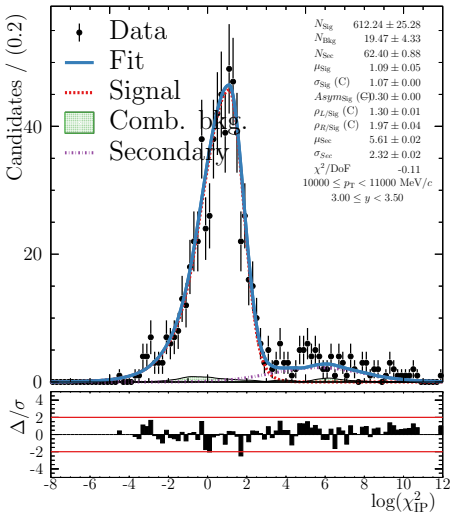

$10 \leq p_{\rm T} < 11\,{\rm GeV},\ 3.0 \leq y < 3.5$

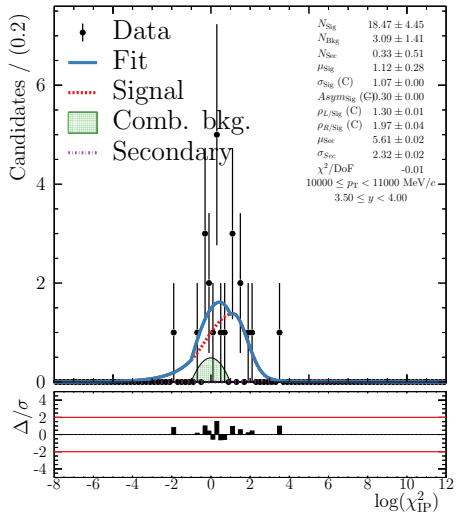

$10 \leq p_{\rm T} < 11\,{\rm GeV},\ 3.5 \leq y < 4.0$

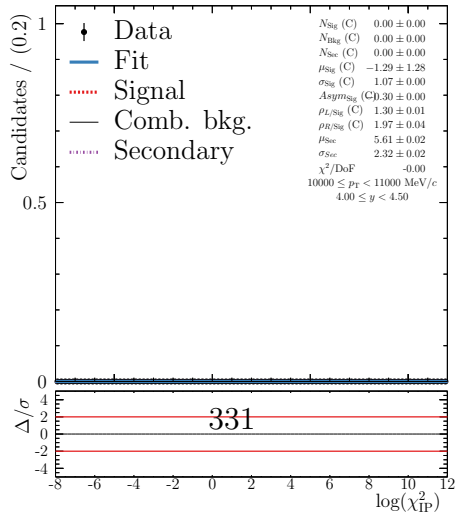

$10 \leq p_{\rm T} < 11\,{\rm GeV},\ 4.0 \leq y < 4.5$

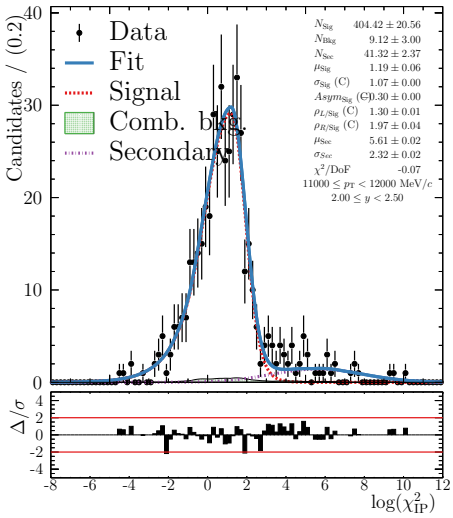

$11 \leq p_{\rm T} < 12\,{\rm GeV},\ 2.0 \leq y < 2.5$

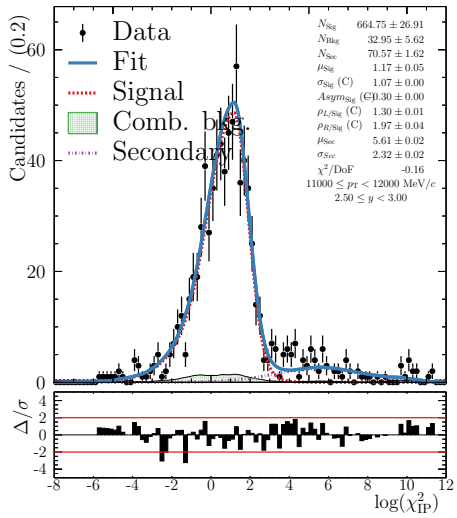

$11 \leq p_{\rm T} < 12\,{\rm GeV},\ 2.5 \leq y < 3.0$

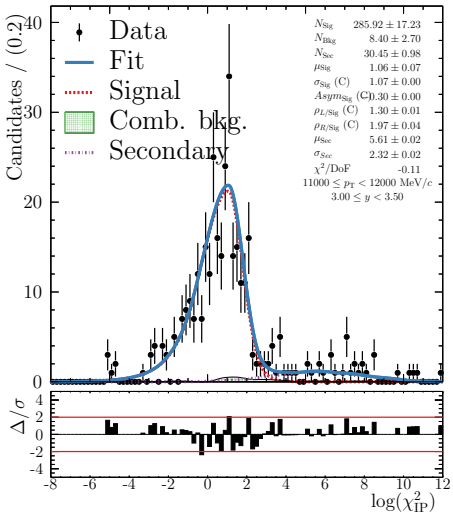

$11 \leq p_{\rm T} < 12\,{\rm GeV},\ 3.0 \leq y < 3.5$

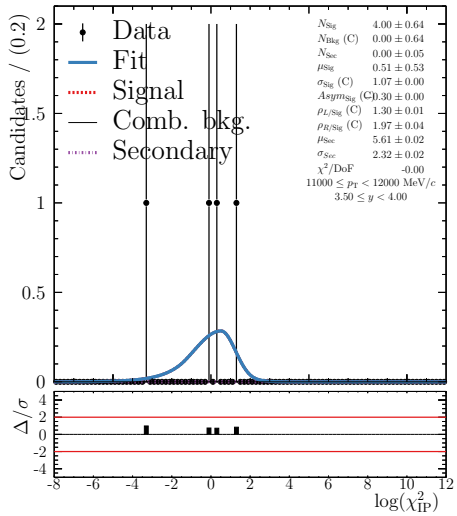

$11 \leq p_{\rm T} < 12\,{\rm GeV},\ 3.5 \leq y < 4.0$

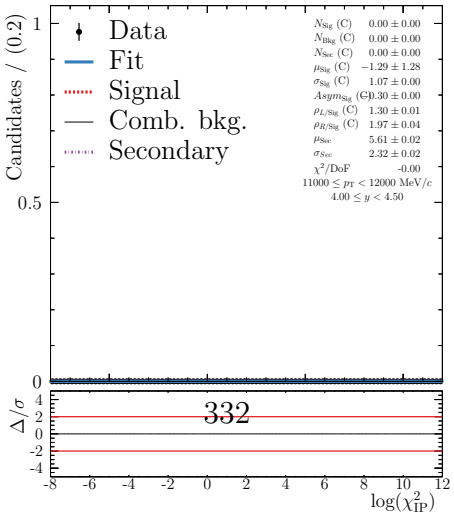

$11 \leq p_{\rm T} < 12\,{\rm GeV},\ 4.0 \leq y < 4.5$

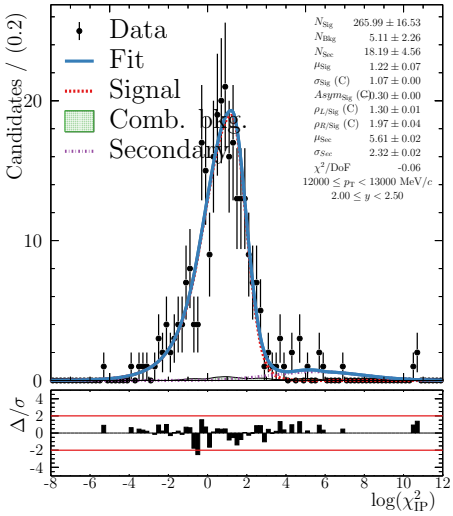

$12 \leq p_{\rm T} < 13\,{\rm GeV},\ 2.0 \leq y < 2.5$

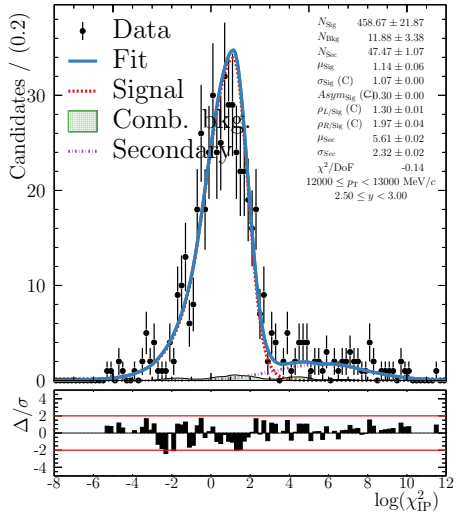

$12 \leq p_{\rm T} < 13\,{\rm GeV},\ 2.5 \leq y < 3.0$

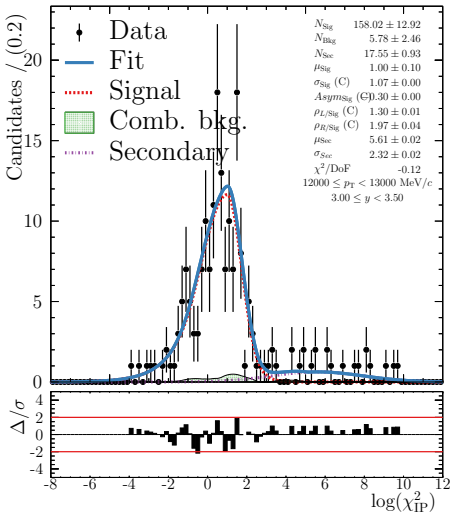

$12 \leq p_{\rm T} < 13\,{\rm GeV},\ 3.0 \leq y < 3.5$

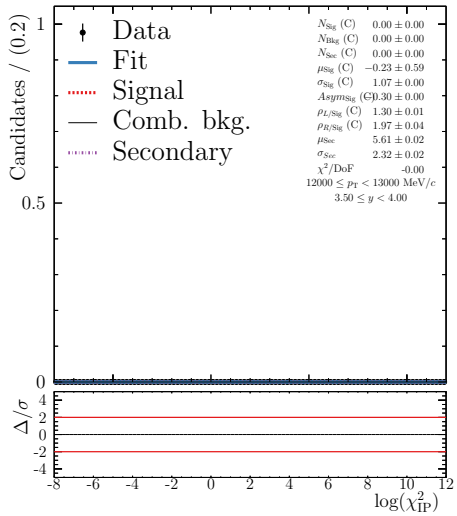

$12 \leq p_{\rm T} < 13\,{\rm GeV},\ 3.5 \leq y < 4.0$

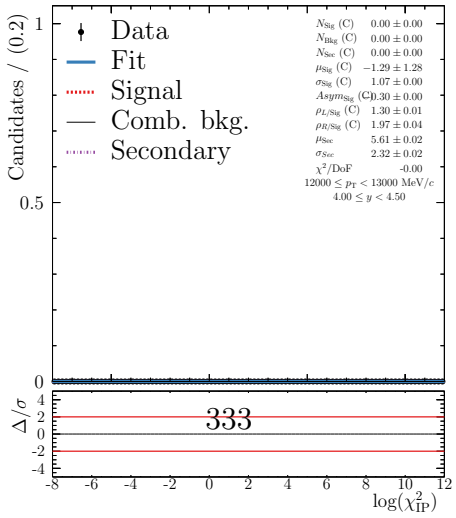

$12 \leq p_{\rm T} < 13\,{\rm GeV},\ 4.0 \leq y < 4.5$

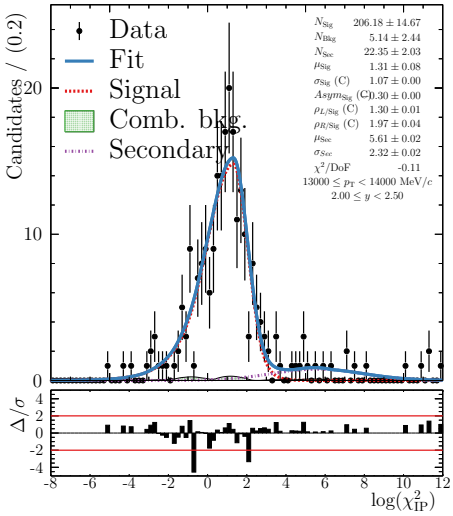

$13 \leq p_{\rm T} < 14\,{\rm GeV},\ 2.0 \leq y < 2.5$

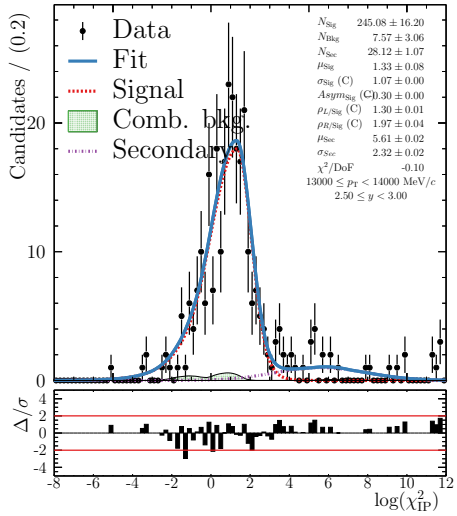

$13 \leq p_{\rm T} < 14\,{\rm GeV},\ 2.5 \leq y < 3.0$

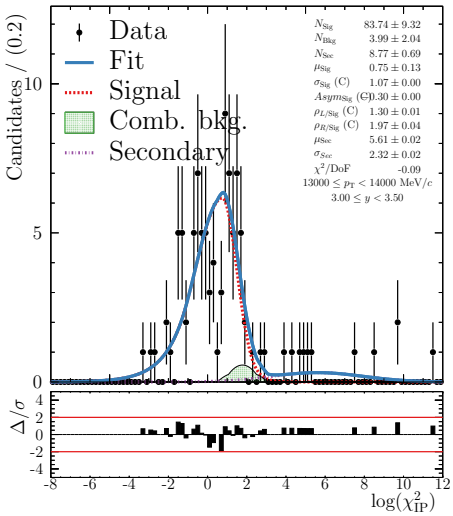

$13 \leq p_{\rm T} < 14\,{\rm GeV},\ 3.0 \leq y < 3.5$

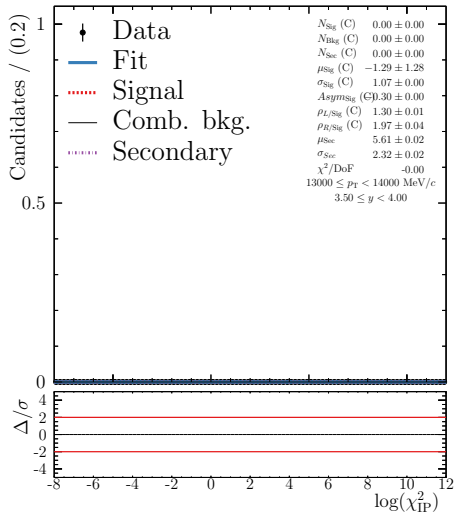

$13 \leq p_{\rm T} < 14\,{\rm GeV},\ 3.5 \leq y < 4.0$

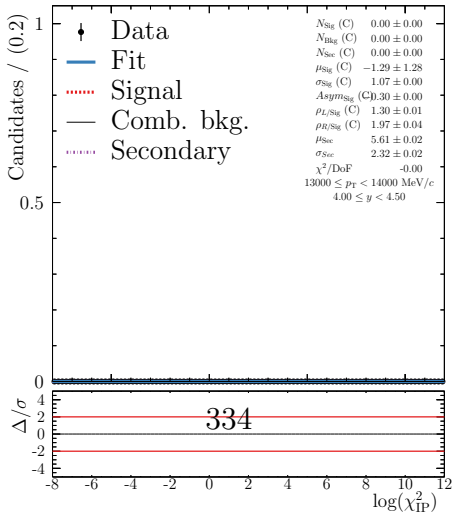

$13 \leq p_{\rm T} < 14\,{\rm GeV},\ 4.0 \leq y < 4.5$

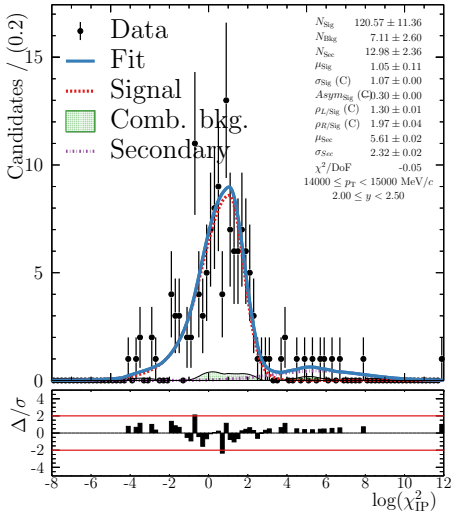

$14 \leq p_{\rm T} < 15\,{\rm GeV},\ 2.0 \leq y < 2.5$

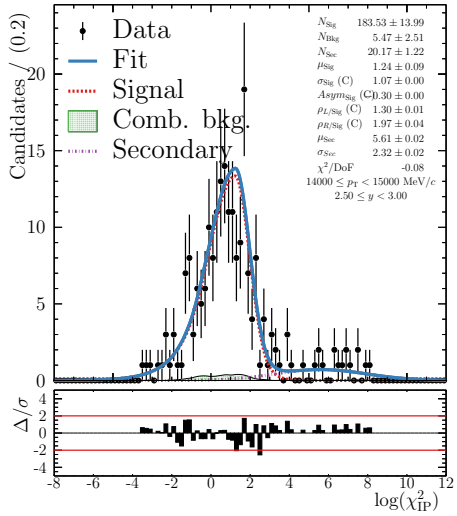

$14 \leq p_{\rm T} < 15\,{\rm GeV},\ 2.5 \leq y < 3.0$

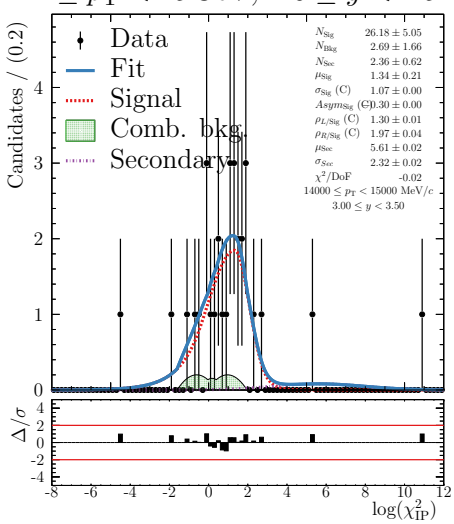

$14 \leq p_{\rm T} < 15\,{\rm GeV},\ 3.0 \leq y < 3.5$

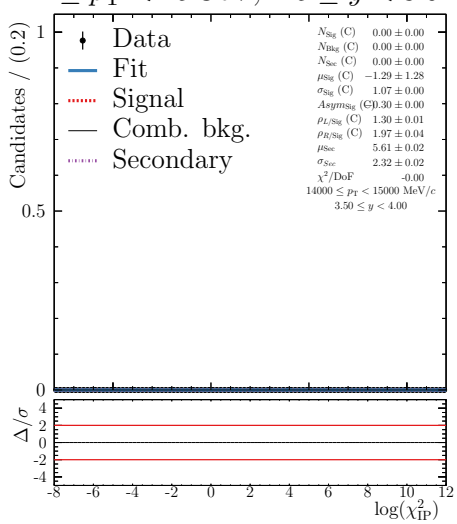

$14 \leq p_{\rm T} < 15\,{\rm GeV},\ 3.5 \leq y < 4.0$

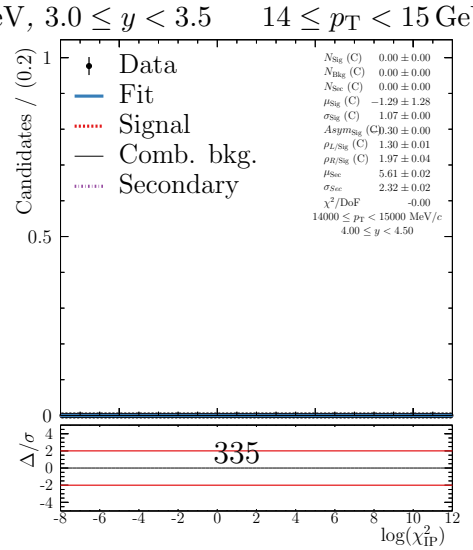

$14 \leq p_{\rm T} < 15\,{\rm GeV},\ 4.0 \leq y < 4.5$

Figure F.0: Fits to the fully selected $D^0 \to K^-\pi^+$, from $D^{*+} \to D^0\pi^+$, $\ln\chi^2_{\rm IP}$ distribution per $p_{\rm T}$-y bin.

F.7 $D^{*+} \to D^0\pi^+$ with $D^0 \to K^-\pi^+\pi^-\pi^+$

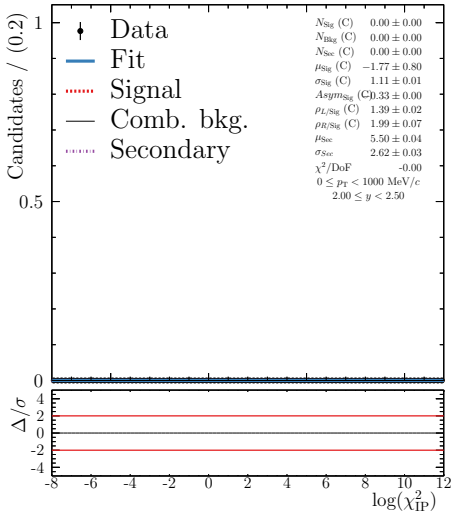

$0 \leq p_{\rm T} < 1\,{\rm GeV},\ 2.0 \leq y < 2.5$

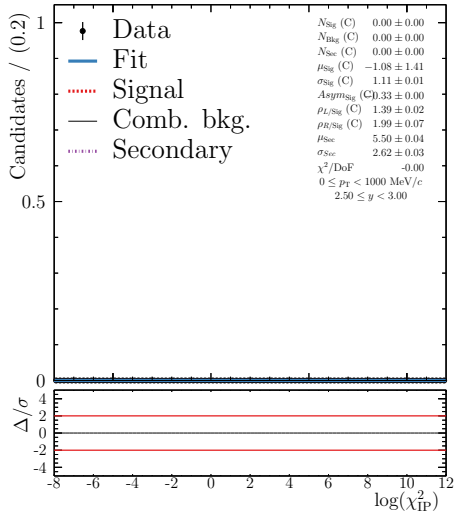

$0 \leq p_{\rm T} < 1\,{\rm GeV},\ 2.5 \leq y < 3.0$

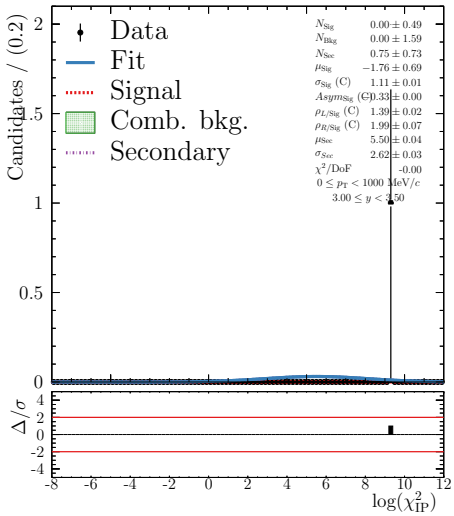

$0 \leq p_{\rm T} < 1\,{\rm GeV},\ 3.0 \leq y < 3.5$

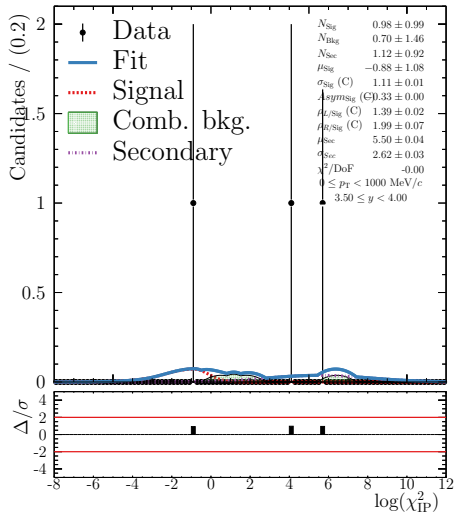

$0 \leq p_{\rm T} < 1\,{\rm GeV},\ 3.5 \leq y < 4.0$

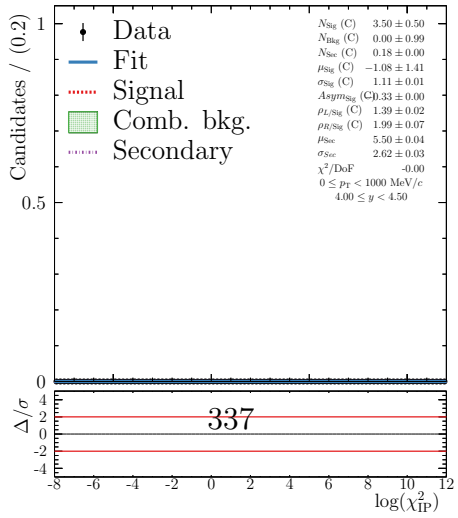

$0 \leq p_{\rm T} < 1\,{\rm GeV},\ 4.0 \leq y < 4.5$

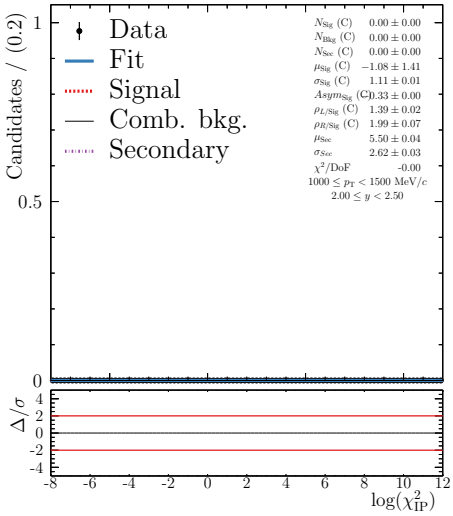

$1 \leq p_{\rm T} < 1.5\,{\rm GeV},\ 2.0 \leq y < 2.5$

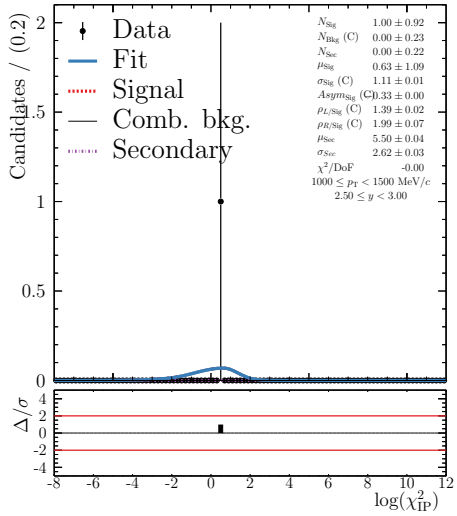

$1 \leq p_{\rm T} < 1.5\,{\rm GeV},\ 2.5 \leq y < 3.0$

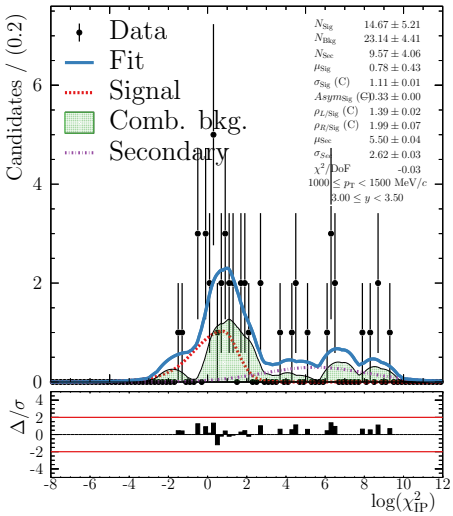

$1 \leq p_{\rm T} < 1.5\,{\rm GeV},\ 3.0 \leq y < 3.5$

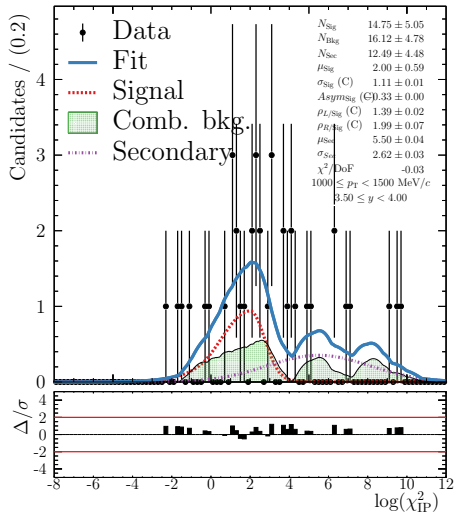

$1 \leq p_{\rm T} < 1.5\,{\rm GeV},\ 3.5 \leq y < 4.0$

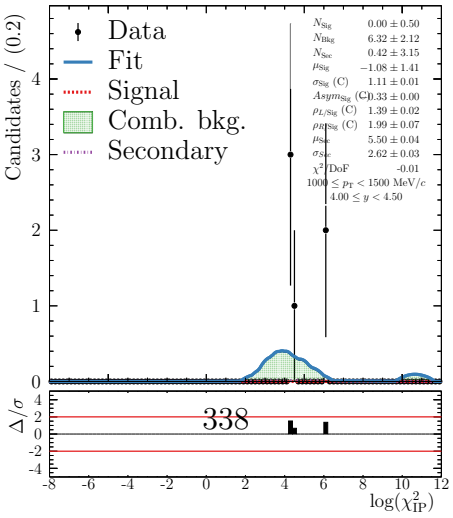

$1 \leq p_{\rm T} < 1.5\,{\rm GeV},\ 4.0 \leq y < 4.5$

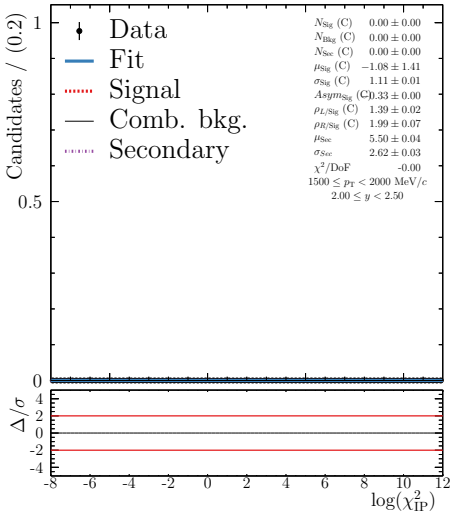

$1.5 \leq p_{\rm T} < 2\,{\rm GeV},\ 2.0 \leq y < 2.5$

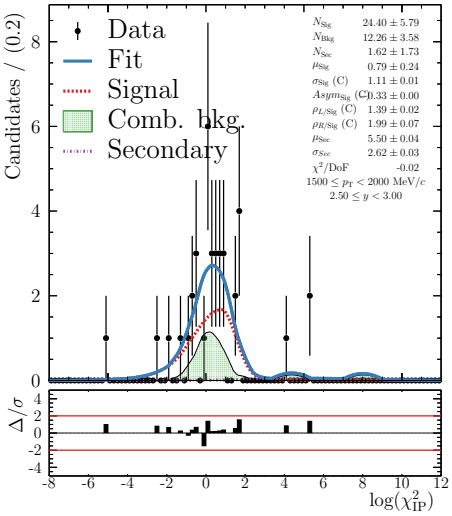

$1.5 \leq p_{\rm T} < 2\,{\rm GeV},\ 2.5 \leq y < 3.0$

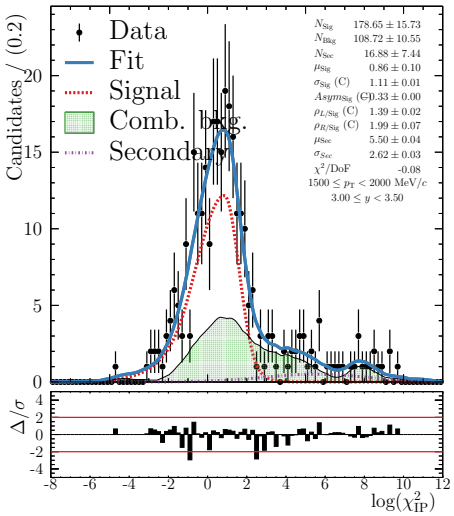

$1.5 \leq p_{\rm T} < 2\,{\rm GeV},\ 3.0 \leq y < 3.5$

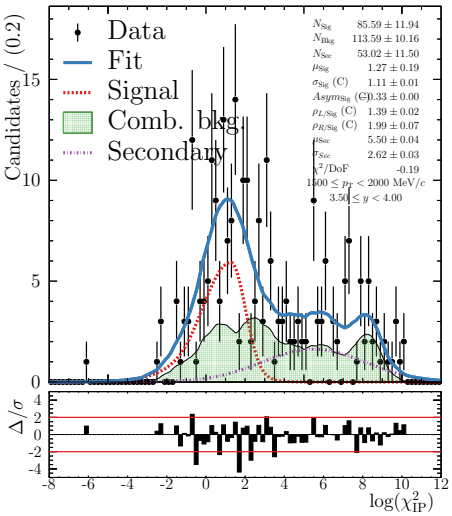

$1.5 \leq p_{\rm T} < 2\,{\rm GeV},\ 3.5 \leq y < 4.0$

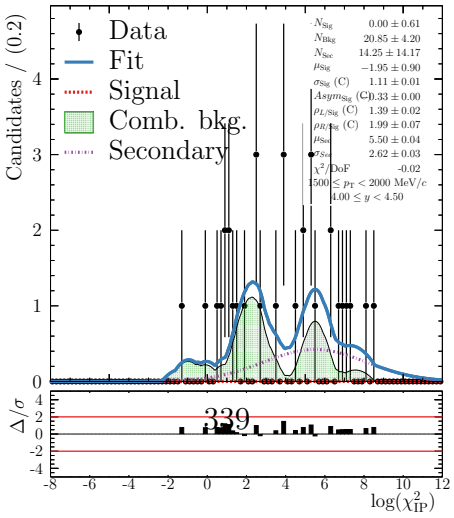

$1.5 \leq p_{\rm T} < 2\,{\rm GeV},\ 4.0 \leq y < 4.5$

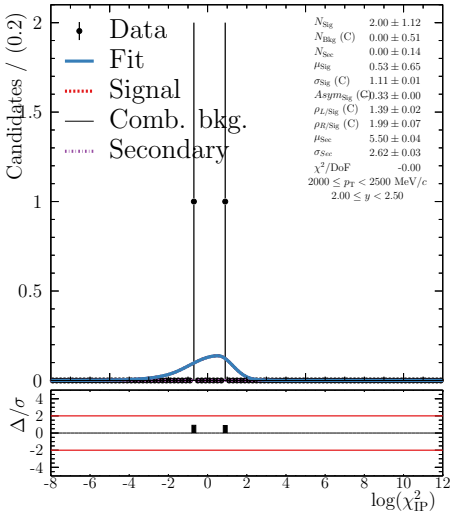

$2 \leq p_{\rm T} < 2.5\,{\rm GeV},\ 2.0 \leq y < 2.5$

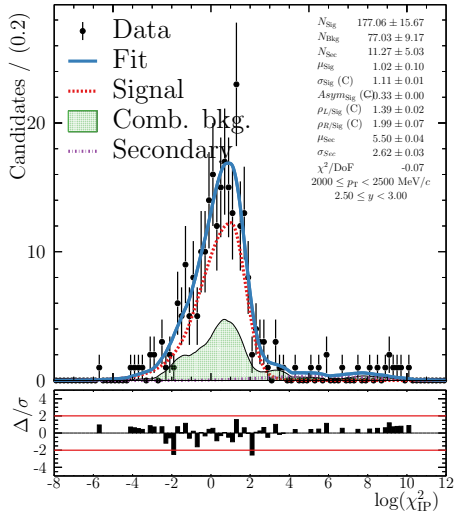

$2 \leq p_{\rm T} < 2.5\,{\rm GeV},\ 2.5 \leq y < 3.0$

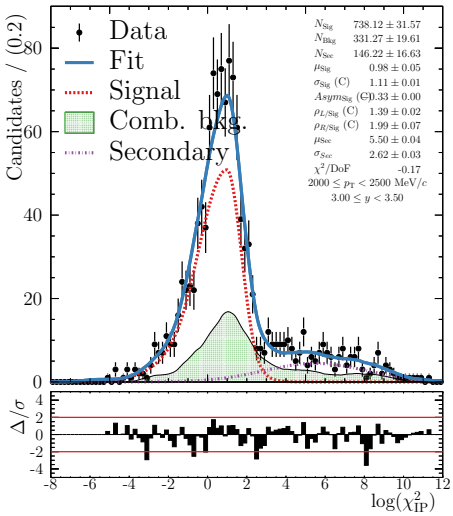

$2 \leq p_{\rm T} < 2.5\,{\rm GeV},\ 3.0 \leq y < 3.5$

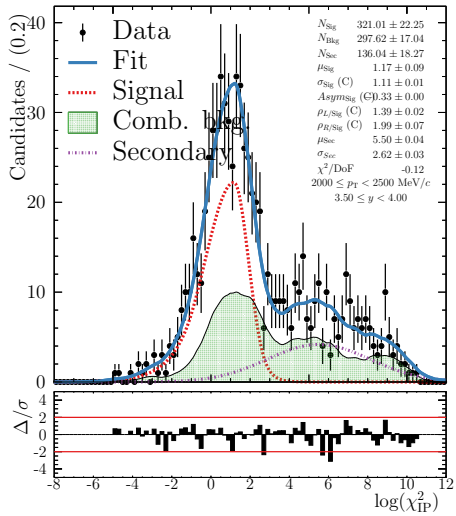

$2 \leq p_{\rm T} < 2.5\,{\rm GeV},\ 3.5 \leq y < 4.0$

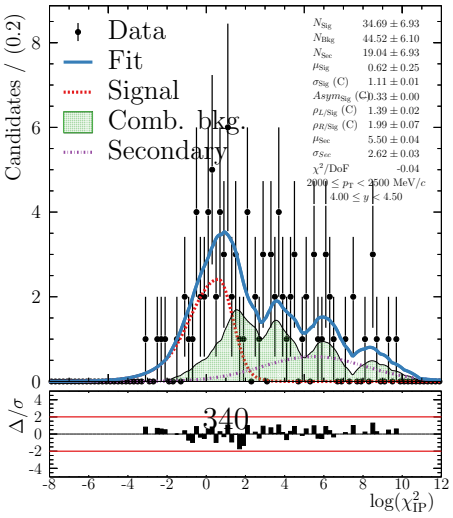

$2 \leq p_{\rm T} < 2.5\,{\rm GeV},\ 4.0 \leq y < 4.5$

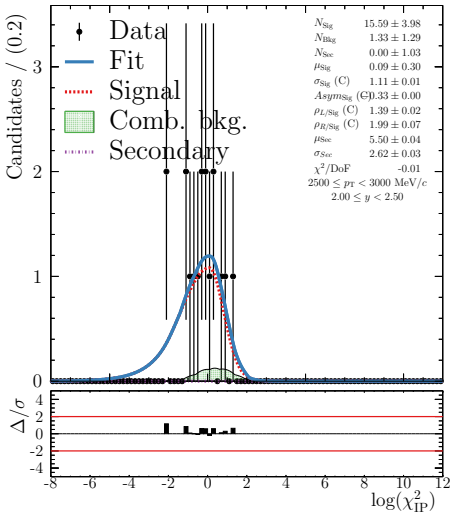

$2.5 \leq p_{\rm T} < 3\,{\rm GeV},\ 2.0 \leq y < 2.5$

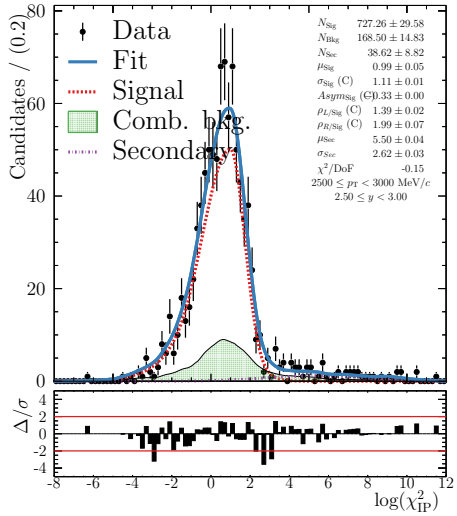

$2.5 \leq p_{\rm T} < 3\,{\rm GeV},\ 2.5 \leq y < 3.0$

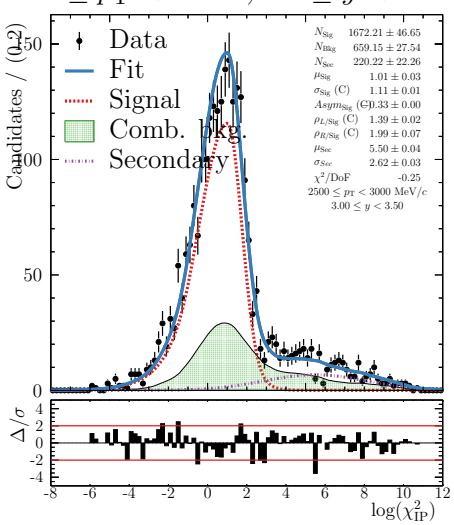

$2.5 \leq p_{\rm T} < 3\,{\rm GeV},\ 3.0 \leq y < 3.5$

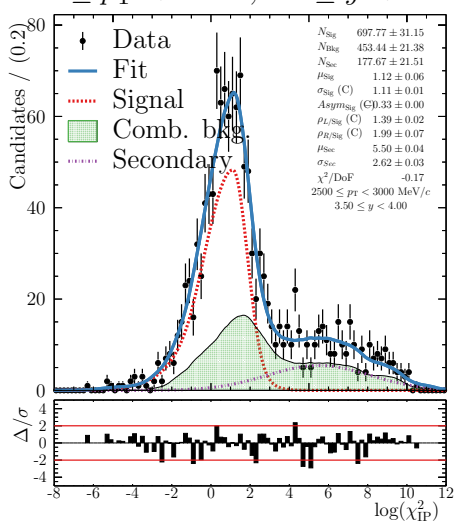

$2.5 \leq p_{\rm T} < 3\,{\rm GeV},\ 3.5 \leq y < 4.0$

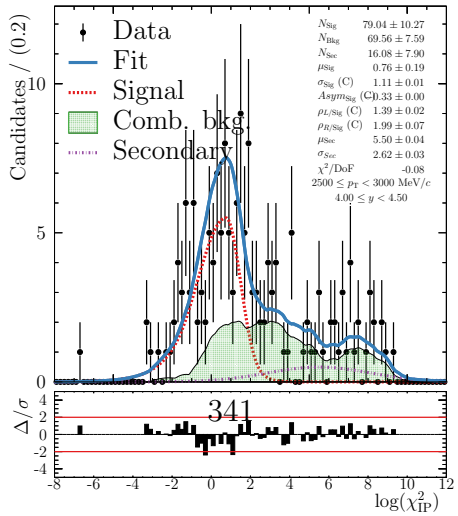

$2.5 \leq p_{\rm T} < 3\,{\rm GeV},\ 4.0 \leq y < 4.5$

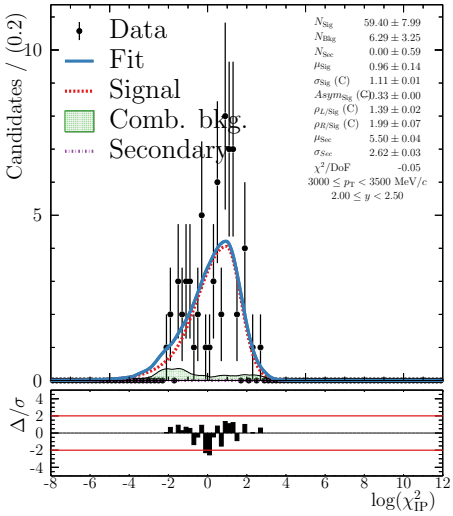

$3 \leq p_{\rm T} < 3.5\,{\rm GeV},\ 2.0 \leq y < 2.5$

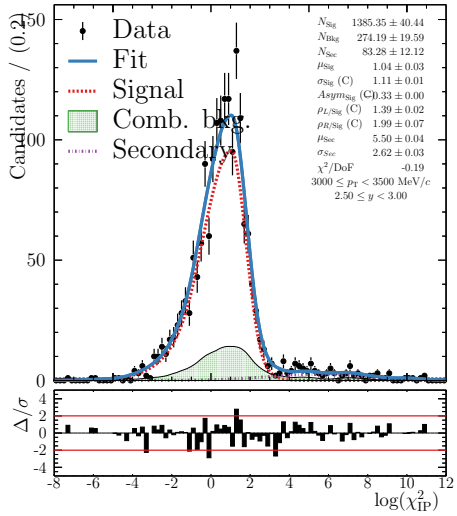

$3 \leq p_{\rm T} < 3.5\,{\rm GeV},\ 2.5 \leq y < 3.0$

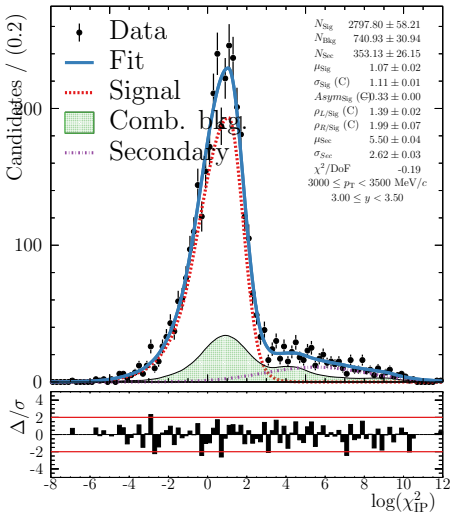

$3 \leq p_{\rm T} < 3.5\,{\rm GeV},\ 3.0 \leq y < 3.5$

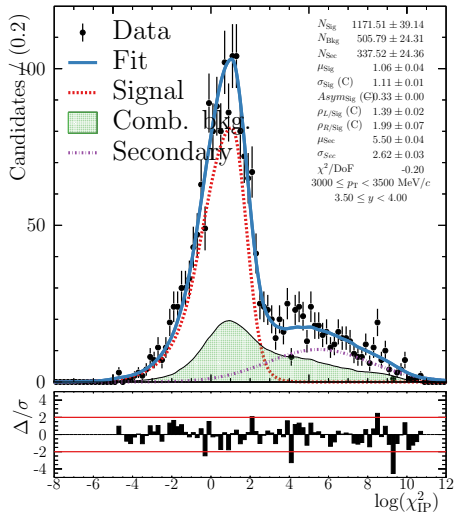

$3 \leq p_{\rm T} < 3.5\,{\rm GeV},\ 3.5 \leq y < 4.0$

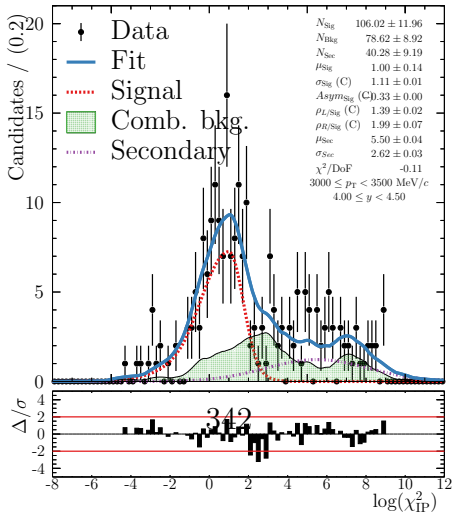

$3 \leq p_{\rm T} < 3.5\,{\rm GeV},\ 4.0 \leq y < 4.5$

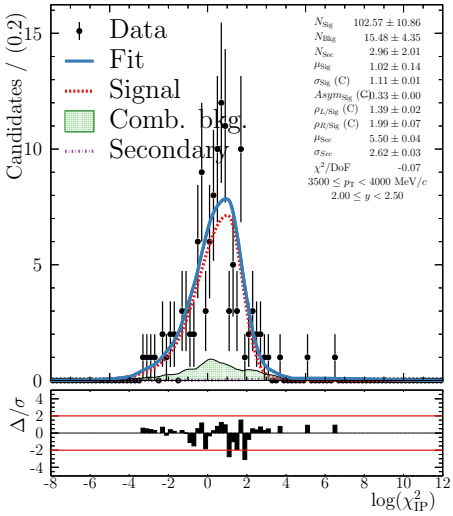

$3.5 \leq p_{\rm T} < 4\,{\rm GeV},\ 2.0 \leq y < 2.5$

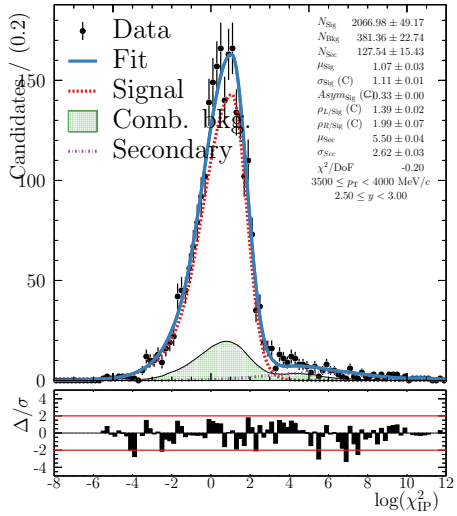

$3.5 \leq p_{\rm T} < 4\,{\rm GeV},\ 2.5 \leq y < 3.0$

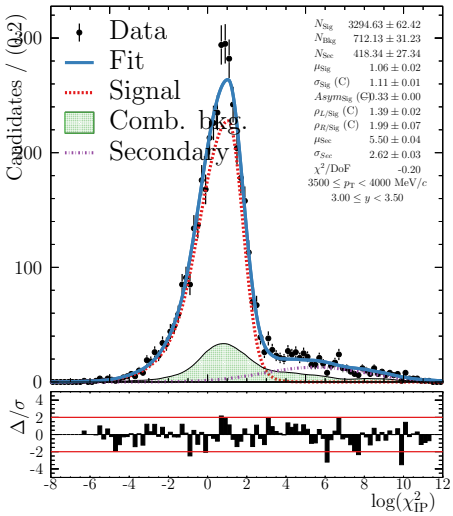

$3.5 \leq p_{\rm T} < 4\,{\rm GeV},\ 3.0 \leq y < 3.5$

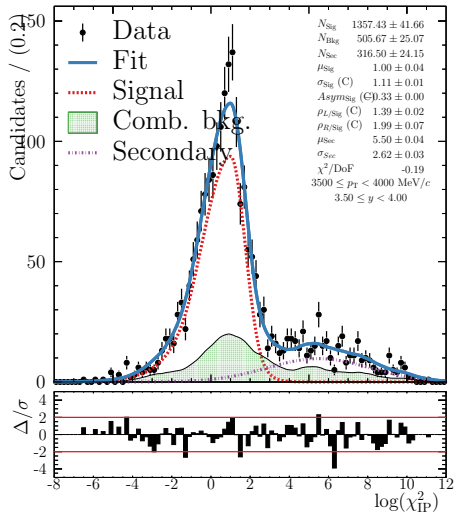

$3.5 \leq p_{\rm T} < 4\,{\rm GeV},\ 3.5 \leq y < 4.0$

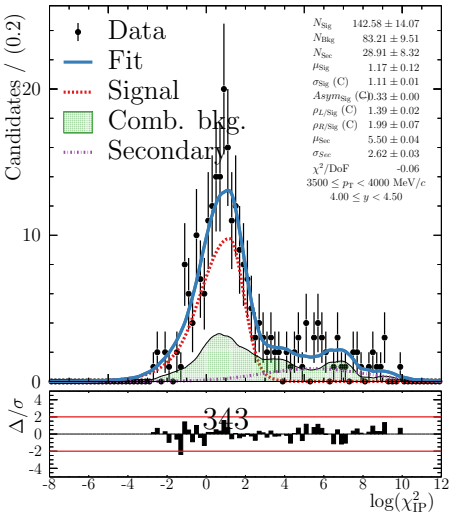

$3.5 \leq p_{\rm T} < 4\,{\rm GeV},\ 4.0 \leq y < 4.5$

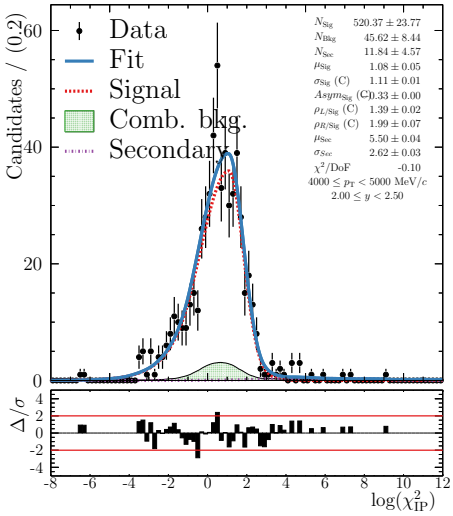

$4 \le p_{\rm T} < 5\,{\rm GeV},\ 2.0 \le y < 2.5$

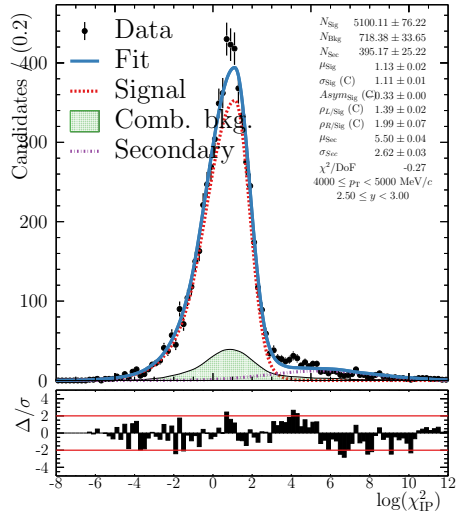

$4 \le p_{\rm T} < 5\,{\rm GeV},\ 2.5 \le y < 3.0$

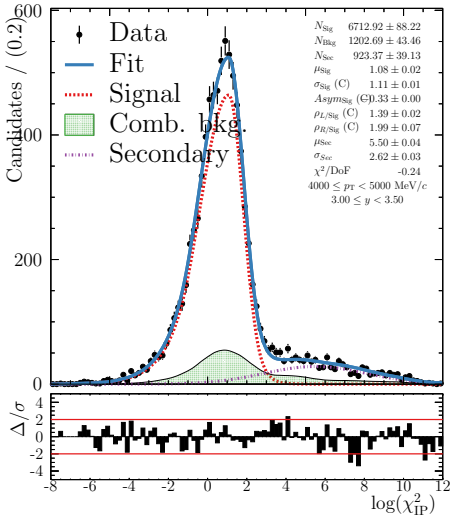

$4 \le p_{\rm T} < 5\,{\rm GeV},\ 3.0 \le y < 3.5$

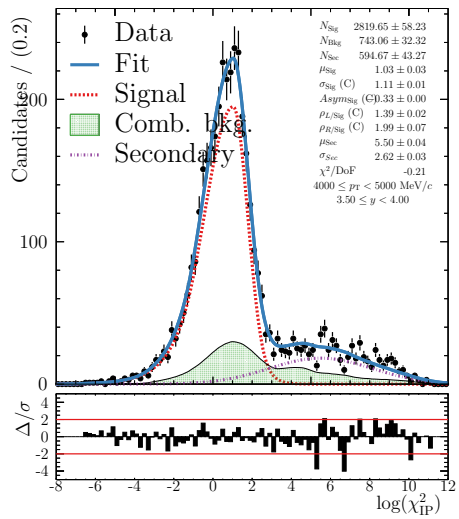

$4 \le p_{\rm T} < 5\,{\rm GeV},\ 3.5 \le y < 4.0$

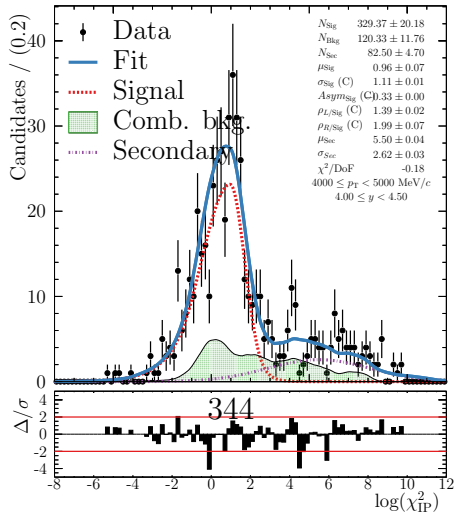

$4 \le p_{\rm T} < 5\,{\rm GeV},\ 4.0 \le y < 4.5$

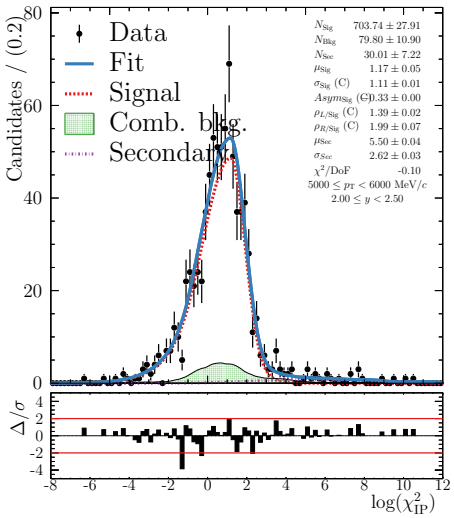

$5 \leq p_{\rm T} < 6\,{\rm GeV},\ 2.0 \leq y < 2.5$

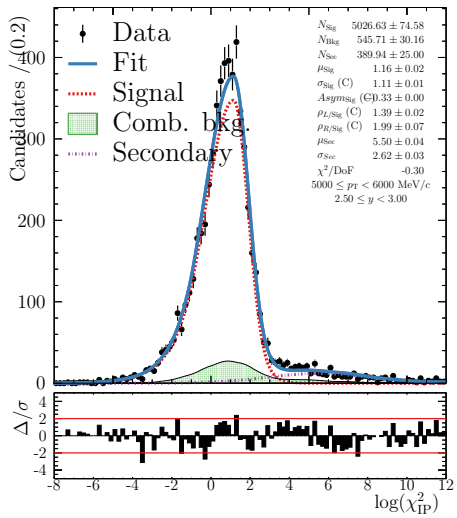

$5 \leq p_{\rm T} < 6\,{\rm GeV},\ 2.5 \leq y < 3.0$

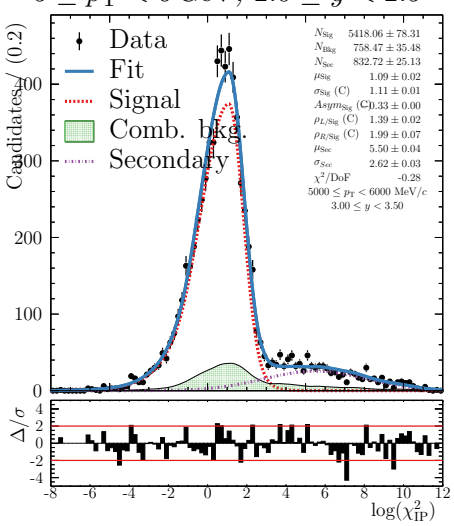

$5 \leq p_{\rm T} < 6\,{\rm GeV},\ 3.0 \leq y < 3.5$

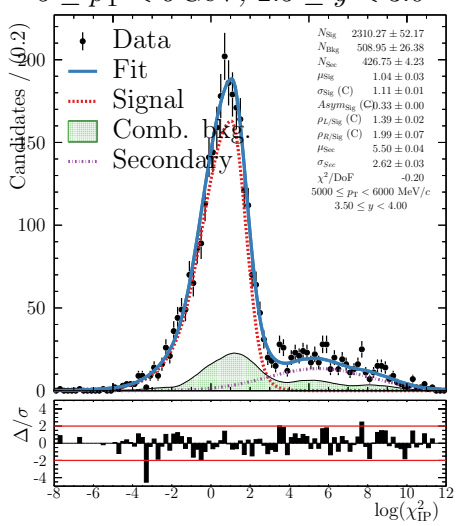

$5 \leq p_{\rm T} < 6\,{\rm GeV},\ 3.5 \leq y < 4.0$

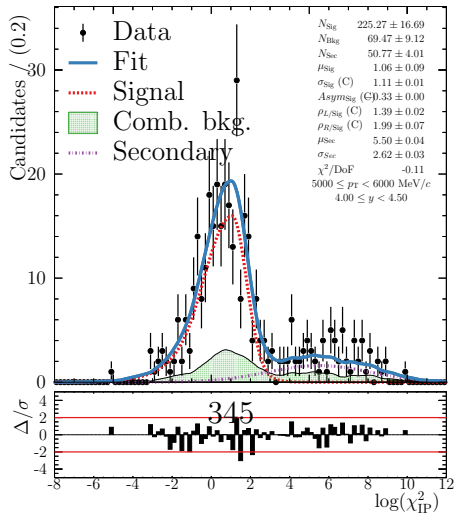

$5 \leq p_{\rm T} < 6\,{\rm GeV},\ 4.0 \leq y < 4.5$

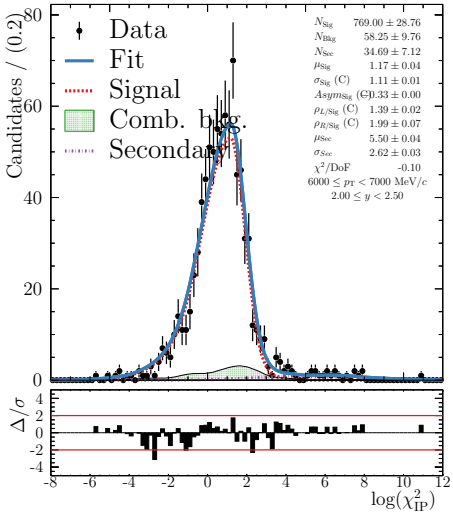

$6 \le p_{\rm T} < 7\,{\rm GeV},\ 2.0 \le y < 2.5$

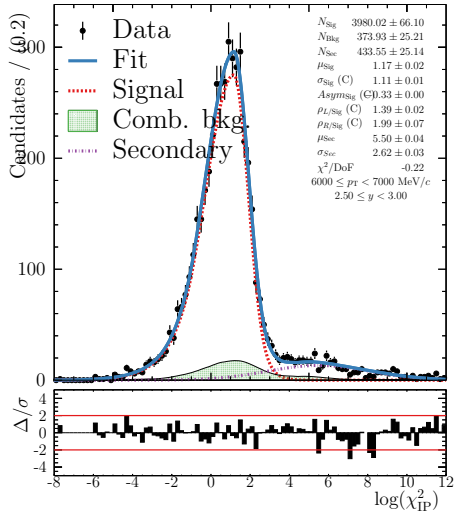

$6 \le p_{\rm T} < 7\,{\rm GeV},\ 2.5 \le y < 3.0$

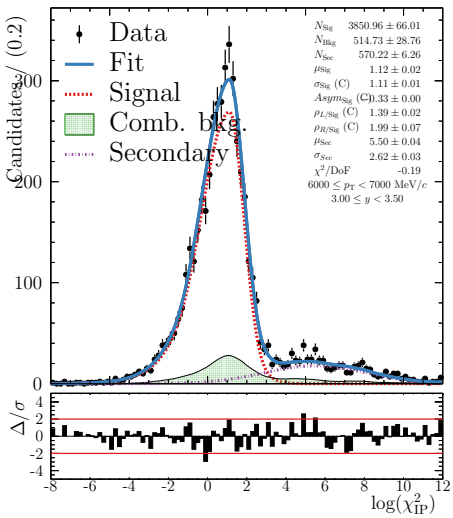

$6 \le p_{\rm T} < 7\,{\rm GeV},\ 3.0 \le y < 3.5$

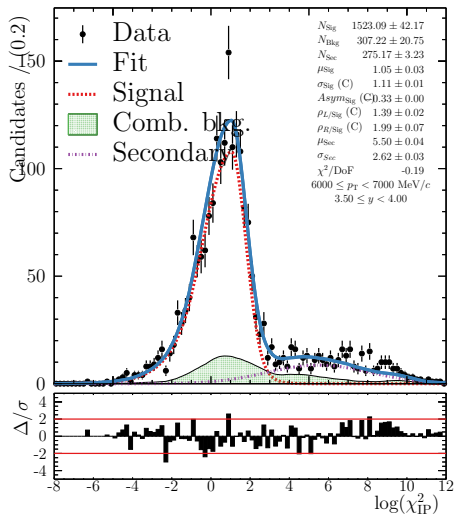

$6 \le p_{\rm T} < 7\,{\rm GeV},\ 3.5 \le y < 4.0$

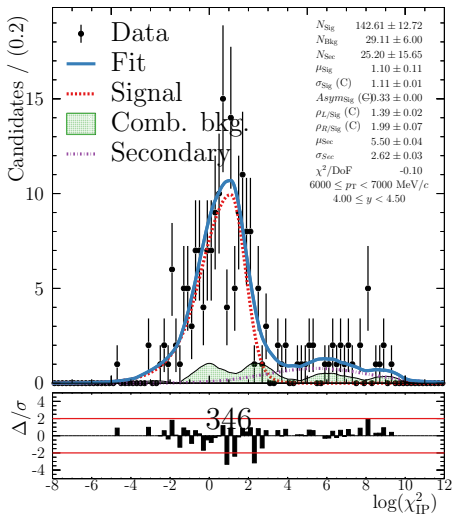

$6 \le p_{\rm T} < 7\,{\rm GeV},\ 4.0 \le y < 4.5$

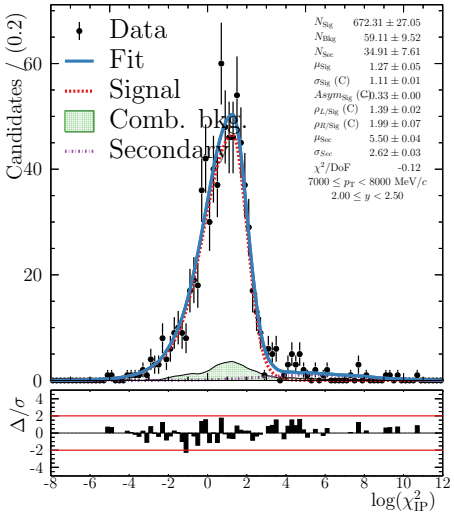

$7 \leq p_{\rm T} < 8\,{\rm GeV},\ 2.0 \leq y < 2.5$

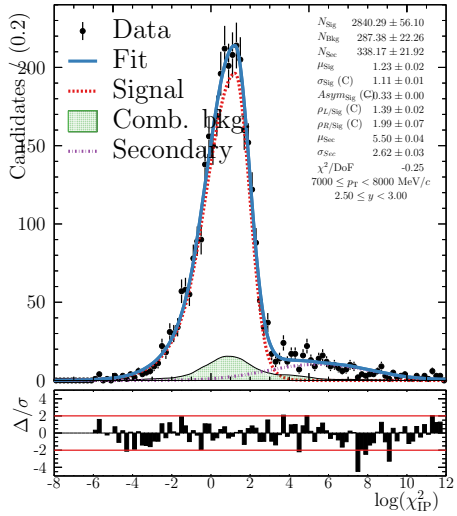

$7 \leq p_{\rm T} < 8\,{\rm GeV},\ 2.5 \leq y < 3.0$

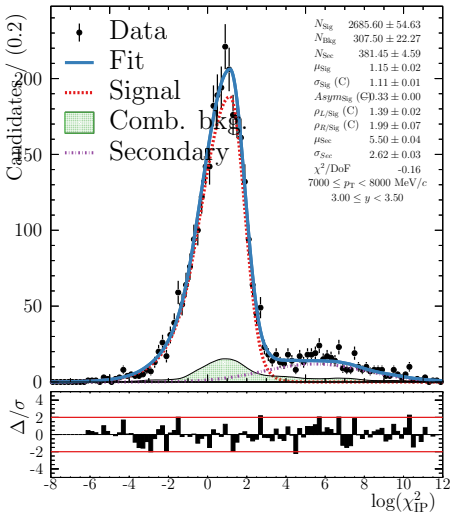

$7 \leq p_{\rm T} < 8\,{\rm GeV},\ 3.0 \leq y < 3.5$

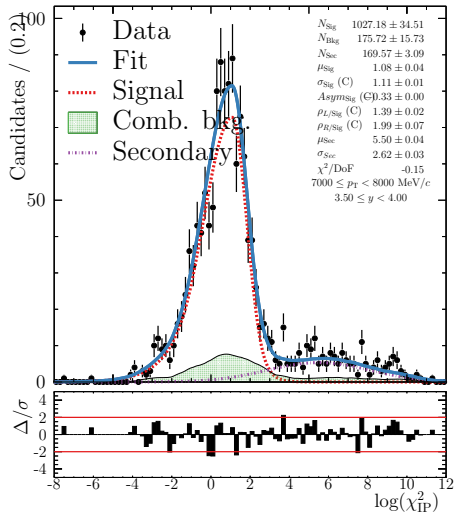

$7 \leq p_{\rm T} < 8\,{\rm GeV},\ 3.5 \leq y < 4.0$

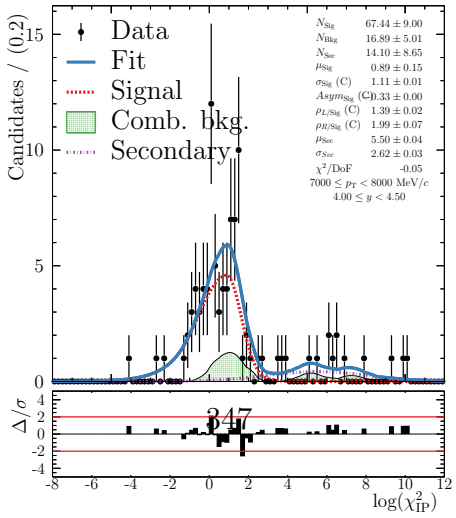

$7 \leq p_{\rm T} < 8\,{\rm GeV},\ 4.0 \leq y < 4.5$

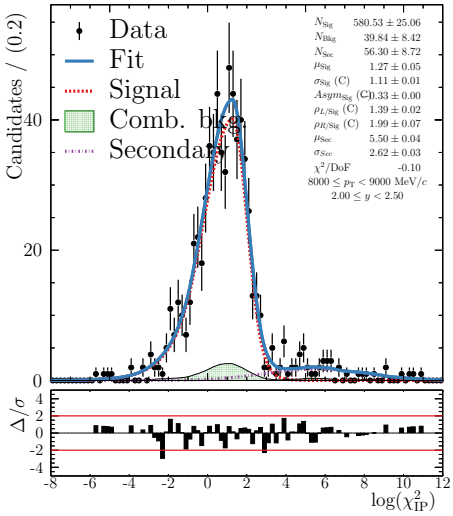

$8 \le p_{\rm T} < 9\,{\rm GeV},\ 2.0 \le y < 2.5$

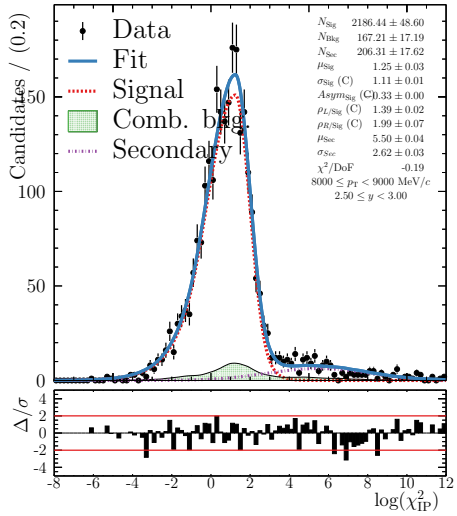

$8 \le p_{\rm T} < 9\,{\rm GeV},\ 2.5 \le y < 3.0$

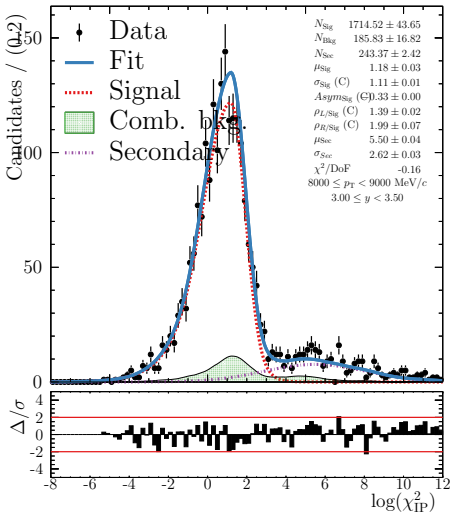

$8 \le p_{\rm T} < 9\,{\rm GeV},\ 3.0 \le y < 3.5$

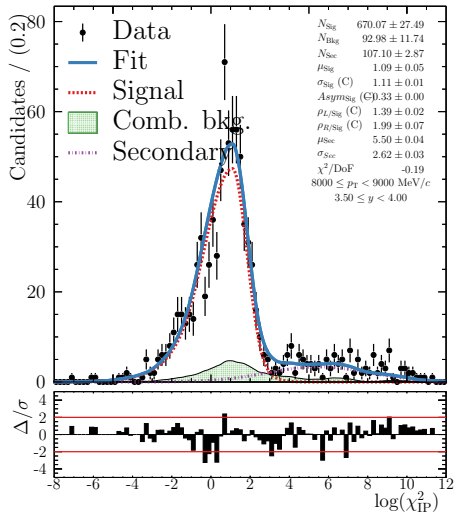

$8 \le p_{\rm T} < 9\,{\rm GeV},\ 3.5 \le y < 4.0$

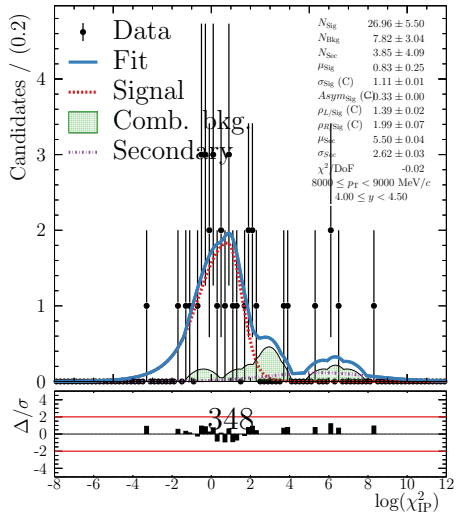

$8 \le p_{\rm T} < 9\,{\rm GeV},\ 4.0 \le y < 4.5$

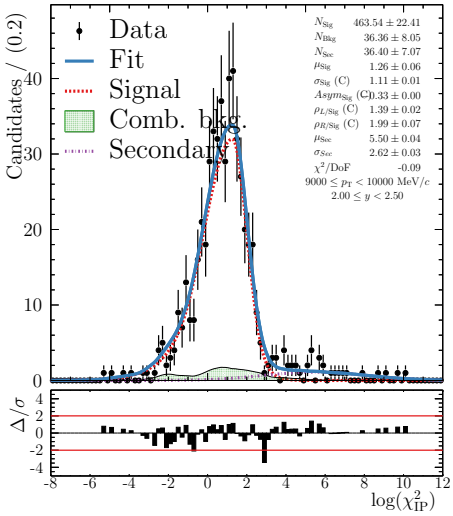

$9 \leq p_{\rm T} < 10\,{\rm GeV},\ 2.0 \leq y < 2.5$

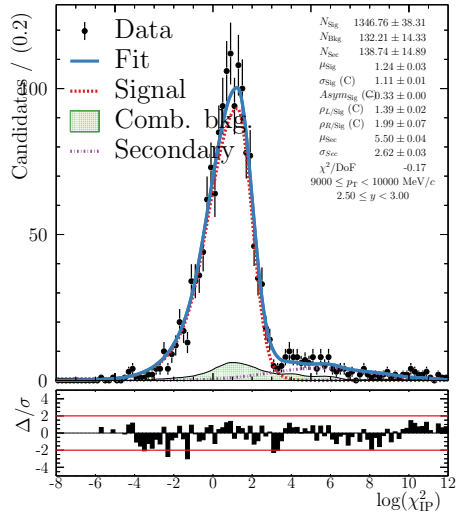

$9 \leq p_{\rm T} < 10\,{\rm GeV},\ 2.5 \leq y < 3.0$

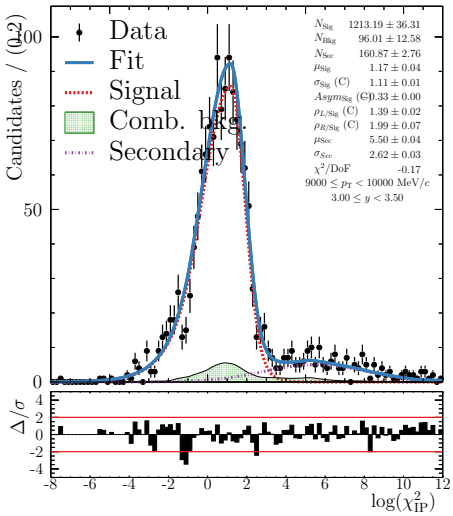

$9 \leq p_{\rm T} < 10\,{\rm GeV},\ 3.0 \leq y < 3.5$

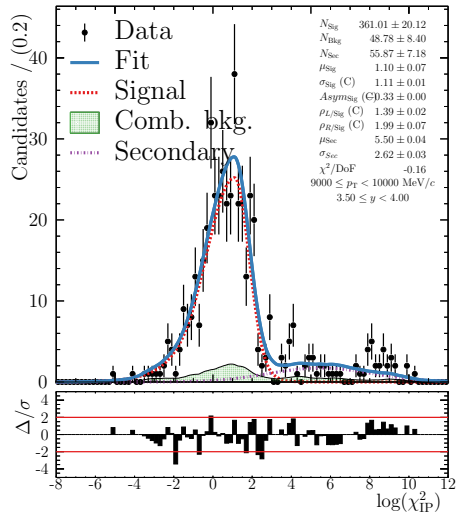

$9 \leq p_{\rm T} < 10\,{\rm GeV},\ 3.5 \leq y < 4.0$

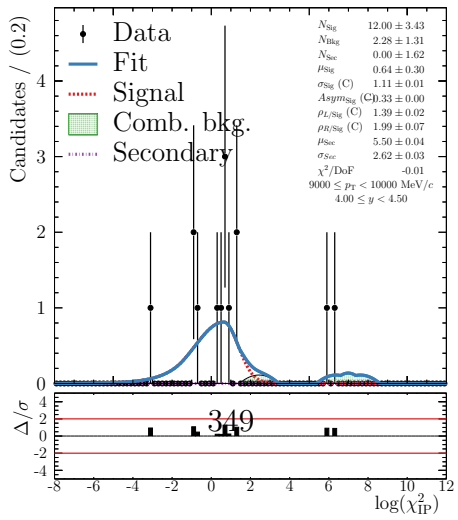

$9 \leq p_{\rm T} < 10\,{\rm GeV},\ 4.0 \leq y < 4.5$

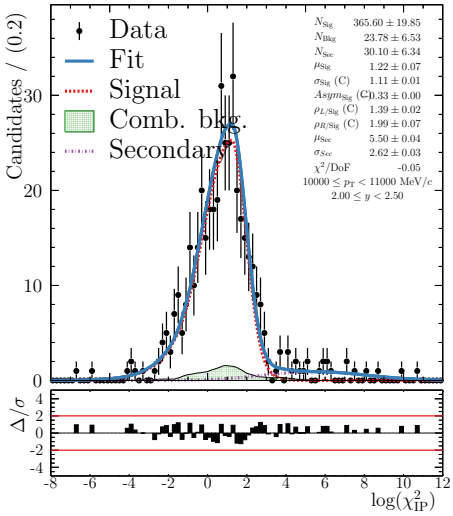

$10 \leq p_{\rm T} < 11\,{\rm GeV},\ 2.0 \leq y < 2.5$

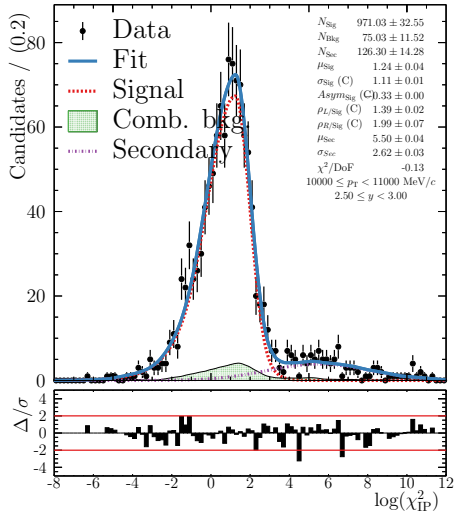

$10 \leq p_{\rm T} < 11\,{\rm GeV},\ 2.5 \leq y < 3.0$

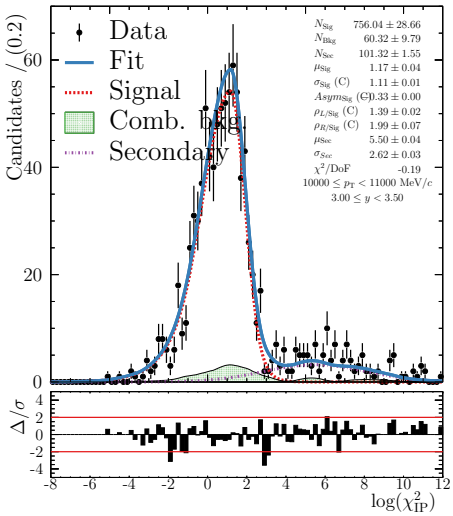

$10 \leq p_{\rm T} < 11\,{\rm GeV},\ 3.0 \leq y < 3.5$

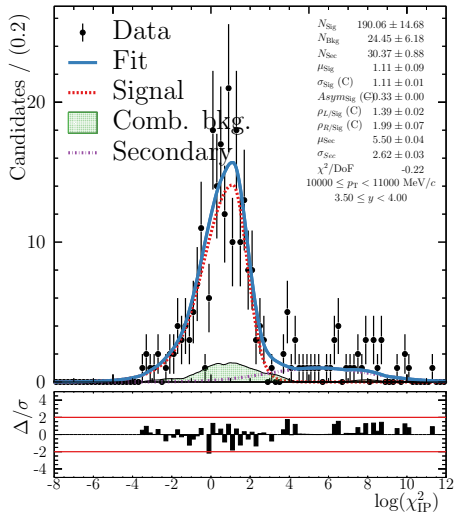

$10 \leq p_{\rm T} < 11\,{\rm GeV},\ 3.5 \leq y < 4.0$

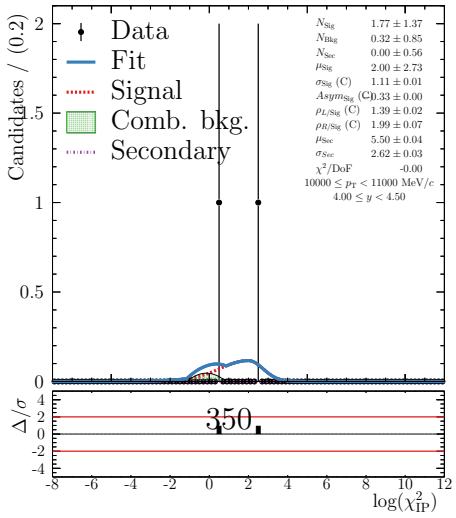

$10 \leq p_{\rm T} < 11\,{\rm GeV},\ 4.0 \leq y < 4.5$

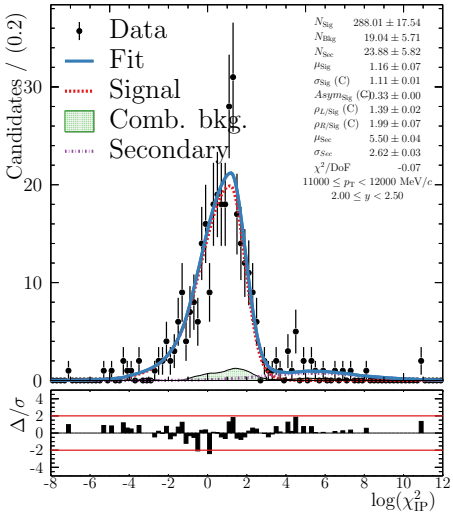

$11 \leq p_{\rm T} < 12\,{\rm GeV},\ 2.0 \leq y < 2.5$

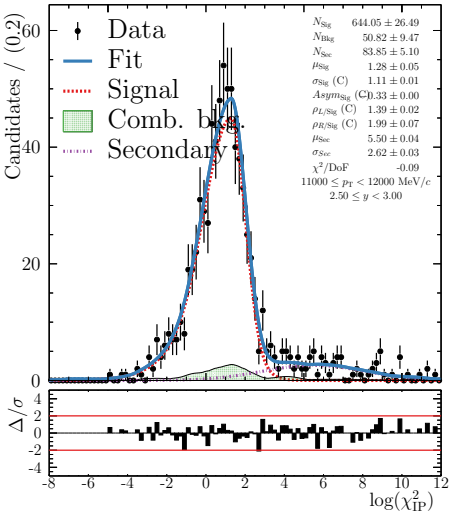

$11 \leq p_{\rm T} < 12\,{\rm GeV},\ 2.5 \leq y < 3.0$

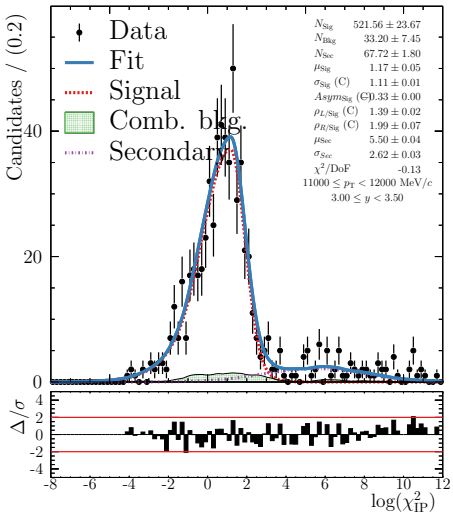

$11 \leq p_{\rm T} < 12\,{\rm GeV},\ 3.0 \leq y < 3.5$

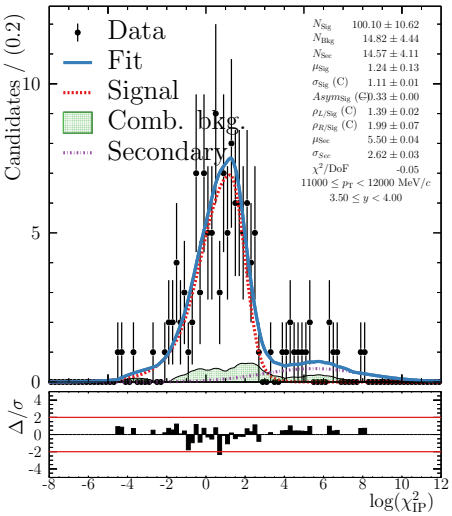

$11 \leq p_{\rm T} < 12\,{\rm GeV},\ 3.5 \leq y < 4.0$

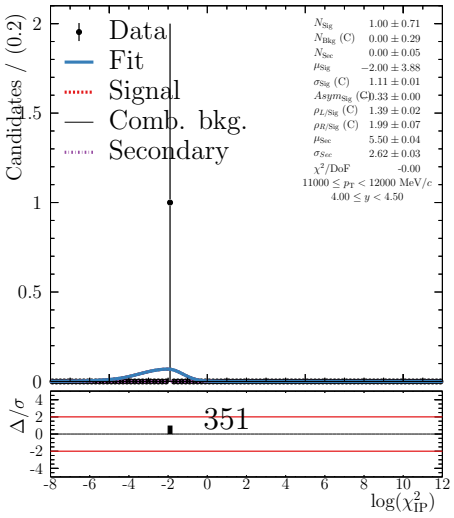

$11 \leq p_{\rm T} < 12\,{\rm GeV},\ 4.0 \leq y < 4.5$

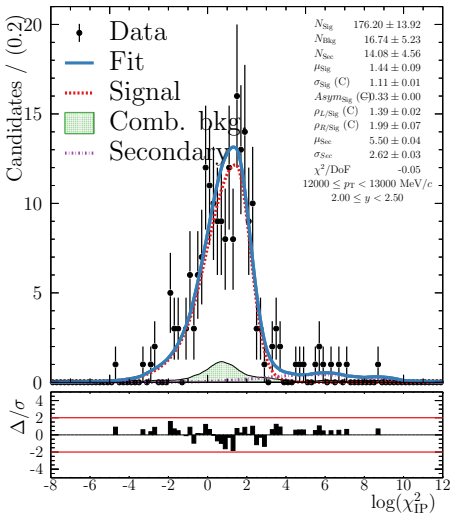

$12 \leq p_{\rm T} < 13\,{\rm GeV},\ 2.0 \leq y < 2.5$

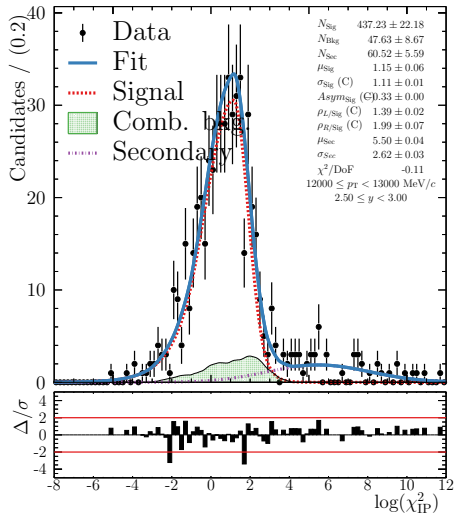

$12 \leq p_{\rm T} < 13\,{\rm GeV},\ 2.5 \leq y < 3.0$

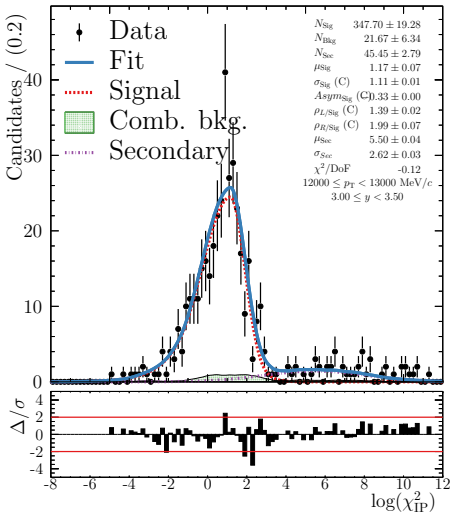

$12 \leq p_{\rm T} < 13\,{\rm GeV},\ 3.0 \leq y < 3.5$

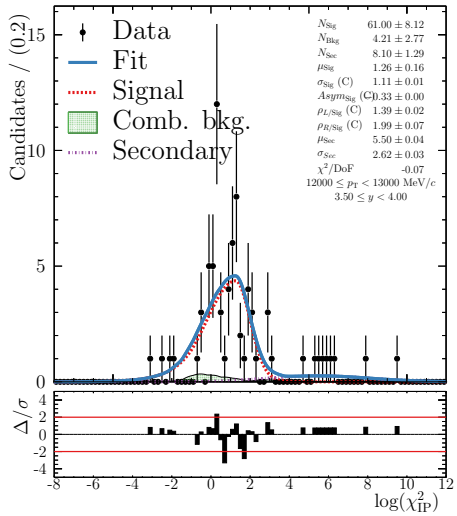

$12 \leq p_{\rm T} < 13\,{\rm GeV},\ 3.5 \leq y < 4.0$

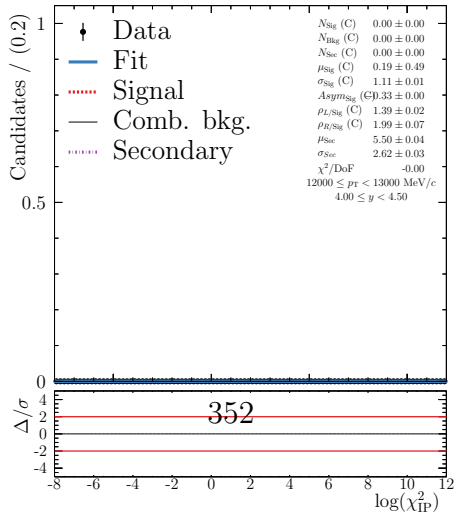

$12 \leq p_{\rm T} < 13\,{\rm GeV},\ 4.0 \leq y < 4.5$

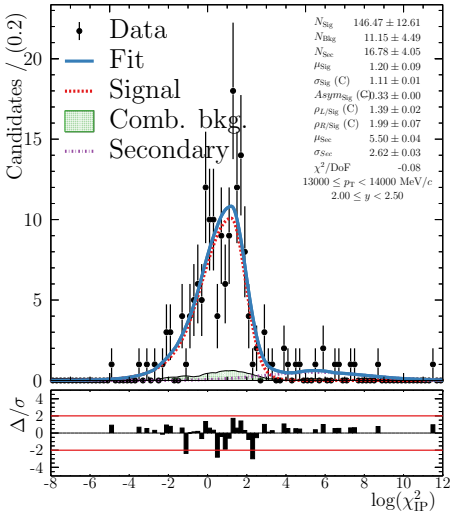

$13 \leq p_{\rm T} < 14\,{\rm GeV},\ 2.0 \leq y < 2.5$

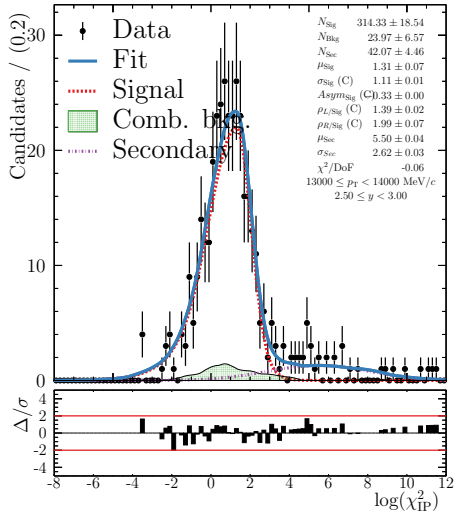

$13 \leq p_{\rm T} < 14\,{\rm GeV},\ 2.5 \leq y < 3.0$

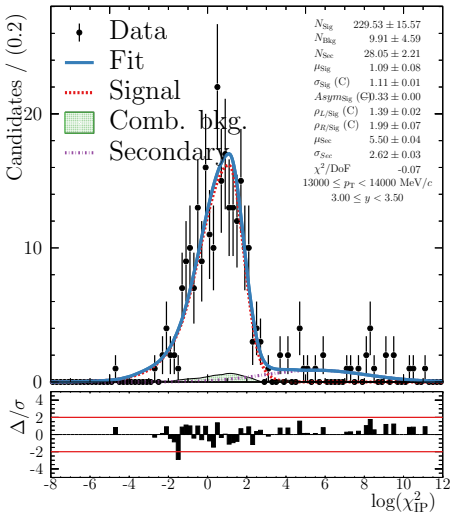

$13 \leq p_{\rm T} < 14\,{\rm GeV},\ 3.0 \leq y < 3.5$

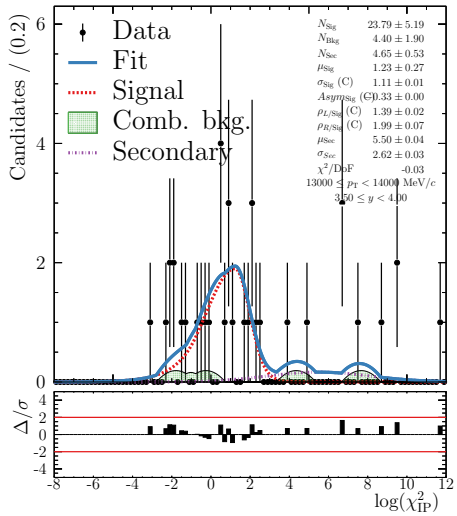

$13 \leq p_{\rm T} < 14\,{\rm GeV},\ 3.5 \leq y < 4.0$

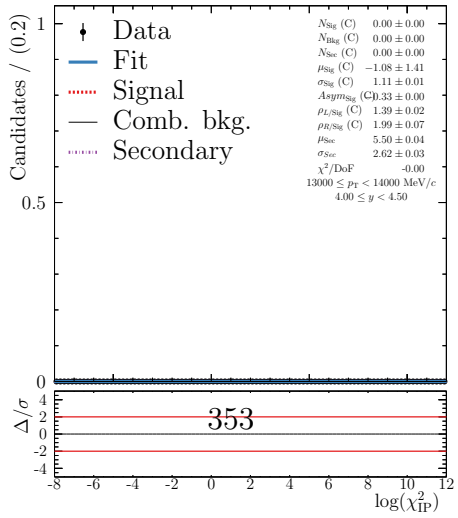

$13 \leq p_{\rm T} < 14\,{\rm GeV},\ 4.0 \leq y < 4.5$

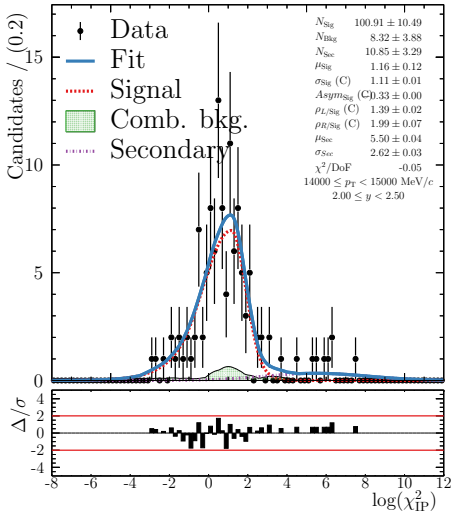

$14 \leq p_{\rm T} < 15\,{\rm GeV},\ 2.0 \leq y < 2.5$

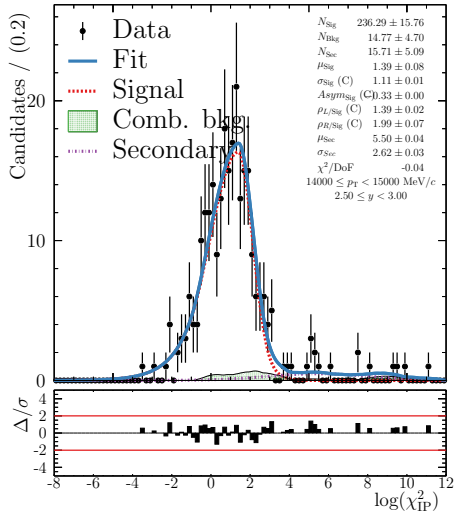

$14 \leq p_{\rm T} < 15\,{\rm GeV},\ 2.5 \leq y < 3.0$

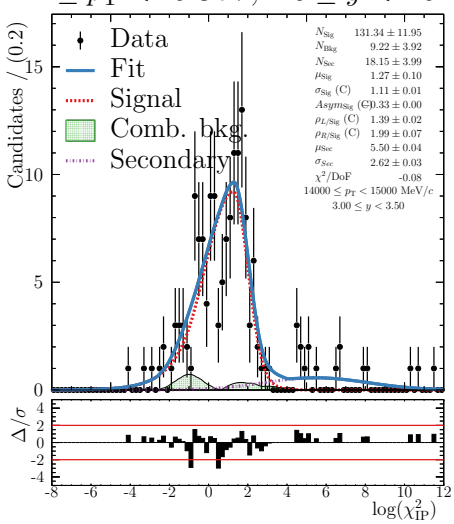

$14 \leq p_{\rm T} < 15\,{\rm GeV},\ 3.0 \leq y < 3.5$

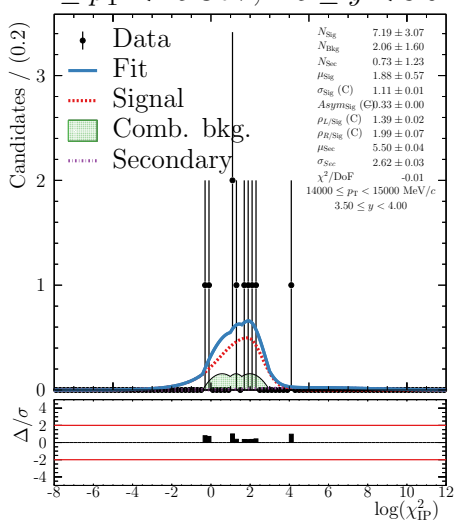

$14 \leq p_{\rm T} < 15\,{\rm GeV},\ 3.5 \leq y < 4.0$

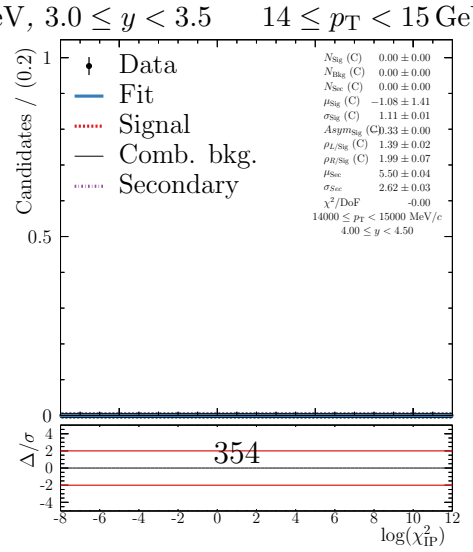

$14 \leq p_{\rm T} < 15\,{\rm GeV},\ 4.0 \leq y < 4.5$

Figure F.0: Fits to the fully selected $D^0 \to K^-\pi^+\pi^-\pi^+$, from $D^{*+} \to D^0\pi^+$, $\ln\chi^2_{\rm IP}$ distribution per $p_{\rm T}$-y bin.

G Tables of generator cut efficiencies

Sections G.1 to G.8 contain tables of 'acceptance' or generator-level cuts for the MC samples as described in Section 5.1.

G.1 $D^0 \to K^-\pi^+$

Table G.1: Efficiency of DaughtersInLHCb for D^0 in MagDown event type 27163003 (Dst_D0pi,Kpi=DecProdCut, $D^{*+} \to D^0(K^-\pi^+)\pi^+$) in bins of (p_{T}, y), where p_{T} and y are computed in the proton-proton CM frame. The numbers are expressed as ratios of the number of signal decays generated into the bin to the number of those decays that satisfy the DaughtersInLHCb requirement.

p_{T}	y				
(GeV)	$[2.0, 2.5[$	$[2.5, 3.0[$	$[3.0, 3.5[$	$[3.5, 4.0[$	$[4.0, 4.5[$
$[0.00, 0.25[$	1318/1748	1399/1611	1257/1537	808/1365	163/1208
$[0.25, 0.50[$	3498/4690	3851/4478	3277/4060	2182/3589	885/3260
$[0.50, 0.75[$	4769/6418	5137/5825	4727/5414	3522/4797	1803/4123
$[0.75, 1.00[$	5356/6940	5864/6370	5531/5844	4353/5170	2411/4298
$[1.00, 1.25[$	5351/6855	5900/6387	5359/5570	4574/4930	2764/4079
$[1.25, 1.50[$	4889/6215	5359/5748	5127/5296	4131/4412	2796/3543
$[1.50, 1.75[$	4516/5581	4714/5004	4271/4396	3550/3778	2569/3134
$[1.75, 2.00[$	4036/4881	4211/4439	3942/4046	3169/3368	2226/2661
$[2.00, 2.25[$	3578/4307	3722/3866	3380/3436	2736/2879	1985/2296
$[2.25, 2.50[$	3134/3662	3234/3366	2830/2884	2348/2461	1627/1835
$[2.50, 2.75[$	2749/3146	2733/2824	2425/2458	1966/2044	1416/1602
$[2.75, 3.00[$	2366/2696	2410/2472	2117/2148	1664/1726	1264/1385
$[3.00, 3.50[$	3943/4408	3756/3832	3357/3389	2667/2746	1878/2056
$[3.50, 4.00[$	3019/3275	2958/2991	2448/2456	1934/1978	1474/1575
$[4.00, 4.50[$	2274/2421	2127/2137	1865/1869	1492/1510	1073/1122
$[4.50, 5.00[$	1773/1871	1585/1591	1362/1367	1039/1045	807/839
$[5.00, 6.00[$	2453/2557	2175/2180	1743/1746	1414/1420	1040/1056
$[6.00, 7.00[$	1483/1528	1226/1230	1042/1043	842/843	586/596
$[7.00, 8.00[$	930/951	739/739	609/609	493/494	341/346
$[8.00, 9.00[$	537/545	479/479	386/386	275/277	201/203
$[9.00, 10.00[$	369/372	293/293	248/248	162/163	116/117
$[10.00, 11.00[$	255/257	212/212	166/166	117/117	65/65
$[11.00, 12.00[$	180/182	144/144	104/104	79/79	42/42
$[12.00, 13.00[$	115/115	97/97	60/60	55/55	42/42
$[13.00, 14.00[$	69/69	70/70	57/57	35/35	13/13

Table G.2: Efficiency of DaughtersInLHCb for D^0 in MagDown event type 27163003 (Dst_D0pi,Kpi=DecProdCut, $D^{*+} \to D^0(K^-\pi^+)\pi^+$) in bins of (p_{T}, y), where p_{T} and y are computed in the proton-proton CM frame. The quoted uncertainties are binomial statistical uncertainties only.

p_{T} (GeV)	y [2.0, 2.5[	[2.5, 3.0[	[3.0, 3.5[	[3.5, 4.0[	[4.0, 4.5[
[0.00, 0.25[	0.754 ± 0.010	0.868 ± 0.008	0.818 ± 0.010	0.592 ± 0.013	0.135 ± 0.010
[0.25, 0.50[	0.746 ± 0.006	0.860 ± 0.005	0.807 ± 0.006	0.608 ± 0.008	0.271 ± 0.008
[0.50, 0.75[	0.743 ± 0.005	0.882 ± 0.004	0.873 ± 0.005	0.734 ± 0.006	0.437 ± 0.008
[0.75, 1.00[	0.772 ± 0.005	0.921 ± 0.003	0.946 ± 0.003	0.842 ± 0.005	0.561 ± 0.008
[1.00, 1.25[	0.781 ± 0.005	0.924 ± 0.003	0.962 ± 0.003	0.928 ± 0.004	0.678 ± 0.007
[1.25, 1.50[	0.787 ± 0.005	0.932 ± 0.003	0.968 ± 0.002	0.936 ± 0.004	0.789 ± 0.007
[1.50, 1.75[	0.809 ± 0.005	0.942 ± 0.003	0.972 ± 0.003	0.940 ± 0.004	0.820 ± 0.007
[1.75, 2.00[	0.827 ± 0.005	0.949 ± 0.003	0.974 ± 0.002	0.941 ± 0.004	0.837 ± 0.007
[2.00, 2.25[	0.831 ± 0.006	0.963 ± 0.003	0.984 ± 0.002	0.950 ± 0.004	0.865 ± 0.007
[2.25, 2.50[	0.856 ± 0.006	0.961 ± 0.003	0.981 ± 0.003	0.954 ± 0.004	0.887 ± 0.007
[2.50, 2.75[	0.874 ± 0.006	0.968 ± 0.003	0.987 ± 0.002	0.962 ± 0.004	0.884 ± 0.008
[2.75, 3.00[	0.878 ± 0.006	0.975 ± 0.003	0.986 ± 0.003	0.964 ± 0.004	0.913 ± 0.008
[3.00, 3.50[	0.895 ± 0.005	0.980 ± 0.002	0.991 ± 0.002	0.971 ± 0.003	0.913 ± 0.006
[3.50, 4.00[	0.922 ± 0.005	0.989 ± 0.002	0.997 ± 0.001	0.978 ± 0.003	0.936 ± 0.006
[4.00, 4.50[	0.939 ± 0.005	0.995 ± 0.001	0.998 ± 0.001	0.988 ± 0.003	0.956 ± 0.006
[4.50, 5.00[	0.948 ± 0.005	0.996 ± 0.002	0.996 ± 0.002	0.994 ± 0.002	0.962 ± 0.007
[5.00, 6.00[	0.959 ± 0.004	0.998 ± 0.001	0.998 ± 0.001	0.996 ± 0.002	0.985 ± 0.004
[6.00, 7.00[	0.971 ± 0.004	0.997 ± 0.002	0.999 ± 0.001	0.999 ± 0.001	0.983 ± 0.005
[7.00, 8.00[	0.978 ± 0.005	1.000 ± 0.000	1.000 ± 0.000	0.998 ± 0.002	0.986 ± 0.006
[8.00, 9.00[	0.985 ± 0.005	1.000 ± 0.000	1.000 ± 0.000	0.993 ± 0.005	0.990 ± 0.007
[9.00, 10.00[	0.992 ± 0.005	1.000 ± 0.000	1.000 ± 0.000	0.994 ± 0.006	0.991 ± 0.009
[10.00, 11.00[	0.992 ± 0.005	1.000 ± 0.000	1.000 ± 0.000	1.000 ± 0.000	1.000 ± 0.000
[11.00, 12.00[	0.989 ± 0.008	1.000 ± 0.000	1.000 ± 0.000	1.000 ± 0.000	1.000 ± 0.000
[12.00, 13.00[	1.000 ± 0.000	1.000 ± 0.000	1.000 ± 0.000	1.000 ± 0.000	1.000 ± 0.000
[13.00, 14.00[	1.000 ± 0.000	1.000 ± 0.000	1.000 ± 0.000	1.000 ± 0.000	1.000 ± 0.000

Table G.3: Efficiency of DaughtersInLHCb for D^0 in MagUp event type 27163003 (Dst_D0pi,Kpi=DecProdCut, $D^{*+} \to D^0(K^-\pi^+)\pi^+$) in bins of (p_{T}, y), where p_{T} and y are computed in the proton-proton CM frame. The numbers are expressed as ratios of the number of signal decays generated into the bin to the number of those decays that satisfy the DaughtersInLHCb requirement.

p_{T}	y				
(GeV)	$[2.0, 2.5[$	$[2.5, 3.0[$	$[3.0, 3.5[$	$[3.5, 4.0[$	$[4.0, 4.5[$
$[0.00, 0.25[$	687/918	752/860	625/751	413/720	83/632
$[0.25, 0.50[$	1758/2412	1915/2235	1749/2146	1131/1898	468/1776
$[0.50, 0.75[$	2454/3307	2823/3169	2426/2786	1810/2574	896/2208
$[0.75, 1.00[$	2768/3668	3106/3374	2992/3154	2295/2688	1228/2215
$[1.00, 1.25[$	2731/3521	3003/3242	2852/2980	2351/2515	1431/2081
$[1.25, 1.50[$	2611/3333	2819/3017	2589/2685	2219/2389	1537/1952
$[1.50, 1.75[$	2379/2931	2497/2649	2357/2441	1864/1985	1389/1644
$[1.75, 2.00[$	2062/2506	2216/2324	2088/2137	1624/1718	1203/1443
$[2.00, 2.25[$	1928/2313	1949/2011	1725/1755	1390/1461	1047/1229
$[2.25, 2.50[$	1606/1913	1631/1696	1431/1460	1287/1337	916/1024
$[2.50, 2.75[$	1433/1650	1444/1489	1284/1304	1083/1119	744/843
$[2.75, 3.00[$	1227/1382	1295/1329	1077/1091	861/897	643/704
$[3.00, 3.50[$	2016/2252	2039/2074	1773/1791	1355/1393	1065/1159
$[3.50, 4.00[$	1627/1754	1503/1520	1295/1299	1033/1050	682/731
$[4.00, 4.50[$	1221/1312	1136/1145	958/960	794/803	568/599
$[4.50, 5.00[$	920/968	849/851	699/701	577/584	401/411
$[5.00, 6.00[$	1245/1299	1127/1130	944/945	742/745	527/539
$[6.00, 7.00[$	729/746	656/656	619/619	379/382	268/270
$[7.00, 8.00[$	500/507	387/387	315/315	217/218	181/182
$[8.00, 9.00[$	295/298	271/271	197/197	153/153	96/97
$[9.00, 10.00[$	183/184	186/186	125/125	93/93	58/58
$[10.00, 11.00[$	128/128	114/114	79/79	58/58	37/37
$[11.00, 12.00[$	103/103	90/90	70/70	41/41	27/27
$[12.00, 13.00[$	59/59	68/68	37/37	36/36	23/23
$[13.00, 14.00[$	51/51	38/38	31/31	15/15	13/13

Table G.4: Efficiency of DaughtersInLHCb for D^0 in MagUp event type 27163003 (Dst_D0pi,Kpi=DecProdCut, $D^{*+} \to D^0(K^-\pi^+)\pi^+$) in bins of (p_{T}, y), where p_{T} and y are computed in the proton-proton CM frame. The quoted uncertainties are binomial statistical uncertainties only.

p_{T} (GeV)	y [2.0, 2.5[	[2.5, 3.0[	[3.0, 3.5[	[3.5, 4.0[	[4.0, 4.5[
[0.00, 0.25[	0.748 ± 0.014	0.874 ± 0.011	0.832 ± 0.014	0.574 ± 0.018	0.131 ± 0.013
[0.25, 0.50[	0.729 ± 0.009	0.857 ± 0.007	0.815 ± 0.008	0.596 ± 0.011	0.264 ± 0.010
[0.50, 0.75[	0.742 ± 0.008	0.891 ± 0.006	0.871 ± 0.006	0.703 ± 0.009	0.406 ± 0.010
[0.75, 1.00[	0.755 ± 0.007	0.921 ± 0.005	0.949 ± 0.004	0.854 ± 0.007	0.554 ± 0.011
[1.00, 1.25[	0.776 ± 0.007	0.926 ± 0.005	0.957 ± 0.004	0.935 ± 0.005	0.688 ± 0.010
[1.25, 1.50[	0.783 ± 0.007	0.934 ± 0.005	0.964 ± 0.004	0.929 ± 0.005	0.787 ± 0.009
[1.50, 1.75[	0.812 ± 0.007	0.943 ± 0.005	0.966 ± 0.004	0.939 ± 0.005	0.845 ± 0.009
[1.75, 2.00[	0.823 ± 0.008	0.954 ± 0.004	0.977 ± 0.003	0.945 ± 0.005	0.834 ± 0.010
[2.00, 2.25[	0.834 ± 0.008	0.969 ± 0.004	0.983 ± 0.003	0.951 ± 0.006	0.852 ± 0.010
[2.25, 2.50[	0.840 ± 0.008	0.962 ± 0.005	0.980 ± 0.004	0.963 ± 0.005	0.895 ± 0.010
[2.50, 2.75[	0.868 ± 0.008	0.970 ± 0.004	0.985 ± 0.003	0.968 ± 0.005	0.883 ± 0.011
[2.75, 3.00[	0.888 ± 0.008	0.974 ± 0.004	0.987 ± 0.003	0.960 ± 0.007	0.913 ± 0.011
[3.00, 3.50[	0.895 ± 0.006	0.983 ± 0.003	0.990 ± 0.002	0.973 ± 0.004	0.919 ± 0.008
[3.50, 4.00[	0.928 ± 0.006	0.989 ± 0.003	0.997 ± 0.002	0.984 ± 0.004	0.933 ± 0.009
[4.00, 4.50[	0.931 ± 0.007	0.992 ± 0.003	0.998 ± 0.001	0.989 ± 0.004	0.948 ± 0.009
[4.50, 5.00[	0.950 ± 0.007	0.998 ± 0.002	0.997 ± 0.002	0.988 ± 0.005	0.976 ± 0.008
[5.00, 6.00[	0.958 ± 0.006	0.997 ± 0.002	0.999 ± 0.001	0.996 ± 0.002	0.978 ± 0.006
[6.00, 7.00[	0.977 ± 0.005	1.000 ± 0.000	1.000 ± 0.000	0.992 ± 0.005	0.993 ± 0.005
[7.00, 8.00[	0.986 ± 0.005	1.000 ± 0.000	1.000 ± 0.000	0.995 ± 0.005	0.995 ± 0.005
[8.00, 9.00[	0.990 ± 0.006	1.000 ± 0.000	1.000 ± 0.000	1.000 ± 0.000	0.990 ± 0.010
[9.00, 10.00[	0.995 ± 0.005	1.000 ± 0.000	1.000 ± 0.000	1.000 ± 0.000	1.000 ± 0.000
[10.00, 11.00[	1.000 ± 0.000	1.000 ± 0.000	1.000 ± 0.000	1.000 ± 0.000	1.000 ± 0.000
[11.00, 12.00[	1.000 ± 0.000	1.000 ± 0.000	1.000 ± 0.000	1.000 ± 0.000	1.000 ± 0.000
[12.00, 13.00[	1.000 ± 0.000	1.000 ± 0.000	1.000 ± 0.000	1.000 ± 0.000	1.000 ± 0.000
[13.00, 14.00[	1.000 ± 0.000	1.000 ± 0.000	1.000 ± 0.000	1.000 ± 0.000	1.000 ± 0.000

G.2 $D^0 \to K^-\pi^+\pi^-\pi^+$

Table G.5: Efficiency of DaughtersInLHCb for D^0 in MagDown event type 27265002 (Dst_D0pi,Kpipipi=DecProdCutMINT, $D^{*+} \to D^0(K^-\pi^+\pi^-\pi^+)\pi^+$) in bins of (p_{T}, y), where p_{T} and y are computed in the proton-proton CM frame. The numbers are expressed as ratios of the number of signal decays generated into the bin to the number of those decays that satisfy the DaughtersInLHCb requirement.

p_{T}	y				
(GeV)	$[2.0, 2.5[$	$[2.5, 3.0[$	$[3.0, 3.5[$	$[3.5, 4.0[$	$[4.0, 4.5[$
$[0.00, 0.25[$	1177/1792	1422/1661	1270/1625	677/1414	90/1241
$[0.25, 0.50[$	3145/4716	3834/4487	3115/3997	1867/3589	565/3081
$[0.50, 0.75[$	4428/6420	5220/5874	4428/5436	3159/4899	1182/4173
$[0.75, 1.00[$	4976/7008	5797/6303	5455/5903	3781/5069	1696/4290
$[1.00, 1.25[$	4991/6994	5836/6188	5295/5677	3982/4825	2093/4090
$[1.25, 1.50[$	4553/6182	5464/5768	4823/5113	3776/4433	2177/3622
$[1.50, 1.75[$	4441/5698	4930/5131	4351/4554	3341/3832	2079/3142
$[1.75, 2.00[$	3974/5017	4567/4719	3776/3918	2904/3315	1934/2727
$[2.00, 2.25[$	3492/4292	3792/3886	3258/3354	2536/2772	1735/2290
$[2.25, 2.50[$	3123/3716	3128/3188	2820/2911	2248/2417	1453/1879
$[2.50, 2.75[$	2731/3170	2790/2829	2386/2439	1915/2039	1279/1563
$[2.75, 3.00[$	2317/2668	2393/2417	2207/2242	1660/1750	1185/1393
$[3.00, 3.50[$	4028/4450	3939/3973	3340/3394	2594/2695	1925/2167
$[3.50, 4.00[$	2942/3193	2997/3005	2478/2504	2057/2105	1419/1538
$[4.00, 4.50[$	2370/2536	2106/2111	1856/1866	1393/1412	1024/1097
$[4.50, 5.00[$	1779/1858	1657/1659	1419/1423	1031/1047	793/825
$[5.00, 6.00[$	2409/2489	2134/2141	1775/1779	1349/1367	975/1007
$[6.00, 7.00[$	1448/1484	1263/1264	1098/1101	807/811	541/551
$[7.00, 8.00[$	943/951	809/810	611/612	458/458	339/341
$[8.00, 9.00[$	609/611	491/491	358/358	273/273	173/173
$[9.00, 10.00[$	359/359	320/320	214/214	179/180	105/105
$[10.00, 11.00[$	237/238	196/196	147/147	127/127	73/73
$[11.00, 12.00[$	167/167	162/162	101/101	78/78	50/50
$[12.00, 13.00[$	118/118	108/108	64/64	50/50	44/44
$[13.00, 14.00[$	83/84	63/63	56/56	33/33	20/20

Table G.6: Efficiency of DaughtersInLHCb for D^0 in MagDown event type 27265002 (Dst_D0pi,Kpipipi=DecProdCutMINT, $D^{*+} \to D^0(K^-\pi^+\pi^-\pi^+)\pi^+$) in bins of (p_{T}, y), where p_{T} and y are computed in the proton-proton CM frame. The quoted uncertainties are binomial statistical uncertainties only.

p_{T}	y				
(GeV)	$[2.0, 2.5[$	$[2.5, 3.0[$	$[3.0, 3.5[$	$[3.5, 4.0[$	$[4.0, 4.5[$
$[0.00, 0.25[$	0.657 ± 0.011	0.856 ± 0.009	0.782 ± 0.010	0.479 ± 0.013	0.073 ± 0.007
$[0.25, 0.50[$	0.667 ± 0.007	0.854 ± 0.005	0.779 ± 0.007	0.520 ± 0.008	0.183 ± 0.007
$[0.50, 0.75[$	0.690 ± 0.006	0.889 ± 0.004	0.815 ± 0.005	0.645 ± 0.007	0.283 ± 0.007
$[0.75, 1.00[$	0.710 ± 0.005	0.920 ± 0.003	0.924 ± 0.003	0.746 ± 0.006	0.395 ± 0.007
$[1.00, 1.25[$	0.714 ± 0.005	0.943 ± 0.003	0.933 ± 0.003	0.825 ± 0.005	0.512 ± 0.008
$[1.25, 1.50[$	0.736 ± 0.006	0.947 ± 0.003	0.943 ± 0.003	0.852 ± 0.005	0.601 ± 0.008
$[1.50, 1.75[$	0.779 ± 0.005	0.961 ± 0.003	0.955 ± 0.003	0.872 ± 0.005	0.662 ± 0.008
$[1.75, 2.00[$	0.792 ± 0.006	0.968 ± 0.003	0.964 ± 0.003	0.876 ± 0.006	0.709 ± 0.009
$[2.00, 2.25[$	0.814 ± 0.006	0.976 ± 0.002	0.971 ± 0.003	0.915 ± 0.005	0.758 ± 0.009
$[2.25, 2.50[$	0.840 ± 0.006	0.981 ± 0.002	0.969 ± 0.003	0.930 ± 0.005	0.773 ± 0.010
$[2.50, 2.75[$	0.862 ± 0.006	0.986 ± 0.002	0.978 ± 0.003	0.939 ± 0.005	0.818 ± 0.010
$[2.75, 3.00[$	0.868 ± 0.007	0.990 ± 0.002	0.984 ± 0.003	0.949 ± 0.005	0.851 ± 0.010
$[3.00, 3.50[$	0.905 ± 0.004	0.991 ± 0.001	0.984 ± 0.002	0.963 ± 0.004	0.888 ± 0.007
$[3.50, 4.00[$	0.921 ± 0.005	0.997 ± 0.001	0.990 ± 0.002	0.977 ± 0.003	0.923 ± 0.007
$[4.00, 4.50[$	0.935 ± 0.005	0.998 ± 0.001	0.995 ± 0.002	0.987 ± 0.003	0.933 ± 0.008
$[4.50, 5.00[$	0.957 ± 0.005	0.999 ± 0.001	0.997 ± 0.001	0.985 ± 0.004	0.961 ± 0.007
$[5.00, 6.00[$	0.968 ± 0.004	0.997 ± 0.001	0.998 ± 0.001	0.987 ± 0.003	0.968 ± 0.006
$[6.00, 7.00[$	0.976 ± 0.004	0.999 ± 0.001	0.997 ± 0.002	0.995 ± 0.002	0.982 ± 0.006
$[7.00, 8.00[$	0.992 ± 0.003	0.999 ± 0.001	0.998 ± 0.002	1.000 ± 0.000	0.994 ± 0.004
$[8.00, 9.00[$	0.997 ± 0.002	1.000 ± 0.000	1.000 ± 0.000	1.000 ± 0.000	1.000 ± 0.000
$[9.00, 10.00[$	1.000 ± 0.000	1.000 ± 0.000	1.000 ± 0.000	0.994 ± 0.006	1.000 ± 0.000
$[10.00, 11.00[$	0.996 ± 0.004	1.000 ± 0.000	1.000 ± 0.000	1.000 ± 0.000	1.000 ± 0.000
$[11.00, 12.00[$	1.000 ± 0.000	1.000 ± 0.000	1.000 ± 0.000	1.000 ± 0.000	1.000 ± 0.000
$[12.00, 13.00[$	1.000 ± 0.000	1.000 ± 0.000	1.000 ± 0.000	1.000 ± 0.000	1.000 ± 0.000
$[13.00, 14.00[$	0.988 ± 0.012	1.000 ± 0.000	1.000 ± 0.000	1.000 ± 0.000	1.000 ± 0.000

Table G.7: Efficiency of DaughtersInLHCb for D^0 in MagUp event type 27265002 (Dst_D0pi,Kpipipi=DecProdCutMINT, $D^{*+} \to D^0(K^-\pi^+\pi^-\pi^+)\pi^+$) in bins of (p_{T}, y), where p_{T} and y are computed in the proton-proton CM frame. The numbers are expressed as ratios of the number of signal decays generated into the bin to the number of those decays that satisfy the DaughtersInLHCb requirement.

p_{T}	y				
(GeV)	$[2.0, 2.5[$	$[2.5, 3.0[$	$[3.0, 3.5[$	$[3.5, 4.0[$	$[4.0, 4.5[$
$[0.00, 0.25[$	1204/1809	1466/1714	1157/1470	721/1466	109/1256
$[0.25, 0.50[$	3119/4691	3784/4404	3174/4096	1948/3723	572/3248
$[0.50, 0.75[$	4257/6387	5283/5943	4463/5342	2952/4752	1202/4157
$[0.75, 1.00[$	4922/6992	5898/6348	5305/5786	3785/5074	1657/4246
$[1.00, 1.25[$	4994/6833	5807/6193	5276/5639	4093/4940	2127/4088
$[1.25, 1.50[$	4736/6358	5385/5673	4956/5221	3700/4352	2257/3673
$[1.50, 1.75[$	4252/5520	4940/5127	4278/4500	3317/3777	2172/3251
$[1.75, 2.00[$	3931/4976	4244/4367	3725/3875	2989/3334	1844/2608
$[2.00, 2.25[$	3497/4277	3783/3864	3307/3415	2555/2823	1683/2243
$[2.25, 2.50[$	3174/3788	3253/3309	2828/2906	2287/2462	1530/1952
$[2.50, 2.75[$	2729/3207	2856/2892	2461/2508	1908/2043	1355/1663
$[2.75, 3.00[$	2379/2728	2492/2516	2125/2164	1653/1741	1190/1413
$[3.00, 3.50[$	3925/4366	3807/3832	3377/3434	2773/2872	1884/2141
$[3.50, 4.00[$	2952/3203	2953/2968	2414/2436	1938/1991	1373/1494
$[4.00, 4.50[$	2278/2430	2192/2200	1830/1842	1472/1512	1074/1141
$[4.50, 5.00[$	1850/1940	1589/1590	1336/1340	1071/1082	739/772
$[5.00, 6.00[$	2394/2469	2193/2194	1835/1840	1408/1417	1015/1052
$[6.00, 7.00[$	1498/1517	1261/1261	1073/1078	806/815	604/616
$[7.00, 8.00[$	912/918	814/814	625/626	470/471	307/312
$[8.00, 9.00[$	578/580	455/455	385/386	280/282	210/211
$[9.00, 10.00[$	389/391	325/325	220/220	163/163	118/118
$[10.00, 11.00[$	241/241	196/196	157/157	107/107	66/66
$[11.00, 12.00[$	186/186	133/133	101/101	76/76	54/54
$[12.00, 13.00[$	101/101	109/109	65/65	61/61	37/37
$[13.00, 14.00[$	69/69	68/68	48/48	35/35	23/23

Table G.8: Efficiency of DaughtersInLHCb for D^0 in MagUp event type 27265002 (Dst_D0pi,Kpipipi=DecProdCutMINT, $D^{*+} \to D^0(K^-\pi^+\pi^-\pi^+)\pi^+$) in bins of (p_{T}, y), where p_{T} and y are computed in the proton-proton CM frame. The quoted uncertainties are binomial statistical uncertainties only.

p_{T} (GeV)	y [2.0, 2.5[	[2.5, 3.0[	[3.0, 3.5[	[3.5, 4.0[	[4.0, 4.5[
[0.00, 0.25[	0.666 ± 0.011	0.855 ± 0.008	0.787 ± 0.011	0.492 ± 0.013	0.087 ± 0.008
[0.25, 0.50[	0.665 ± 0.007	0.859 ± 0.005	0.775 ± 0.007	0.523 ± 0.008	0.176 ± 0.007
[0.50, 0.75[	0.667 ± 0.006	0.889 ± 0.004	0.835 ± 0.005	0.621 ± 0.007	0.289 ± 0.007
[0.75, 1.00[	0.704 ± 0.005	0.929 ± 0.003	0.917 ± 0.004	0.746 ± 0.006	0.390 ± 0.007
[1.00, 1.25[	0.731 ± 0.005	0.938 ± 0.003	0.936 ± 0.003	0.829 ± 0.005	0.520 ± 0.008
[1.25, 1.50[	0.745 ± 0.005	0.949 ± 0.003	0.949 ± 0.003	0.850 ± 0.005	0.614 ± 0.008
[1.50, 1.75[	0.770 ± 0.006	0.964 ± 0.003	0.951 ± 0.003	0.878 ± 0.005	0.668 ± 0.008
[1.75, 2.00[	0.790 ± 0.006	0.972 ± 0.003	0.961 ± 0.003	0.897 ± 0.005	0.707 ± 0.009
[2.00, 2.25[	0.818 ± 0.006	0.979 ± 0.002	0.968 ± 0.003	0.905 ± 0.006	0.750 ± 0.009
[2.25, 2.50[	0.838 ± 0.006	0.983 ± 0.002	0.973 ± 0.003	0.929 ± 0.005	0.784 ± 0.009
[2.50, 2.75[	0.851 ± 0.006	0.988 ± 0.002	0.981 ± 0.003	0.934 ± 0.005	0.815 ± 0.010
[2.75, 3.00[	0.872 ± 0.006	0.990 ± 0.002	0.982 ± 0.003	0.949 ± 0.005	0.842 ± 0.010
[3.00, 3.50[	0.899 ± 0.005	0.993 ± 0.001	0.983 ± 0.002	0.966 ± 0.003	0.880 ± 0.007
[3.50, 4.00[	0.922 ± 0.005	0.995 ± 0.001	0.991 ± 0.002	0.973 ± 0.004	0.919 ± 0.007
[4.00, 4.50[	0.937 ± 0.005	0.996 ± 0.001	0.993 ± 0.002	0.974 ± 0.004	0.941 ± 0.007
[4.50, 5.00[	0.954 ± 0.005	0.999 ± 0.001	0.997 ± 0.001	0.990 ± 0.003	0.957 ± 0.007
[5.00, 6.00[	0.970 ± 0.003	1.000 ± 0.000	0.997 ± 0.001	0.994 ± 0.002	0.965 ± 0.006
[6.00, 7.00[	0.987 ± 0.003	1.000 ± 0.000	0.995 ± 0.002	0.989 ± 0.004	0.981 ± 0.006
[7.00, 8.00[	0.993 ± 0.003	1.000 ± 0.000	0.998 ± 0.002	0.998 ± 0.002	0.984 ± 0.007
[8.00, 9.00[	0.997 ± 0.002	1.000 ± 0.000	0.997 ± 0.003	0.993 ± 0.005	0.995 ± 0.005
[9.00, 10.00[	0.995 ± 0.004	1.000 ± 0.000	1.000 ± 0.000	1.000 ± 0.000	1.000 ± 0.000
[10.00, 11.00[	1.000 ± 0.000	1.000 ± 0.000	1.000 ± 0.000	1.000 ± 0.000	1.000 ± 0.000
[11.00, 12.00[	1.000 ± 0.000	1.000 ± 0.000	1.000 ± 0.000	1.000 ± 0.000	1.000 ± 0.000
[12.00, 13.00[	1.000 ± 0.000	1.000 ± 0.000	1.000 ± 0.000	1.000 ± 0.000	1.000 ± 0.000
[13.00, 14.00[	1.000 ± 0.000	1.000 ± 0.000	1.000 ± 0.000	1.000 ± 0.000	1.000 ± 0.000

G.3 $D^+ \to K^-\pi^+\pi^+$

Table G.9: Efficiency of DaughtersInLHCb for D^+ in MagDown event type 21263010 (D+_K-pi+pi+=res,DecProdCut, $D^+ \to K^-\pi^+\pi^+$) in bins of (p_{T}, y), where p_{T} and y are computed in the proton-proton CM frame. The numbers are expressed as ratios of the number of signal decays generated into the bin to the number of those decays that satisfy the DaughtersInLHCb requirement.

p_{T}	y				
(GeV)	$[2.0, 2.5[$	$[2.5, 3.0[$	$[3.0, 3.5[$	$[3.5, 4.0[$	$[4.0, 4.5[$
$[0.00, 0.25[$	1122/1690	1414/1601	1321/1443	1060/1308	630/1142
$[0.25, 0.50[$	2932/4477	3556/4036	3622/3938	2808/3501	1654/2941
$[0.50, 0.75[$	4095/6095	5109/5801	4963/5326	3814/4614	2364/4011
$[0.75, 1.00[$	4424/6491	5512/6140	5337/5651	4173/4841	2617/4146
$[1.00, 1.25[$	4531/6543	5506/6018	5049/5342	4093/4664	2692/3928
$[1.25, 1.50[$	4384/6083	5050/5458	4771/4980	3824/4290	2565/3597
$[1.50, 1.75[$	4023/5395	4596/4874	4155/4287	3450/3761	2248/3000
$[1.75, 2.00[$	3650/4763	4105/4317	3624/3728	2897/3155	1984/2531
$[2.00, 2.25[$	3265/4104	3499/3619	3164/3234	2548/2704	1777/2177
$[2.25, 2.50[$	2864/3553	3056/3167	2668/2703	2139/2259	1546/1842
$[2.50, 2.75[$	2468/2974	2646/2705	2269/2313	1925/2004	1311/1513
$[2.75, 3.00[$	2179/2571	2261/2298	1973/1997	1663/1721	1190/1324
$[3.00, 3.50[$	3768/4324	3907/3952	3284/3317	2549/2629	1944/2134
$[3.50, 4.00[$	2794/3109	2689/2716	2310/2326	1929/1972	1358/1450
$[4.00, 4.50[$	2082/2280	2064/2076	1753/1766	1396/1415	1011/1067
$[4.50, 5.00[$	1667/1781	1590/1593	1343/1346	1053/1075	715/746
$[5.00, 6.00[$	2325/2423	2107/2112	1808/1816	1308/1326	983/1011
$[6.00, 7.00[$	1385/1431	1242/1242	999/1004	814/821	558/574
$[7.00, 8.00[$	894/906	748/749	614/617	478/480	304/305
$[8.00, 9.00[$	557/560	494/495	376/376	291/296	182/184
$[9.00, 10.00[$	370/372	337/337	263/263	172/173	112/114
$[10.00, 11.00[$	249/250	188/188	178/178	112/113	69/69
$[11.00, 12.00[$	159/159	135/135	94/94	87/87	45/45
$[12.00, 13.00[$	114/114	114/114	73/73	45/45	24/24
$[13.00, 14.00[$	79/79	62/62	58/58	30/30	33/33

Table G.10: Efficiency of DaughtersInLHCb for D^+ in MagDown event type 21263010 (D+_K-pi+pi+=res,DecProdCut, $D^+ \to K^-\pi^+\pi^+$) in bins of (p_{T}, y), where p_{T} and y are computed in the proton-proton CM frame. The quoted uncertainties are binomial statistical uncertainties only.

p_{T} (GeV)	y [2.0, 2.5[	[2.5, 3.0[	[3.0, 3.5[	[3.5, 4.0[	[4.0, 4.5[
[0.00, 0.25[	0.664 ± 0.011	0.883 ± 0.008	0.915 ± 0.007	0.810 ± 0.011	0.552 ± 0.015
[0.25, 0.50[	0.655 ± 0.007	0.881 ± 0.005	0.920 ± 0.004	0.802 ± 0.007	0.562 ± 0.009
[0.50, 0.75[	0.672 ± 0.006	0.881 ± 0.004	0.932 ± 0.003	0.827 ± 0.006	0.589 ± 0.008
[0.75, 1.00[	0.682 ± 0.006	0.898 ± 0.004	0.944 ± 0.003	0.862 ± 0.005	0.631 ± 0.007
[1.00, 1.25[	0.692 ± 0.006	0.915 ± 0.004	0.945 ± 0.003	0.878 ± 0.005	0.685 ± 0.007
[1.25, 1.50[	0.721 ± 0.006	0.925 ± 0.004	0.958 ± 0.003	0.891 ± 0.005	0.713 ± 0.008
[1.50, 1.75[	0.746 ± 0.006	0.943 ± 0.003	0.969 ± 0.003	0.917 ± 0.004	0.749 ± 0.008
[1.75, 2.00[	0.766 ± 0.006	0.951 ± 0.003	0.972 ± 0.003	0.918 ± 0.005	0.784 ± 0.008
[2.00, 2.25[	0.796 ± 0.006	0.967 ± 0.003	0.978 ± 0.003	0.942 ± 0.004	0.816 ± 0.008
[2.25, 2.50[	0.806 ± 0.007	0.965 ± 0.003	0.987 ± 0.002	0.947 ± 0.005	0.839 ± 0.009
[2.50, 2.75[	0.830 ± 0.007	0.978 ± 0.003	0.981 ± 0.003	0.961 ± 0.004	0.866 ± 0.009
[2.75, 3.00[	0.848 ± 0.007	0.984 ± 0.003	0.988 ± 0.002	0.966 ± 0.004	0.899 ± 0.008
[3.00, 3.50[	0.871 ± 0.005	0.989 ± 0.002	0.990 ± 0.002	0.970 ± 0.003	0.911 ± 0.006
[3.50, 4.00[	0.899 ± 0.005	0.990 ± 0.002	0.993 ± 0.002	0.978 ± 0.003	0.937 ± 0.006
[4.00, 4.50[	0.913 ± 0.006	0.994 ± 0.002	0.993 ± 0.002	0.987 ± 0.003	0.948 ± 0.007
[4.50, 5.00[	0.936 ± 0.006	0.998 ± 0.001	0.998 ± 0.001	0.980 ± 0.004	0.958 ± 0.007
[5.00, 6.00[	0.960 ± 0.004	0.998 ± 0.001	0.996 ± 0.002	0.986 ± 0.003	0.972 ± 0.005
[6.00, 7.00[	0.968 ± 0.005	1.000 ± 0.000	0.995 ± 0.002	0.991 ± 0.003	0.972 ± 0.007
[7.00, 8.00[	0.987 ± 0.004	0.999 ± 0.001	0.995 ± 0.003	0.996 ± 0.003	0.997 ± 0.003
[8.00, 9.00[	0.995 ± 0.003	0.998 ± 0.002	1.000 ± 0.000	0.983 ± 0.007	0.989 ± 0.008
[9.00, 10.00[	0.995 ± 0.004	1.000 ± 0.000	1.000 ± 0.000	0.994 ± 0.006	0.982 ± 0.012
[10.00, 11.00[	0.996 ± 0.004	1.000 ± 0.000	1.000 ± 0.000	0.991 ± 0.009	1.000 ± 0.000
[11.00, 12.00[	1.000 ± 0.000	1.000 ± 0.000	1.000 ± 0.000	1.000 ± 0.000	1.000 ± 0.000
[12.00, 13.00[	1.000 ± 0.000	1.000 ± 0.000	1.000 ± 0.000	1.000 ± 0.000	1.000 ± 0.000
[13.00, 14.00[	1.000 ± 0.000	1.000 ± 0.000	1.000 ± 0.000	1.000 ± 0.000	1.000 ± 0.000

Table G.11: Efficiency of DaughtersInLHCb for D^+ in MagUp event type 21263010 (D+_K-pi+pi+=res,DecProdCut, $D^+ \to K^-\pi^+\pi^+$) in bins of (p_{T}, y), where p_{T} and y are computed in the proton-proton CM frame. The numbers are expressed as ratios of the number of signal decays generated into the bin to the number of those decays that satisfy the DaughtersInLHCb requirement.

p_{T}	y				
(GeV)	$[2.0, 2.5[$	$[2.5, 3.0[$	$[3.0, 3.5[$	$[3.5, 4.0[$	$[4.0, 4.5[$
$[0.00, 0.25[$	1150/1726	1370/1591	1350/1466	1090/1343	659/1187
$[0.25, 0.50[$	2838/4392	3623/4122	3575/3874	2788/3451	1767/3120
$[0.50, 0.75[$	4071/6163	5022/5664	4821/5171	3822/4617	2455/4070
$[0.75, 1.00[$	4498/6669	5710/6383	5201/5533	4165/4903	2583/4128
$[1.00, 1.25[$	4573/6545	5504/6029	5049/5321	4038/4640	2674/3919
$[1.25, 1.50[$	4268/5893	5180/5584	4763/4944	3780/4209	2484/3502
$[1.50, 1.75[$	4054/5453	4660/4928	4159/4295	3418/3734	2275/3032
$[1.75, 2.00[$	3599/4714	4074/4262	3691/3814	2957/3182	2068/2599
$[2.00, 2.25[$	3211/4017	3620/3757	3304/3369	2508/2675	1770/2182
$[2.25, 2.50[$	2956/3601	3040/3124	2593/2636	2194/2325	1523/1792
$[2.50, 2.75[$	2525/3054	2715/2768	2273/2293	1885/1973	1331/1574
$[2.75, 3.00[$	2126/2522	2297/2328	2060/2087	1618/1670	1130/1267
$[3.00, 3.50[$	3711/4241	3713/3757	3268/3307	2453/2522	1917/2114
$[3.50, 4.00[$	2739/3043	2888/2909	2354/2368	2019/2050	1345/1439
$[4.00, 4.50[$	2249/2445	2080/2088	1761/1770	1409/1427	1038/1089
$[4.50, 5.00[$	1667/1795	1609/1613	1271/1275	1051/1064	779/815
$[5.00, 6.00[$	2293/2381	2060/2062	1749/1757	1397/1412	1007/1044
$[6.00, 7.00[$	1426/1477	1195/1195	1011/1013	831/837	534/547
$[7.00, 8.00[$	885/904	797/797	638/640	473/478	311/318
$[8.00, 9.00[$	559/568	519/519	394/395	315/318	187/190
$[9.00, 10.00[$	373/377	313/313	267/267	163/163	91/94
$[10.00, 11.00[$	242/242	219/219	188/188	110/111	69/69
$[11.00, 12.00[$	146/146	127/127	95/95	80/80	59/59
$[12.00, 13.00[$	129/129	93/93	63/63	45/45	28/28
$[13.00, 14.00[$	105/105	76/76	63/63	35/35	19/19

Table G.12: Efficiency of DaughtersInLHCb for D^+ in MagUp event type 21263010 (D+_K-pi+pi+=res,DecProdCut, $D^+ \to K^-\pi^+\pi^+$) in bins of (p_{T}, y), where p_{T} and y are computed in the proton-proton CM frame. The quoted uncertainties are binomial statistical uncertainties only.

p_{T} (GeV)	y [2.0, 2.5[	[2.5, 3.0[	[3.0, 3.5[	[3.5, 4.0[	[4.0, 4.5[
[0.00, 0.25[	0.666 ± 0.011	0.861 ± 0.009	0.921 ± 0.007	0.812 ± 0.011	0.555 ± 0.014
[0.25, 0.50[	0.646 ± 0.007	0.879 ± 0.005	0.923 ± 0.004	0.808 ± 0.007	0.566 ± 0.009
[0.50, 0.75[	0.661 ± 0.006	0.887 ± 0.004	0.932 ± 0.003	0.828 ± 0.006	0.603 ± 0.008
[0.75, 1.00[	0.674 ± 0.006	0.895 ± 0.004	0.940 ± 0.003	0.849 ± 0.005	0.626 ± 0.008
[1.00, 1.25[	0.699 ± 0.006	0.913 ± 0.004	0.949 ± 0.003	0.870 ± 0.005	0.682 ± 0.007
[1.25, 1.50[	0.724 ± 0.006	0.928 ± 0.003	0.963 ± 0.003	0.898 ± 0.005	0.709 ± 0.008
[1.50, 1.75[	0.743 ± 0.006	0.946 ± 0.003	0.968 ± 0.003	0.915 ± 0.005	0.750 ± 0.008
[1.75, 2.00[	0.763 ± 0.006	0.956 ± 0.003	0.968 ± 0.003	0.929 ± 0.005	0.796 ± 0.008
[2.00, 2.25[	0.799 ± 0.006	0.964 ± 0.003	0.981 ± 0.002	0.938 ± 0.005	0.811 ± 0.008
[2.25, 2.50[	0.821 ± 0.006	0.973 ± 0.003	0.984 ± 0.002	0.944 ± 0.005	0.850 ± 0.008
[2.50, 2.75[	0.827 ± 0.007	0.981 ± 0.003	0.991 ± 0.002	0.955 ± 0.005	0.846 ± 0.009
[2.75, 3.00[	0.843 ± 0.007	0.987 ± 0.002	0.987 ± 0.002	0.969 ± 0.004	0.892 ± 0.009
[3.00, 3.50[	0.875 ± 0.005	0.988 ± 0.002	0.988 ± 0.002	0.973 ± 0.003	0.907 ± 0.006
[3.50, 4.00[	0.900 ± 0.005	0.993 ± 0.002	0.994 ± 0.002	0.985 ± 0.003	0.935 ± 0.007
[4.00, 4.50[	0.920 ± 0.005	0.996 ± 0.001	0.995 ± 0.002	0.987 ± 0.003	0.953 ± 0.006
[4.50, 5.00[	0.929 ± 0.006	0.998 ± 0.001	0.997 ± 0.002	0.988 ± 0.003	0.956 ± 0.007
[5.00, 6.00[	0.963 ± 0.004	0.999 ± 0.001	0.995 ± 0.002	0.989 ± 0.003	0.965 ± 0.006
[6.00, 7.00[	0.965 ± 0.005	1.000 ± 0.000	0.998 ± 0.001	0.993 ± 0.003	0.976 ± 0.007
[7.00, 8.00[	0.979 ± 0.005	1.000 ± 0.000	0.997 ± 0.002	0.990 ± 0.005	0.978 ± 0.008
[8.00, 9.00[	0.984 ± 0.005	1.000 ± 0.000	0.997 ± 0.003	0.991 ± 0.005	0.984 ± 0.009
[9.00, 10.00[	0.989 ± 0.005	1.000 ± 0.000	1.000 ± 0.000	1.000 ± 0.000	0.968 ± 0.018
[10.00, 11.00[	1.000 ± 0.000	1.000 ± 0.000	1.000 ± 0.000	0.991 ± 0.009	1.000 ± 0.000
[11.00, 12.00[	1.000 ± 0.000	1.000 ± 0.000	1.000 ± 0.000	1.000 ± 0.000	1.000 ± 0.000
[12.00, 13.00[	1.000 ± 0.000	1.000 ± 0.000	1.000 ± 0.000	1.000 ± 0.000	1.000 ± 0.000
[13.00, 14.00[	1.000 ± 0.000	1.000 ± 0.000	1.000 ± 0.000	1.000 ± 0.000	1.000 ± 0.000

G.4 $D^+ \to \phi\pi^+$

Table G.13: Efficiency of DaughtersInLHCb for D^+ in MagDown event type 21263002 (D+_K-K+pi+=res,DecProdCut, $D^+ \to K^-K^+\pi^+$) in bins of (p_{T}, y), where p_{T} and y are computed in the proton-proton CM frame. The numbers are expressed as ratios of the number of signal decays generated into the bin to the number of those decays that satisfy the DaughtersInLHCb requirement.

p_{T}	y				
(GeV)	$[2.0, 2.5[$	$[2.5, 3.0[$	$[3.0, 3.5[$	$[3.5, 4.0[$	$[4.0, 4.5[$
$[0.00, 0.25[$	2647/3255	2794/3036	2677/2951	1934/2587	961/2316
$[0.25, 0.50[$	7244/8783	7676/8309	6771/7575	5181/6859	2720/5897
$[0.50, 0.75[$	9965/12026	10280/11149	9059/10031	7167/9143	3947/7912
$[0.75, 1.00[$	11087/13339	11324/12124	10106/10892	7778/9541	4582/8108
$[1.00, 1.25[$	10833/12862	11259/11842	9969/10532	7906/9211	4869/7698
$[1.25, 1.50[$	10078/11797	10339/10754	9427/9833	7329/8344	4786/6904
$[1.50, 1.75[$	9226/10677	9201/9495	8236/8521	6558/7195	4577/6080
$[1.75, 2.00[$	8283/9395	8120/8341	7338/7540	5735/6191	3961/5007
$[2.00, 2.25[$	7063/7850	7295/7439	6294/6398	4990/5274	3637/4335
$[2.25, 2.50[$	6401/7076	6209/6297	5302/5384	4329/4514	3040/3505
$[2.50, 2.75[$	5554/6043	5299/5361	4690/4726	3685/3799	2715/2999
$[2.75, 3.00[$	4622/5013	4616/4648	3941/3962	3246/3308	2463/2668
$[3.00, 3.50[$	7844/8359	7413/7445	6439/6458	5126/5197	3858/4090
$[3.50, 4.00[$	5754/6064	5305/5318	4564/4578	3798/3844	2799/2914
$[4.00, 4.50[$	4446/4640	4176/4186	3434/3444	2820/2836	2189/2239
$[4.50, 5.00[$	3332/3447	3041/3044	2590/2595	2133/2148	1531/1559
$[5.00, 6.00[$	4553/4659	4105/4107	3462/3469	2771/2783	1965/1991
$[6.00, 7.00[$	2800/2837	2524/2526	1987/1990	1554/1559	1094/1104
$[7.00, 8.00[$	1803/1816	1496/1496	1161/1161	931/933	581/585
$[8.00, 9.00[$	1077/1085	1008/1008	743/743	573/574	413/415
$[9.00, 10.00[$	742/742	635/635	490/490	363/363	240/240
$[10.00, 11.00[$	492/492	402/402	317/317	225/225	125/126
$[11.00, 12.00[$	347/347	244/244	219/219	161/161	81/81
$[12.00, 13.00[$	237/237	171/171	168/168	94/94	67/67
$[13.00, 14.00[$	159/159	135/135	97/97	84/84	36/36

Table G.14: Efficiency of DaughtersInLHCb for D^+ in MagDown event type 21263002 (D+_K-K+pi+=res,DecProdCut, $D^+ \to K^-K^+\pi^+$) in bins of (p_{T}, y), where p_{T} and y are computed in the proton-proton CM frame. The quoted uncertainties are binomial statistical uncertainties only.

p_{T} (GeV)	y [2.0, 2.5[	[2.5, 3.0[	[3.0, 3.5[	[3.5, 4.0[	[4.0, 4.5[
[0.00, 0.25[	0.813 ± 0.007	0.920 ± 0.005	0.907 ± 0.005	0.748 ± 0.009	0.415 ± 0.010
[0.25, 0.50[	0.825 ± 0.004	0.924 ± 0.003	0.894 ± 0.004	0.755 ± 0.005	0.461 ± 0.006
[0.50, 0.75[	0.829 ± 0.003	0.922 ± 0.003	0.903 ± 0.003	0.784 ± 0.004	0.499 ± 0.006
[0.75, 1.00[	0.831 ± 0.003	0.934 ± 0.002	0.928 ± 0.002	0.815 ± 0.004	0.565 ± 0.006
[1.00, 1.25[	0.842 ± 0.003	0.951 ± 0.002	0.947 ± 0.002	0.858 ± 0.004	0.633 ± 0.005
[1.25, 1.50[	0.854 ± 0.003	0.961 ± 0.002	0.959 ± 0.002	0.878 ± 0.004	0.693 ± 0.006
[1.50, 1.75[	0.864 ± 0.003	0.969 ± 0.002	0.967 ± 0.002	0.911 ± 0.003	0.753 ± 0.006
[1.75, 2.00[	0.882 ± 0.003	0.974 ± 0.002	0.973 ± 0.002	0.926 ± 0.003	0.791 ± 0.006
[2.00, 2.25[	0.900 ± 0.003	0.981 ± 0.002	0.984 ± 0.002	0.946 ± 0.003	0.839 ± 0.006
[2.25, 2.50[	0.905 ± 0.003	0.986 ± 0.001	0.985 ± 0.002	0.959 ± 0.003	0.867 ± 0.006
[2.50, 2.75[	0.919 ± 0.004	0.988 ± 0.001	0.992 ± 0.001	0.970 ± 0.003	0.905 ± 0.005
[2.75, 3.00[	0.922 ± 0.004	0.993 ± 0.001	0.995 ± 0.001	0.981 ± 0.002	0.923 ± 0.005
[3.00, 3.50[	0.938 ± 0.003	0.996 ± 0.001	0.997 ± 0.001	0.986 ± 0.002	0.943 ± 0.004
[3.50, 4.00[	0.949 ± 0.003	0.998 ± 0.001	0.997 ± 0.001	0.988 ± 0.002	0.961 ± 0.004
[4.00, 4.50[	0.958 ± 0.003	0.998 ± 0.001	0.997 ± 0.001	0.994 ± 0.001	0.978 ± 0.003
[4.50, 5.00[	0.967 ± 0.003	0.999 ± 0.001	0.998 ± 0.001	0.993 ± 0.002	0.982 ± 0.003
[5.00, 6.00[	0.977 ± 0.002	1.000 ± 0.000	0.998 ± 0.001	0.996 ± 0.001	0.987 ± 0.003
[6.00, 7.00[	0.987 ± 0.002	0.999 ± 0.001	0.998 ± 0.001	0.997 ± 0.001	0.991 ± 0.003
[7.00, 8.00[	0.993 ± 0.002	1.000 ± 0.000	1.000 ± 0.000	0.998 ± 0.002	0.993 ± 0.003
[8.00, 9.00[	0.993 ± 0.003	1.000 ± 0.000	1.000 ± 0.000	0.998 ± 0.002	0.995 ± 0.003
[9.00, 10.00[	1.000 ± 0.000	1.000 ± 0.000	1.000 ± 0.000	1.000 ± 0.000	1.000 ± 0.000
[10.00, 11.00[	1.000 ± 0.000	1.000 ± 0.000	1.000 ± 0.000	1.000 ± 0.000	0.992 ± 0.008
[11.00, 12.00[	1.000 ± 0.000	1.000 ± 0.000	1.000 ± 0.000	1.000 ± 0.000	1.000 ± 0.000
[12.00, 13.00[	1.000 ± 0.000	1.000 ± 0.000	1.000 ± 0.000	1.000 ± 0.000	1.000 ± 0.000
[13.00, 14.00[	1.000 ± 0.000	1.000 ± 0.000	1.000 ± 0.000	1.000 ± 0.000	1.000 ± 0.000

Table G.15: Efficiency of DaughtersInLHCb for D^+ in MagUp event type 21263002 (D+_K-K+pi+=res,DecProdCut, $D^+ \to K^-K^+\pi^+$) in bins of (p_{T}, y), where p_{T} and y are computed in the proton-proton CM frame. The numbers are expressed as ratios of the number of signal decays generated into the bin to the number of those decays that satisfy the DaughtersInLHCb requirement.

p_{T}	y				
(GeV)	$[2.0, 2.5[$	$[2.5, 3.0[$	$[3.0, 3.5[$	$[3.5, 4.0[$	$[4.0, 4.5[$
$[0.00, 0.25[$	2726/3309	3002/3262	2601/2907	2051/2735	1021/2305
$[0.25, 0.50[$	7338/8954	7765/8425	6997/7767	5271/7002	2703/6040
$[0.50, 0.75[$	10012/12122	10434/11305	9349/10265	7064/9156	4023/7913
$[0.75, 1.00[$	11182/13454	11842/12624	10303/11093	7903/9648	4860/8463
$[1.00, 1.25[$	10891/12920	11288/11904	10342/10866	7861/9261	5025/7806
$[1.25, 1.50[$	10327/12157	10491/10938	9365/9769	7417/8375	4928/7129
$[1.50, 1.75[$	9441/10804	9631/9960	8554/8853	6719/7410	4483/5981
$[1.75, 2.00[$	8229/9311	8405/8595	7233/7412	5903/6376	4051/5096
$[2.00, 2.25[$	7294/8146	7295/7431	6237/6344	5290/5583	3729/4481
$[2.25, 2.50[$	6312/6987	6180/6274	5405/5480	4287/4453	3284/3790
$[2.50, 2.75[$	5579/6084	5511/5572	4692/4723	3853/3983	2805/3116
$[2.75, 3.00[$	4830/5213	4615/4653	4083/4122	3204/3283	2443/2658
$[3.00, 3.50[$	8028/8560	7407/7437	6507/6533	5207/5283	3858/4090
$[3.50, 4.00[$	5938/6219	5573/5586	4778/4794	3927/3974	2895/3002
$[4.00, 4.50[$	4562/4750	4159/4167	3623/3636	2720/2743	2091/2154
$[4.50, 5.00[$	3411/3518	3169/3174	2644/2650	2118/2131	1538/1567
$[5.00, 6.00[$	4644/4743	4234/4239	3495/3501	2815/2831	2058/2090
$[6.00, 7.00[$	2802/2840	2488/2490	2029/2035	1562/1567	1063/1069
$[7.00, 8.00[$	1761/1780	1592/1592	1233/1234	923/925	624/628
$[8.00, 9.00[$	1135/1138	980/981	794/794	580/580	363/364
$[9.00, 10.00[$	756/760	619/619	486/486	380/380	214/215
$[10.00, 11.00[$	502/502	411/411	353/353	223/223	148/148
$[11.00, 12.00[$	313/313	268/268	242/242	171/171	72/72
$[12.00, 13.00[$	240/241	201/201	151/151	102/102	69/69
$[13.00, 14.00[$	168/168	160/160	105/105	65/65	49/49

Table G.16: Efficiency of DaughtersInLHCb for D^+ in MagUp event type 21263002 (D+_K-K+pi+=res,DecProdCut, $D^+ \to K^-K^+\pi^+$) in bins of (p_{T}, y), where p_{T} and y are computed in the proton-proton CM frame. The quoted uncertainties are binomial statistical uncertainties only.

p_{T} (GeV)	y [2.0, 2.5[	[2.5, 3.0[	[3.0, 3.5[	[3.5, 4.0[	[4.0, 4.5[
[0.00, 0.25[	0.824 ± 0.007	0.920 ± 0.005	0.895 ± 0.006	0.750 ± 0.008	0.443 ± 0.010
[0.25, 0.50[	0.820 ± 0.004	0.922 ± 0.003	0.901 ± 0.003	0.753 ± 0.005	0.448 ± 0.006
[0.50, 0.75[	0.826 ± 0.003	0.923 ± 0.003	0.911 ± 0.003	0.772 ± 0.004	0.508 ± 0.006
[0.75, 1.00[	0.831 ± 0.003	0.938 ± 0.002	0.929 ± 0.002	0.819 ± 0.004	0.574 ± 0.005
[1.00, 1.25[	0.843 ± 0.003	0.948 ± 0.002	0.952 ± 0.002	0.849 ± 0.004	0.644 ± 0.005
[1.25, 1.50[	0.849 ± 0.003	0.959 ± 0.002	0.959 ± 0.002	0.886 ± 0.003	0.691 ± 0.005
[1.50, 1.75[	0.874 ± 0.003	0.967 ± 0.002	0.966 ± 0.002	0.907 ± 0.003	0.750 ± 0.006
[1.75, 2.00[	0.884 ± 0.003	0.978 ± 0.002	0.976 ± 0.002	0.926 ± 0.003	0.795 ± 0.006
[2.00, 2.25[	0.895 ± 0.003	0.982 ± 0.002	0.983 ± 0.002	0.948 ± 0.003	0.832 ± 0.006
[2.25, 2.50[	0.903 ± 0.004	0.985 ± 0.002	0.986 ± 0.002	0.963 ± 0.003	0.866 ± 0.006
[2.50, 2.75[	0.917 ± 0.004	0.989 ± 0.001	0.993 ± 0.001	0.967 ± 0.003	0.900 ± 0.005
[2.75, 3.00[	0.927 ± 0.004	0.992 ± 0.001	0.991 ± 0.002	0.976 ± 0.003	0.919 ± 0.005
[3.00, 3.50[	0.938 ± 0.003	0.996 ± 0.001	0.996 ± 0.001	0.986 ± 0.002	0.943 ± 0.004
[3.50, 4.00[	0.955 ± 0.003	0.998 ± 0.001	0.997 ± 0.001	0.988 ± 0.002	0.964 ± 0.003
[4.00, 4.50[	0.960 ± 0.003	0.998 ± 0.001	0.996 ± 0.001	0.992 ± 0.002	0.971 ± 0.004
[4.50, 5.00[	0.970 ± 0.003	0.998 ± 0.001	0.998 ± 0.001	0.994 ± 0.002	0.981 ± 0.003
[5.00, 6.00[	0.979 ± 0.002	0.999 ± 0.001	0.998 ± 0.001	0.994 ± 0.001	0.985 ± 0.003
[6.00, 7.00[	0.987 ± 0.002	0.999 ± 0.001	0.997 ± 0.001	0.997 ± 0.001	0.994 ± 0.002
[7.00, 8.00[	0.989 ± 0.002	1.000 ± 0.000	0.999 ± 0.001	0.998 ± 0.002	0.994 ± 0.003
[8.00, 9.00[	0.997 ± 0.002	0.999 ± 0.001	1.000 ± 0.000	1.000 ± 0.000	0.997 ± 0.003
[9.00, 10.00[	0.995 ± 0.003	1.000 ± 0.000	1.000 ± 0.000	1.000 ± 0.000	0.995 ± 0.005
[10.00, 11.00[	1.000 ± 0.000	1.000 ± 0.000	1.000 ± 0.000	1.000 ± 0.000	1.000 ± 0.000
[11.00, 12.00[	1.000 ± 0.000	1.000 ± 0.000	1.000 ± 0.000	1.000 ± 0.000	1.000 ± 0.000
[12.00, 13.00[	0.996 ± 0.004	1.000 ± 0.000	1.000 ± 0.000	1.000 ± 0.000	1.000 ± 0.000
[13.00, 14.00[	1.000 ± 0.000	1.000 ± 0.000	1.000 ± 0.000	1.000 ± 0.000	1.000 ± 0.000

G.5 $D_s^+ \to \phi\pi^+$

Table G.17: Efficiency of DaughtersInLHCb for D_s^+ in MagDown event type 23263020 (Ds+_K-K+pi+=res,DecProdCut, $D_s^+ \to K^-K^+\pi^+$) in bins of (p_{T}, y), where p_{T} and y are computed in the proton-proton CM frame. The K^- K^+ invariant mass is required to be in the interval $|m(K^-K^+) - 1019.5\,\mathrm{MeV}| < 20\,\mathrm{MeV}$ for both the numerator and denominator.The numbers are expressed as ratios of the number of signal decays generated into the bin to the number of those decays that satisfy the DaughtersInLHCb requirement.

p_{T}	y				
(GeV)	$[2.0, 2.5[$	$[2.5, 3.0[$	$[3.0, 3.5[$	$[3.5, 4.0[$	$[4.0, 4.5[$
$[0.00, 0.25[$	479/614	539/593	480/519	370/462	233/432
$[0.25, 0.50[$	1279/1576	1283/1436	1308/1440	1021/1280	572/1115
$[0.50, 0.75[$	1797/2228	1846/2056	1709/1900	1329/1734	787/1502
$[0.75, 1.00[$	2047/2502	2072/2280	1859/2043	1461/1848	954/1576
$[1.00, 1.25[$	2044/2505	2003/2199	1881/2023	1546/1853	978/1503
$[1.25, 1.50[$	1910/2305	1977/2106	1781/1864	1409/1585	985/1377
$[1.50, 1.75[$	1706/2020	1818/1923	1614/1669	1336/1471	856/1176
$[1.75, 2.00[$	1568/1825	1470/1555	1515/1559	1169/1266	862/1055
$[2.00, 2.25[$	1418/1635	1385/1431	1294/1313	1081/1156	713/831
$[2.25, 2.50[$	1243/1428	1239/1265	1125/1136	901/939	677/787
$[2.50, 2.75[$	1079/1214	1144/1173	929/937	809/838	594/663
$[2.75, 3.00[$	934/1055	918/929	832/833	684/699	480/512
$[3.00, 3.50[$	1589/1726	1590/1613	1172/1174	1053/1066	796/837
$[3.50, 4.00[$	1199/1278	1158/1164	922/925	790/799	582/604
$[4.00, 4.50[$	911/972	835/844	737/738	617/628	408/424
$[4.50, 5.00[$	694/733	702/704	525/526	452/454	292/299
$[5.00, 6.00[$	1043/1077	890/892	752/755	551/553	411/419
$[6.00, 7.00[$	569/586	530/530	438/439	349/352	263/264
$[7.00, 8.00[$	415/421	321/321	263/263	198/199	130/131
$[8.00, 9.00[$	240/241	189/190	163/163	122/122	84/86
$[9.00, 10.00[$	158/161	125/125	96/96	93/93	50/51
$[10.00, 11.00[$	95/97	94/94	42/43	43/43	37/37
$[11.00, 12.00[$	83/83	54/54	43/43	24/24	21/21
$[12.00, 13.00[$	49/49	43/43	34/34	24/24	10/10
$[13.00, 14.00[$	46/46	34/34	24/24	6/6	6/6

Table G.18: Efficiency of DaughtersInLHCb for D_s^+ in MagDown event type 23263020 (Ds+_K-K+pi+=res,DecProdCut, $D_s^+ \to K^-K^+\pi^+$) in bins of $(p_{\rm T}, y)$, where $p_{\rm T}$ and y are computed in the proton-proton CM frame. The K^- K^+ invariant mass is required to be in the interval $|m(K^-K^+) - 1019.5\,{\rm MeV}| < 20\,{\rm MeV}$ for both the numerator and denominator.The quoted uncertainties are binomial statistical uncertainties only.

$p_{\rm T}$	y				
(GeV)	$[2.0, 2.5[$	$[2.5, 3.0[$	$[3.0, 3.5[$	$[3.5, 4.0[$	$[4.0, 4.5[$
$[0.00, 0.25[$	0.780 ± 0.017	0.909 ± 0.012	0.925 ± 0.012	0.801 ± 0.019	0.539 ± 0.024
$[0.25, 0.50[$	0.812 ± 0.010	0.893 ± 0.008	0.908 ± 0.008	0.798 ± 0.011	0.513 ± 0.015
$[0.50, 0.75[$	0.807 ± 0.008	0.898 ± 0.007	0.899 ± 0.007	0.766 ± 0.010	0.524 ± 0.013
$[0.75, 1.00[$	0.818 ± 0.008	0.909 ± 0.006	0.910 ± 0.006	0.791 ± 0.009	0.605 ± 0.012
$[1.00, 1.25[$	0.816 ± 0.008	0.911 ± 0.006	0.930 ± 0.006	0.834 ± 0.009	0.651 ± 0.012
$[1.25, 1.50[$	0.829 ± 0.008	0.939 ± 0.005	0.955 ± 0.005	0.889 ± 0.008	0.715 ± 0.012
$[1.50, 1.75[$	0.845 ± 0.008	0.945 ± 0.005	0.967 ± 0.004	0.908 ± 0.008	0.728 ± 0.013
$[1.75, 2.00[$	0.859 ± 0.008	0.945 ± 0.006	0.972 ± 0.004	0.923 ± 0.007	0.817 ± 0.012
$[2.00, 2.25[$	0.867 ± 0.008	0.968 ± 0.005	0.986 ± 0.003	0.935 ± 0.007	0.858 ± 0.012
$[2.25, 2.50[$	0.870 ± 0.009	0.979 ± 0.004	0.990 ± 0.003	0.960 ± 0.006	0.860 ± 0.012
$[2.50, 2.75[$	0.889 ± 0.009	0.975 ± 0.005	0.991 ± 0.003	0.965 ± 0.006	0.896 ± 0.012
$[2.75, 3.00[$	0.885 ± 0.010	0.988 ± 0.004	0.999 ± 0.001	0.979 ± 0.005	0.938 ± 0.011
$[3.00, 3.50[$	0.921 ± 0.007	0.986 ± 0.003	0.998 ± 0.001	0.988 ± 0.003	0.951 ± 0.007
$[3.50, 4.00[$	0.938 ± 0.007	0.995 ± 0.002	0.997 ± 0.002	0.989 ± 0.004	0.964 ± 0.008
$[4.00, 4.50[$	0.937 ± 0.008	0.989 ± 0.004	0.999 ± 0.001	0.982 ± 0.005	0.962 ± 0.009
$[4.50, 5.00[$	0.947 ± 0.008	0.997 ± 0.002	0.998 ± 0.002	0.996 ± 0.003	0.977 ± 0.009
$[5.00, 6.00[$	0.968 ± 0.005	0.998 ± 0.002	0.996 ± 0.002	0.996 ± 0.003	0.981 ± 0.007
$[6.00, 7.00[$	0.971 ± 0.007	1.000 ± 0.000	0.998 ± 0.002	0.991 ± 0.005	0.996 ± 0.004
$[7.00, 8.00[$	0.986 ± 0.006	1.000 ± 0.000	1.000 ± 0.000	0.995 ± 0.005	0.992 ± 0.008
$[8.00, 9.00[$	0.996 ± 0.004	0.995 ± 0.005	1.000 ± 0.000	1.000 ± 0.000	0.977 ± 0.016
$[9.00, 10.00[$	0.981 ± 0.011	1.000 ± 0.000	1.000 ± 0.000	1.000 ± 0.000	0.980 ± 0.019
$[10.00, 11.00[$	0.979 ± 0.014	1.000 ± 0.000	0.977 ± 0.023	1.000 ± 0.000	1.000 ± 0.000
$[11.00, 12.00[$	1.000 ± 0.000	1.000 ± 0.000	1.000 ± 0.000	1.000 ± 0.000	1.000 ± 0.000
$[12.00, 13.00[$	1.000 ± 0.000	1.000 ± 0.000	1.000 ± 0.000	1.000 ± 0.000	1.000 ± 0.000
$[13.00, 14.00[$	1.000 ± 0.000	1.000 ± 0.000	1.000 ± 0.000	1.000 ± 0.000	1.000 ± 0.000

Table G.19: Efficiency of DaughtersInLHCb for D_s^+ in MagUp event type 23263020 (Ds+_K-K+pi+=res,DecProdCut, $D_s^+ \to K^-K^+\pi^+$) in bins of $(p_{\rm T}, y)$, where $p_{\rm T}$ and y are computed in the proton-proton CM frame. The K^- K^+ invariant mass is required to be in the interval $|m(K^-K^+) - 1019.5\,{\rm MeV}| < 20\,{\rm MeV}$ for both the numerator and denominator.The numbers are expressed as ratios of the number of signal decays generated into the bin to the number of those decays that satisfy the DaughtersInLHCb requirement.

$p_{\rm T}$	y				
(GeV)	$[2.0, 2.5[$	$[2.5, 3.0[$	$[3.0, 3.5[$	$[3.5, 4.0[$	$[4.0, 4.5[$
$[0.00, 0.25[$	478/583	485/534	482/529	384/493	221/435
$[0.25, 0.50[$	1246/1609	1279/1425	1176/1290	977/1241	509/1054
$[0.50, 0.75[$	1779/2255	1808/2007	1707/1899	1280/1634	737/1437
$[0.75, 1.00[$	1993/2509	1960/2185	1818/2010	1399/1760	863/1545
$[1.00, 1.25[$	1947/2375	2084/2269	1931/2080	1451/1708	916/1453
$[1.25, 1.50[$	1816/2192	2051/2190	1738/1811	1408/1624	933/1310
$[1.50, 1.75[$	1722/2037	1791/1900	1612/1664	1277/1424	846/1120
$[1.75, 2.00[$	1553/1828	1524/1608	1434/1475	1221/1311	806/994
$[2.00, 2.25[$	1372/1569	1397/1453	1178/1198	1026/1097	687/815
$[2.25, 2.50[$	1135/1303	1199/1236	1074/1084	848/878	639/732
$[2.50, 2.75[$	1110/1237	1030/1059	942/947	777/787	585/653
$[2.75, 3.00[$	968/1072	951/970	789/795	664/670	499/529
$[3.00, 3.50[$	1588/1728	1491/1505	1328/1333	1099/1116	750/793
$[3.50, 4.00[$	1255/1339	1034/1043	991/998	788/796	564/586
$[4.00, 4.50[$	872/927	846/850	645/648	561/568	376/393
$[4.50, 5.00[$	660/694	625/626	546/548	447/449	310/316
$[5.00, 6.00[$	968/1009	865/865	765/767	533/537	425/436
$[6.00, 7.00[$	547/557	495/497	426/428	327/329	220/221
$[7.00, 8.00[$	345/351	309/309	260/260	185/185	152/153
$[8.00, 9.00[$	240/240	211/211	140/140	129/129	90/90
$[9.00, 10.00[$	153/155	113/113	122/123	72/72	40/40
$[10.00, 11.00[$	108/108	105/105	66/66	59/59	26/26
$[11.00, 12.00[$	67/67	68/68	57/57	40/40	11/11
$[12.00, 13.00[$	45/45	39/39	37/37	22/22	9/9
$[13.00, 14.00[$	44/44	29/29	18/18	11/11	8/8

Table G.20: Efficiency of DaughtersInLHCb for D_s^+ in MagUp event type 23263020 (Ds+_K-K+pi+=res,DecProdCut, $D_s^+ \to K^-K^+\pi^+$) in bins of $(p_{\rm T}, y)$, where $p_{\rm T}$ and y are computed in the proton-proton CM frame. The K^- K^+ invariant mass is required to be in the interval $|m(K^-K^+) - 1019.5\,{\rm MeV}| < 20\,{\rm MeV}$ for both the numerator and denominator.The quoted uncertainties are binomial statistical uncertainties only.

$p_{\rm T}$	y				
(GeV)	$[2.0, 2.5[$	$[2.5, 3.0[$	$[3.0, 3.5[$	$[3.5, 4.0[$	$[4.0, 4.5[$
$[0.00, 0.25[$	0.820 ± 0.016	0.908 ± 0.012	0.911 ± 0.012	0.779 ± 0.019	0.508 ± 0.024
$[0.25, 0.50[$	0.774 ± 0.010	0.898 ± 0.008	0.912 ± 0.008	0.787 ± 0.012	0.483 ± 0.015
$[0.50, 0.75[$	0.789 ± 0.009	0.901 ± 0.007	0.899 ± 0.007	0.783 ± 0.010	0.513 ± 0.013
$[0.75, 1.00[$	0.794 ± 0.008	0.897 ± 0.007	0.904 ± 0.007	0.795 ± 0.010	0.559 ± 0.013
$[1.00, 1.25[$	0.820 ± 0.008	0.918 ± 0.006	0.928 ± 0.006	0.850 ± 0.009	0.630 ± 0.013
$[1.25, 1.50[$	0.828 ± 0.008	0.937 ± 0.005	0.960 ± 0.005	0.867 ± 0.008	0.712 ± 0.013
$[1.50, 1.75[$	0.845 ± 0.008	0.943 ± 0.005	0.969 ± 0.004	0.897 ± 0.008	0.755 ± 0.013
$[1.75, 2.00[$	0.850 ± 0.008	0.948 ± 0.006	0.972 ± 0.004	0.931 ± 0.007	0.811 ± 0.012
$[2.00, 2.25[$	0.874 ± 0.008	0.961 ± 0.005	0.983 ± 0.004	0.935 ± 0.007	0.843 ± 0.013
$[2.25, 2.50[$	0.871 ± 0.009	0.970 ± 0.005	0.991 ± 0.003	0.966 ± 0.006	0.873 ± 0.012
$[2.50, 2.75[$	0.897 ± 0.009	0.973 ± 0.005	0.995 ± 0.002	0.987 ± 0.004	0.896 ± 0.012
$[2.75, 3.00[$	0.903 ± 0.009	0.980 ± 0.004	0.992 ± 0.003	0.991 ± 0.004	0.943 ± 0.010
$[3.00, 3.50[$	0.919 ± 0.007	0.991 ± 0.002	0.996 ± 0.002	0.985 ± 0.004	0.946 ± 0.008
$[3.50, 4.00[$	0.937 ± 0.007	0.991 ± 0.003	0.993 ± 0.003	0.990 ± 0.004	0.962 ± 0.008
$[4.00, 4.50[$	0.941 ± 0.008	0.995 ± 0.002	0.995 ± 0.003	0.988 ± 0.005	0.957 ± 0.010
$[4.50, 5.00[$	0.951 ± 0.008	0.998 ± 0.002	0.996 ± 0.003	0.996 ± 0.003	0.981 ± 0.008
$[5.00, 6.00[$	0.959 ± 0.006	1.000 ± 0.000	0.997 ± 0.002	0.993 ± 0.004	0.975 ± 0.008
$[6.00, 7.00[$	0.982 ± 0.006	0.996 ± 0.003	0.995 ± 0.003	0.994 ± 0.004	0.995 ± 0.005
$[7.00, 8.00[$	0.983 ± 0.007	1.000 ± 0.000	1.000 ± 0.000	1.000 ± 0.000	0.993 ± 0.007
$[8.00, 9.00[$	1.000 ± 0.000	1.000 ± 0.000	1.000 ± 0.000	1.000 ± 0.000	1.000 ± 0.000
$[9.00, 10.00[$	0.987 ± 0.009	1.000 ± 0.000	0.992 ± 0.008	1.000 ± 0.000	1.000 ± 0.000
$[10.00, 11.00[$	1.000 ± 0.000	1.000 ± 0.000	1.000 ± 0.000	1.000 ± 0.000	1.000 ± 0.000
$[11.00, 12.00[$	1.000 ± 0.000	1.000 ± 0.000	1.000 ± 0.000	1.000 ± 0.000	1.000 ± 0.000
$[12.00, 13.00[$	1.000 ± 0.000	1.000 ± 0.000	1.000 ± 0.000	1.000 ± 0.000	1.000 ± 0.000
$[13.00, 14.00[$	1.000 ± 0.000	1.000 ± 0.000	1.000 ± 0.000	1.000 ± 0.000	1.000 ± 0.000

G.6 $D_s^+ \to \pi^-\pi^+\pi^+$

Table G.21: Efficiency of DaughtersInLHCb for D_s^+ in MagDown event type 23263011 (Ds+_pi-pi+pi+=res,DecProdCut, $D_s^+ \to \pi^-\pi^+\pi^+$) in bins of (p_{T}, y), where p_{T} and y are computed in the proton-proton CM frame. The numbers are expressed as ratios of the number of signal decays generated into the bin to the number of those decays that satisfy the DaughtersInLHCb requirement.

p_{T}	y				
(GeV)	$[2.0, 2.5[$	$[2.5, 3.0[$	$[3.0, 3.5[$	$[3.5, 4.0[$	$[4.0, 4.5[$
$[0.00, 0.25[$	740/1449	1139/1362	1201/1297	1017/1207	688/1032
$[0.25, 0.50[$	2059/4047	3180/3812	3261/3491	2701/3094	1851/2728
$[0.50, 0.75[$	2910/5608	4224/5117	4309/4610	3733/4274	2490/3587
$[0.75, 1.00[$	3266/6094	4864/5759	4816/5167	4031/4550	2730/3785
$[1.00, 1.25[$	3354/6030	4751/5515	4839/5091	3831/4274	2609/3598
$[1.25, 1.50[$	3183/5514	4680/5306	4371/4556	3610/4009	2496/3295
$[1.50, 1.75[$	3128/5050	4211/4702	4016/4165	3321/3593	2176/2843
$[1.75, 2.00[$	2861/4553	3803/4145	3592/3710	2886/3128	1966/2456
$[2.00, 2.25[$	2672/4000	3398/3665	3076/3164	2460/2630	1766/2160
$[2.25, 2.50[$	2422/3515	2956/3132	2776/2826	2135/2269	1544/1838
$[2.50, 2.75[$	2116/2943	2579/2700	2383/2427	1878/1981	1340/1597
$[2.75, 3.00[$	1967/2634	2235/2334	2080/2105	1672/1772	1160/1328
$[3.00, 3.50[$	3315/4237	3768/3880	3198/3244	2588/2718	1802/2050
$[3.50, 4.00[$	2653/3184	2709/2771	2493/2512	1822/1891	1359/1538
$[4.00, 4.50[$	2000/2342	2026/2052	1792/1809	1457/1507	1017/1121
$[4.50, 5.00[$	1650/1841	1631/1650	1293/1304	1006/1033	791/849
$[5.00, 6.00[$	2262/2495	2127/2139	1825/1831	1500/1521	1034/1098
$[6.00, 7.00[$	1395/1505	1318/1324	1100/1105	828/836	522/549
$[7.00, 8.00[$	880/921	792/793	642/644	453/457	322/328
$[8.00, 9.00[$	568/589	536/536	407/408	284/285	198/200
$[9.00, 10.00[$	418/430	338/338	248/249	185/186	125/127
$[10.00, 11.00[$	276/279	176/176	177/177	105/105	79/81
$[11.00, 12.00[$	182/185	153/153	124/124	83/83	52/52
$[12.00, 13.00[$	114/115	96/96	80/80	58/58	32/32
$[13.00, 14.00[$	89/89	80/80	64/64	41/41	22/22

Table G.22: Efficiency of DaughtersInLHCb for D_s^+ in MagDown event type 23263011 (Ds+_pi-pi+pi+=res,DecProdCut, $D_s^+ \to \pi^-\pi^+\pi^+$) in bins of (p_{T}, y), where p_{T} and y are computed in the proton-proton CM frame. The quoted uncertainties are binomial statistical uncertainties only.

p_{T} (GeV)	y [2.0, 2.5[	[2.5, 3.0[	[3.0, 3.5[	[3.5, 4.0[	[4.0, 4.5[
[0.00, 0.25[	0.511 ± 0.013	0.836 ± 0.010	0.926 ± 0.007	0.843 ± 0.010	0.667 ± 0.015
[0.25, 0.50[	0.509 ± 0.008	0.834 ± 0.006	0.934 ± 0.004	0.873 ± 0.006	0.679 ± 0.009
[0.50, 0.75[	0.519 ± 0.007	0.825 ± 0.005	0.935 ± 0.004	0.873 ± 0.005	0.694 ± 0.008
[0.75, 1.00[	0.536 ± 0.006	0.845 ± 0.005	0.932 ± 0.004	0.886 ± 0.005	0.721 ± 0.007
[1.00, 1.25[	0.556 ± 0.006	0.861 ± 0.005	0.951 ± 0.003	0.896 ± 0.005	0.725 ± 0.007
[1.25, 1.50[	0.577 ± 0.007	0.882 ± 0.004	0.959 ± 0.003	0.900 ± 0.005	0.758 ± 0.007
[1.50, 1.75[	0.619 ± 0.007	0.896 ± 0.004	0.964 ± 0.003	0.924 ± 0.004	0.765 ± 0.008
[1.75, 2.00[	0.628 ± 0.007	0.917 ± 0.004	0.968 ± 0.003	0.923 ± 0.005	0.800 ± 0.008
[2.00, 2.25[	0.668 ± 0.007	0.927 ± 0.004	0.972 ± 0.003	0.935 ± 0.005	0.818 ± 0.008
[2.25, 2.50[	0.689 ± 0.008	0.944 ± 0.004	0.982 ± 0.002	0.941 ± 0.005	0.840 ± 0.009
[2.50, 2.75[	0.719 ± 0.008	0.955 ± 0.004	0.982 ± 0.003	0.948 ± 0.005	0.839 ± 0.009
[2.75, 3.00[	0.747 ± 0.008	0.958 ± 0.004	0.988 ± 0.002	0.944 ± 0.005	0.873 ± 0.009
[3.00, 3.50[	0.782 ± 0.006	0.971 ± 0.003	0.986 ± 0.002	0.952 ± 0.004	0.879 ± 0.007
[3.50, 4.00[	0.833 ± 0.007	0.978 ± 0.003	0.992 ± 0.002	0.964 ± 0.004	0.884 ± 0.008
[4.00, 4.50[	0.854 ± 0.007	0.987 ± 0.002	0.991 ± 0.002	0.967 ± 0.005	0.907 ± 0.009
[4.50, 5.00[	0.896 ± 0.007	0.988 ± 0.003	0.992 ± 0.003	0.974 ± 0.005	0.932 ± 0.009
[5.00, 6.00[	0.907 ± 0.006	0.994 ± 0.002	0.997 ± 0.001	0.986 ± 0.003	0.942 ± 0.007
[6.00, 7.00[	0.927 ± 0.007	0.995 ± 0.002	0.995 ± 0.002	0.990 ± 0.003	0.951 ± 0.009
[7.00, 8.00[	0.955 ± 0.007	0.999 ± 0.001	0.997 ± 0.002	0.991 ± 0.004	0.982 ± 0.007
[8.00, 9.00[	0.964 ± 0.008	1.000 ± 0.000	0.998 ± 0.002	0.996 ± 0.004	0.990 ± 0.007
[9.00, 10.00[	0.972 ± 0.008	1.000 ± 0.000	0.996 ± 0.004	0.995 ± 0.005	0.984 ± 0.011
[10.00, 11.00[	0.989 ± 0.006	1.000 ± 0.000	1.000 ± 0.000	1.000 ± 0.000	0.975 ± 0.017
[11.00, 12.00[	0.984 ± 0.009	1.000 ± 0.000	1.000 ± 0.000	1.000 ± 0.000	1.000 ± 0.000
[12.00, 13.00[	0.991 ± 0.009	1.000 ± 0.000	1.000 ± 0.000	1.000 ± 0.000	1.000 ± 0.000
[13.00, 14.00[	1.000 ± 0.000	1.000 ± 0.000	1.000 ± 0.000	1.000 ± 0.000	1.000 ± 0.000

Table G.23: Efficiency of DaughtersInLHCb for D_s^+ in MagUp event type 23263011 (Ds+_pi-pi+pi+=res,DecProdCut, $D_s^+ \to \pi^-\pi^+\pi^+$) in bins of $(p_{\rm T}, y)$, where $p_{\rm T}$ and y are computed in the proton-proton CM frame. The numbers are expressed as ratios of the number of signal decays generated into the bin to the number of those decays that satisfy the DaughtersInLHCb requirement.

$p_{\rm T}$	y				
(GeV)	$[2.0, 2.5[$	$[2.5, 3.0[$	$[3.0, 3.5[$	$[3.5, 4.0[$	$[4.0, 4.5[$
$[0.00, 0.25[$	683/1435	1197/1455	1161/1282	1034/1184	727/1066
$[0.25, 0.50[$	1946/3946	2982/3654	3191/3413	2706/3112	1818/2682
$[0.50, 0.75[$	2768/5445	4147/5026	4404/4722	3581/4096	2466/3539
$[0.75, 1.00[$	3221/6112	4603/5511	4591/4932	3956/4463	2729/3822
$[1.00, 1.25[$	3352/6045	4833/5569	4630/4889	3815/4259	2660/3662
$[1.25, 1.50[$	3259/5680	4503/5174	4408/4610	3582/3949	2308/3157
$[1.50, 1.75[$	3079/5096	4141/4602	3940/4105	3120/3432	2193/2842
$[1.75, 2.00[$	2781/4355	3765/4120	3407/3526	2889/3096	1966/2452
$[2.00, 2.25[$	2639/3899	3350/3630	3123/3214	2436/2629	1771/2118
$[2.25, 2.50[$	2321/3399	2927/3121	2615/2676	2125/2262	1543/1844
$[2.50, 2.75[$	2116/2940	2546/2662	2302/2353	1838/1959	1317/1546
$[2.75, 3.00[$	1966/2623	2209/2300	2003/2030	1583/1665	1157/1322
$[3.00, 3.50[$	3332/4261	3746/3833	3180/3216	2537/2672	1837/2062
$[3.50, 4.00[$	2710/3308	2783/2828	2371/2400	1828/1896	1326/1474
$[4.00, 4.50[$	2051/2392	2028/2048	1846/1856	1385/1422	1049/1141
$[4.50, 5.00[$	1589/1813	1542/1557	1277/1284	1042/1059	756/808
$[5.00, 6.00[$	2271/2497	2170/2179	1802/1814	1369/1400	977/1027
$[6.00, 7.00[$	1395/1488	1273/1279	1110/1111	791/798	555/579
$[7.00, 8.00[$	858/887	902/903	642/647	487/492	356/365
$[8.00, 9.00[$	543/558	526/527	395/395	280/280	175/179
$[9.00, 10.00[$	352/360	312/312	274/275	182/184	112/113
$[10.00, 11.00[$	246/250	231/231	184/184	129/129	77/77
$[11.00, 12.00[$	182/184	137/137	125/125	100/101	46/46
$[12.00, 13.00[$	132/132	82/82	67/67	58/58	26/26
$[13.00, 14.00[$	86/87	79/79	52/52	41/41	22/22

Table G.24: Efficiency of DaughtersInLHCb for D_s^+ in MagUp event type 23263011 (Ds+_pi-pi+pi+=res,DecProdCut, $D_s^+ \to \pi^-\pi^+\pi^+$) in bins of $(p_{\rm T}, y)$, where $p_{\rm T}$ and y are computed in the proton-proton CM frame. The quoted uncertainties are binomial statistical uncertainties only.

$p_{\rm T}$	y				
(GeV)	$[2.0, 2.5[$	$[2.5, 3.0[$	$[3.0, 3.5[$	$[3.5, 4.0[$	$[4.0, 4.5[$
$[0.00, 0.25[$	0.476 ± 0.013	0.823 ± 0.010	0.906 ± 0.008	0.873 ± 0.010	0.682 ± 0.014
$[0.25, 0.50[$	0.493 ± 0.008	0.816 ± 0.006	0.935 ± 0.004	0.870 ± 0.006	0.678 ± 0.009
$[0.50, 0.75[$	0.508 ± 0.007	0.825 ± 0.005	0.933 ± 0.004	0.874 ± 0.005	0.697 ± 0.008
$[0.75, 1.00[$	0.527 ± 0.006	0.835 ± 0.005	0.931 ± 0.004	0.886 ± 0.005	0.714 ± 0.007
$[1.00, 1.25[$	0.555 ± 0.006	0.868 ± 0.005	0.947 ± 0.003	0.896 ± 0.005	0.726 ± 0.007
$[1.25, 1.50[$	0.574 ± 0.007	0.870 ± 0.005	0.956 ± 0.003	0.907 ± 0.005	0.731 ± 0.008
$[1.50, 1.75[$	0.604 ± 0.007	0.900 ± 0.004	0.960 ± 0.003	0.909 ± 0.005	0.772 ± 0.008
$[1.75, 2.00[$	0.639 ± 0.007	0.914 ± 0.004	0.966 ± 0.003	0.933 ± 0.004	0.802 ± 0.008
$[2.00, 2.25[$	0.677 ± 0.007	0.923 ± 0.004	0.972 ± 0.003	0.927 ± 0.005	0.836 ± 0.008
$[2.25, 2.50[$	0.683 ± 0.008	0.938 ± 0.004	0.977 ± 0.003	0.939 ± 0.005	0.837 ± 0.009
$[2.50, 2.75[$	0.720 ± 0.008	0.956 ± 0.004	0.978 ± 0.003	0.938 ± 0.005	0.852 ± 0.009
$[2.75, 3.00[$	0.750 ± 0.008	0.960 ± 0.004	0.987 ± 0.003	0.951 ± 0.005	0.875 ± 0.009
$[3.00, 3.50[$	0.782 ± 0.006	0.977 ± 0.002	0.989 ± 0.002	0.949 ± 0.004	0.891 ± 0.007
$[3.50, 4.00[$	0.819 ± 0.007	0.984 ± 0.002	0.988 ± 0.002	0.964 ± 0.004	0.900 ± 0.008
$[4.00, 4.50[$	0.857 ± 0.007	0.990 ± 0.002	0.995 ± 0.002	0.974 ± 0.004	0.919 ± 0.008
$[4.50, 5.00[$	0.876 ± 0.008	0.990 ± 0.002	0.995 ± 0.002	0.984 ± 0.004	0.936 ± 0.009
$[5.00, 6.00[$	0.909 ± 0.006	0.996 ± 0.001	0.993 ± 0.002	0.978 ± 0.004	0.951 ± 0.007
$[6.00, 7.00[$	0.938 ± 0.006	0.995 ± 0.002	0.999 ± 0.001	0.991 ± 0.003	0.959 ± 0.008
$[7.00, 8.00[$	0.967 ± 0.006	0.999 ± 0.001	0.992 ± 0.003	0.990 ± 0.005	0.975 ± 0.008
$[8.00, 9.00[$	0.973 ± 0.007	0.998 ± 0.002	1.000 ± 0.000	1.000 ± 0.000	0.978 ± 0.011
$[9.00, 10.00[$	0.978 ± 0.008	1.000 ± 0.000	0.996 ± 0.004	0.989 ± 0.008	0.991 ± 0.009
$[10.00, 11.00[$	0.984 ± 0.008	1.000 ± 0.000	1.000 ± 0.000	1.000 ± 0.000	1.000 ± 0.000
$[11.00, 12.00[$	0.989 ± 0.008	1.000 ± 0.000	1.000 ± 0.000	0.990 ± 0.010	1.000 ± 0.000
$[12.00, 13.00[$	1.000 ± 0.000	1.000 ± 0.000	1.000 ± 0.000	1.000 ± 0.000	1.000 ± 0.000
$[13.00, 14.00[$	0.989 ± 0.011	1.000 ± 0.000	1.000 ± 0.000	1.000 ± 0.000	1.000 ± 0.000

G.7 $D^{*+} \to D^0\pi^+$, $D^0 \to K^-\pi^+$

Table G.25: Efficiency of DaughtersInLHCb for D^{*+} in MagDown event type 27163003 (Dst_D0pi,Kpi=DecProdCut, $D^{*+} \to D^0(K^-\pi^+)\pi^+$) in bins of (p_{T}, y), where p_{T} and y are computed in the proton-proton CM frame. The numbers are expressed as ratios of the number of signal decays generated into the bin to the number of those decays that satisfy the DaughtersInLHCb requirement.

p_{T}	y				
(GeV)	$[2.0, 2.5[$	$[2.5, 3.0[$	$[3.0, 3.5[$	$[3.5, 4.0[$	$[4.0, 4.5[$
$[0.00, 0.25[$	1132/1513	1190/1379	1042/1297	649/1189	94/1023
$[0.25, 0.50[$	3044/4111	3323/3897	2827/3583	1856/3179	685/2883
$[0.50, 0.75[$	4239/5713	4699/5332	4257/4904	3119/4339	1470/3721
$[0.75, 1.00[$	4959/6406	5385/5879	5079/5403	3937/4743	2173/4017
$[1.00, 1.25[$	4978/6433	5536/6018	5009/5214	4263/4656	2503/3878
$[1.25, 1.50[$	4720/6058	5212/5588	4877/5058	4005/4276	2693/3501
$[1.50, 1.75[$	4381/5431	4738/5058	4362/4471	3607/3840	2568/3135
$[1.75, 2.00[$	3949/4886	4043/4284	3788/3907	3093/3294	2180/2681
$[2.00, 2.25[$	3609/4331	3746/3927	3511/3589	2781/2938	2002/2331
$[2.25, 2.50[$	3184/3797	3284/3413	2892/2938	2398/2522	1766/2028
$[2.50, 2.75[$	2827/3299	2972/3077	2513/2561	2100/2195	1445/1630
$[2.75, 3.00[$	2477/2826	2409/2493	2237/2266	1784/1860	1291/1458
$[3.00, 3.50[$	4098/4646	4035/4130	3576/3626	2876/2970	2063/2266
$[3.50, 4.00[$	3296/3623	3134/3191	2663/2677	2102/2165	1541/1667
$[4.00, 4.50[$	2466/2654	2395/2408	2074/2083	1607/1631	1212/1293
$[4.50, 5.00[$	1990/2108	1819/1827	1591/1596	1247/1259	932/963
$[5.00, 6.00[$	2698/2834	2495/2504	2020/2023	1649/1657	1229/1260
$[6.00, 7.00[$	1777/1835	1491/1494	1199/1200	964/967	724/735
$[7.00, 8.00[$	1098/1132	898/899	758/759	620/621	408/416
$[8.00, 9.00[$	688/700	567/567	495/495	352/353	246/249
$[9.00, 10.00[$	454/460	398/398	291/291	238/239	167/168
$[10.00, 11.00[$	297/299	235/235	217/217	131/132	93/94
$[11.00, 12.00[$	228/230	186/186	137/137	97/97	49/49
$[12.00, 13.00[$	155/157	129/129	96/96	72/72	33/33
$[13.00, 14.00[$	106/106	93/93	53/53	53/53	42/42

Table G.26: Efficiency of DaughtersInLHCb for D^{*+} in MagDown event type 27163003 (Dst_D0pi,Kpi=DecProdCut, $D^{*+} \to D^0(K^-\pi^+)\pi^+$) in bins of (p_{T}, y), where p_{T} and y are computed in the proton-proton CM frame. The quoted uncertainties are binomial statistical uncertainties only.

p_{T} (GeV)	y [2.0, 2.5[	[2.5, 3.0[	[3.0, 3.5[	[3.5, 4.0[	[4.0, 4.5[
[0.00, 0.25[	0.748 ± 0.011	0.863 ± 0.009	0.803 ± 0.011	0.546 ± 0.014	0.092 ± 0.009
[0.25, 0.50[	0.740 ± 0.007	0.853 ± 0.006	0.789 ± 0.007	0.584 ± 0.009	0.238 ± 0.008
[0.50, 0.75[	0.742 ± 0.006	0.881 ± 0.004	0.868 ± 0.005	0.719 ± 0.007	0.395 ± 0.008
[0.75, 1.00[	0.774 ± 0.005	0.916 ± 0.004	0.940 ± 0.003	0.830 ± 0.005	0.541 ± 0.008
[1.00, 1.25[	0.774 ± 0.005	0.920 ± 0.003	0.961 ± 0.003	0.916 ± 0.004	0.645 ± 0.008
[1.25, 1.50[	0.779 ± 0.005	0.933 ± 0.003	0.964 ± 0.003	0.937 ± 0.004	0.769 ± 0.007
[1.50, 1.75[	0.807 ± 0.005	0.937 ± 0.003	0.976 ± 0.002	0.939 ± 0.004	0.819 ± 0.007
[1.75, 2.00[	0.808 ± 0.006	0.944 ± 0.004	0.970 ± 0.003	0.939 ± 0.004	0.813 ± 0.008
[2.00, 2.25[	0.833 ± 0.006	0.954 ± 0.003	0.978 ± 0.002	0.947 ± 0.004	0.859 ± 0.007
[2.25, 2.50[	0.839 ± 0.006	0.962 ± 0.003	0.984 ± 0.002	0.951 ± 0.004	0.871 ± 0.007
[2.50, 2.75[	0.857 ± 0.006	0.966 ± 0.003	0.981 ± 0.003	0.957 ± 0.004	0.887 ± 0.008
[2.75, 3.00[	0.877 ± 0.006	0.966 ± 0.004	0.987 ± 0.002	0.959 ± 0.005	0.885 ± 0.008
[3.00, 3.50[	0.882 ± 0.005	0.977 ± 0.002	0.986 ± 0.002	0.968 ± 0.003	0.910 ± 0.006
[3.50, 4.00[	0.910 ± 0.005	0.982 ± 0.002	0.995 ± 0.001	0.971 ± 0.004	0.924 ± 0.006
[4.00, 4.50[	0.929 ± 0.005	0.995 ± 0.001	0.996 ± 0.001	0.985 ± 0.003	0.937 ± 0.007
[4.50, 5.00[	0.944 ± 0.005	0.996 ± 0.002	0.997 ± 0.001	0.990 ± 0.003	0.968 ± 0.006
[5.00, 6.00[	0.952 ± 0.004	0.996 ± 0.001	0.999 ± 0.001	0.995 ± 0.002	0.975 ± 0.004
[6.00, 7.00[	0.968 ± 0.004	0.998 ± 0.001	0.999 ± 0.001	0.997 ± 0.002	0.985 ± 0.004
[7.00, 8.00[	0.970 ± 0.005	0.999 ± 0.001	0.999 ± 0.001	0.998 ± 0.002	0.981 ± 0.007
[8.00, 9.00[	0.983 ± 0.005	1.000 ± 0.000	1.000 ± 0.000	0.997 ± 0.003	0.988 ± 0.007
[9.00, 10.00[	0.987 ± 0.005	1.000 ± 0.000	1.000 ± 0.000	0.996 ± 0.004	0.994 ± 0.006
[10.00, 11.00[	0.993 ± 0.005	1.000 ± 0.000	1.000 ± 0.000	0.992 ± 0.008	0.989 ± 0.011
[11.00, 12.00[	0.991 ± 0.006	1.000 ± 0.000	1.000 ± 0.000	1.000 ± 0.000	1.000 ± 0.000
[12.00, 13.00[	0.987 ± 0.009	1.000 ± 0.000	1.000 ± 0.000	1.000 ± 0.000	1.000 ± 0.000
[13.00, 14.00[	1.000 ± 0.000	1.000 ± 0.000	1.000 ± 0.000	1.000 ± 0.000	1.000 ± 0.000

Table G.27: Efficiency of DaughtersInLHCb for D^{*+} in MagUp event type 27163003 (Dst_D0pi,Kpi=DecProdCut, $D^{*+} \to D^0(K^-\pi^+)\pi^+$) in bins of (p_{T}, y), where p_{T} and y are computed in the proton-proton CM frame. The numbers are expressed as ratios of the number of signal decays generated into the bin to the number of those decays that satisfy the DaughtersInLHCb requirement.

p_{T}	y				
(GeV)	$[2.0, 2.5[$	$[2.5, 3.0[$	$[3.0, 3.5[$	$[3.5, 4.0[$	$[4.0, 4.5[$
$[0.00, 0.25[$	598/813	655/747	533/646	331/631	43/552
$[0.25, 0.50[$	1536/2104	1684/1984	1513/1887	956/1678	345/1550
$[0.50, 0.75[$	2112/2892	2467/2803	2159/2495	1569/2305	770/2032
$[0.75, 1.00[$	2662/3454	2908/3157	2719/2887	2097/2489	1078/2074
$[1.00, 1.25[$	2512/3327	2888/3105	2726/2850	2224/2421	1306/1962
$[1.25, 1.50[$	2501/3150	2640/2843	2508/2615	2091/2235	1444/1881
$[1.50, 1.75[$	2311/2918	2486/2628	2290/2368	1898/2035	1369/1646
$[1.75, 2.00[$	2071/2546	2139/2280	2015/2070	1647/1750	1227/1456
$[2.00, 2.25[$	1866/2261	1973/2060	1845/1886	1418/1497	1029/1218
$[2.25, 2.50[$	1696/2026	1733/1792	1486/1515	1256/1319	932/1084
$[2.50, 2.75[$	1477/1735	1495/1551	1313/1341	1137/1182	818/917
$[2.75, 3.00[$	1283/1481	1290/1325	1126/1138	990/1015	687/776
$[3.00, 3.50[$	2126/2391	2158/2209	1889/1911	1440/1500	1093/1192
$[3.50, 4.00[$	1715/1881	1690/1712	1405/1412	1127/1147	823/890
$[4.00, 4.50[$	1353/1461	1260/1273	1043/1046	842/856	590/631
$[4.50, 5.00[$	1029/1096	940/946	813/815	694/702	481/496
$[5.00, 6.00[$	1407/1481	1295/1299	1087/1090	874/880	618/631
$[6.00, 7.00[$	880/902	753/753	684/684	467/470	323/330
$[7.00, 8.00[$	567/579	496/496	432/432	272/274	190/191
$[8.00, 9.00[$	377/382	323/323	231/231	182/182	149/150
$[9.00, 10.00[$	255/258	205/205	163/163	130/130	72/73
$[10.00, 11.00[$	122/122	157/157	113/113	70/70	45/45
$[11.00, 12.00[$	132/132	100/100	65/65	51/51	35/35
$[12.00, 13.00[$	85/85	84/84	67/67	36/36	23/23
$[13.00, 14.00[$	46/46	60/60	33/33	33/33	20/20

Table G.28: Efficiency of DaughtersInLHCb for D^{*+} in MagUp event type 27163003 (Dst_D0pi,Kpi=DecProdCut, $D^{*+} \to D^0(K^-\pi^+)\pi^+$) in bins of $(p_{\rm T}, y)$, where $p_{\rm T}$ and y are computed in the proton-proton CM frame. The quoted uncertainties are binomial statistical uncertainties only.

$p_{\rm T}$	y				
(GeV)	$[2.0, 2.5[$	$[2.5, 3.0[$	$[3.0, 3.5[$	$[3.5, 4.0[$	$[4.0, 4.5[$
$[0.00, 0.25[$	0.736 ± 0.015	0.877 ± 0.012	0.825 ± 0.015	0.525 ± 0.020	0.078 ± 0.011
$[0.25, 0.50[$	0.730 ± 0.010	0.849 ± 0.008	0.802 ± 0.009	0.570 ± 0.012	0.223 ± 0.011
$[0.50, 0.75[$	0.730 ± 0.008	0.880 ± 0.006	0.865 ± 0.007	0.681 ± 0.010	0.379 ± 0.011
$[0.75, 1.00[$	0.771 ± 0.007	0.921 ± 0.005	0.942 ± 0.004	0.843 ± 0.007	0.520 ± 0.011
$[1.00, 1.25[$	0.755 ± 0.007	0.930 ± 0.005	0.956 ± 0.004	0.919 ± 0.006	0.666 ± 0.011
$[1.25, 1.50[$	0.794 ± 0.007	0.929 ± 0.005	0.959 ± 0.004	0.936 ± 0.005	0.768 ± 0.010
$[1.50, 1.75[$	0.792 ± 0.008	0.946 ± 0.004	0.967 ± 0.004	0.933 ± 0.006	0.832 ± 0.009
$[1.75, 2.00[$	0.813 ± 0.008	0.938 ± 0.005	0.973 ± 0.004	0.941 ± 0.006	0.843 ± 0.010
$[2.00, 2.25[$	0.825 ± 0.008	0.958 ± 0.004	0.978 ± 0.003	0.947 ± 0.006	0.845 ± 0.010
$[2.25, 2.50[$	0.837 ± 0.008	0.967 ± 0.004	0.981 ± 0.004	0.952 ± 0.006	0.860 ± 0.011
$[2.50, 2.75[$	0.851 ± 0.009	0.964 ± 0.005	0.979 ± 0.004	0.962 ± 0.006	0.892 ± 0.010
$[2.75, 3.00[$	0.866 ± 0.009	0.974 ± 0.004	0.989 ± 0.003	0.975 ± 0.005	0.885 ± 0.011
$[3.00, 3.50[$	0.889 ± 0.006	0.977 ± 0.003	0.988 ± 0.002	0.960 ± 0.005	0.917 ± 0.008
$[3.50, 4.00[$	0.912 ± 0.007	0.987 ± 0.003	0.995 ± 0.002	0.983 ± 0.004	0.925 ± 0.009
$[4.00, 4.50[$	0.926 ± 0.007	0.990 ± 0.003	0.997 ± 0.002	0.984 ± 0.004	0.935 ± 0.010
$[4.50, 5.00[$	0.939 ± 0.007	0.994 ± 0.003	0.998 ± 0.002	0.989 ± 0.004	0.970 ± 0.008
$[5.00, 6.00[$	0.950 ± 0.006	0.997 ± 0.002	0.997 ± 0.002	0.993 ± 0.003	0.979 ± 0.006
$[6.00, 7.00[$	0.976 ± 0.005	1.000 ± 0.000	1.000 ± 0.000	0.994 ± 0.004	0.979 ± 0.008
$[7.00, 8.00[$	0.979 ± 0.006	1.000 ± 0.000	1.000 ± 0.000	0.993 ± 0.005	0.995 ± 0.005
$[8.00, 9.00[$	0.987 ± 0.006	1.000 ± 0.000	1.000 ± 0.000	1.000 ± 0.000	0.993 ± 0.007
$[9.00, 10.00[$	0.988 ± 0.007	1.000 ± 0.000	1.000 ± 0.000	1.000 ± 0.000	0.986 ± 0.014
$[10.00, 11.00[$	1.000 ± 0.000	1.000 ± 0.000	1.000 ± 0.000	1.000 ± 0.000	1.000 ± 0.000
$[11.00, 12.00[$	1.000 ± 0.000	1.000 ± 0.000	1.000 ± 0.000	1.000 ± 0.000	1.000 ± 0.000
$[12.00, 13.00[$	1.000 ± 0.000	1.000 ± 0.000	1.000 ± 0.000	1.000 ± 0.000	1.000 ± 0.000
$[13.00, 14.00[$	1.000 ± 0.000	1.000 ± 0.000	1.000 ± 0.000	1.000 ± 0.000	1.000 ± 0.000

G.8 $D^{*+} \to D^0\pi^+$, $D^0 \to K^-\pi^+\pi^-\pi^+$

Table G.29: Efficiency of DaughtersInLHCb for D^{*+} in MagDown event type 27265002 (Dst_D0pi,Kpipipi=DecProdCutMINT, $D^{*+} \to D^0(K^-\pi^+\pi^-\pi^+)\pi^+$) in bins of (p_{T}, y), where p_{T} and y are computed in the proton-proton CM frame. The numbers are expressed as ratios of the number of signal decays generated into the bin to the number of those decays that satisfy the DaughtersInLHCb requirement.

p_{T}	y				
(GeV)	$[2.0, 2.5[$	$[2.5, 3.0[$	$[3.0, 3.5[$	$[3.5, 4.0[$	$[4.0, 4.5[$
$[0.00, 0.25[$	1017/1540	1227/1452	1058/1385	537/1220	57/1103
$[0.25, 0.50[$	2721/4153	3321/3933	2687/3522	1569/3198	417/2725
$[0.50, 0.75[$	3939/5740	4672/5298	3980/4927	2709/4366	995/3793
$[0.75, 1.00[$	4571/6488	5416/5869	4995/5459	3513/4747	1466/3954
$[1.00, 1.25[$	4671/6582	5328/5706	4953/5302	3745/4614	1866/3846
$[1.25, 1.50[$	4331/5952	5310/5606	4672/4979	3546/4197	2096/3612
$[1.50, 1.75[$	4290/5626	4820/5040	4221/4443	3322/3862	1958/3071
$[1.75, 2.00[$	3891/4934	4389/4559	3794/3955	2948/3361	1864/2727
$[2.00, 2.25[$	3579/4475	4028/4138	3313/3417	2494/2810	1801/2457
$[2.25, 2.50[$	3095/3745	3300/3382	2890/2979	2296/2504	1463/1911
$[2.50, 2.75[$	2740/3255	2863/2911	2533/2605	2007/2150	1369/1735
$[2.75, 3.00[$	2497/2893	2452/2489	2093/2133	1722/1821	1129/1392
$[3.00, 3.50[$	4150/4695	4240/4286	3709/3776	2824/2957	2003/2310
$[3.50, 4.00[$	3223/3529	3165/3178	2700/2740	2175/2243	1572/1735
$[4.00, 4.50[$	2558/2758	2420/2427	2061/2075	1615/1646	1198/1296
$[4.50, 5.00[$	1996/2110	1807/1811	1610/1616	1203/1218	852/891
$[5.00, 6.00[$	2730/2831	2483/2489	2068/2074	1590/1615	1169/1220
$[6.00, 7.00[$	1697/1745	1497/1501	1276/1280	936/943	672/689
$[7.00, 8.00[$	1081/1102	966/966	781/782	561/564	382/385
$[8.00, 9.00[$	734/739	609/610	456/456	346/346	251/251
$[9.00, 10.00[$	479/480	414/414	299/299	219/219	130/130
$[10.00, 11.00[$	331/332	247/247	172/172	140/141	95/95
$[11.00, 12.00[$	189/189	176/176	122/122	115/115	64/64
$[12.00, 13.00[$	141/141	140/140	102/102	63/63	45/45
$[13.00, 14.00[$	115/115	105/105	54/54	49/49	39/39

Table G.30: Efficiency of DaughtersInLHCb for D^{*+} in MagDown event type 27265002 (Dst_D0pi,Kpipipi=DecProdCutMINT, $D^{*+} \to D^0(K^-\pi^+\pi^-\pi^+)\pi^+$) in bins of (p_{T}, y), where p_{T} and y are computed in the proton-proton CM frame. The quoted uncertainties are binomial statistical uncertainties only.

p_{T}	y				
(GeV)	$[2.0, 2.5[$	$[2.5, 3.0[$	$[3.0, 3.5[$	$[3.5, 4.0[$	$[4.0, 4.5[$
$[0.00, 0.25[$	0.660 ± 0.012	0.845 ± 0.009	0.764 ± 0.011	0.440 ± 0.014	0.052 ± 0.007
$[0.25, 0.50[$	0.655 ± 0.007	0.844 ± 0.006	0.763 ± 0.007	0.491 ± 0.009	0.153 ± 0.007
$[0.50, 0.75[$	0.686 ± 0.006	0.882 ± 0.004	0.808 ± 0.006	0.620 ± 0.007	0.262 ± 0.007
$[0.75, 1.00[$	0.705 ± 0.006	0.923 ± 0.003	0.915 ± 0.004	0.740 ± 0.006	0.371 ± 0.008
$[1.00, 1.25[$	0.710 ± 0.006	0.934 ± 0.003	0.934 ± 0.003	0.812 ± 0.006	0.485 ± 0.008
$[1.25, 1.50[$	0.728 ± 0.006	0.947 ± 0.003	0.938 ± 0.003	0.845 ± 0.006	0.580 ± 0.008
$[1.50, 1.75[$	0.763 ± 0.006	0.956 ± 0.003	0.950 ± 0.003	0.860 ± 0.006	0.638 ± 0.009
$[1.75, 2.00[$	0.789 ± 0.006	0.963 ± 0.003	0.959 ± 0.003	0.877 ± 0.006	0.684 ± 0.009
$[2.00, 2.25[$	0.800 ± 0.006	0.973 ± 0.003	0.970 ± 0.003	0.888 ± 0.006	0.733 ± 0.009
$[2.25, 2.50[$	0.826 ± 0.006	0.976 ± 0.003	0.970 ± 0.003	0.917 ± 0.006	0.766 ± 0.010
$[2.50, 2.75[$	0.842 ± 0.006	0.984 ± 0.002	0.972 ± 0.003	0.933 ± 0.005	0.789 ± 0.010
$[2.75, 3.00[$	0.863 ± 0.006	0.985 ± 0.002	0.981 ± 0.003	0.946 ± 0.005	0.811 ± 0.010
$[3.00, 3.50[$	0.884 ± 0.005	0.989 ± 0.002	0.982 ± 0.002	0.955 ± 0.004	0.867 ± 0.007
$[3.50, 4.00[$	0.913 ± 0.005	0.996 ± 0.001	0.985 ± 0.002	0.970 ± 0.004	0.906 ± 0.007
$[4.00, 4.50[$	0.927 ± 0.005	0.997 ± 0.001	0.993 ± 0.002	0.981 ± 0.003	0.924 ± 0.007
$[4.50, 5.00[$	0.946 ± 0.005	0.998 ± 0.001	0.996 ± 0.002	0.988 ± 0.003	0.956 ± 0.007
$[5.00, 6.00[$	0.964 ± 0.003	0.998 ± 0.001	0.997 ± 0.001	0.985 ± 0.003	0.958 ± 0.006
$[6.00, 7.00[$	0.972 ± 0.004	0.997 ± 0.001	0.997 ± 0.002	0.993 ± 0.003	0.975 ± 0.006
$[7.00, 8.00[$	0.981 ± 0.004	1.000 ± 0.000	0.999 ± 0.001	0.995 ± 0.003	0.992 ± 0.004
$[8.00, 9.00[$	0.993 ± 0.003	0.998 ± 0.002	1.000 ± 0.000	1.000 ± 0.000	1.000 ± 0.000
$[9.00, 10.00[$	0.998 ± 0.002	1.000 ± 0.000	1.000 ± 0.000	1.000 ± 0.000	1.000 ± 0.000
$[10.00, 11.00[$	0.997 ± 0.003	1.000 ± 0.000	1.000 ± 0.000	0.993 ± 0.007	1.000 ± 0.000
$[11.00, 12.00[$	1.000 ± 0.000	1.000 ± 0.000	1.000 ± 0.000	1.000 ± 0.000	1.000 ± 0.000
$[12.00, 13.00[$	1.000 ± 0.000	1.000 ± 0.000	1.000 ± 0.000	1.000 ± 0.000	1.000 ± 0.000
$[13.00, 14.00[$	1.000 ± 0.000	1.000 ± 0.000	1.000 ± 0.000	1.000 ± 0.000	1.000 ± 0.000

Table G.31: Efficiency of DaughtersInLHCb for D^{*+} in MagUp event type 27265002 (Dst_D0pi,Kpipipi=DecProdCutMINT, $D^{*+} \to D^0(K^-\pi^+\pi^-\pi^+)\pi^+$) in bins of (p_{T}, y), where p_{T} and y are computed in the proton-proton CM frame. The numbers are expressed as ratios of the number of signal decays generated into the bin to the number of those decays that satisfy the DaughtersInLHCb requirement.

p_{T}	y				
(GeV)	$[2.0, 2.5[$	$[2.5, 3.0[$	$[3.0, 3.5[$	$[3.5, 4.0[$	$[4.0, 4.5[$
$[0.00, 0.25[$	1039/1563	1260/1490	990/1277	562/1269	65/1100
$[0.25, 0.50[$	2729/4152	3295/3862	2727/3584	1644/3263	427/2852
$[0.50, 0.75[$	3867/5755	4751/5378	3933/4791	2633/4374	1007/3804
$[0.75, 1.00[$	4457/6371	5400/5848	4925/5384	3363/4613	1442/3933
$[1.00, 1.25[$	4629/6460	5466/5843	4999/5354	3800/4646	1863/3847
$[1.25, 1.50[$	4520/6125	5206/5522	4629/4915	3667/4357	2097/3578
$[1.50, 1.75[$	4148/5459	4770/4967	4282/4500	3234/3742	2111/3197
$[1.75, 2.00[$	3829/4918	4264/4409	3777/3951	2960/3353	1870/2703
$[2.00, 2.25[$	3452/4327	3842/3938	3238/3379	2615/2884	1652/2276
$[2.25, 2.50[$	3145/3808	3308/3371	3005/3073	2269/2490	1544/2031
$[2.50, 2.75[$	2891/3441	2927/2979	2497/2565	2039/2197	1385/1739
$[2.75, 3.00[$	2480/2902	2604/2631	2235/2275	1732/1848	1198/1465
$[3.00, 3.50[$	4136/4678	4105/4144	3597/3661	2894/3022	2029/2368
$[3.50, 4.00[$	3148/3462	3182/3197	2705/2746	2168/2243	1560/1731
$[4.00, 4.50[$	2499/2688	2424/2433	2044/2058	1661/1702	1145/1230
$[4.50, 5.00[$	1909/2023	1850/1856	1482/1489	1194/1223	860/905
$[5.00, 6.00[$	2822/2931	2453/2455	2134/2142	1645/1660	1161/1216
$[6.00, 7.00[$	1719/1753	1543/1543	1234/1239	947/955	695/713
$[7.00, 8.00[$	1102/1111	968/968	780/782	600/604	442/447
$[8.00, 9.00[$	691/697	583/583	493/494	364/364	250/253
$[9.00, 10.00[$	477/479	359/359	299/299	217/219	154/155
$[10.00, 11.00[$	324/325	266/266	185/185	137/137	94/94
$[11.00, 12.00[$	222/222	167/167	139/139	96/96	57/57
$[12.00, 13.00[$	161/161	131/131	90/90	67/67	49/49
$[13.00, 14.00[$	94/94	97/97	59/59	54/54	33/33

Table G.32: Efficiency of DaughtersInLHCb for D^{*+} in MagUp event type 27265002 (Dst_D0pi,Kpipipi=DecProdCutMINT, $D^{*+} \to D^0(K^-\pi^+\pi^-\pi^+)\pi^+$) in bins of (p_{T}, y), where p_{T} and y are computed in the proton-proton CM frame. The quoted uncertainties are binomial statistical uncertainties only.

p_{T} (GeV)	y [2.0, 2.5[	[2.5, 3.0[	[3.0, 3.5[	[3.5, 4.0[	[4.0, 4.5[
[0.00, 0.25[	0.665 ± 0.012	0.846 ± 0.009	0.775 ± 0.012	0.443 ± 0.014	0.059 ± 0.007
[0.25, 0.50[	0.657 ± 0.007	0.853 ± 0.006	0.761 ± 0.007	0.504 ± 0.009	0.150 ± 0.007
[0.50, 0.75[	0.672 ± 0.006	0.883 ± 0.004	0.821 ± 0.006	0.602 ± 0.007	0.265 ± 0.007
[0.75, 1.00[	0.700 ± 0.006	0.923 ± 0.003	0.915 ± 0.004	0.729 ± 0.007	0.367 ± 0.008
[1.00, 1.25[	0.717 ± 0.006	0.935 ± 0.003	0.934 ± 0.003	0.818 ± 0.006	0.484 ± 0.008
[1.25, 1.50[	0.738 ± 0.006	0.943 ± 0.003	0.942 ± 0.003	0.842 ± 0.006	0.586 ± 0.008
[1.50, 1.75[	0.760 ± 0.006	0.960 ± 0.003	0.952 ± 0.003	0.864 ± 0.006	0.660 ± 0.008
[1.75, 2.00[	0.779 ± 0.006	0.967 ± 0.003	0.956 ± 0.003	0.883 ± 0.006	0.692 ± 0.009
[2.00, 2.25[	0.798 ± 0.006	0.976 ± 0.002	0.958 ± 0.003	0.907 ± 0.005	0.726 ± 0.009
[2.25, 2.50[	0.826 ± 0.006	0.981 ± 0.002	0.978 ± 0.003	0.911 ± 0.006	0.760 ± 0.009
[2.50, 2.75[	0.840 ± 0.006	0.983 ± 0.002	0.973 ± 0.003	0.928 ± 0.006	0.796 ± 0.010
[2.75, 3.00[	0.855 ± 0.007	0.990 ± 0.002	0.982 ± 0.003	0.937 ± 0.006	0.818 ± 0.010
[3.00, 3.50[	0.884 ± 0.005	0.991 ± 0.001	0.983 ± 0.002	0.958 ± 0.004	0.857 ± 0.007
[3.50, 4.00[	0.909 ± 0.005	0.995 ± 0.001	0.985 ± 0.002	0.967 ± 0.004	0.901 ± 0.007
[4.00, 4.50[	0.930 ± 0.005	0.996 ± 0.001	0.993 ± 0.002	0.976 ± 0.004	0.931 ± 0.007
[4.50, 5.00[	0.944 ± 0.005	0.997 ± 0.001	0.995 ± 0.002	0.976 ± 0.004	0.950 ± 0.007
[5.00, 6.00[	0.963 ± 0.003	0.999 ± 0.001	0.996 ± 0.001	0.991 ± 0.002	0.955 ± 0.006
[6.00, 7.00[	0.981 ± 0.003	1.000 ± 0.000	0.996 ± 0.002	0.992 ± 0.003	0.975 ± 0.006
[7.00, 8.00[	0.992 ± 0.003	1.000 ± 0.000	0.997 ± 0.002	0.993 ± 0.003	0.989 ± 0.005
[8.00, 9.00[	0.991 ± 0.003	1.000 ± 0.000	0.998 ± 0.002	1.000 ± 0.000	0.988 ± 0.007
[9.00, 10.00[	0.996 ± 0.003	1.000 ± 0.000	1.000 ± 0.000	0.991 ± 0.006	0.994 ± 0.006
[10.00, 11.00[	0.997 ± 0.003	1.000 ± 0.000	1.000 ± 0.000	1.000 ± 0.000	1.000 ± 0.000
[11.00, 12.00[	1.000 ± 0.000	1.000 ± 0.000	1.000 ± 0.000	1.000 ± 0.000	1.000 ± 0.000
[12.00, 13.00[	1.000 ± 0.000	1.000 ± 0.000	1.000 ± 0.000	1.000 ± 0.000	1.000 ± 0.000
[13.00, 14.00[	1.000 ± 0.000	1.000 ± 0.000	1.000 ± 0.000	1.000 ± 0.000	1.000 ± 0.000

Table H.1: Differences in yield between the a tighter, efficiency corrected, cut on D0_DIRA_OWNPV and the nominal selection

p_{T} [MeV/c]	y [2, 2.5[	[2.5, 3[	[3, 3.5[	[3.5, 4[	[4, 4.5[
[9000, 10000[	7553/6123	9233/8208	2687/3227	0/0	0/0
[8000, 9000[	11177/9228	14090/13026	7846/9382	991/1185	0/0
[7000, 8000[	23035/14289	24444/21255	15231/17051	3912/4009	0/0
[6000, 7000[	8335/22182	40036/35888	26458/30357	9941/11565	92/87
[5000, 6000[	47085/34886	72976/61270	45831/53200	33688/27657	1337/1541
[4000, 5000[	39913/52387	92293/106551	81457/93118	45642/57388	6385/7875
[3000, 4000[	90931/69846	188517/170546	174146/154314	123834/98903	17294/23788
[2000, 3000[	65859/74507	205316/221653	192255/218456	169811/135560	28270/40683
[1000, 2000[	54309/59721	191991/203640	208530/223735	109225/140174	25439/40938
[0, 1000[	22794/24399	87535/97953	102396/117554	55371/76978	32634/21281

H Monte Carlo modelling systematic

H.1 An example with $D^0 \to K^-\pi^+$

- For each variable which a cut is applied to (excluding ghost probability, PID and mass variables):
  - Using sWeights, obtain a signal yield for a tighter cut with 50% MC efficiency with respect to the main selection
  - The PID efficiency is included by correcting each sWeight with the per track PID efficiencies
  - See Tables H.1–H.12.
  - Find the difference between the efficiency corrected tighter cut and the nominal selection
- Sum the differences for each variable to obtain a difference per pT/y bin, Table H.13
- Finally sum over all pT/y bins to obtain an uncertainty which is applied to each pT/y bin

Table H.2: Differences in yield between the a tighter, efficiency corrected, cut on D0_ENDVERTEX_CHI2/D0_ENDVERTEX_NDOF and the nominal selection

p_{T} [MeV/c]	y [2, 2.5[	[2.5, 3[	[3, 3.5[	[3.5, 4[	[4, 4.5[
[9000, 10000[	5599/6123	8544/8208	3585/3227	0/0	0/0
[8000, 9000[	10292/9228	13260/13026	8183/9382	1473/1185	0/0
[7000, 8000[	12012/14289	22015/21255	16577/17051	3748/4009	0/0
[6000, 7000[	21433/22182	36388/35888	30018/30357	12483/11565	57/87
[5000, 6000[	35830/34886	62647/61270	53960/53200	26827/27657	1757/1541
[4000, 5000[	55894/52387	103165/106551	95193/93118	56666/57388	7779/7875
[3000, 4000[	74337/69846	172965/170546	157346/154314	98777/98903	24115/23788
[2000, 3000[	79568/74507	230517/221653	215492/218456	136308/135560	39312/40683
[1000, 2000[	61902/59721	203464/203640	228897/223735	137647/140174	43300/40938
[0, 1000[	29490/24399	99371/97953	122413/117554	79721/76978	22422/21281

Table H.3: Differences in yield between the a tighter, efficiency corrected, cut on D0_Loki_AMINDOCA and the nominal selection

p_{T} [MeV/c]	y [2, 2.5[	[2.5, 3[	[3, 3.5[	[3.5, 4[	[4, 4.5[
[9000, 10000[	5561/6123	8507/8208	3222/3227	0/0	0/0
[8000, 9000[	9591/9228	12223/13026	10750/9382	1400/1185	0/0
[7000, 8000[	12896/14289	19927/21255	17942/17051	4141/4009	0/0
[6000, 7000[	21039/22182	36738/35888	28819/30357	12256/11565	169/87
[5000, 6000[	35259/34886	59286/61270	53892/53200	27074/27657	1527/1541
[4000, 5000[	58006/52387	110143/106551	91835/93118	59401/57388	7162/7875
[3000, 4000[	62380/69846	172893/170546	150634/154314	101591/98903	23125/23788
[2000, 3000[	78794/74507	230301/221653	212501/218456	136088/135560	40207/40683
[1000, 2000[	63268/59721	204261/203640	227188/223735	135885/140174	44292/40938
[0, 1000[	19864/24399	96827/97953	119296/117554	79152/76978	22142/21281

Table H.4: Differences in yield between the a tighter, efficiency corrected, cut on D0_Loki_BPVVDCHI2 and the nominal selection

p_{T} [MeV/c]	y [2, 2.5[	[2.5, 3[	[3, 3.5[	[3.5, 4[	[4, 4.5[
[9000, 10000[	6933/6123	9318/8208	4225/3227	0/0	0/0
[8000, 9000[	10211/9228	9702/13026	10738/9382	1457/1185	0/0
[7000, 8000[	13002/14289	19218/21255	18828/17051	4979/4009	0/0
[6000, 7000[	25065/22182	31791/35888	26346/30357	13990/11565	135/87
[5000, 6000[	29674/34886	53927/61270	47178/53200	24369/27657	1513/1541
[4000, 5000[	60771/52387	114583/106551	80423/93118	66585/57388	6533/7875
[3000, 4000[	90059/69846	183944/170546	174799/154314	113959/98903	27256/23788
[2000, 3000[	90846/74507	214237/221653	248022/218456	162374/135560	31768/40683
[1000, 2000[	53242/59721	210016/203640	194427/223735	166480/140174	51132/40938
[0, 1000[	24630/24399	103151/97953	99711/117554	49428/76978	23959/21281

Table H.5: Differences in yield between the a tighter, efficiency corrected, cut on D0_h1_TRACK_CHI2NDOF and the nominal selection

p_{T} [MeV/c]	y [2, 2.5[	[2.5, 3[	[3, 3.5[	[3.5, 4[	[4, 4.5[
[9000, 10000[	5685/6123	10862/8208	1472/3227	0/0	0/0
[8000, 9000[	8501/9228	8277/13026	13992/9382	399/1185	0/0
[7000, 8000[	14416/14289	14974/21255	9821/17051	2256/4009	0/0
[6000, 7000[	19642/22182	45780/35888	15021/30357	6838/11565	129/87
[5000, 6000[	36505/34886	77195/61270	76033/53200	16195/27657	1056/1541
[4000, 5000[	50064/52387	84422/106551	128687/93118	37001/57388	5668/7875
[3000, 4000[	61517/69846	141670/170546	208332/154314	65070/98903	30637/23788
[2000, 3000[	86369/74507	235285/221653	149304/218456	96498/135560	33292/40683
[1000, 2000[	71544/59721	189832/203640	282789/223735	182915/140174	46148/40938
[0, 1000[	30835/24399	98707/97953	89425/117554	60645/76978	19473/21281

Table H.6: Differences in yield between the a tighter, efficiency corrected, cut on D0_h2_TRACK_CHI2NDOF and the nominal selection

p_{T} [MeV/c]	y [2, 2.5[	[2.5, 3[	[3, 3.5[	[3.5, 4[	[4, 4.5[
[9000, 10000[	5358/6123	11407/8208	1545/3227	0/0	0/0
[8000, 9000[	8543/9228	8813/13026	4323/9382	697/1185	0/0
[7000, 8000[	12100/14289	13889/21255	8766/17051	6044/4009	0/0
[6000, 7000[	19067/22182	46384/35888	17201/30357	17050/11565	109/87
[5000, 6000[	36220/34886	45055/61270	76240/53200	38521/27657	853/1541
[4000, 5000[	50192/52387	81938/106551	53755/93118	78990/57388	5833/7875
[3000, 4000[	69992/69846	133854/170546	99035/154314	67041/98903	17677/23788
[2000, 3000[	68936/74507	186392/221653	156260/218456	95599/135560	32782/40683
[1000, 2000[	69820/59721	215954/203640	280681/223735	98952/140174	47705/40938
[0, 1000[	29961/24399	97984/97953	87014/117554	57362/76978	17798/21281

Table H.7: Differences in yield between the a tighter, efficiency corrected, cut on D0_h1_ETA and the nominal selection

p_{T} [MeV/c]	y [2, 2.5[	[2.5, 3[	[3, 3.5[	[3.5, 4[	[4, 4.5[
[9000, 10000[	5576/6123	8062/8208	3173/3227	0/0	0/0
[8000, 9000[	8927/9228	12440/13026	9335/9382	1082/1185	0/0
[7000, 8000[	13388/14289	20949/21255	17725/17051	3634/4009	0/0
[6000, 7000[	24501/22182	34660/35888	32156/30357	11740/11565	49/87
[5000, 6000[	38784/34886	59480/61270	50589/53200	27025/27657	1529/1541
[4000, 5000[	57545/52387	103510/106551	93549/93118	58672/57388	9675/7875
[3000, 4000[	69689/69846	174481/170546	150017/154314	95998/98903	25807/23788
[2000, 3000[	70815/74507	208992/221653	230077/218456	142162/135560	36644/40683
[1000, 2000[	55556/59721	199780/203640	223431/223735	137432/140174	37338/40938
[0, 1000[	21651/24399	100763/97953	118179/117554	79059/76978	19855/21281

Table H.8: Differences in yield between the a tighter, efficiency corrected, cut on D0_h2_ETA and the nominal selection

p_{T} [MeV/c]	y [2, 2.5[	[2.5, 3[	[3, 3.5[	[3.5, 4[	[4, 4.5[
[9000, 10000[	7015/6123	7423/8208	3645/3227	0/0	0/0
[8000, 9000[	9548/9228	12720/13026	8867/9382	945/1185	0/0
[7000, 8000[	12798/14289	21656/21255	17903/17051	3828/4009	0/0
[6000, 7000[	21850/22182	34030/35888	31668/30357	11491/11565	152/87
[5000, 6000[	34258/34886	57390/61270	50833/53200	28372/27657	1612/1541
[4000, 5000[	51249/52387	105256/106551	97831/93118	57394/57388	6775/7875
[3000, 4000[	67175/69846	164347/170546	156502/154314	95998/98903	23853/23788
[2000, 3000[	72395/74507	221185/221653	218148/218456	133710/135560	38953/40683
[1000, 2000[	55411/59721	208069/203640	231453/223735	140130/140174	44000/40938
[0, 1000[	23298/24399	96004/97953	117437/117554	81232/76978	20244/21281

Table H.9: Differences in yield between the a tighter, efficiency corrected, cut on D0_h1_P and the nominal selection

p_{T} [MeV/c]	y [2, 2.5[	[2.5, 3[	[3, 3.5[	[3.5, 4[	[4, 4.5[
[9000, 10000[	7341/6123	8594/8208	2773/3227	0/0	0/0
[8000, 9000[	10997/9228	13650/13026	10239/9382	631/1185	0/0
[7000, 8000[	14177/14289	22614/21255	18180/17051	3308/4009	0/0
[6000, 7000[	22986/22182	33801/35888	28427/30357	11370/11565	160/87
[5000, 6000[	36062/34886	59163/61270	52038/53200	26583/27657	2253/1541
[4000, 5000[	52515/52387	105263/106551	91416/93118	53615/57388	9460/7875
[3000, 4000[	67752/69846	166974/170546	154529/154314	96768/98903	24730/23788
[2000, 3000[	71558/74507	219470/221653	206925/218456	134210/135560	40566/40683
[1000, 2000[	54526/59721	200295/203640	218958/223735	144912/140174	43883/40938
[0, 1000[	23870/24399	93718/97953	120523/117554	72499/76978	21962/21281

Table H.10: Differences in yield between the a tighter, efficiency corrected, cut on D0_h2_P and the nominal selection

p_{T} [MeV/c]	y [2, 2.5[	[2.5, 3[	[3, 3.5[	[3.5, 4[	[4, 4.5[
[9000, 10000[	5272/6123	8541/8208	2899/3227	0/0	0/0
[8000, 9000[	7744/9228	13019/13026	10597/9382	966/1185	0/0
[7000, 8000[	14857/14289	20948/21255	18182/17051	3650/4009	0/0
[6000, 7000[	22695/22182	36515/35888	29492/30357	10158/11565	102/87
[5000, 6000[	37466/34886	62065/61270	53112/53200	26469/27657	1219/1541
[4000, 5000[	50968/52387	100468/106551	95541/93118	59778/57388	8253/7875
[3000, 4000[	70953/69846	177683/170546	160893/154314	102246/98903	24856/23788
[2000, 3000[	75084/74507	236625/221653	215644/218456	129207/135560	40660/40683
[1000, 2000[	50537/59721	197938/203640	227650/223735	142128/140174	39823/40938
[0, 1000[	27777/24399	98017/97953	123230/117554	79392/76978	22282/21281

Table H.11: Differences in yield between the a tighter, efficiency corrected, cut on D0_h1_PT and the nominal selection

p_{T} [MeV/c]	y [2, 2.5[	[2.5, 3[	[3, 3.5[	[3.5, 4[	[4, 4.5[
[9000, 10000[	5060/6123	7852/8208	3664/3227	0/0	0/0
[8000, 9000[	7783/9228	12475/13026	10411/9382	1806/1185	0/0
[7000, 8000[	13675/14289	19833/21255	16242/17051	3269/4009	0/0
[6000, 7000[	20962/22182	33986/35888	32147/30357	12265/11565	34/87
[5000, 6000[	35617/34886	62530/61270	53399/53200	28372/27657	1213/1541
[4000, 5000[	51836/52387	103629/106551	93025/93118	51628/57388	7725/7875
[3000, 4000[	69967/69846	170867/170546	154118/154314	98685/98903	24629/23788
[2000, 3000[	76091/74507	215078/221653	218787/218456	135761/135560	40635/40683
[1000, 2000[	64245/59721	208732/203640	222169/223735	143957/140174	42270/40938
[0, 1000[	25314/24399	104302/97953	119256/117554	77086/76978	25234/21281

Table H.12: Differences in yield between the a tighter, efficiency corrected, cut on D0_h2_PT and the nominal selection

p_{T} [MeV/c]	y [2, 2.5[	[2.5, 3[	[3, 3.5[	[3.5, 4[	[4, 4.5[
[9000, 10000[	4948/6123	8669/8208	2914/3227	0/0	0/0
[8000, 9000[	7443/9228	12768/13026	10508/9382	1734/1185	0/0
[7000, 8000[	13191/14289	22390/21255	15951/17051	3489/4009	0/0
[6000, 7000[	20725/22182	33991/35888	29633/30357	10996/11565	175/87
[5000, 6000[	34000/34886	61815/61270	50926/53200	26911/27657	1230/1541
[4000, 5000[	52923/52387	111783/106551	91003/93118	62626/57388	7893/7875
[3000, 4000[	72517/69846	167624/170546	149431/154314	99817/98903	22840/23788
[2000, 3000[	73277/74507	230655/221653	220188/218456	137942/135560	40662/40683
[1000, 2000[	65481/59721	199428/203640	220416/223735	148500/140174	41132/40938
[0, 1000[	21611/24399	93938/97953	116529/117554	77113/76978	20797/21281

Table H.13: Total per bin differences between the tighter cut and nominal selection, from Tables H.1–H.12..

p_{T} [MeV/c]	y [2, 2.5[	[2.5, 3[	[3, 3.5[	[3.5, 4[	[4, 4.5[
[9000, 10000[	$1571.29^{+1734.46}_{-1735.11}$	$-8510.64^{+2150.49}_{-2145.87}$	$2921.89^{+870.10}_{-862.21}$	$0.00^{+0.00}_{-0.00}$	$0.00^{+0.00}_{-0.00}$
[8000, 9000[	$-23.12^{+2601.17}_{-2555.23}$	$12872.48^{+2421.56}_{-2430.53}$	$-3207.69^{+2032.74}_{-2010.78}$	$636.30^{+677.26}_{-680.85}$	$0.00^{+0.00}_{-0.00}$
[7000, 8000[	$1925.40^{+3057.11}_{-3034.13}$	$12199.19^{+3086.38}_{-3096.65}$	$13257.58^{+2595.93}_{-2575.38}$	$1846.51^{+1197.86}_{-1213.09}$	$0.00^{+0.00}_{-0.00}$
[6000, 7000[	$17883.21^{+3821.03}_{-3823.04}$	$-13449.47^{+4648.79}_{-4704.44}$	$36894.95^{+3505.41}_{-3520.51}$	$-1793.38^{+2252.34}_{-2248.72}$	$-313.98^{+210.64}_{-204.69}$
[5000, 6000[	$-18126.47^{+5373.40}_{-5300.10}$	$1715.25^{+6150.82}_{-6144.76}$	$-25631.79^{+5322.14}_{-5314.64}$	$1483.89^{+3579.70}_{-3499.61}$	$1400.57^{+785.78}_{-776.19}$
[4000, 5000[	$-3236.09^{+6545.88}_{-6494.66}$	$62161.40^{+7979.47}_{-8031.46}$	$23698.32^{+7028.72}_{-6974.14}$	$659.95^{+5433.48}_{-5428.19}$	$5359.43^{+1864.70}_{-1898.51}$
[3000, 4000[	$-29119.05^{+8263.80}_{-8311.81}$	$30728.37^{+10897.98}_{-11096.02}$	$-38010.36^{+10143.33}_{-10060.39}$	$27053.58^{+7561.75}_{-7524.26}$	$-1365.30^{+3458.09}_{-3409.89}$
[2000, 3000[	$-15512.77^{+8819.89}_{-8650.75}$	$25777.90^{+13960.19}_{-13757.14}$	$137868.69^{+12175.39}_{-12206.29}$	$17048.15^{+9601.90}_{-9708.89}$	$44448.30^{+4396.46}_{-4428.29}$
[1000, 2000[	$-3184.67^{+8485.57}_{-8522.60}$	$13926.14^{+13985.64}_{-13924.52}$	$-81768.71^{+14260.83}_{-14294.08}$	$-6069.86^{+10570.71}_{-10711.28}$	$-15206.38^{+5731.22}_{-5810.29}$
[0, 1000[	$-8309.98^{+5564.42}_{-5565.01}$	$5115.15^{+9973.96}_{-10003.58}$	$75239.86^{+9633.80}_{-9627.68}$	$75681.69^{+7589.25}_{-7694.06}$	$-13428.41^{+5528.02}_{-5555.46}$

H.2 $D^0 \to K^-\pi^+$ distributions and result

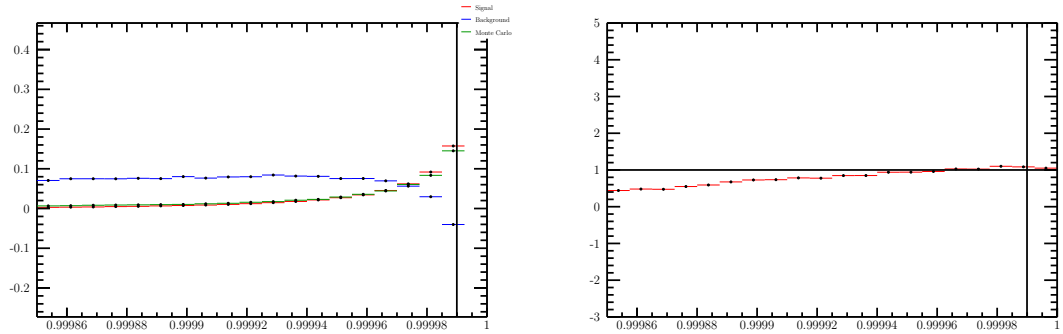

(a) Distributions *(b) Signal data/MC pull*

Figure H.1: Difference in the error corrected yield of 2015 MagDown $D^0 \to K^-\pi^+$ when split by D0_DIRA_OWNPV into two bins, each containing 50% of the simulated events. H.1a shows signal, background and simulated distributions and the pull between signal and simulation is given in H.1b.

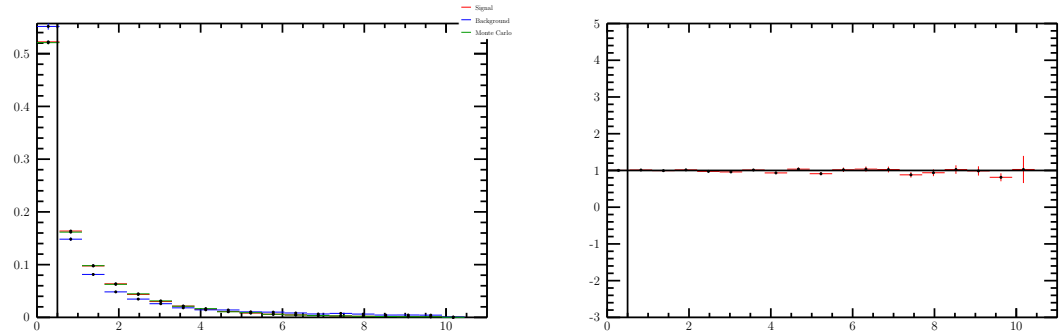

(a) Distributions *(b) Signal data/MC pull*

Figure H.2: Difference in the error corrected yield of 2015 MagDown $D^0 \to K^-\pi^+$ when split by D0_ENDVERTEX_CHI2/D0_ENDVERTEX_NDOF into two bins, each containing 50% of the simulated events. H.2a shows signal, background and simulated distributions and the pull between signal and simulation is given in H.2b.

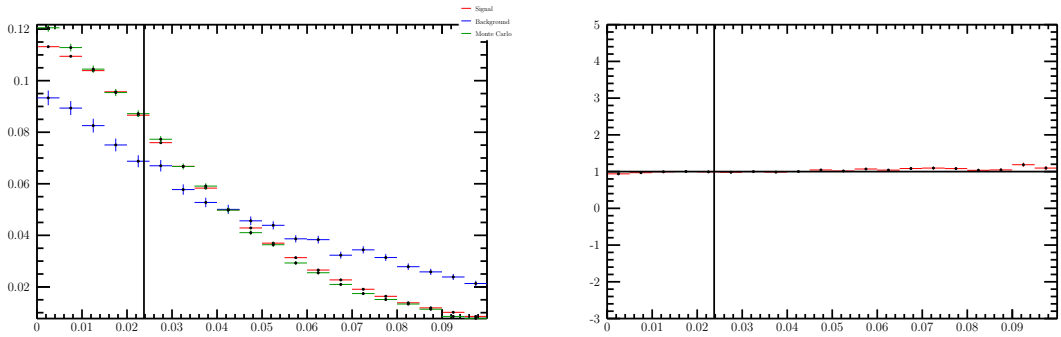

(a) Distributions *(b) Signal data/MC pull*

Figure H.3: Difference in the error corrected yield of 2015 MagDown $D^0 \to K^-\pi^+$ when split by D0_Loki_AMINDOCA into two bins, each containing 50% of the simulated events. H.3a shows signal, background and simulated distributions and the pull between signal and simulation is given in H.3b.

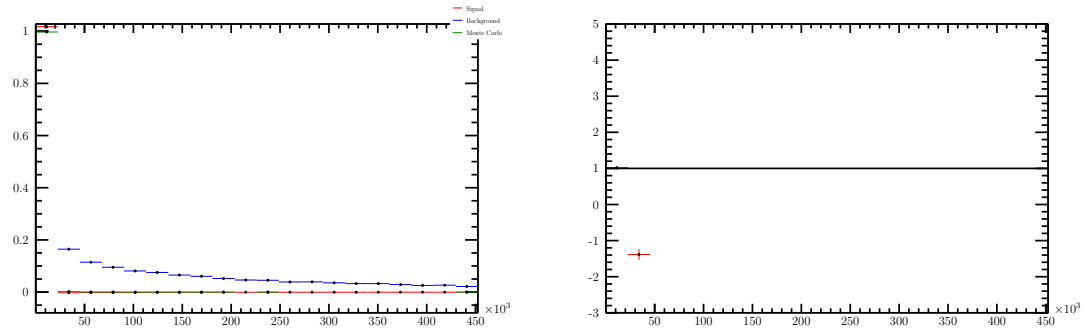

(a) Distributions *(b) Signal data/MC pull*

Figure H.4: Difference in the error corrected yield of 2015 MagDown $D^0 \to K^-\pi^+$ when split by D0_Loki_BPVVDCHI2 into two bins, each containing 50% of the simulated events. H.4a shows signal, background and simulated distributions and the pull between signal and simulation is given in H.4b.

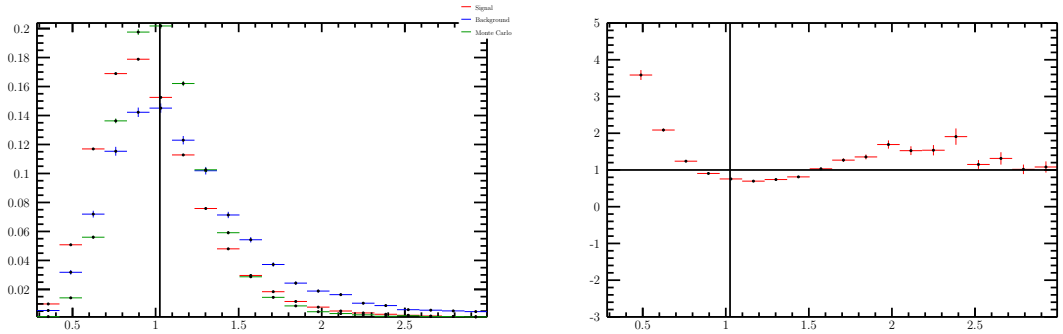

(a) Distributions *(b) Signal data/MC pull*

Figure H.5: Difference in the error corrected yield of 2015 MagDown $D^0 \to K^-\pi^+$ when split by D0_h1_TRACK_CHI2NDOF into two bins, each containing 50% of the simulated events. H.5a shows signal, background and simulated distributions and the pull between signal and simulation is given in H.5b.

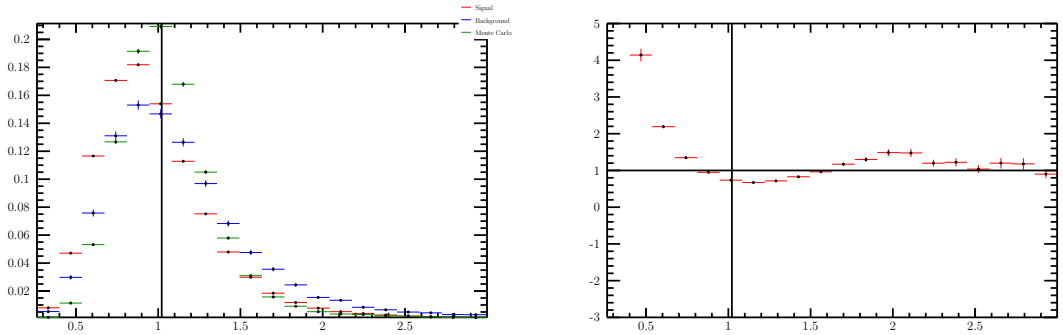

(a) Distributions *(b) Signal data/MC pull*

Figure H.6: Difference in the error corrected yield of 2015 MagDown $D^0 \to K^-\pi^+$ when split by D0_h2_TRACK_CHI2NDOF into two bins, each containing 50% of the simulated events. H.6a shows signal, background and simulated distributions and the pull between signal and simulation is given in H.6b.

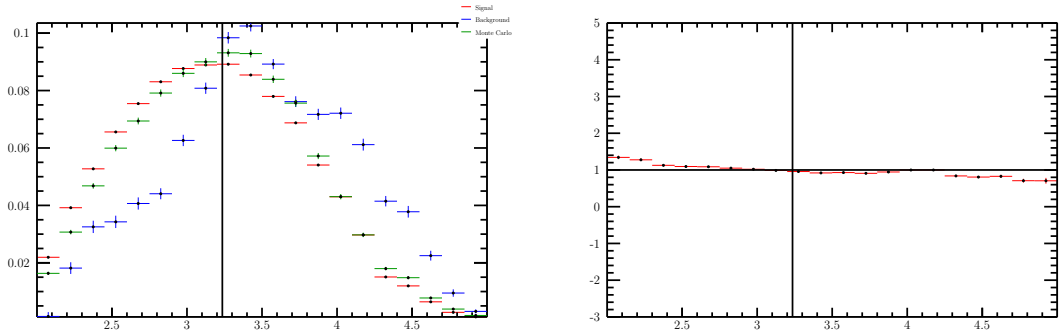

(a) Distributions *(b) Signal data/MC pull*

Figure H.7: Difference in the error corrected yield of 2015 MagDown $D^0 \to K^-\pi^+$ when split by D0_h1_ETA into two bins, each containing 50% of the simulated events. H.7a shows signal, background and simulated distributions and the pull between signal and simulation is given in H.7b.

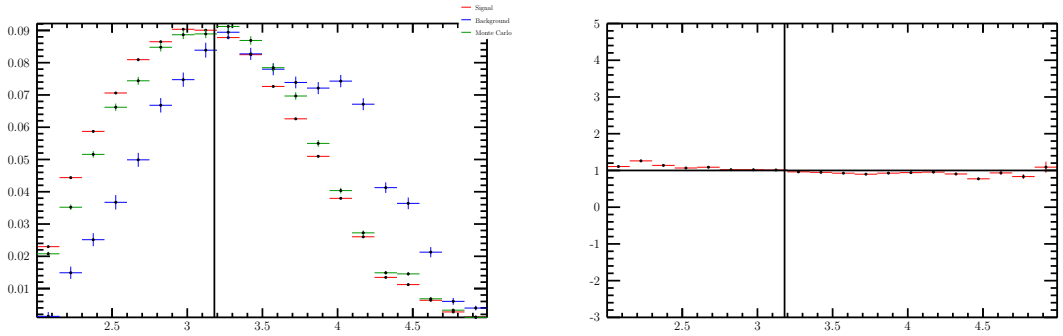

(a) Distributions *(b) Signal data/MC pull*

Figure H.8: Difference in the error corrected yield of 2015 MagDown $D^0 \to K^-\pi^+$ when split by D0_h2_ETA into two bins, each containing 50% of the simulated events. H.8a shows signal, background and simulated distributions and the pull between signal and simulation is given in H.8b.

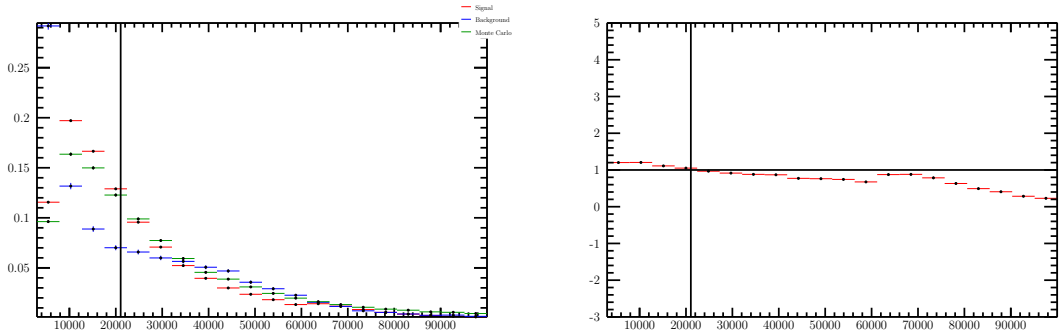

(a) Distributions *(b) Signal data/MC pull*

Figure H.9: Difference in the error corrected yield of 2015 MagDown $D^0 \to K^-\pi^+$ when split by D0_h1_P into two bins, each containing 50% of the simulated events. H.9a shows signal, background and simulated distributions and the pull between signal and simulation is given in H.9b.

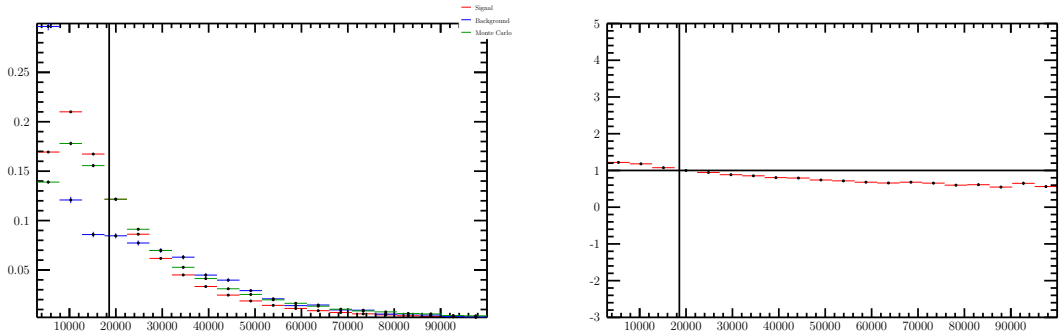

(a) Distributions *(b) Signal data/MC pull*

Figure H.10: Difference in the error corrected yield of 2015 MagDown $D^0 \to K^-\pi^+$ when split by D0_h2_P into two bins, each containing 50% of the simulated events. H.10a shows signal, background and simulated distributions and the pull between signal and simulation is given in H.10b.

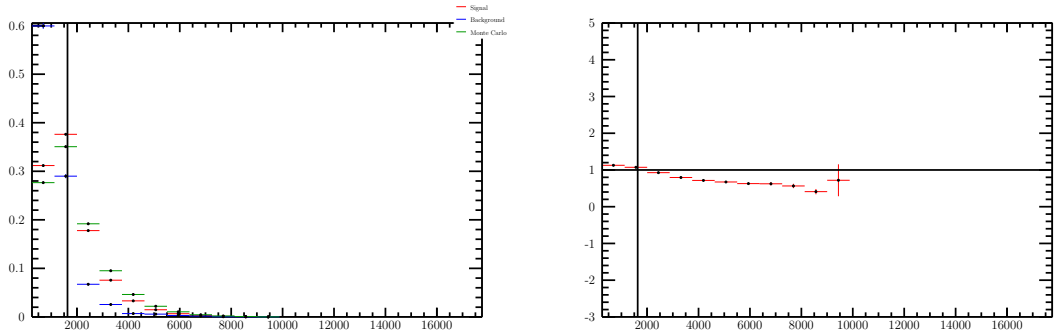

(a) Distributions *(b) Signal data/MC pull*

Figure H.11: Difference in the error corrected yield of 2015 MagDown $D^0 \to K^-\pi^+$ when split by D0_h1_PT into two bins, each containing 50% of the simulated events. H.11a shows signal, background and simulated distributions and the pull between signal and simulation is given in H.11b.

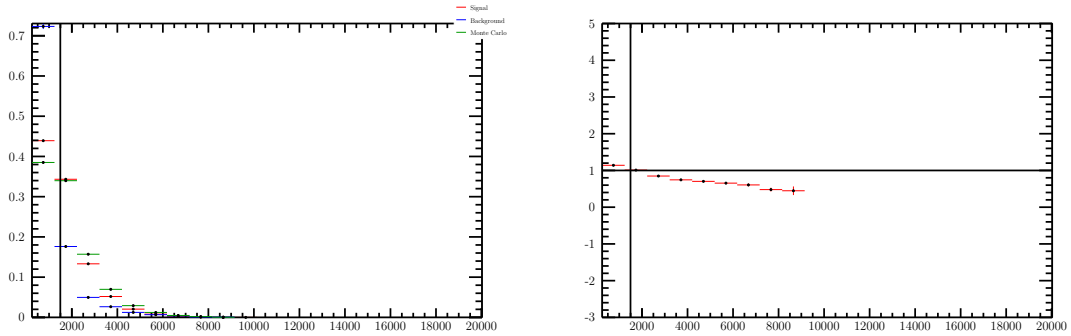

(a) Distributions *(b) Signal data/MC pull*

Figure H.12: Difference in the error corrected yield of 2015 MagDown $D^0 \to K^-\pi^+$ when split by D0_h2_PT into two bins, each containing 50% of the simulated events. H.12a shows signal, background and simulated distributions and the pull between signal and simulation is given in H.12b.

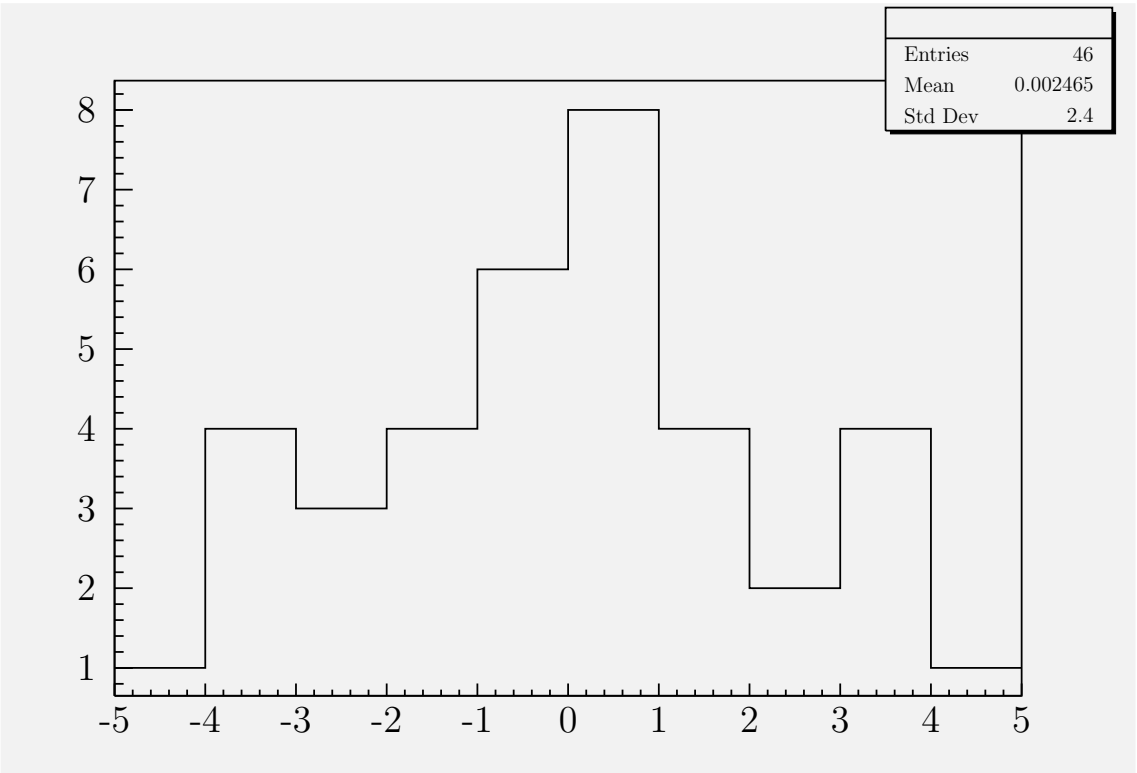

Figure H.13: Histogram of the deviation, in units of the standard deviation, for the Monte Carlo modelling systematic of each kinematic bin in 2015 MagDown $D^0 \to K^-\pi^+$ data.

H.3 $D^{*+} \to D^0\pi^+$ with $D^0 \to K^-\pi^+$ distributions and result

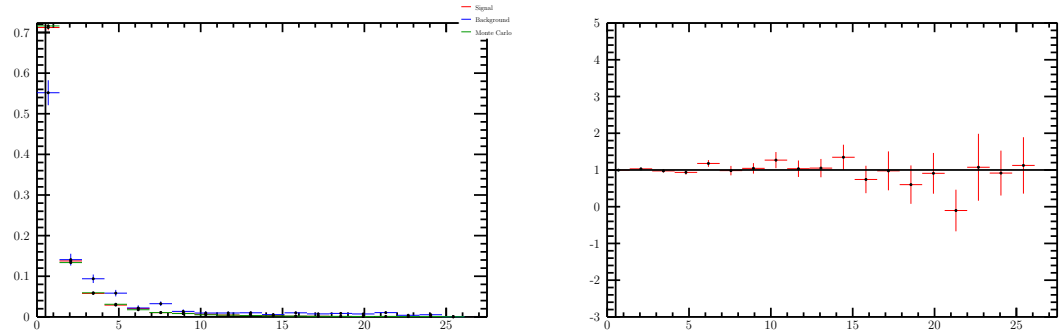

(a) Distributions *(b) Signal data/MC pull*

Figure H.14: Difference in the error corrected yield of 2015 MagDown $D^{*+} \to D^0\pi^+$ with $D^0 \to K^-\pi^+$ when split by Dst_ENDVERTEX_CHI2/Dst_ENDVERTEX_NDOF into two bins, each containing 50% of the simulated events. H.14a shows signal, background and simulated distributions and the pull between signal and simulation is given in H.14b.

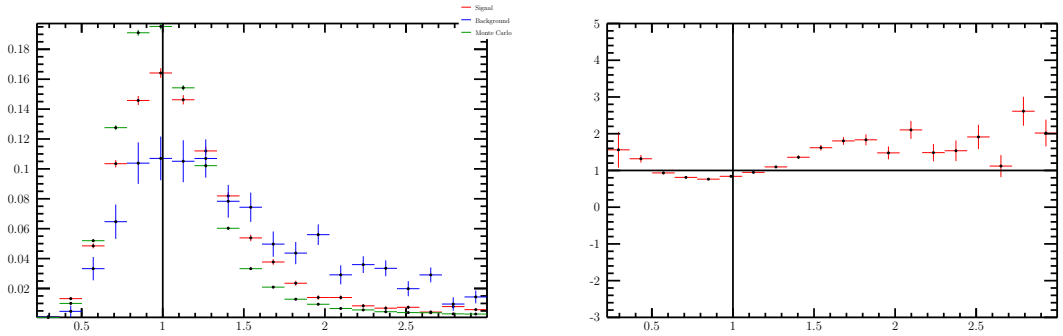

(a) Distributions *(b) Signal data/MC pull*

Figure H.15: Difference in the error corrected yield of 2015 MagDown $D^{*+} \to D^0\pi^+$ with $D^0 \to K^-\pi^+$ when split by Dst_pi_TRACK_CHI2NDOF into two bins, each containing 50% of the simulated events. H.15a shows signal, background and simulated distributions and the pull between signal and simulation is given in H.15b.

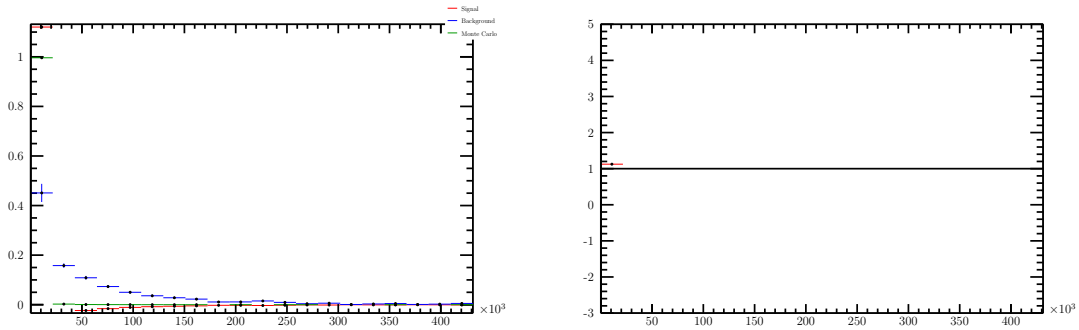

(a) Distributions *(b) Signal data/MC pull*

Figure H.16: Difference in the error corrected yield of 2015 MagDown $D^{*+} \to D^0\pi^+$ with $D^0 \to K^-\pi^+$ when split by D0_FDCHI2_OWNPV into two bins, each containing 50% of the simulated events. H.16a shows signal, background and simulated distributions and the pull between signal and simulation is given in H.16b.

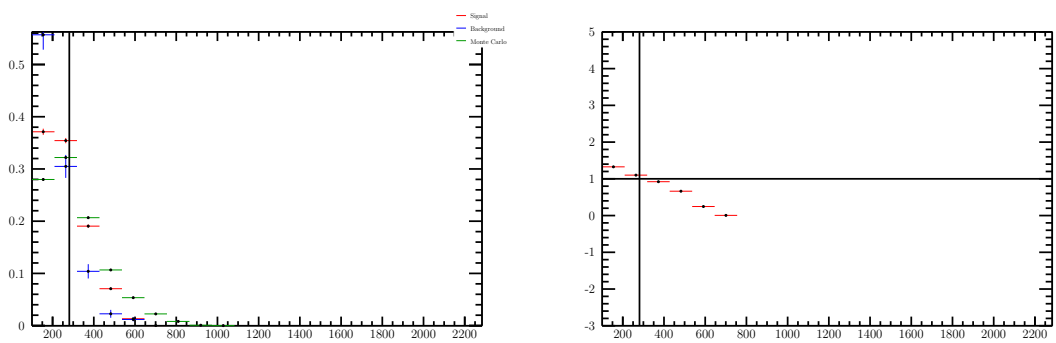

(a) Distributions *(b) Signal data/MC pull*

Figure H.17: Difference in the error corrected yield of 2015 MagDown $D^{*+} \to D^0\pi^+$ with $D^0 \to K^-\pi^+$ when split by Dst_pi_PT into two bins, each containing 50% of the simulated events. H.17a shows signal, background and simulated distributions and the pull between signal and simulation is given in H.17b.

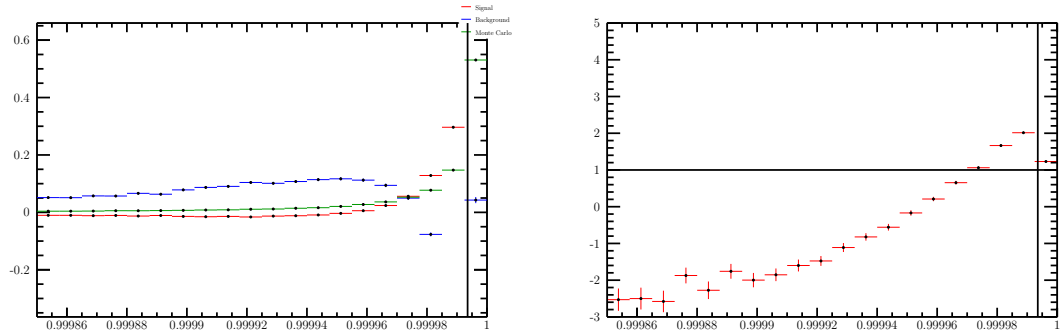

(a) Distributions *(b) Signal data/MC pull*

Figure H.18: Difference in the error corrected yield of 2015 MagDown $D^{*+} \to D^0\pi^+$ with $D^0 \to K^-\pi^+$ when split by D0_DIRA_OWNPV into two bins, each containing 50% of the simulated events. H.18a shows signal, background and simulated distributions and the pull between signal and simulation is given in H.18b.

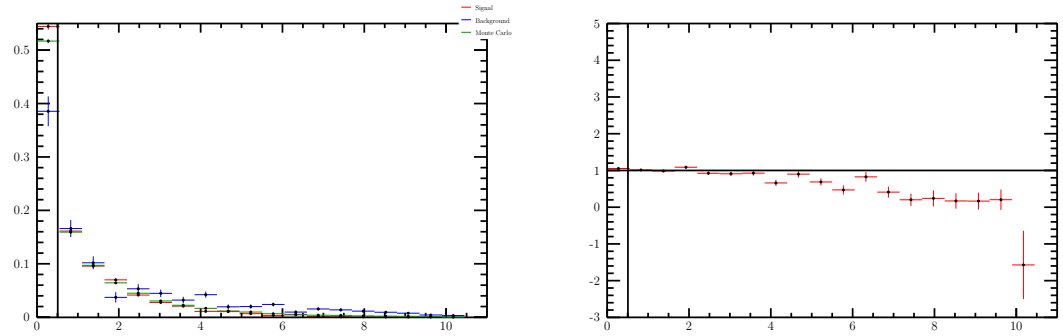

(a) Distributions *(b) Signal data/MC pull*

Figure H.19: Difference in the error corrected yield of 2015 MagDown $D^{*+} \to D^0\pi^+$ with $D^0 \to K^-\pi^+$ when split by D0_ENDVERTEX_CHI2/D0_ENDVERTEX_NDOF into two bins, each containing 50% of the simulated events. H.19a shows signal, background and simulated distributions and the pull between signal and simulation is given in H.19b.

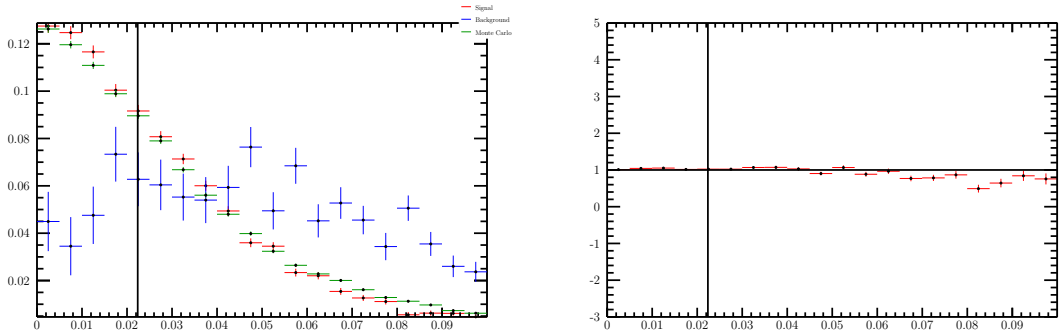

(a) Distributions *(b) Signal data/MC pull*

Figure H.20: Difference in the error corrected yield of 2015 MagDown $D^{*+} \to D^0\pi^+$ with $D^0 \to K^-\pi^+$ when split by D0_Loki_DOCAMAX into two bins, each containing 50% of the simulated events. H.20a shows signal, background and simulated distributions and the pull between signal and simulation is given in H.20b.

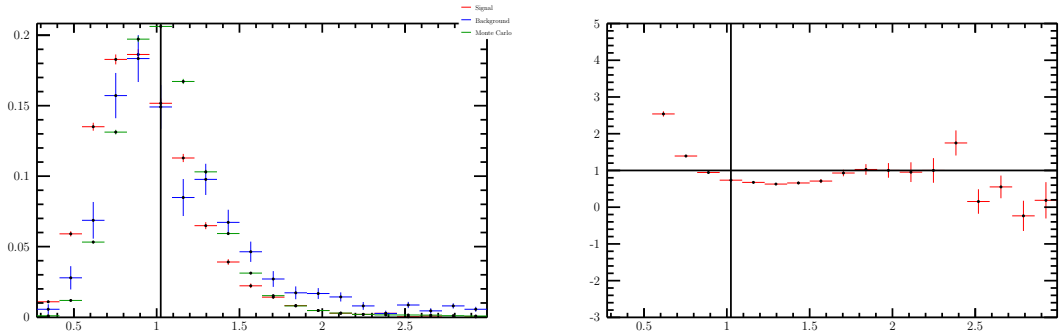

(a) Distributions *(b) Signal data/MC pull*

Figure H.21: Difference in the error corrected yield of 2015 MagDown $D^{*+} \to D^0\pi^+$ with $D^0 \to K^-\pi^+$ when split by D0_h1_TRACK_CHI2NDOF into two bins, each containing 50% of the simulated events. H.21a shows signal, background and simulated distributions and the pull between signal and simulation is given in H.21b.

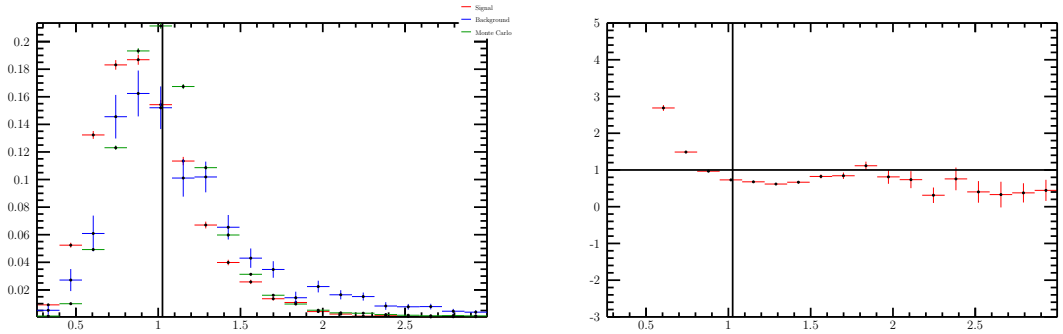

(a) Distributions *(b) Signal data/MC pull*

Figure H.22: Difference in the error corrected yield of 2015 MagDown $D^{*+} \to D^0\pi^+$ with $D^0 \to K^-\pi^+$ when split by D0_h2_TRACK_CHI2NDOF into two bins, each containing 50% of the simulated events. H.22a shows signal, background and simulated distributions and the pull between signal and simulation is given in H.22b.

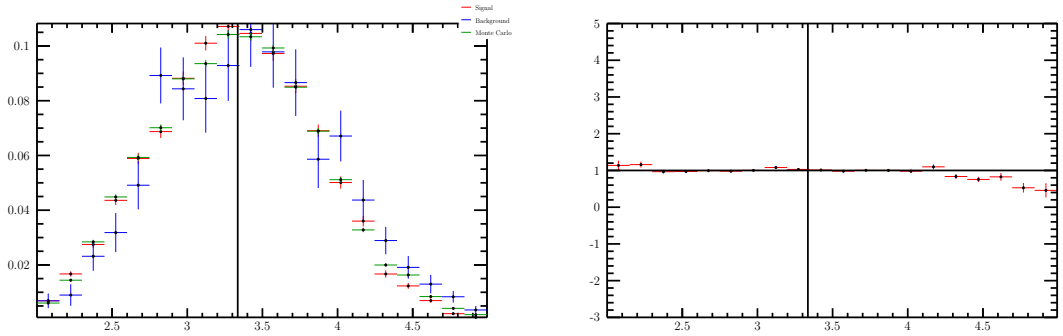

(a) Distributions *(b) Signal data/MC pull*

Figure H.23: Difference in the error corrected yield of 2015 MagDown $D^{*+} \to D^0\pi^+$ with $D^0 \to K^-\pi^+$ when split by D0_h1_ETA into two bins, each containing 50% of the simulated events. H.23a shows signal, background and simulated distributions and the pull between signal and simulation is given in H.23b.

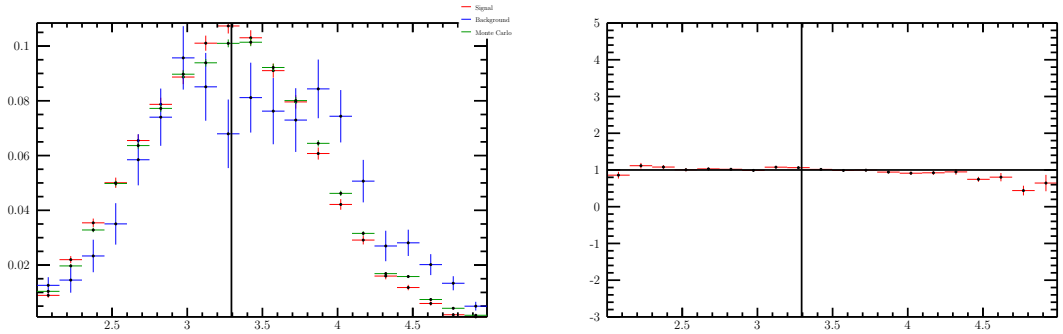

(a) Distributions *(b) Signal data/MC pull*

Figure H.24: Difference in the error corrected yield of 2015 MagDown $D^{*+} \to D^0\pi^+$ with $D^0 \to K^-\pi^+$ when split by D0_h2_ETA into two bins, each containing 50% of the simulated events. H.24a shows signal, background and simulated distributions and the pull between signal and simulation is given in H.24b.

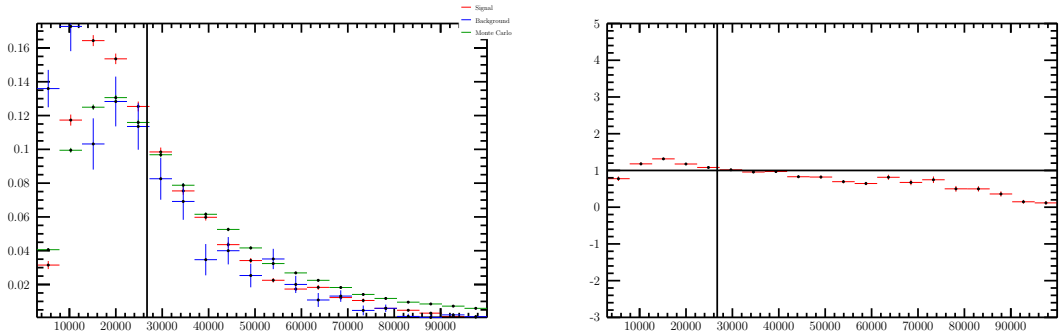

(a) Distributions *(b) Signal data/MC pull*

Figure H.25: Difference in the error corrected yield of 2015 MagDown $D^{*+} \to D^0\pi^+$ with $D^0 \to K^-\pi^+$ when split by D0_h1_P into two bins, each containing 50% of the simulated events. H.25a shows signal, background and simulated distributions and the pull between signal and simulation is given in H.25b.

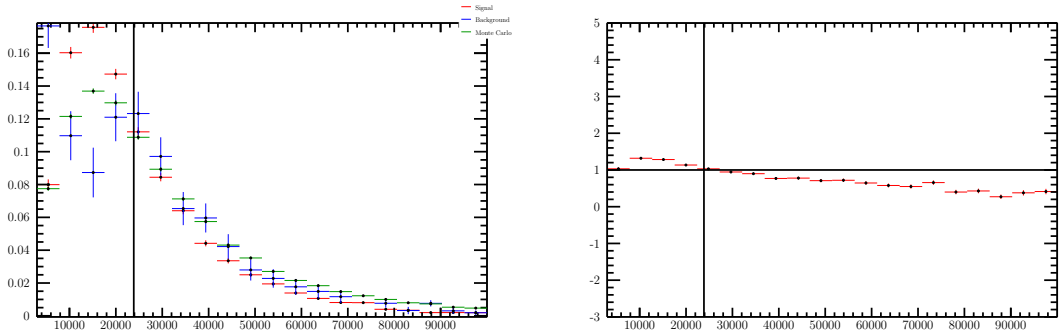

(a) Distributions *(b) Signal data/MC pull*

Figure H.26: Difference in the error corrected yield of 2015 MagDown $D^{*+} \to D^0\pi^+$ with $D^0 \to K^-\pi^+$ when split by D0_h2_P into two bins, each containing 50% of the simulated events. H.26a shows signal, background and simulated distributions and the pull between signal and simulation is given in H.26b.

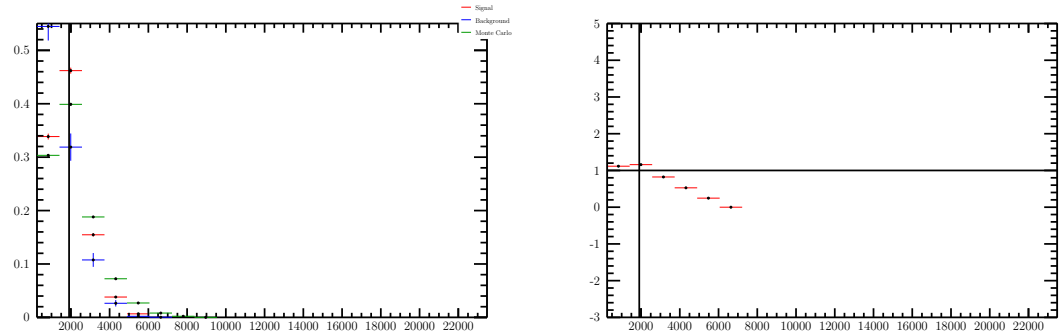

(a) Distributions *(b) Signal data/MC pull*

Figure H.27: Difference in the error corrected yield of 2015 MagDown $D^{*+} \to D^0\pi^+$ with $D^0 \to K^-\pi^+$ when split by D0_h1_PT into two bins, each containing 50% of the simulated events. H.27a shows signal, background and simulated distributions and the pull between signal and simulation is given in H.27b.

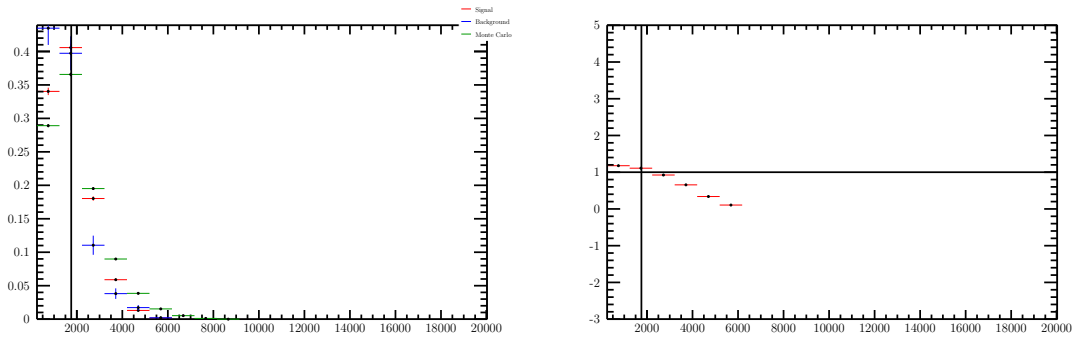

(a) Distributions *(b) Signal data/MC pull*

Figure H.28: Difference in the error corrected yield of 2015 MagDown $D^{*+} \to D^0\pi^+$ with $D^0 \to K^-\pi^+$ when split by D0_h2_PT into two bins, each containing 50% of the simulated events. H.28a shows signal, background and simulated distributions and the pull between signal and simulation is given in H.28b.

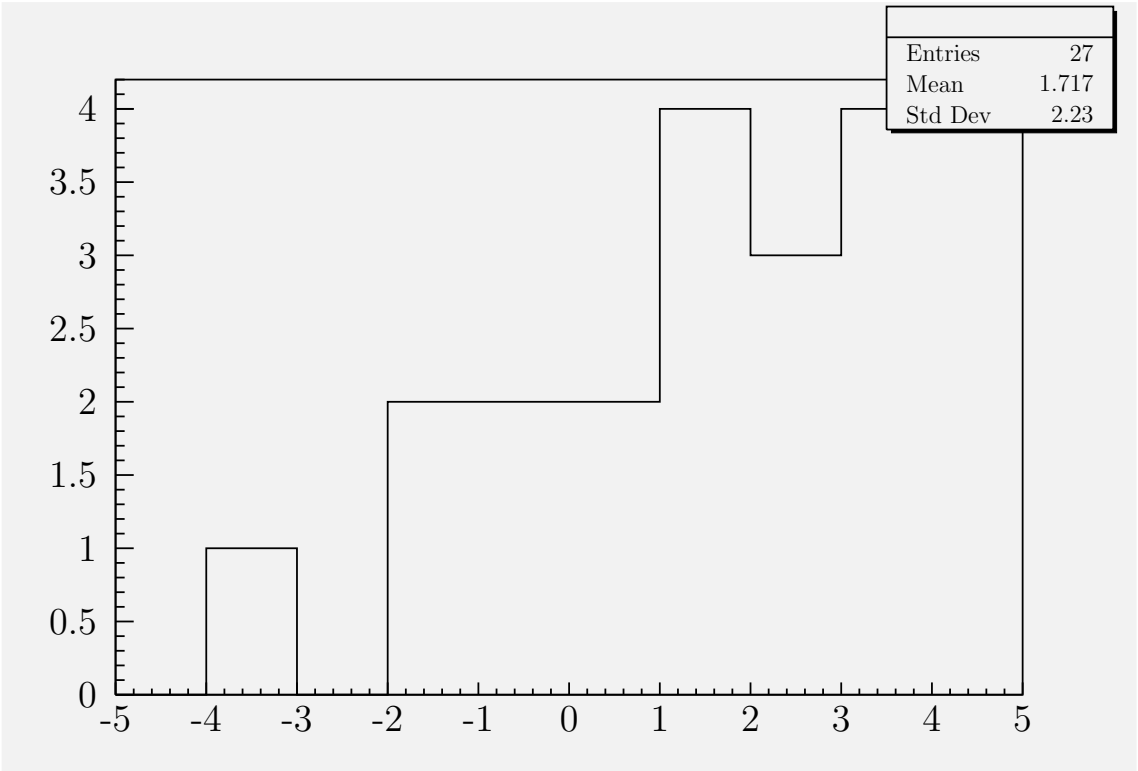

Figure H.29: Histogram of the deviation, in units of the standard deviation, for the Monte Carlo modelling systematic of each kinematic bin in 2015 MagDown $D^{*+} \to D^0\pi^+$ with $D^0 \to K^-\pi^+$ data.

H.4 $D^{*+} \to D^0\pi^+$ with $D^0 \to K^-\pi^+\pi^-\pi^+$ distributions and result

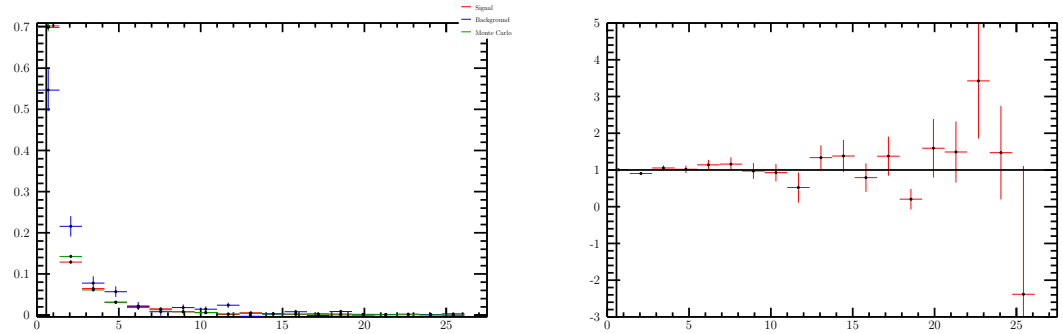

(a) Distributions *(b) Signal data/MC pull*

Figure H.30: Difference in the error corrected yield of 2015 MagDown $D^{*+} \to D^0\pi^+$ with $D^0 \to K^-\pi^+\pi^-\pi^+$ when split by Dst_ENDVERTEX_CHI2/Dst_ENDVERTEX_NDOF into two bins, each containing 50% of the simulated events. H.30a shows signal, background and simulated distributions and the pull between signal and simulation is given in H.30b.

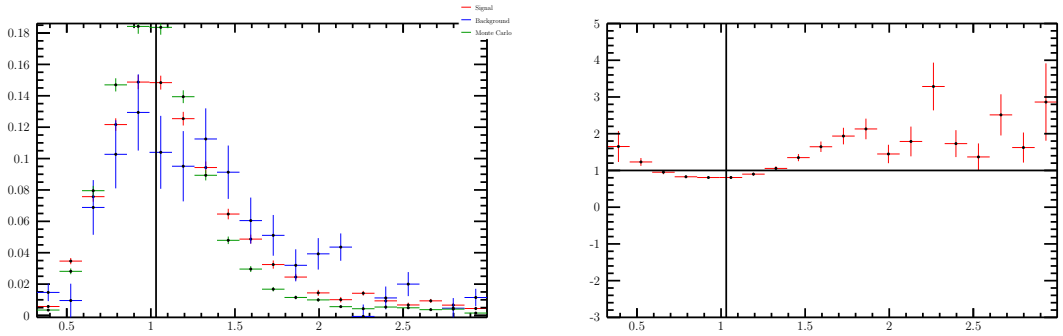

(a) Distributions *(b) Signal data/MC pull*

Figure H.31: Difference in the error corrected yield of 2015 MagDown $D^{*+} \to D^0\pi^+$ with $D^0 \to K^-\pi^+\pi^-\pi^+$ when split by Dst_pi_TRACK_CHI2NDOF into two bins, each containing 50% of the simulated events. H.31a shows signal, background and simulated distributions and the pull between signal and simulation is given in H.31b.

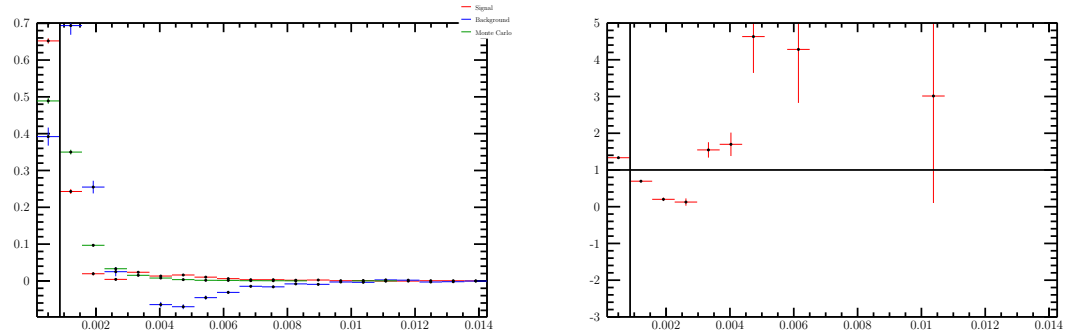

(a) Distributions *(b) Signal data/MC pull*

Figure H.32: Difference in the error corrected yield of 2015 MagDown $D^{*+} \to D^0\pi^+$ with $D^0 \to K^-\pi^+\pi^-\pi^+$ when split by D0_Loki_BPVLTIME into two bins, each containing 50% of the simulated events. H.32a shows signal, background and simulated distributions and the pull between signal and simulation is given in H.32b.

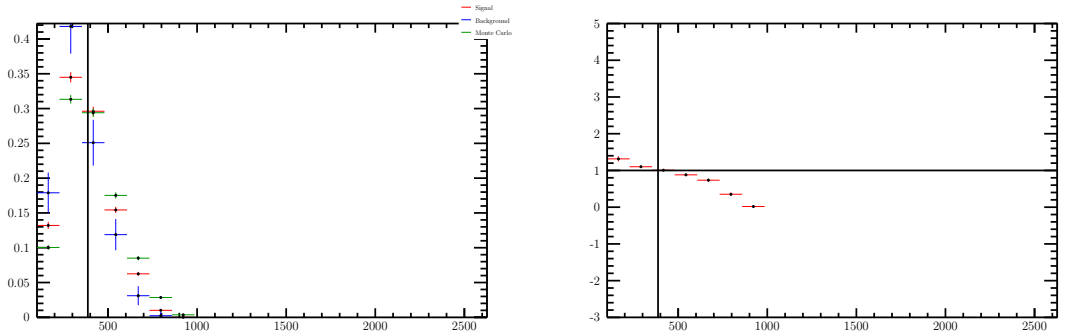

(a) Distributions *(b) Signal data/MC pull*

Figure H.33: Difference in the error corrected yield of 2015 MagDown $D^{*+} \to D^0\pi^+$ with $D^0 \to K^-\pi^+\pi^-\pi^+$ when split by Dst_pi_PT into two bins, each containing 50% of the simulated events. H.33a shows signal, background and simulated distributions and the pull between signal and simulation is given in H.33b.

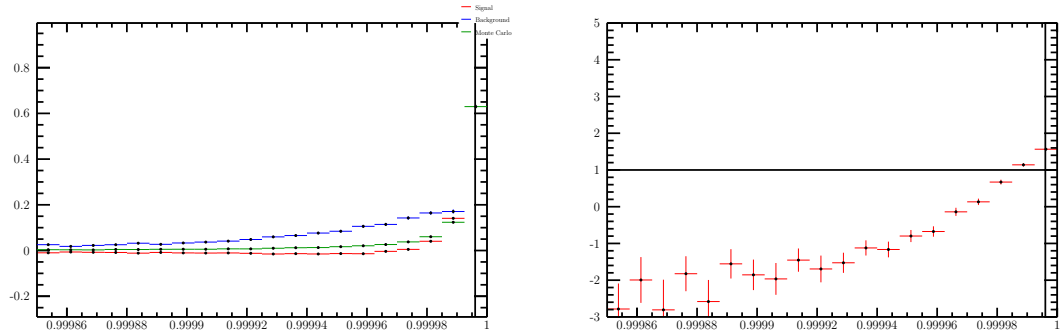

(a) Distributions *(b) Signal data/MC pull*

Figure H.34: Difference in the error corrected yield of 2015 MagDown $D^{*+} \to D^0\pi^+$ with $D^0 \to K^-\pi^+\pi^-\pi^+$ when split by D0_DIRA_OWNPV into two bins, each containing 50% of the simulated events. H.34a shows signal, background and simulated distributions and the pull between signal and simulation is given in H.34b.

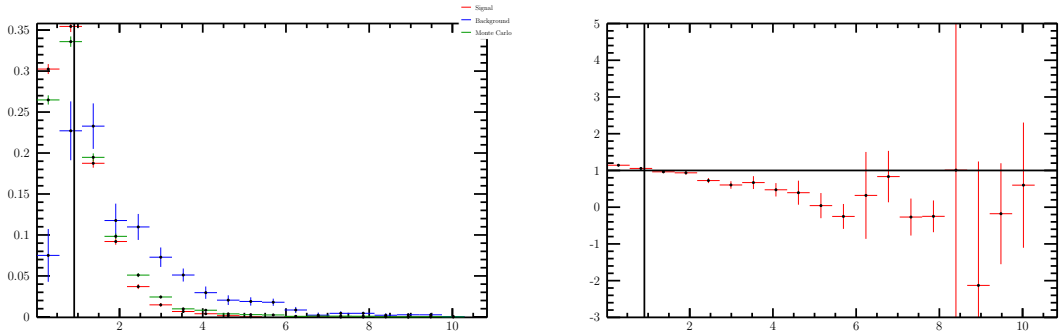

(a) Distributions *(b) Signal data/MC pull*

Figure H.35: Difference in the error corrected yield of 2015 MagDown $D^{*+} \to D^0\pi^+$ with $D^0 \to K^-\pi^+\pi^-\pi^+$ when split by D0_ENDVERTEX_CHI2/D0_ENDVERTEX_NDOF into two bins, each containing 50% of the simulated events. H.35a shows signal, background and simulated distributions and the pull between signal and simulation is given in H.35b.

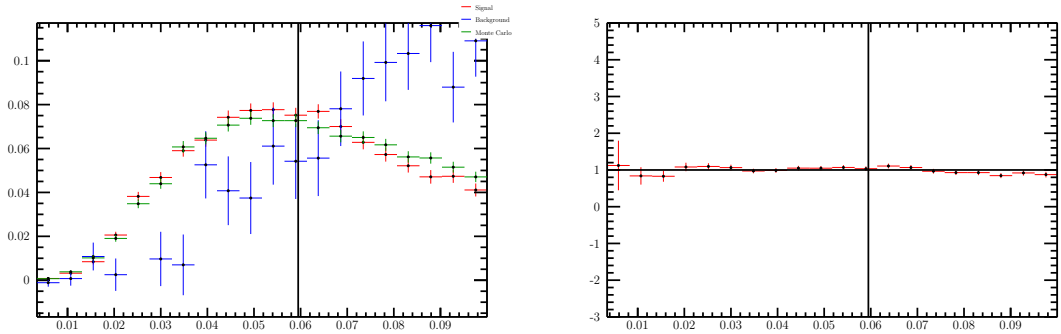

(a) Distributions *(b) Signal data/MC pull*

Figure H.36: Difference in the error corrected yield of 2015 MagDown $D^{*+} \to D^0\pi^+$ with $D^0 \to K^-\pi^+\pi^-\pi^+$ when split by D0_Loki_DOCAMAX into two bins, each containing 50% of the simulated events. H.36a shows signal, background and simulated distributions and the pull between signal and simulation is given in H.36b.

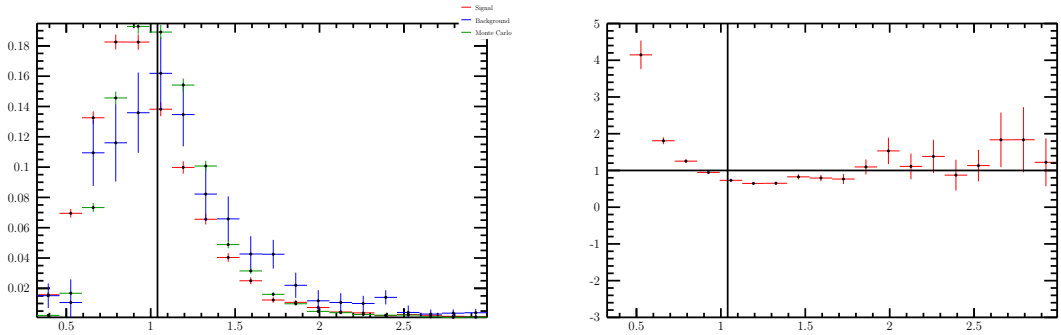

(a) Distributions *(b) Signal data/MC pull*

Figure H.37: Difference in the error corrected yield of 2015 MagDown $D^{*+} \to D^0\pi^+$ with $D^0 \to K^-\pi^+\pi^-\pi^+$ when split by D0_h1_TRACK_CHI2NDOF into two bins, each containing 50% of the simulated events. H.37a shows signal, background and simulated distributions and the pull between signal and simulation is given in H.37b.

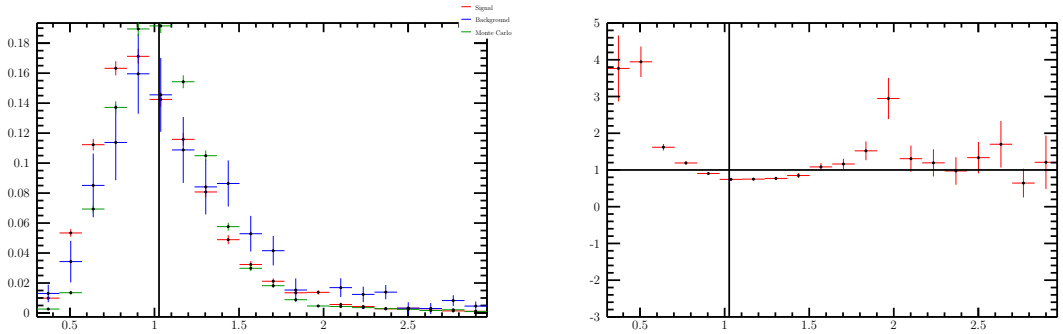

(a) Distributions *(b) Signal data/MC pull*

Figure H.38: Difference in the error corrected yield of 2015 MagDown $D^{*+} \to D^0\pi^+$ with $D^0 \to K^-\pi^+\pi^-\pi^+$ when split by D0_h2_TRACK_CHI2NDOF into two bins, each containing 50% of the simulated events. H.38a shows signal, background and simulated distributions and the pull between signal and simulation is given in H.38b.

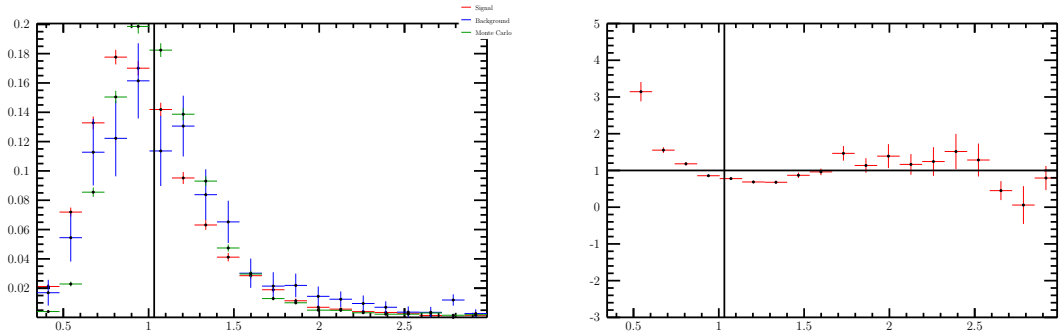

(a) Distributions *(b) Signal data/MC pull*

Figure H.39: Difference in the error corrected yield of 2015 MagDown $D^{*+} \to D^0\pi^+$ with $D^0 \to K^-\pi^+\pi^-\pi^+$ when split by D0_h3_TRACK_CHI2NDOF into two bins, each containing 50% of the simulated events. H.39a shows signal, background and simulated distributions and the pull between signal and simulation is given in H.39b.

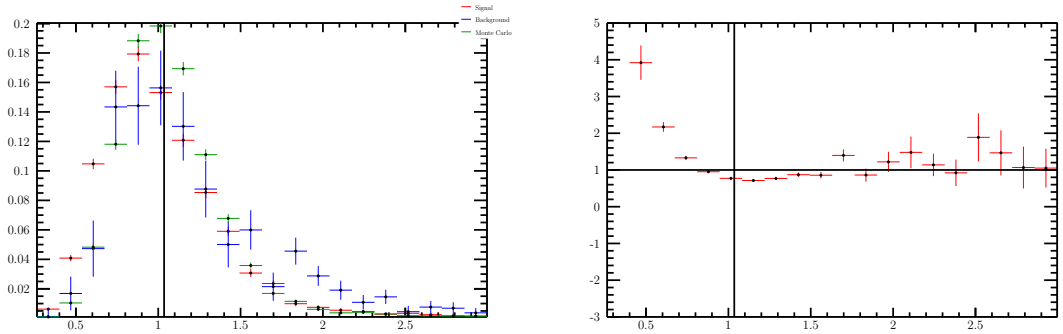

(a) Distributions *(b) Signal data/MC pull*

Figure H.40: Difference in the error corrected yield of 2015 MagDown $D^{*+} \to D^0\pi^+$ with $D^0 \to K^-\pi^+\pi^-\pi^+$ when split by D0_h4_TRACK_CHI2NDOF into two bins, each containing 50% of the simulated events. H.40a shows signal, background and simulated distributions and the pull between signal and simulation is given in H.40b.

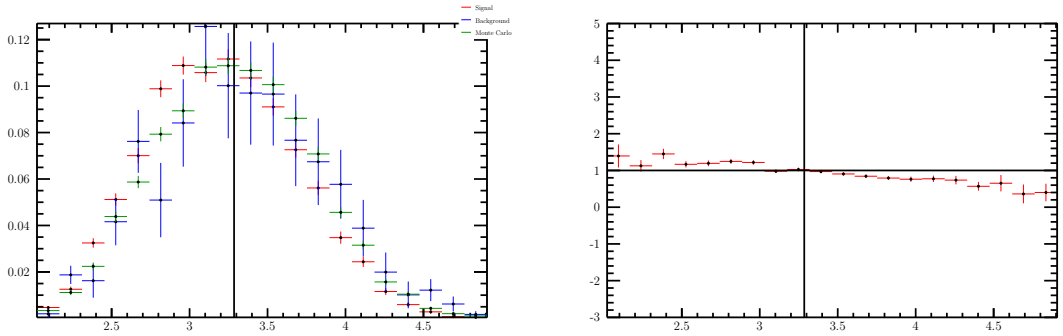

(a) Distributions *(b) Signal data/MC pull*

Figure H.41: Difference in the error corrected yield of 2015 MagDown $D^{*+} \to D^0\pi^+$ with $D^0 \to K^-\pi^+\pi^-\pi^+$ when split by D0_h1_ETA into two bins, each containing 50% of the simulated events. H.41a shows signal, background and simulated distributions and the pull between signal and simulation is given in H.41b.

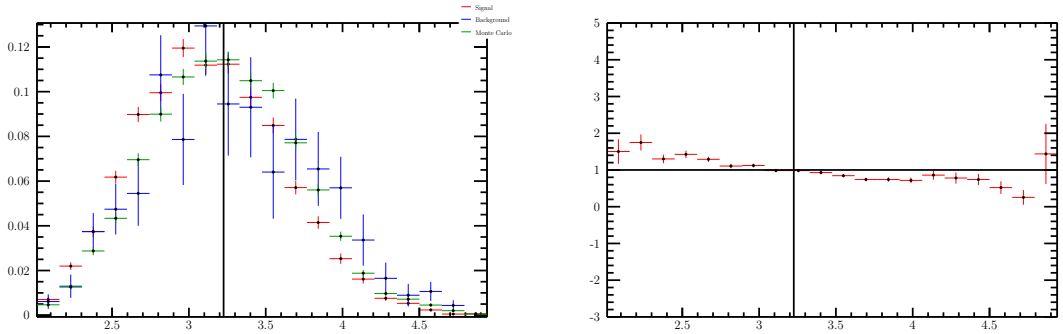

(a) Distributions *(b) Signal data/MC pull*

Figure H.42: Difference in the error corrected yield of 2015 MagDown $D^{*+} \to D^0\pi^+$ with $D^0 \to K^-\pi^+\pi^-\pi^+$ when split by D0_h2_ETA into two bins, each containing 50% of the simulated events. H.42a shows signal, background and simulated distributions and the pull between signal and simulation is given in H.42b.

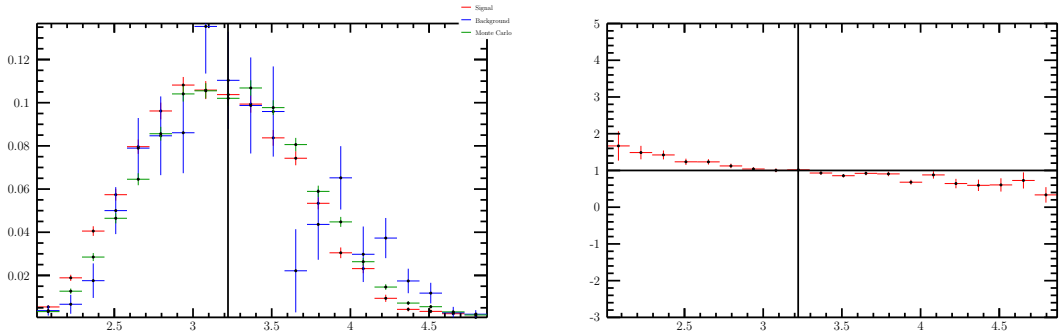

(a) Distributions *(b) Signal data/MC pull*

Figure H.43: Difference in the error corrected yield of 2015 MagDown $D^{*+} \to D^0\pi^+$ with $D^0 \to K^-\pi^+\pi^-\pi^+$ when split by D0_h3_ETA into two bins, each containing 50% of the simulated events. H.43a shows signal, background and simulated distributions and the pull between signal and simulation is given in H.43b.

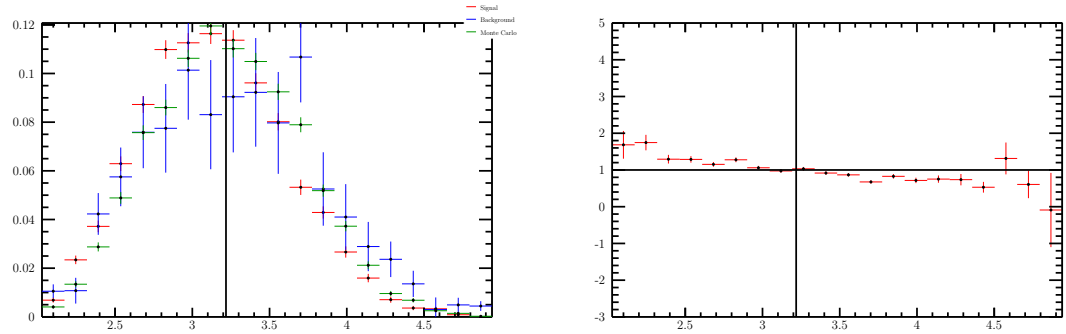

(a) Distributions *(b) Signal data/MC pull*

Figure H.44: Difference in the error corrected yield of 2015 MagDown $D^{*+} \to D^0\pi^+$ with $D^0 \to K^-\pi^+\pi^-\pi^+$ when split by D0_h4_ETA into two bins, each containing 50% of the simulated events. H.44a shows signal, background and simulated distributions and the pull between signal and simulation is given in H.44b.

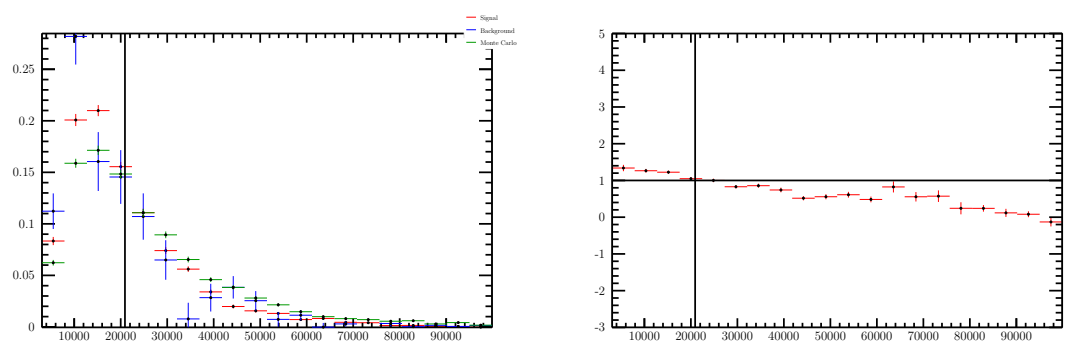

(a) Distributions *(b) Signal data/MC pull*

Figure H.45: Difference in the error corrected yield of 2015 MagDown $D^{*+} \to D^0\pi^+$ with $D^0 \to K^-\pi^+\pi^-\pi^+$ when split by D0_h1_P into two bins, each containing 50% of the simulated events. H.45a shows signal, background and simulated distributions and the pull between signal and simulation is given in H.45b.

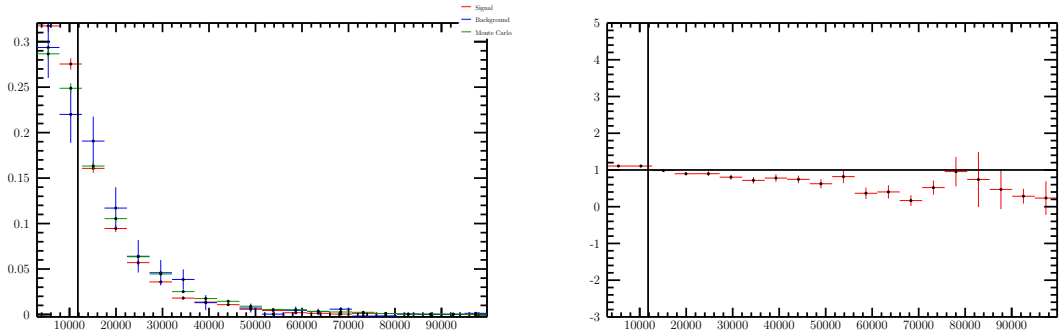

(a) Distributions *(b) Signal data/MC pull*

Figure H.46: Difference in the error corrected yield of 2015 MagDown $D^{*+} \to D^0\pi^+$ with $D^0 \to K^-\pi^+\pi^-\pi^+$ when split by D0_h2_P into two bins, each containing 50% of the simulated events. H.46a shows signal, background and simulated distributions and the pull between signal and simulation is given in H.46b.

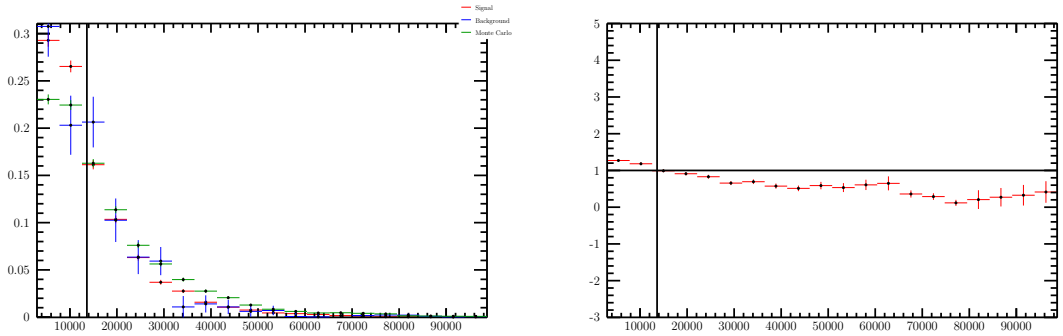

(a) Distributions *(b) Signal data/MC pull*

Figure H.47: Difference in the error corrected yield of 2015 MagDown $D^{*+} \to D^0\pi^+$ with $D^0 \to K^-\pi^+\pi^-\pi^+$ when split by D0_h3_P into two bins, each containing 50% of the simulated events. H.47a shows signal, background and simulated distributions and the pull between signal and simulation is given in H.47b.

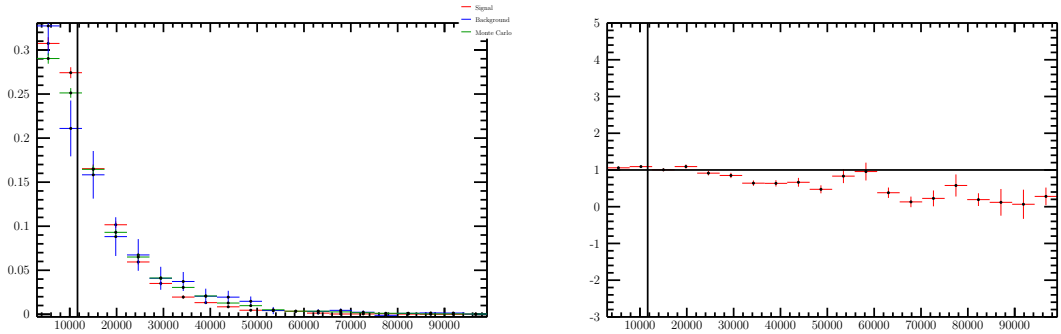

(a) Distributions *(b) Signal data/MC pull*

Figure H.48: Difference in the error corrected yield of 2015 MagDown $D^{*+} \to D^0\pi^+$ with $D^0 \to K^-\pi^+\pi^-\pi^+$ when split by D0_h4_P into two bins, each containing 50% of the simulated events. H.48a shows signal, background and simulated distributions and the pull between signal and simulation is given in H.48b.

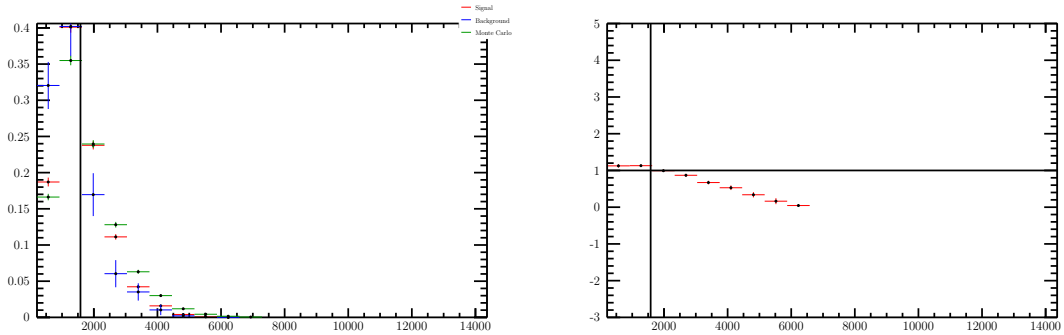

(a) Distributions *(b) Signal data/MC pull*

Figure H.49: Difference in the error corrected yield of 2015 MagDown $D^{*+} \to D^0\pi^+$ with $D^0 \to K^-\pi^+\pi^-\pi^+$ when split by D0_h1_PT into two bins, each containing 50% of the simulated events. H.49a shows signal, background and simulated distributions and the pull between signal and simulation is given in H.49b.

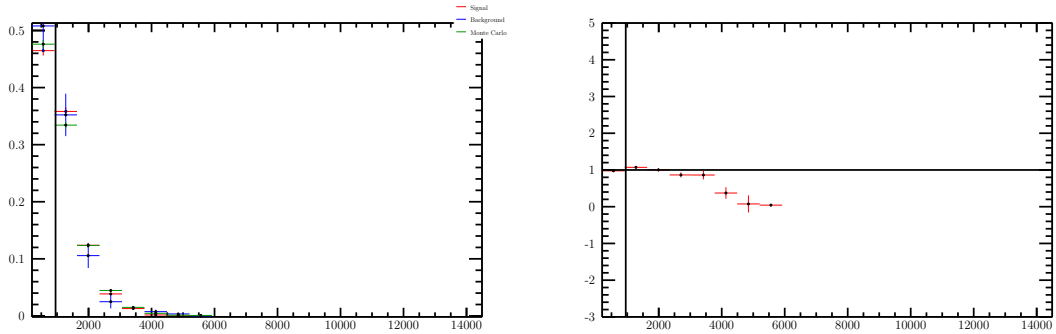

(a) Distributions *(b) Signal data/MC pull*

Figure H.50: Difference in the error corrected yield of 2015 MagDown $D^{*+} \to D^0\pi^+$ with $D^0 \to K^-\pi^+\pi^-\pi^+$ when split by D0_h2_PT into two bins, each containing 50% of the simulated events. H.50a shows signal, background and simulated distributions and the pull between signal and simulation is given in H.50b.

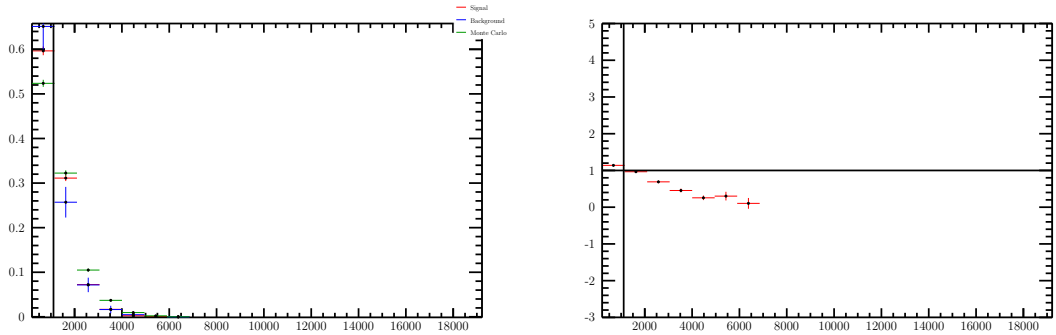

(a) Distributions *(b) Signal data/MC pull*

Figure H.51: Difference in the error corrected yield of 2015 MagDown $D^{*+} \to D^0\pi^+$ with $D^0 \to K^-\pi^+\pi^-\pi^+$ when split by D0_h3_PT into two bins, each containing 50% of the simulated events. H.51a shows signal, background and simulated distributions and the pull between signal and simulation is given in H.51b.

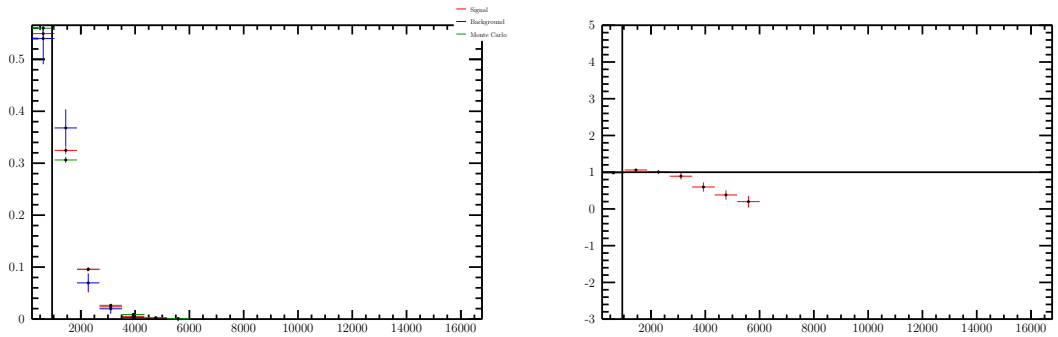

(a) Distributions *(b) Signal data/MC pull*

Figure H.52: Difference in the error corrected yield of 2015 MagDown $D^{*+} \to D^0\pi^+$ with $D^0 \to K^-\pi^+\pi^-\pi^+$ when split by D0_h4_PT into two bins, each containing 50% of the simulated events. H.52a shows signal, background and simulated distributions and the pull between signal and simulation is given in H.52b.

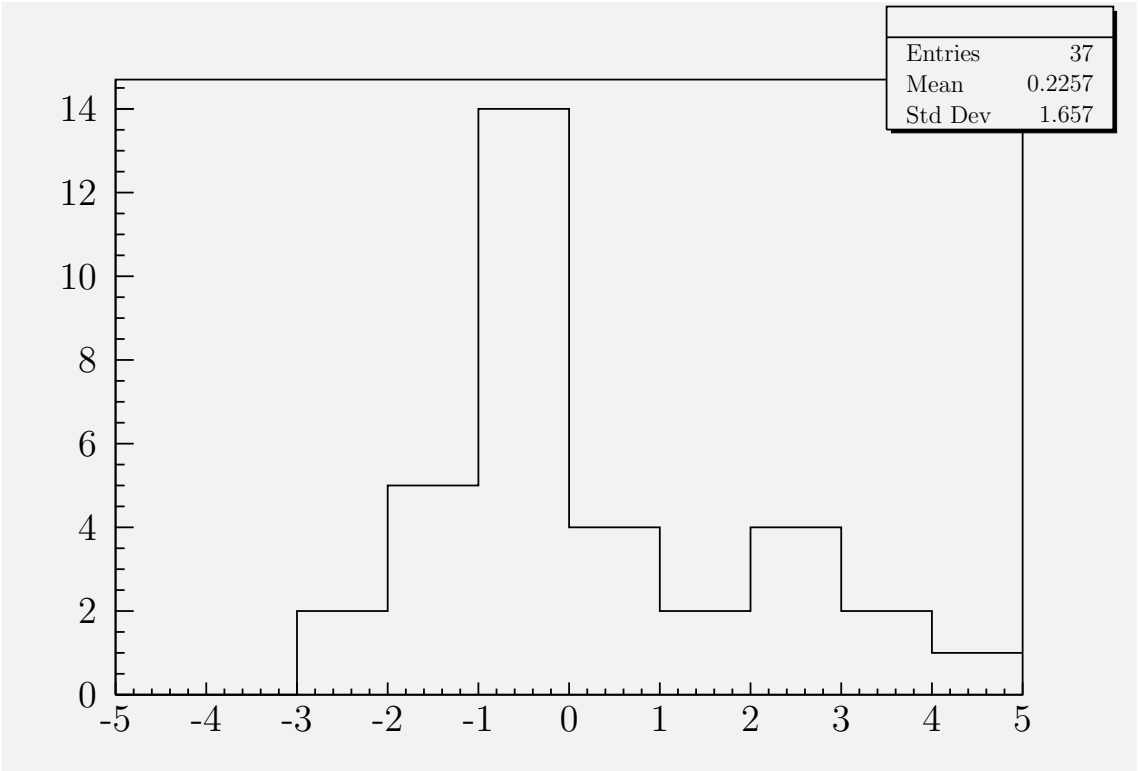

Figure H.53: Histogram of the deviation, in units of the standard deviation, for the Monte Carlo modelling systematic of each kinematic bin in 2015 MagDown $D^{*+} \to D^0\pi^+$ with $D^0 \to K^-\pi^+\pi^-\pi^+$ data.

H.5 $D^+ \to K^-\pi^+\pi^+$ distributions and result

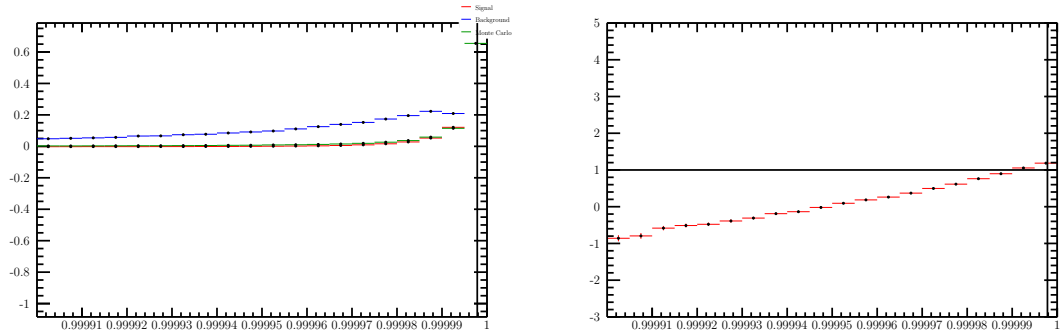

(a) Distributions *(b) Signal data/MC pull*

Figure H.54: Difference in the error corrected yield of 2015 MagDown $D^+ \to K^-\pi^+\pi^+$ when split by Dp_DIRA_OWNPV into two bins, each containing 50% of the simulated events. H.54a shows signal, background and simulated distributions and the pull between signal and simulation is given in H.54b.

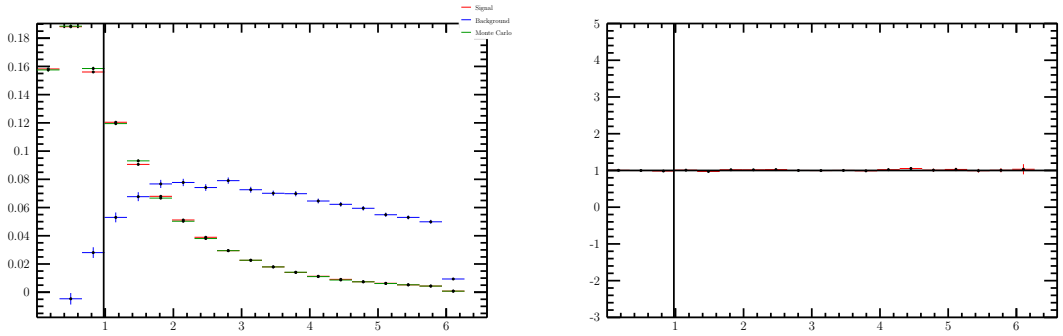

(a) Distributions *(b) Signal data/MC pull*

Figure H.55: Difference in the error corrected yield of 2015 MagDown $D^+ \to K^-\pi^+\pi^+$ when split by Dp_ENDVERTEX_CHI2/Dp_ENDVERTEX_NDOF into two bins, each containing 50% of the simulated events. H.55a shows signal, background and simulated distributions and the pull between signal and simulation is given in H.55b.

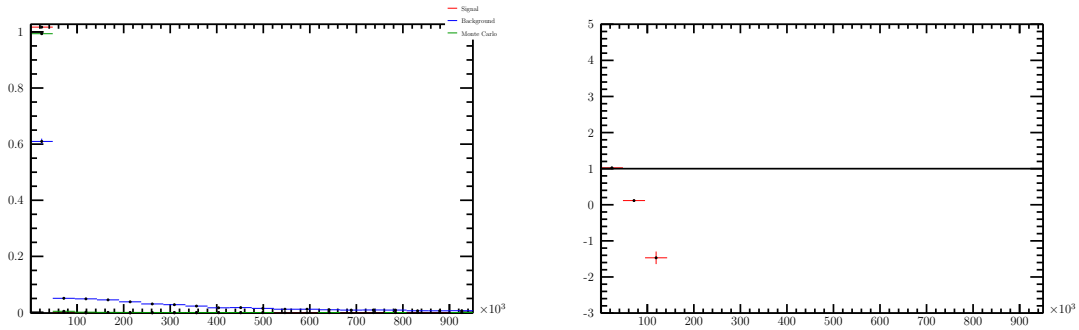

(a) Distributions *(b) Signal data/MC pull*

Figure H.56: Difference in the error corrected yield of 2015 MagDown $D^+ \to K^-\pi^+\pi^+$ when split by Dp_FDCHI2_OWNPV into two bins, each containing 50% of the simulated events. H.56a shows signal, background and simulated distributions and the pull between signal and simulation is given in H.56b.

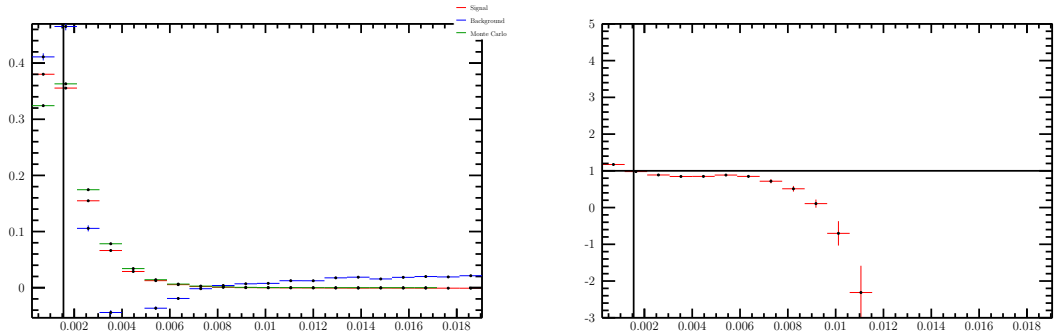

(a) Distributions *(b) Signal data/MC pull*

Figure H.57: Difference in the error corrected yield of 2015 MagDown $D^+ \to K^-\pi^+\pi^+$ when split by Dp_Loki_BPVLTIME into two bins, each containing 50% of the simulated events. H.57a shows signal, background and simulated distributions and the pull between signal and simulation is given in H.57b.

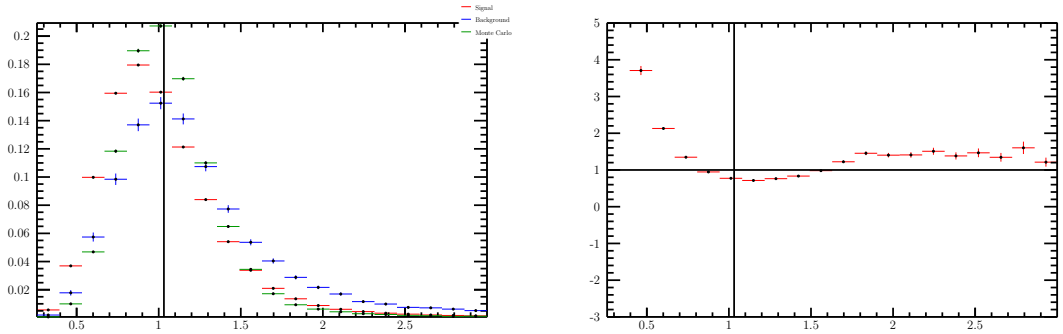

(a) Distributions *(b) Signal data/MC pull*

Figure H.58: Difference in the error corrected yield of 2015 MagDown $D^+ \to K^-\pi^+\pi^+$ when split by Dp_h1_TRACK_CHI2NDOF into two bins, each containing 50% of the simulated events. H.58a shows signal, background and simulated distributions and the pull between signal and simulation is given in H.58b.

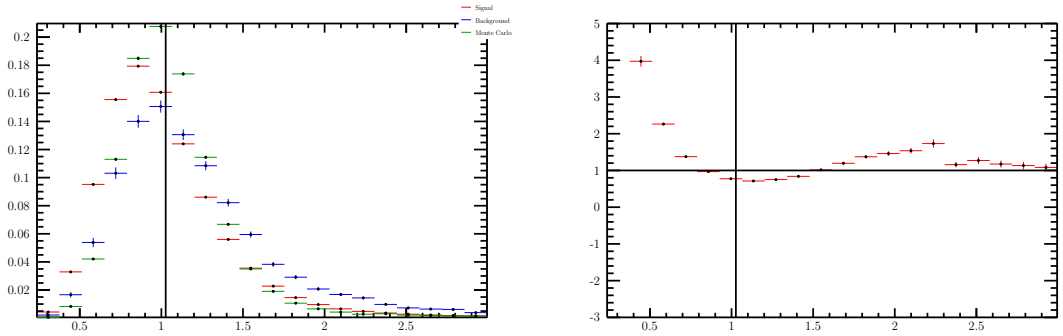

(a) Distributions *(b) Signal data/MC pull*

Figure H.59: Difference in the error corrected yield of 2015 MagDown $D^+ \to K^-\pi^+\pi^+$ when split by Dp_h2_TRACK_CHI2NDOF into two bins, each containing 50% of the simulated events. H.59a shows signal, background and simulated distributions and the pull between signal and simulation is given in H.59b.

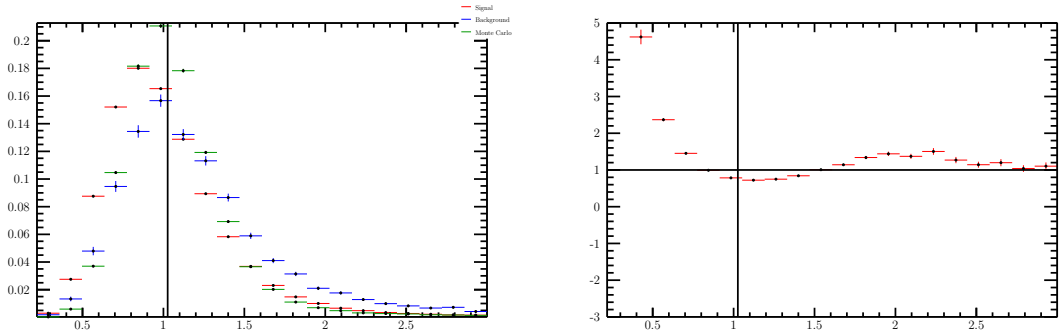

(a) Distributions *(b) Signal data/MC pull*

Figure H.60: Difference in the error corrected yield of 2015 MagDown $D^+ \to K^-\pi^+\pi^+$ when split by Dp_h3_TRACK_CHI2NDOF into two bins, each containing 50% of the simulated events. H.60a shows signal, background and simulated distributions and the pull between signal and simulation is given in H.60b.

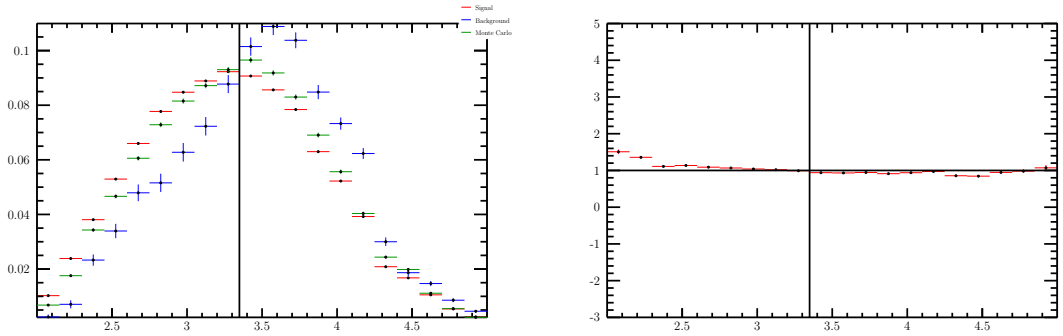

(a) Distributions *(b) Signal data/MC pull*

Figure H.61: Difference in the error corrected yield of 2015 MagDown $D^+ \to K^-\pi^+\pi^+$ when split by Dp_h1_ETA into two bins, each containing 50% of the simulated events. H.61a shows signal, background and simulated distributions and the pull between signal and simulation is given in H.61b.

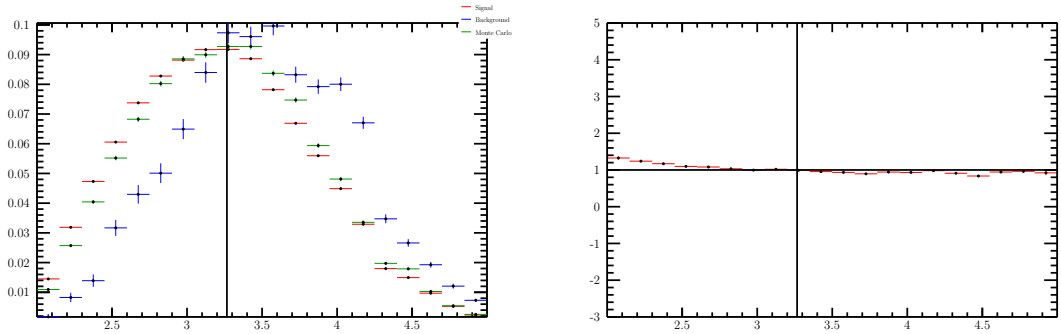

(a) Distributions *(b) Signal data/MC pull*

Figure H.62: Difference in the error corrected yield of 2015 MagDown $D^+ \to K^-\pi^+\pi^+$ when split by Dp_h2_ETA into two bins, each containing 50% of the simulated events. H.62a shows signal, background and simulated distributions and the pull between signal and simulation is given in H.62b.

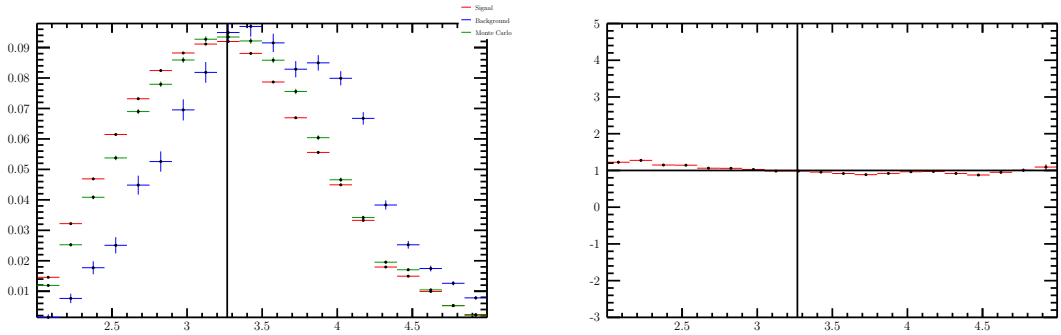

(a) Distributions *(b) Signal data/MC pull*

Figure H.63: Difference in the error corrected yield of 2015 MagDown $D^+ \to K^-\pi^+\pi^+$ when split by Dp_h3_ETA into two bins, each containing 50% of the simulated events. H.63a shows signal, background and simulated distributions and the pull between signal and simulation is given in H.63b.

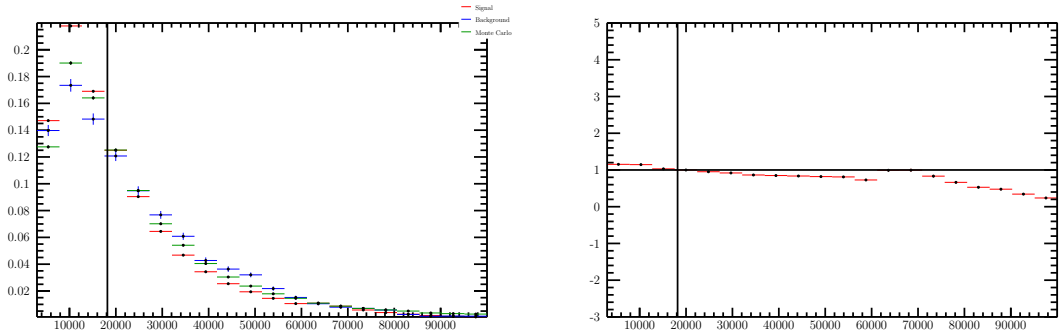

(a) Distributions *(b) Signal data/MC pull*

Figure H.64: Difference in the error corrected yield of 2015 MagDown $D^+ \to K^-\pi^+\pi^+$ when split by Dp_h1_P into two bins, each containing 50% of the simulated events. H.64a shows signal, background and simulated distributions and the pull between signal and simulation is given in H.64b.

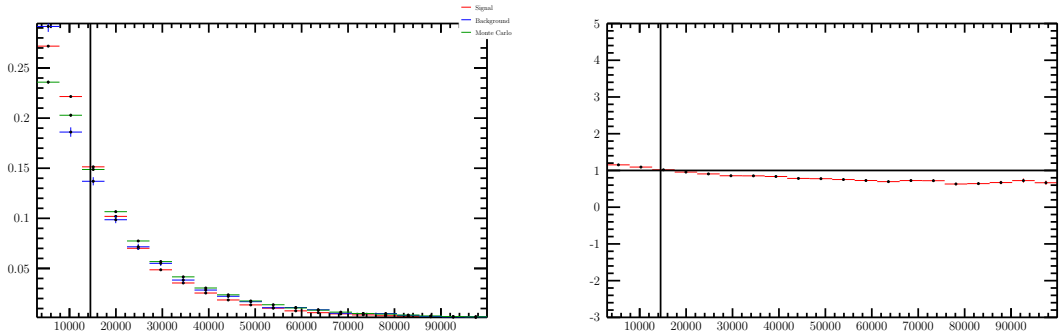

(a) Distributions *(b) Signal data/MC pull*

Figure H.65: Difference in the error corrected yield of 2015 MagDown $D^+ \to K^-\pi^+\pi^+$ when split by Dp_h2_P into two bins, each containing 50% of the simulated events. H.65a shows signal, background and simulated distributions and the pull between signal and simulation is given in H.65b.

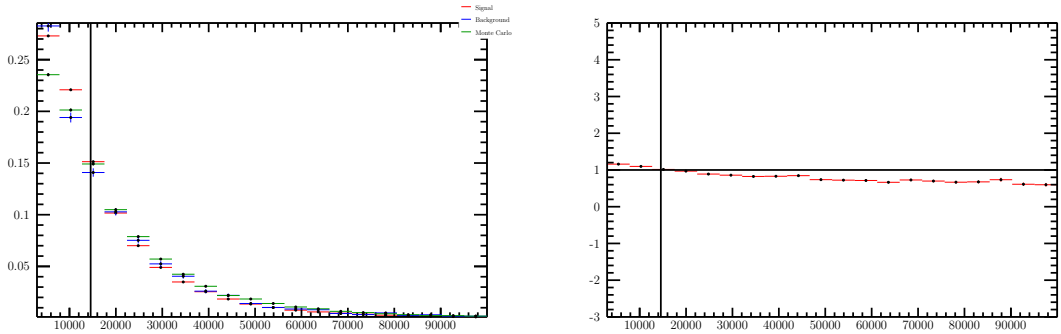

(a) Distributions *(b) Signal data/MC pull*

Figure H.66: Difference in the error corrected yield of 2015 MagDown $D^+ \to K^-\pi^+\pi^+$ when split by Dp_h3_P into two bins, each containing 50% of the simulated events. H.66a shows signal, background and simulated distributions and the pull between signal and simulation is given in H.66b.

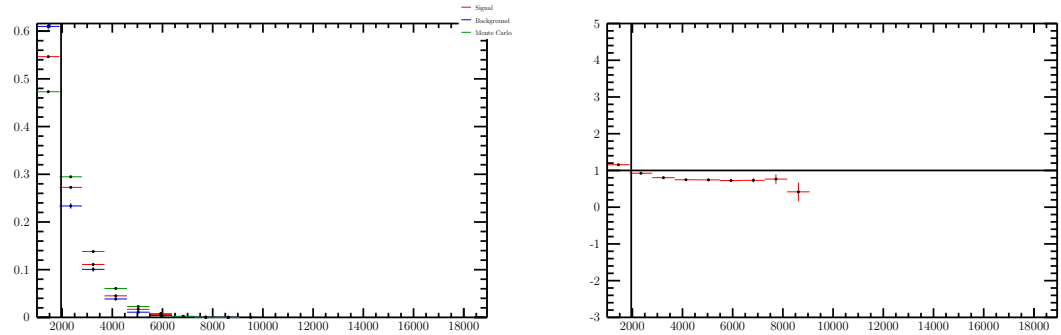

(a) Distributions *(b) Signal data/MC pull*

Figure H.67: Difference in the error corrected yield of 2015 MagDown $D^+ \to K^-\pi^+\pi^+$ when split by Dp_PT_First into two bins, each containing 50% of the simulated events. H.67a shows signal, background and simulated distributions and the pull between signal and simulation is given in H.67b.

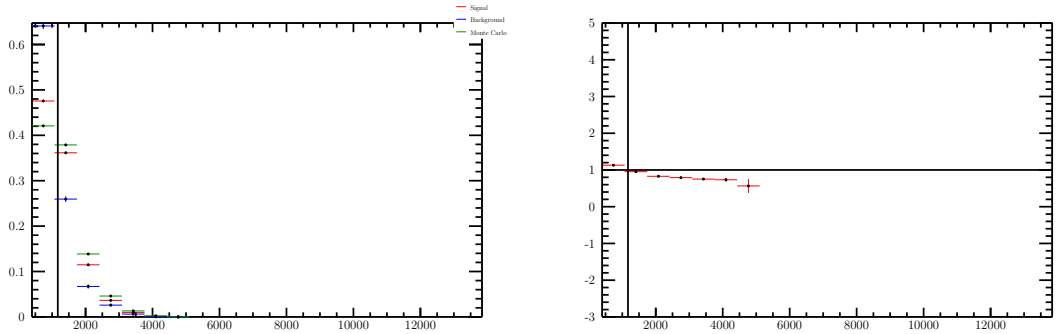

(a) Distributions *(b) Signal data/MC pull*

Figure H.68: Difference in the error corrected yield of 2015 MagDown $D^+ \to K^-\pi^+\pi^+$ when split by Dp_PT_Second into two bins, each containing 50% of the simulated events. H.68a shows signal, background and simulated distributions and the pull between signal and simulation is given in H.68b.

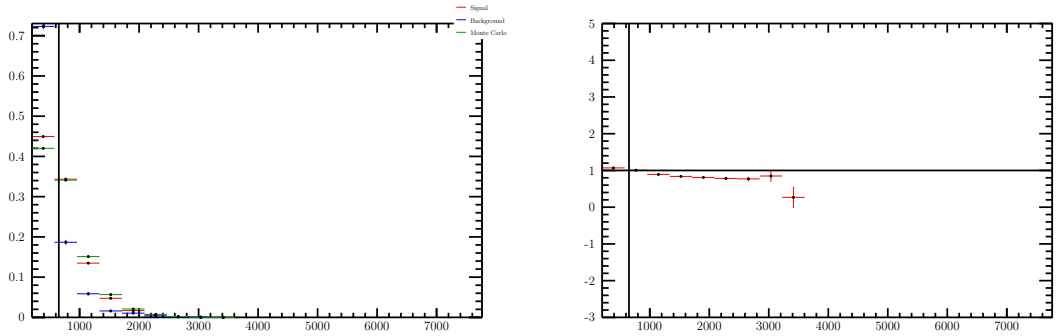

(a) Distributions *(b) Signal data/MC pull*

Figure H.69: Difference in the error corrected yield of 2015 MagDown $D^+ \to K^-\pi^+\pi^+$ when split by Dp_PT_Third into two bins, each containing 50% of the simulated events. H.69a shows signal, background and simulated distributions and the pull between signal and simulation is given in H.69b.

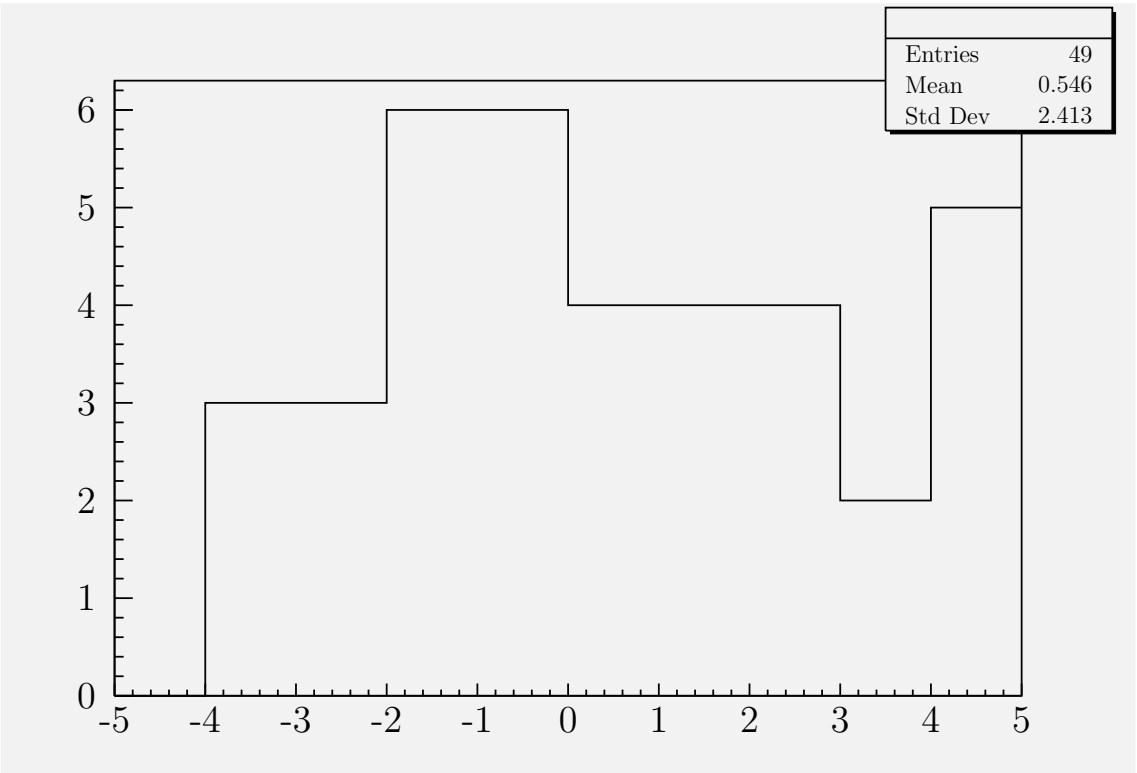

Figure H.70: Histogram of the deviation, in units of the standard deviation, for the Monte Carlo modelling systematic of each kinematic bin in 2015 MagDown $D^+ \to K^-\pi^+\pi^+$ data.

H.6 $D^+ \to K^- K^+ \pi^+$ distributions and result

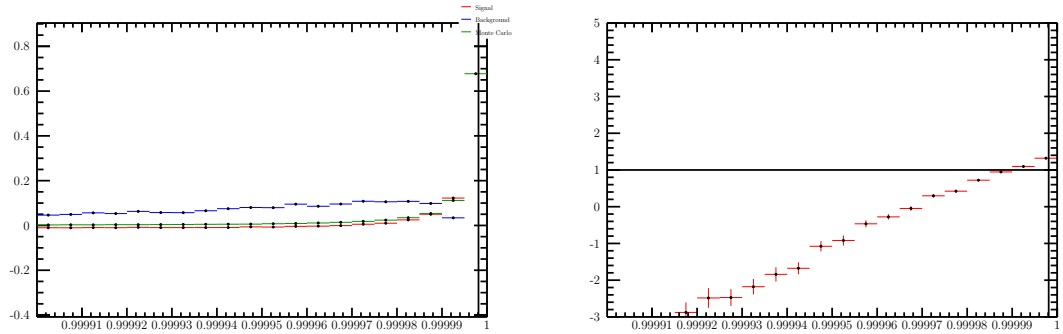

(a) Distributions *(b) Signal data/MC pull*

Figure H.71: Difference in the error corrected yield of 2015 MagDown $D^+ \to K^-K^+\pi^+$ when split by Dp_DIRA_OWNPV into two bins, each containing 50% of the simulated events. H.71a shows signal, background and simulated distributions and the pull between signal and simulation is given in H.71b.

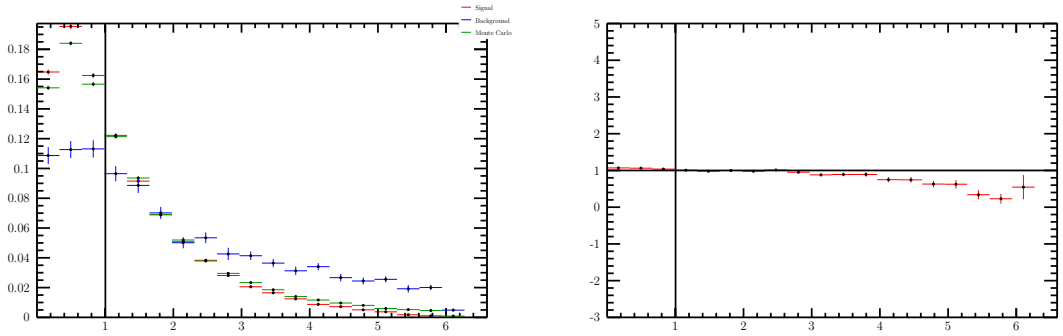

(a) Distributions *(b) Signal data/MC pull*

Figure H.72: Difference in the error corrected yield of 2015 MagDown $D^+ \to K^-K^+\pi^+$ when split by Dp_ENDVERTEX_CHI2/Dp_ENDVERTEX_NDOF into two bins, each containing 50% of the simulated events. H.72a shows signal, background and simulated distributions and the pull between signal and simulation is given in H.72b.

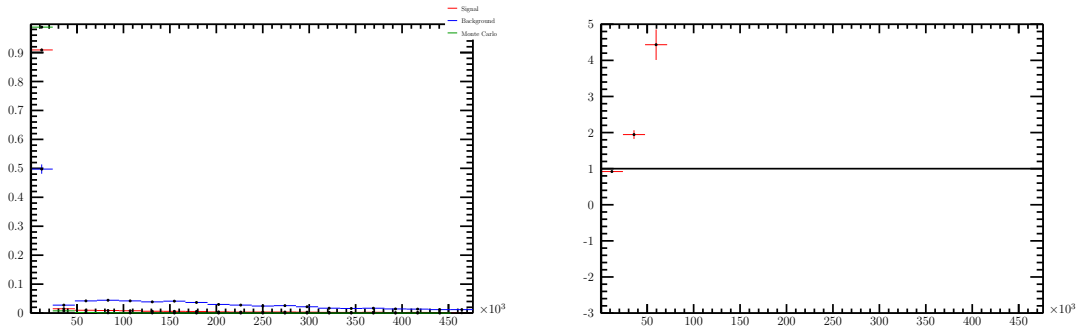

(a) Distributions *(b) Signal data/MC pull*

Figure H.73: Difference in the error corrected yield of 2015 MagDown $D^+ \to K^-K^+\pi^+$ when split by Dp_FDCHI2_OWNPV into two bins, each containing 50% of the simulated events. H.73a shows signal, background and simulated distributions and the pull between signal and simulation is given in H.73b.

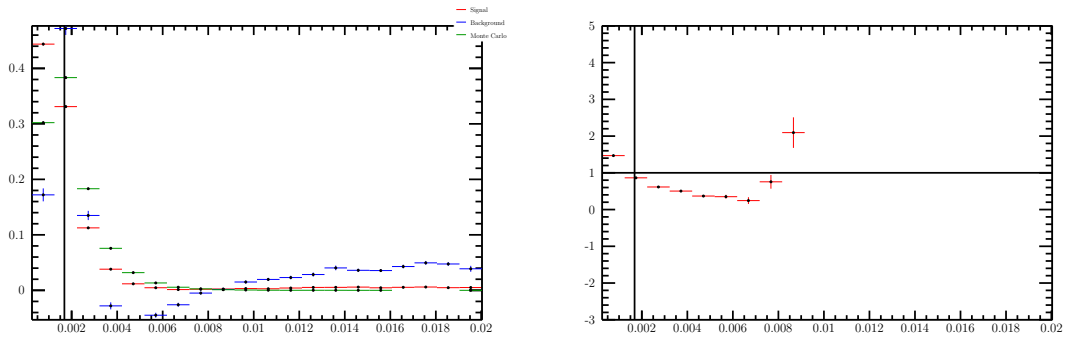

(a) Distributions *(b) Signal data/MC pull*

Figure H.74: Difference in the error corrected yield of 2015 MagDown $D^+ \to K^-K^+\pi^+$ when split by Dp_Loki_BPVLTIME into two bins, each containing 50% of the simulated events. H.74a shows signal, background and simulated distributions and the pull between signal and simulation is given in H.74b.

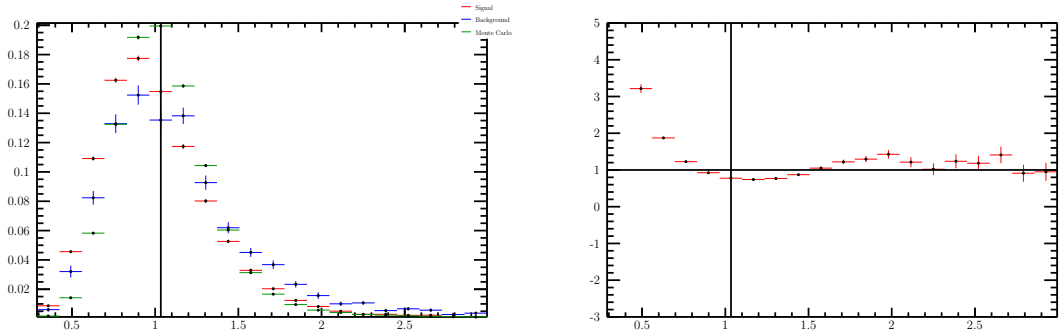

(a) Distributions *(b) Signal data/MC pull*

Figure H.75: Difference in the error corrected yield of 2015 MagDown $D^+ \to K^-K^+\pi^+$ when split by Dp_h1_TRACK_CHI2NDOF into two bins, each containing 50% of the simulated events. H.75a shows signal, background and simulated distributions and the pull between signal and simulation is given in H.75b.

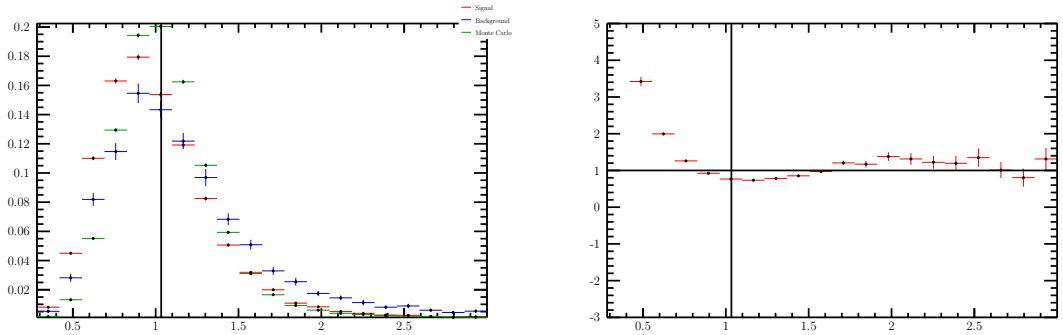

(a) Distributions *(b) Signal data/MC pull*

Figure H.76: Difference in the error corrected yield of 2015 MagDown $D^+ \to K^-K^+\pi^+$ when split by Dp_h2_TRACK_CHI2NDOF into two bins, each containing 50% of the simulated events. H.76a shows signal, background and simulated distributions and the pull between signal and simulation is given in H.76b.

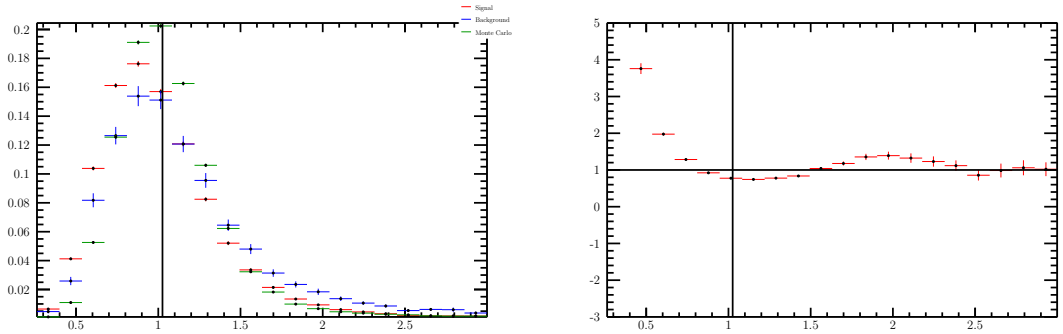

(a) Distributions *(b) Signal data/MC pull*

Figure H.77: Difference in the error corrected yield of 2015 MagDown $D^+ \to K^-K^+\pi^+$ when split by Dp_h3_TRACK_CHI2NDOF into two bins, each containing 50% of the simulated events. H.77a shows signal, background and simulated distributions and the pull between signal and simulation is given in H.77b.

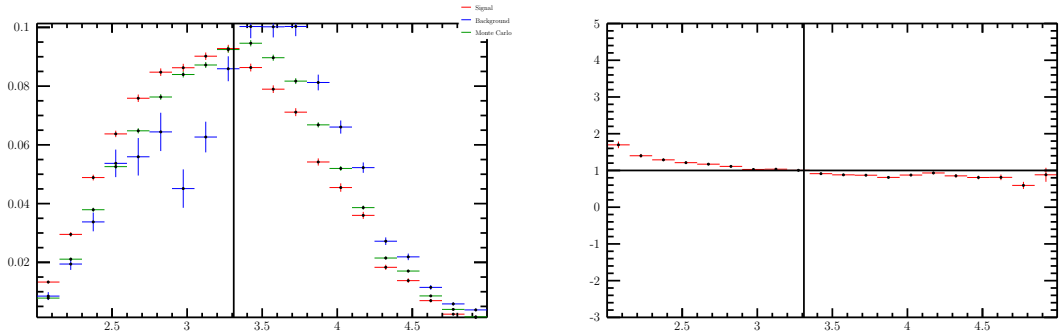

(a) Distributions *(b) Signal data/MC pull*

Figure H.78: Difference in the error corrected yield of 2015 MagDown $D^+ \to K^-K^+\pi^+$ when split by Dp_h1_ETA into two bins, each containing 50% of the simulated events. H.78a shows signal, background and simulated distributions and the pull between signal and simulation is given in H.78b.

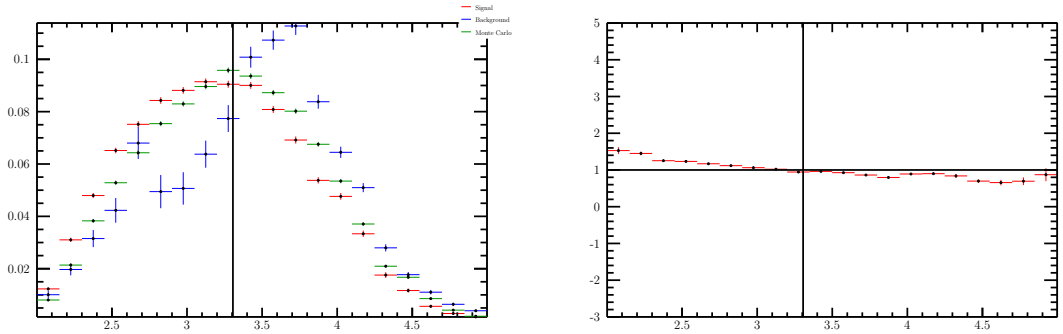

(a) Distributions *(b) Signal data/MC pull*

Figure H.79: Difference in the error corrected yield of 2015 MagDown $D^+ \to K^-K^+\pi^+$ when split by Dp_h2_ETA into two bins, each containing 50% of the simulated events. H.79a shows signal, background and simulated distributions and the pull between signal and simulation is given in H.79b.

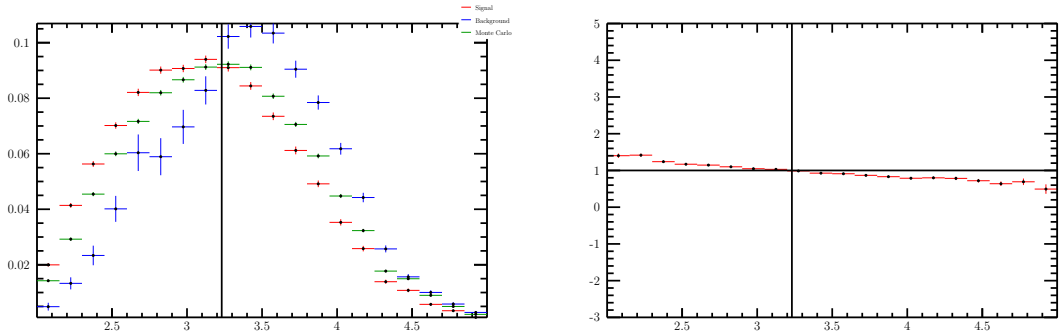

(a) Distributions *(b) Signal data/MC pull*

Figure H.80: Difference in the error corrected yield of 2015 MagDown $D^+ \to K^-K^+\pi^+$ when split by Dp_h3_ETA into two bins, each containing 50% of the simulated events. H.80a shows signal, background and simulated distributions and the pull between signal and simulation is given in H.80b.

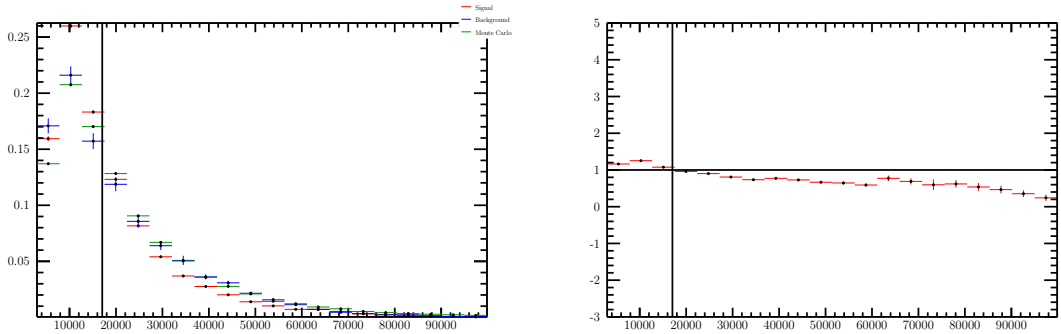

(a) Distributions *(b) Signal data/MC pull*

Figure H.81: Difference in the error corrected yield of 2015 MagDown $D^+ \to K^-K^+\pi^+$ when split by Dp_h1_P into two bins, each containing 50% of the simulated events. H.81a shows signal, background and simulated distributions and the pull between signal and simulation is given in H.81b.

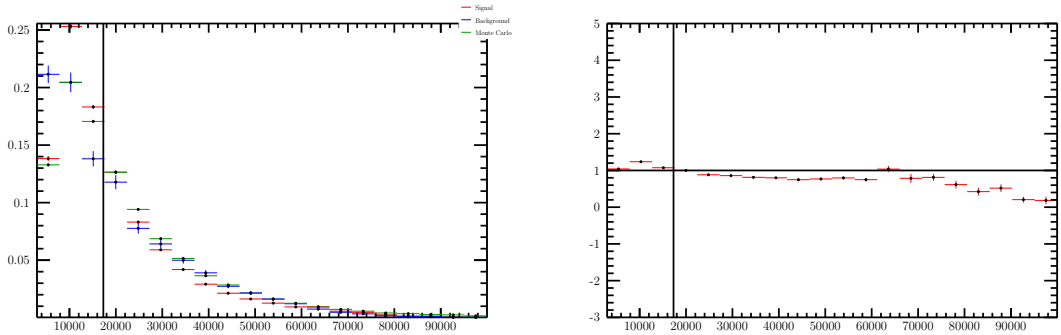

(a) Distributions *(b) Signal data/MC pull*

Figure H.82: Difference in the error corrected yield of 2015 MagDown $D^+ \to K^-K^+\pi^+$ when split by Dp_h2_P into two bins, each containing 50% of the simulated events. H.82a shows signal, background and simulated distributions and the pull between signal and simulation is given in H.82b.

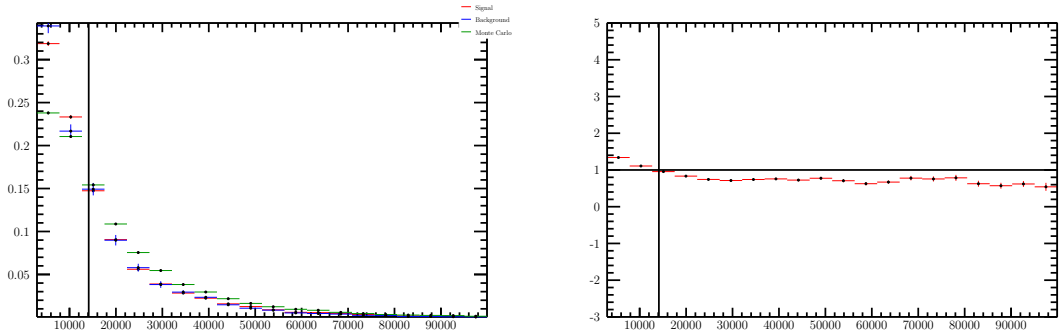

(a) Distributions *(b) Signal data/MC pull*

Figure H.83: Difference in the error corrected yield of 2015 MagDown $D^+ \to K^-K^+\pi^+$ when split by Dp_h3_P into two bins, each containing 50% of the simulated events. H.83a shows signal, background and simulated distributions and the pull between signal and simulation is given in H.83b.

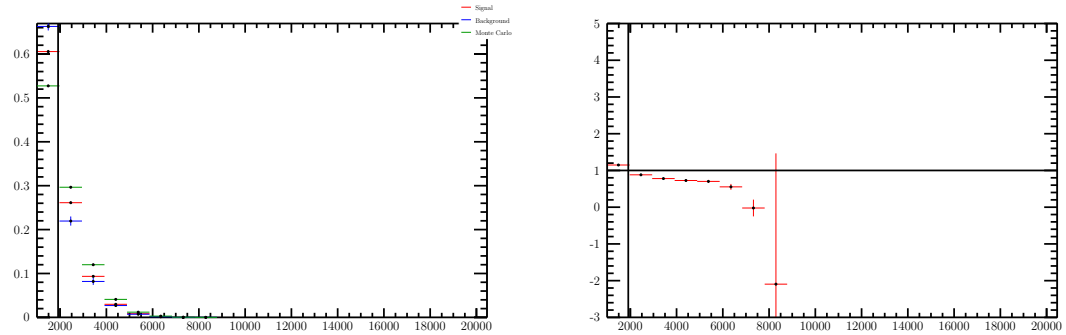

(a) Distributions *(b) Signal data/MC pull*

Figure H.84: Difference in the error corrected yield of 2015 MagDown $D^+ \to K^-K^+\pi^+$ when split by Dp_PT_First into two bins, each containing 50% of the simulated events. H.84a shows signal, background and simulated distributions and the pull between signal and simulation is given in H.84b.

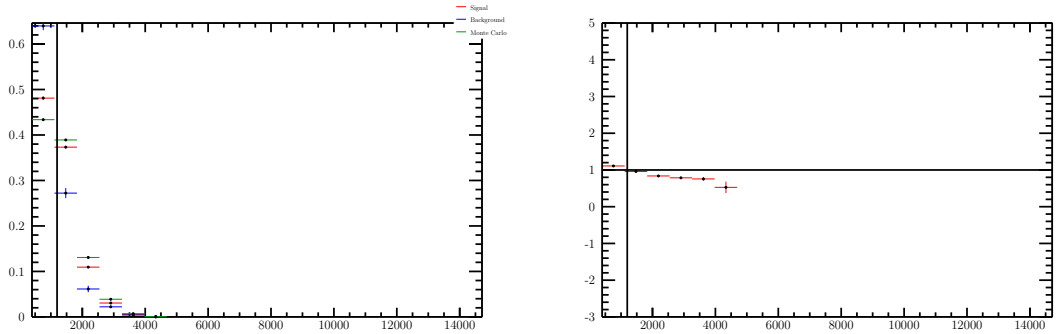

(a) Distributions *(b) Signal data/MC pull*

Figure H.85: Difference in the error corrected yield of 2015 MagDown $D^+ \to K^-K^+\pi^+$ when split by Dp_PT_Second into two bins, each containing 50% of the simulated events. H.85a shows signal, background and simulated distributions and the pull between signal and simulation is given in H.85b.

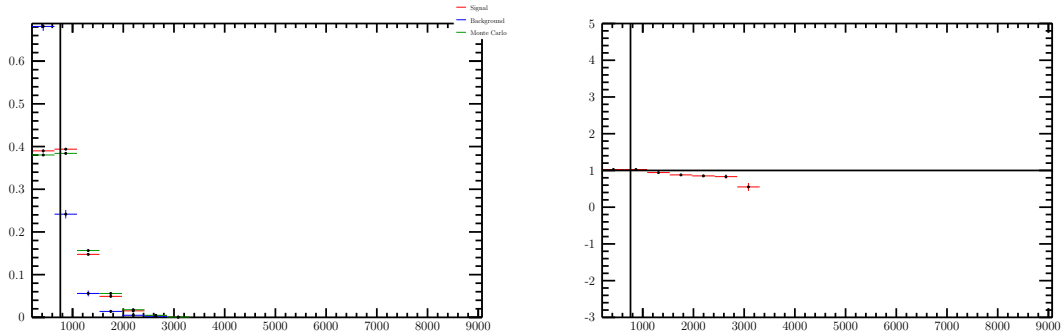

(a) Distributions *(b) Signal data/MC pull*

Figure H.86: Difference in the error corrected yield of 2015 MagDown $D^+ \to K^-K^+\pi^+$ when split by Dp_PT_Third into two bins, each containing 50% of the simulated events. H.86a shows signal, background and simulated distributions and the pull between signal and simulation is given in H.86b.

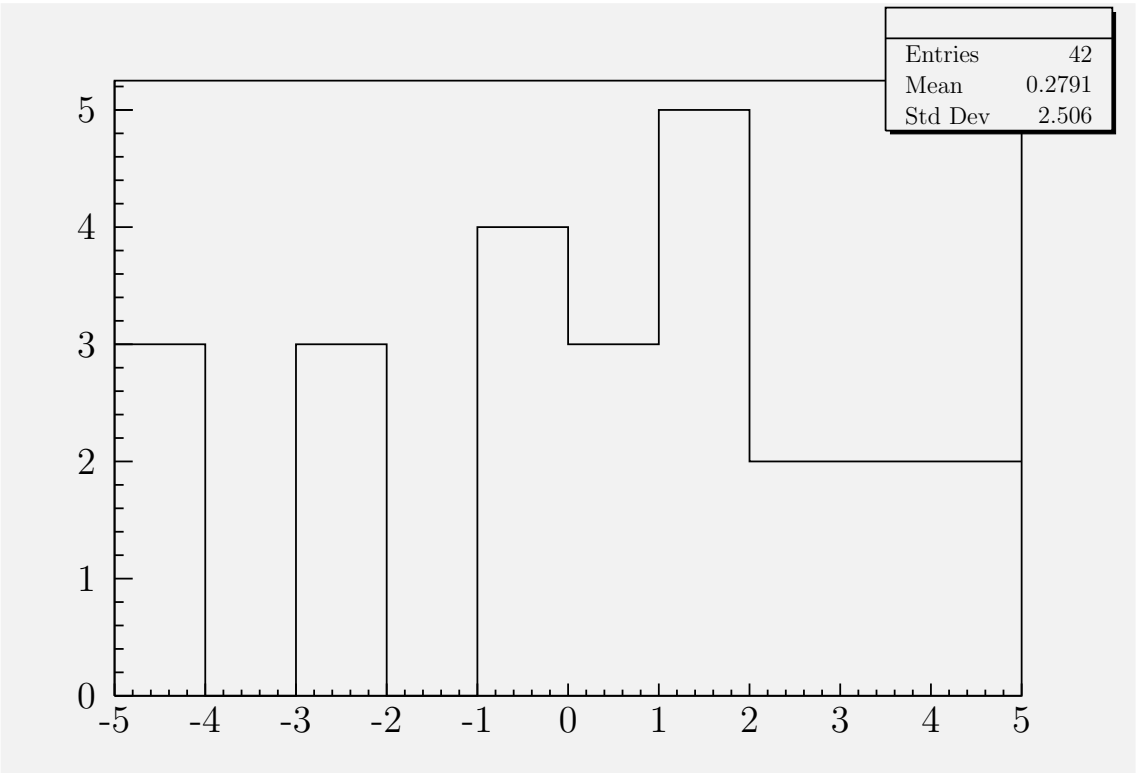

Figure H.87: Histogram of the deviation, in units of the standard deviation, for the Monte Carlo modelling systematic of each kinematic bin in 2015 MagDown $D^+ \to K^-K^+\pi^+$ data.

H.7 $D_s^+ \to K^- K^+ \pi^+$ distributions and result

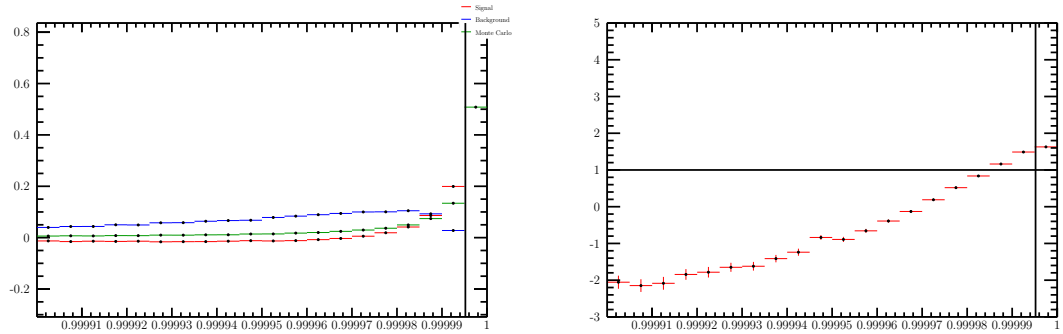

(a) Distributions *(b) Signal data/MC pull*

Figure H.88: Difference in the error corrected yield of 2015 MagDown $D_s^+ \to K^-K^+\pi^+$ when split by Ds_DIRA_OWNPV into two bins, each containing 50% of the simulated events. H.88a shows signal, background and simulated distributions and the pull between signal and simulation is given in H.88b.

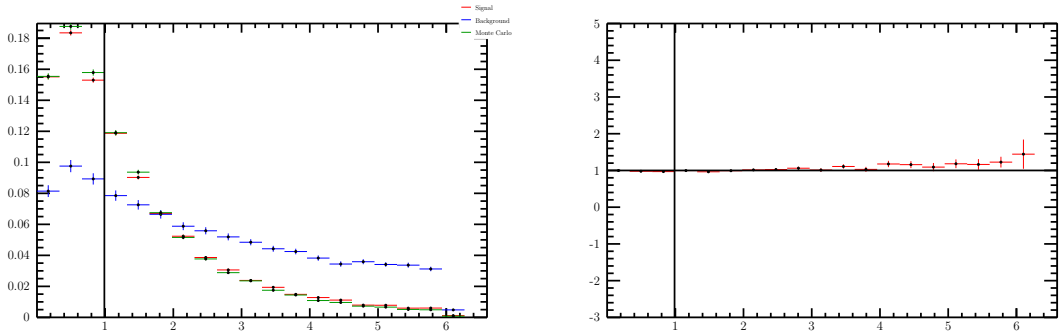

(a) Distributions *(b) Signal data/MC pull*

Figure H.89: Difference in the error corrected yield of 2015 MagDown $D_s^+ \to K^-K^+\pi^+$ when split by Ds_ENDVERTEX_CHI2/Ds_ENDVERTEX_NDOF into two bins, each containing 50% of the simulated events. H.89a shows signal, background and simulated distributions and the pull between signal and simulation is given in H.89b.

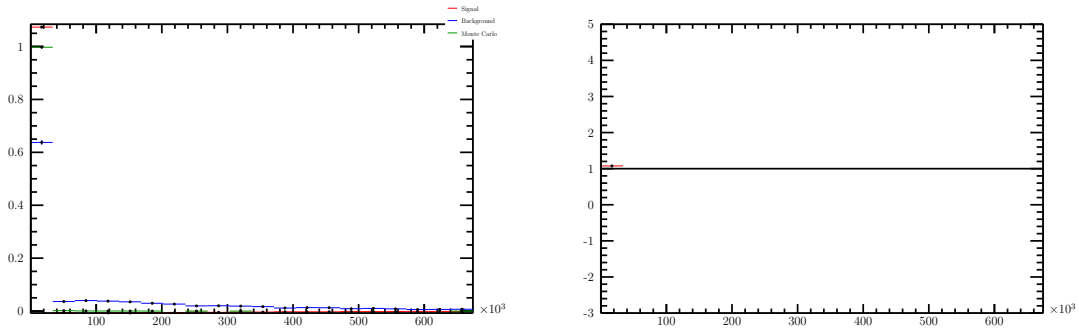

(a) Distributions *(b) Signal data/MC pull*

Figure H.90: Difference in the error corrected yield of 2015 MagDown $D_s^+ \to K^-K^+\pi^+$ when split by Ds_FDCHI2_OWNPV into two bins, each containing 50% of the simulated events. H.90a shows signal, background and simulated distributions and the pull between signal and simulation is given in H.90b.

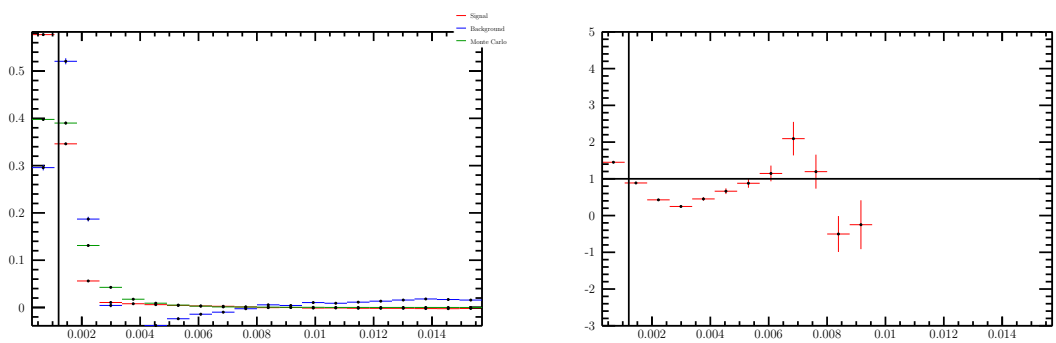

(a) Distributions *(b) Signal data/MC pull*

Figure H.91: Difference in the error corrected yield of 2015 MagDown $D_s^+ \to K^-K^+\pi^+$ when split by Ds_Loki_BPVLTIME into two bins, each containing 50% of the simulated events. H.91a shows signal, background and simulated distributions and the pull between signal and simulation is given in H.91b.

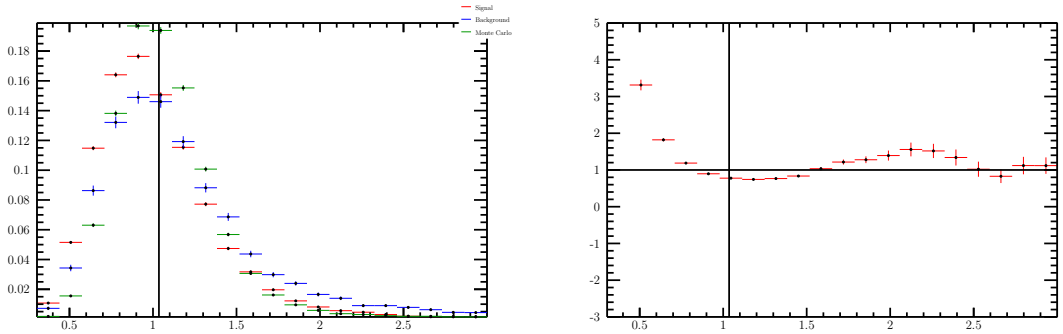

(a) Distributions *(b) Signal data/MC pull*

Figure H.92: Difference in the error corrected yield of 2015 MagDown $D_s^+ \to K^-K^+\pi^+$ when split by Ds_h1_TRACK_CHI2NDOF into two bins, each containing 50% of the simulated events. H.92a shows signal, background and simulated distributions and the pull between signal and simulation is given in H.92b.

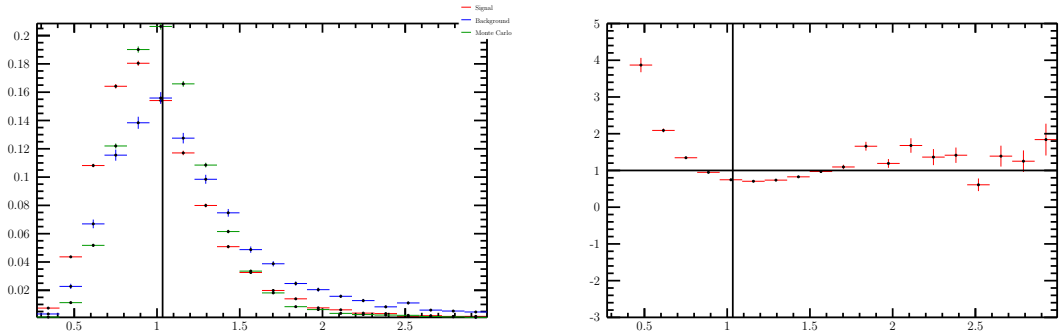

(a) Distributions *(b) Signal data/MC pull*

Figure H.93: Difference in the error corrected yield of 2015 MagDown $D_s^+ \to K^-K^+\pi^+$ when split by Ds_h2_TRACK_CHI2NDOF into two bins, each containing 50% of the simulated events. H.93a shows signal, background and simulated distributions and the pull between signal and simulation is given in H.93b.

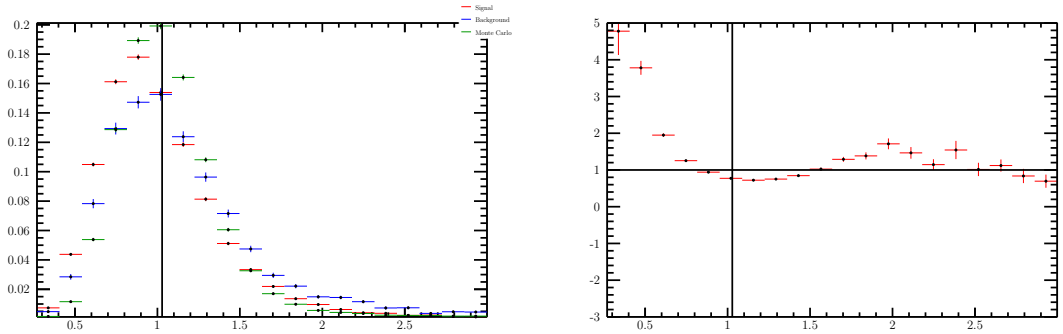

(a) Distributions *(b) Signal data/MC pull*

Figure H.94: Difference in the error corrected yield of 2015 MagDown $D_s^+ \to K^-K^+\pi^+$ when split by Ds_h3_TRACK_CHI2NDOF into two bins, each containing 50% of the simulated events. H.94a shows signal, background and simulated distributions and the pull between signal and simulation is given in H.94b.

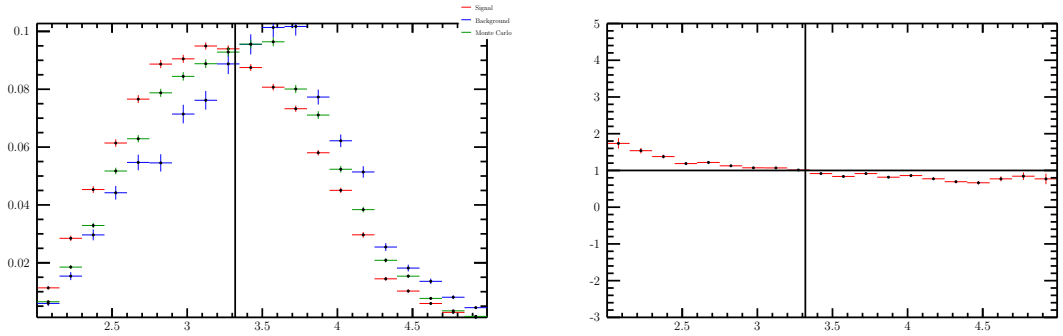

(a) Distributions *(b) Signal data/MC pull*

Figure H.95: Difference in the error corrected yield of 2015 MagDown $D_s^+ \to K^-K^+\pi^+$ when split by Ds_h1_ETA into two bins, each containing 50% of the simulated events. H.95a shows signal, background and simulated distributions and the pull between signal and simulation is given in H.95b.

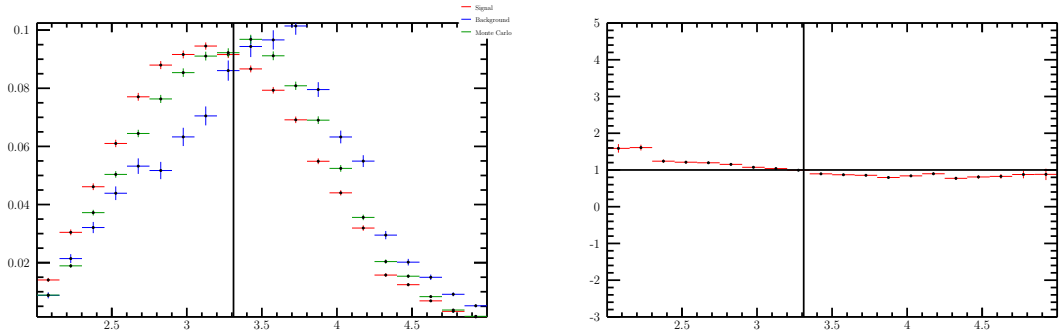

(a) Distributions *(b) Signal data/MC pull*

Figure H.96: Difference in the error corrected yield of 2015 MagDown $D_s^+ \to K^-K^+\pi^+$ when split by Ds_h2_ETA into two bins, each containing 50% of the simulated events. H.96a shows signal, background and simulated distributions and the pull between signal and simulation is given in H.96b.

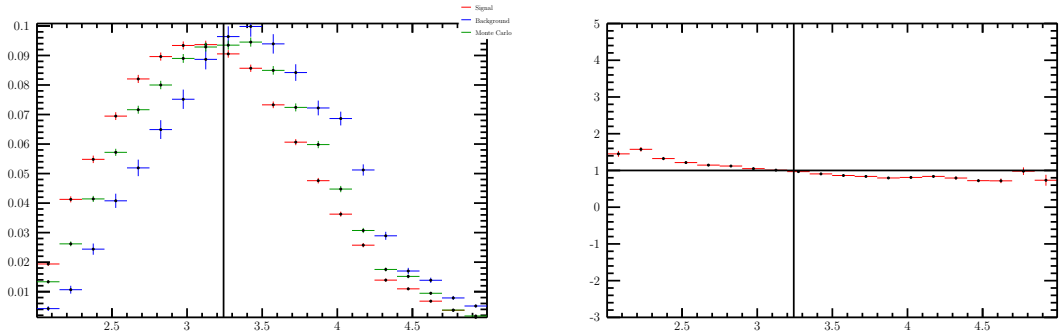

(a) Distributions *(b) Signal data/MC pull*

Figure H.97: Difference in the error corrected yield of 2015 MagDown $D_s^+ \to K^-K^+\pi^+$ when split by Ds_h3_ETA into two bins, each containing 50% of the simulated events. H.97a shows signal, background and simulated distributions and the pull between signal and simulation is given in H.97b.

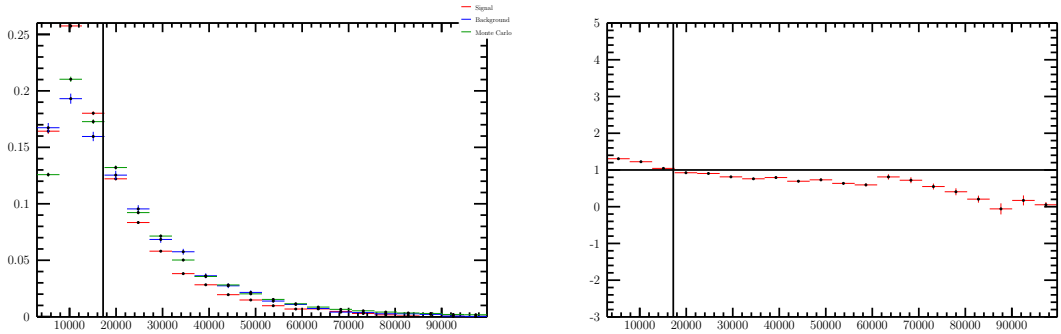

(a) Distributions *(b) Signal data/MC pull*

Figure H.98: Difference in the error corrected yield of 2015 MagDown $D_s^+ \to K^-K^+\pi^+$ when split by Ds_h1_P into two bins, each containing 50% of the simulated events. H.98a shows signal, background and simulated distributions and the pull between signal and simulation is given in H.98b.

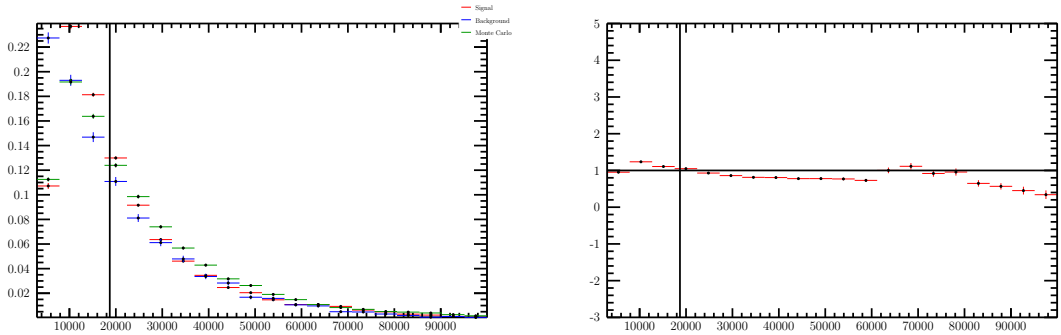

(a) Distributions *(b) Signal data/MC pull*

Figure H.99: Difference in the error corrected yield of 2015 MagDown $D_s^+ \to K^-K^+\pi^+$ when split by Ds_h2_P into two bins, each containing 50% of the simulated events. H.99a shows signal, background and simulated distributions and the pull between signal and simulation is given in H.99b.

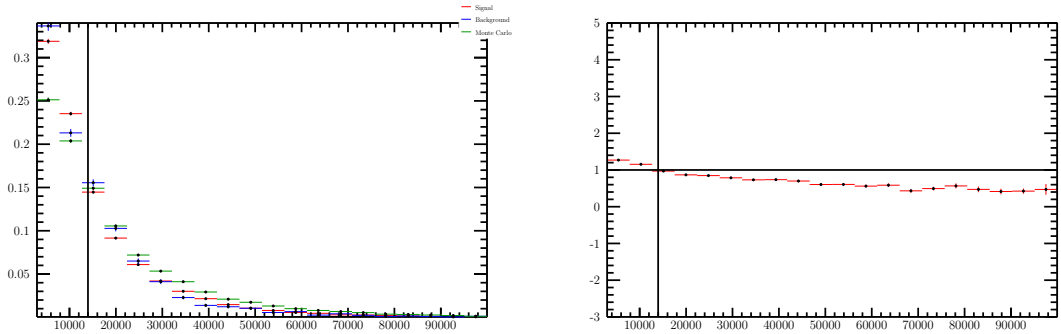

(a) Distributions *(b) Signal data/MC pull*

Figure H.100: Difference in the error corrected yield of 2015 MagDown $D_s^+ \to K^-K^+\pi^+$ when split by Ds_h3_P into two bins, each containing 50% of the simulated events. H.100a shows signal, background and simulated distributions and the pull between signal and simulation is given in H.100b.

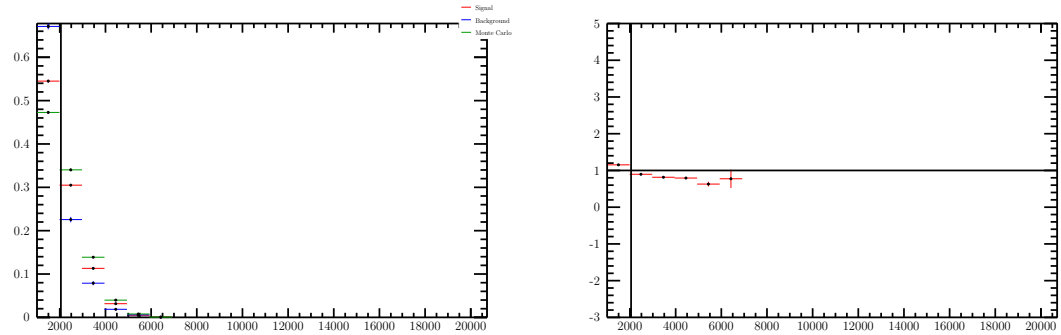

(a) Distributions *(b) Signal data/MC pull*

Figure H.101: Difference in the error corrected yield of 2015 MagDown $D_s^+ \to K^-K^+\pi^+$ when split by Ds_PT_First into two bins, each containing 50% of the simulated events. H.101a shows signal, background and simulated distributions and the pull between signal and simulation is given in H.101b.

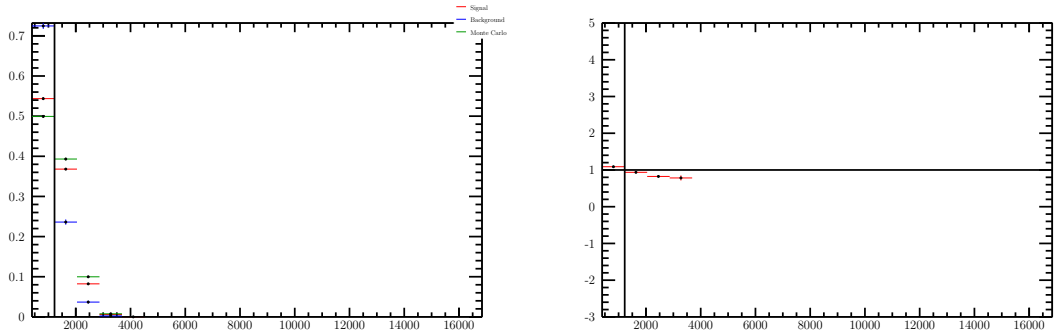

(a) Distributions *(b) Signal data/MC pull*

Figure H.102: Difference in the error corrected yield of 2015 MagDown $D_s^+ \to K^-K^+\pi^+$ when split by Ds_PT_Second into two bins, each containing 50% of the simulated events. H.102a shows signal, background and simulated distributions and the pull between signal and simulation is given in H.102b.

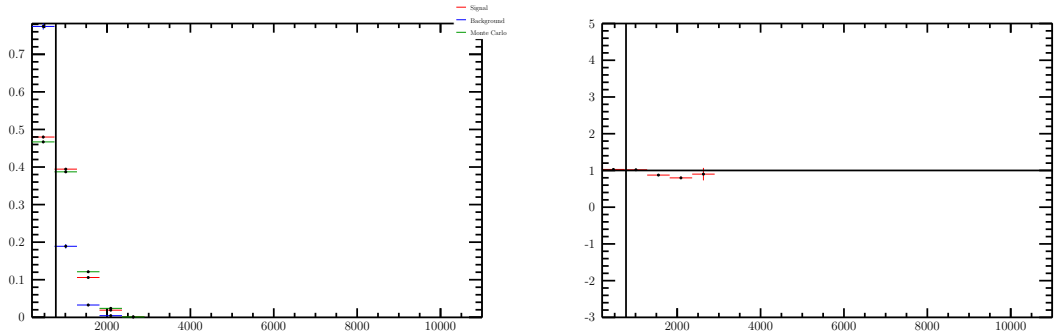

(a) Distributions *(b) Signal data/MC pull*

Figure H.103: Difference in the error corrected yield of 2015 MagDown $D_s^+ \to K^-K^+\pi^+$ when split by Ds_PT_Third into two bins, each containing 50% of the simulated events. H.103a shows signal, background and simulated distributions and the pull between signal and simulation is given in H.103b.

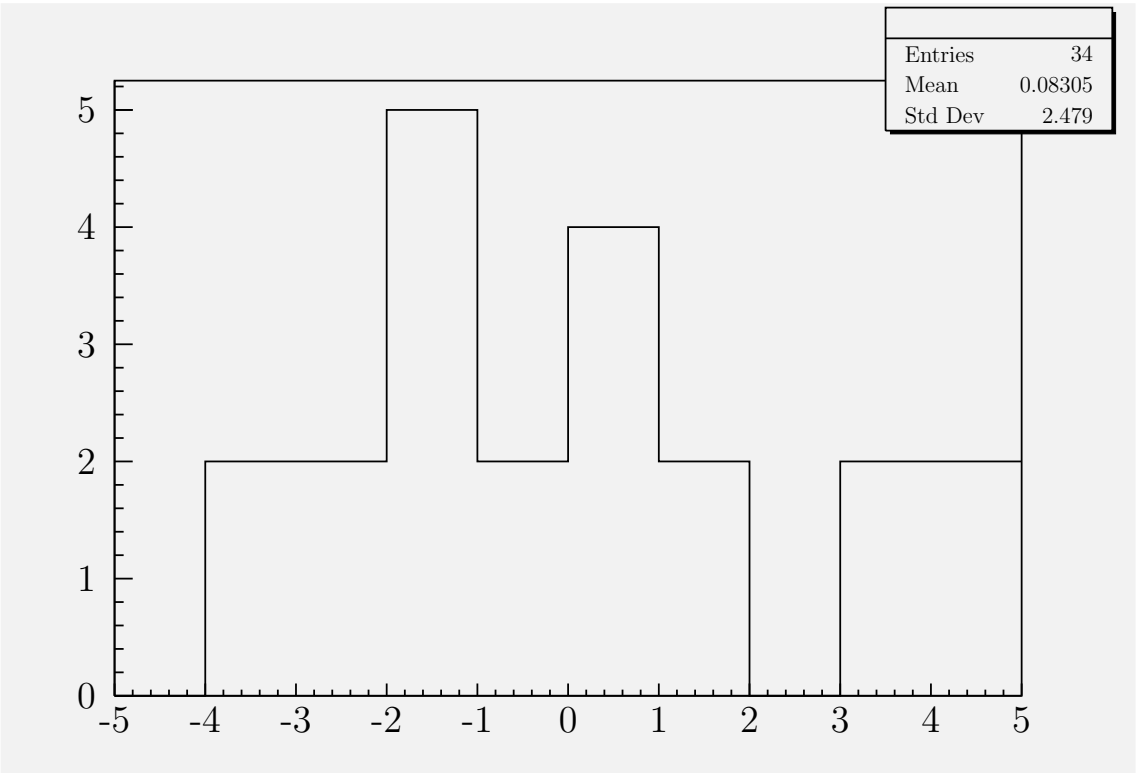

Figure H.104: Histogram of the deviation, in units of the standard deviation, for the Monte Carlo modelling systematic of each kinematic bin in 2015 MagDown $D_s^+ \to K^-K^+\pi^+$ data.

H.8 $D_s^+ \to \phi\pi^+$ distributions and result

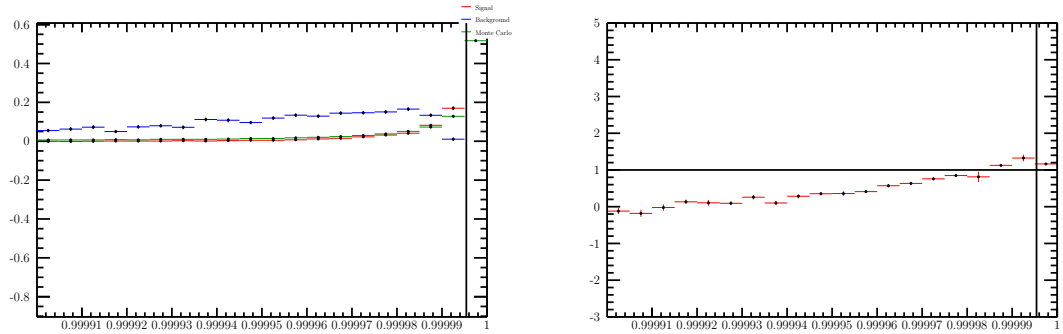

(a) Distributions *(b) Signal data/MC pull*

Figure H.105: Difference in the error corrected yield of 2015 MagDown $D_s^+ \to \phi\pi^+$ when split by Ds_DIRA_OWNPV into two bins, each containing 50% of the simulated events. H.105a shows signal, background and simulated distributions and the pull between signal and simulation is given in H.105b.

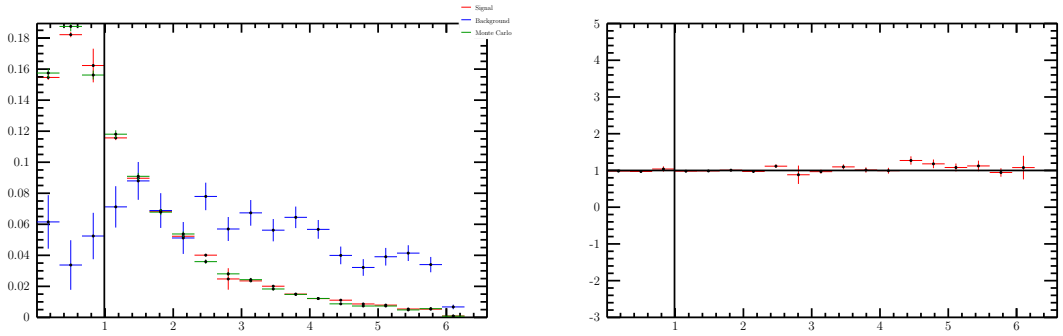

(a) Distributions *(b) Signal data/MC pull*

Figure H.106: Difference in the error corrected yield of 2015 MagDown $D_s^+ \to \phi\pi^+$ when split by Ds_ENDVERTEX_CHI2/Ds_ENDVERTEX_NDOF into two bins, each containing 50% of the simulated events. H.106a shows signal, background and simulated distributions and the pull between signal and simulation is given in H.106b.

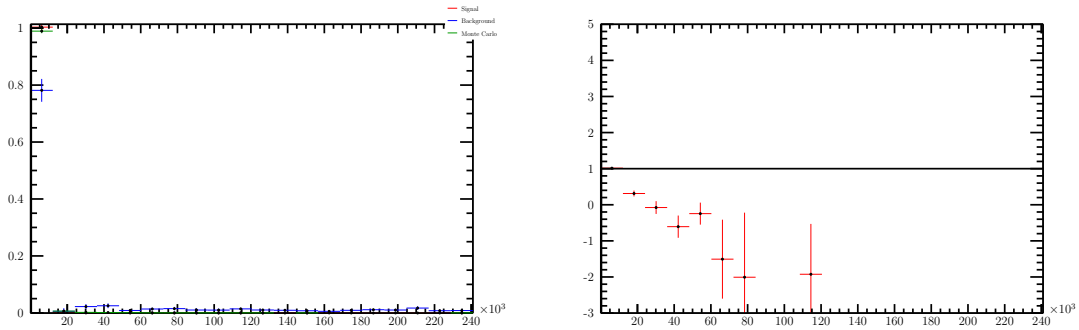

(a) Distributions *(b) Signal data/MC pull*

Figure H.107: Difference in the error corrected yield of 2015 MagDown $D_s^+ \to \phi\pi^+$ when split by Ds_FDCHI2_OWNPV into two bins, each containing 50% of the simulated events. H.107a shows signal, background and simulated distributions and the pull between signal and simulation is given in H.107b.

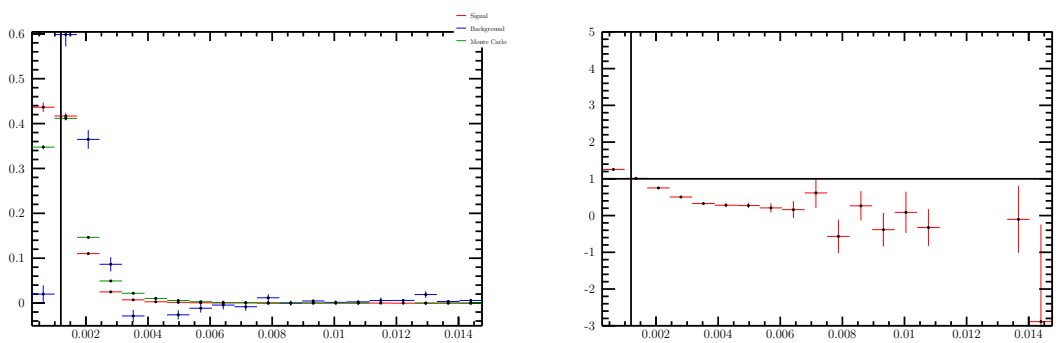

(a) Distributions *(b) Signal data/MC pull*

Figure H.108: Difference in the error corrected yield of 2015 MagDown $D_s^+ \to \phi\pi^+$ when split by Ds_Loki_BPVLTIME into two bins, each containing 50% of the simulated events. H.108a shows signal, background and simulated distributions and the pull between signal and simulation is given in H.108b.

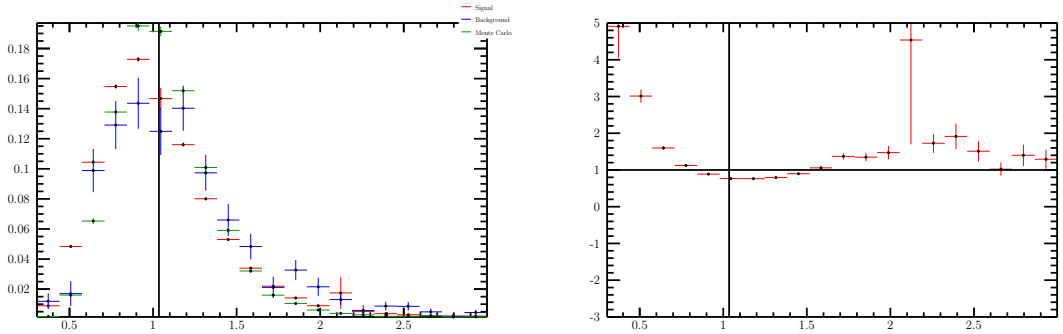

(a) Distributions *(b) Signal data/MC pull*

Figure H.109: Difference in the error corrected yield of 2015 MagDown $D_s^+ \to \phi\pi^+$ when split by Ds_h1_TRACK_CHI2NDOF into two bins, each containing 50% of the simulated events. H.109a shows signal, background and simulated distributions and the pull between signal and simulation is given in H.109b.

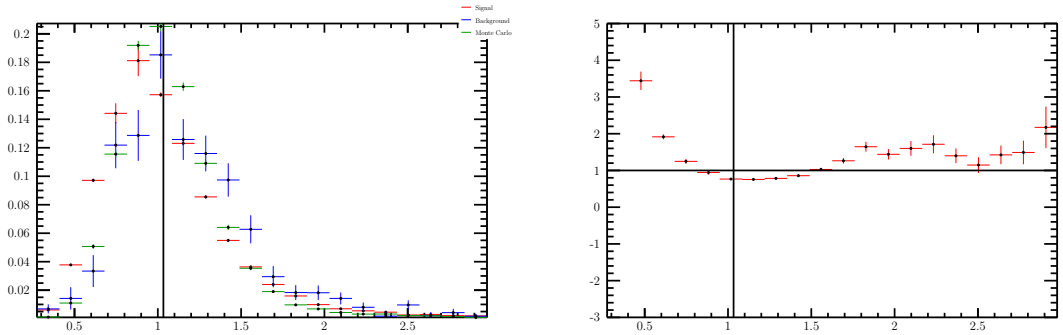

(a) Distributions *(b) Signal data/MC pull*

Figure H.110: Difference in the error corrected yield of 2015 MagDown $D_s^+ \to \phi\pi^+$ when split by Ds_h2_TRACK_CHI2NDOF into two bins, each containing 50% of the simulated events. H.110a shows signal, background and simulated distributions and the pull between signal and simulation is given in H.110b.

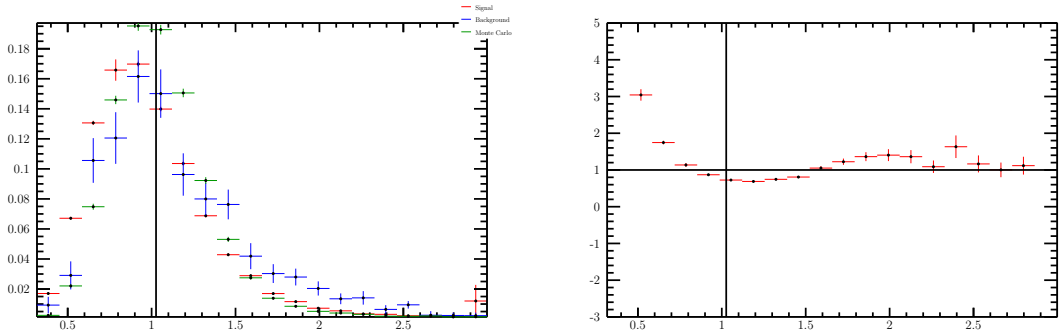

(a) Distributions *(b) Signal data/MC pull*

Figure H.111: Difference in the error corrected yield of 2015 MagDown $D_s^+ \to \phi\pi^+$ when split by Ds_h3_TRACK_CHI2NDOF into two bins, each containing 50% of the simulated events. H.111a shows signal, background and simulated distributions and the pull between signal and simulation is given in H.111b.

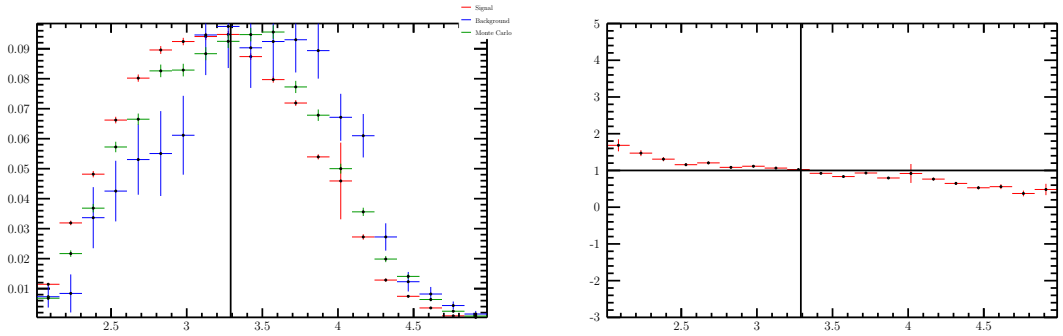

(a) Distributions *(b) Signal data/MC pull*

Figure H.112: Difference in the error corrected yield of 2015 MagDown $D_s^+ \to \phi\pi^+$ when split by Ds_h1_ETA into two bins, each containing 50% of the simulated events. H.112a shows signal, background and simulated distributions and the pull between signal and simulation is given in H.112b.

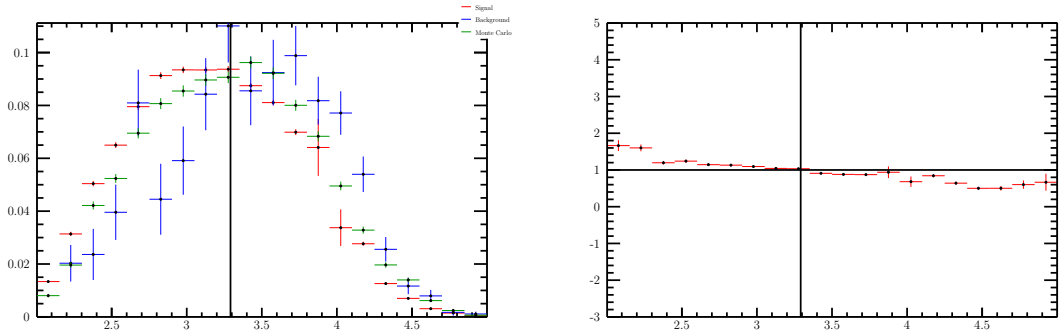

(a) Distributions *(b) Signal data/MC pull*

Figure H.113: Difference in the error corrected yield of 2015 MagDown $D_s^+ \to \phi\pi^+$ when split by Ds_h2_ETA into two bins, each containing 50% of the simulated events. H.113a shows signal, background and simulated distributions and the pull between signal and simulation is given in H.113b.

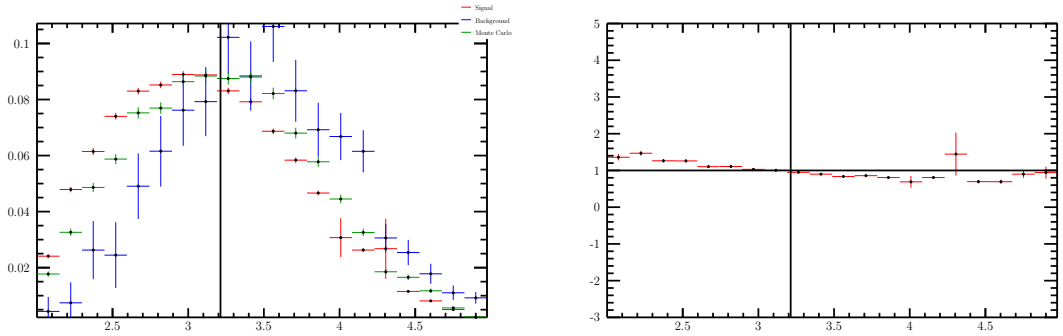

(a) Distributions *(b) Signal data/MC pull*

Figure H.114: Difference in the error corrected yield of 2015 MagDown $D_s^+ \to \phi\pi^+$ when split by Ds_h3_ETA into two bins, each containing 50% of the simulated events. H.114a shows signal, background and simulated distributions and the pull between signal and simulation is given in H.114b.

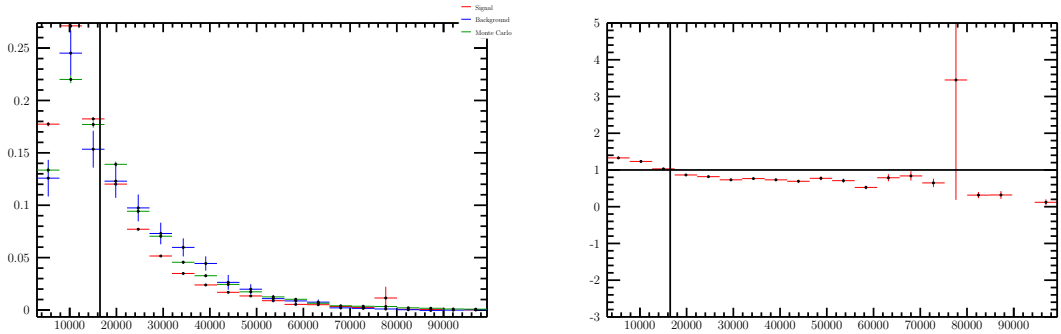

(a) Distributions *(b) Signal data/MC pull*

Figure H.115: Difference in the error corrected yield of 2015 MagDown $D_s^+ \to \phi\pi^+$ when split by Ds_h1_P into two bins, each containing 50% of the simulated events. H.115a shows signal, background and simulated distributions and the pull between signal and simulation is given in H.115b.

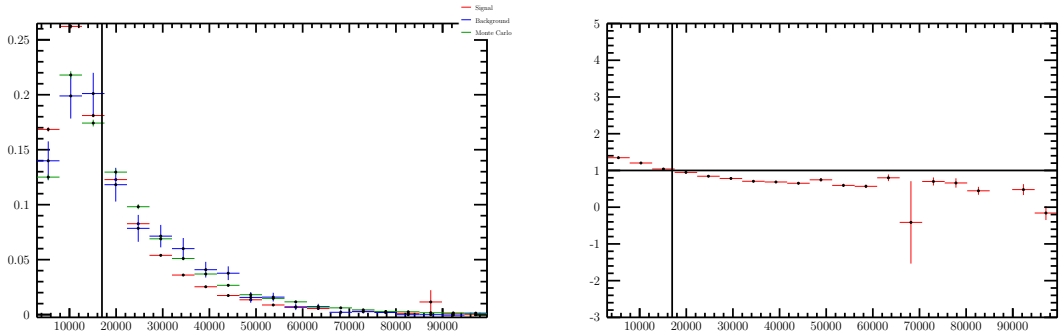

(a) Distributions *(b) Signal data/MC pull*

Figure H.116: Difference in the error corrected yield of 2015 MagDown $D_s^+ \to \phi\pi^+$ when split by Ds_h2_P into two bins, each containing 50% of the simulated events. H.116a shows signal, background and simulated distributions and the pull between signal and simulation is given in H.116b.

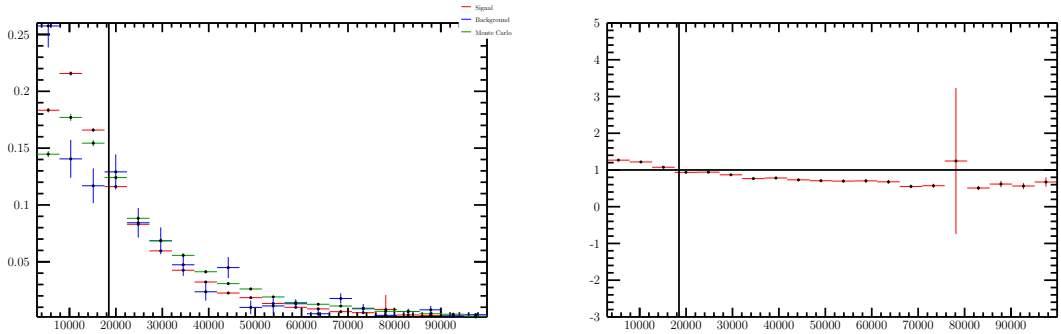

(a) Distributions *(b) Signal data/MC pull*

Figure H.117: Difference in the error corrected yield of 2015 MagDown $D_s^+ \to \phi\pi^+$ when split by Ds_h3_P into two bins, each containing 50% of the simulated events. H.117a shows signal, background and simulated distributions and the pull between signal and simulation is given in H.117b.

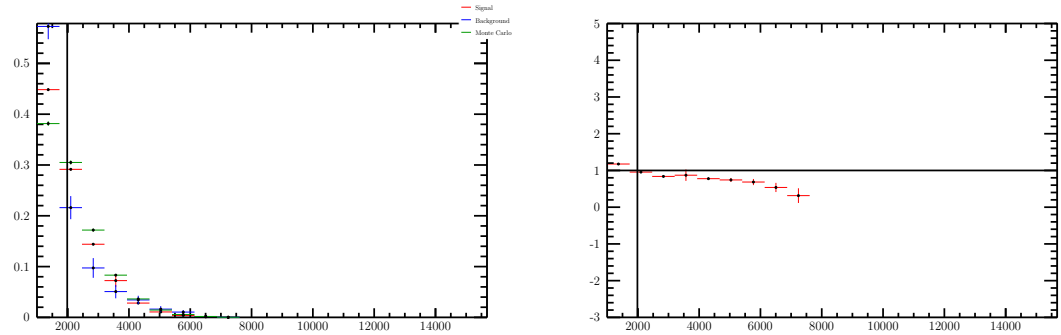

(a) Distributions *(b) Signal data/MC pull*

Figure H.118: Difference in the error corrected yield of 2015 MagDown $D_s^+ \to \phi\pi^+$ when split by Ds_PT_First into two bins, each containing 50% of the simulated events. H.118a shows signal, background and simulated distributions and the pull between signal and simulation is given in H.118b.

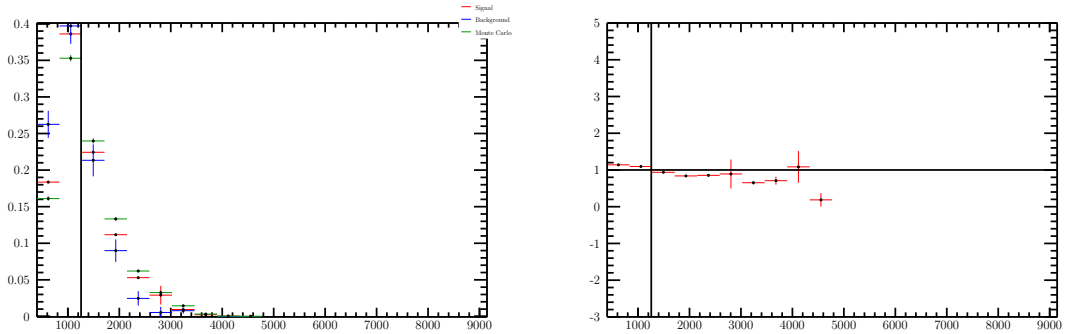

(a) Distributions *(b) Signal data/MC pull*

Figure H.119: Difference in the error corrected yield of 2015 MagDown $D_s^+ \to \phi\pi^+$ when split by Ds_PT_Second into two bins, each containing 50% of the simulated events. H.119a shows signal, background and simulated distributions and the pull between signal and simulation is given in H.119b.

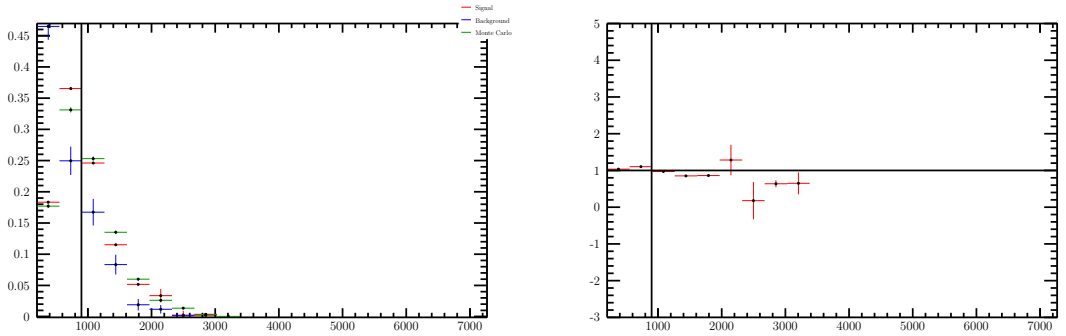

(a) Distributions *(b) Signal data/MC pull*

Figure H.120: Difference in the error corrected yield of 2015 MagDown $D_s^+ \to \phi\pi^+$ when split by Ds_PT_Third into two bins, each containing 50% of the simulated events. H.120a shows signal, background and simulated distributions and the pull between signal and simulation is given in H.120b.

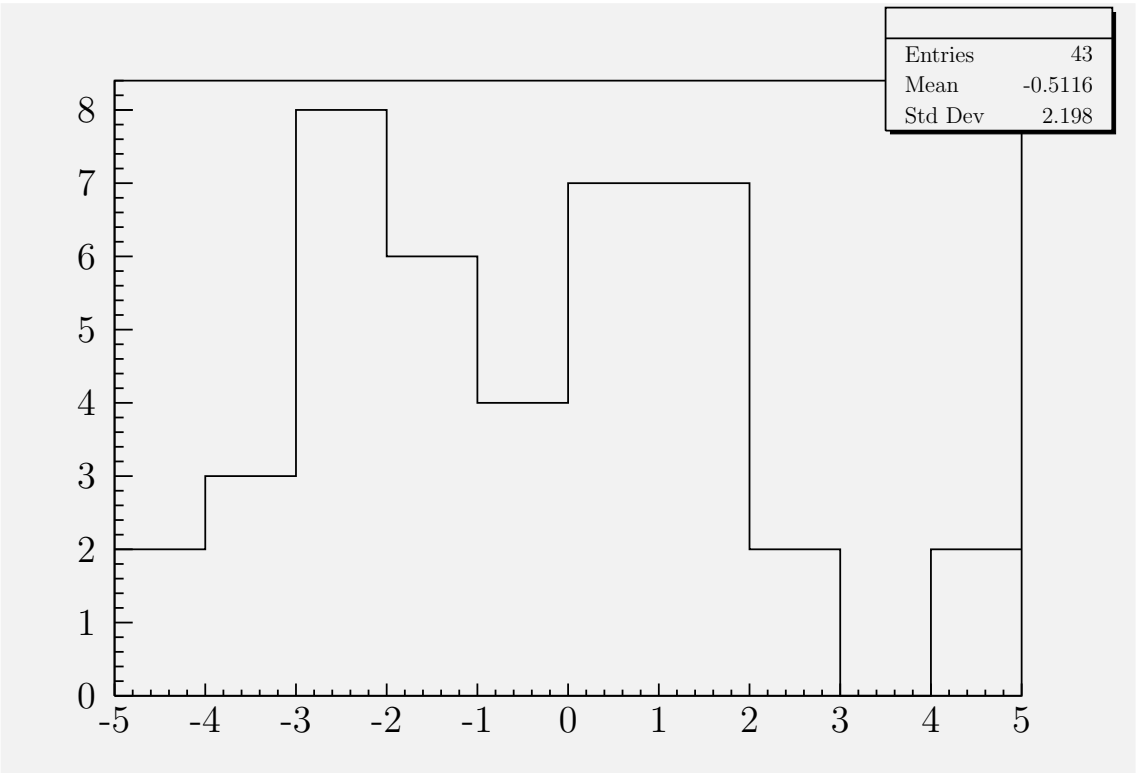

Figure H.121: Histogram of the deviation, in units of the standard deviation, for the Monte Carlo modelling systematic of each kinematic bin in 2015 MagDown $D_s^+ \to \phi\pi^+$ data.

H.9 $D_s^+ \to K^- K^+ \pi^+$ excluding ϕ distributions and result

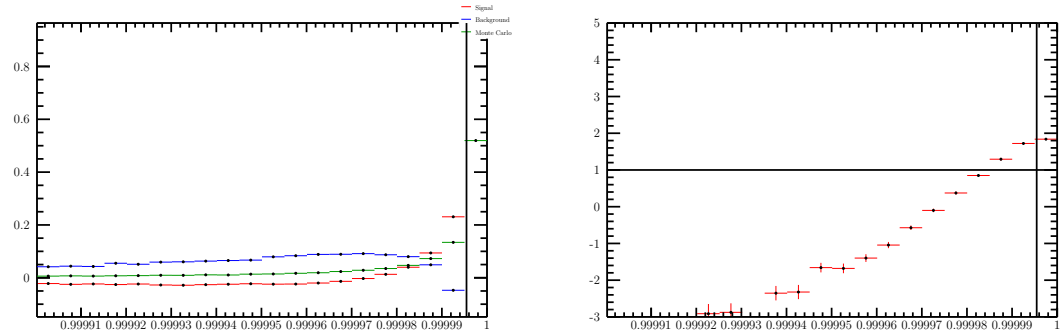

(a) Distributions *(b) Signal data/MC pull*

Figure H.122: Difference in the error corrected yield of 2015 MagDown $D_s^+ \to K^-K^+\pi^+$ excluding ϕ when split by Ds_DIRA_OWNPV into two bins, each containing 50% of the simulated events. H.122a shows signal, background and simulated distributions and the pull between signal and simulation is given in H.122b.

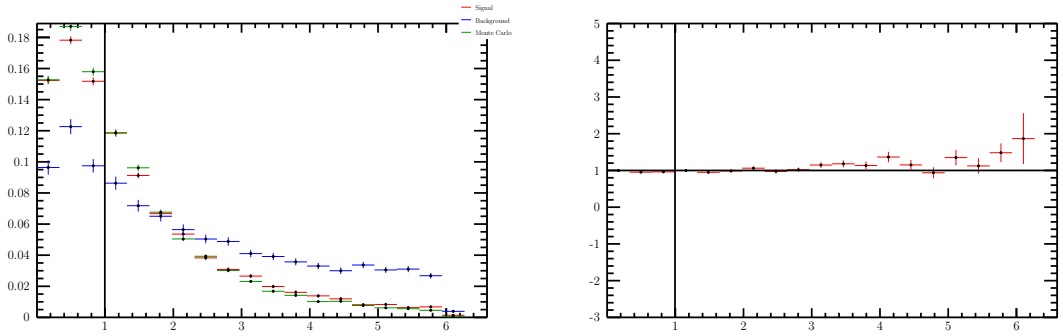

(a) Distributions *(b) Signal data/MC pull*

Figure H.123: Difference in the error corrected yield of 2015 MagDown $D_s^+ \to K^-K^+\pi^+$ excluding ϕ when split by Ds_ENDVERTEX_CHI2/Ds_ENDVERTEX_NDOF into two bins, each containing 50% of the simulated events. H.123a shows signal, background and simulated distributions and the pull between signal and simulation is given in H.123b.

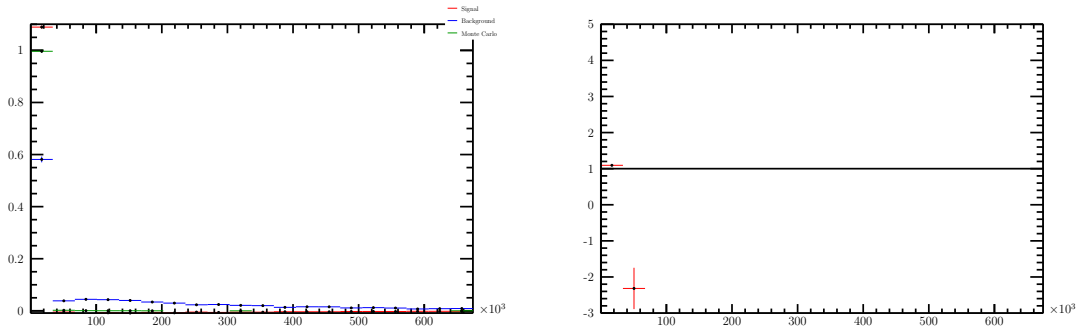

(a) Distributions *(b) Signal data/MC pull*

Figure H.124: Difference in the error corrected yield of 2015 MagDown $D_s^+ \to K^-K^+\pi^+$ excluding ϕ when split by Ds_FDCHI2_OWNPV into two bins, each containing 50% of the simulated events. H.124a shows signal, background and simulated distributions and the pull between signal and simulation is given in H.124b.

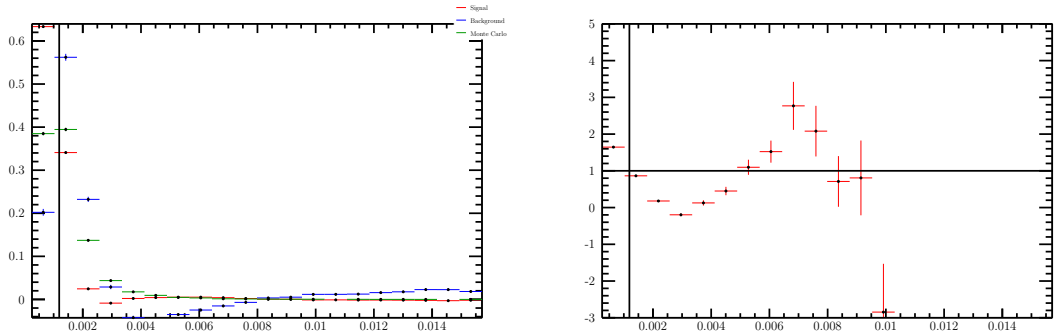

(a) Distributions *(b) Signal data/MC pull*

Figure H.125: Difference in the error corrected yield of 2015 MagDown $D_s^+ \to K^-K^+\pi^+$ excluding ϕ when split by Ds_Loki_BPVLTIME into two bins, each containing 50% of the simulated events. H.125a shows signal, background and simulated distributions and the pull between signal and simulation is given in H.125b.

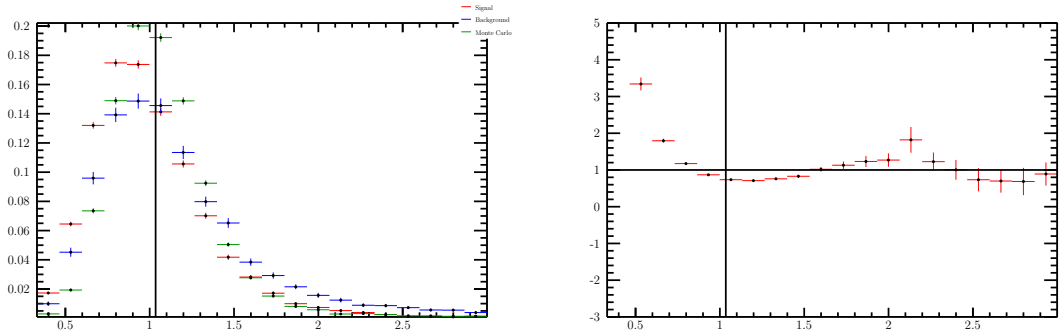

(a) Distributions *(b) Signal data/MC pull*

Figure H.126: Difference in the error corrected yield of 2015 MagDown $D_s^+ \to K^-K^+\pi^+$ excluding ϕ when split by Ds_h1_TRACK_CHI2NDOF into two bins, each containing 50% of the simulated events. H.126a shows signal, background and simulated distributions and the pull between signal and simulation is given in H.126b.

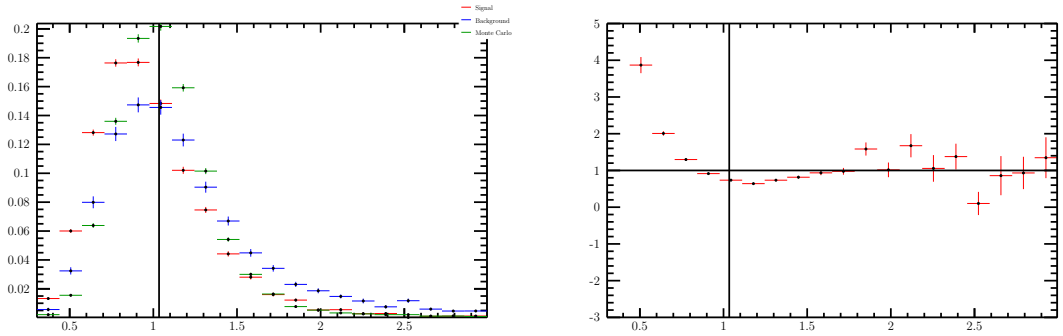

(a) Distributions *(b) Signal data/MC pull*

Figure H.127: Difference in the error corrected yield of 2015 MagDown $D_s^+ \to K^-K^+\pi^+$ excluding ϕ when split by Ds_h2_TRACK_CHI2NDOF into two bins, each containing 50% of the simulated events. H.127a shows signal, background and simulated distributions and the pull between signal and simulation is given in H.127b.

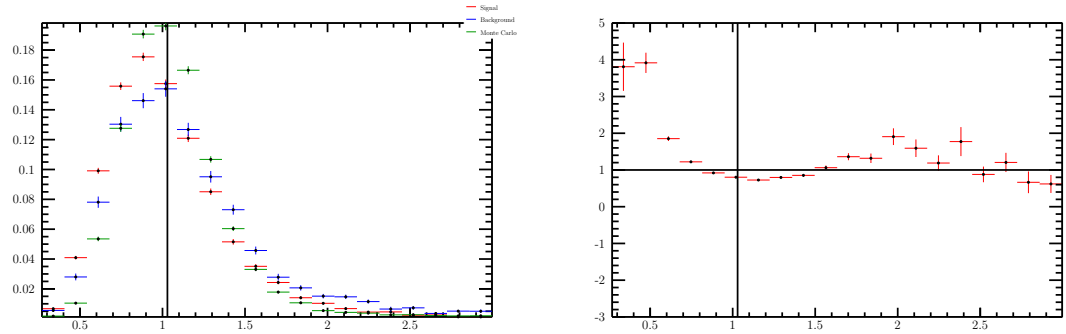

(a) Distributions *(b) Signal data/MC pull*

Figure H.128: Difference in the error corrected yield of 2015 MagDown $D_s^+ \to K^-K^+\pi^+$ excluding ϕ when split by Ds_h3_TRACK_CHI2NDOF into two bins, each containing 50% of the simulated events. H.128a shows signal, background and simulated distributions and the pull between signal and simulation is given in H.128b.

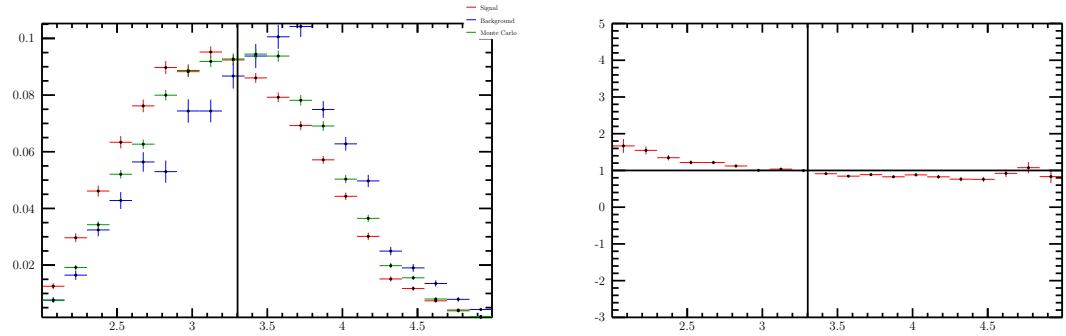

(a) Distributions *(b) Signal data/MC pull*

Figure H.129: Difference in the error corrected yield of 2015 MagDown $D_s^+ \to K^-K^+\pi^+$ excluding ϕ when split by Ds_h1_ETA into two bins, each containing 50% of the simulated events. H.129a shows signal, background and simulated distributions and the pull between signal and simulation is given in H.129b.

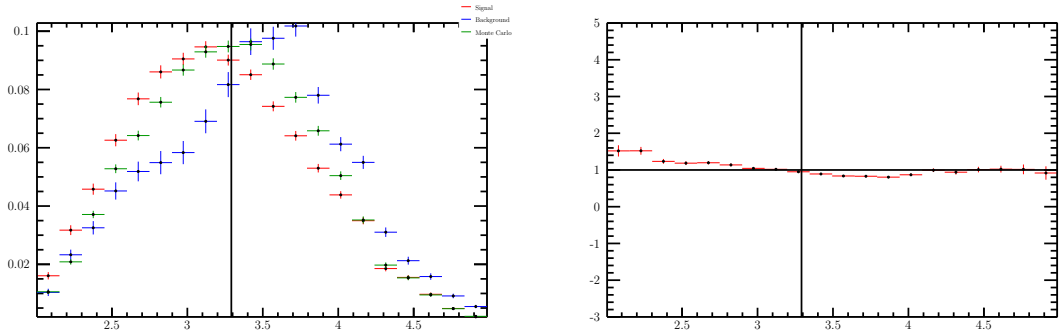

(a) Distributions *(b) Signal data/MC pull*

Figure H.130: Difference in the error corrected yield of 2015 MagDown $D_s^+ \to K^-K^+\pi^+$ excluding ϕ when split by Ds_h2_ETA into two bins, each containing 50% of the simulated events. H.130a shows signal, background and simulated distributions and the pull between signal and simulation is given in H.130b.

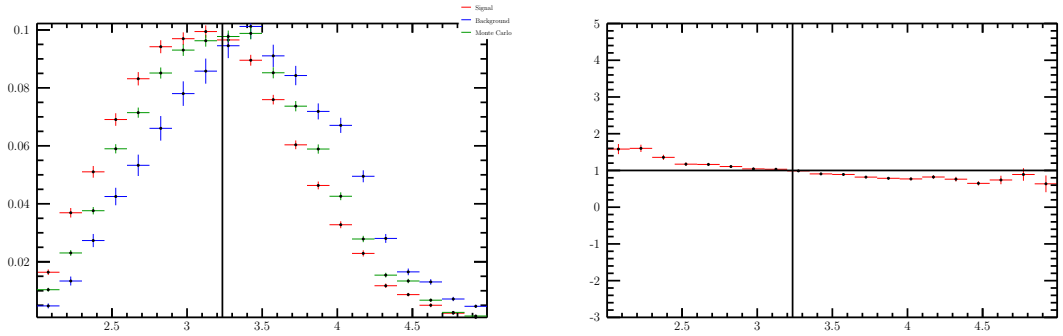

(a) Distributions *(b) Signal data/MC pull*

Figure H.131: Difference in the error corrected yield of 2015 MagDown $D_s^+ \to K^-K^+\pi^+$ excluding ϕ when split by Ds_h3_ETA into two bins, each containing 50% of the simulated events. H.131a shows signal, background and simulated distributions and the pull between signal and simulation is given in H.131b.

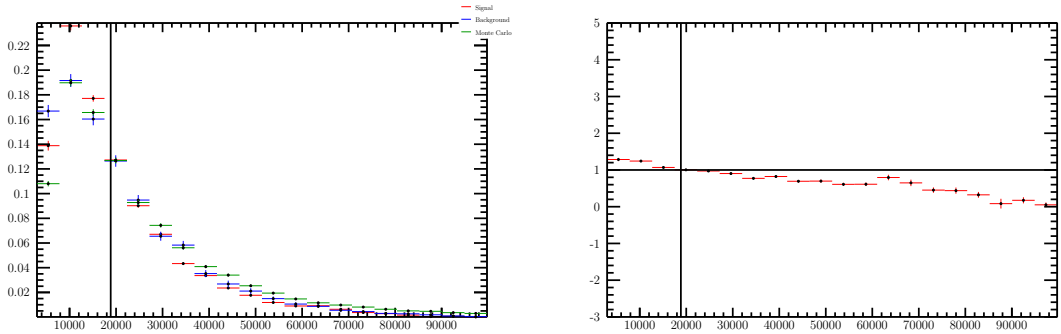

(a) Distributions *(b) Signal data/MC pull*

Figure H.132: Difference in the error corrected yield of 2015 MagDown $D_s^+ \to K^-K^+\pi^+$ excluding ϕ when split by Ds_h1_P into two bins, each containing 50% of the simulated events. H.132a shows signal, background and simulated distributions and the pull between signal and simulation is given in H.132b.

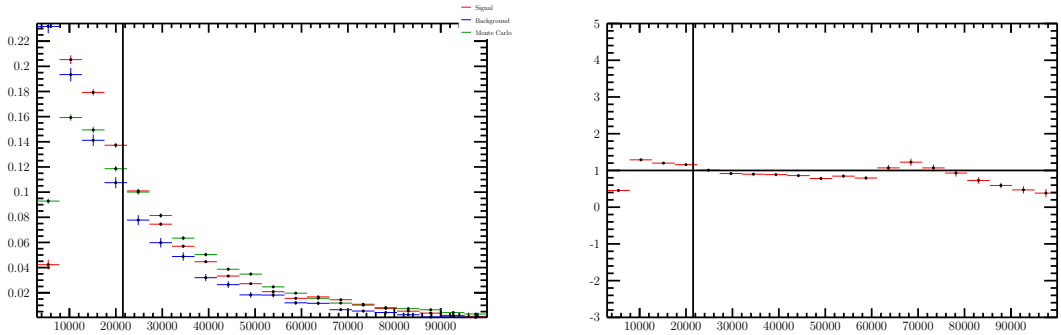

(a) Distributions *(b) Signal data/MC pull*

Figure H.133: Difference in the error corrected yield of 2015 MagDown $D_s^+ \to K^-K^+\pi^+$ excluding ϕ when split by Ds_h2_P into two bins, each containing 50% of the simulated events. H.133a shows signal, background and simulated distributions and the pull between signal and simulation is given in H.133b.

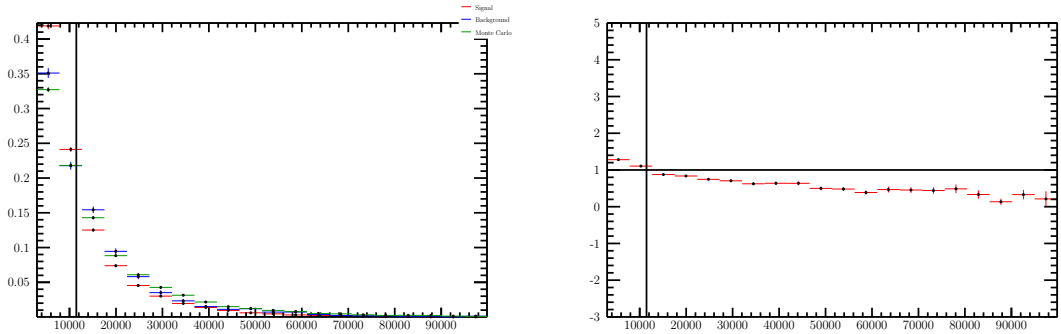

(a) Distributions *(b) Signal data/MC pull*

Figure H.134: Difference in the error corrected yield of 2015 MagDown $D_s^+ \to K^-K^+\pi^+$ excluding ϕ when split by Ds_h3_P into two bins, each containing 50% of the simulated events. H.134a shows signal, background and simulated distributions and the pull between signal and simulation is given in H.134b.

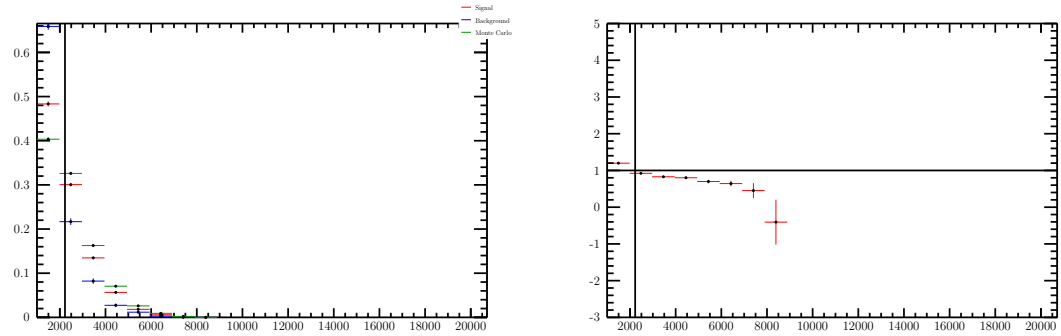

(a) Distributions *(b) Signal data/MC pull*

Figure H.135: Difference in the error corrected yield of 2015 MagDown $D_s^+ \to K^-K^+\pi^+$ excluding ϕ when split by Ds_PT_First into two bins, each containing 50% of the simulated events. H.135a shows signal, background and simulated distributions and the pull between signal and simulation is given in H.135b.

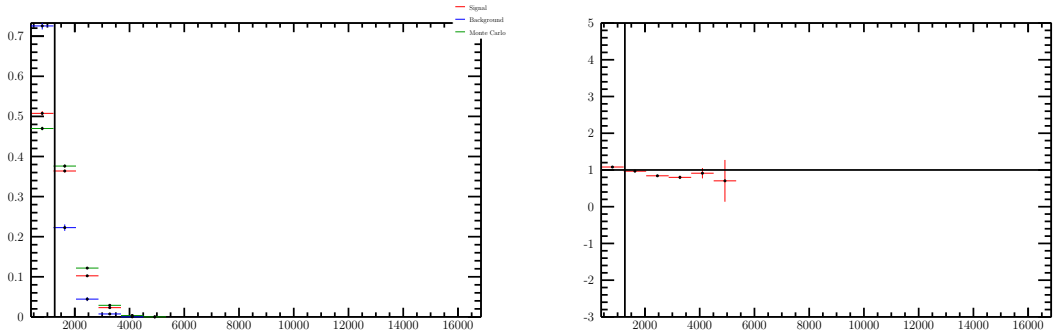

(a) Distributions *(b) Signal data/MC pull*

Figure H.136: Difference in the error corrected yield of 2015 MagDown $D_s^+ \to K^-K^+\pi^+$ excluding ϕ when split by Ds_PT_Second into two bins, each containing 50% of the simulated events. H.136a shows signal, background and simulated distributions and the pull between signal and simulation is given in H.136b.

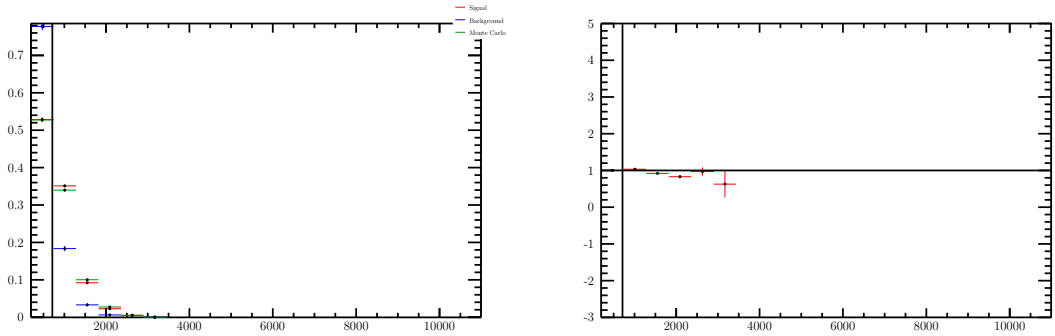

(a) Distributions *(b) Signal data/MC pull*

Figure H.137: Difference in the error corrected yield of 2015 MagDown $D_s^+ \to K^-K^+\pi^+$ excluding ϕ when split by Ds_PT_Third into two bins, each containing 50% of the simulated events. H.137a shows signal, background and simulated distributions and the pull between signal and simulation is given in H.137b.

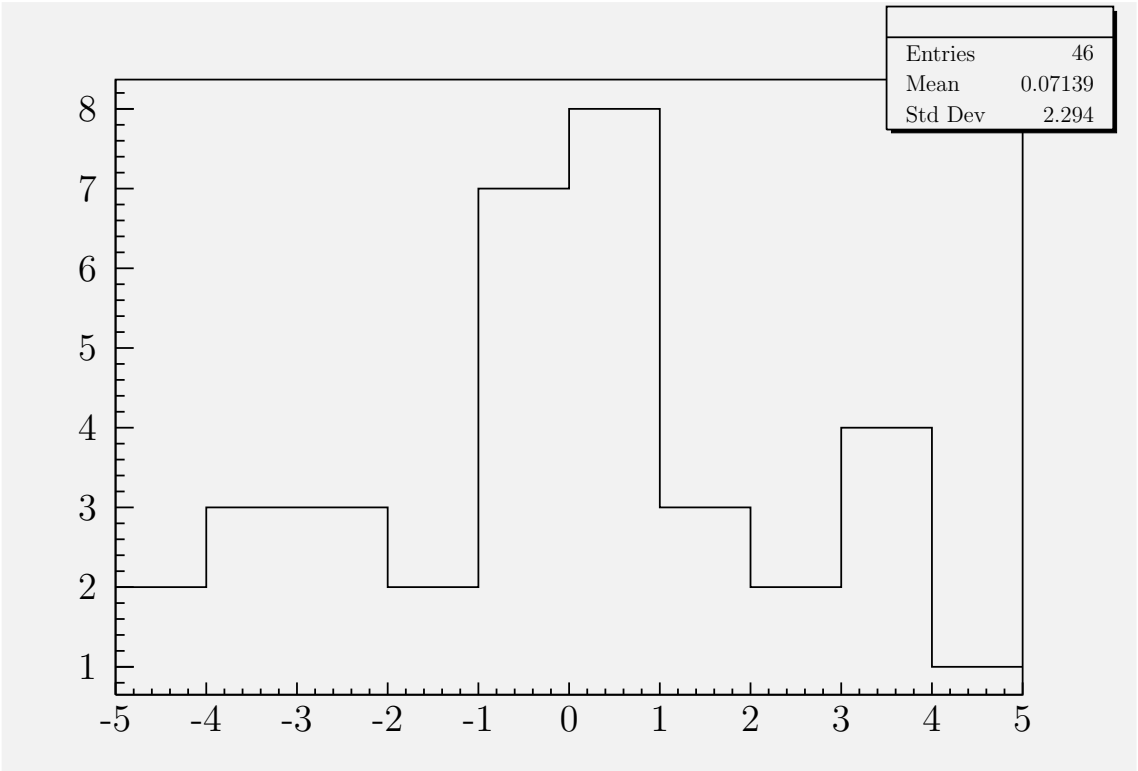

Figure H.138: Histogram of the deviation, in units of the standard deviation, for the Monte Carlo modelling systematic of each kinematic bin in 2015 MagDown $D_s^+ \to K^-K^+\pi^+$ excluding ϕ data.

References

[1] R. Gauld, J. Rojo, L. Rottoli, and J. Talbert, *Charm production in the forward region: constraints on the small-x gluon and backgrounds for neutrino astronomy*, arXiv:1506.0802.

[2] M. Cacciari, M. L. Mangano, and P. Nason, *Gluon PDF constraints from the ratio of forward heavy quark production at the LHC at $\sqrt{s} = 7$ and 13 TeV*, arXiv:1507.0619.

[3] A. Bhattacharya *et al.*, *Perturbative charm production and the prompt atmospheric neutrino flux in light of RHIC and LHC*, arXiv:1502.0107.

[4] O. Zenaiev *et al.*, *Impact of heavy-flavour production cross sections measured by the LHCb experiment on parton distribution functions at low x*, arXiv:1503.0458.

[5] LHCb collaboration, R. Aaij *et al.*, *Prompt charm production in pp collisions at $\sqrt{s} = 7$ TeV*, Nucl. Phys. **B871** (2013) 1, arXiv:1302.2864.

[6] T. Bauer *et al.*, *Prompt charm production in pp collisions at $\sqrt{s} = 7$ TeV in 2010 data*, .

[7] ISO, *Quantities and units — Part 11: Mathematical signs and symbols for use in the physical sciences and technology*, ISO 31-11:1992, International Organization for Standardization, Geneva, Switzerland, 1992.

[8] B. Kniehl, G. Kramer, I. Schienbein, and H. Spiesberger, *Inclusive charmed-meson production at the CERN LHC*, Eur. Phys. J. **C72** (2012) 2082, arXiv:1202.0439.

[9] M. Cacciari *et al.*, *Theoretical predictions for charm and bottom production at the LHC*, JHEP **10** (2012) 137, arXiv:1205.6344.

[10] NNPDF, R. D. Ball *et al.*, *Parton distributions for the LHC Run II*, JHEP **1504** (2015) 040, arXiv:1410.8849.

[11] Particle Data Group, C. Amsler *et al.*, *Fragmentation functions in e^+e^- annihilation and lepton-nucleon DIS*, in *Review of particle physics*, vol. B667, ch. 17, p. 1. 2008. doi: 10.1016/j.physletb.2008.07.018.

[12] T. Sjstrand *et al.*, *An introduction to PYTHIA 8.2*, Comput. Phys. Commun. **191** (2015) 159, arXiv:1410.3012.

[13] J. Alwall *et al.*, *The automated computation of tree-level and next-to-leading order differential cross sections, and their matching to parton shower simulations*, JHEP **1407** (2014) 079, arXiv:1405.0301.

[14] P. Skands, S. Carrazza, and J. Rojo, *Tuning PYTHIA 8.1: the Monash 2013 tune*, Eur. Phys. J. **C74** (2014), no. 8 3024, arXiv:1404.5630.

[15] T. Kneesch, B. A. Kniehl, G. Kramer, and I. Schienbein, *Charmed-meson fragmentation functions with finite-mass corrections*, Nucl. Phys. **B799** (2008) 34, arXiv:0712.0481.

[16] B. A. Kniehl and G. Kramer, *Charmed-hadron fragmentation functions from CERN LEP1 revisited*, Phys. Rev. **D74** (2006) 037502, arXiv:hep-ph/0607306.

[17] H.-L. Lai *et al.*, *New parton distributions for collider physics*, Phys. Rev. **D82** (2010) 074024, arXiv:1007.2241.

[18] P. M. Nadolsky *et al.*, *Implications of CTEQ global analysis for collider observables*, Phys. Rev. **D78** (2008) 013004, arXiv:0802.0007.

[19] W. K. Tung *et al.*, *Heavy Quark Mass Effects in Deep Inelastic Scattering and Global QCD Analysis*, JHEP **02** (2007) 053, arXiv:hep-ph/0611254.

[20] J. Pumplin, H. L. Lai, and W. K. Tung, *The Charm Parton Content of the Nucleon*, Phys. Rev. **D75** (2007) 054029, arXiv:hep-ph/0701220.

[21] LHCb collaboration, R. Aaij *et al.*, *Measurement of the track reconstruction efficiency at LHCb*, arXiv:1408.1251, submitted to JINST.

[22] Particle Data Group, K. A. Olive *et al.*, *Review of particle physics*, Chin. Phys. **C38** (2014) 090001.

[23] M. Pivk and F. R. Le Diberder, *Plots: A statistical tool to unfold data distributions*, Nuclear Instruments and Methods in Physics Research A **555** (2005) 356, arXiv:physics/0402083.

[24] A. Poluektov, *Kernel density estimation of a multidimensional efficiency profile*, Journal of Instrumentation **10** (2015), no. 02 P02011.

[25] Particle Data Group, K. Olive *et al.*, *Review of Particle Physics*, Chin. Phys. **C38** (2014) 090001.

[26] CLEO Collaboration, J. P. Alexander *et al.*, *Absolute measurement of hadronic branching fractions of the D_s^+ meson*, Phys. Rev. Lett. **100** (2008) 161804.

[27] T. M. Karbach and M. Schlupp, *Constraints on Yield Parameters in Extended Maximum Likelihood Fits*, ArXiv e-prints (2012) `arXiv:1210.7141`.

[28] C. Burr and S. Easo, *Measuring open charm hadron production at 7 TeV using the LHCb detector*, PhD thesis, Southampton, University of Southampton, May, 2015, Presented 01 Jun 2015.

[29] Particle Data Group, C. Amsler *et al.*, *Review of Particle Physics*, Phys. Lett. **B667** (2008) 1.

[30] L. Lyons, D. Gibaut, and P. Clifford, *How to combine correlated estimates of a single physical quantity*, Nuclear Instruments and Methods in Physics Research Section A **270** (1988), no. 1 110 .

[31] R. Barlow, *Asymmetric Errors*, ArXiv Physics e-prints (2004) `arXiv:physics/0401042`.

[32] M. Gersabeck and M. Alexander, *Measurement of the charm mixing and CP violation parameter y_{CP} with 2011 data*, .